EQUINE SCINTIGRAPHY

Edited by S. J. Dyson, R. C. Pilsworth, A. R. Twardock and M. J. Martinelli

EQUINE VETERINARY JOURNAL LTD

Equine Veterinary Journal, 351 Exning Road, Newmarket, Suffolk CB8 0AU, UK.
Tel: +44 (0) 1638 666160 ▪ Fax: +44 (0) 1638 668665 ▪ Website: www.evj.co.uk ▪ Email: viv@evj.co.uk

Equine Veterinary Journal is the official journal of the British Equine Veterinary Association. It is produced and published by Equine Veterinary Journal Ltd.

▪ ISBN 0-9545689-0-7
▪ First Published 2003

Front Cover Image Courtesy of *Dr Mark Holmes, School of Veterinary Medicine, University of Cambridge, Cambridgeshire, UK.*
Subject Indexes Prepared by *Indexing Specialists (UK) Ltd., Hove, West Sussex, UK.*
Typeset and Published by *Equine Veterinary Journal Ltd., Newmarket, Suffolk, UK.*
Printed in Great Britain by *Geerings of Ashford Ltd., Ashford, Kent, UK.*

CONTENTS

FOREWORD

Modern veterinary medicine is confronted in a persistent way by basic sciences and new techniques. Various developments in chemistry, biochemistry and physics allow new diagnostic and therapeutic procedures and force the veterinarian to engage in interdisciplinary problems.

Nuclear medicine sets a typical example for these tendencies. The use of radioactive substances in medical diagnosis has gained a high standing because of large clinical experiences, numerous experimental results, advances in physics, radiochemistry and marked improvements of the technical equipment. The development of human nuclear medicine in the last two decades has been amazing.

In the 1980s and 1990s, turf battles started between nuclear medicine and new imaging modalities such as computer assisted tomography and magnetic resonance imaging. Nuclear medicine seemed to be on the losing end. However, new techniques like positron emission tomography and imaging with radioactive labelled antibodies kindled new interest.

The development of nuclear medicine in the veterinary field was much less spectacular. The first publications of the applications of radioisotope imaging techniques appeared in the late 1960s and early 1970s. Usually these were very limited investigations in selected cases with exotic nuclides such as ^{85}Sr and ^{87m}Sr. Routine application of the radioactive labelled tracers became possible after the introduction of ^{99m}Tc and the availability of suited labels for the different target organs. In small animal medicine, nearly all procedures known to the human nuclear medicine were tested and became routine examinations in specialised centres. However, large scale availability never became reality.

In equine radiology, only the application of ^{99m}Tc-labelled substances for the demonstration of bone metabolism and the airways became accepted examination methods. All other possibilities for the demonstration of organ metabolism never gained acceptance on a larger scale.

The duties of the veterinarian using radioactive imaging are varied. Indications for the use of the radioactive label, the assessment of radioactive risk, differentiation and interpretation of results are some of the points to be considered.

The aim of this book is to substantiate the application of the radioisotope imaging method in the horse by physical, chemical, biochemical, physiological and pharmacological means and to outline its advantages against other imaging methods. It is not a book containing all the information to interpret bone scans in the different regions. Instead, it tries to give the necessary information on how to perform the examination and which possibilities exist for the interpretation process. Examinations can be performed in different ways. Most veterinarians like to perform scintigraphic examination in the standing horse. This limits the total number of counts that generate the image. Movement of the patient is the limiting factor. Examination in the anaesthetised horse allows the acquisition of large count numbers and images with better resolution and more anatomical detail, but at the cost of the anaesthetic risk.

Professor Gottlieb Ueltschi
University of Berne, Switzerland

ACKNOWLEDGEMENTS

Peter Rossdale - who first proposed this book to the Editors, for his help and encouragement throughout its production.
Professor Ueltschi, University of Berne, Switzerland, not only for contributing our Forword, but also for setting standards in scintigraphy we all feel motivated to aspire to.
Ann Monteith (*EVJ*) - who set up the initial commissioning of the chapters from authors and put the book on a firm foundation.
Anita Boole (*EVJ*) - who took over the production of the book from Ann Monteith, designed the cover, and designed such an attractive style and layout for the text.
Lindsey Abeyasekere (*EVJ*) - who painstakingly proof read the manuscripts as they were produced in the *EVJ* office.
Rachel Green (*EVJ*) - for dealing with the business of making a pile of chapters into a book.
All of our authors, for giving so freely of their time and expertise.
All those who supplied illustrations for the book, and who are credited individually in the figure legends.
We would also like to pay tribute to the pioneers of equine scintigraphy, on several continents, who set up this science for us to explore and and document.

All Editors

I thank Tim Donovan, John Palmer and Jo Weekes, the imaging technicians past and present at the *Animal Health Trust*, for technical support and being sources of knowledge and experience. A succession of interns has also provided technical assistance during image acquisition and, by testing the hypothesis that by teaching you learn, has encouraged both the development of knowledge and distilling clarity of thought. Steve Bloomer from *Nuclear Diagnostics* has been a constant inspiration to learn more and to try to achieve the best standards of imaging. Many colleagues from around the world have over the years provided thought-provoking questions, shared their experiences and presented a challenge to improve our levels of diagnosis. I am indebted to our co-authors, without whom this project could not have been achieved. The completion of this book would not have been possible without Anita Boole and her colleagues at the *Equine Veterinary Journal*, to whom we are indebted. My husband, John Wilkinson, has again showed extreme patience and tolerance during the many hours spent on this project, but also encouragement, support, friendship and humour.

Sue Dyson

I would like to thank: my co-editors, for agreeing without hesitation to devote endless unpaid hours to this project when I first approached them; my colleagues and technicians at *Beaufort Cottage Diagnostic Centre* for their encouragement in first setting up the scintigraphy facility and their hard work in running it; my wife Lynn, and children Anna and Ellen, for tolerating my absence both physically and mentally on numerous evenings and weekends whilst this book was in preparation, and for their constant love and support.

Rob Pilsworth

I thank Mike Molnar (*Diagnostic Services, Inc.*) for his review and suggestions regarding Part I, Chapter 3, The Gamma Camera; Deryl Markgraf (*Enhanced Technologies Corp.*) for information and photographs of gamma camera installations; Greg Daniel for returning (on loan) Sorenson and Phelps' 'Physics in Nuclear Medicine', which I didn't think I needed after retirement (an oxymoronic word, I've discovered); my co-editors for including me in this project, allowing me to stay in touch with developments and veterinarians involved in this intriguing discipline of nuclear scintigraphy; all of my colleagues and friends who encouraged and participated in the development of nuclear medicine at the *University of Illinois College of Veterinary Medicine*; lastly, my wife Mary, for her blessing, encouragement and wisdom knowing I should do this.

Bob Twardock

I have numerous people to thank for my academic and clinical development over the 11 years that I have been involved with nuclear scintigraphy. This includes all the referring veterinarians in Scotland, the Mid-western United States and southern California, who recognised what this advance in diagnostic imaging could do for their cases. I would also like to thank my co-editors for their stimulating dialogues on scintigraphy over the years and for including me in this project. I would like to thank Rachel Green and Peter Rossdale in the *EVJ* office for their support and friendship over the last 8 years. Finally, I need to thank my other co-editor, Bob Twardock, for his mentorship, patience and friendship over the last 11 years. Dr Twardock was truly a pioneer and champion of nuclear scintigraphy long before the industry really understood the diagnostic implications it would have on the equine performance industry. Bob, thanks for your foresight and tutelage.

Mark Martinelli

PREFACE

Nuclear scintigraphy has been widely used in equine veterinary medicine in institutions and referral practices for approximately 15 years, and in recent years more private practices have been establishing nuclear medicine facilities. It has become very apparent to us that although a number of excellent general review papers and chapters in books discuss the potential usefulness of equine nuclear scintigraphy, and some much more specific articles have been published, there has been a lack of a general text covering all aspects of equine nuclear medicine. We are also aware that, as with many imaging modalities, practitioners sometimes attempt to diagnose abnormalities without a comprehensive knowledge of normal, and the full range of normal variations, and sometimes without adequately criticising their own basic image quality. We therefore set out to harness the collective expertise of a number of people experienced with nuclear scintigraphy from a variety of geographical locations, and involved with different populations of sports and pleasure horses.

The book is divided into two sections. In *Part I*, we aimed to provide a comprehensive but essentially practical guide to how to perform equine nuclear scintigraphy to achieve the best possible results, whilst complying with safety legislation, and how to interpret the resultant images. We are aware that the legislation concerning the use of radiopharmaceuticals varies worldwide, but the basic guidelines provided should encompass the requirements of most countries.

The majority of equine nuclear scintigraphic examinations are used to evaluate the musculoskeletal system and a large proportion of the book is devoted to this. We have therefore provided guidelines for image interpretation and also, in *Part II*, a comprehensive, but not exhaustive, atlas of normal images from horses involved in different athletic disciplines and examples of some of the more common conditions causing lameness or poor performance. However, there are also extensive chapters in *Part II* devoted to other aspects of nonorthopaedic nuclear medicine. We hope that, by providing many high quality illustrations, we will encourage practitioners to strive to match the image standard reproduced here.

In order to keep the figure legends as concise as possible, we introduced a number of standard abbreviations which are listed on the following pages. We recognise that some readers may find this more difficult, but space constraints made this essential.

We feel strongly that nuclear scintigraphy is not a tool to be used in isolation. It should be used selectively and the results must always be related to those of clinical examination and other diagnostic techniques. It is not going to provide an answer in every horse and we have attempted to highlight both the limitations of nuclear scintigraphy and some artefacts that may confound interpretation.

We, the Editors, learnt a lot by sharing our collective experiences and sincerely hope that anyone reading this text or browsing through the figures will be both stimulated and challenged to improve their level of diagnosis.

The Editors

TERMS & ABBREVIATIONS

ANATOMICAL ABBREVIATIONS

ABC Antebrachiocarpal (joint)
ACB Accessory carpal bone
ALDDFT Accessory ligament of the DDFT
CD Centrodistal (joint)
CF Coxofemoral (joint)
CMC Carpometacarpal (joint)
C1 First carpal bone
C2 Second carpal bone
C3 Third carpal bone
C4 Fourth carpal bone
DDFT Deep digital flexor tendon
DJD Degenerative joint disease
DIP Distal interphalangeal joint
DSP Dorsal spinous process
ELL Enostosis-like lesion
FP Femoropatellar (joint)
FT Femorotibial (joint)
HR Humeroradial/elbow (joint)
IC Intermediate carpal (bone)
LFT Lateral femorotibial (joint)
MC Middle carpal (joint)
MCP Metacarpophalangeal (joint)
McII Second metacarpal bone
McIII Third metacarpal bone
McIV Fourth metacarpal bone
MFT Medial femorotibial joint
MTP Metatarsophalangeal (joint)
MtII Second metatarsal bone
MtIII Third metatarsal bone
MtIV Fourth metatarsal bone
OA Osteoarthritis
OCD *Osteochondritis dissecans*
OCLL Osseous cyst-like lesion
PIP Proximal interphalangeal (joint)
PSB Proximal sesamoid bone
PSD Proximal suspensory desmitis
RC Radial carpal (bone)
SBC Subchondral bone cyst
SDFT Superficial digital flexor tendon
SH Scapulohumeral (joint)
SL Suspensory ligament
TC Tarsocrural (joint)
TMT Tarsometatarsal (joint)
T3 Third tarsal bone
UC Ulnar carpal (bone)

USE

Am. Competition Amateur Competition
Am. Dressage Amateur Dressage
Dressage
Dressage (Nov.) Novice
Dressage (Med.) Medium
Dressage (Adv.Med.) Advanced Medium
Dressage (Prix St George)
Potential Dressage
Driving
Endurance Riding
Eventing (Int.) Intermediate
Eventing (Adv.) Advanced
3-Day Eventing
Flat Racing
General Purpose
Hunting
National Hunt Racing
Native Showing
Pacer
Pony Club Activities
Showing
Showjumping
Am. Showjumping Amateur Showjumping
Showjumping (Grand Prix)
Showjumping (International)
Trotter

FIGURE ORIENTATION

L Left
R Right
LF Left Fore
RF Right Fore
LH Left Hind
RH Right Hind
DORS Dorsal
PALM Palmar
CRAN Cranial
CAUD Caudal
MED Medial
LAT Lateral
PROX Proximal
DIST Distal
VENT Ventral
ROST Rostral

BREED

AxW Arab x Welsh
AxWxTB Arab x Welsh x Thoroughbred
Am.TB American Thoroughbred
BWB Belgian Warmblood
Brit.WB British Warmblood
Cob
Conn. Connemara
Conn.xA Connemara x Arab
DanWB Danish Warmblood
DWB Dutch Warmblood
GWB German Warmblood
Han. Hanoverian
Han.x Hanoverian x
IDx Irish Draught x
IDxTB Irish Draught x Thoroughbred
Irish
Irish SH Irish Sports Horse
Irish TB Irish Thoroughbred
O Oldenburg
Pony
SB Standardbred
SF Selle Française
Shire
TB Thoroughbred
TBx Thoroughbred x
TBxCB Thoroughbred x Cleveland Bay
Trak. Trakehner
WB Warmblood
Welsh(A) Welsh Section A
Welsh(D) Welsh Section D

SEX

F Filly
M Mare
C Colt
S Stallion
G Gelding

EQUINE SCINTIGRAPHY PART I

Chapter 1

BASIC PRINCIPLES OF EQUINE SCINTIGRAPHY

ADAM J. DRIVER
Dubai Equine Hospital, PO Box 9373, Dubai, UAE.

INTRODUCTION

The basic principle of nuclear scintigraphy is the detection of γ-rays, emitted from the decay of a radionuclide, by a gamma camera. When the radionuclide is attached to a specific pharmaceutical, a graphical representation of the physiological function, shape, size and position of the target organ can be made. The clinical information obtained from the images depends on the biochemistry of the pharmaceutical, its interactions with the target organ specifically, and its transport through other tissues and organs.

While scintigraphic images give anatomical information about the target organ, the spatial resolution is poor compared to other imaging modalities such as radiography, magnetic resonance imaging (MRI) and computed tomography (CT). The main information obtained from the images is based on a physiological process of the target organ, e.g. in bone scans the turnover of bone and blood flow to the bone are assessed; in renal scans the glomerular filtration rate, tubular clearance or drainage can be assessed, depending on the radiopharmaceutical used. This is a fundamental principle when interpreting the images formed; it is not the anatomy of the organ that is being investigated but a physiological process associated with that organ. Therefore, as with all imaging modalities, scintigraphy should never be used in isolation for diagnosis, but in conjunction with a full clinical evaluation, and other imaging or diagnostic modalities, as required. It is commonly agreed that full body indiscriminate skeletal scanning in the horse, without clinical guidance is of little or no diagnostic value, and leads to unnecessary exposure of personnel to radiation[1].

Scintigraphy has progressed a long way since Hal Anger's invention of the gamma camera in 1957, to modern digital gamma cameras and single photon emission tomography (SPECT) and positron emission tomography (PET) scanners. With the advent of digital imaging and a dedicated nuclear medicine computer, scintigraphy has further evolved to provide more information from the same images. We now have the ability to manipulate images using algorithmic functions such as smoothing or sharpening filters, motion correction, interpolation and windowing to improve subjectively the detection of abnormal regions. We also have the option to assess images quantitatively with region of interest software, time activity curves and profiling software. In the horse, scintigraphy has been used predominantly for the detection of bone pathology, particularly stress fractures and entheseopathies. Even in the human field, the bone scan was considered the 'gold standard' for the detection of stress fractures until the advent of MRI[2]. The improved diagnosis of stress fractures in the horse has been of great benefit in reducing the mortality rate from these injuries by preventing them developing into catastrophic fractures. Scintigraphy is not only more sensitive in the detection of stress fractures than radiography[3], but allows imaging of sites in which radiography would be difficult or contraindicated, such as the pelvis. Because of its sensitivity, it allows monitoring of the healing process so that horses may be returned to training at the correct time.

Nuclear medicine has also been useful for research because of its ability to image physiological properties. It has been used to investigate exercise-induced pulmonary haemorrhage (EIPH), chronic obstructive pulmonary disease (COPD) and laminitis. As newer and more stable pharmaceuticals are developed in the human field, especially those that are bound to technetium (^{99m}Tc), further areas of investigative imaging will be opened up to the veterinarian. One such field is the investigation of infectious or inflammatory processes in the horse. Many non-ideal radiopharmaceuticals have been utilised in the detection of occult sites of infection or inflammation, but with varying success, and often with large amounts of image manipulation and extended scanning times required. A new radiopharmaceutical, ^{99m}Tc-ciprofloxacin (Infecton), has recently been used successfully in a dog to image an occult site of infection in a hip prosthesis[4]. In human trials, the results have also been promising as a specific bacterial-seeking agent[5]. With the development of further pharmaceuticals or the development of labelling of specific markers such as inflammatory mediators or monoclonal antibodies, the role of scintigraphy in research will continue to grow, giving us an insight into pathophysiological processes. As in many areas, we shall learn from, and follow in the footsteps of, our human counterparts, to adapt and utilise new developments in nuclear medicine, to research further into disease processes.

The commonest form of radionuclide imaging employs elements that emit γ-ray photons at single or multiple energies. The equipment used to detect and image these emissions is the gamma camera, which is a position-sensitive γ-ray detector.

THE RADIONUCLIDE

The radionuclide (also known as the radioisotope) is the radioactive component of the radiopharmaceutical. The commonest radionuclides used in scintigraphy emit single energy γ-rays as part of their decay process and are chosen with reference to the following important criteria:

- The radionuclide must be easily attached to the pharmaceutical to be used to assess the physiological function under investigation.

Table 1: Common radionuclides used in nuclear medicine imaging

Element	Isotope	Half-life ($T^{1/2}$)	Principle γ-ray energies (KeV)
Technetium	Tc-99m	6 h	140.5
Krypton	Kr-81	13 secs	190
Thallium	Tl-201	3.05 days	68–80
Indium	In-111	2.8 days	173, 247
Iodine	I-123	13.2 h	(28), 159

- It must have a short half-life ($T^{1/2}$) to limit the radiation dose to the patient and facilitate early and safe disposal.
- The gamma radiation should interact minimally with body tissues, thereby minimising patient dose and allowing radiation to escape the patient so that it can be detected.
- The radiation emitted should be of sufficiently low energy to minimise scatter, which would compromise spatial information. As gamma energy increases, the relative amount of scatter in the spectrum increases, because the probability of Compton interaction (see *Detection of Radiation*) relative to photoelectric interaction increases.
- The scattered radiation must be able to be absorbed by the collimator, allowing the primary radiation to be detected by the scintillation crystal. The energy of the gamma radiation must be of an energy suitable for efficient detection by the scintillating crystal.

Therefore, radioisotopes that produce γ-rays with energies between 80 and 247 KeV and that have short half-lives are used. Some common radionuclides used in scintigraphy are included in **Table 1**.

For some studies, non-ideal isotopes are required due to the organ being imaged. The radioactive gas Krypton-81 (^{81}Kr) used in ventilation studies is non-ideal because of its short $T^{1/2}$ (13 secs), meaning that the generator must be sited close to or in the area where the procedure will be performed. Even the parent isotope for ^{81}Kr has a short $T^{1/2}$ (4.5 h), and has to be produced from a cyclotron, making it an expensive isotope to produce. Therefore, only specialist centres with an on-site pharmacy, close to or with a cyclotron, can perform such procedures.

Indium-111 (^{111}In) has been used in the equine field to label equine leucocytes for imaging an abdominal abscess[6], but is a non-ideal isotope and the majority of indium labelling of radiopharmaceuticals has been replaced by ^{99m}Tc.

The most commonly used radioisotope in equine scintigraphy is ^{99m}Tc. This has a $T^{1/2}$ of 6.02 h and emits γ-rays at an energy of 140 KeV. The short $T^{1/2}$ results in low radiation dose for the patient, but is long enough to allow for production of radiopharmaceuticals and transportation from a pharmacy, while still maintaining sufficient radioactivity to produce diagnostic images. The energy value of 140 KeV allows a significant quantity of γ-radiation to escape the patient, as 50% of γ-rays will escape from a depth of 4.6 cm of soft tissue, the half value layer (HVL)[a], but are of sufficiently low energy to be absorbed easily by lead (HVL 0.3 mm) and to interact with the scintillating material (sodium iodide HVL of 2.5 mm). It can also be used to radiolabel a wide range of clinically useful pharmaceuticals.

The radionuclide emits ionising radiation during the process of radioactive decay. Decay is an exponential process, following the equation:

Equation 1

$A_t = A_o e^{-\lambda t}$ where A_t = Radioactivity at time t
A_o = Original activity at time 0
λ = Decay constant = $^{0.693}/_{T^{1/2}}$

The fractional decay of a radioisotope can also be calculated by rearranging the equation.

Equation 2

$$A_t/A_o = e^{\lambda t}$$

Table 2 shows the fractions of ^{99m}Tc remaining at hourly intervals post calibration, calculated using equation 2. Alternatively, a decay factor can be used to calculate the residual activity, by dividing the original quantity by the decay factor for the time elapsed.

THE RADIOPHARMACEUTICAL

The radiopharmaceutical used is dependent on the organ, body component or biological function to be targeted. This topic is covered in depth in *Part I, Chapter 2*. An ideal radiopharmaceutical should rapidly localise to the target organ once administered, be nontoxic and be easily eliminated from the body, to minimise radiation dose to the patient[7]. Some common radiopharmaceuticals used include the following.

Diphosphonate Salts

Several of the diphosphonate salts are the most commonly used in equine scintigraphy, as they selectively localise in the bone. These include methylene diphosphonate (MDP), disodium oxidronate (HDP) and methylene hydroxydiphosphonate (MHDP).

The diphosphonate salt binds to hydroxyapatite in the bone, and its uptake is relative to the osteoblastic activity or metabolism of the bone and the blood flow to the bone in a specific area. Increased osteoblastic activity or blood flow result in an increased uptake of the radiopharmaceutical.

Simple Salts

$Na^{123}I$ is used for thyroid imaging, but is expensive and not readily available because it is produced in a cyclotron. For this reason, pertechnetate is more commonly used for routine thyroid examinations

Nanocolloids

Nanocolloids have been used in horses as a cheap alternative to labelled antibodies or blood cells, to image sites of inflammation. They consist of very small human albumin particles. The method of localisation is due to small blood

[a]HVL: the thickness of an absorbing material that absorbs half of the incident γ-rays.

Table 2: Fractional decay of ^{99m}technetium

Time (h)	Activity fraction post calibration (A_0)	Decay factor
0	1.000	
1	0.891	1.12
2	0.794	1.26
3	0.707	1.42
4	0.630	1.59
5	0.561	1.78
6	0.500	2.00

Example: If 7000 MBq of ^{99m}Tc is assayed at 08.00 h, then the activity when injected at 11.00 h would be 7000 x 0.707 = 4949 MBq. Alternatively, using the decay factor, 7000 ÷ 3 h (1.42) = 4930 MBq.

vessels leaking, in the inflamed state, so allowing these molecules to extravasate in areas of inflammation. Trials have been disappointing, showing many false positive results, and that it is no more reliable than second-phase scanning with HDP or MDP. The primary use of nanocolloids in human medicine is to image the bone marrow and lymphatic systems.

Labelled Cells

White blood cells (WBCs) are labelled with ^{111}In or ^{99m}Tc HMPAO as a method of imaging areas of inflammation or infection, but interpretation can be difficult, with both false negative and positive results. There is a normal large accumulation in the spleen, liver and lungs[8]. Results of trials in the horse have not been convincing, although inflammatory bowel disease has recently been successfully imaged[9].

Labelled red blood cells (RBCs) have been used in horses to image areas of EIPH. ^{99m}Tc-stannous fluoride RBCs are given at exercise, and the horse is imaged post exercise[10].

Labelled Antibodies

Labelled monoclonal antibodies are being used increasingly to target specific processes or receptor sites in human medicine. Human polyclonal nonspecific immunoglobulins (HIG) have been shown to be among the most effective radiopharmaceuticals to localise areas of musculoskeletal infection or inflammation[11]. High molecular weight melanoma associated antibody, labelled with ^{99m}Tc, is a sensitive method of detecting metastatic spread of malignant melanoma in humans[12].

Labelled Biochemicals

See *Part I, Chapter 2* for further information.

Macroalbumin Aggregates

^{99m}Tc macroalbumin aggregates (MAA) are used to assess pulmonary perfusion and distribution. The radiopharmaceutical is injected as a bolus into the jugular vein and the MAA particles lodge in the small pulmonary capillaries and arterioles, showing the distribution of pulmonary perfusion. Used together with ventilation studies, ventilation perfusion (V/Q) mismatches can be determined (see *Part II, Chapter 7*).

THE GAMMA CAMERA AND COLLIMATORS

The gamma camera is discussed in depth in *Part I, Chapter 3*, but it is important to have an overview of its construction and function in understanding the basic principles of scintigraphy.

The Collimator

The first function of the gamma camera is to filter the cloud of γ-photons being emitted in all directions from the patient, to those that are travelling along the line of sight of the gamma camera. This enables their origin to be determined and attributed to a corresponding position on the image that is being produced. This function is fulfilled by the collimator. The collimator basically acts in a similar way to a grid in radiography. Collimators need to be made of a material with a high atomic number (Z), which will absorb photons that are not travelling perpendicular to the camera. Therefore, a collimator in its simplest form is a sheet of lead with holes in it. The holes may be parallel, diverging or converging, or pinhole, but the most efficient shape to filter the photons, while maximising spatial resolution and sensitivity, is hexagonal. The septa between the holes will not stop all of the photons, but normally a small level of septal penetration such as 5% is acceptable. The size of the holes affects the resolution of the image produced. The smaller or deeper the holes, the better the resolution, as fewer scattered γ-rays reach the crystal. However, it takes longer to produce an image (acquisition time), as the number of γ-rays reaching the crystal is reduced. As the acquisition time is increased, so patient movement has a greater effect on image definition, which is a particular problem in horses. There is always a trade-off, as in all imaging modalities, between competing factors for overall image quality.

The detailed structure and function of collimators is discussed in *Part I, Chapter 3*.

Detection of Radiation

The gamma camera detects γ-rays using a scintillation material, usually a single, thallium-activated, sodium iodide crystal (see *Part I, Chapter 3*, **Figure 1**). The thickness of the crystal within the camera depends on the function of the camera and the range of common radionuclides to be used, and determines the sensitivity for detecting the electromagnetic radiation. The thicker the crystal, the more photons/unit area will be detected. However, this is at the expense of intrinsic spatial resolution; when a γ-ray enters the crystal, the thicker the crystal, the more likely it is that there will be multiple Compton events (see **Figure 1**), degrading the spatial resolution. The depth of the light flash affects the relative intensity of the light photons reaching the photomultiplier tubes (PMTs), which also affects the intrinsic resolution. If the crystal is too thin, then there is poor detection of the γ-rays and a correspondingly poor count rate and long acquisition times. If low-energy gamma-emitting radionuclides, such as ^{99m}Tc, are to be used predominantly, then the crystal should be approximately 9–12 mm thick. The crystal itself is extremely fragile and requires protection from thermal and mechanical stresses, and also from moisture. It is is usually sealed by a thin layer of aluminium at the front and sides, and with transparent plastic or glass at the rear to allow the light photons to pass to the PMTs, but prevent moisture exposure.

Figure 1

Compton scatter indicating different energy transfer from the photon to the recoil electron. The greater the transfer, the more acute the angle between incident and scattered photon.

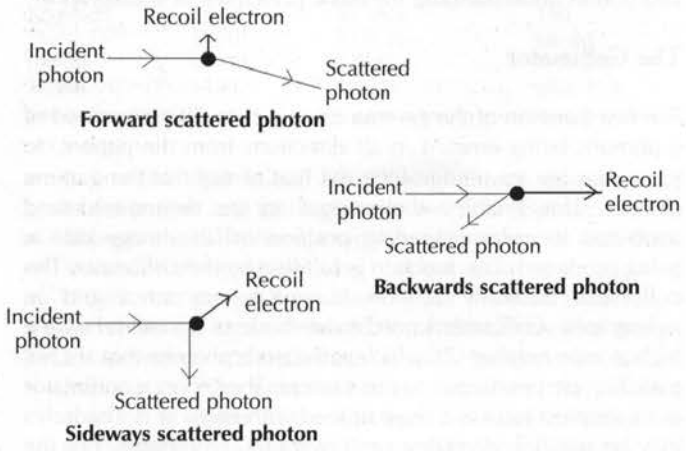

Figure 2

Graphical representation of Compton scatter and photopeak in a pulse height analyser.

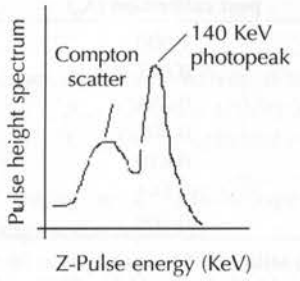

When a γ-ray photon interacts with the sodium iodide crystal, it can do so in one of two ways: photoelectric interaction or Compton scatter. Basically, photoelectric interactions are the events which provide the information to produce the final image. Compton scatter corrupts that image information. The visible light photons produced from photoelectric interactions pass via the light guide to the PMTs. The PMTs are arranged in an hexagonal pattern, and matched with areas of holes in the collimator. There are up to 91 PMTs in a modern gamma camera. The light photons from the sodium iodide crystal diverge in all directions, with those passing through the light guide falling on the surface of multiple PMTs. A PMT is an evacuated glass tube, which has a photocathode at one end, coated with a material that absorbs light photons and emits photoelectrons. Normally, one electron is emitted for every 5–10 light photons absorbed. These electrons are accelerated through the vacuum towards the positive anode at the opposite end. As the electrons are accelerated through the tube they impinge on dynodes, 'knocking' out 3–4 further electrons. In a typical PMT there are around 10 dynodes, so multiplying the electron number by 10^6, creating a voltage high enough to be measured. Each light flash from the sodium iodide crystal illuminates the array of PMTs differentially, depending on its position. This leads to different voltages within each of the illuminated PMTs, with the highest voltage being in the PMT nearest to the collimator hole through which the γ-ray passed. The positional circuitry within the gamma camera calculates the x and y coordinates from the differential voltages. The circuitry also calculates what is known as the z value, by summing all the voltages from the PMTs. This value is proportional to the original energy of the γ photon.

The resolution of the image can be improved by reducing the effect of Compton scatter. The radioisotope emits γ-ray photons at a particular energy level (e.g. 140 KeV). If the gamma camera was perfect and the photons travelled unhindered from their source to the detector, every γ-ray detected would be assigned exactly the same energy value. The energy spectrum would appear as a vertical spike (delta function). However, due to the statistical nature of the scintillator light output and the photomultipliers' response, the gamma camera can only estimate the energy of each incoming γ-ray photon. The energy spectrum for a single-energy γ-ray source therefore appears to form a sharp peak around the expected value, with a half-height, full width (FWHM) of about ± 10% at 140 KeV. This is called the 'photopeak'. In addition to this limitation, sometimes some of the energy of the gamma photon escapes from the camera; not all of the energy is deposited from the γ-ray in the crystal. Some of the incident γ-ray energy in the crystal will also fall under the photopeak and be recorded as a second small peak at a slightly lower (KeV) energy. This may lead to a second small peak at a slightly lower energy. Worse still, the photons may be deflected (scattered) from their direct line of flight from their source within the patient to the camera due to 'Compton scattering' (**Figure 1**). In a Compton scattering interaction, the photon bounces off an outer shell electron (see *Part I, Chapter 2*) in an atom (in the same manner as snooker balls will bounce off each other). When a photon is scattered in this way it changes direction, so the origin of its path is lost and it also loses some energy. Generally, the higher the energy of the incident photon, the more forward the direction of the scattered photon (**Figure 1**).

By losing the information about the spatial location of its origin, this photon, if used in the image, would reduce resolution and contrast. However, because the scattered photons have lower energies than unscattered photons, the z value from the PMTs will be lower. From this information, their contribution to the image may be reduced. This is achieved by setting the camera to exclude those γ-rays outside a narrow range around the centre of the photopeak (e.g. for ^{99m}Tc around 140 KeV). This range is known as the energy window, which will reject photons with lower energy, many of which have been Compton scattered (**Figure 2**). This window is usually set at about ± 10% either side of the peak because of the energy resolution of the camera.

It is imperative that the energy window is centred on the correct photopeak. Simply setting the window controls to 140 ± 10% is not adequate. It must be certain that the camera is correctly adjusted and that the photopeak is correctly positioned relative to the window, to ensure that the correct photons are being imaged. Only the ^{99m}Tc source should be used to do this and never the patient, because of corruption of the spectrum of radiation by scatter in the patient.

The output signal from the PMTs or counting and positional circuitry can be either analogue or digital, depending on the equipment used. The majority of gamma cameras used in equine facilities are of the analogue type, meaning that the

Figure 3

Poisson distribution of 100 counts/pixel in a uniform image.

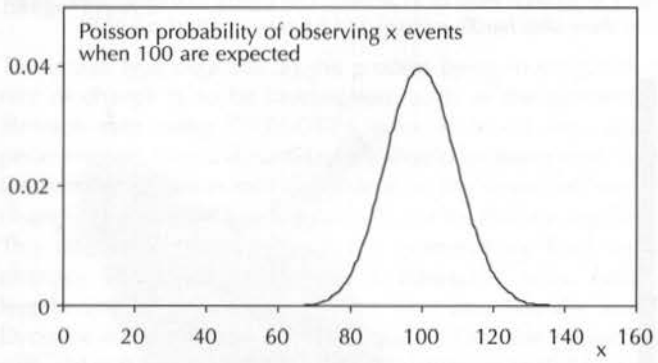

signal must be converted to a digital format for it to be used by a dedicated nuclear medicine computer system and allow post processing of the image. This is achieved by passing the signal through an analogue to digital converter (ADC). This samples the analogue signal at a set frequency and converts the voltage at each point in time to a binary number, used to build the image matrix within the computer. The frequency of sampling is determined by the matrix size and the highest frequency of the analogue signal. This is known as the 'Nyquist criterion', which states that the sampling rate must be at least twice the highest frequency present in the signal. If this is not true then high frequency information is lost from the image. This is not as large a problem for nuclear medicine as it is for imaging modalities such as Doppler, MRI or CT, where 'aliasing' artefacts occur due to undersampling.

The information used to produce the image and the matrix size used to display the image are closely interrelated, and must be taken into account when setting protocols. The following section outlines the basic principles, but this topic is covered in more detail in *Part I, Chapter 5*.

SCANNING PROTOCOL

Before scanning, several questions must be answered, including: the likely count rate from the area of interest; length of time or number of counts required to produce the image; matrix size used to display the images; isotope to be used; and study type that is to be acquired. All of these factors are interrelated and determine not only the diagnostic quality but also the statistical validity of the image produced. These factors also affect some of the post processing functions, including the ability to quantify or semiquantify activity in regions of interest. An understanding of their principles is required before these parameters can be determined.

Matrix Size

The matrix size is the number of pixels used to display the image on the monitor. It also affects the sampling frequency of the ADC and the size of memory required to store each image. The standard matrix sizes available are 64 x 64, 128 x 128, 256 x 256, 512 x 512 and 1024 x 1024. Each pixel within the matrix corresponds to a location on the camera face, and the information stored in that pixel represents the number of γ-ray events detected at that location over the acquisition time. Determining the correct matrix size to view the image is dependent on several subjective and objective criteria. Because each pixel relates to a specific area on the camera face, the larger the matrix size (smaller individual pixels), the smaller the area each pixel represents, and so the higher the perceived spatial resolution. For a standard 40 cm field of view camera, a 128 x 128 matrix has a pixel size which corresponds to 3.1 mm^2, and a 256 x 256 matrix has pixels which correspond to a size of 1.56 mm^2. From a subjective aspect, the higher the matrix size the higher the apparent spatial resolution and so the image appears to show greater detail rather than looking 'pixelated' or coarse. Why are images then not acquired in the highest matrix size possible? There are several reasons why this should not be done. The perceived gains in spatial resolution are not true gains, as it is not the matrix size that determines the system resolution (R^s), but the resolution of the collimator used and the intrinsic resolution of the camera. This relationship is shown by the following equation:

Equation 3

$(R^s)^2 = (R^i)^2 + (R^c)^2$ where R^i = Intrinsic resolution of camera
R^c = Collimator resolution

The intrinsic resolution, measured at the face of the crystal, is normally between 1–2 mm. The collimator resolution for a low-energy, general purpose collimator is about 4–5 mm at the collimator surface and 9–10 mm at 10 cm from the surface. For a high resolution collimator, this is improved to 2–3 mm at the surface and 6–7 mm at 10 cm. From this, it can be seen that by far the largest factor in the total system resolution is the collimator. By setting the matrix size at greater than 128 x 128, no real gain in spatial resolution is achieved. The second reason why care must be taken when choosing the matrix size relates to the amount of information that is available to produce the image, and the information in each pixel. If, for example, 100,000 counts are acquired into a 128 x 128 matrix from a uniform field source, then there should be approximately 6 counts/pixel. If the same number of counts were acquired into a 256 x 256 matrix, then there would be approximately 1.5 counts/pixel, so the amount of information in each pixel is quartered by doubling the matrix. Unfortunately, in scintigraphy there is a lot of 'noise' in the imaging process, which corrupts both the image contrast and spatial resolution. Compton scatter is one form of noise that has already been discussed. There are other sources of noise, including inherent noise within the camera system and, more importantly, Poisson noise, which is due to the random nature of radioactive decay. It is important to understand Poisson noise to see how it affects the image quality, statistical reliability of the image and any quantitative analysis of the image.

The radionuclide source emits an average number of events (γ-rays) per second (the activity), but the exact timing and direction of each γ-ray event is random. The gamma camera creates an image by counting the number of γ-ray events from a particular direction, within a given time. The resultant distribution of the number of events infers the distribution of radioactivity within the target organ. Going back to a uniform field source and the resultant image, it would be seen that the absolute number of events counted in each pixel was not the

Figure 4

Percentage Poisson error relationship with count number.

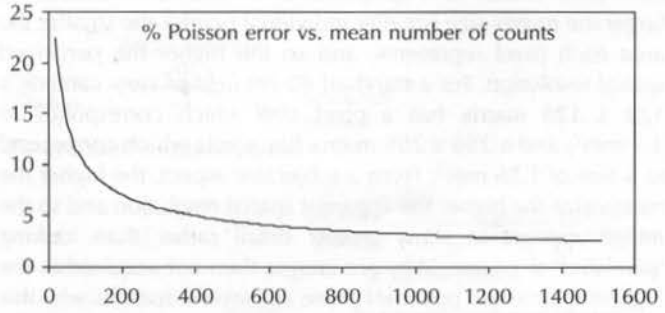

same. The distribution of the number of counts in each pixel is known as the Poisson distribution, an example of which is seen in **Figure 3**.

Therefore, if the mean (μ) number of counts/pixel were known, then the standard deviation (σ) of the counts is the square-root of the mean ($\sqrt{\mu}$). Therefore, 68% of the pixels counted will fall within $\pm 1\ \sigma$.

The noise within an image can also be calculated by the following equation:

Equation 4

$$\% \text{ Image noise} = 100/\sqrt{\mu}$$

Because the % noise varies as the square-root of the mean, the percentage error decreases as the mean number of counts increases. This is the most important fact to remember, and is seen in **Figure 4**.

As a practical example, suppose there is a region of interest (ROI) containing 100 counts and a second containing 115 counts. At face value, it would seem that the second ROI is 15% hotter than the first but, because so few events have been sampled from the underlying distribution, that simply cannot be said. The underlying distribution value in each case is not known (μ_1 or μ_2), but an estimate of what it is likely can be made from what has been sampled in each ROI; that is, an uncertainty can be attributed in each result using the knowledge of Poisson statistics. It is known that the uncertainty is proportional to the square root of μ, but as we do not know μ we have to estimate the uncertainty from the value we measure: x (100 and 115).

Therefore, all we can say about the underlying value for ROI 1 is that 68% (1 standard deviation) of the times we sample it, it is somewhere in the range 100 ± 10. Similarly, all we can say about the underlying value for ROI 2 is that 68% of the time it is likely to be in the range 115 ± 11.

If we want to estimate the difference B - A, then we add the uncorrelated uncertainties in quadrature to get the final result:

Equation 5

$$(115 \pm 11) - (100 \pm 10) = 15 \pm 15$$

This difference of 15 is not statistically significant. Actually, in this case even a difference of 30 wouldn't be significant, but merely suggestive. You really need 3 standard errors clear (in this case a clearance of 45) before the difference could be claimed to be significant. Although this is an extreme example, this is a crucial issue for image interpretation.

Figure 5

Effect of active physes in a young horse on image interpretation (count capture). The very high counts from the physeal region give this set count acquisition most of its activity. This means that other areas away from these sites hardly register, and have no contrast gradient.

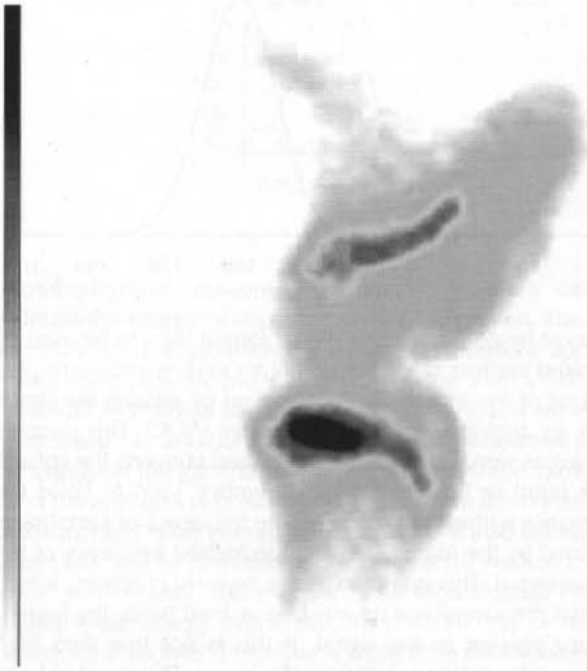

- ***Lateral view, right stifle, 2-year-old TB colt***
- ***Matrix 256 x 256***

How does this affect which matrix is to be used in a practical sense? The larger the matrix size, the fewer the counts in each pixel, and so the greater the percentage noise present in the image. If ROI or counts/pixel analysis are to be used, it can be seen that an appropriately high number of counts has to be acquired within the area to make any differences significant. For larger matrices this entails prolonged acquisition times, so movement blur would have a greater effect and radiation safety issues would be introduced. Therefore, 512 x 512 or 1024 x 1024 are not practicably achievable matrices for scintigraphic imaging. If low count rates are found, there is significant motion, or ROI assessment is to be performed, then a smaller matrix should be used, such as 64 x 64 or 128 x 128. When higher count rates or total count numbers are attained, then a matrix size of 256 x 256 can be used. As a rule of thumb, the greater the number of counts acquired or counts/pixel in an image, the smaller the % noise in the image, and the more sensitive to identifying subtle areas of increased activity.

It must be remembered that there is no hard and fast rule, and influences such as the brain's ability to recognise patterns within noisy data should be taken into account for subjective assessment of an image. A larger matrix can always be converted down, but this process cannot be performed in the other direction. Interpolation allows a matrix to be enlarged, but no new information is added; the additional pixel values

are made from averaging the values in the surrounding pixels, and noise is still an issue.

Image Type

The image type depends on the process being investigated. If rate of change is to be investigated, such as the glomerular filtration rate using ^{99m}Tc-DTPA scan or blood flow using pertechnetate, then a dynamic study should be performed, with the number of frames/min dependent on the suspected rate of change, or the scaling of time/activity curves that are required. This rate may change through the examination, from rapid changes at the start requiring 1 frame/1–2 secs, before lengthening to 1 frame/30–60 secs, or it may stay the same. Dynamic frames should also be acquired if motion correction software is to be used to produce a final composite static image of the area of interest.

Gated studies are dynamic studies in which a physiological process is studied in real time. The initiating trigger for the acquisition of a sequence of frames is linked to a physiological process, for instance one event of an electrocardiographic (ECG) cycle in studies of cardiac output. The count acquired from a single cardiac cycle is too small to produce an image, but the specific phases of the image can be related to the ECG and rapid, multiple acquisition images of a large number of cycles can be matched to produce final composite images of the different phases at set times within the cycle. This method of acquisition is known as multiple gated acquisition. Normally, between 16 and 30 frames are acquired in each R–R interval, with 100,000–200,000 counts/frame.

Static studies are used to show the distribution pattern of a radiopharmaceutical within the target organ when rate of change is not important.

Set Count or Set Time Acquisition

The majority of gamma cameras allow the acquisition of frames to be set for a length of time, or for a set number of counts. Both have distinct advantages and disadvantages, some specific to equine skeletal scintigraphy.

The set count acquisition method sets the number of counts to be recorded to produce an image, e.g. 100,000–5,000,000. The image produced represents the distribution of those counts using a colour or grey scale. This method of acquisition is only useful when looking subjectively at the distribution pattern of the radiopharmaceutical, such as in skeletal imaging or any other imaging where rate of change is not a factor. This method of acquisition also ensures that a statistically significant amount of information is acquired to produce the image for the matrix size that is being used.

Set time acquisition predetermines the time taken to acquire an image based on the count rate, or expected count rate, in the area being imaged. When the count rates are the same or nearly the same, the static images produced can again be assessed subjectively for the distribution pattern or assessed quantitatively with ROI software. When the count rates are altered because of a pathological site in the target organ, the images can be compared subjectively or quantitatively. There are several artefacts which detrimentally affect this method of acquisition that should be recognised. Some of these artefacts pose a major problem in equine skeletal scintigraphy and are discussed in detail in *Part I, Chapter 9*. They include:

- Poor radiopharmaceutical uptake (RU) in the distal limb, especially when affecting single limbs.
- Muscle wastage artefacts.
- Chronic lameness/cold limb.
- Diffuse perilesional increased radiopharmaceutical uptake (IRU).

These artefacts change the count rate and the perceived activity within an area if acquired over a set time, so producing a misleading increase or decrease activity when compared to the contralateral area or limb. They make subjective assessment of the distribution pattern between the two sides difficult and, most dangerously in the distal limb with poor uptake, can lead to statistically irrelevant images being produced. When set count acquisition is used, it ensures that the same amount of information is used to produce the images in contralateral areas, so that a distribution pattern of activity can be assessed subjectively or using ROI analysis. This is the cornerstone of image interpretation of skeletal scintigraphy. There are, however, also negative issues associated with set-count acquisition. These include count capture and how it may mask pathology in other areas or affect quantitative comparisons.

Count capture or stealing counts refers to the highly uneven distribution of counts in an image; for instance, if there is a marked focal IRU. In such instances, there may be less intense RU in another site associated with a lesion but, because the area of marked IRU takes the largest proportion of the counts, other areas may have a statistically invalid number of counts. Comparing such a region between images, either subjectively or with ROI analysis, is statistically unreliable. **Figure 5** shows an example of active physes in a young horse. If these images were obtained using a set-count method, there would be inadequate counts in other regions to assess safely for pathology, despite masking or windowing the images. If images showing a potential count capture are observed post acquisition, they should be reacquired using a sufficiently long acquisition time to ensure that pixels away from the area of marked IRU contain a statistically valid count. For subjective appraisal of the image, the area of highest IRU should be masked (see *Part I, Chapter 5*).

As with many areas in scintigraphy there is no right or wrong method of acquisition, but knowledge of the dangers and reliability of the results will ensure diagnostic images and valid interpretation. A sensible compromise protocol would be to obtain the first images for the distal limb and pelvis for a set number of counts, and then base the rest of the examination on the time period required to obtain these counts. Alternatively, the count rate can be assessed prior to commencing image acquisition, and a set-time based on this count rate, which ensures sufficient counts, used throughout.

In conclusion, nuclear medicine is a sensitive, although often nonspecific, imaging modality that allows the veterinarian to investigate many physiological processes in the horse. A thorough understanding of scintigraphy and digital imaging not only allows the clinician to gain the full potential of this modality, but also ensures the production of diagnostic

quality and statistically reliable images. It also enables the clinician to avoid misinterpretation and to recognise the limitations of the technique.

ACKNOWLEDGEMENTS

The author would like to acknowledge the help and direction received in the writing of this chapter from Dr Steve Bloomer, Nuclear Diagnostics, UK.

REFERENCES

1. Easton, S. (2000) The influence of clinical examination on bone scintigraphy findings in the equine case. *Presented at the International Veterinary Radiology Association*, Obihito, Japan.
2. Sterling, J.C., Edelstein, D.W., Calvo, R.D. *et al.* (1992) Stress fractures in the athlete: diagnosis and management. *Sports Med.* **14**, 336-345.
3. Mattheson, G., Clement, D.B., McKenzie, D.C. *et al.* (1987) Scintigraphic uptake of ^{99m}technetium at non-painful sites in athletes with stress fracture. The concept of bone strain. *Sports Med.* **4**, 65-75.
4. Peremans, K., De Winter, F., Janssens, L. *et al.* (2002) An infected hip prosthesis in a dog diagnosed with a 99m-Tc- ciprofloxacin (Infecton) scan. *Vet. Radiol. Ultrasound* **43**, 178-182.
5. Britton, K.E., Vinjamuri, S., Hall, A.V. *et al.* (1997) Clinical evaluation of technetium-99m Infecton for the localisation of bacterial infection. *Eur. J. Nucl. Med.* **24**, 553-556.
6. Koblik, P.D., Lofstedt, J., Jakowski, R.M. *et al.* (1985) Use of 111-indium labelled leucocytes to image an abdominal abscess in a horse. *J. Am. vet. med. Ass.* **186**, 1319-1322
7. Sharp, P. (1998) Nuclear medicine imaging. In: *Practical Nuclear Medicine*, Eds: P. Sharp, H. Gemmell and F. Smith, Oxford University Press, Oxford. pp 1-12.
8. Butson, R., Webbon, P. and Fairburn, S. (1995) Tc-99m HMPAO-labelled leucocytes and their biodistribution in the horse: a preliminary investigation. *Equine vet. J.* **27**, 313-315.
9. Weller, R., Weaver, M., Livesey, L. *et al.* (2000) Nuclear scintigraphy with 99m-Tc-HMPAO labelled leukocytes in the assessment of horses with malabsorption. *Vet. Radiol. Ultrasound* **41**, 563.
10. Votion, D.M., Roberts, C.A., Marlin, D.J. *et al.* (1999) Feasibility of scintigraphy in exercise-induced pulmonary haemorrhage detection and quantification: preliminary studies. *Equine vet. J., Suppl.* **30**, 137-142.
11. Peters, A. (1998) Infection. In: *Practical Nuclear Medicine*, Eds: P. Sharp, H. Gemmell and F. Smith, Oxford University Press, Oxford. pp 285-315.
12. Perkins, A.C. (1998) Tumour imaging. In: *Practical Nuclear Medicine*, Eds: P. Sharp, H. Gemmell and F. Smith, Oxford University Press, Oxford. pp 279-280.

Chapter 2a

RADIOPHARMACY

ADAM J. DRIVER
Dubai Equine Hospital, PO Box 9373, Dubai, UAE.

INTRODUCTION

The aim of this chapter is to give a basic understanding of the workings of the radiopharmacy, the products available and their function. With such an understanding, the veterinarian will be able to work in conjunction with his or her radiopharmacy to gain the most out of their nuclear medicine facility. The unique pressures placed on a radiopharmacy by an equine facility require the pharmacist and veterinarian to work in close conjunction. Forward planning is essential to maintain a supply of radiopharmaceutical to the veterinarian, to minimise or avoid radiation exposure and to ensure the production and delivery of a sterile, pyrogen-free and suitable radiopharmaceutical, to be used within its shelf-life. This chapter concentrates mainly on the production of ^{99m}technetium (^{99m}Tc) radiopharmaceuticals (**Table 1**), as this is the predominant γ-emitting isotope used in equine scintigraphy. It outlines the management of the supply of these radiopharmaceuticals, the quality control practiced within the radiopharmacy and the principles of the organ-seeking agents. The majority of pharmaceuticals are prepared from kits supplied and guaranteed by their manufacturers.

BASIC PRINCIPLES OF THE ATOM AND IONISATION

To understand the production of the radionuclides, we should first review some of the basic details of the atom and ionisation. All atoms consist of a central nucleus, with electrons which orbit round the nucleus. The nucleus contains protons and neutrons, both of which have the same mass of one atomic mass unit (a.m.u.) (An a.m.u. is 1/12 the mass of a carbon-12 atom).

All protons have a positive charge and neutrons have no charge. All electrons have a negative charge and a mass of 1/1840 a.m.u. The atomic number, Z, of an atom is the number of protons within the nucleus. The number of neutrons within the nucleus is known as N. The atomic mass number A = Z + N. For example, the carbon-12 atom has an A of 12, a Z of 6 and an N of 6. Radioactive decay of unstable atoms leads to changes within the structure of the nucleus and the release of energy. The different forms of decay result in γ-radiation, α-emission and β-emission. The release of a helium nucleus (2 protons and 2 neutrons) is α-emission; β-emission is the release of an electron from the nucleus. This occurs when a neutron within the nucleus decays to form a proton and an electron. The electron is then released from the nucleus, and the atom changes from one element to another. This is referred to as β^- decay. Alternatively, some isotopes may become stable by the decay of a proton within the nucleus to a neutron and a positively charged electron. The positively charged electron, or positron, is then expelled from the nucleus. This is referred to as β^+ decay. Positron emitters are used in positron emission tomography (PET) scans. γ-radiation is the release of a photon of γ-radiation from an excited nucleus, at a single or several energies. These energy levels are specific to the nuclide[a] which emits them. The energy of the emitted γ-ray is measured in electron volts (eV). An electron volt is the energy acquired by an electron when it is accelerated through 1 volt. For example, an electron moving through 60,000 V acquires the energy of 60,000 eV, or 60 KeV. In a practical example, when the KV is set on an x-ray machine, this is the voltage between the cathode and anode and, in turn, is also the maximal energy of the x-ray spectrum that will be produced when the exposure is made.

The basic elements are often represented by their abbreviated symbols from the periodic table. Therefore, molybdenum is written 'Mo' and technetium 'Tc'. Many of the elements can exist in several different forms, or isotopes, with varying numbers of neutrons within the nucleus. The atomic number (Z) for a specific element is always the same, but the atomic mass number (A) can be variable. The convention when writing the abbreviated form is to include either the atomic mass number (A) alone, or with the atomic number (Z) as well. For example molybdenum-99 can be written ^{99}Mo or $^{99}_{42}$Mo, and technetium-99m can be written as ^{99m}Tc or $^{99}_{43}$Tc. As can be seen from this example, both molybdenum and technetium have the same atomic mass number (A), but a different atomic number (Z). The ^{m} in the abbreviated form for technetium refers to the isotope being in a metastable state; i.e. the nucleus is stable with reference to the number of protons and neutrons present, but still has an excess amount of energy. This energy is released during radioactive decay as γ-radiation of a specific energy, as described above. In the case of ^{99m}Tc, the photons of γ-radiation released have an energy of 140 KeV.

The electrons which orbit the nucleus of an atom do so within specific energy levels. These levels are known as 'electron shells'. Each of these shells has a fixed energy, dependent on the atomic number of the atom, and each shell also has a fixed maximum number of electrons. The shells are called K, L, M, N, etc. and the negatively charged electrons in each shell are attracted to the positively charged nucleus (see **Figure 1**). The work or energy needed to remove an electron

[a]The terms radioisotope and radionuclide are often used interchangeably, although this is not technically correct. A nuclide refers to a species of atom of any element distinguished by the number of neutrons and protons in its nucleus and its energy state. An isotope is one of a set of chemically identical species of atom which have the same atomic number, but different mass numbers. A nucleotide refers to a subcomponent of nucleic acids and this term should not be used.

Figure 1

Schematic representation of an atom, showing the 'electron shells' K, L and M, all of which require different energy levels to retain an electron.

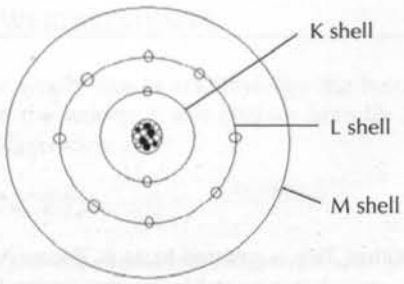

from the atom is known as the binding energy. The binding energy is greatest for the electrons in the K shell, as they have the greatest attraction to the nucleus, and less for the outer shells. When an electron is removed from an atom, it produces an 'ion pair'; that is a negatively charged electron and the positively charged atom (or positive ion). Ion pairs are unstable and react with other molecules around them, especially water. This reaction leads to the production of free radicals and hydrogen peroxide which, in turn, react with other molecules, for example DNA in the human body. This can lead to cellular damage. The damage can be evident immediately (analagous to sunburn), but is usually seen at a later date. X-radiation, γ-radiation, α-particles and β-particles when they collide with the electrons of atoms, transfer energy to the electrons, which can then overcome the binding energy and so produce ion pairs and disrupted molecular bonds. This is the basis of the cellular damage that occurs following exposure to ionising radiation. Minimising exposure to ionising radiation by following the 'as low as reasonably achievable' (ALARA) principles, by minimising time with, maximising distance from and avoiding exposure to or contamination from ionising radiation, must always be foremost in the actions of both the pharmacist and veterinarian (see *Part I, Chapter 12*).

The ^{99}Molybdenum/^{99m}Technetium Generator

The molybdenum used as the parent isotope within the generator is produced by one of two methods; from either reactor irradiation or nuclear fission, as shown, respectively, by the equations below:

Equation 1

$n + {}^{98}Mo \rightarrow {}^{99}Mo + \gamma$ where n = neutron
γ = photon of gamma radiation

Equation 2

$^{235}U^{b} + n \rightarrow {}^{236}U \rightarrow {}^{99}Mo + {}^{133}Sn^{c} + 4n$ where n = neutron

Both of the above reactions occur within nuclear reactors, and ^{99}Mo is a byproduct of the nuclear industry. ^{99}Mo has a relatively long half-life ($T^{1/2}$) of 66 h and decays by β-particle emission to ^{99m}Tc. Several companies produce and supply ^{99}Mo/^{99m}Tc generators, including Amersham International and CIS Bio International (a subsidiary of Schering Health Care Ltd.), but the general design is similar in most cases. This basic design is outlined below.

Figure 2

The inner alumina column of a ^{99}Mo/^{99m}Tc generator.

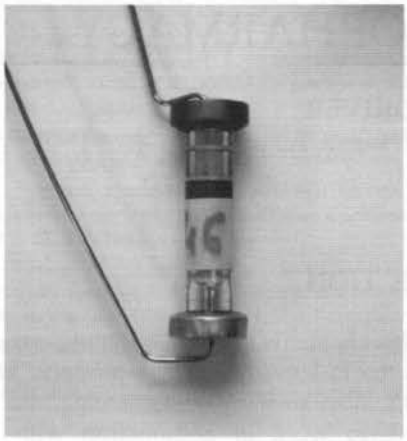

Figure 3

The inner lead casing around the alumina column.

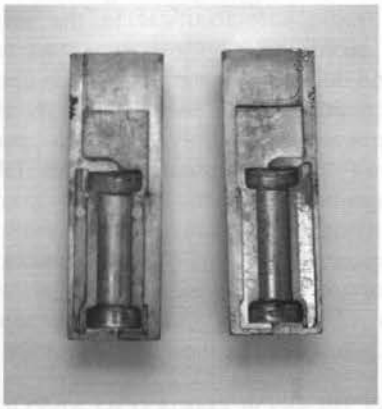

The ^{99}Mo/^{99m}Tc generator consists of an inner alumina column, onto which the parent isotope, ^{99}Mo, has been adsorbed as the salt ammonium molybdate $(NH^4)^+(MoO^4)$ (**Figure 2**). The column is shielded by a lead or depleted uranium jacket, depending on the maximal activity of the ^{99}Mo, at the time of delivery (**Figure 3**).

The other components of the generator consist of a reservoir of sterile 0.9% w/v saline, which flows through the column and into a 15 ml sterile, evacuated vial.

The vials are supplied with the generator and contain a vacuum equal to 5 ml, although alternate volumes of 10 ml or 15 ml can be supplied (**Figures 4 and 5**). This allows the pharmacist to produce varying radioactivity concentrations of the eluate.

There are 2 main types of generator, the 'wet' and 'dry' types. The dry system has only a small reservoir of saline,

[b]Uranium; [c]Tin.

Figure 4

The reservoir, column and elution vial of a $^{99}Mo/^{99m}Tc$ generator.

Figure 5

Schematic overview of a $^{99}Mo/^{99m}Tc$ generator.

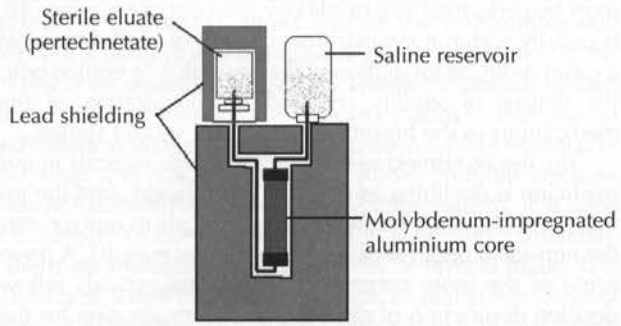

enough for a single elution, which is connected prior to elution. After the saline has been drawn through the column, air is then also drawn through the column to dry it. The dry generators contain filters, normally a 0.22 μm hydrophobic filter, through which the air passes to dry the alumina column after it has been eluted. The filter maintains sterility within the generator. The air is drawn through the column to prevent radiolysis from occurring. Radiolysis of the water results in oxidation of the ^{99m}Tc on the column, and leads to a lower yield of ^{99m}Tc at subsequent elutions. The wet system has the column bathed in the saline solution from a large saline reservoir, and each time the elution volume is drawn through an evacuated vial is attached to the system. The photograph in **Figure 4** is of a wet system. Manufacturers have now overcome the problem of radiolysis, and the yield of ^{99m}Tc is not compromised in either system.

The vials themselves are placed in a lead pot designed to fit into the top of the generator, and the elution needle allowed to penetrate the vial within. The lead pots shield the operator from radiation. The elution needle is protected by one of two methods. Either a sterile, single-use, disposable needle guard is placed over the needle between elutions, or a sterile bacteriostatic solution, such as lauryl bromide dimethylbenzylammonium (0.02%), within a vial, is placed over the needle. A photograph of a complete generator is seen in **Figure 6**.

The elution takes place in a sterile environment, and should be performed as directed by the manufacturer's instructions and the appropriate regulations. Ensure that the valve to the saline

Figure 6

A commercially available molybdenum/technetium generator.

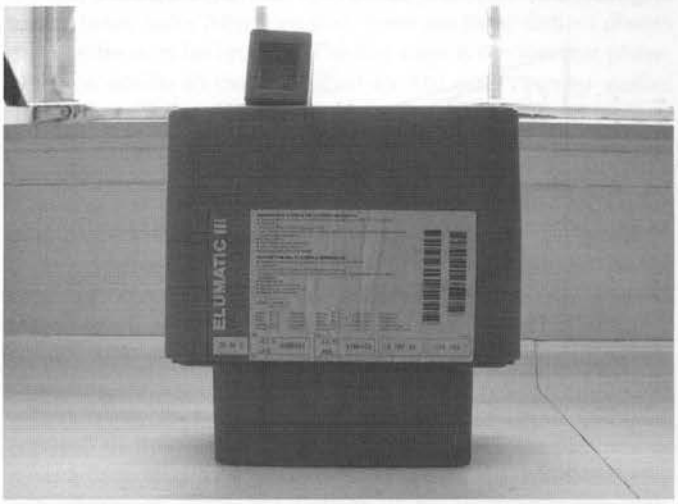

reservoir is open. Replace the needle guard or bacteriostatic solution vial with the shielded elution container. It is recommended that at least 2 mins be waited to ensure that elution is complete, before removing the elution container and replacing the bacteriostatic vial or needle guard.

When the sterile saline passes through the alumina column, the ^{99m}Tc is removed as sodium pertechnetate ($Na^{99m}TcO_4$) within the solution. It is this solution which can then be used as a radiopharmaceutical for imaging purposes, or to produce a wide variety of other radiopharmaceuticals from the various commercially available kits (see **Table 1**).

The parent molybdenum within the generator decays to the daughter ^{99m}Tc at such a rate that the ^{99m}Tc radioactivity grows to 50% of a new maximum equilibrium value within 6 h of elution. Within 12 h that activity is 75%, and within 24 h the activity is at a maximum. At this stage, the activity of the ^{99m}Tc and ^{99}Mo decay at the same rate. This is known as a transient equilibrium, with the ^{99m}Tc decaying as quickly as it is being produced, giving the appearance that the daughter and parent isotopes are decaying with the same $T^{1/2}$ of 67 h (**Figure 7**).

To maintain sterility of the generator, it must be sited in a clean environment and handled using full aseptic technique. Each country has its own specific legislation for storage and use of a generator. The level of controlled environment required in human medicine is neither necessary nor appropriate for preparation of radiopharmaceuticals for the horse. However, strict aseptic technique, such as that used for preparation of medicines in the equine hospital environment, should be employed.

The pharmaceutical being produced is a source of ionising radiation and is covered by the Ionising Radiation Regulations 1999 (IRR99) in the UK, or similar legislation in other countries, which means that all work carried out with the radionuclides must adhere to these regulations and the ALARA principles. The workstations or laminar flow cabinets must provide shielding of personnel from ionising radiation arising from the production of the radiopharmaceuticals. Purpose-built systems are available from companies such as Amersham International (see *Part I, Chapter 12*).

Figure 7

Logarithmic graph showing the decay of ^{99}Mo, and growth and regrowth, after elution, of activity of ^{99m}Tc in a generator.

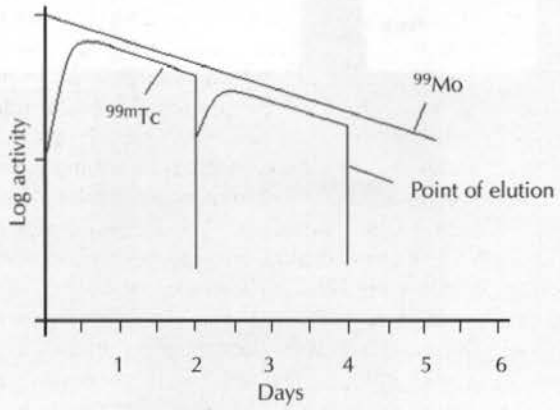

Figure 8

The typical appearance of a radiopharmaceutical kit, ready for labelling.

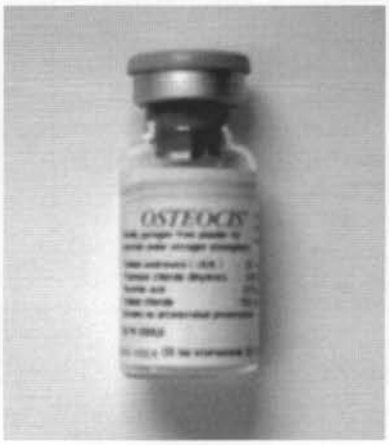

The management of a generator within a radiopharmacy, especially when serving one or several equine nuclear medicine facilities, requires much skill to ensure an adequate supply of pertechnetate for all requirements each day from the finite activity available. This may not be a problem at the start of a week, when a new generator has been purchased, but towards the end of a week when the activity is falling, it may require the radiopharmacy to obtain a second generator, especially if the equine clinic caseload is heavier at that time.

Forward planning is essential, taking into account decay constants, so that the correct amount of isotope is available for injection at the right time, particularly if the radiopharmaceutical is supplied by the local hospital. It must also be remembered that all veterinary practices in the UK must be licensed by the Environment Agency, for both use of and storage and/or disposal of open sources, for a specific activity of radionuclide. When setting this limit, one should include an adequate margin to allow for the delay that occurs between delivery of the isotope to the clinic and its eventual injection into the horse. Because of the short half-life of technetium (6 h), a delay of only 2–3 h between delivery and injection results in a license requirement 30% greater than the actual dose required for each horse.

PRODUCTION OF RADIOPHARMACEUTICALS

The vast majority of radiopharmaceuticals are produced from kits. A kit is simply a sterile reaction vial containing the nonradioactive chemicals required to produce a specific ^{99m}Tc radiopharmaceutical[1] (see **Figure 8**). The kits are supplied in vial form. The vial is filled with the kit ingredients, usually freeze dried, within a nitrogen environment.

Kit for the Production of Methylene Diphosphonate

The ingredients of the kit comprise the following:

- The ligand; this is the compound to be complexed to the ^{99m}Tc (e.g. methylene diphosphonate).
- Stannous ions (Sn^{2+}); the stannous ion is present in various chemical forms, and acts as a reducing agent for the ^{99m}Tc.
- Stabilisers, antioxidants, buffers and bacteriocides[2].

The production of the radiopharmaceutical from the kit must be performed in a sterile environment; for human use, this is usually within a laminar flow cabinet or workstation, within a clean room, as for elution of the generator. In equine practice, the degree of sterility required for preparation of normal medications in the hospital environment should suffice.

The use of nontechnetium radiopharmaceuticals in nuclear medicine is declining as new kits are brought onto the market that use technetium-bound pharmaceuticals to replace many of the non-ideal organ-seeking radiopharmaceuticals. A review of some of the more common radiopharmaceuticals follows. A detailed description of protocols and interpretation for the use of these pharmaceuticals is given in *Part II, Chapters 6 and 7*.

Pertechnetate

Sodium pertechnetate ($Na^+TcO_4^-$) is the chemical form of the radionuclide in the eluate that is removed from the generator, as described previously. Without any further manufacturing procedures, it can be used for a number of scintigraphic imaging protocols. The pertechnetate anion is accumulated and excreted by a number of organs within the body and can therefore be used to assess the function of these organs. The gastric parietal cells, salivary glands, choroid plexus, thyroid glands and kidneys all accumulate pertechnetate after it has been administered either orally, rectally or, more commonly, by the intravenous route. After intravenous injection of pertechnetate, 100% of the substance is found in the bloodstream, of which 75% is bound to plasma proteins[3]. This is used in people for vascular studies, also known as first pass studies. It is a noninvasive method of assessing cardiac shunts in children and imaging vascular occlusive disease or for post operative assessment of vascular surgery. With the advent and advancement of magnetic resonance imaging (MRI) and echocardiography, these techniques are, however, becoming less popular in the human field. In the horse, it has been used for vascular studies including the investigation of laminitis and aortoiliac thromboembolism (see *Part II, Chapter 6*). The unbound pertechnetate diffuses into the interstitial compartment. As this shift occurs, more protein-bound pertechnetate is released, to maintain an equilibrium. This

continues to occur until 75% of the injected dose has shifted into the interstitium[3]. Several organs, as detailed above, are able to remove pertechnetate from the interstitial fluid compartment and accumulate it. Within 30 mins of injection, the highest activity of pertechnetate is found within the stomach. This is because an internal recycling occurs. The gastric parietal cells are able to accumulate pertechnetate from the interstitial fluid actively. Within the cell, the pertechnetate is treated in a similar way to the chloride ion, and is substituted for it, to be excreted as pertechnic acid. Once in the stomach, the acid dissociates back to pertechnetate and so an internal recycling occurs, leading to very high levels within the gastric lining. This characteristic of pertechnetate is used in human medicine to search for ectopic gastric mucosa, as would be found in a Merkel's diverticulum.

Pertechnetate is also actively removed from the interstitial fluid by the thyroid glands. The acinar cells trap the pertechnetate because of its chemical structure and its ionic weight. Pertechnetate is said to be nonorganified within the thyroids, unlike radioactive iodine, because it is not subsequently used in the formation of thyroxine. The activity of pertechnetate reaches 10 times that of the surrounding soft tissues, and 3 times that of the salivary glands in people[4]. In the cat, it has been reported that activity within the normal thyroid is similar to that within the salivary glands[5]. The use of pertechnetate to image the thyroids has been widely reported in people, dogs and cats, but not in the horse, probably because they do not commonly suffer from hyperthyroidism. It is used prior to surgery to assess if the condition is unilateral, bilateral, or if there are metastatic or ectopic sites of thyroid tissue. It is also used post surgery to identify ectopic or malignant sites not removed. If hyperthyroidism were suspected in a horse, then it would be a logical imaging modality to use to assess the function of the thyroids.

The use of pertechnetate for nuclear portal angiography after rectal administration has been described in the dog[6]. The pertechnetate is rapidly absorbed after rectal administration. A dynamic study follows the movement of the pertechnetate through the portal system, via the liver and then into the heart. The relative time taken for activity to increase in the liver and heart is both specific and sensitive for portosystemic shunts. It is a noninvasive method compared to contrast portography. Portosystemic shunts have been described in the foal and, although this method of diagnosis has not been described in the literature, it probably could be utilised for foals.

The salivary glands also actively take up the pertechnetate from the interstitial fluid, due to its ionic structure. The pertechnetate is secreted in the saliva, so can be used for assessing the function, size, shape and position of the salivary glands, as well as duct patency. This procedure has not been described in the horse, but could probably be utilised if an abnormality was suspected. In people, 50% of pertechnetate administered is excreted by the kidneys; the rest is lost via the faecal route, with a small amount of loss via sweat and salivary excretions[4].

The Diphosphonate Salts

The diphosphonate salts are a stable group of phosphonates, with the phosphorus bound to carbon. There are many kit forms available, including methylene diphosphonate (MDP), methylene hydroxydiphosphonate (MHDP), disodium oxidronate (HDP) and ethane-1-hydroxyl-1,1-diphosphonate (EHDP). Once injected intravenously, they rapidly localise to the bone and are cleared from the blood and soft tissues, giving an excellent bone to soft tissue ratio. After injection, there are three distinct phases that can be used for imaging. The first stage is the vascular phase, which is similar to that described for first pass vascular studies using pertechnetate. In the second stage, known as the pool or soft tissue phase, ^{99m}Tc diphosphonate diffuses into the interstitial fluid. The interstitial phase is relatively short as the uptake of the diphosphonate into bone significantly affects the pool phase images within 15–20 mins after injection. The third, or bone, phase is the binding of the diphosphonate to the exposed surface of the hydroxyapatite crystals in bone. It is not known whether this process is active or passive, but it is relatively rapid, with maximal activity seen 2–4 h after injection. Hydroxyapatite is the largest component of the inorganic matrix within bone, and only a very small percentage is normally exposed to the interstitial fluid. Increases in bone turnover or remodelling lead to increased exposure of the hydroxyapatite and, therefore, increased uptake of the diphosphonate salt. During the third phase of scanning, it is therefore the process of bone turnover which is being imaged. The blood supply to the bone is the other major factor that determines the relative uptake of diphosphonate in the third phase. Maximal pathophysiological blood flow to bone produces a 3-fold increase in activity in the bone, whereas maximal bone turnover, as seen in areas of fractures or neoplasia, causes up to a 5-fold increase in activity. Therefore, the rate-limiting step in the localisation of diphosphonate is the amount of hydroxyapatite exposed to the interstitial fluid[7]. Other factors which affect the uptake of diphosphonate by bone include the quantity of mineralised bone, autonomic tone, capillary permeability, local acid-base balance, fluid pressure within the bone, vitamins and hormones[8].

The diphosphonate salts are the most commonly used radiopharmaceuticals in the horse. They are used for the detection of bone pathology, as scintigraphy has been shown to be more sensitive than radiography[8]. The use of MDP has also been shown to be sensitive in the detection of dental disease in the horse[9] (see *Part II, Chapter 5*).

Hexamethyl-propylene-amine (HMPAO) and Indium Chloride

These radiopharmaceuticals are used for conditions in which labelled white blood cells (WBCs) are required. HMPAO is also known as 'exametazime', and is used bound to ^{99m}Tc. The radiopharmaceutical produced is relatively unstable, and the manufacturer identifies several restrictions in the production and use of the pharmaceutical. These restrictions include a limit of 0.37–1.1GBq of activity that the kit can be reconstituted with; that the ^{99m}Tc used to reconstitute the kit should have been eluted from the generator within 2 h previously; and that the generator should have been eluted within 24 h before the current elution. These criteria ensure the quality of the pertechnetate used in the reconstitution, and hence limit the quantity of free pertechnetate within the kit. A further restriction of 30 mins on the useful life of the kit once it has been reconstituted is due to changes in the chemical complex that occur after administration to the patient. These changes relate to the use of HMPAO for cerebral regional blood flow scans, where the highly lipophilic nature of the pharmaceutical allows

Table 1: Radiopharmaceuticals used to investigate a range of physiological or pathological processes

Target organ	Pathophysiological process or disease	Radiopharmaceutical
Bone	Metabolism	MDP, HDP, MHDP, EHDP
Renal	Glomerular filtration rate	DTPA, ^{51}Cr EDTA
	Tubular excretion	MAG_3
	Blood flow	Pertechnetate
Lung	Ventilation distribution	Technegas (^{99m}Tc-carbon particles), DTPA aerosol
	Perfusion distribution	MAA
	EIPH	^{99m}Tc-labelled RBCs, MAA
Infection and inflammation	Inflammation (soft tissue)	Gallium citrate, pertechnetate, indium chloride, HMPAO-labelled WBCs, leucoscan
	Inflammation (bowel)	HMPAO-labelled WBCs
	Infection (general)	Gallium citrate, indium chloride, Tc-HMPAO
	Infection (dental)	MDP
Liver	Hepatobiliary function	Mebrofenin
	Morphology	Sulphur-colloid
Vascular	Angiography	Pertechnetate
	Portosystemic shunt	Pertechnetate
Thyroid	Hypothyroidism	Pertechnetate

it to cross the blood-brain barrier. With time, the chemical structure changes to become less lipophilic, so it will not cross the blood-brain barrier.

In the horse, HMPAO is used for labelling leucocytes. Its lipophilic nature is required to penetrate the leucocytes, specifically the granulocytes, so time is a factor in labelling the cells. It is also relatively less stable than other leucocyte-labelling radiopharmaceuticals, such as ^{111}Indium compounds, as it elutes from cells at a rate of 5%/h[10]. The use of ^{99m}Tc-HMPAO labelled WBCs has been described in the horse for the investigation of abdominal disorders[11]. The WBCs first accumulate within the lung, but are normally cleared within 1–2 h. There is normal accumulation within the spleen, liver and bone marrow in the horse[12]. Activity also appears rapidly within the kidneys, ureters and bladder because of the elution of the ^{99m}Tc-HMPAO complexes from the WBCs. In the horse, it has been used in the investigation of malabsorption[11]. In people, ^{99m}Tc-HMPAO is useful in the detection of occult abscesses in the abdomen, lung, liver and kidney. It is also useful in demonstrating inflammatory bowel disease, acute respiratory distress syndrome and osteomyelitis, although this last syndrome can be confusing due to normal activity within the bone marrow. Indium can also be used to label WBCs, but has a number of disadvantages over ^{99m}Tc complexes, including poorer image resolution, longer scanning times, longer $T^{1/2}$ and high photon energy, leading to higher patient radiation dose. ^{111}Indium-labelled leucocytes have been used in a horse to identify an abdominal abscess[13].

Diethylene-triamine-penta-acetic Acid (DTPA)

DTPA is used for a variety of scanning protocols in people, including blood brain perfusion, cerebrospinal fluid (CSF), cysternography, gastric emptying, renal function and morphology studies, and pulmonary ventilation studies. In the horse, it has been used mainly for ventilation and renal function studies. DTPA is rapidly distributed throughout the extracellular space after intravenous injection, and is excreted exclusively by glomerular filtration. DTPA excretion gives a good correlation with the standard measurements of glomerular filtration rate[14]. However, in people, the use of MAG_3 has superceded the use of DTPA for several reasons. MAG_3 has a greater extraction efficiency, resulting in better quality images because of a higher target to background ratio. Moreover, although DPTA is a glomerular-filtrated agent, contaminants and variable protein binding may invalidate its use for measurement of the true glomerular filtration rate. Methods have been described for nonimaging studies to determine the GFR in horses using blood clearance techniques. This method requires serial blood samples to be collected and the plasma activity of the DTPA compared to the activity in a standard solution retained from the original dose, to correct for decay and calculate % dose per unit volume of plasma. The calculations required to determine the glomerular filtration rate and interpretation of the results can be found in several texts[15,16] (see *Part II, Chapter 6*).

Aerosolised ^{99m}Tc-DTPA can be used to image pulmonary ventilation. However, it is not an ideal pharmaceutical for this purpose for several reasons, including:

- Diffusion into the pulmonary circulation, causing loss of activity from airways.
- Simultaneous ventilation and perfusion studies cannot be performed because both use ^{99m}Tc as the radionuclide.
- Increased radioactive dose is required for the delayed macroaggregated albumen (MAA) perfusion distribution study to swamp the activity of the ventilation study, or a delay of at least 1–2 h before perfusion scanning.
- Nebulisation must produce droplets of between 0.5–1 μm, to ensure deposition in the alveoli to produce a true image of lung ventilation distribution.
- It is important to understand that only the distribution of blood perfusion and air flow are being imaged. The technique is not quantitative.

- Turbulent air flow, as found with many lung pathologies, may adversely affect the deposition of the aerosol.
- It is possible to have formation of areas of apparent increased distribution due to clumping of particles.
- Ventilating a horse safely without contaminating personnel and equipment is a technically demanding process.

Despite these limitations, DTPA is a useful radiopharmaceutical for ventilation studies and its use has been documented in the horse. Some clinicians prefer to term it an inhalation study because of the many factors that may restrict the deposition of particles more than gas throughout the ventilated lung[17]. Inhalation studies, combined with perfusion studies, have been used to investigate COPD and EIPH pathologies in the horse (see *Part II, Chapter 7*).

Carbon Particles (Technegas)

Technegas comprises ultra-small carbon particles in argon gas that are labelled with ^{99m}Tc. The particles are a maximum of 5 nm in diameter[18]. Because of their size they have gas-like penetration properties, but adhere to alveolar walls like aerosols[17]. Technegas is not cleared by passive diffusion so loss of activity from the lungs is not a problem, unlike DTPA. Technegas is used for ventilation studies in people using the same protocol as for DTPA aerosol studies; therefore, it could probably be successfully used instead of DTPA in the horse. The equipment required to perform this technique is expensive.

Macro-aggregates of Albumin (MAA)

Albumin macro-aggregates have a diameter of 10–40 µm, compared to alveolar capillary diameters of 7–10 µm. When injected into the jugular vein, the MAA particles are cleared on their first passage through the pulmonary circulation by becoming lodged in the alveolar capillaries and terminal arterioles. The distribution of the MAA is therefore proportional to the relative blood flow to the different areas of the lungs. In people, a relative safety margin is assured based on the number of MAA particles injected, compared to the proportion of arterioles blocked. When 200,000 particles are injected, less than 0.1% of the total number of arterioles are blocked, giving a safety margin of 1000:1[18]. In people, more than 60,000 particles need to be injected to produce an artefact-free scan, but increasing the number to greater than 200,000 does not improve the quality further. In the horse, a range between 300,000–500,000 particles has been quoted as being used safely[19]. When injecting the MAA, there are several protocols which must be followed to ensure a diagnostic scan. The syringe must be agitated prior to injection to free and mix all particles in the injection suspension. Blood must not be drawn into the syringe prior to injection to avoid clot formation in the syringe. The injection should be performed slowly.

RADIOPHARMACY QUALITY CONTROL

The radionuclide produced from the generator and the radiopharmaceuticals produced from the kits must be guaranteed for certain parameters to ensure that they produce a diagnostic quality image, that the radiation dose to the patient is minimised, and that they are safe to administer to the patient. The tests involved include:

- Sterility.
- Pyrogen-free (only for volumes larger than 15 ml in the UK).
- Radionuclide purity.
- Radiochemical purity.
- Chemical purity.

The sterility testing of a batch of radiopharmaceuticals is performed in retrospect due to the short $T^{1/2}$ of the nuclide and the requirement to administer the product prior to the completion of testing. A normal protocol for this is to send the first or second and the final eluate from the generator for culture and sterility testing. Random radiopharmaceutical samples are also chosen on a weekly basis to be sent for sterility testing.

Pyrogen testing is performed if required, although not routinely by the radiopharmacy. The standard test is the limulus amoebocyte lysate (LAL) test. It is a sensitive test performed to detect the presence of endotoxins.

The chemical purity test is performed on the first and last eluates from the generator to detect abnormally high levels of aluminium (Al^{3+}) in the eluate from the generator. This is important when producing colloid radiopharmaceuticals, as the Al^{3+} adversely affects their stability, leading to dissociation and the potential for corrupted images. Commercial kits are available which determine if the concentration is below a maximum level (10 µg/ml).

The radiochemical purity is the percentage of the total radioactivity of the radionuclide concerned that is present in the source in the declared chemical form[2]. This is to guarantee that the radiopharmaceutical dispensed contains an acceptable percentage of the correct radiochemical form, e.g. for a bone scan dose, ^{99m}Tc-MDP, and only low levels of various other ^{99m}Tc chemical forms, which would have a different biodistribution from the ^{99m}Tc-MDP and therefore corrupt the image. The other chemical forms include free $^{99m}TcO_4^-$ (pertechnetate) and TcO_2 (technetium dioxide), which is known as hydrolysed/reduced technetium. All commercial kits produced under licence are guaranteed for their radiochemical purity if they are produced following the licensing instructions. It is common practice to test the first kit in a new batch and then at monthly intervals from commercial supplies. If a kit is produced within the radiopharmacy or is reconstituted in an unlicensed manner, then each radiopharmaceutical should be tested. Planar chromatography is used to determine the percentage radiochemical purity.

Radionuclide purity is defined as the percentage of the radioactivity of the radionuclide concerned to the total radioactivity of the source[20]. For example, from the eluate of the molybdenum/technetium generator, this would be expressed as the percentage of ^{99m}Tc in the eluate. Other radionuclides present include the parent radionuclide, other daughter radionuclides or fission byproducts. All commercially manufactured generators have a radionuclide purity guaranteed. There can be an accidental elution of ^{99}Mo from the generator, and a limited radionuclide purity test can be performed in the radiopharmacy. Usually, the first and last eluate from a new generator is tested in this manner. The eluate is placed in a 6 mm thick lead pot, which attenuates the radiation from the ^{99m}Tc by

a factor of 10^6. The radioactivity from the ^{99}Mo can then be measured by placing the pot in a radionuclide calibrator. A loss of radionuclide purity can potentially increase the patient dose and deleteriously affect the image quality.

Occasionally, the quality of images being produced from a scan is poor, with the radiopharmaceutical not localising in the target organ, or high background activity resulting in poor contrast. Practical measures that can be assessed at the time of the scan include:

1. Checking the photopeak and energy window settings of the gamma camera.
2. Checking that no extraneous source of radiation is present in the scanning room.
3. If the pharmaceutical is administered by injection, scanning the area of injection to ensure that it has not inadvertently been injected perivascularly.
4. For ^{99m}Tc pharmaceuticals, if isotope dissociation has occurred (rare), large amounts of free pertechnetate would result. These accumulate in the thyroid glands. This phenomenon can therefore be checked by imaging the thyroid glands, which will be well above background levels in this instance.

It is clear that much work and expense is involved in setting up and managing an effective radiopharmacy. This can be avoided altogether if radiopharmaceuticals are supplied to the equine clinic from a local hospital pharmacy, already calibrated and labelled.

ACKNOWLEDGEMENTS

The following people have been invaluable in helping to produce this chapter. Their advice, knowledge and practical support are deeply appreciated: Miss Elizabeth Pitcher, Medical Physicist, Bristol General Hospital, UK and Dr Adrian Parkin, Medical Physicist, Addenbrooke's Hospital, Cambridge, UK.

REFERENCES

1. Kowalsky, R.J. (1987) Principles of radioactive decay, radioactivity, 99m-Tc generators and radiopharmacy. In: *Handbook of Veterinary Nuclear Medicine*, Eds: C.R. Berry and G.B. Daniel, North Carolina State University, North Carolina. pp 1-24.
2. Doherty, J. and Graham, D. (1998) The radiopharmacy. In: *Practical Nuclear Medicine*, Eds: P.F. Sharp, H.G. Gemmell and F.W. Smith, Oxford University Press, Oxford. pp 72-99.
3. Nicolini, M., Bandoll, G. and Mazzi, V. (1986) *Technetium Chemistry and Nuclear Medicine 2*, Vol. 2, Verona/Raven Press, New York.
4. Smith, F.W. (1998) 99m-technetium pertechnetate. In: *Practical Nuclear Medicine*, Eds: P.F. Sharp, H.G. Gemmell and F.W. Smith, Oxford University Press, Oxford.
5. Beck, K.A. and Hornoff, W.J. (1985) The normal feline thyroid. *Vet. Radiol.* **26**, 35-38.
6. Koblik, P.D., Komtebedde, J., Yen, C.K. *et al.* (1990) Use of transcolonic technetium-99m pertechnetate as a screening test for portosystemic shunts in dogs. *J. Am. vet. med. Ass.* **196**, 925-929.
7. Chambers, M.D. (1987) Bone imaging: the diphosphonates. In: *Handbook of Veterinary Nuclear Medicine*, Eds: C.R. Berry and G. Daniel, North Carolina State University, North Carolina.
8. Smith, F.W. (1998) The skeletal system. In: *Practical Nuclear Medicine*, Eds: P.F. Sharp, H.G. Gemmell and F.W. Smith, Oxford University Press, Oxford. pp 235-252.
9. Weller, R., Livesey, L., Maierl, J. *et al.* (2001) Comparison of radiography and scintigraphy in the diagnosis of dental disorders in the horse. *Equine vet. J.* **33**, 49-58.
10. Peters, A.M. (1998) Infection. In: *Practical Nuclear Medicine*, Eds: P.F. Sharp, H.G. Gemmell and F.W. Smith, Oxford University Press, Oxford. pp 285-315.
11. Weller, R., Weaver, M., Livesey, L. *et al.* (2000) Nuclear scintigraphy with 99m-Tc-HMPAO labelled leukocytes in the assessment of horses with malabsorption. *Vet. Radiol. Ultrasound* **41**, 563.
12. Butson, R.J., Webbon, P.M. and Fairbairn, S.M. (1995) Tc-99m-HMPAO labeled leukocytes and their biodistribution in the horse: a preliminary investigation. *Equine vet. J.* **27**, 313-315.
13. Koblik, P.D., Lofstedt, J., Jakowski, R.M. *et al.* (1985) Use of 111-Indium labelled leukocytes to image an abdominal abscess in a horse. *J. Am. vet. med. Ass.* **186**, 1319-1322.
14. Smith, F.W. and Gemmell, H.G. (1998) The urinary tract. In: *Practical Nuclear Medicine*, Eds: F.W. Smith, H.G. Gemmell and P.F. Sharp, Oxford University Press, Oxford. pp 213-234.
15. Twardock, A.R., Krawiec, D.R. and Itkin, R.J. (1987) Renal imaging. 1: Renal scintigraphy. In: *Handbook of Veterinary Nuclear Medicine*, Eds: C.R. Berry and G.B. Daniel, North Carolina State University, North Carolina.
16. Matthews, H.K., Andrews, F.M., Daniel, G.B. *et al.* (1992) Comparison of standard and radionuclide methods for measurement of glomerular filtration rate and effective renal blood flow in female horses. *Am. J. vet. Res.* **53**, 1612-1616.
17. Votion, D.M. and Lekeux, P.M. (1997) Equine lung scintigraphy. In: *Dubai International Equine Symposium: The Diagnosis and Treatment of Respiratory Disease*, Eds: N.W. Rantanen and M.L. Hauser, Matthew R. Rantanen Design, Dubai.
18. Gray, H.W. (1998) The lung. In: *Practical Nuclear Medicine*, Eds: P.F. Sharp, H.G. Gemmell and F.W. Smith, Oxford University Press, Oxford. pp 159-175.
19. Berry, C.R., Daniel, G. and O'Callaghan, M. (1987) Pulmonary scintigraphy. In: *Handbook of Veterinary Nuclear Medicine*, Eds: C.R. Berry and G.B. Daniel, North Carolina State University, North Carolina. pp 143-153.
20. Anon (1993) *British Pharmacopoeia (XV)*, The Medicines Commission, HMSO, London.

Chapter 2b

PRACTICAL RADIOPHARMACY FOR EQUINE BONE SCINTIGRAPHY

JO WEEKES
Centre for Equine Studies, Animal Health Trust, Lanwades Park, Kentford, Newmarket, Suffolk CB8 7UU, UK.

^{99}MOLYBDENUM/^{99m}TECHNETIUM GENERATOR

All radiopharmacies involved in the supply of ^{99m}Tc-labelled radiopharmaceuticals store and use a generator. Several commercial generators are available, all consisting of ^{99}Mo adsorbed onto a sterile aluminium oxide column. The $^{99}TcO_4^-$ (pertechnetate) is eluted from the column with sterile 0.9% w/v sodium chloride solution.

The generator is a sterile system which can be used over a period of 1–2 weeks, although the ^{99m}Tc-pertechnetate eluted should be used only for up to 12 h after elution. Generators are now supplied with large quantities of ^{99}Mo loaded onto the column to supply the high demand for ^{99m}Tc. This is especially useful for equine practices that perform skeletal scintigraphy, as the high concentration of ^{99m}Tc allows small injectable volumes (2–5 ml) to be drawn up to give the required dose for equine skeletal scintigraphy (10 MBq/kg bwt). A new generator provides ^{99m}Tc in a high radioactive concentration that is ideal for equine skeletal scintigraphy, but the concentration is probably too high for respiratory or gastric use, for which it is necessary to dilute the eluate using 0.9% w/v sodium chloride solution. The quantity of eluted and dispensed ^{99m}Tc should be measured in a suitable radioisotope ionisation chamber.

The generator should be stored and eluted under conditions which maintain the sterility of the column and protect operatives from radiation. For veterinary use, a clean area on a bench within a clean room is sufficient. Although the column is shielded with lead, it may be necessary to use secondary lead shielding to reduce radiation to desirable levels. ^{99}Mo/^{99m}Tc generators are examples of closed systems and, in order to maintain sterility and integrity of the system, they should be eluted strictly in accordance with the manufacturer's instructions using the eluting solvent and collection vials provided. All staff who perform radiopharmacy procedures must have undergone training that local radiopharmacy staff can provide.

Ordering a Generator

Several companies produce and supply ^{99}Mo/^{99m}Tc generators, including Amersham International[a] and CIS Bio International[b] in the UK. Local hospitals will often be able to supply contact details for suppliers in other countries.

Prior to ordering a ^{99}Mo/^{99m}Tc generator, it is necessary to calculate the required activity of ^{99m}Tc required each day. By using the reference table supplied here (**Table 1**), it can be determined which generator size will give the desired daily activity. Consideration of the date of delivery and reference date of the generator may enable the purchase of a smaller generator to provide the desired ^{99m}Tc activity (**Table 1**). Prior to ordering, it is essential to check that the maximum activity of the generator on delivery does not exceed the maximum permissible storage activity levels for both ^{99}Mo and ^{99m}Tc on the Environment Agency licence.

Instructions for Use/Handling

Only trained staff must perform any handling or elution of a ^{99}Mo/^{99m}Tc generator.

To elute a ^{99}Mo/^{99m}Tc generator to produce ^{99m}Tc-pertechnetate to be used for scintigraphy, the following are typical general working instructions. However, it is necessary to check the working instructions supplied by the manufacturer and to ensure that this system of work is approved by the person responsible for advice on radiation safety. In the UK, this is the Radiation Protection Advisor (RPA).

1. On receipt of a ^{99}Mo/^{99m}Tc generator, details of the date of arrival, activity (GBq), reference date, batch number (serial and lot number) and expiry date, together with location of storage, must be recorded on an appropriate form (**Form 1**).
2. Place generator in position behind lead shielding.
3. Open safety valve to position 1 at least 3 mins prior to first elution. Do not turn off safety valve between elutions. The

Form 1: Record of receipt, storage and dispatch of ^{99}Mo/^{99m}Tc generators

Date of receipt	Lot No.	Serial No.	Calibration		Expiry date	Storage			Packaged		Collection Date	Destination
			Activity	Date/Time		Location	From	To	Date	Signature		

Table 1: Reference table showing the maximal radioactivity of elutable ^{99m}Tc sodium pertechnetate for each size of generator

Generator size		Days																							
		-8	-7	-6	-5	-4	-3	-2	-1	0	+1	+2	+3	+4	+5	+6	+7	+8	+9	+10	+11	+12	+13	+14	
GBq	**2**	15.02	11.67	9.07	7.05	5.48	4.26	3.31	2.57	2	1.55	1.21	0.94	0.73	0.57	0.44	0.34	0.27	0.21	0.16	0.13	0.10	0.08	0.06	**2**
mCi	**54**	405	315	245	190	148	115	89	69	54	42	33	25	20	15	12	9	7	6	4	3	3	2	2	**54**
GBq	**4**	30.03	23.34	18.14	14.10	10.96	8.52	6.62	5.15	4	3.11	2.42	1.88	1.46	1.13	0.88	0.69	0.53	0.41	0.32	0.25	0.19	0.15	0.12	**4**
mCi	**108**	811	630	490	381	296	230	179	139	108	84	65	51	39	31	24	19	14	11	9	7	5	4	3	**108**
GBq	**6**	45.05	35.01	27.21	21.15	16.44	12.78	9.93	7.72	6	4.66	3.62	2.82	2.19	1.70	1.32	1.03	0.80	0.62	0.48	0.38	0.29	0.23	0.18	**6**
mCi	**162**	1216	945	735	571	444	345	268	208	162	126	98	76	59	46	36	28	22	17	13	10	8	6	5	**162**
GBq	**8**	60.07	46.96	36.29	28.20	21.92	17.04	13.24	10.29	8	6.22	4.83	3.76	2.92	2.27	1.76	1.37	1.07	0.83	0.64	0.50	0.39	0.30	0.24	**8**
mCi	**216**	1622	1261	980	761	592	460	358	278	216	168	130	101	79	61	48	37	29	22	17	14	10	8	6	**216**
GBq	**10**	75.08	58.36	45.36	35.25	27.40	21.3	16.55	12.87	10	7.77	6.04	4.70	3.65	2.84	2.20	1.71	1.33	1.04	0.80	0.63	0.49	0.38	0.29	**10**
mCi	**270**	2027	1576	1225	952	740	575	447	347	270	210	163	127	99	77	60	46	36	28	22	17	13	10	8	**270**
GBq	**12**	90.10	70.03	54.43	42.31	32.88	25.56	19.86	15.44	12	9.33	7.25	5.63	4.38	3.40	2.65	2.06	1.60	1.24	0.96	0.75	0.58	0.45	0.35	**12**
mCi	**324**	2433	1891	1470	1142	888	690	536	417	324	252	196	152	118	61	71	56	43	34	26	20	16	12	10	**324**
GBq	**16**	120.13	93.37	72.57	56.41	43.84	34.08	26.49	20.59	16	12.44	9.67	7.51	5.84	4.54	3.53	2.74	2.13	1.66	1.29	1.00	0.78	0.60	0.47	**16**
mCi	**432**	3244	2521	1959	1523	1184	920	715	556	432	336	261	203	158	123	95	74	58	45	35	27	21	16	13	**432**
GBq	**20**	150.16	116.71	90.72	70.51	54.80	42.59	33.11	25.73	20	15.54	12.08	9.39	7.30	5.67	4.41	3.43	2.66	2.07	1.61	1.25	0.97	0.76	0.60	**20**
mCi	**540**	4054	3151	2449	1904	1480	1150	894	695	540	420	326	254	197	153	119	93	72	56	43	34	26	20	16	**540**

NB: The days with a minus sign are the days preceding the date shown on the label (calibration date); those with a plus sign are the days after this date.

safety valve is to be turned off (to position 0) only when the generator is being packaged for return to manufacturer.

4. To elute the generator, place a sterile elution vial within the elution shield.
5. Dial up an appropriate eluate volume on the generator.
6. Swab the exposed elution vial septum with an alcohol wipe.
7. Remove and discard the needle protector from the generator. Check that the elution needle is straight, and replace if necessary.
8. Place the elution shield firmly upside-down over the needle.
9. Turn valve from position 1 to 2 and leave the vial until elution is complete (this can take up to 10 mins; it is important to wait until all bubbling has ceased).
10. Turn valve back to position 1, remove the elution vial shield and place a new needle protector over the needle.
11. Replace any protective lead shielding.
12. Assay the activity of the eluate.
13. Complete the eluate label provided using a solvent-resistant pen, specifying the date and time of elution, elution number, eluate activity and volume at that time, and name of the member of staff performing elution.
14. Attach the completed label to the elution vial and replace the vial within the shield.
15. Record elution details on an appropriate form (**Form 2**).

Reconstitution of a Kit

Any handling of ^{99m}Tc-pertechnetate or reconstitution of kits must be performed only by trained staff.

A kit can be defined as 'a prepackaged set of sterile ingredients designed for the preparation of a specific radiopharmaceutical'. There are many advantages of using kits for the preparation of radiopharmaceuticals:

- Closed procedure.
- Rapid and easy preparation of product.
- Low radiation hazard to operative.
- Sterile and pyrogen-free product.
- Reproducable and reliable product.
- Readily available.
- Long shelf-life of unreconstituted kit.

The following are typical general working instructions to reconstitute a multidose vial of, for example, methylene diphosphonate (MDP) with ^{99m}Tc-sodium pertechnetate, to form an agent suitable for skeletal scintigraphy. However, it is necessary to check the working instructions supplied by the manufacturer of the kit you want to reconstitute:

1. The MDP vial may be reconstituted with between 2 and 8 ml of eluate containing a maximum of 18.5 GBq ^{99m}Tc pertechnetate.
2. Calculate the activity and volume required of the kit.
3. Swab the MDP vial septum and place vial in a tungsten lead vial shield.
4. Swab the elution vial septum, draw a volume of air equal to the required volume of eluate into the syringe, add the needle and syringe shield, and pressurise the elution vial with this air.
5. Invert the vial and allow the eluate to fill the syringe slowly to the required volume.

Form 2: Record of $^{99}Mo/^{99m}Tc$ generator elution

Generator No.	Elution No.	Date	Time	Activity (GBq)	Volume (ml)	Comments	Signature

Form 3: Record of radiopharmaceutical preparation

		Pharmaceutical kit				Diluent					Eluate					
Date	Time	Type	Manu-facturer	Batch No.	Expiry date	Type	Manu-facturer	Batch No.	Expiry date	Volume (ml)	No.	Volume (ml)	Activity (MBq)	Final volume (ml)	Visual check	Prepared by

6. Inject the eluate into the MDP vial and remove an equal volume of nitrogen from the space above the liquid before withdrawing the needle.
7. If necessary, swab the saline ampoule, draw up the required volume of saline and inject it into the MDP vial to dilute the preparation to the required concentration of radioactivity (GBq/ml). Remove an equal volume of nitrogen from the space above the liquid before withdrawing the needle. Any remaining saline should be discarded.
8. Shake the MDP vial in its shield for 10 secs to ensure complete dissolution of the powder.
9. Remove the MDP vial from its vial shield using tongs and visually inspect the contents for gross particulate contamination, viewing it from behind a lead glass shield.
10. Assay the activity of the MDP vial.
11. Complete the kit label provided using a solvent-resistant pen, specifying the date and time of reconstitution, elution number, eluate activity, final volume of the kit, any dilution required and name of the member of staff performing reconstitution.
12. Attach the completed label to the kit vial and replace the vial within its shield.
13. Record kit details on an appropriate form (**Form 3**).
14. The kit has an expiry time of approximately 8 h after reconstitution, but this differs for different types of kit and manufacturers.

MANUFACTURERS' ADDRESSES

[a]Amersham International Plc, Little Chalfont, Buckinghamshire, UK.
[b]CIS Bio International, Schering Health Care Ltd, Burgess Hill, West Sussex, UK.

FURTHER READING

1. Sharp, P.F., Gemmel, H.G. and Smith, F.W. (1989) *Practical Nuclear Medicine*, Oxford University Press, Oxford, UK.
2. Sampson, C.B. (1990) *Textbook of Radiopharmacy*, Gordon and Breach Science Publishers.

Chapter 3

BASIC STRUCTURE AND FUNCTION OF THE CAMERA

A. ROBERT TWARDOCK
2517 Prairie Ridge, Champaign, Illinois 61822, USA.

As its name implies, the gamma camera functions to detect γ-rays emitted by a radiopharmaceutical after its administration to the patient and to produce an image showing the distribution of that radiopharmaceutical within the tissues of the patient. The quality of the image is greatly dependent upon the quality of the camera, its care and maintenance (including routine quality control measures), and its proper use. Therefore, it behoves the equine scintigrapher to possess a good, fundamental knowledge of the components of the camera and how they contribute to the production of the image. The large majority of scintigraphy in equine practices is performed by technicians; it is therefore equally important that they have the same basic understanding of the camera. Nothing is more frustrating than producing and attempting to interpret a poor quality scintigraphic image.

Figure 1 illustrates the basic components of a gamma camera. ^{99m}Tc-labelled diphosphonate in the patient emits γ-rays, many of which are scattered and absorbed in the patient, some of which leave the patient with or without interacting and enter the camera with energies as high as their initial 140 KeV or below. The collimator allows only those rays moving parallel to its holes to reach the crystal, and these are a very small fraction of the radiation leaving the horse. This explains why gamma camera images take so long to 'build', while measurement of the radiation dose at the site being imaged shows a level which should give a 100,000 count (100K) acquisition quite quickly. Most of the γ-rays leaving the horse in the direction of the camera are stopped by the collimator. Rays that interact in the crystal deposit energy that is re-emitted as scintillation light having visible and ultraviolet wavelengths. The scintillation light is detected and converted to electrical pulses by an array of photomultiplier tubes (PMTs) that are optically coupled to the crystal. Electric pulses from the PMTs that fall within the ^{99m}Tc photopeak energy window (Z pulses) are registered in the image in terms of where the scintillation light is emitted in the crystal (X and Y signals) and hence, indirectly, where the diphosphonate molecules are located in the patient. Most of the components are housed in a heavy, lead-lined shield called the 'head', that protects the detector from environmental background radiation. Cameras used for veterinary applications are mounted on a variety of systems, including stands, gantries, jib cranes and chain hoists, that allow the operator to move them around the patient (see *Part I, Chapter 4*).

The NaI(Tl) Crystal

The crystal functions as a transducer of high energy, ionising γ-ray photon energy to low energy, ultraviolet and visible scintillation photon light energy. High energy γ-rays interact and lose energy in the crystal because of its composition (thallium activated sodium iodide), density and thickness. The detectors of early gamma cameras had relatively small diameter crystals (25 cm, for example) and a relatively small number (typically 19) of large diameter (7.5 cm) PMTs, giving them restricted fields-of-view and poor spatial resolution. The crystals of these early cameras were 1.25 cm thick, which also limited resolution. In the intervening years, camera manufacturers have

Figure 1

The basic components of a gamma camera. The crystal, PMTs and much of the signal processing circuitry are enclosed in a heavy, lead-lined housing that shields the detector from background radiation.

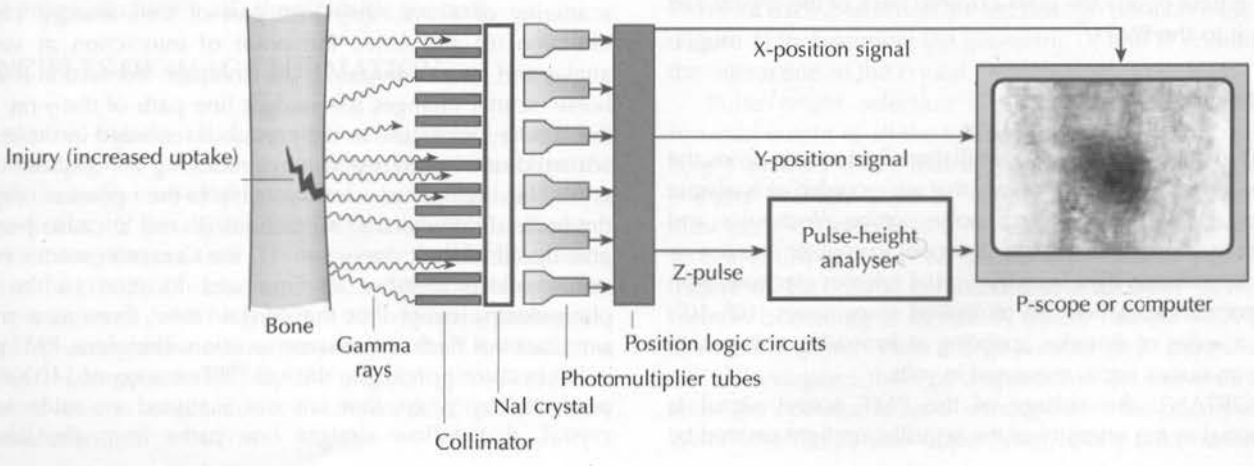

Figure 2

The sight no nuclear medicine clinician ever wants to see on the computer screen, the image of a broken crystal. This example resulted from a full-force kick from a horse to the surface of the collimator. (Courtesy of D. Reid, Scantek, Northampton.)

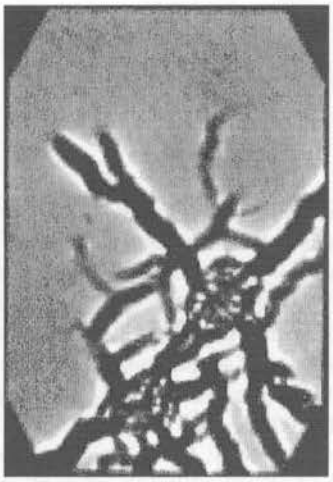

improved spatial resolution to its practical limit by using thinner crystals (6–9 mm) and larger numbers of smaller diameter PMTs. Because most cameras employed in equine practices are procured as second or third generation used or reconditioned instruments, it is important to understand and evaluate the level of camera technology used at the time the camera was built when considering one for purchase. Large field-of-view cameras with thin crystals are now considered to be 'state of the art' for equine scintigraphy.

Thinner crystals are almost as efficient in stopping 140 KeV γ-rays as thicker ones, and their resolution is better because scintillation light is less scattered and absorbed before reaching the PMTs. Great care must be taken to avoid exposing any crystal to rapid temperature changes or mechanical shock, which can crack a very expensive component of the camera; thin crystals are especially susceptible (**Figure 2**). The front and outer rim of the crystal are sealed within an aluminum 'can' and the back is covered by glass that protects it from the environment. Sodium iodide is hygroscopic and absorbs water and becomes yellowed, losing detection efficiency and resolution, if the 'can' leaks and allows moist air to reach the crystal. The aluminium 'can' also protects the crystal from mechanical shock and stray light. Optical grease covers the glass-covered back of the crystal and couples it to the PMTs.

The Photomultiplier Tube

The PMT (**Figure 3**) converts scintillation light energy from the crystal to pulses of electrical energy that are recorded as analogue or digital signals, sent through pulse sorting electronics and displayed by a positioning scope (P-scope), computer monitor, or on film. Scintillation light from the crystal releases electrons from the photocathode, which are multiplied many times (10^6–10^8) through a series of dynodes operating at increasing voltages, to produce an output signal measured in volts.

IMPORTANT: the voltage of the PMT output signal is proportional to the intensity of the scintillation light emitted by

Figure 3

Basic principles of a photomultiplier tube (PMT). The entrance window is optically coupled to the back of the crystal, allowing scintillation light photons to release electrons from the photocathode. Each photoelectron is multiplied 10^6–10^8 times in the output signal, producing a relatively large pulse of current when the PMT is stimulated by a relatively weak light signal.

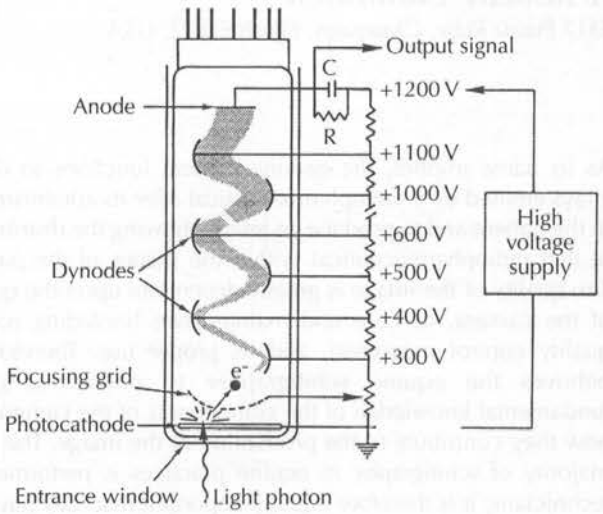

the crystal, which in turn is proportional to the γ-ray energy deposited in the crystal:

Equation 1

γ-ray energy deposited in crystal	α	scintillation light output of crystal	α	PMT signal voltage

Because of this proportional relationship, the spectrum of energies deposited by γ-rays in the crystal can be displayed, and a specific range of γ-ray energies (the photopeak) can be selected from which to create the scintigraphic image.

The Gamma-Ray Spectrum and Photopeak

When γ-rays deposit their energies in the crystal, causing scintillations, they do so by means of Compton and photoelectric interactions. **Figure 4** illustrates these interactions and their resultant energy deposition spectrum, as measured by the size of their PMT signal output voltages. As shown in **Figure 4**, Compton interactions (C, D, and E) cause scattering of γ-rays; they lose part of their energy, change direction (θ) and leave the point of interaction at varying angles and lower energies. If the Compton interaction is in the horse, scatter changes the straight line path of the γ-ray from the labelled molecule to the crystal. If recorded in the image, scattered rays would distort it by producing scintillations in the crystal having little or no relationship to their point of origin in the horse. Photoelectric interactions (B and E) cause γ-rays to give up all of their energy. In 'E', the Compton scatter events are so close together in time and location to the final photoelectric event that the crystal 'sees' them as a single, simultaneous flash at the same location. Therefore, PMT pulse voltages corresponding to the full ^{99m}Tc energy of 140 KeV are produced by γ-rays that are not scattered *en route* to the crystal, that follow straight line paths from the labelled

Figure 4

Gamma-ray interactions in the crystal (A–E) and the γ-ray energy spectrum produced by those interactions. The camera operator positions an electronic window around the photopeak, allowing only those interactions depositing the entire 140 KeV energy of the ^{99m}Tc γ-ray in the crystal (B and E) to be registered in the scintigraphic image. pe = photoelectric event; ce = Compton event; LLD = lower level discriminator; ULD = upper level discriminator.

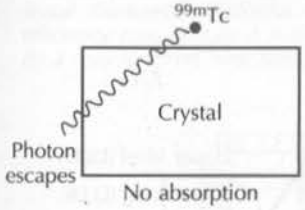

A
No interaction
Energy absorbed by crystal = 0 MeV
No flash of light
No pulse

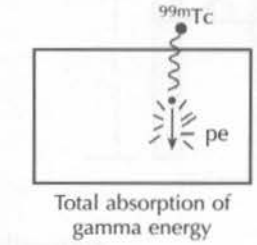

B
One photoelectric interaction
Energy absorbed by crystal = full 140 KeV of the incident gamma photon
One flash of light
Pulse counted under photopeak energy (=140 KeV)

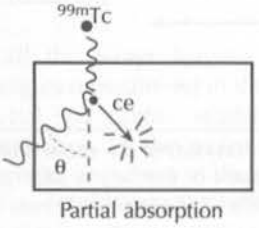

C
One Compton interaction with escape of scattered photon
Energy absorbed by crystal <140 KeV
Flash of light less bright than in B
Pulse counted under energy lower than that of the photopeak

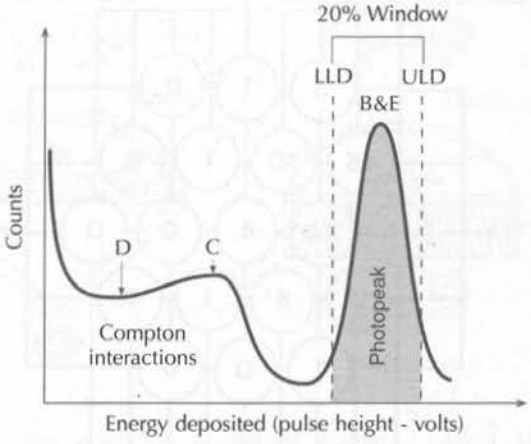

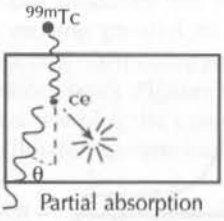

D
One Compton interaction with escape of scattered photon
Energy absorbed by crystal <energy absorbed in C (because of smaller θ)
Flash of light less bright than in C
Pulse counted under energy lower than in C

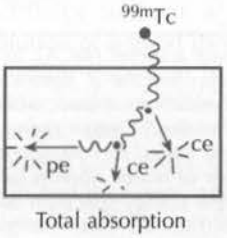

E
Two Compton interactions followed by a photoelectric interaction
Energy absorbed by crystal = 140 KeV
Three flashes of light almost simultaneous
Intensity of composite flash as in B
Pulse counted under photopeak

molecules to the crystal, and that produce the highest quality image. The locations in the spectrum of PMT pulses produced by Compton scatter that escapes the crystal (C and D), and by photoelectric (B) or Compton followed by photoelectric interactions (E), are shown in **Figure 4**. The pulses produced by 'B' and 'E' fall under the 'photopeak'. 'Peaking' the camera refers to electronically selecting those pulses to be registered in the image, excluding all others outside the peak.

PRINCIPLES OF IMAGE FORMATION

The gamma camera produces the scintigraphic image by: 1) collimating the γ-rays that are allowed to interact in the crystal, usually restricting access to γ-rays travelling perpendicular to the crystal with a parallel hole collimator; 2) determining the position (X,Y location) of each scintillation event in the crystal; 3) including in the image only those events having energies (Z pulse heights) that fall within the photopeak; and 4) registering those events according to their X,Y locations in a digital computer for display and processing. Collimation is discussed later, in conjunction with camera detection efficiency and resolution.

Position registration (step 2) is illustrated in **Figure 5**. Scintillation light is most intense at the point of γ-ray interaction in the crystal (star), and diminishes with distance. PMTs closest to the point of interaction intercept the most light photons and produce the greatest pulse voltages, with progressively decreasing pulse sizes from PMTs located at increasing distances from that point. The relative output voltages from all PMTs for each interaction are fed through position logic circuits (**Figure 1**) to determine the geometric (X and Y) coordinates of the interaction in the crystal.

Pulse height selection is accomplished by sending the summed output of all the tubes, called the 'Z pulse', to a pulse height analyser (PHA) that selects only pulses with photopeak energies for registration as 'counts' in the image. The PHA of most gamma cameras is a multichannel analyser (MCA), that sorts and displays PMT 'Z' pulses according to their energies (**Figure 6**). Each pulse is recorded in a 'channel' in the MCA's memory according to its size. A typical camera MCA has 100 channels or more. When a large number of 'Z' pulses is sorted, the MCA displays them as a spectrum. The camera's controls allow the operator to set a 'window' over the photopeak, with lower level (LLD) and upper level (ULD) discriminators that

Figure 5

Schematic diagram of the arrangement of PMTs in a 19-tube camera, illustrating the principle of registering the location (star) of a scintillation event in the crystal. PMT output signals (represented as arbitrary numbers) decrease with distance from the event. The PMT outputs are summed for each of four sets of coordinates (X^+, X^-, Y^+, Y^-), measured from vertical and horizontal lines passing through the centre of the crystal. The X,Y address of the location is calculated from the summed outputs, digitised and stored in the corresponding pixel of the image array.

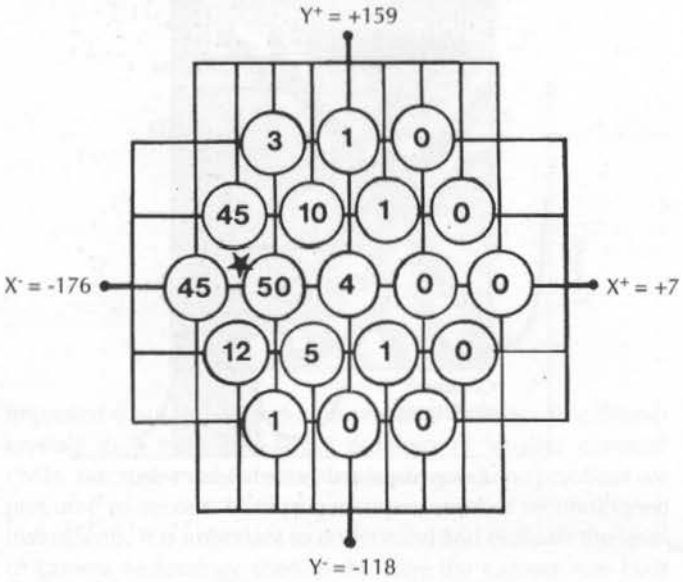

Figure 6

Illustration of pulse sorting by a multichannel analyser (MCA). In this example, output pulses from the amplifier represent the 'Z' signals from a camera. For ease of illustration only 12 channels are shown, whereas the MCA of a gamma camera has many hundred. Output pulses are digitised according to their magnitudes and stored in corresponding channels in the MCA's memory. The number of pulses stored/channel during a counting interval is displayed as the energy spectrum of the gamma emitter.

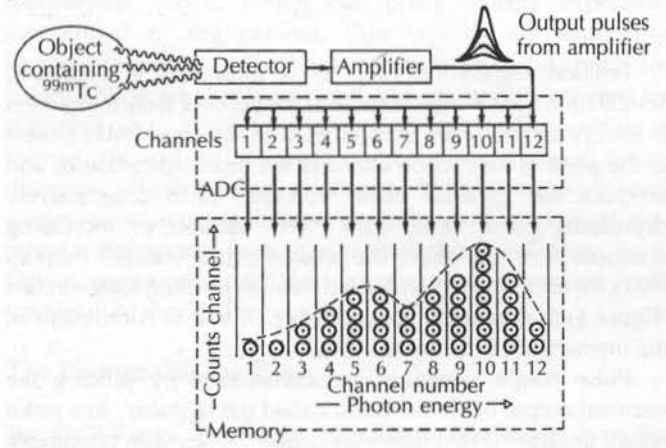

define the lower and upper edges of the photopeak. By setting the window over the photopeak, only those γ-rays moving directly, unscattered, from the labelled molecule contribute as counts in the image (**Figure 7**). Those that are scattered by Compton interactions are at lower energies before striking the crystal; their pulses fall outside the window, thereby eliminating the 'noise' they would otherwise contribute to the image.

Figure 7

Example of pulse sorting in the window of a pulse height analyser. Only the pulse that falls within the window (between the LLD and ULD) is registered as a count. ***a)*** *An example of real-time electrical pulses.* ***b)*** *How only one pulse would register after pulse height analysis.*

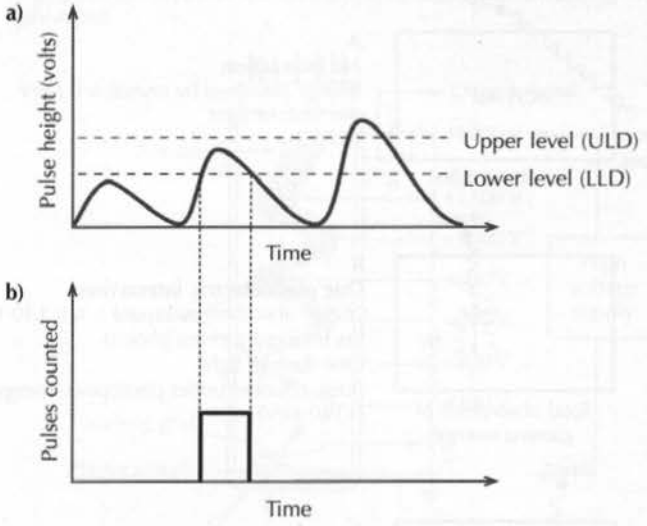

Figure 8

Determining full width at half maximum (FWHM) of the count profile (point or line spread function) from a point or line source of γ-rays. FWHM is measured in cm or mm of collimator or crystal face.

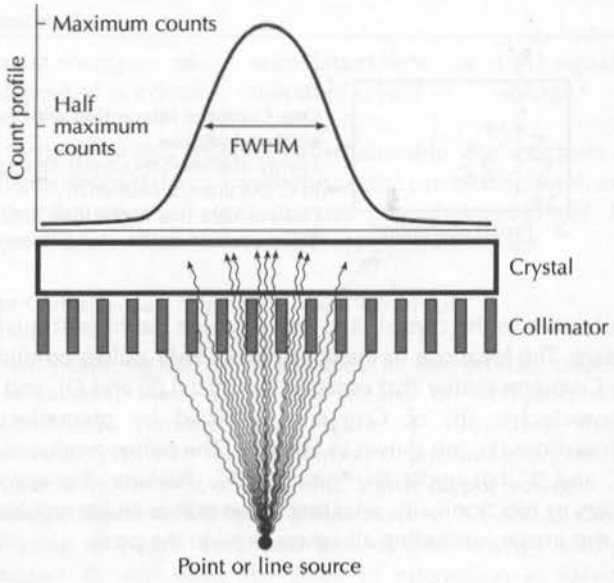

Window Width

For most scintigraphic procedures using ^{99m}Tc, the width of the window, the difference between the LLD and ULD, is set at 20% of the 140 KeV photopeak energy. For example, if the ^{99m}Tc photopeak is centred at channel 140 of the MCA, a 20% window would be 28 channels wide, 14 channels below and 14 channels above 140 (LLD = channel 126 and ULD = channel 154), allowing interactions in the crystal between 126 KeV and 154 KeV to be recorded as counts in the image.

Figure 9

Factors determining collimator resolution and efficiency, vs. septal penetration by γ-rays travelling nonparallel to the collimator holes. The septal thickness (T) required to limit penetration to 5% or less is determined by septal length (L) and hole diameter (D). For a given septal thickness, resolution is improved only at the expense of efficiency (sensitivity). W = shortest path length through the septum for a γ-ray to travel from one hole to the next.

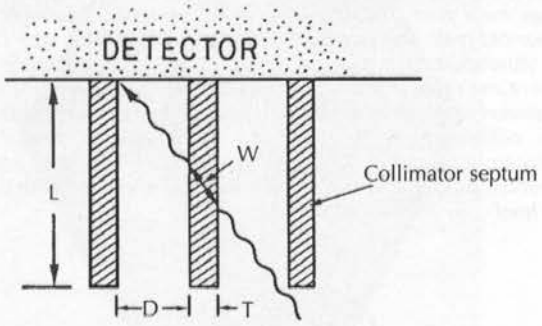

Collimation

If all the γ-rays leaving the patient that have photopeak energies (unscattered in the patient) were allowed to strike the crystal, no useful, readable image of radiopharmaceutical distribution in the patient could be produced. They could originate anywhere in the body and still hit the crystal, having no useful relationship between site of anatomical origin and the X,Y coordinates of the scintillation event in the crystal. The collimator produces that relationship by allowing only those γ-rays moving parallel to its openings to reach the crystal. Gamma rays not moving parallel to its holes are stopped by the collimator's septa (**Figures 1 and 9**). Because a large proportion of γ-rays reaching the camera from the patient are stopped by the collimator, gamma cameras are very inefficient detectors.

Equation 2

$$\text{Percentage detection efficiency} = \frac{\text{Counts recorded/time x 100}}{\text{γ-rays emitted by source/time}}$$

The lower a camera's efficiency, the more time it takes to acquire an image of a given number of counts, obviously a very important factor in equine scintigraphy because movement by the horse during acquisition blurs the image.

Optimising the camera's efficiency (sensitivity) for all imaging purposes might seem to be an obvious objective of scintigraphers. However, that goal is a trade-off against the camera's spatial resolution. Spatial resolution can be defined as:

'The fidelity with which an imaging device reproduces an object or defines the presence of an abnormality'[1], or 'the minimum distance between two points at which the detecting system can distinguish them as two points rather than one'.

A commonly used measure of gamma camera resolution is 'full width at half maximum' (FWHM). FWHM is measured by placing a very small point source or a very thin line source on the camera, acquiring a high count image of the source, plotting its count profile, and measuring the profile's width at half its maximum count (**Figure 8**). The smaller the FWHM value, the better the camera's resolution. Camera resolution can also be evaluated using bar phantoms, to be discussed later.

Figure 10

Different collimator designs, showing their effects on image size and orientation on the crystal. Converging and diverging collimators magnify and minify the image, respectively, and the pinhole both magnifies and inverts it. Pinholes have excellent resolution, but very low efficency.

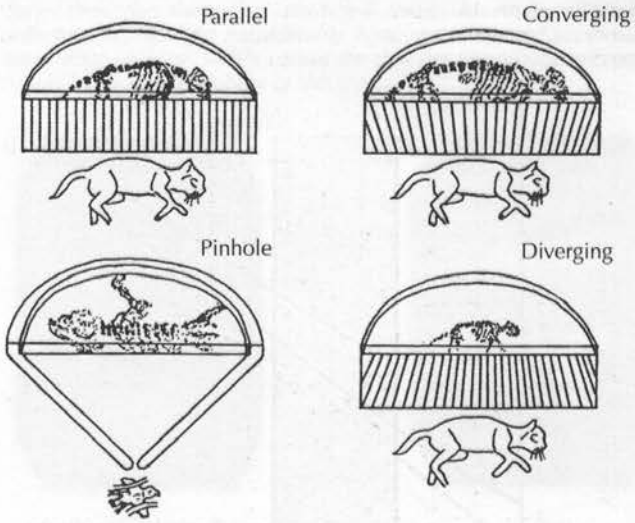

The resolution of a gamma camera, called system resolution, is the combined result of: 1) intrinsic resolution and 2) collimator resolution.

Intrinsic resolution is the resolution of the detector and its electronics without a collimator in place. The intrinsic resolution of a good gamma camera is around 3 mm FWHM. Collimator resolution is the resolution of the collimator itself. As discussed previously, intrinsic resolution depends on crystal thickness, the number and diameter of PMTs, and their associated electronics. Collimator resolution depends on septal length and thickness, and hole geometry (**Figure 9**). Collimator designers aim for minimal septal thickness, to obstruct the smallest possible area of detector surface and maintain maximum efficiency, and also ensure minimal septal penetration (<5%) by impinging γ-rays. A geometry of long, narrow holes provides the best resolution, but results in reduced efficiency and longer image acquisition times.

Manufacturers provide collimators with different combinations of resolutions and sensitivities, and for differing γ-rays energies. 'Low energy' collimators are designed for an upper limit of about 150 KeV, suitable for 140 KeV ^{99m}Tc but not, for example, for Indium-111's gammas of 172 and 247 KeV which require a 'medium energy' collimator. For most equine scintigraphy applications, a parallel hole, low energy, all (or general) purpose (LEAP) collimator gives best results in terms of image quality versus counting times. Converging hole, diverging hole and pin-hole collimators are also available (**Figure 10**) but are more useful in small animal scintigraphy than in equine work.

Resolution vs. Lesion Detectability

There is a large difference between intrinsic or system resolutions quoted by gamma camera manufacturers and actual lesion size that can be detected in a patient. At typical organ depths, collimator resolution is the primary determinant

Figure 11

Camera (system) resolution versus source-to-collimator distance for a typical parallel-hole collimator on two cameras differing two-fold in their intrinsic (without collimator) resolutions. At typical organ depths, camera resolution is determined primarily by collimator resolution. R_i = Intrinsic resolution of camera; FWHM = full width at half maximum.

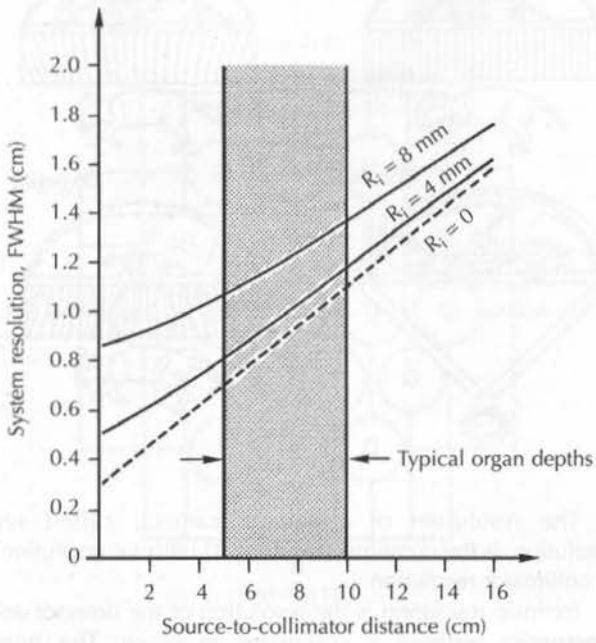

of the system (the camera's) resolution. As shown in **Figure 11**, at organ depths of 10 cm, system FWHM varies only between 1.2–1.4 cm for cameras differing two-fold (4 vs. 8 mm) in their intrinsic resolutions.

Other factors affecting lesion detectability include the 'count density' of the image and 'object contrast'. Count density refers to the number of counts recorded/unit area of the image (typically counts/pixel). Image quality increases with count density, but obviously requires a longer counting time and/or a larger dose of radiopharmaceutical. Object contrast refers to the relative count densities of a lesion and of normal tissues surrounding the lesion, which are properties of the radiopharmaceutical and the pathophysiology of the organ system being imaged. In general, 'hot' lesions against a 'cold' background are more detectable than *vice versa*. In summary, lesion sizes that are detectable vary greatly from one imaging situation to another, depending on the relative influences of all the factors just discussed. The camera's resolution is only one factor, and is not the major determinant in most equine scintigraphic applications.

Probably, the most important factors affecting image quality in equine scintigraphy, assuming that a well tuned camera with at least 37 PMTs is used, are patient motion during acquisition and camera-to-subject distance. If the patient and/or camera move relative to one another during image acquisition, the image will obviously blur. Although motion correction software (discussed in *Part I, Chapter 5*) is available with newer computers, it should not be relied on entirely to counteract the effects of motion. Such motion can be very subtle during a

Figure 12

a) *The effect on resolution of increased subject-to-camera distance. Close to the camera (A), γ-rays from the subject reach the crystal through a limited number of collimator holes, producing an image confined to area 'a' in the crystal. Further from the camera (B), more collimator holes are available for straight line travel to the crystal, increasing the image size to area 'b' and decreasing resolution. Provided that the projected image of the subject remains within the edges of the crystal, there is no decrease in the count-rate or total counts in the image for a given counting time.* ***b)*** *Lateral view, distal right forelimb, 4-year-old male Thoroughbred (TB) racehorse. Matrix size 128 x 128. An illustration of the actual effect of increasing distance between patient and collimator on image quality. Note particularly the decreased resolution of the pastern joint and foot. Distances were measured from the collimator surface to the skin surface lateral to the metacarpophalangeal joint: (i) 6 cm (this was the unavoidable minimum produced with the collimator in firm contact with the edge of the hoof); (ii) 30 cm; (iii) 60 cm.*

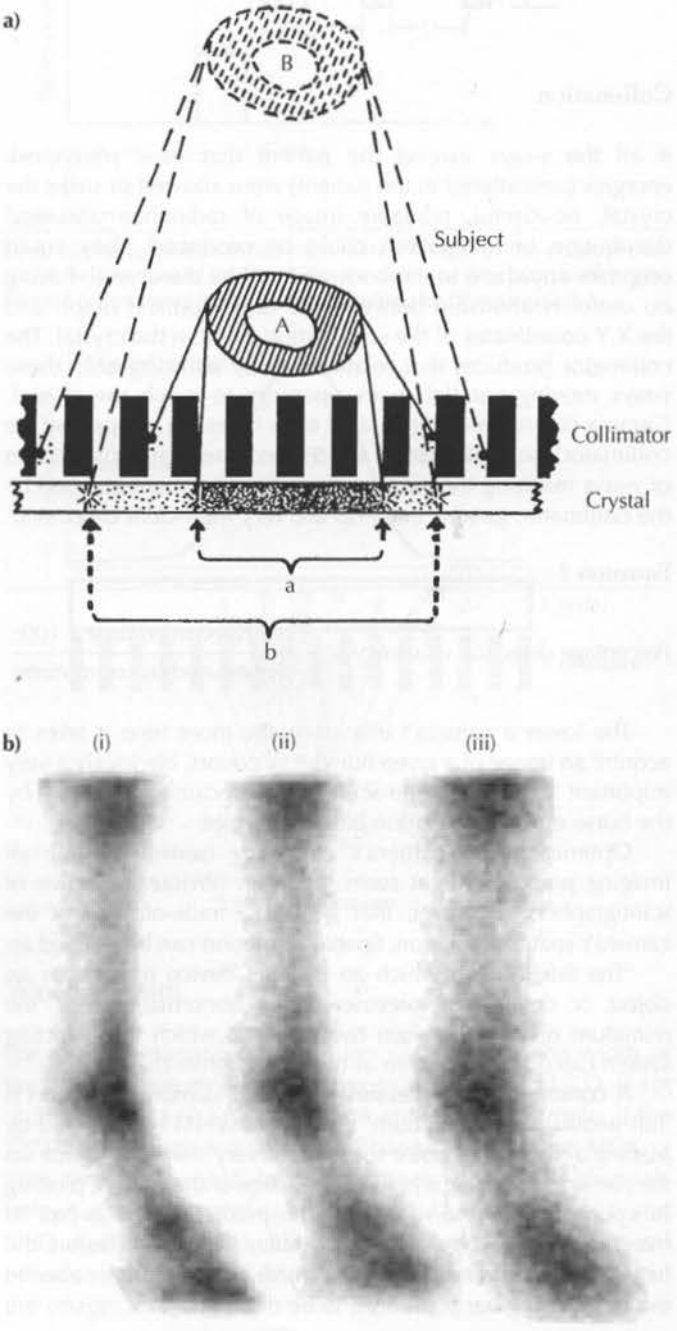

Figure 13

Intrinsic flood field of a 37-PMT gamma camera that is 'off-peak'. Note mottled pattern showing locations of individual PMTs. When properly tuned, the field uniformity of the same camera is excellent.

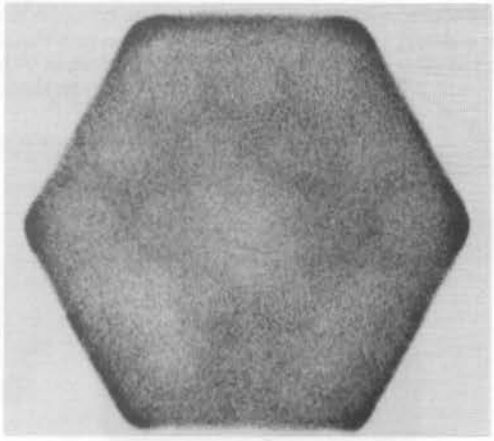

minute's acquisition and requires close, constant observation of the horse and the image as it forms on the computer monitor. Trade-offs are required between longer counting times to acquire higher count densities and the likelihood of motion degrading the image. Short of anaesthetising the patient, 300,000–400,000 total counts is a typical upper limit for a bone phase image of a large equine joint within an acquisition time of 1–2 mins.

Figure 12 illustrates the major impact of camera-to-subject distance on image resolution. Even a relatively small (5–6 cm) space between the collimator and horse's limb noticeably degrades the image. This distance is unavoidable, because when, for instance, the wall of the hoof is in contact with the collimator in a lateral view, the natural taper of the limb will move the fetlock itself more distally. The image degradation becomes worse with increasing distance (**Figure 12b**).

Note that the count-rate and total counts in the image do not decrease with distance, but the object being imaged is spread over a larger area of the crystal (from width 'a' to width 'b'; **Figure 12a**) decreasing resolution and image quality. Placing the horse as close as possible to the camera may involve extra work and time, but is critical to obtain the best possible scintigraphic images. The camera's suspension system and surrounding space, which affect the manoeuverability of both horse and camera, are very important considerations when designing a gamma camera facility. Ample room and an easily moved camera may cost more initially, but will pay off over time in reduced technician imaging hours, increased throughput, safety for horse and operator, and the greatest confidence in one's diagnostic interpretation (see *Part I, Chapter 4*).

GAMMA CAMERA QUALITY CONTROL (QC)

Peaking the Camera

To be performed daily: The photopeak window setting must be checked at the start of each day that imaging is performed, whether other QC tests are performed the same day or not. In the rush of a hectic work day, it is tempting to 'fire up' the

Figure 14

*Another less marked example of an 'off-peak' image, and the improvement in image quality obtained by setting the correct photopeak. In **a)**, the tubes are giving out different voltage signals from the same input signal, a flood source. This gives the field a patchy appearance, as the counts from adjacent tubes are either higher or lower than the theoretical predicted value. **b)** After tuning, the uniformity is improved considerably. Note the continued presence of some 'edge-packing', which causes the thin rim of apparent increased counts in the very periphery of the image.*

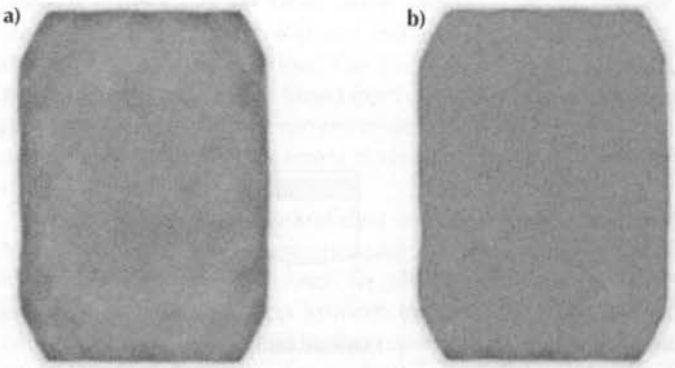

camera and go without any QC, but the old adage of 'haste makes waste' is especially applicable here. The stabilities of power line voltages, power supplies, amplifiers and pulse height analysers are not to be taken for granted, and much frustration and lost time can occur for lack of a simple check. Hopefully, a camera will remain stable during an entire day, but for some cameras and in some circumstances (such as significant room temperature changes), photopeak checks could be needed more frequently. Flood images from an off-peak camera (photopeak not centred in the 20% window) have a mottled pattern showing the locations of individual PMTs (**Figures 13 and 14**). The daily photopeak check can be done with the collimator in place, since removing the collimator is time-consuming and involves some risk to the crystal. When performed that way the peak represents the output of only those PMTs nearest the source, but all other components that might contribute to an off-peak camera are properly checked. 'Peaking' must utilise the pure isotope source, and should not be done using the patient as the source of activity.

Uniformity and Efficiency Tests

To be performed weekly: The performance of all the PMTs and the structural integrity of the collimator are tested by 'flooding' the camera both with (extrinsic flood) and without (intrinsic flood) the collimator in place (**Figure 15**), and evaluating the uniformity of count distribution throughout the image field. These tests should be carried out no less often than weekly, or more frequently depending on how well the camera holds its 'tune'. They must be redone any time the camera is turned off at the mains supply or there is a power failure that affects the camera.

PMTs are not absolutely identical in their pulse size outputs to a given amount of scintillation light input. If uncorrected, even relatively small PMT output differences result in significant nonuniformities in a flood image. An individual PMT can go out of tune due to ageing or changes to its electronic circuitry. To

Figure 15

Source-to-camera arrangements for uniformity and efficiency quality control tests. The point source for intrinsic testing must be located directly perpendicular to the centre of the crystal, at a distance 3–5 times the diameter or longest dimension of the camera. The distance must be exactly the same between tests for efficiency results to be comparable week-to-week.

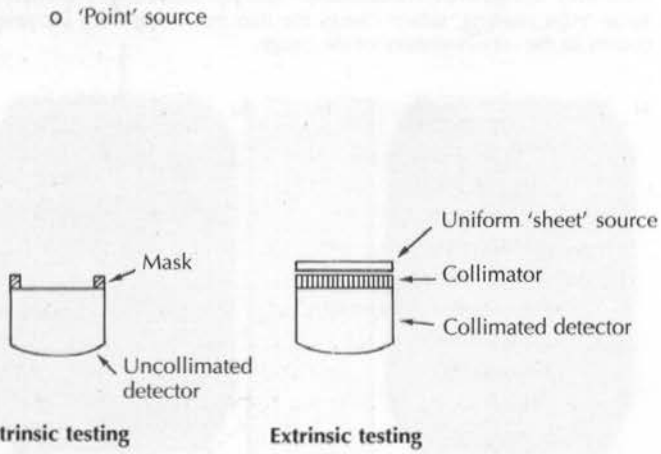

Figure 16

The result of an electrical pre-amplifier problem (A), on a Technicare Omega 500 camera, in conjunction with poor optical grease coupling of one tube (B). This degree of nonuniformity would overwhelm the ability of the UFCs to correct the flood field image, and should trigger a call to the engineer.

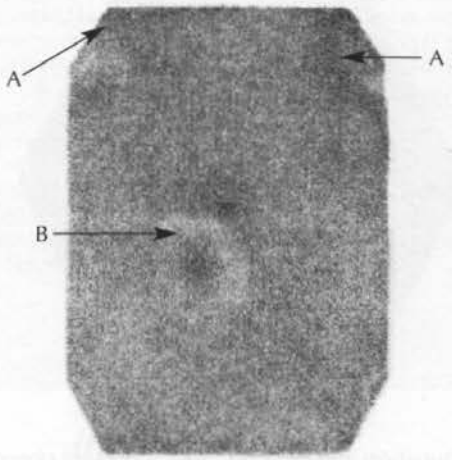

correct for such differences, gamma camera electronics include a package to create uniformity between individual PMTs. This has traditionally been known as the 'uniformity flood correction circuit' (UFC). The methods by which such electronics operate differ among cameras, depending on the manufacturer, model and age of technology employed. Older camera UFCs employ count 'skimming' or count addition, artificially subtracting or adding counts to pixels of flood images that are significantly hotter or colder than a reference pixel count in the centre of the field. Newer camera UFCs work by adjusting the Z pulse magnitude or the location of the photopeak window for each pixel of a flood field image matrix, thereby avoiding artificial loss or addition of counts in the image. In newer digital cameras, PMT output pulses are digitised at each tube, allowing individual tube tuning and uniformity correction electronics to be located in the camera head. Uniformity, the variation in counts between the highest and lowest counting pixels in a flood field image, in a modern, well tuned camera, should not exceed 5% and hopefully be less. Uniformities of less than 2% are claimed for digital cameras.

To perform an intrinsic flood (no collimator), a flood or tuning mask is attached to the camera. A ^{99m}Tc point source (approximately 8–16 mBq) is positioned over the centre of the camera at a distance of 3-5 times the diameter or longest dimension of the camera. The source must be located directly perpendicular to the centre of the camera (**Figure 15**). If it is positioned above the camera, be absolutely certain that it cannot fall and hit the camera, risking a cracked crystal and the major cost of replacing it. Also, cover the crystal with a thin sheet of foam rubber or polystyrene to protect from the shock of such an event. For efficiency calculations, the source-to-camera distance must be exactly the same from week to week, and the source size (megaBecquerels) must be measured accurately and recorded within 15–20 mins of the time of flooding, or source size must be decay corrected. With the source in place, 2–4 million count images are acquired, ideally as follows: 1) prior to deactivating the UFC, to evaluate field uniformity changes during the previous week; 2) with the UFC turned off, to accentuate effects of improperly tuned or malfunctioning PMTs and circuits (**Figure 16**); and 3) after flooding with the UFC operating, to store a newly corrected flood field for the next week's imaging. Computer software is available for calculating uniformity in flood field images; however, evaluation by visual inspection is quite adequate for most equine scintigraphic studies. Not all cameras allow the operator to deactivate the the UFC, in which case step 2 cannot be performed.

A camera's efficiency (or sensitivity) is calculated from the count-rate during the final intrinsic flooding, relative to the size of the point source. Efficiency should be the same from week to week; any significant change, usually a reduction, requires immediate diagnosis and correction of the cause. Reduced efficiency indicates malfunctioning components that may or may not be seen in flood images, and impacts the time required to acquire images and complete a study. One way to calculate a camera's relative efficiency is:

Equation 3

$$\text{Relative Efficiency} = \frac{\text{Total counts in image/mBq in source}}{\text{Acquisition time in secs}}$$

$$= \text{Counts/sec/mBq}$$

To repeat, source-to-camera distance must be the same and source activity (mBq) must be measured accurately within 15–20 mins of flooding in order to compare relative efficiency values over an extended period of time. Gradual loss of camera performance, such as that due to slow hydration and discolouration of the crystal, may not be apparent any other way.

Linearity and Intrinsic Resolution (Phantom) Tests

To be performed weekly: Bar phantoms are made of parallel lead bars thick enough to stop ^{99m}Tc γ-rays, of equal or varying widths, separated by spaces of the same width as the bars, and held in place in plastic sheets. Flood images are obtained as previously described (no collimator) with the bar phantom

Figure 17

Bone scans with a small photopenic area (arrows) that could be misinterpreted as a lesion, but is actually an artefact caused by a collimator dent denying γ-rays impinging on that site access to the crystal. This 'cold spot' is constant in position from image to image. If the collimator is removed and re-attached upside down, the position of the artefact should also move with it. If it does not, the problem must be in the crystal, or in the tube electronics. ***a)*** *Lateral right stifle.* ***b)*** *Lateral right stifle.* ***c)*** *Lateral right tarsus.* ***d)*** *Lateral right distal limb.*

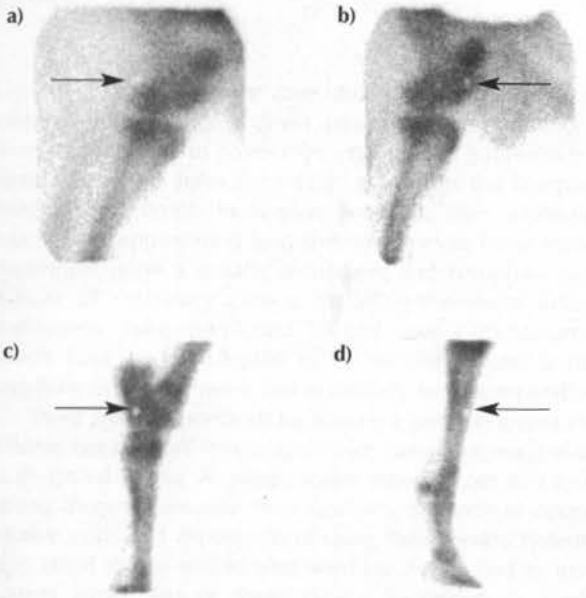

placed on the camera. Linearity of the camera is evaluated by observing that the images of bars and spaces are parallel and not wavy or distorted. Intrinsic resolution is evaluated by determining the narrowest widths of bars and spaces that can be seen in the image. These tests are convenient to do on a weekly basis by obtaining a bar phantom flood image following the last uniformity flood image acquisition.

Collimator (Extrinsic) Uniformity Test

Performed monthly or after physical impact to the collimator, this test is used to detect damage to or contamination of the collimator. This test requires that a 'sheet' source large enough to cover the entire detector be placed in contact with the collimator's face (**Figure 15**). A sheet source can be prepared by uniformly mixing 40–100 mBq of ^{99m}Tc in a flat, water-filled plastic container. Sheet sources of ^{57}Co embedded in a plastic sheet are available commercially, but are quite expensive and decay fairly rapidly (^{57}Co half-life = 270 days). ^{57}Co's γ-ray energies of 122–136 KeV are close enough to ^{99m}Tc 140 Kev for flooding purposes. Although using a ^{57}Co source avoids the time and effort of mixing a ^{99m}Tc source and doesn't risk contaminating the camera, its cost is difficult to justify for a veterinary practice. This test is recommended as a monthly routine, but it is well worth doing after any incident that could dent or loosen the septa of the collimator (such as dropping it). Collimator artefacts are not uncommon[2], and are not detected by the weekly intrinsic floods, for which the collimator is removed. Artefacts produced by dented or folded septa appear as 'cold' areas in a flood image (**Figures 17a–d**), and those produced by separated septa as 'hot spots'.

Gamma Camera Care and Maintenance

Gamma cameras, especially their crystals, must be carefully protected from both physical and thermal shocks. Considering the essential need to position horses' feet and limbs in contact with the collimator, crystals are surprisingly tolerant of the equine scintigraphy environment - but they do occasionally get broken (see **Figure 2**). A 6 mm thick 'lucite' or 'perspex' sheet can be applied to the collimator face, to help absorb glancing impacts. These can be fitted using industrial grade 'Velcro' stuck to the edge of the collimator and the back of the protector, outside the imaging window. The thick shielding surrounding the detector protects from blows from other directions. Even so, the handlers of horse and camera must take every precaution to avoid sharp blows to the camera occurring. This is also for their own and the horse's safety.

Temperature, humidity and dust control are also important to the welfare of the camera, meaning that it should be located in a dedicated room - not in the usual equine stable environment. A rapid drop in room temperature, such as that caused by leaving an outside door open on a wintry day, can cause the crystal to crack. Excess heat and humidity may affect the camera's electronics, so an air conditioned room is required in most circumstances. These matters are dealt with in more detail in *Part I, Chapter 4*. When the camera is not in use, the head should be positioned facing down, which helps to maintain the optical grease seal and contact between the PMTs and the crystal.

Power Cuts and Failures

If an unavoidable power failure is anticipated, the camera should be turned off at the mains. When power is reconnected, the camera should be 'warmed up' for 10 mins before turning up the voltage (gain) to the PMTs. If the power failure is for more than a few hours, the batteries which maintain the information in the UFC will often be drained, and the stored flood lost. A new flood should then be stored once the camera is ready for use. When unexpected power cuts occur, again the camera should be turned off and the same protocol followed on resumption of supply. Following any interruption of power supply, for whatever reason, uniformity and efficiency tests should be repeated (see earlier this chapter).

ACKNOWLEDGEMENTS

With kind permission from Elvesier Science, Figures 3, 6, 9, 11 and 13 are reprinted from: Sorenson, J.A. and Phelps, M.E. (1987) *Physics in Nuclear Medicine*, pp 74, 98, 332, 341 and 386. Also, Figures 5, 10, and 12a are reprinted with permission from W.B. Saunders Co. from: O'Callaghan, M.W. (1991) Nuclear medicine equipment. *Semin. Vet. Med. Surg.: Small Anim.* **6**, 113.

REFERENCES

1. Rollo, F.D. and C.C. Harris (1977) Factors affecting image formation. In: *Nuclear Medicine, Physics, Instrumentation, and Agents*, Ed: F.D. Rollo, C.V. Mosby. pp 387-435.
2. Daniel, G.B. (1991) Nuclear medicine artifacts and image quality. *Semin. Vet. Med. Surg.: Small Anim.* **6**, 119-130.

Chapter 4

GAMMA CAMERA INSTALLATIONS

ROB C. PILSWORTH and MIKE C. SHEPHERD
Rossdale & Partners, Beaufort Cottage Stables, High Street, Newmarket, Suffolk CB8 8JS, UK.

Gamma cameras are, by their nature, extremely heavy and cumbersome. This is a direct result of the amount of lead shielding required to protect the crystal from γ-rays other than those which will form the image, as well as the complicated internal electronics. In human hospitals, very sophisticated mechanical apparatus is available to carry out bone scanning, dependent upon a usually recumbent and compliant patient. Almost all veterinary clinics, including the major academic institutions, have purchased second user gamma cameras, which have to be adapted to be moved around a patient weighing 500 kg or more that is unlikely to be cooperative.

There are many methods for moving a gamma camera around a horse, but they fall into several major categories, each of which is illustrated below. A questionnaire was sent out to 15 clinics asking them to describe their facilities, methods of operation, relative costs and experience of using their chosen system. We also asked if they would alter anything if they had to install a system again. Ten of these clinics responded, 5 academic institutions and 5 private practices. The results of the questionnaire are summarised below. The authors would sincerely like to thank those who responded for their time and help.

GAMMA CAMERA SUPPORT AND OPERATION

There are 3 primary ways of moving a gamma camera around a horse. The advantages and disadvantages of each are considered in turn.

1. Forklift Truck

The unit illustrated in **Figure 1** was used by Donald Attenburrow in Exeter, who pioneered the use of the gamma camera in equine practice in the UK. This particular unit is mounted on compressed air driven casters, which make it manually moveable. The compressor is situated outside the gamma camera room. The horse stands in stocks with a raised platform so that the legs of the forklift truck can access immediately underneath the horse. Commercial battery-operated forklift trucks can also be used. The main disadvantage with this system is the inappropriate placement of the legs of the forklift truck. These tend to touch the horse's feet as the truck is moved backwards and forwards. This can be mitigated by the use of raised stocks as shown in this example. Other disadvantages are the danger associated with lack of ability to move the gamma camera quickly away from the horse in case of emergency and the noise associated with moving the truck backwards and forwards. The compressed air system shown in the figure would help in this respect. Other disadvantages include the room size required to manoeuvre a forklift truck and the excessive time it takes to orient the camera head perpendicular to the site to be imaged. Only one user out of ten in our gamma camera user survey still used a forklift truck.

Figure 1

A forklift truck being used in Don Attenburrow's clinic in Exeter, UK. The floor casters are operated by compressed air, which gives so little friction contact that the entire apparatus is moveable by hand by one person. The raised stocks allow access by the forklift truck legs beneath the horse. (Courtesy of D. Attenburrow, Exeter, UK.)

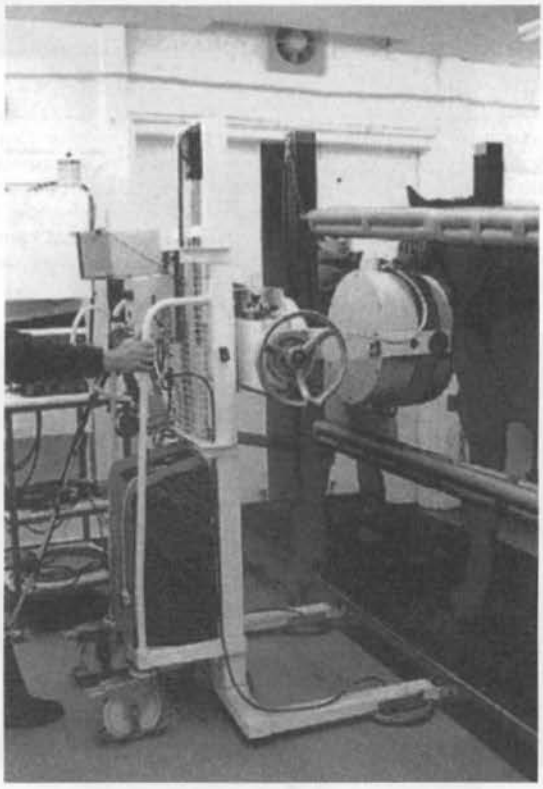

2. Overhead Gantry plus Winch using Chain or Wire

This was a popular system in the survey (5/10; see **Figure 2**). Its main advantages are that it is extremely cheap to install and can be moved all around the horse without the animal having to be moved. Once the horse is stable under sedation, this is a great advantage, as turning and moving horses tends to wake them up.

Most users listed as a disadvantage the noise levels produced by the winch directly over the horse, and the relative instability of the camera, which tends to swing gently like a pendulum. One modification which may be of interest is shown in **Figure 3**. Here, a cable suspension system has had a telescopic box

Figure 2

The most simple kind of overhead gantry suspension, involving an electric winch with a wire or chain hoist. (Courtesy of Paul Proctor, Proctor and Wainwright, Northumberland, UK.)

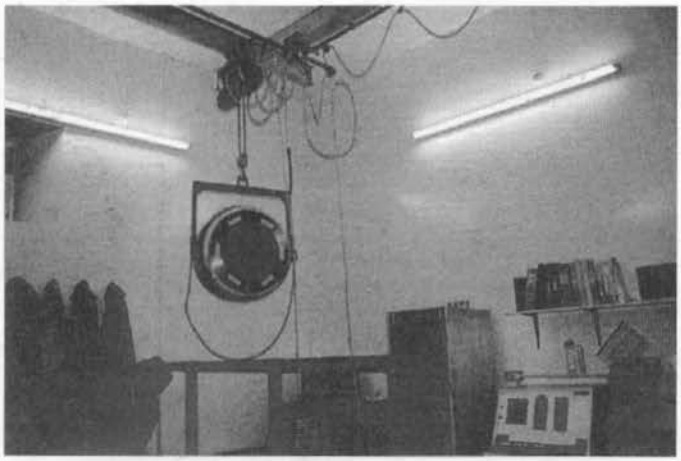

Figure 3

In this overhead suspension system at the New Bolton Centre in Pennsylvania, USA, extra stability has been imparted to the camera head by the use of a telescopic box section fitted around the suspension wire. The camera is dropped part-way into the pit for weightbearing lateral images of the distal limb. A second small field of view camera is permanently positioned in a pit for solar views of the feet (arrow). (Courtesy M. W. Ross, New Bolton Centre, USA.)

section added around the outside of it. This box section is fixed to the camera yoke at the bottom and the winch at the top and introduces some extra stability to stop the camera swinging on the end of the chain. The box section itself bears no weight.

One advantage of the chain- or cable-hoisted camera is that it can be held on to the surface of the horse for imaging of the spine, pelvis and neck so that the minor oscillations in skeletal movement produced by respiration can be eliminated, by gently moving with the horse.

3. Hydraulic Cargo Crane (*Figures 4a and b*), Overhead Chain-Driven Gantry (*Figure 5*) or Custom-Designed Hydraulic or Screw-Operated Stand (*Figures 6 a–d*)

In the gamma camera user survey, 4 of the current users expressed a view that, although they were relatively happy

Figure 4

A commercially available hydraulic cargo crane, seen here in the Dolly Green Scintigraphy Suite, Santa Anita Race Track, California, USA. ***a)*** *This type of crane can now be purchased with a wireless remote control, which adds even further to its flexibility in use. The pit pictured* ***b)*** *is used for solar views, and weightbearing lateral images.* (Courtesy of R. M. Arthur, Santa Anita, USA.)

a)

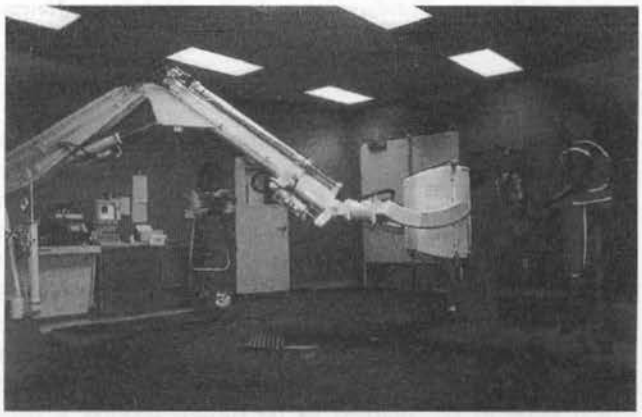

b)

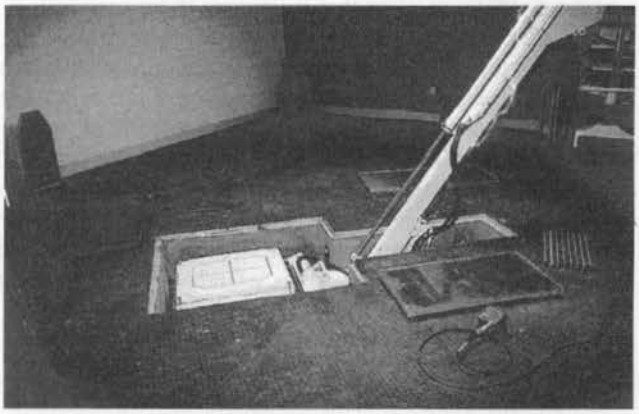

Figure 5

An overhead chain-driven mechanical gantry system. This again gives great flexibility for movement all around the horse and is operated from a hand control. The facility illustrated is at the Rood and Riddle Equine Hospital, Kentucky. (Courtesy of Rood and Riddle, Lexington, USA.)

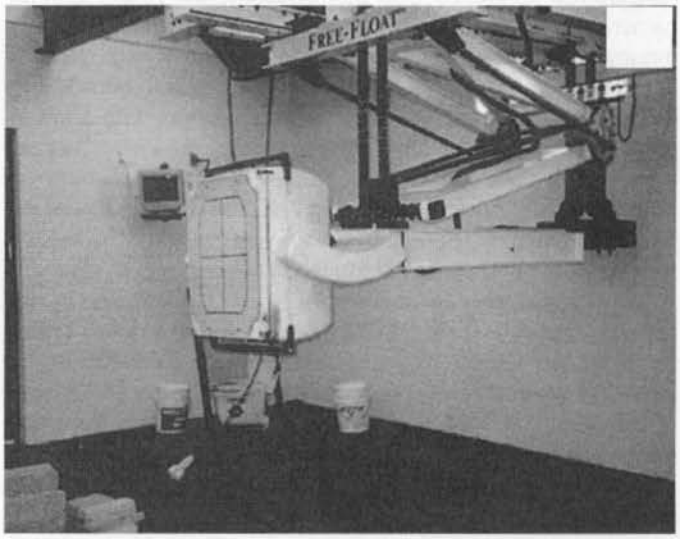

Figure 6

a) *and* ***b)*** *show the custom-made hydraulic stand at the Donnington Grove Equine Hospital, Newbury, UK. The stand rolls backwards and forwards on rails beside the horse and the camera head can move in every direction and rotate. The horse stands on a hydraulic platform which can be raised to acquire weightbearing images of the distal limb.* (Courtesy of B. Bladon, Newbury, UK.) ***c), d)*** *and* ***e)*** *show the 'Ultra Scan' lift system offered by Advanced Technologies as a commercially available package in the USA. Here, the head is moved manually in the horizontal plane on a Gorbel overhead crane system. The vertical movement is by a motor-driven screw drive. The head can be rotated at the end of the arm in both planes, giving complete flexibility. This unit is seen in the Alamo Pintado Equine Clinic in California, USA.* (Courtesy of Deryl Markgraf, Enhanced Technologies, USA.)

a)

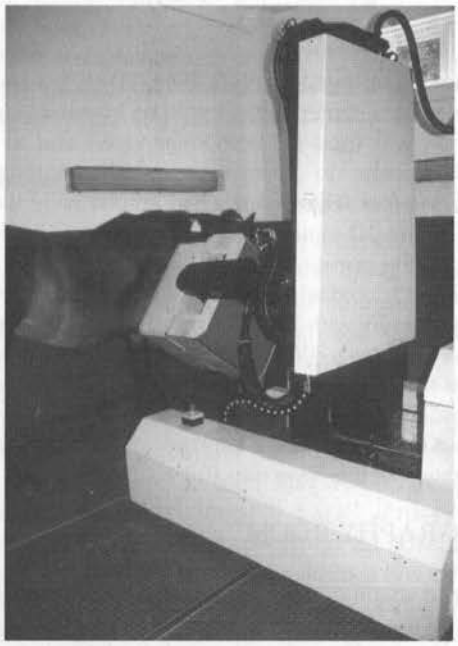

b)

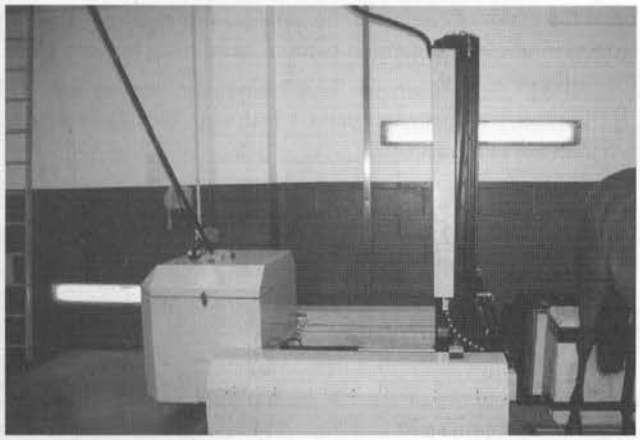

c)

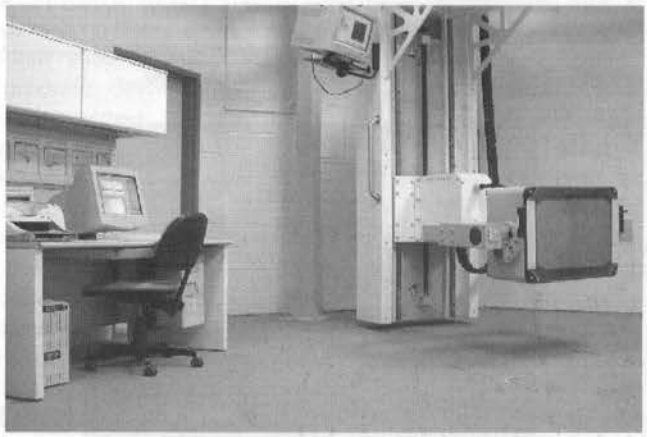

d)

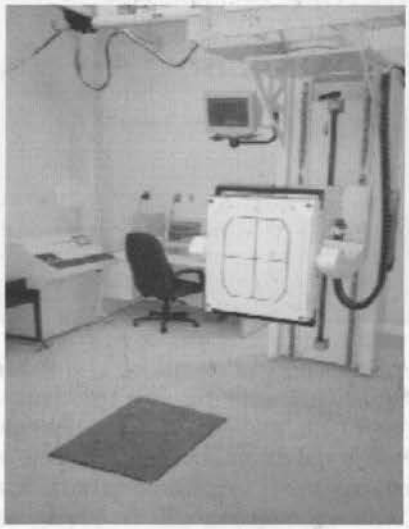

e)

with this system, were they to re-install they would use a hydraulic cargo crane, having seen these cranes in operation in other clinics.

The hydraulic cargo crane probably presents the optimal system for moving the gamma camera. It can access all parts of the horse and the hydraulic motors are kept outside the camera room so that the crane is virtually silent in operation. Wireless remote controls, which are hand-held, are now available. This allows the crane operator to stand immediately adjacent to the horse. The camera is completely moveable in all directions. One disadvantage is that the horse has to be turned around to image the contralateral side. Secondly, as with all fixed systems, it is not possible to hold the camera head onto the horse during

Figure 7

A 'high-lift' winch in operation at Beaufort Cottage Equine Hospital, Newmarket, UK. The design of the winch allows almost no dead space between the yoke of the gamma camera and the overhead beam, which is particularly useful if ceiling height is at a premium.

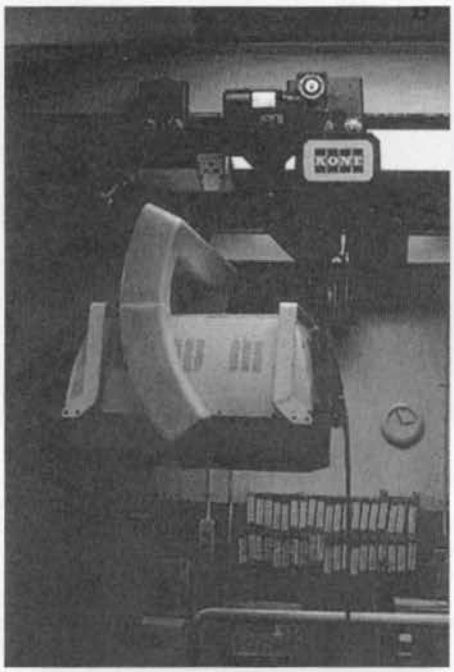

imaging of the spine and pelvis. This introduces some extra respiratory movement. Motion correction programmes can eliminate this to some extent, but most of these would use a count window of 2–3 secs to gain sufficient counts for a frame of data. This will often involve part or all of one respiratory movement, and so does not eliminate all 'blurring'. Unless the camera can pivot independently at the end of the crane arm, the horse has to be moved repeatedly in order to keep the camera head perpendicular to it.

Some clinics have designed purpose-built one-off hydraulic stands (**Figures 6a and b**). One example, at the Donnington Grove Equine Hospital, Newbury, UK, offers complete flexibility of head position, with very economical use of space. This facility also has a rising platform under the horse, so that weightbearing lateral views can be obtained easily. This ingenious set-up appears to offer an ideal solution to the problems faced by use of the gamma camera around a horse. A similar system, which shares many of these design features, the Ultra-scan Lift System[a] is available 'off the peg' in North America (**Figures 6c, d and e**). Here, the head is moved around the room by means of a Gorbel industrial overhead crane. The vertical motion is achieved by means of a motor-driven screw drive. All of these movements are extremely smooth and quiet, and the system provides an ideal answer to the problem of moving the camera around a horse.

In the gamma camera survey, all of the users of fixed systems (4/10) were completely satisfied with their systems and would employ the identical system again were they to re-install.

Table 1 shows the remaining survey results. Methods of suspension used in the 10 clinics were as follows:

Overhead gantry plus crane (chain or wire cable)	4
Hydraulic cargo crane or mechanical stand	5
Mobile forklift truck	1

Stocks were utilised by only 3 of the 10 clinics and a pit into which the gamma camera head could be lowered was available in 7. The pit was used for both solar views and to lower the head sufficiently to allowed lateral imaging of the weightbearing foot (**Figure 4b**). Lead aprons were worn by the staff in 3 of the 10 clinics. Two of the clinics employed lead screening on the horse.

Significant overdosing of horses with technetium was relatively common, with a third of the clinics administering more than 10 MBq/kg bwt. Four of the 10 clinics were administering 50% more than this dose. This has important repercussions on radiation safety (see *Part I, Chapter 12*) and dose rates received by staff, but may not actually improve image quality because of dose saturation of the bone (see *Part I, Chapter 2*).

SCINTIGRAPHY ROOM

The size and shape of the room is often determined by what is available. In the survey, the minimum room size was 4 x 4 m. If a pit is to be used for solar views, its depth has to be estimated once the make of camera to be used is known, as the false floor slotted in above the gamma camera head must be very close to the collimator face.

Floor

One problem which has to be addressed by every gamma camera user is the fact that there is a certain amount of 'dead space' from the bottom of the edge of the imaging window of the collimator to the floor. In order to obtain lateral weightbearing images of the foot and fetlock, some method has to be found to lower the camera so that the bottom of the collimator window edge coincides with the sole of the foot.

Table 1: Remaining survey results

	Minimum	Maximum	Mean
Cost of camera and support mechanism	£2,000	£120,000	£36,000
Size of room	4 x 4 m	10 x 12 m	6.4 x 5.4 m
Personnel requirement	2	4	3
Cost of isotope (5 GBq)	£32	£205	£84
Dose (MBq/kg bwt)	10	16	12
Discharge time for horse (from injection)	24 (USA only x 2)	72	48
Time elapsed for muck and urine disposal	48 h	72 h	60 h
Scans performed annually	60	530	240

This can be addressed either by use of the camera in a pit, with the horse standing on the floor, or a raised platform to align the sole of the foot with the bottom of the collimator. When constructing a scintigraphy unit, if a platform is to be used, then prior measurement of the distance from the floor to the bottom of the collimator window, when the camera is in the vertical position, is essential. A hydraulic platform (**Figure 6b**) offers a very flexible solution to this problem. Clinicians appear to be divided over the relative advantages of pit vs. platform, and the reader is advised to see both in action before making a choice.

Drainage

In the UK at least, it is probably preferable that the scintigraphy room has no floor drains, so that urine spills can be cleared up via absorption and storage to eventual decay. The possibility of radioactive discharges into sewers opens up an extra set of rules and regulations which are best avoided.

Ceiling Height

In order to scan above the horse's spine and pelvis, at least 2 m should be allowed from the floor to the lower surface of the collimator of the gamma camera. The gamma camera itself will often occupy half a metre, and the winch and supporting chain, if this method of suspension is used, will introduce a further 'dead space' until the ceiling is reached.

If ceiling height is no problem, then the supporting girders can be arranged to compensate for this. However, if ceiling height is at a premium, a 'high lift' winch, in which the weightbearing chain is looped back across an axle immediately under the ceiling, might be an advantage. This means that the winch is able to lift within a few centimetres of the ceiling rather than to the underside of the winch unit itself (**Figure 7**).

TEMPERATURE CONTROL

All of the clinics concerned had thermostatically controlled heating systems but only 3 of 10 had installed air conditioning, 2 in the USA and 1 in Australia, presumably a direct result of the climatic need to control both ends of the temperature spectrum.

Gamma cameras have a reputation for being extremely sensitive in relation to temperature change. While care in this respect is justified, the situation is probably somewhat overstated, and the gamma camera is a lot less temperature-sensitive than its reputation suggests. The sensitive item in the gamma camera is the sodium iodide crystal, which is a large crystal only a few millimetres thick, sandwiched between sheets of perspex. It is certainly true that this cannot stand rapid fluctuations in temperature. However, the crystal itself is sandwiched in the middle of the gamma camera head, often covered with a large lead collimator which gives the whole unit a significant amount of thermal inertia.

It is not really critical that gamma cameras are used in a warm or cold environment, as long as rapid changes in temperature are avoided. For this reason, the most pragmatic approach to temperature control is often thorough insulation of the room concerned. Application of 10 cm polystyrene insulation to the inside of the walls covered with a composite board nailed to battens has been an effective solution.

Similarly, one can fit a false ceiling such as those used in modern shop fittings. These are relatively inexpensive, can incorporate down-lighter units, which avoid glare on the computer screen, and give one the facility to insulate above the false ceiling with fibreglass loft insulation. The combined effect of this insulation is that the gamma camera room is like a cave, in that the temperature inside it fluctuates very little between summer and winter. Combined with a simple night storage heater for use during the winter and a ventilation fan to bring fresh air into the room, the temperature is always ±5°C. Air conditioning certainly makes for a more pleasant working environment, and the electronics in the console and camera head are temperature- and humidity-sensitive. In the summer, horses injected with sedatives often sweat profusely, creating a saturated atmosphere within the scintigraphy room. Air conditioning avoids this problem to some extent. There are, therefore, sound quality control factors to encourage the fitting of air conditioning. An air conditioning unit costs no more than £3000 ($4500) and is a 'one-off' investment which will certainly be of benefit.

Radiopharmacy Preparation Area

Local regulatory requirements in each country will differ and should be explored well in advance of drawing up plans. Almost all regulatory authorities will insist that isotope handling is performed in a defined site, which can be clearly marked at its entrance point, and to which it is physically possible to restrict access. If isotopes are to be obtained from a hospital radiopharmacy already labelled, then the facility can be quite simple, but should include:

1. A means of securing the delivered transit container from the time of delivery to the time of use.
2. A bench area, covered with an absorbent, disposable paper or card coating.
3. A record-keeping book, in which to log all delivered isotope and account for its eventual fate.
4. Lead storage vessels, for storage of contaminated needles, syringes and other 'disposables' until decay allows safe disposal in normal waste (60 h).
5. A supply of disposable protective gloves, face shields or goggles, to use during isotope handling.
6. A suitably calibrated contamination monitor, to survey the work area after each use (see *Part I, Chapter 12*).

If a generator is to be used, to generate isotope for labelling 'in house', a much more extensive radiopharmacy is required, as outlined in *Part I, Chapters 2 and 12*.

The authors realise that many clinics which have already installed scintigraphy equipment will have to tolerate the inadequacies of their system. It is hoped that the review carried out in this chapter, and the examples illustrated, will allow clinics considering installation to assess the pros and cons of each type of camera support system.

MANUFACTURER'S ADDRESS

[a]Ultra-Scan Lift System, Enhanced Technologies, Bedford, Texas, USA.

Chapter 5

IMAGE ACQUISITION, POST PROCESSING, DISPLAY AND STORAGE

JO WEEKES and SUE J. DYSON
Centre for Equine Studies, Animal Health Trust, Lanwades Park, Kentford, Newmarket, Suffolk CB8 7UU, UK.

Nuclear medicine is potentially more quantitative and less subjective than other methods of diagnostic imaging. It is therefore important to understand the quantitative features, in order to achieve the best possible diagnostic accuracy. Computer processing of the images generated in nuclear medicine is now an accepted part of daily practice, but for accurate interpretation it is necessary to appreciate how both images can be enhanced and artefacts created. In this chapter, we examine the principles of image acquisition and the processing techniques which are most commonly used in equine scintigraphy.

THE DIGITAL IMAGE

A signal may be defined as a function that carries information. For most nuclear medicine applications, the signal originates from the output of a gamma camera, and is usually viewed in the form of a digital image. The information the signal carries concerns the distribution of the radionuclide and, after its interpretation, provides clinical information.

For a conventional gamma camera, both the X and Y analogue signals are converted to digital signals using analogue to digital converters (ADCs), and the Z signal is used to control the transmission of these digital signals into the computer and gives information about the energy range of the original γ-ray event. The digital X and Y signals and the Z signal for each event detected by the camera crystal are used by the computer to generate a digital image.

TYPES OF COMPUTER

In its simplest form, the system consists of a computer with ancillary electronics to digitise the gamma camera signals. While computer manufacturers initially produced these systems, gamma camera manufacturers and suppliers now supply them as part of an integrated digital camera system. With one or two exceptions, most hardware is not specific to nuclear medicine, while almost all software is specific to nuclear medicine image handling and processing.

All gamma camera vendors now offer the computer as an integral and inseparable part of the total gamma camera system. It is commonplace to purchase a secondhand refurbished gamma camera and new PC-based computer software. Manufacturers offer processing packages with considerable flexibility and programming capability. Human programmes used in animal studies must be tested for applicability and accuracy. Typically, some programmes are useful and some are not, and this should be taken into account as you may be paying for a lot of software you will not be able to use. Fortunately, most vendors are willing to customise processing packages for equine use.

Before choosing a computer system, it is important to produce a comprehensive specification of intended use and requirements for the system. These considerations include:

1. What type of studies are to be performed?
2. How much data will need to be stored?
3. Is long-term archiving important?
4. Is the system intended for routine clinical use?
5. Is it to be used in a research environment with several users?
6. How many gamma cameras can the computer support?
7. Can the system be interfaced to other computers and image processing systems?
8. Does the clinic have other digital imaging systems for which the computer might be used?

The final choice will be limited by the available products and, probably most importantly, cost.

IMAGE ACQUISITION TECHNIQUE

Matrix Mode

The most common form of image acquisition is called matrix or frame mode. This is achieved by dividing the camera field of view into a regular matrix of pixels. Each pixel is assigned a unique memory location in the computer. The value stored in this location is the number of γ-ray events which have been detected in the corresponding location on the camera face. The number, and hence the size, of the pixels used is of practical importance and depends on:

1. The available computer memory.
2. The total number of images to be acquired.
3. The number of counts contained in each image.
4. The required temporal[a] and spatial resolution.

Matrix Size and Reason for Selection

Matrices used in nuclear medicine range from 64 x 64–1024 x 1024

[a]Temporal resolution: the speed at which successive images (frames) are acquired in dynamic studies.

and the choice of a suitable matrix size depends upon a number of factors:

1. Resolution cannot be better than the size of an individual matrix element or pixel. For a 128 x 128 matrix and a 40 x 40 cm field of view (FOV) gamma camera, the pixel size is about 3 mm^2. Note that the pixel size is governed by the FOV, e.g. with a FOV of 20 x 30 cm, a 128 x 128 matrix would give a pixel size of 1.5 mm^2.
2. If pixellation ($pixels/mm^2$) is very course, a finer pixellation will improve resolution.
3. There is nothing to be gained by decreasing the pixel size below the resolving capability of the imaging equipment. For example, the system spatial resolution of a gamma camera at 10 cm distance from the patient using a low energy general purpose collimator is 9–10 mm and when using a low energy high resolution collimator it is 6–7 mm.
4. As the pixel size becomes smaller, the size of its signal gets smaller and the ratio of its signal to noise gets smaller. Therefore, the size of the signal (number of γ-rays) is a limiting factor in determining the smallest useful pixel size. Noise becomes a greater problem as signal size is decreased.
5. Finer pixellation places a greater burden on the computer in terms of data storage and manipulation. A 256 x 256 matrix contains over 65,000 pixels and each one must be stored and examined individually. A factor of 2 change of matrix size brings about a factor of 4 change in the storage space required.

In clinical practice, dynamic acquisitions (where you are looking for higher temporal resolution than spatial resolution) are much more subject to low count statistics than static acquisitions (where you are looking for lower temporal resolution than spatial resolution) because of the smaller time unit during which the acquisition matrix actually acquires signal data from the gamma camera. In general, if the photon flux is low and frame rate high, then a smaller matrix (64 x 64 or 128 x 128) should be used in order to obtain adequate statistics per pixel. However, this is not the case if you are going to motion correct the dynamically acquired images because the statistics of the summed image are important. If the count rate is high enough to provide adequate statistics then a larger matrix can be used (256 x 256 matrix) to improve the spatial resolution of the image, but this requires more disk space (HERMES standard storage capacity 280 Gb).

CONTROL OF ACQUISITION

Static Acquisition

The concept of 'static acquisition' refers to the acquisition of a single image of a particular anatomical region of the patient. In the static mode, a preset time or number of counts determines the length of time for the study. Statistics determine the number of counts or the time of acquisition necessary to achieve the resolution, contrast and image density required for the image. However, when comparing symmetrical structures (e.g. lateral views of fetlocks) we prefer a preset time (e.g. 2 mins), as this allows quantitative and qualitative interpretation of the relative radiopharmaceutical uptake (RU) by the two structures. The term 'preset time' refers to an image acquisition technique that is terminated after a fixed period and is not related to count rate. Preset time acquisitions can be risky because the photon flux from the horse is unknown. One might not acquire enough counts to obtain a statistically adequate image for interpretation. This is particularly the case in old horses, or in horses with cold limbs (see *Part I, Chapter 6*). However, in our experience, a preset time of 2 mins in the majority of horses provides sufficient count density (200,000 counts) to produce a high quality image. The proximal parts of a limb are relatively count rich and at least 200,000–300,000 counts are easily achievable. In young, immature horses with higher bone turnover, shorter acquisition times may provide sufficient data. If the total counts acquired in 2 mins is not sufficient, the view must be repeated for a longer acquisition time (3–4 mins), and the same acquisition time should then be used on the opposite joint to ensure a direct comparison of RU.

Alternatively, images can be obtained until a preset number of counts is achieved. The duration of acquisition may vary between 2 limbs because of differences in distal limb perfusion (see *Part I, Chapter 6*), the presence of a lesion with high RU in the field of view, or the tendency of the entire lame limb to have generalised increased RU compared to the nonlame limb.

Static images are obtained using a 128 x 128 matrix size for blood pool images and a 256 x 256 matrix size for osseous phase images when higher spatial resolution is required. Any number of static acquisitions can be acquired, each view being uniquely labelled; e.g. Dorsal Front Fetlocks. Image description is discussed in *Part I, Chapter 9*. Routinely, we acquire static images only of regions distal to the carpi and hocks, because the risk of slight movement is relatively low. Motion correction cannot be applied to static images.

Dynamic Studies

Dynamic acquisitions in nuclear medicine are used for studies in which there is a time-varying distribution of the radiopharmaceutical activity, or when motion needs to be corrected prior to forming a static image. Most computers in nuclear medicine allow for two different types of dynamic acquisition, frame mode and list mode.

Frame mode dynamic acquisition is used mostly in equine scintigraphy and is conceptually similar to static acquisition. A rapid series of sequential images is acquired, each for a preset time. Data for the first image is stored in a section of memory called a buffer for the preset time. Storage of the next image is immediately commenced in another buffer, while the first image data is simultaneously transferred to disk for storage. This process is repeated until the required number of frames is acquired. This process is known as 'double buffering'. Several segments of different frame times and number of frames can be specified by the operator, but the maximum number of frames and minimum frame time is dependent on the available memory and disk transfer rate.

In order to record a rapidly changing distribution of radiopharmaceutical within the horse (for example, in blood flow studies), a series of sequential images per frame are acquired, each for a preset time. In our experience, a series of 80 x 1 sec frames is sufficient to demonstrate blood flow to the area of interest, but the acquisition is initiated only when the activity starts to appear on the p-scope; otherwise frames, time

Figure 1

a) *Left lateral bone phase image of the caudal thoracic region of a Warmblood gelding obtained with a general purpose collimator. The image was acquired dynamically and then motion corrected. Image definition is rather poor because of scattered radiation.* ***b)*** *Left lateral bone phase of the caudal thoracic region of the same horse as (a). This image was acquired using a high resolution collimator. Image acquisition time was increased compared with (a), to ensure a high enough total count was acquired. Despite the longer acquisition time, image quality is much better.*

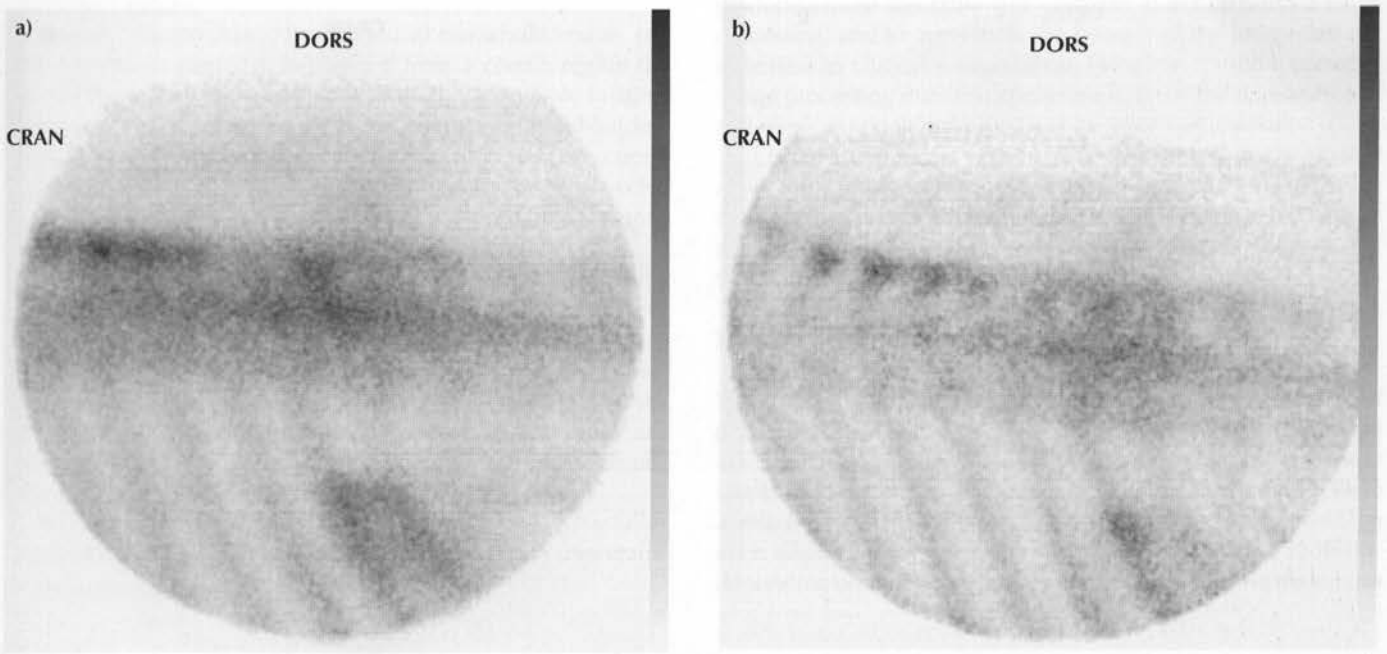

and computer space are wasted. The time between injection and the start of the acquisition is variable; in a study of the distal forelimbs of 270 horses, it ranged between 19 and 123 secs, with a mean of 47 secs after injection[1].

Evaluation of blood flow to the distal limbs can be helpful in interpreting subsequent pool and bone phase images[2]. Blood flow or first pass angiography studies are also potentially valuable in the assessment of a horse with suspected aortoiliac thrombosis[3,4] and femoral artery thrombosis[5].

In equine scintigraphy, motion is often a problem during image acquisition, especially proximal to the fetlocks. Although horses are sedated to try to minimise gross movements, inevitably there is a variable degree of swaying movement. This becomes a greater problem in the more proximal parts of the limbs and the thoracolumbar and pelvic regions. The degree of motion can result in images with excessive movement blur, prohibiting accurate interpretation and, in some instances, creating artefactual lesions[6]. Acquisition of a dynamic sequence of 35 x 2-sec frames usually provides a sufficient count density to produce a high quality static image once motion correction has been performed. If the total counts acquired is not sufficient (e.g. cold limb), the view must be repeated for a longer acquisition time (60 x 2-sec frames) and the same acquisition parameters should then be used on the opposite joint to ensure a direct comparison of RU. For certain areas, for example the thoracic and lumbar spine where there is large overlying muscle mass, we have found that it is essential to use a low energy high resolution collimator in order to reduce the amount of scattered gamma photons being detected. These degrade the final image, thereby reducing resolution (**Figure 1**). In order to compensate for the reduced number of gamma photons being detected by the gamma camera, the acquisition time must be increased routinely to 60 x 2-sec frames. Prior to movement correction, high resolution collimators prolonged acquisition time to such an extent that the improvement in resolution was negated by movement blur. With modern motion correction programmes this no longer applies.

As far as we are aware, the list mode dynamic acquisition is not used in equine scintigraphy, but is available in most nuclear medicine computer software packages. During a list mode acquisition the individual signals (X, Y and Z) of every detected event are stored as a function of time in a list. List mode data may be processed directly and a series of frames of varying matrix sizes and acquisition times may be formed from the list at the operator's choice. List mode data collection is more supple, but it is limited both in terms of storage capacity and in data capture rate.

Dual Isotope Studies

Most gamma cameras have the facility to record events from more than one energy signal, either from a multiple gamma emitter or from 2 different gamma emitters (e.g. ^{99m}Tc and ^{81m}Kr used in pulmonary scintigraphy). Static or dynamic images of each set of X and Y signals corresponding to the 2 energy (Z) signals can be obtained simultaneously using the computer, provided enough memory buffers are available.

PRINCIPLES AND PRACTICE OF MOVEMENT CORRECTION

Movement of the limb or region being imaged causes a displacement of the image as a function of time and can considerably degrade the image resolution. To overcome image blurring, it is preferable that images proximal to the fetlocks are

Figure 2

Dorsal image of the sacroiliac joints without motion correction. The lumbar and sacral spines have been masked out by computer processing after acquisition. Note the blurred image of the tubera sacrale (A) and the right tuber coxae (B). Compare with Figure 3.

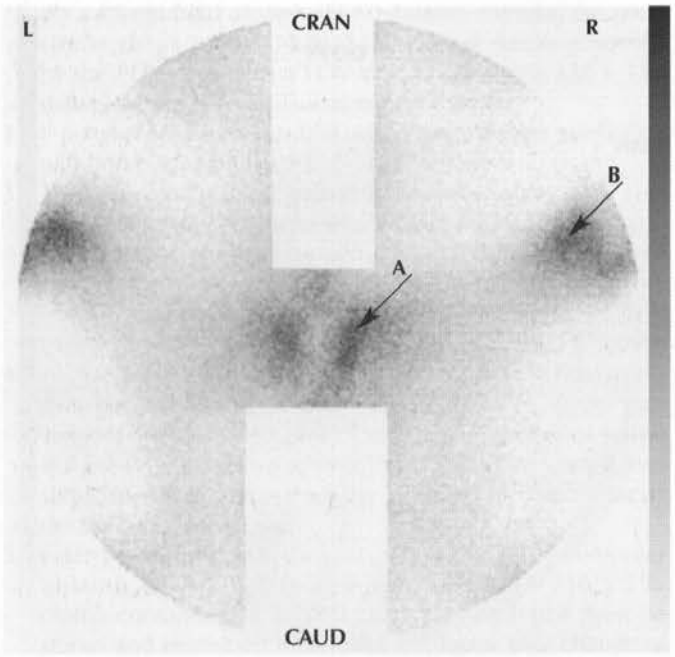

Figure 3

Dorsal image of the sacroiliac joints of the same image acquisition as Figure 2, but after motion correction. The lumbar and sacral spines have been masked out. Note the much crisper outline of the tubera sacrale (arrows) compared to Figure 2.

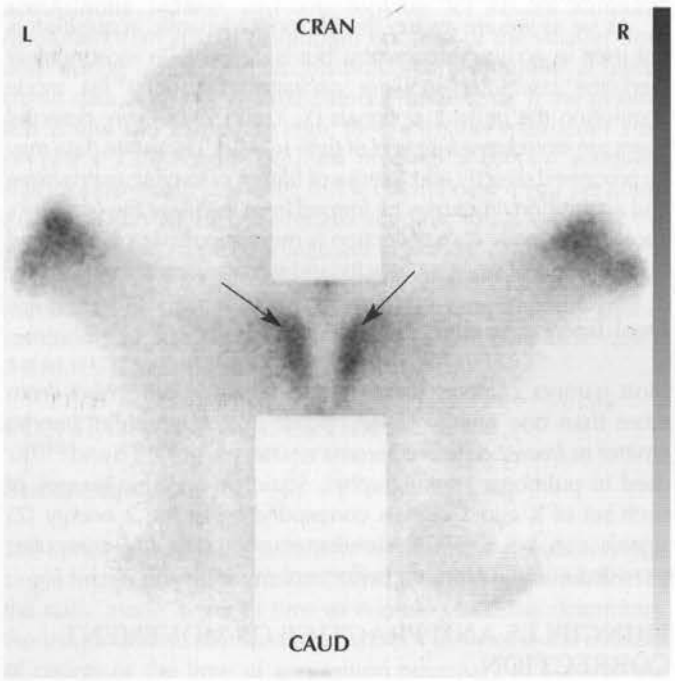

acquired as a dynamic study and then motion correction is performed on the dynamic sequence, prior to all the images being summed to produce a final static image of high spatial resolution.

There are various motion correction software packages

Figure 4

Dorsal image of the sacroiliac joints after motion correction has been performed. Excessive movement during image acquisition resulted in failure of the motion correction programme to eliminate the results of movement. Note the halo artefact around the periphery of the image on the left side (arrows).

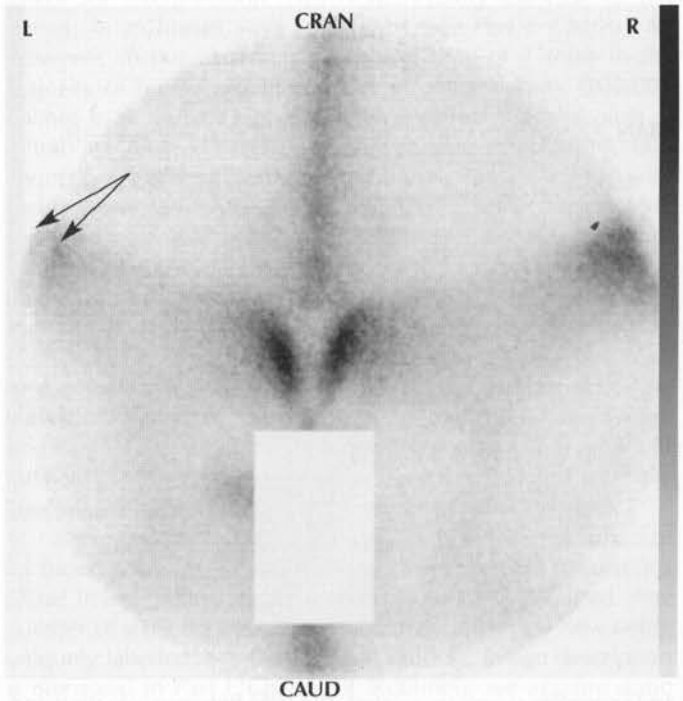

available from most nuclear medicine software suppliers. However, the basic principles and practice of motion correction software are similar. The software programme is designed to correct dynamic studies of any matrix size for movement in both the horizontal and vertical directions. The programme checks for movement by performing a correlation between successive images, with the second image in various positions relative to the first, in order to find the position in which the correlation is best. This position is then assumed to be the correct position and when the study is corrected the image is moved accordingly. The image is initially filtered with a low pass filter to reduce the amount of high-frequency noise, thereby making the process less prone to the effects of this noise in low-statistics images. Next, the data is checked for movement in both X and Y directions; usually this is represented graphically on the display and shows the integral movement throughout the study. The differential shifts curves for X and Y are calculated and then used to correct the data. Images can be shifted (image translation) by a number of pixels in both X and Y directions. The repaired study is then saved as a new study either in its original form (i.e. dynamic study) or by summing the individual frames to produce a final static image. Motion correction software packages can, in the majority of cases, correct for small amounts of motion to produce a high resolution image, but they cannot adequately correct for large amounts of motion. In these cases, the resultant image is blurred and of no diagnostic value; therefore, the acquisition must be repeated (**Figures 2–4**). To evaluate the effectiveness of motion correction, assess the crispness of the outline of the perimeter of the image and the uniformity of its shape, as well as looking at the anatomical resolution.

The efficacy of motion correction is also influenced by the presence of a moving region of intense RU. For example, if the bladder containing radioactive urine is on the periphery of an image and keeps moving in and out of the image, the computer will find it very difficult to perform motion correction properly.

Motion correction can be applied to the whole image, or correction parameters can be derived from a certain region of interest (ROI)[b] from the image and applied to the whole image. For example, when performing motion correction on a shoulder image, it is preferable to derive the motion correction parameters only from the shoulder area and exclude the neck, which, if included, would result in a more blurred image, since there is always more neck movement.

In addition to an automated method of motion correction, it should also be possible to remove individual frames. For example, if a horse made a gross movement during frames 34 and 35, these 2 frames could be deleted before running the automated motion correction programme. This should improve the resolution of the final static image. A similar number of frames should be removed from the image of the contralateral limb, for accurate comparisons.

Not all commercially available software packages have fully automated motion correction programmes, but this is important for daily clinical use.

TECHNIQUES FOR IMAGE PRESENTATION AND PROCESSING

The term 'image processing' covers a variety of procedures, including any operation that alters the appearance of an image to produce a more 'desirable' form. We aim to reduce noise through processing, and to accentuate the features of the image that are important to clinical interpretation. However, if used incorrectly image processing may also create or eliminate the appearance of pathological conditions, so it must be used with caution.

Using a computer system, it is hoped that image quality may be improved or optimised by various display manipulations and additional information extracted which is not readily available from viewing the images directly (e.g. time-activity curves).

Display Lookuptables

The display of digital images is achieved by using a matrix of pixels in which different pixel count values within the image are displayed as pixels of different intensities, or colours. These intensities are defined in a lookuptable. Most lookuptables have a maximum of 256 different intensities or display levels, so each display pixel in an image is assigned one of the 256 levels, depending on that pixel's count value. Normally, the maximum

Figure 5

Display format. A dynamic sequence of 35 2-sec frames of a lateral view of a carpus.

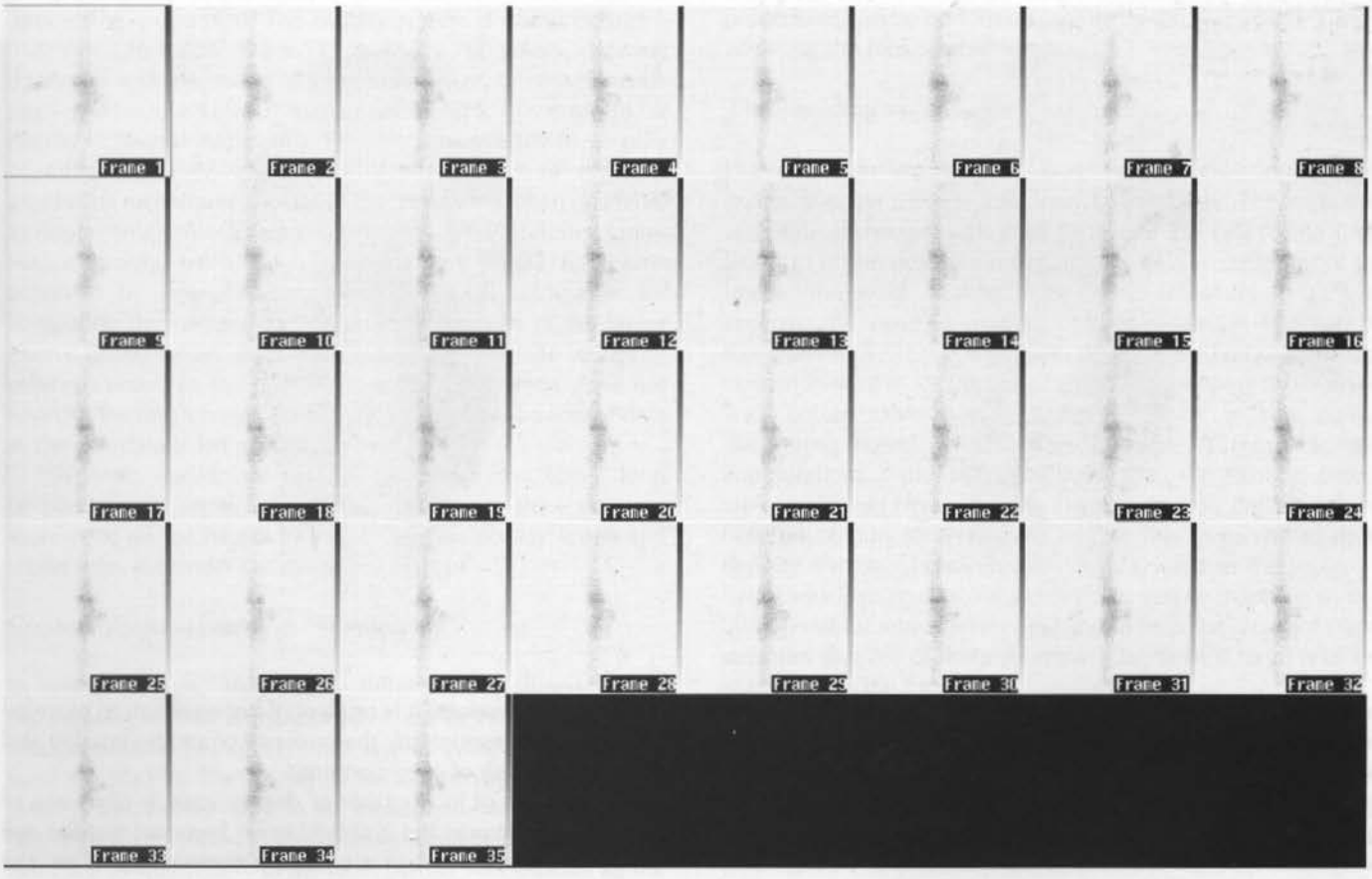

[b]A region of interest (ROI) is an area of pixels within an image or set of images that is defined or outlined for analytical or curve generating purposes.

Figure 6

Left lateral images of the mid cervical region obtained dynamically using 35 2-sec frames, after motion correction. The left image ***a)*** *has a large matrix size (256 x 256), whereas the inferior right image* ***b)*** *has a small matrix size (64 x 64).*

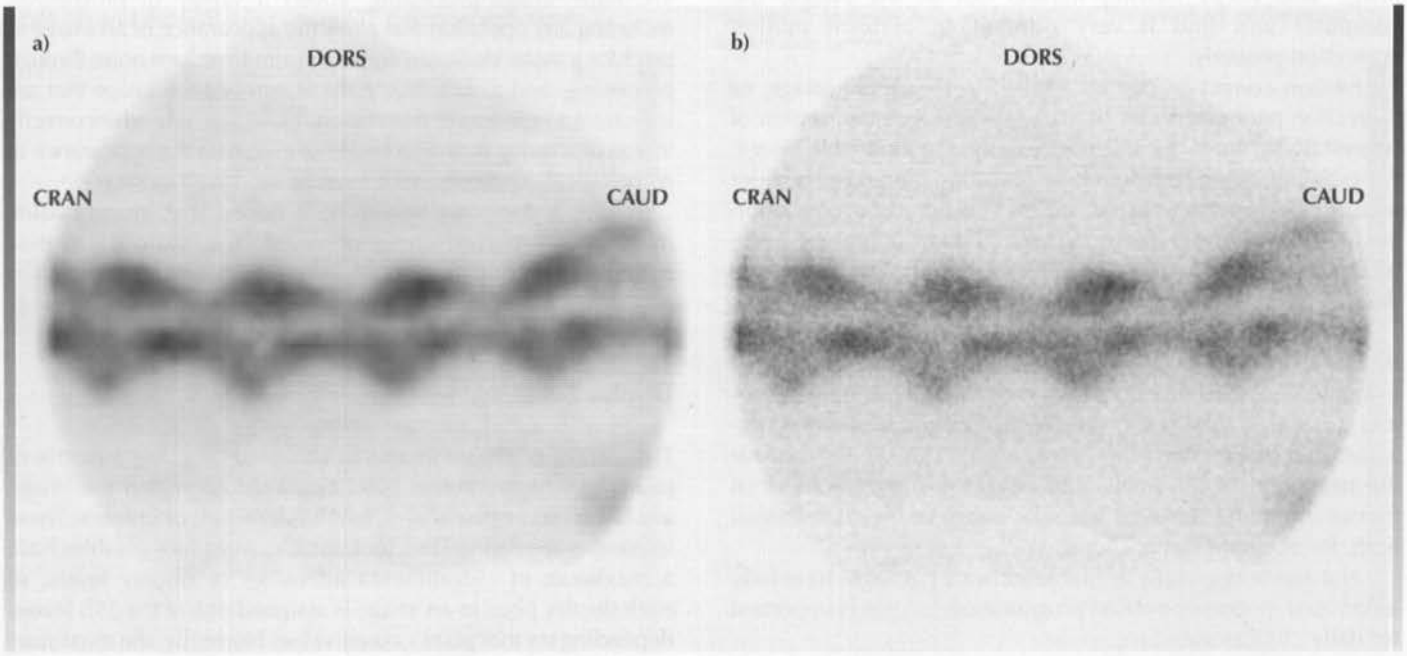

Figure 7

Dorsal images of the head. In image ***a)****, marked RU in the right side of the head makes visualisation of other structures difficult. In image* ***b)*** *the upper threshold range has been reduced (55 compared to 100) so that RU in the right mandible can be better visualised. This is an example of contrast enhancement.*

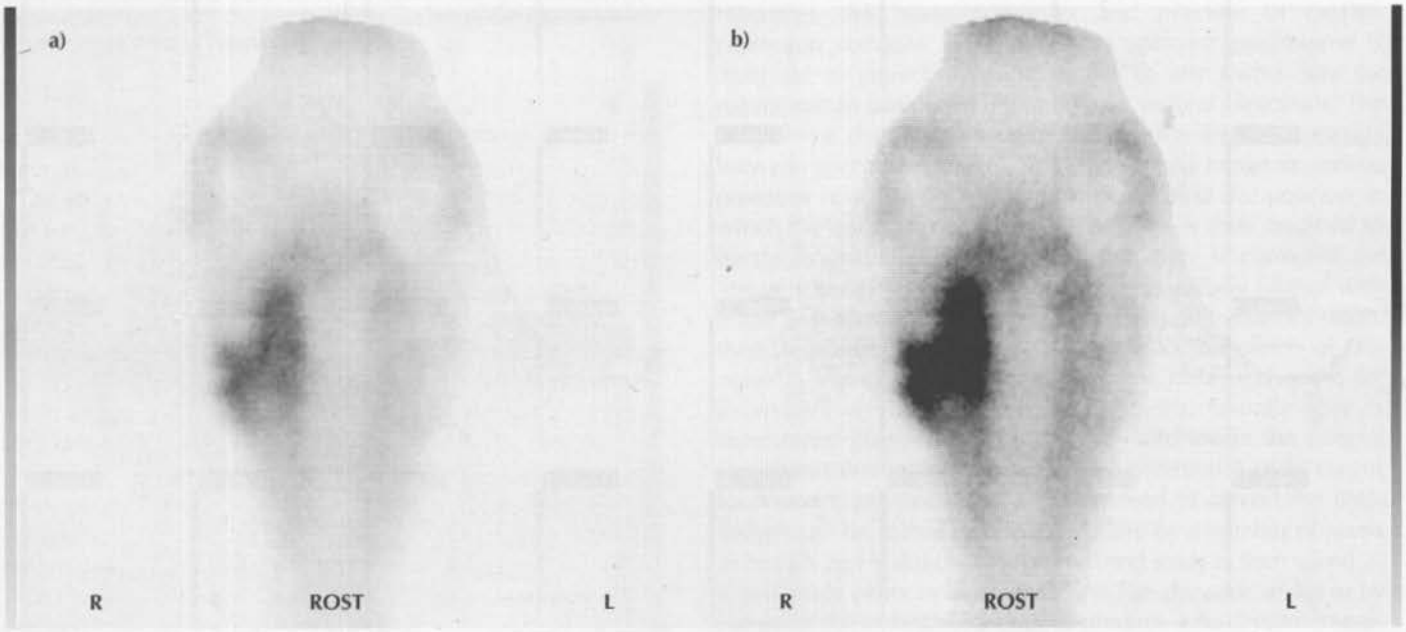

pixel value within the image is set to the highest level (often black) and the minimum value set to the lowest value (often white). Much has been written about the relative merits of greyscale and colour images. The sharp visual transition from one colour to another may alert the eye to the possibility of an abnormal area of RU. However, this colour change may represent an increase or decrease of only 1 or 2 counts/pixel depending on the colour scale used and may not be significant statistically. Therefore, it is prudent, if not essential, to examine greyscale images to verify the presence of an abnormality and minimise the risk of over-reporting.

The choice of lookuptable or display scale is often one of personal preference, but it should again be noted that the eye views different colours in a nonlinear manner. Therefore, the use of a multicolour lookuptable can lead to 'false contours' within the image.

Figure 8

a) Summated image of a lateral view of the carpus of a 3-year-old horse and b) the individual 2-sec frames collected dynamically from which the summed image was formed. Note the IRU in the distal radial physis typical of an immature horse.

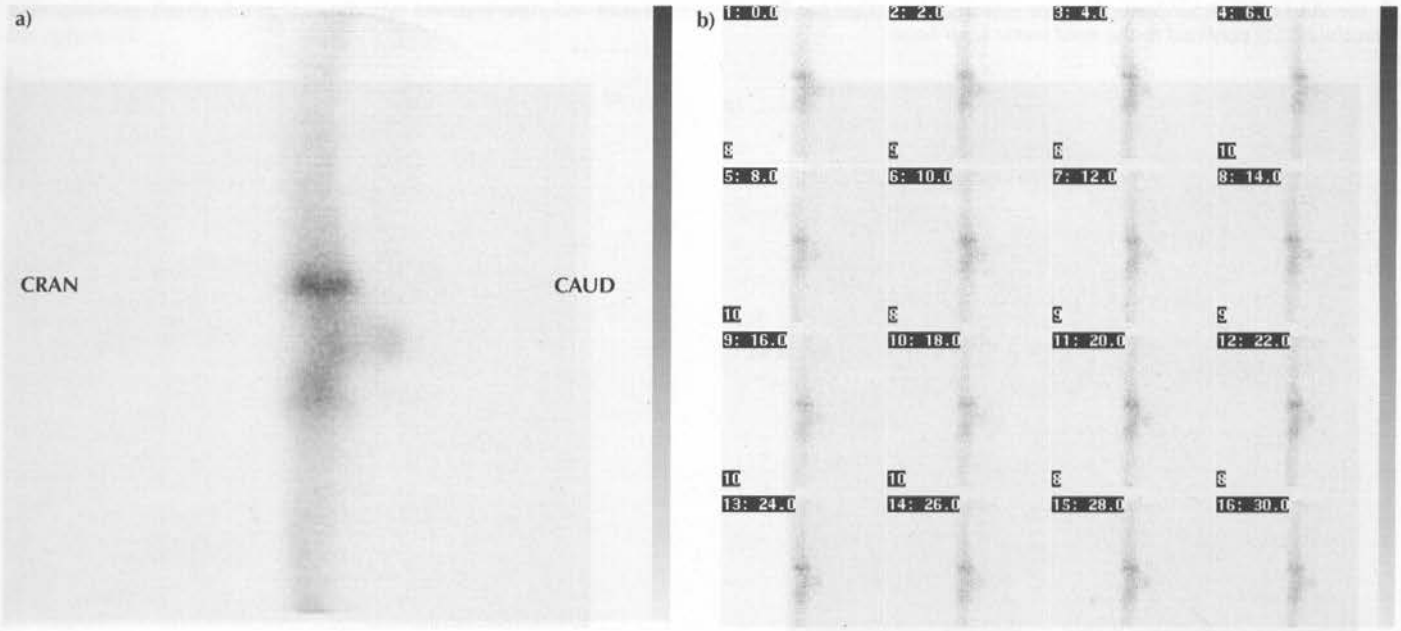

Display Format

Image display is probably the most common form of 'processing' performed. The display screen is comprised of a matrix of 256 x 256, 512 x 512 or 768 x 768 pixels, allowing display of a single image of large matrix size, or simultaneous display of many images of smaller matrix size. This is useful for display of several frames of a dynamic study (**Figure 5**), display of different views, or display of the results of different processing techniques applied to the image. It is often desirable to display small matrix size images, such as 64 x 64, in a larger matrix, thereby using the full display size (**Figure 6**). This is achieved by interpolation, a mathematical technique for computing the contents of the additional pixels in the larger matrix. These values are obtained by averaging the values of adjacent pixels in the original image. Interpolation does not improve the resolution of the image, and there is no loss of data as the raw data is left unaltered.

Dynamic studies are usefully displayed in a 'cine' loop (a continuous, rapid, sequential display on the computer monitor of all the frames in the study). The display levels and replay rates are under the operator's control.

Contrast Enhancement or 'Windowing'

In some images, the count difference between pixels representing normal and abnormal areas in the image may be small compared to the maximum counts in the image, such as from the bladder. The display of such an image using the full range of the display levels in the lookuptable would not depict this difference clearly. Contrast enhancement of the image is achieved by adjustment of the lookuptable. This enables all the display levels to be used specifically for displaying the range of pixel values of interest (**Figure 7**). Pixels containing more than a certain number of counts may be saturated (set to maximum level), or pixels containing less than a certain number of counts may be suppressed (set to minimum level). Such windowing procedures can be performed rapidly by the operator by simply adjusting the lookuptable levels.

Thresholding vs. Rescale

Example: There is a maximum pixel value of 1024 counts in the image. You are using a 256 level colour table. The computer automatically maps each pixel to one of the 256 colour table levels to fit the dynamic range (minimum to maximum) of the image. You want to reduce the upper threshold to 25% to improve the contrast in a low-count region. A fast way to threshold is to use the lower 64 entries of the colour table (the bottom 25% of it) for the greyscale range, mapping those pixels with colour table entries higher than 64 to one colour (saturating them). This is fast because it requires little computation; it just reassigns colours to the existing colour table mapping. However, this also means you are now using only 64 colours to render the image. This gives rise to more definite contours between each colour value in the image. A better way is to rescale (recalculate) the colour mapping so that all 256 colour table entries are used to map the range of count densities that are of interest (in this case from 0 to 25% of the maximum in the image).

Image Arithmetic

Pixel values within images can be changed by conventional arithmetic operations on a pixel by pixel basis. Examples of use are:

1. When defining an ROI on a dynamic study, it is best performed on an image of summed frames which contain

Figure 9

a) Dorsopalmar radiographic view of the right carpus and proximal metacarpal region of an 8-year-old advanced event horse with moderately severe lameness eliminated by palmar metacarpal (subcarpal) nerve blocks. There is no significant radiological abnormality. b) Dorsal and lateral scintigraphic images showing marked focal IRU in the right carpal/metacarpal area; it is not easy to determine anatomically whether this is confined to the third metacarpal bone. In c) the scintigraphic image has been registered with and superimposed over the radiograph, clearly demonstrating that the IRU is confined to the third metacarpal bone.

sufficient counts to demonstrate accurately the areas of interest you want to delineate within the image (**Figure 8**).

2. Two images of different frame times can be compared directly by multiplying one image by the ratio of frame times.
3. Fast frame dynamic studies often contain a small number of counts in each frame, resulting in noisy images. Addition of several frames can improve the image quality (spatial resolution) at the expense of some reduction in the temporal resolution of the study.

Image Translation

Images can be shifted by a number of pixels in both X and Y directions or by rotation or inversion (flipping). This is used in motion correction and image registration software.

Image registration is of particular value when you need to:

1. Accurately identify the anatomical site of an area of increased or decreased RU by overlaying the scintigraphic image over the corresponding radiograph view (**Figure 9**).
2. Compare identical regions quantitatively on opposite joints e.g. lateral views of the hocks (**Figure 10**) (see *Regions of Interest* and *Profile Analysis*).

In order to compare RU accurately, ideally the 2 limbs must be similarly orientated, e.g. dorsal to the left; therefore, one image is reversed about the Y axis. The 2 images should then be co-registered so that they are aligned exactly. This may be performed by selecting similar anatomical points on each image, and the software then matches these points. Some software packages allow you to co-register images automatically. This

Figure 10

Lateral images of ***a)*** *left and* ***b)*** *right hocks that have been registered so that identical ROIs can automatically be located on the left and right limbs. The image of the right hock was 'flipped' post acquisition. The ROI tool window demonstrates the number of pixels in each of the 2 ROIs, the mean counts/pixel, minimum and maximum counts/cell and the standard deviation of counts within the ROI. The relative percentage of counts in the left and right images is calculated both for the raw data and after normalisation of the image. There is focal IRU in the central and third tarsal bones of the right hock.*

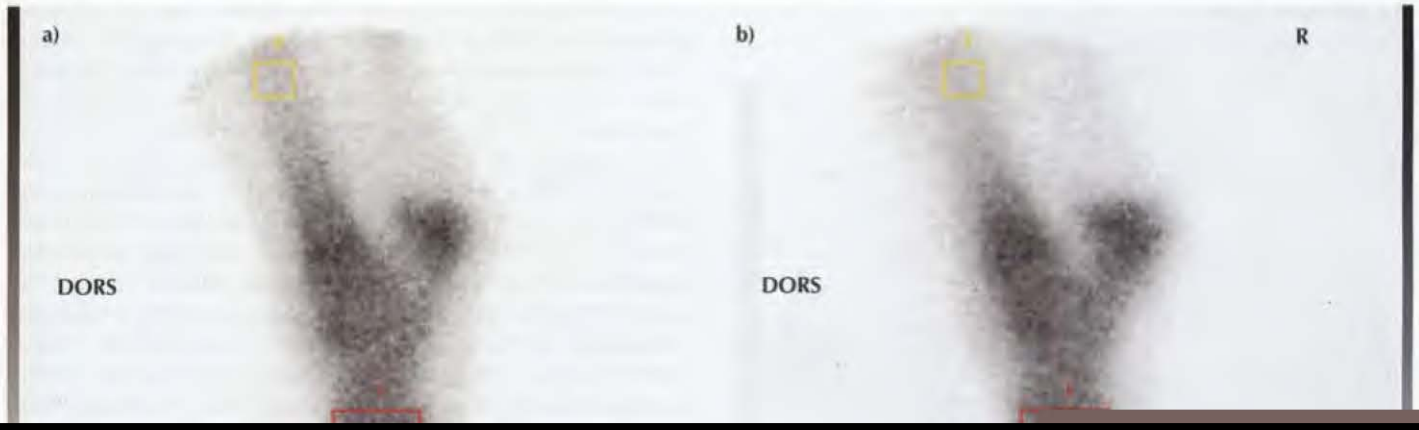

Figure 12

Dorsal image of the pelvic region: the same acquisition as Figure 11. The region of the bladder and the lumbar spine have been masked out. This results in better visualisation of RU in the tubera sacrale, sacroiliac joints and tuber coxae compared to Figure 11. There is rather blurred demarcation between RU in the tubera sacrale and the sacroiliac joint regions, suggestive of sacroiliac joint disease. Compare with Figure 3.

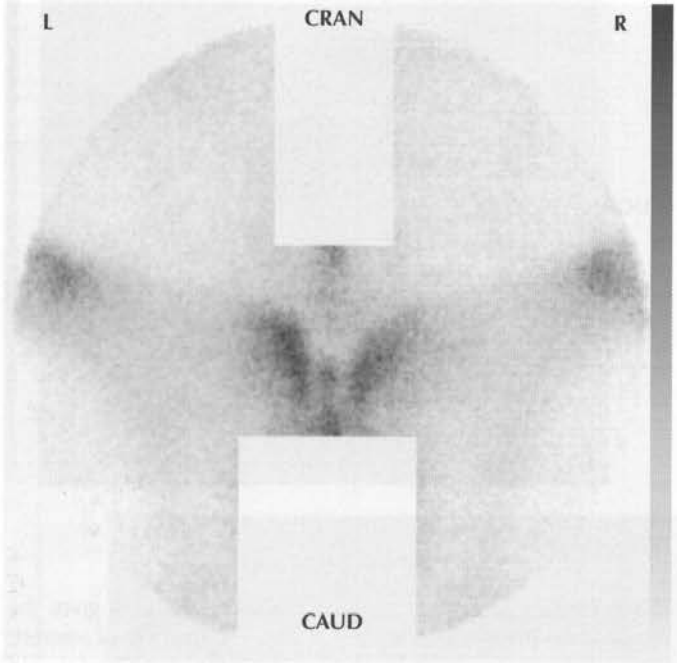

of the foot is then outlined and the areas external to the foot are masked out or deleted (**Figure 14**).

Image Filtering

Image filtering results in the modification of data values in the image itself, rather than simply of the lookuptable, as in display manipulation. Image filtering is applied to images to reduce their granular appearance, which is distracting to the interpreter, and to provide improved visualisation or detection of boundaries and edges (see *Part I, Chapter 9*). However, although filters improve the signal to noise ratio, they do this at the expense of losing detail. The most commonly used technique for filtering is to convolve the image with an array of numbers known as the filter function. Most data processing systems are supplied with a selection of filter functions (**Table 1**). One of the most commonly used filters is for image smoothing (see *Image Smoothing*) to reduce noise in a low count density image. Unfortunately, it also blurs out the edges of the structures. When a clear definition of an edge is necessary, as for example when it is necessary to draw an ROI around an organ, edge enhancement filters are available (see *Edge Enhancement*). However, care must be taken when using filters, as their application cannot compensate for poor image data and inappropriate or overzealous application of filters can introduce artefacts (**Figure 15**), which may be mistaken for abnormal pathology. It is therefore important that the original image be displayed together with the filtered version (**Figure 16**). It has been suggested that scintigraphic images with low count statistics, due to reduced dosage of the radiopharmaceutical or reduced acquisition time, may be equally diagnostic if digital

Figure 13

*Right lateral image of the mid and caudal thoracic vertebrae and ribs. In **a)** RU in the kidney results in poor definition of the vertebrae. In **b)** the kidney has been masked out. There is now much clearer definition of the thoracic vertebrae and ribs. There is IRU in the summits of the dorsal spinous processes of the 15th and 16th thoracic vertebrae (arrows). However, there is rather poor correlation between such IRU and either radiographic evidence of impingement of the dorsal spinous processes or clinical signs of thoracolumbar pain.*

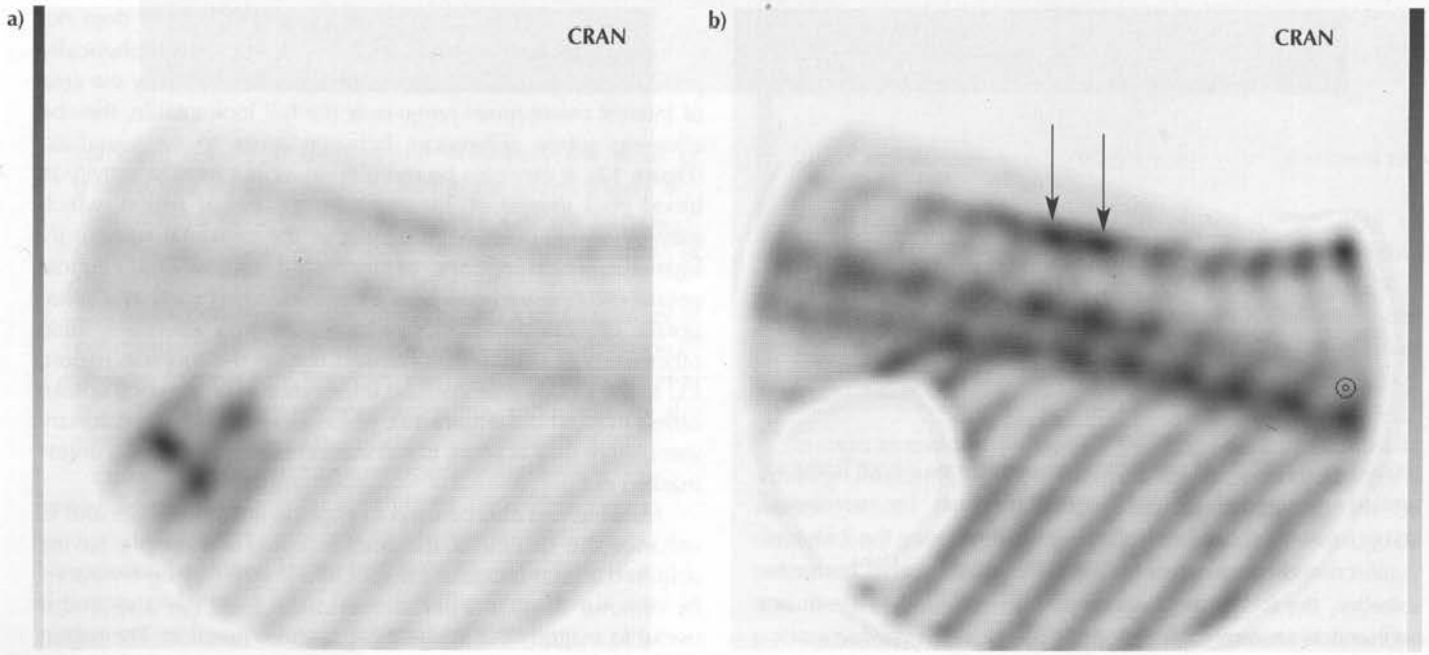

Figure 14

Solar images of the left front foot. Image ***a)*** *is the raw data. Image* ***b)*** *has been 'zoomed' (magnified x 2), smoothed and areas peripheral to the foot have been masked out, giving clearer definition in this image. There is IRU in the centre of the navicular bone (arrow).*

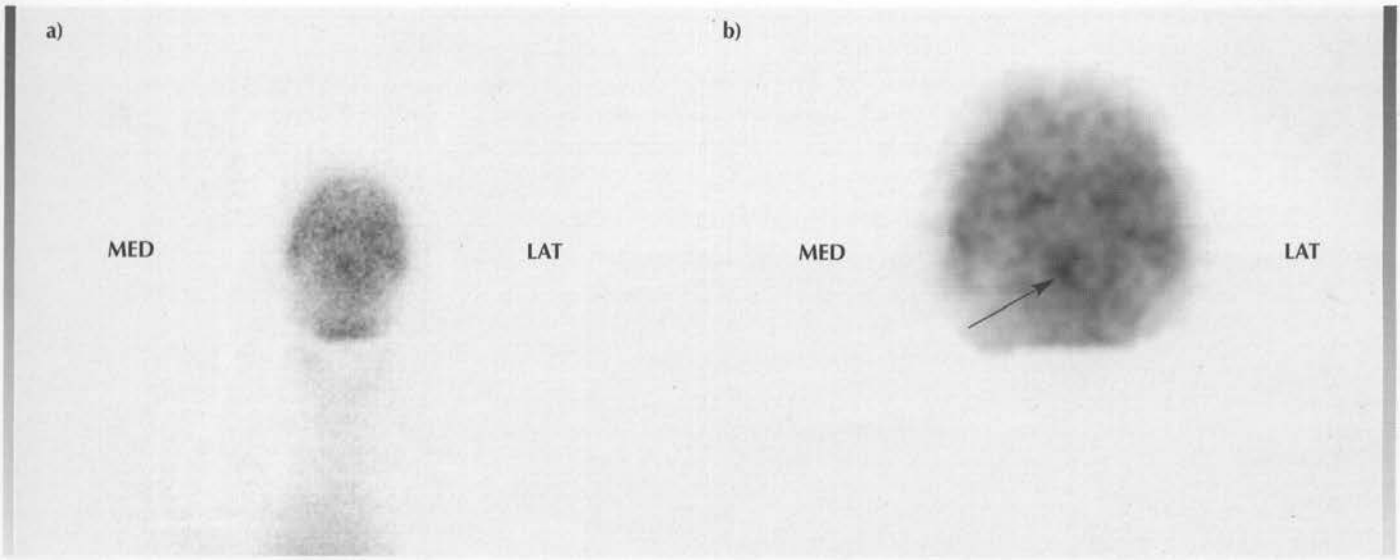

Figure 15

Lateral images of the left hock. A high resolution Metz filter has been used in ***b)****. The original image* ***a)*** *gives much more information than the inappropriately filtered image (b). Artefacts can be created by inappropriate use of a filter.*

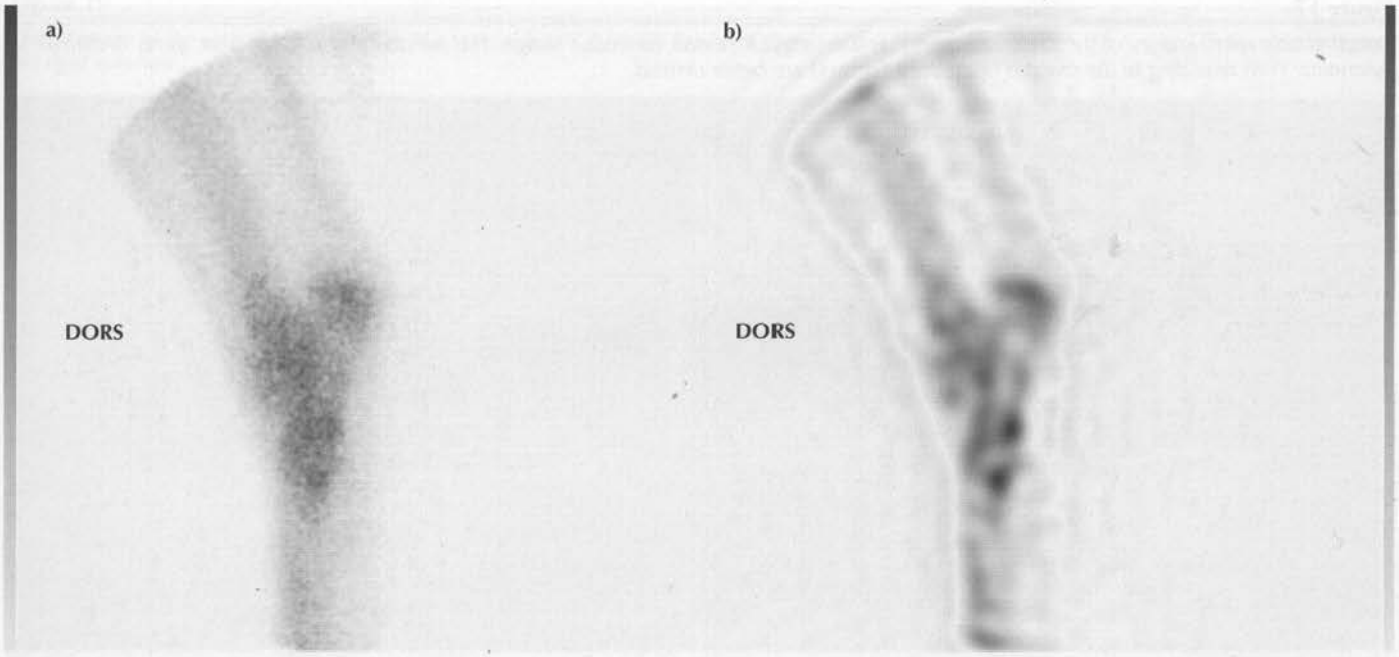

Table 1: Common filter types and their uses

Filter type	Use
Low pass	Noise reducing. No contrast enhancement.
Butterworth	Modified low pass filter. No contrast enhancement.
Metz	Noise reducing, contrast enhancing. Gentle filter not likely to introduce artefacts. Recommend contrast enhancing filter.
Wiener	Provides both noise reduction and contrast enhancement. Capable of introducing artefacts.
Scramp	Contrast enhancement. Gives greatest contrast enhancement of all filters. Capable of introducing artefacts.
Inverse MTF	Contrast enhancement. Capable of introducing artefacts.

The authors have direct practical experience of the use of the Metz filter in many situations. The use of the other filters in equine scintigraphy does not appear to be widespread, but they are included for completeness, since they are often included in software packages.

Figure 16

Caudal images of the right stifle. ***a)*** *Original image.* ***b)*** *Image filtered using a high resolution Metz filter. In this example, the filtered image highlights IRU in the medial femoral condyle (arrow) which was associated with a subchondral bone cyst.*

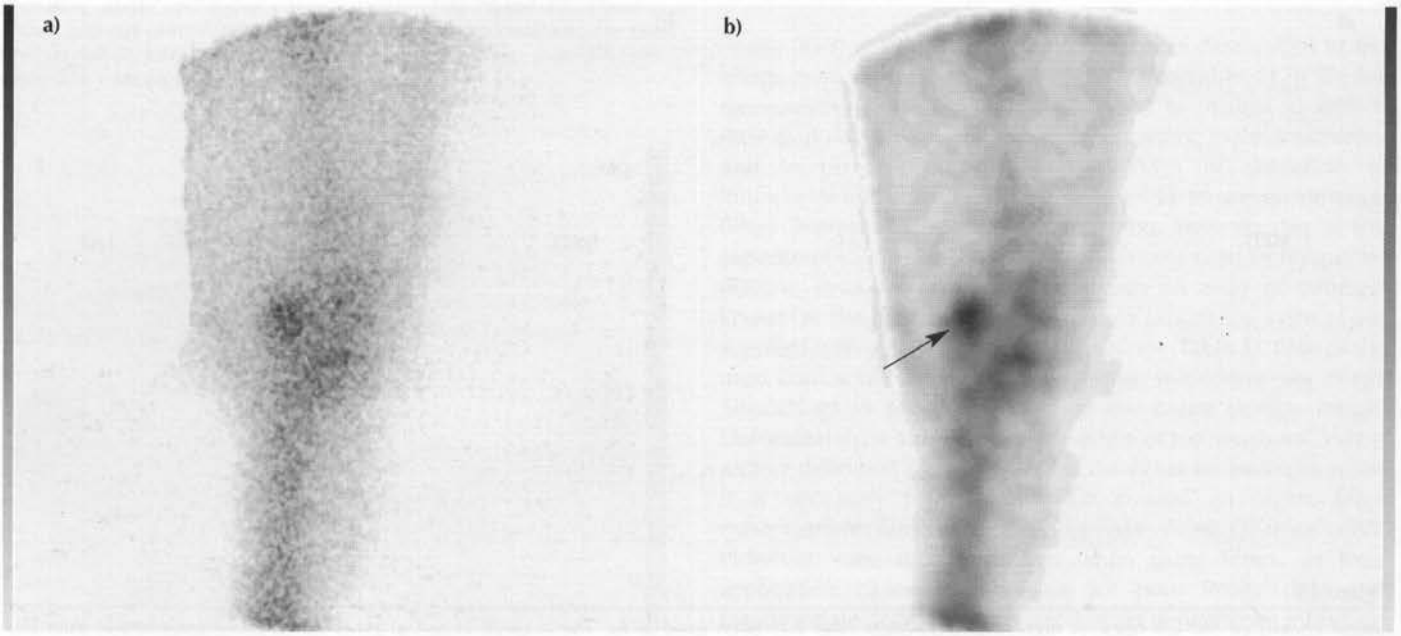

Figure 17

Dorsal scintigraphic images of the sacroiliac region. ***a)*** *The original motion correction image. The periphery of the sacroiliac joints is difficult to determine. With re-scaling* ***b)*** *the margins of the joint (arrows) are better defined.*

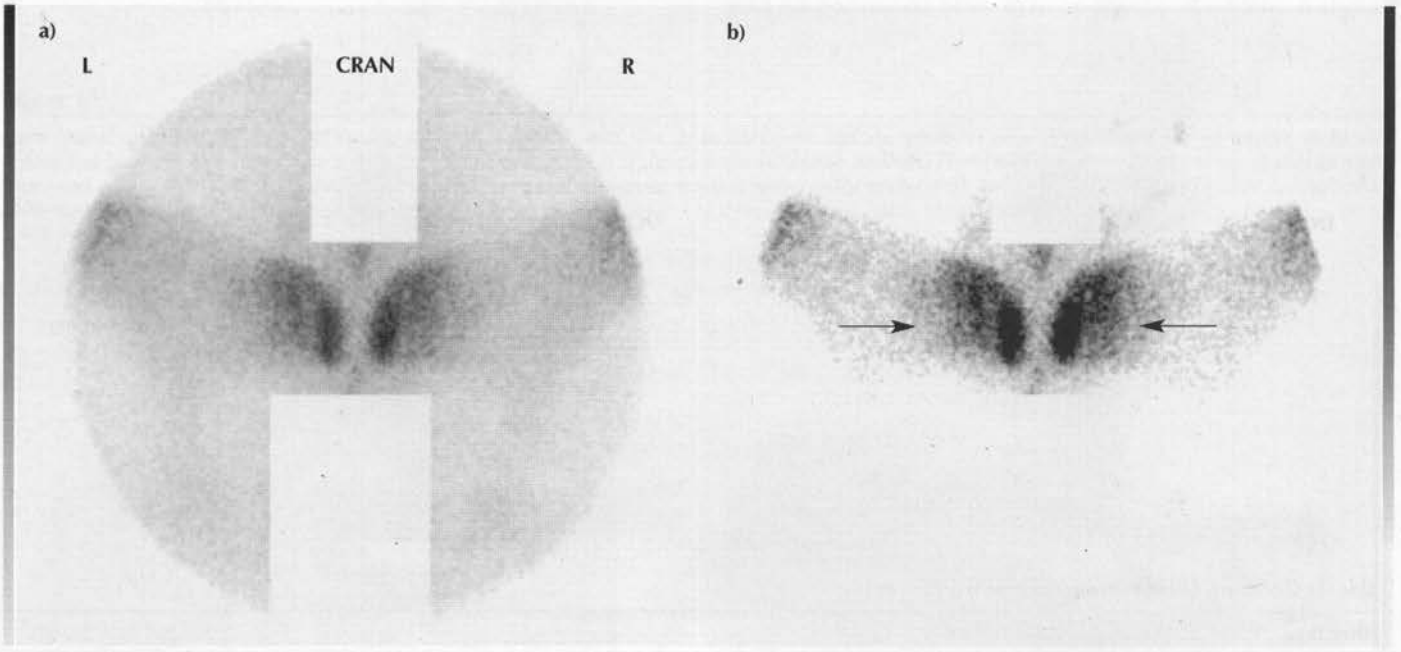

filtering is used correctly[7]. However, as previously mentioned, filters only improve the signal to noise ratio and they do so at the expense of losing detail and with the chance of introducing artefacts within the image that could be mistaken for pathology. With a low count statistic image of poor detail, the final processed image is going to be of even further reduced detail and is therefore not suitable for diagnostic purposes.

Image Smoothing

There are two types of image smoothing filters that are useful in nuclear medicine; spatial and temporal filters (see **Table 1**). Spatial filters are usually used on static images to attempt to remove statistical fluctuations in the image. This is accomplished by modifying the values of the data points

Figure 18

a) Image summed from dynamic acquisition of blood flow to plantar distal hindlimbs. b) Time activity curves from ROIs drawn around left and right distal phalanges.

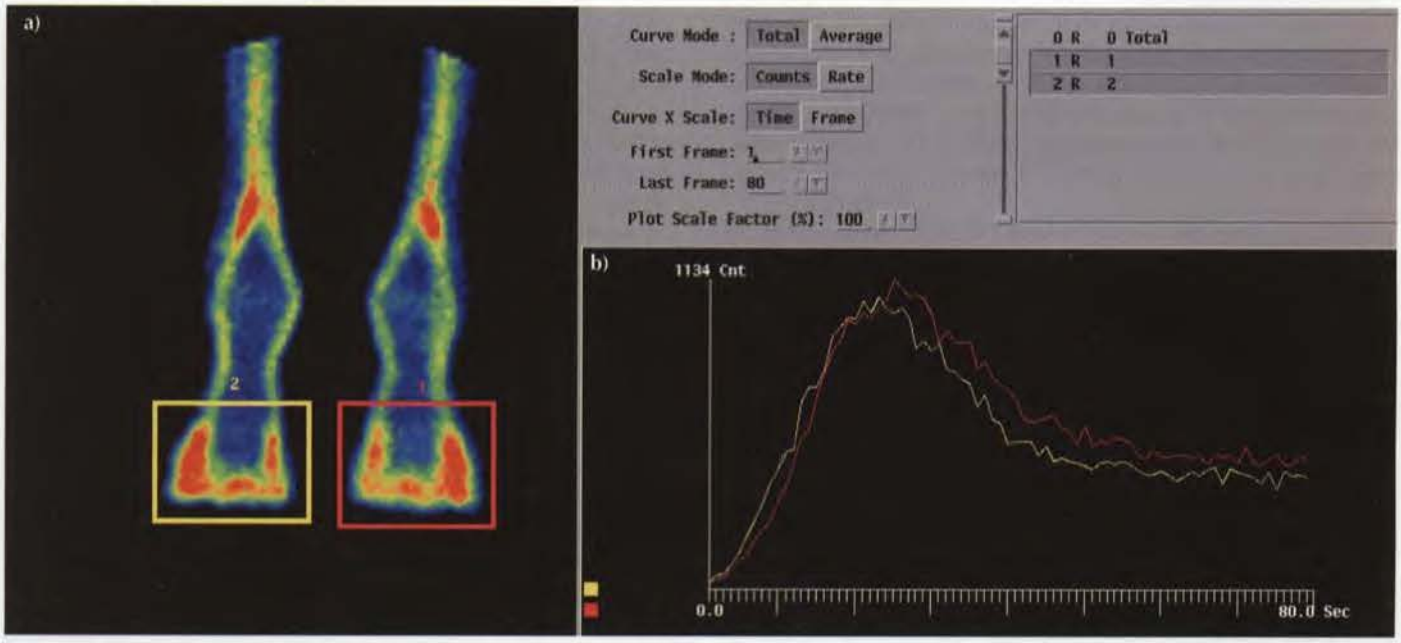

Figure 19

Dorsal image of the sacroiliac joint region of a normal horse. A profile has been drawn across the joints (between the two red lines), demonstrating left right symmetry.

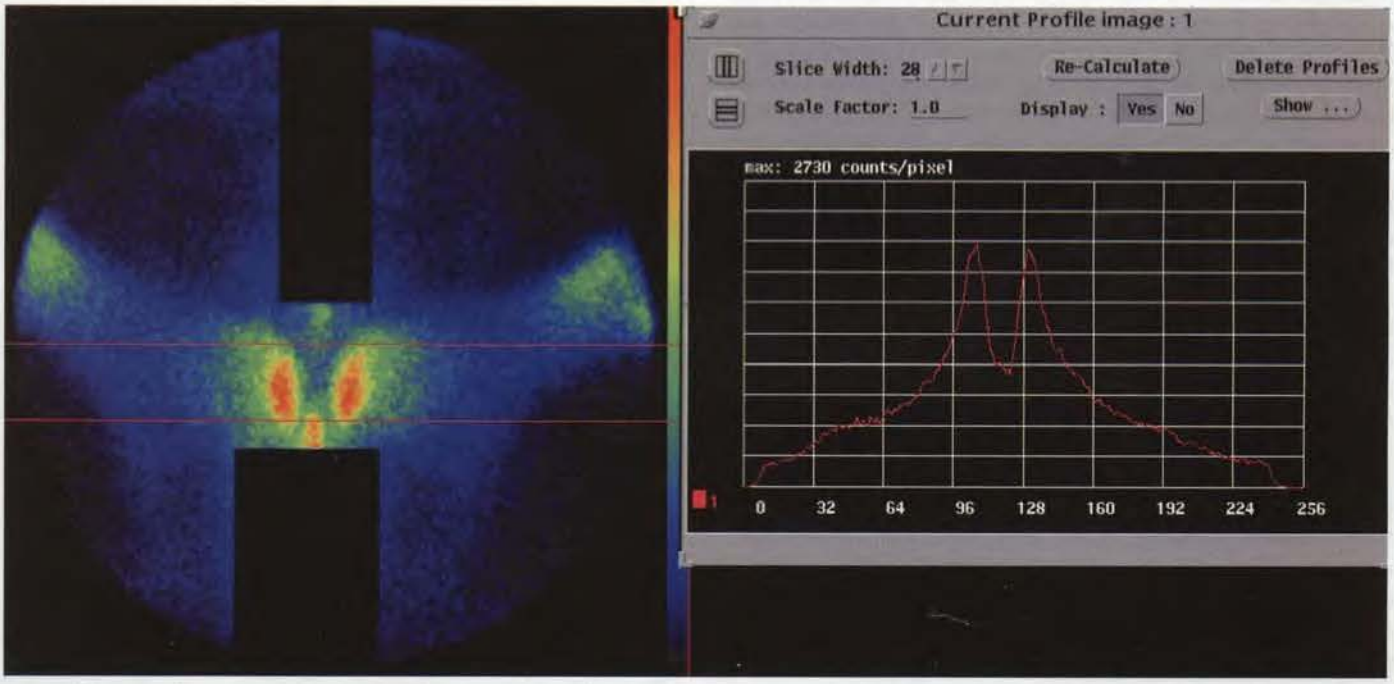

within the image. A 2-dimensional 9-point smoothing programme is the standard. This technique operates by reducing the statistical fluctuations in each pixel by averaging the pixel with its closest neighbours.

Noise smoothing is an application of spatial smoothing that attempts to decrease the visual prominence of noise so that those low contrast objects of moderate to large size may be better appreciated. All methods of smoothing noise sacrifice some resolution in the process of smoothing the image. In our experience, use of a high resolution Metz filter can be helpful in evaluation of lateral images of the thoracolumbar region, making it easier to discern accurately areas of IRU.

Temporal filters can be used only on dynamic images, since they involve a weighted averaging technique between

each pixel in one image and the same pixel in the frame immediately preceding and following the image. These values are added together to develop a weighted average that replaces the original pixel value of the central image. The filter then moves to another image, and the procedure is repeated until all images are smoothed and a filtered dynamic study is created. There is some loss of spatial resolution using this technique; however, the ability to view the images without flicker more than compensates for the small loss of resolution.

Edge Enhancement

Quantification of activity within a volume such as an organ requires that the volume be delimited. Edge enhancement is intended to increase the visibility of small structures with moderate to high contrast. For this reason, edge detection algorithms are of importance (e.g. drawing an ROI over a kidney for a renal function study requires accurate detection of the kidney's edges). The simplest method of edge detection relies on estimating the gradient and the second derivative (rate of change of gradient) at various points in the image. A

at least 10% and preferably >20% difference in RU for clinical significance, provided that there are similar total counts in each ROI and that there is a large enough number of total counts in the image (>200,000). ROI analysis can also be used to assess ratios of uptake between 2 or more defined areas within the same limb, which can be particularly helpful if similar abnormalities are present bilaterally.

However, variable total counts in 2 ROIs introduces what is called Poisson error. For example, there is no statistical significance in a 15% difference between 2 ROIs, one with 100 counts in it and another with 115 counts. This is because the uncertainty in the measured value from the average of the underlying distribution is around 10% for each region (the difference is therefore 15 ± 14). The system uniformity of the camera must also be considered. Even with a system integral uniformity index of 3%, there could be a 6% difference between any two regions of the field of view, especially if one or both of the regions are near the edge.

It is important to realise that the count density information obtained using an ROI defined around a specific area of uptake does not represent the quantity of radiopharmaceutical. In order to estimate

images obtained under these circumstances are of superior quality but, in the majority of cases, do not reveal anything further that is clinically significant than that visualised on images obtained using a high quality acquisition technique, especially including motion correction, with the horse sedated.

Other factors that can be used to increase the quality of the images obtained are:

1. Use of a low energy high resolution collimator instead of a general purpose collimator. However, to achieve good count statistics the acquisition time must be increased, which increases the risk of movement artefact in the final image.
2. Injecting a larger dose of the radiopharmaceutical/kg bwt. Increased count statistics would be obtained with the same acquisition time, thereby improving spatial resolution of the final image. However, the increased radiation dose to staff is a risk and is not justified.
3. Use of frusemide or catheterisation of the bladder prior to imaging. This enhances the quality of the images obtained over the pelvic region by reducing the amount of radiopharmaceutical activity seen in the bladder.
4. Use of various computer manipulations to the raw image data (filtering). The advantages/disadvantages of this have already been described.

IMAGE STORAGE AND RECORDING

The most common display is a persistence oscilloscope in which the X and Y signals from the gamma camera are applied to the deflection plates, giving the tube beam the same position on the face of the persistence oscilloscope as that on the gamma camera face. For each successive γ-ray the oscilloscope beam shifts to the new position, and an image of low count rate density is quickly built up and renewed at rates controlled by the operator. Modern acquisition software often uses the persistence image as the default image on the computer monitor. This image assists and is ideal for positioning, but it is totally unsuitable for diagnosis.

Image Storage

There are 2 types of storage devices, internal and external. The main internal storage device of any computer is a hard disk, which can be mirrored (copied) for security. Data/image files are written magnetically onto this hard disk. External storage devices include floppy disks, CD/DVD-R, RAID devices, magneto optical disks and tape drives. Nowadays, CD-R/DVD-R disks are commonly used for backing-up data because they are robust, relatively inexpensive, can store 700 Mb/4.5 Gb of data and have fast data access times.

Image Recording

Before selecting a printer, it is important to produce a comprehensive specification of intended use and requirements of the printer. Cost, speed, quality, colour capability, reliability, print cost and network options are important criteria when choosing a printer. Throughput and paper handling options should also be considered.

Various types of printers can be connected to the imaging computer to produce a hard copy of the final images. All have strengths and weaknesses.

1. Inkjet printer: Inkjet printers gradually build up the hard copy one line at a time. Therefore, they are comparatively slow to produce the complete final image and are not suitable for high volume work. Additionally, inkjet printers are only semipermanent because the ink tends to be water based. In some cases, the print can be spoiled by physical damage such as smearing. The newest generation of inkjet printers offers high resolution and their print quality is comparable to that of a laser printer. Cost per print is low, although not as low as laser prints, because inkjets use expensive inks and papers.

2. Laser printer: Laser printers create an entire page at a time using optical technology similar to that found in photocopiers. A laser imposes an image on a light sensitive drum. The image is then transferred to the paper by electromagnetically fusing toner onto the paper at very high temperatures. Laser printers can be networked and used by other workers within the clinic. They offer relatively fast print speeds, high print resolution and overall robustness, which allows for a very high duty cycle. The cost per page for laser prints is low, because paper and toner are relatively inexpensive. The most expensive consumable component of a laser printer is the optical print cartridge, which is usually rated for tens of thousands of prints. Colour laser printers are still relatively expensive by comparison to colour inkjet printers, but their low cost per print is comparable to that of a colour photocopier. Therefore, they are used when fast, high quality, high quantity colour output is a requirement.

3. Thermal printer: Thermal printers are exceptionally high quality colour printers producing a much higher quality print than most inkjets and lasers. The most common types are dye-sublimation and thermal wax printers. All function in the same manner, using heat to impose inks from a coloured ribbon onto coated paper. These prints are of a quality approaching that of colour photographs. Thermal printers are relatively expensive and their cost per page is exceptionally high. Additionally, these printers are very slow[8].

Input Devices

Scanners translate optical information into digital information that a computer can understand. This allows manipulation of images into reports that may be printed out as a hard copy and also facilitates image registration of scintigraphy, MRI, CT and/or radiographs to aid localisation of any abnormal RU.

REFERENCES

1. Dyson, S. Unpublished data.
2. Dyson, S., Lakhani, K. and Wood, J. (2001) Factors influencing blood flow in the equine digit and their effect on uptake of ^{99m}technetium methylene diphosphonate into bone. *Equine vet. J.* **33**, 591-598.
3. Ross, M., Maxson, A., Stacy, V. *et al.* (1997) First-pass radionuclide angiography in the diagnosis of aortoiliac thromboembolism in a horse. *Vet. Radiol. Ultrasound* **38**, 226-230.
4. Boswell, J., Marr, C., Cauvin, E. *et al.* (1999) The use of scintigraphy in the diagnosis of aortic-iliac thrombosis in a horse. *Equine vet. J.* **31**, 537-541.
5. Dyson, S. Unpublished data.
6. Dyson, S., Murray, R., Branch, M. *et al.* (2003) The sacroiliac joints: evaluation using nuclear scintigraphy. Part I: The normal horse. *Equine vet. J.* **35**, 226-232.
7. Eksell, P., Carlsson, S., Lord, P. *et al.* (2000) Effects of a digital filter on detectability of a phantom lesion in a scintigram of the equine tarsus. *Vet. Radiol. Ultrasound* **41**, 365-370.

8. Martinelli. M.J. (1998) *A Handbook of Computers in Veterinary Medicine*, Romney Publications, Newmarket, UK.

FURTHER READING

1. Sharp, P.F., Gemmell, H.G. and Smith F.W. (1989) *Practical Nuclear Medicine*, Oxford University Press.
2. Williams, A.G. and Eckel, C.G. (1987) *Practical Computer Applications in Radionuclide Imaging*, Churchill Livingstone.
3. Pokropek, T. (1980) *Image Processing in Nuclear Medicine*, Grune and Stratton.
4. Dendy, P.P. and Heaton, B. (1987) *Physics for Radiologists*, Blackwell Scientific Publications.
5. Curry, T.S., Dowdey, J.E. and Murry, R.C. (1990) *Christensen's Physics of Diagnostic Radiology*, Lea and Febiger.

Chapter 6

PATIENT PREPARATION

SUE J. DYSON
Centre for Equine Studies, Animal Health Trust, Lanwades Park, Kentford, Newmarket, Suffolk CB8 7UU, UK.

Acquisition of high quality nuclear scintigraphic images requires attention to detail and a regular system for preparation of the horse. This chapter focuses on patient preparation for musculoskeletal imaging. We find that horses are much more cooperative and less likely to behave dangerously if they have been hospitalised overnight, prior to image acquisition.

ESTIMATION OF RADIOPHARMACEUTICAL DOSE

Ideally, horses should be weighed so that an accurate dose of the radiopharmaceutical is administered. For ^{99m}Tc-methylene diphosphonate (MDP), a dose of at least 1 GBq for each 100 kg bwt is required. If a weighbridge is not available, reasonably accurate 'guesstimates' can be made using girth tape measurements[1], together with assessment of the overall build of the horse. Doses of less than 1 GBq/100 kg bwt may result in satisfactory radiopharmaceutical uptake (RU), and hence adequate image quality, in young immature athletes, but in mature horses count rates will be low, resulting in either increased acquisition times to obtain satisfactory count rates or inadequate image quality with insufficient counts per image to provide reliable statistical information.

THE EFFECTS OF RECENTLY PERFORMED NERVE BLOCKS

There is conflicting evidence about the effects of recently performed nerve blocks on uptake of ^{99m}Tc-diphosphonate in soft tissue and bone phase scintigraphic images[2-6]. This probably reflects the type of local anaesthetic solution used, volumes employed, sites of injection and skill of the administrator. In most studies assessing bone phase images obtained within 4–24 h after experimental intra-articular or perineural injection of lidocaine, mepivacaine and bupivacine in the carpus or tarsus or further distally, there was no abnormal uptake[3-5]. Up to 4 ml of local anaesthetic solution per site was used for perineural injections. However, perineural analgesia of the palmar and palmar metacarpal nerves using 8 ml butanilicain per site resulted in a diffuse region of markedly increased soft tissue diphosphonate uptake in bone phase images, completely confounding interpretation. Abnormal RU in muscle in bone phase images has been reported after perineural analgesia in the antebrachium[2]. Both perineural and intra-articular analgesia may be more likely to result in abnormalities in pool or soft tissue phase images[4,5]. Perineural analgesia of the palmar (abaxial sesamoid) nerves (2 ml lidocaine/site) had no effect, whereas perineural analgesia of the palmar digital nerves or the palmar and palmar metacarpal nerves in the proximal or distal metacarpal region (4 ml lidocaine/site) resulted in abnormal pool phase images for up to 7 days for the palmar digital nerves or 17 days for the palmar and palmar metacarpal nerves. Most of these studies looked at the effects of 1 or 2 injections per limb whereas, in the clinical situation, it is likely that many more nerve blocks may have been performed prior to nuclear scintigraphy being performed.

In my experience, if several perineural blocks have been performed in the metacarpal or metatarsal and pastern regions within 7 days of image acquisition, there are frequently diffuse areas of increased radiopharmaceutical uptake (IRU) in soft tissue images and often in bone phase images as well, which can completely confound interpretation. However, a single block with good technique, for example perineural analgesia of the palmar metacarpal nerves at subcarpal level, may have no effect. Perineural analgesia of either the palmar digital or palmar (abaxial sesamoid) nerves using 1–2 ml mepivacaine per site is generally not associated with abnormal uptake. Recent intrathecal analgesia of the navicular bursa may result in abnormal uptake in pool phase images. There is a high risk of abnormal RU following perineural analgesia of the median and ulnar nerves or the fibular and tibial nerves (see *Part I, Chapter 10*). This probably reflects the larger volumes of local anaesthetic solution employed, deposition in muscle and, for the deep fibular nerve, its close proximity to the distal cranial aspect of the tibia, with the possibility of the needle impacting the bone. In my experience, carefully performed intra-articular analgesia or intrathecal analgesia of tendon sheaths does not influence RU in either pool or bone phase images.

It is therefore recommended that there should ideally be a delay of at least 7 days between performing multiple perineural local analgesic techniques and nuclear scintigraphy. If there is any adverse soft tissue response to perineural analgesia, scintigraphic examination should be delayed until this has resolved. Scintigraphic examination can proceed soon after most single perineural injections, intra-articular analgesia or analgesia of tendon sheaths using mepivacaine, provided that the injections were performed atraumatically, the needle did not impact onto bone, and that there was no adverse reaction to injection. If any problems arose during or after injection, scintigraphic examination should be delayed. Imaging of the foot should always be delayed for at least 7 days after intrathecal analgesia of the navicular bursa.

WOUNDS, BANDAGE RUBS, LOCAL CONTUSIONS

Rub sores, the result of overtight bandaging, recent soft tissue injuries, and contusions sustained during transport can all result in abnormal RU in pool phase images and sometimes also in bone phase images. There is often diffuse mild IRU which, if in

an area of clinical suspicion, makes interpretation difficult. Occasionally, IRU may be quite marked following trauma to a superficial bony structure such as the tuber ischium, tuber coxae or tuber calcanei.

AVOIDING THE COLD LIMB SYNDROME

The cold limb syndrome in the horse results in markedly reduced uptake of the diphosphonate into bone from the carpus or tarsus distally, or distal to the fetlock, or affecting only the feet, either unilaterally or bilaterally[7]. It is the result of transient ischaemia of unknown aetiology in sites of variable locations in the distal parts of the limbs and may occur in one or more limbs. Poor image quality due to low count rates and poor bone to soft tissue contrast may result in lesions being missed and, although image acquisition times could be increased to compensate, this is frequently impractical. Asymmetrical bone uptake of the radiopharmaceutical between 2 limbs may confuse interpretation and, although modern computer software permits normalisation of images, the problem is not solved. The problem tends to be worse in cold environmental conditions, or when there are large diurnal temperature fluctuations[8]. The problem is not prevented by bandaging the limbs for at least 15 h prior to image acquisition. Poor RU was seen in 20 of 75 horses (27%) in one or both forelimbs, all of which had been bandaged previously. This was associated with poor blood flow to the distal limb, evaluated using vascular phase images[8]. The use of peripheral vasodilating agents does not reliably eliminate the problem[9].

Exercise at trot and canter for 15 mins prior to injection of the diphosphonate has a marked positive effect on both distal limb perfusion and RU into bone[7]. Two hundred and two horses undergoing routine scintigraphic examination between November 1998 and November 1999 were randomly assigned to one of 4 groups: no bandages and no exercise; bandages and no exercise; no bandages and exercise; bandages and exercise. Bandages consisted of a Fybagee wrap[a] covered by a woollen stable bandage, and were applied from immediately distal to the carpus to the coronary band, at least 16 h prior to injection of the radiopharmaceutical. If it was clinically contraindicated to exercise a horse, it was randomly re-assigned to a nonexercise group. Foot surface temperature was measured thermographically prior to injection of the radiopharmaceutical to determine whether uptake could be predicted. There was an association between low environmental temperature and reduced perfusion of the digits. There was a strong positive relationship between foot surface temperature and perfusion and, although cold feet could have good perfusion, it was very unusual for hot feet to have poor perfusion. Foot temperature was influenced by bandaging only in nonexercised horses. Exercise had highly significant positive effects on both distal limb perfusion and RU into bone. Although there was some interaction between bandaging and exercise and RU into bone, bandaging alone had no effect. It is therefore recommended that, whenever practically possible, horses should be lunged at trot and canter for 15 mins prior to injection of radiopharmaceutical, if examination of the regions distal to the carpus and tarsus is to be performed. Walking exercise can also reduce the risk of poor RU into bone, but less reliably.

An alternative approach is to warm the entire horse to improve distal limb circulation, by placing the horse in a heated stable for at least 1 h prior to injection of the radiopharmaceutical and for 2 h afterwards[10]. The effect of exercise (walking) for 30 mins was compared with placing horses in a stable heated using two 2 kW radiant heaters. The horses in the stabled group were injected when the limbs were palpably warm. The time taken to acquire a lateral view of a distal forelimb or hindlimb of 50,000 counts was compared. 50,000 counts were achieved within 50 secs in 18 of 23 horses kept in the hot box, but in only 9 of 38 exercised horses. Therefore, warming the horse may both facilitate rapid image acquisition and help to ensure good image quality.

USE OF A PREPLACED INTRAVENOUS CATHETER

Use of a preplaced jugular catheter should ensure accurate injection of the radiopharmaceutical and provides a conduit for subsequent injections of diuretic and sedative drugs, without having to repeatedly restimulate the horse by needle injections, especially during the period of image acquisition. If the hair coat is fine it is unnecessary to clip, provided that the area is cleansed thoroughly, but if thick, clipping is preferable. If problems are encountered during catheter placement prior to injection and it is necessary to use a second catheter, it is preferable to place it in the opposite jugular vein, since a pre-existing hole in the first side may allow escape of radiopharmaceutical into the local soft tissues, with subsequent very poor distribution elsewhere in the body. It is important that the catheter is sutured or taped in place. It is preferable that the horse is then housed in a stable with a full grill, to avoid displacement of the catheter by the horse rubbing on the door margins.

The use of a catheter is not essential and radiopharmaceutical can be administered by direct needle injection. However, the use of a catheter is recommended, particularly in horses that are difficult to inject.

Inadvertent perivascular injection of a significant proportion of the dose results in very poor distribution of the radiopharmaceutical and images of nondiagnostic quality, due to very low count rates. There will be focal perivascular uptake in the soft tissues around the injection site and uptake in local lymph nodes.

REMOVAL OF THE SHOES

In some circumstances, it is necessary to remove the shoes to obtain adequate solar images of the feet. Egg bar shoes, bar shoes and heart bar shoes all interfere with count acquisition, acting as an effective mask. Therefore, shoes of these types must be removed for solar views. Normal open shoes can be left on, provided that the branches do not shield parts of the bones of the foot. A shoe fitted tightly at the heel may shield RU in the cartilages of the foot in solar images. Comparison of lateral and solar images is crucial to differentiate between RU in the cartilages of the foot, navicular bone or both.

If a foot becomes contaminated with radioactive urine between radiopharmaceutical injection and image acquisition, urine may sometimes track under a shoe, especially a wide-web shoe with a concave solar surface. This contamination can only be removed effectively by removal of the shoe and wiping the foot with a cationic detergent solution, such as

Radiac wash[b]. Sometimes it is even necessary to immerse and scrub the lower part of the foot in a bucket containing Radiac wash solution.

TAPING THE FEET

If images of the feet are required, the feet should be covered with tough impermeable material to prevent urine contamination. This should be done before injection of the radiopharmaceutical, so that personnel are not unnecessarily exposed to radiation immediately after injection. Gaffer tape or Elephant ('Duck') tape[c] are useful products, but a sufficiently thick layer should be applied so that the horse does not wear through it as it walks around the stable in the 2–3 h interval between injection and image acquisition. The tape is removed prior to image acquisition, preferably prior to entering the scintigraphy room.

BANDAGING THE LIMBS

The potential benefits and shortcomings of bandaging the limbs to prevent the cold limb syndrome are discussed above. If images of the limbs distal to the carpus or tarsus are required the limbs should be bandaged from immediately distal to the carpus or tarsus to the level of the coronary band prior to radiopharmaceutical injection, to avoid contamination from radioactive urine. The forelimbs are most at risk in geldings and stallions and the hindlimbs in mares. Mares in season can be particularly problematic. It is suggested that a mare's tail should be folded up and taped, to avoid a contaminated tail swishing and further contaminating the limbs. Avoid standing a horse in a stable without absorbent bedding, since urine splashing is more likely in a stable with rubber mats and minimal bedding. A light rug placed over the horse can protect the trunk if the horse lies down.

USE OF DIURETICS

^{99m}Tc-diphosphonate and ^{99m}Tc-pertechnetate are excreted principally in the urine. Therefore, radioactive urine in the bladder can be a major problem when trying to interpret images of the pelvic region, the coxofemoral and sometimes the stifle joints. Even with the ability to post process images and mask out the region of the bladder, this is inadequate to compensate for significant amounts of urine in the bladder superimposed over, or in close proximity to, a region of interest. It is therefore essential to administer a diuretic to encourage urination at a suitable time between radiopharmaceutical injection and image acquisition. The timing aims to induce urination as soon before image acquisition as possible, so the bladder is as empty as possible, but so that the horse is not stimulated to urinate repeatedly during image acquisition. The alpha-2 agonist sedative drugs themselves have some diuretic activity and this combined with recent administration of a diuretic can make a horse become very restless during image acquisition, because it wants to urinate. Generally, frusemide (Lasix 5%)[d] (0.1mg/kg bwt) is administered intravenously 1.5 h after injection of radiopharmaceutical. In addition, the bladder can be catheterised prior to image acquisition, but great care must be taken to avoid inadvertent contamination of personnel.

We now routinely administer frusemide to all patients, because the use of this standard dose reliably reduces the radiation dose rate of the horse 24 h after injection by approximately 50% compared to without frusemide. Therefore, at 24 h the dose rate of the horse is 0.5 microsieverts/h, equivalent to background level.

TIMING OF RADIOPHARMACEUTICAL INJECTION

For musculoskeletal imaging, vascular, pool (or soft tissue) and bone (or delayed) phase images can be obtained. Vascular images are obtained almost immediately after radiopharmaceutical injection. The time interval between injection and radiopharmaceutical appearing in the limb vasculature varies between horses, ranging from 19 to 123 secs in a series of 270 horses, with a mean of 43 secs[11]. There is also variation of uptake into soft tissues between horses and sometimes between limbs, depending on the symmetry of blood flow. It is generally considered that pool phase images can be obtained between 2 and 20 mins after injection. However, even a difference of 2 mins between acquisition of left and right lateral images can have a large effect on the pattern of uptake. In addition, in the presence of an active bone lesion there is frequently very early uptake of radiopharmaceutical into bone, limiting the sensitivity of pool phase images. Bone phase images are ideally obtained between 2.5 and 4 h after injection of radiopharmaceutical, when bone to soft tissue contrast is highest. Count rates tend to decline after this time.

MANUFACTURERS' ADDRESSES

[a]Fybragate, Leeds, Yorkshire, UK.
[b]Biodex Medical Systems, Atomic Products Corp., Shirley, New York, USA.
[c]The Sellotape Company, Dunstable, Bedfordshire, UK.
[d]Intervet UK Ltd., Milton Keynes, Buckinghamshire, UK.

REFERENCES

1. Ellis, J. and Hollands, T. (2002) Use of height-specific weigh tapes to estimate the bodyweight of horses. *Vet. Rec.* **150**, 632-634.
2. Allhands, F., Twardock, A. and Boero, M. (1987) Uptake of ^{99m}TcMDP in muscle associated with a peripheral nerve block. *Vet. Radiol.* **28**, 181-184.
3. Gaughan, E., Wallace, R. and Kallfelz, F. (1990) Local anesthetics and nuclear medical bone images of the equine forelimb. *Vet. Surg.* **19**, 131-135.
4. Trout, D., Hornof, W., Liskey, C. *et al.* (1991) The effects of regional perineural anesthesia on soft tissue and bone phase scintigraphy in the horse. *Vet. Radiol.* **32**, 140-144.
5. Trout, D., Hornof, W. and Fisher, P. (1991) The effects of intra-articular anesthesia on soft tissue- and bone-phase scintigraphy in the horse. *Vet. Radiol.* **32**, 251-255.
6. Rohs, E., Ueltschi, G. and Lauk, H. (1994) Untersuchungen zur lokalen interaktion zwischen lokalanasthetika und ^{99m}Tc-DPD. *Pferdheilkunde* **10**, 289-300.
7. Dyson, S., Lakhani, K. and Wood, J. (2002) Factors affecting blood flow in the equine digit and their effect on uptake on ^{99m}technetium methylene diphosphonate into bone. *Equine vet. J.* **33**, 591-598.
8. Dyson, S. (1999) Observations on nuclear scintigraphic examination of the equine foot: an investigation of factors which may influence blood flow to the equine digit. In: *Proceedings of the 6th Geneva Congress on Equine Medicine and Surgery*. pp 71-72.
9. Ueltschi, G. (1997) Personal communication.
10. Jones, N. and Bladon, B. (2001) Halogen radiant heaters reduce circulatory cut-off during gamma scintigraphy. In: *Proceedings of the 10th British Equine Veterinary Association Congress*. p 44.
11. Dyson, S. Unpublished data.

Chapter 7

PRACTICAL SCINTIGRAPHIC EXAMINATION OF THE HORSE

ROB C. PILWSORTH and SUE J. DYSON

Rossdale & Partners, Beaufort Cottage Stables, High Street, Newmarket, Suffolk CB8 8JS, UK.
Centre for Equine Studies, Animal Health Trust, Lanwades Park, Kentford, Newmarket CB8 7UU, UK.

In order to carry out any scintigraphic examination, whether orthopaedic imaging or other forms of targeted imaging, it is necessary to bring together the horse and a gamma camera. Unlike in human medicine, we have a noncompliant patient that may be apprehensive of such a large piece of equipment, and the noise involved in moving it around. There are several practical steps that can be taken to facilitate safe and relatively straightforward handling of the horse during scintigraphic examination. These have obvious benefits to the horse, but also enhance the safety of both personnel and the expensive and delicate equipment that was never designed to come into contact with a horse.

RESTRAINT

Manual Restraint

A headcollar and lead does not give sufficient control to ensure safety. A bridle or chain shank, looped through the headcollar and across the nose, should always be employed. All other restraint necessary for scintigraphic examinations should rely on sedation rather than the use of twitches, lip chains etc., as these present a real hazard, both to the equipment and to personnel involved in scanning procedures

Physical Restraint

Some clinicians prefer the use of stocks to confine the patient, with removable sections to allow access of the gamma camera. The stocks stop the horse shuffling away from the camera head as it is moved, and can also limit movement of the horse if it panics. However, moving sections of the stocks to permit access of the gamma camera makes the examination slower.

Chemical Restraint

The ideal sedative combination results in profound sedation without ataxia. Unfortunately, it is rarely possible to achieve this ideal. Horses vary in the degree of sedation they require for safe and speedy examination. Some clinicians prefer that horses should always be admitted to the clinic the day before scintigraphic examination so that they are more settled at the time of examination, and their temperament can be evaluated more fully prior to sedation.

All drugs are given intravenously so that the dose can be carefully tifrated to effect. A good compromise in sedation vs.

Figure 1

A horse wearing half-cup blinkers which are useful in screening the patient from movements of the gamma camera. Note the use of a free-standing chin rest, used for imaging the neck to avoid respiratory movement.

ataxia is a combination of detomidine and butorphanol. An initial sedative dose of 0.3 ml detomidine (Domosedan)[a] (10 mg/ml formulation) and 0.6 ml butorphanol (Torbugesic Injection)[b] (10 mg/ml formulation) per 450 kg horse is a satisfactory start. This works out at 0.0066 mg/kg bwt detomidine and 0.013 mg/kg bwt butorphanol. The weight assessment of the horse used for calculation of the technetium dose can be used to predict sedative requirements accurately.

In our experience, horses that still show anxiety towards the presence and noise associated with the equipment often respond well to injection of 10 mg acetylpromazine (ACP Injection)[c] (10 mg/ml formulation). This appears to reduce anxiety, without producing marked ataxia. Increasing doses of detomidine and butorphanol can be used, but this often results in a marked increase in ataxia once the initial dose levels have been passed. For long scintigraphic procedures, incremental doses of detomidine and butorphanol may be necessary, at approximately one third of the initial dose. However, these almost always result in further sudden 'sagging' of the horse,

Figure 2

a) *A head rest (after Neuwirth and Romine)[3] attached to the gamma camera.* ***b)*** *The head rest in use to eliminate motion in imaging the head.*

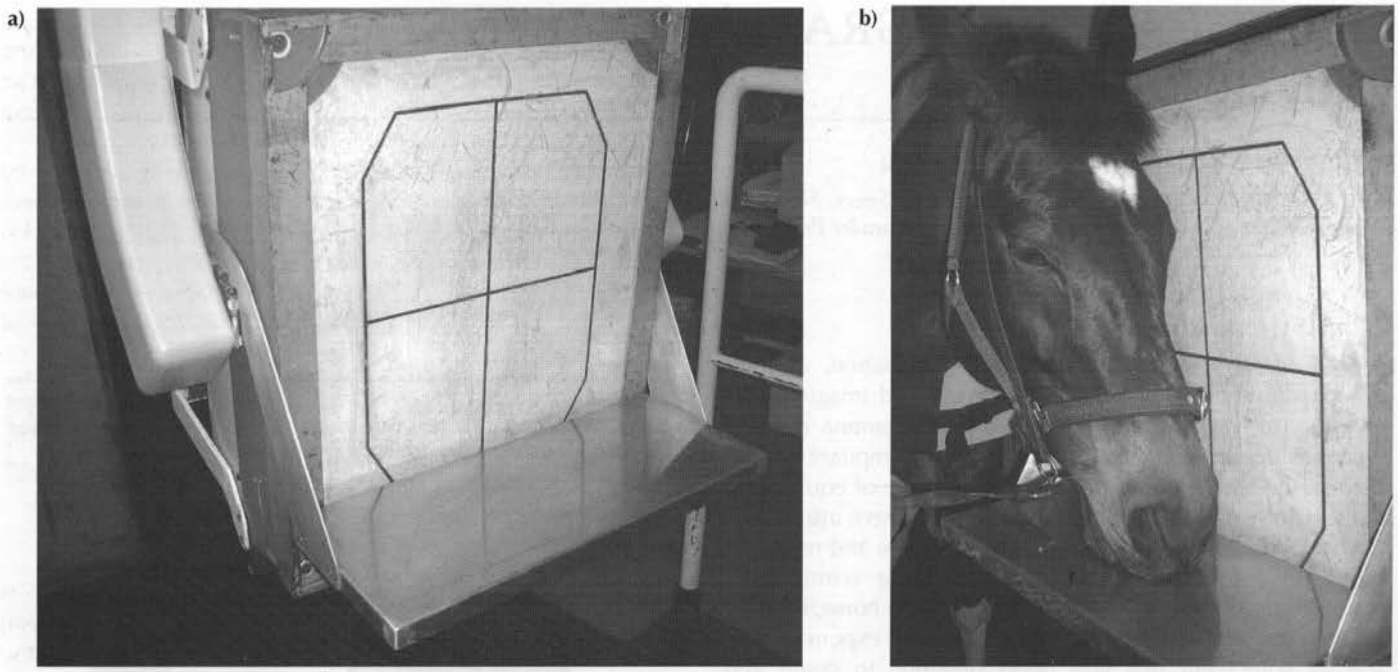

which will ruin partially acquired images, approximately 1–2 mins after injection as the sedative takes full effect. Therefore, after top-up doses, scintigraphic examination should be discontinued for approximately 3 mins to allow full sedation.

Some clinicians use an alpha-2 agonist alone (detomidine or romifidine) because of the difficulty of lifting feet for solar views in a heavily sedated horse (see *Part I, Chapter 8*). This, however, must be weighed against the risk of sudden unexpected kicking in response to inadvertent touching of the legs, which has been well documented when alpha-2 agonist drugs are used in isolation. If the solar views are left to the end of the examination, prior administration of both detomidine and butorphanol is not usually a problem.

There are also less conventional drug combinations which are reported to have excellent sedative properties, with less ataxia and rocking; e.g. a mixture of acetylpromazine, romifidine and morphine given as follows: acetylpromazine 0.3 mg/kg bwt, followed 30 secs later by romifidine 0.05 mg/kg bwt, then followed 10 mins later by morphine 0.1 mg/kg bwt[1]. Additional incremental doses of romifidine (0.025 mg/kg bwt) can be administered as required. However, the use of a strictly controlled drug (morphine) creates additional paperwork.

An alternative is a combination of detomidine (0.015 mg/kg bwt) and acetylpromazine (0.04 mg/kg bwt) administered concurrently, which is reported to give good sedation with minimal ataxia[2].

Behavioural Procedures

Horses which are apprehensive of the movement of the gamma camera behind their heads and around their quarters can be helped by fitting half cup blinkers (**Figure 1**). Those which are particularly bothered by the noise of the chain hoist or hydraulics involved in moving the camera often respond well to the insertion of gauze-wrapped cotton wool plugs into both ears. These must be removed at the end of the procedure! If both the fore- and hindlimbs are to be examined, it may be preferable to start with the forelimbs while the horse becomes accustomed to the movement of the camera.

A mare that is in season may prove to be particularly difficult to position since, when the camera comes into contact, the mare may lean against it. She may also squirt urine episodically, resulting in localised contamination. Contamination of the tail may present a particular problem, since contamination may become widely dispersed if the mare flicks her tail. Bandaging the tail in a tied-up position may therefore be beneficial.

POSITIONING AIDS

Certain examinations are best performed using mechanical aids to prevent or minimise movement of the horse during image acquisition. The head is notoriously difficult to image well in a free-standing horse because sedated horses often have a recurrent cyclical head droop. Holding the head manually should be resisted because of the resultant radiation dose to the handler. A simple chin rest allows good static images of the head (**Figure 2**)[3]. Obviously, the exact design of this depends on the configuration of the gamma camera head, but all cameras should be able to have a chin rest adapted to fit. For lateral scintigraphic examination of the cervical spine, an adjustable, free-standing chin rest is an effective way of preventing head movements (**Figure 1**). A V-shaped wooden support can be constructed to stabilise the foot and reduce the chance of it sliding on the camera during acquisition of solar views[3].

CAMERA POSITIONING AND SHIELDING

An organised system of scintigraphic examination should be rehearsed and carried out methodically. While each clinic will have its preference for the order of image acquisition, once a

Figure 3

Free-standing half-curved lead divider used to image a single limb, screening out the contralateral limb.

pattern has been established, it should be adhered to so that the examination is completed as speedily as possible. This helps to reduce the radiation dose received by staff during scintigraphic examinations. The horse should be moved minimally during the examination, because movement tends to arouse the horse from a stable degree of sedation. If facilities are available for image co-registration with x-ray images, then the limb position for scintigraphic imaging must closely match that for the radiographic projection, e.g. for a lateral view of a metacarpo- or metatarsophalangeal joint the limb should be bearing full weight, with the metacarpal or metatarsal region positioned vertically.

When imaging the distal parts of the limb, the opposite limb must be shielded from the view of the camera. The contralateral limb is too far from the camera to have acceptable resolution and adds counts that provide no useful information. Also, γ-rays from the hindlimbs must be shielded when acquiring dorsal views of the forelimbs. Similarly, the forelimbs must be shielded when acquiring plantar images of the hindlimbs. The neck should be shielded when acquiring dorsal views of the head. The use of free-standing lead screens between the fore- and hindlimbs allows for single limb imaging of the distal limb (**Figure 3**)[3]. For the more proximal joints (tarsus upwards) the horse's stance has to be adjusted so that the limb under investigation is advanced cranially when compared to that not required in the image, or a lead rubber screen can be used. For joints such as the elbow, a lead rubber screen must be used, held wrapped around the medial aspect of the contralateral elbow because separation of these joints is difficult. Fortunately, the chest provides good attenuation of the γ-rays from the distal aspect of the contralateral humerus. For the shoulder joints and scapulae and the coxofemoral joints, there is sufficient attenuation of signal between the two sides that superimposition is usually not a problem.

Flexed lateral views are often useful in discriminating between the exact site of increased uptake in the carpus and metacarpo- or metatarsophalangeal joints. A padded 'rest' can be used for the carpus. For the fetlock joints, the toe of the foot can be placed in a radiography positioning block.

Solar (palmar) views of front feet are readily acquired by positioning the foot to be examined on the gamma camera which is positioned horizontally. The limb should be extended to avoid superimposition of the fetlock and pastern and the horse's head moved to one side so that it does not contribute to counts. A lead apron may be placed over the distal part of the limb.

Solar (plantar) views of hind feet are achieved most readily with the gamma camera positioned vertically and the foot held against the camera, supported on blocks of suitable height. The contralateral hindlimb should be shielded.

PERSONNEL REQUIREMENTS

The minimum team to carry out scintigraphic examination is three people. One person holds and controls the horse, one moves the gamma camera and the third person runs the acquisition station or computer. It is dangerous to leave an unattended gamma camera adjacent to a horse; therefore, one person should not both control the camera and run the acquisitions. Full concentration has to be given to the horse by the person responsible for moving the gamma camera so that rapid evasive action can be taken if needed. Some computers have a remote start and stop capability which theoretically means that one person can control both the camera and the computer, but in practice this markedly slows acquisition. Ideally, the computer work station should be positioned some distance from the examination area to reduce the radiation dose to the computer operator. The gamma camera itself often shields the body of the camera operator. The horse holder potentially receives the biggest dose of radiation and protective measures such as those described in *Part I, Chapter 12* should be followed to minimise this dose.

MANUFACTURERS' ADDRESSES

[a]Pfizer Limited, Sandwich, Kent, UK.
[b]Fort Dodge Animal Health, Hedge End, Southampton, UK.
[c]Vericore, Novartis Animal Health UK Ltd, Litlington, Hertfordshire, UK.

REFERENCES

1. Walmsley, J.P. (2002) Personal communication.
2. Nelson, A. (2002) Personal communication.
3. Neuwirth, L. and Romine, C. (2000) Ancillary equipment to increase quality and reduce radiation exposure in the equine nuclear medicine laboratory. *Vet. Radiol. Ultrasound* **41**, 470-475.

Chapter 8

ORTHOPAEDIC IMAGING

SUE J. DYSON and JO WEEKES
Centre for Equine Studies, Animal Health Trust, Lanwades Park, Kentford, Newmarket, Suffolk CB8 7UU, UK.

PRINCIPLES OF MUSCULOSKELETAL IMAGING

^{99m}Tc polyphosphonate radiopharmaceuticals have a high degree of incorporation into bone and are rapidly cleared from the soft tissues, giving good quality bone images. Hydroxymethylene diphosphonate (HMDP) is cleared from the blood slightly more quickly than methylene diphosphonate (MDP), but the latter is usually cheaper and has more widespread availability. For studies evaluating only pool or soft tissue phase images, ^{99m}Tc-pertechnetate is preferable because it does not bind to areas of rapidly remodelling bone, and therefore interpretation is not confounded by early bone radiopharmaceutical uptake (RU), which can occur within minutes of injection of ^{99m}Tc-MDP. Usually, however, information about both soft tissues and bone is required and, if pertechnetate is used, a delay of at least 24 h is required before repeating imaging using MDP, to allow time for decay and clearance of most of the pertechnetate.

The musculoskeletal scan can be divided into 3 phases: vascular or first pass; pool or soft tissue; and bone, osseous or delayed.

Vascular Phase

After intravenous injection, ^{99m}Tc-diphosphonate is first distributed in the vessels and vascular images are obtained as soon as radiopharmaceutical is seen in the area being imaged. This takes approximately 20–70 secs in most horses. Dynamic images are obtained at 1 or 2 sec intervals for up to 90 secs. Obviously, the horse must be positioned adjacent to the gamma camera prior to radiopharmaceutical injection. Only one area can be imaged. With a large field of view (FOV) (i.e. 500 mm diameter) camera, dorsal views of a selected region of both forelimbs or plantar views of both hindlimbs can be obtained simultaneously, but only a single lateral view can be obtained, unless 2 gamma cameras are available for simultaneous bilateral image acquisitions. Physiological changes, such as local variations in capillary bed recruitment or regional changes of flow in large vessels, influence the vascular phase images. Blood flow may be markedly reduced either unilaterally or bilaterally in some horses with 'cold limbs' and there will be a predictable poor uptake of ^{99m}Tc-diphosphonate into bone (see *Part I, Chapter 6*). Decreased blood flow due to vascular infarcts or severe soft tissue trauma may result in reduced distribution of the radiopharmaceutical. Reduced perfusion of regions of the foot may be seen in association with laminitis. Increased blood flow may be associated with acute inflammation, infectious osteitis or osteomyelitis or, rarely in the horse, tumours. Dorsal images of the pelvic region can be used to assess blood flow in the terminal aorta and iliac arteries (see *Part II, Chapter 6*). With dual camera acquisitions, evaluation of blood flow in the femoral arteries can also be assessed[1]. Thus diagnosis of suspected aortoiliacofemoral thrombosis can be substantiated[2,3].

Pool Phase

Phase II, or the pool or soft tissue phase, represents the distribution of the radiopharmaceutical in the capillary bed and extracellular fluid, but within a few minutes there is also uptake into bone, the intensity of which depends on the local activity of the bone. Therefore, phase II is not specific for soft tissues and early bone uptake can confound interpretation. Early bone uptake is most likely to occur with relatively acute lesions. Phase II lasts until the bone image is discernible, which usually takes between 10 and 20 mins, but uptake in both soft tissue and bone changes quite quickly and comparison between 2 limbs is not easy unless images are obtained simultaneously. The first image should be obtained approximately 2 mins after injection. Images are best obtained for a preset time because there is too much variability in uptake to rely on preset total counts for the image. The contralateral limb should be examined as soon as possible after the first limb for meaningful comparisons to be made. It may be useful to repeat both sides immediately to follow the progression of uptake. Bone uptake starts to dominate within 10–20 mins; therefore, pool phase images are usually restricted to a single site.

Phase II is not particularly sensitive to soft tissue injuries and a negative result does not preclude the presence of a significant soft tissue injury. Of 33 horses with proximal suspensory desmitis (PSD) confirmed ultrasonographically, and for which pool phase images were obtained, only 7 had detectable abnormalities of soft tissue RU[4]. It must be borne in mind that relatively intense RU in muscle in the antebrachium or crus may mask a much lesser degree of uptake in the proximal metacarpal or metatarsal region. Masking out the muscle area (see *Part I, Chapter 5*) may reveal abnormal uptake. In some horses with acute tendon or ligament damage, abnormal uptake in pool phase images is readily seen; however, care must be taken not to confuse it with RU in an adjacent vascular plexus. This is common in the distal third of the metacarpal region. Marked RU in the coronary plexuses may mask abnormal RU in the pastern or foot regions. Radiopharmaceutical may persist in distal limb veins for up to 15 mins, confounding interpretation of pool phase images. Recently performed local analgesic techniques can also confound interpretation of pool phase images (see *Part I, Chapter 10*).

The amount of radiopharmaceutical accumulating in the extracellular fluid depends on the rate of vascular delivery, autonomic tone in the local area, rate of diffusion into and out of the local extracellular fluid space and the size of that space. Lateral pool phase images of the foot have been useful in the detection of abnormal uptake in the region of the deep digital flexor tendon (DDFT), which has correlated with lesions confirmed during bursoscopy of the navicular bursa, using magnetic resonance imaging (MRI), or at *post mortem* examination[5,6]. Muscle uptake in horses with recurrent exertional rhabdomyolysis is often normal in pool phase images, but in some affected horses is abnormal in the bone phase images.

When clinical examination and the use of diagnostic analgesia have localised pain specifically to a region, maximum information about this area can be obtained by combining vascular, pool and bone phase images. Ideally, both dorsal or plantar and lateral pool phase images should be obtained, with the shortest possible time interval between obtaining the lateral images of the left and right limbs.

Bone Phase

Bone phase imaging should start 2–3 h after injection of the radiopharmaceutical, by which time there will be good uptake in bone, with reasonable clearance from the soft tissues. However, if there is poor uptake in bone, as may occur in older horses, greater than approximately 15 years of age, the definition between the bone and soft tissues will be poor. The diphosphonate binds to hydroxyapatite crystals, the inorganic component of bone, and uptake is determined by delivery of the radiopharmaceutical to bone (i.e. blood flow) and by its deposition, influenced by changes in capillary permeability, local extracellular fluid volume and the available bone crystal surface area. Subnormal blood flow limits delivery of diphosphonate to bone, but at normal and higher rates of blood flow, uptake is determined by the available bone crystal area. Mild increases in RU may reflect increased blood flow, but intense activity reflects abnormal bone turnover. Binding sites are exposed under normal and pathological conditions in areas of actively modelled bone and in soft tissues undergoing mineralisation. Uptake occurs by chemical adsorption onto, and by direct integration into, the crystalline structure[7]. However, in rat models, ^{99m}Tc has also been shown to be incorporated into the organic matrix of bone[8-10]. Bone turnover involves both resorption, mediated by osteoclasts, and bone formation, mediated by osteoblasts. Accumulation of radiopharmaceutical is predominantly mediated by osteoblastic activity, although other mechanisms may exist, since positive bone scans may be seen in people with osteomalacia, in which there is high matrix turnover but failure of mineralisation[11]. In experimental models, maximum RU occurred 8–12 days after injury[12]. Periarticular regions have increased radiopharmaceutical uptake (IRU) compared with diaphyseal regions of long bone due to greater amounts of cancellous bone. Physes with active osteogenesis have intense RU.

Abnormal RU into bone can be described as mild, moderate or intense, and diffuse or focal; although it is usually a region of increased uptake, areas of reduced uptake can also be seen due to acute bone infarction, thrombosis, or sequestrum formation. It is vitally important to recognise that IRU does not necessarily reflect a pathological lesion, and is not necessarily associated with a source of pain causing lameness.

INDICATIONS FOR NUCLEAR SCINTIGRAPHY

Since abnormal RU can be seen unassociated with a painful lesion causing lameness, it is important that nuclear scintigraphy is not used as a substitute for comprehensive clinical examination and other basic tools of lameness diagnosis such as local analgesia, radiography and ultrasonography. Images must be interpreted in the light of all other available information. It is also important to recognise that many lesions causing lameness are not associated with scintigraphic abnormalities. It is vitally important to recognise that a negative bone scan does not mean that the areas that have been examined are therefore not the source of the problem causing lameness. For example, 19 of 30 (63%) horses with hindlimb PSD had a negative bone scan of the proximal metatarsal region[4].

PRINCIPLES OF IMAGE ACQUISITION

Indications for nuclear scintigraphic examination include:

- Localisation of pain to a region, but inability to identify a potential cause of pain using radiography and ultrasonography. In this situation, a targeted 3 phase examination should be performed.
- Assessment of the possible significance of equivocal radiological abnormalities.
- Acute onset of lameness and clinical suspicion of a fracture, or stress-related bone injury that cannot be identified radiographically.
- Failure to localise the source of pain using local analgesic techniques.
- Inability to perform local analgesic techniques safely due to the dangerous behaviour of the horse.
- Lameness in several limbs, which may make local analgesic techniques difficult to interpret if blocks in one limb are wearing off when those in another limb are taking effect.
- A racehorse with a history of lameness at high speeds, which is not currently lame but is suspected of having stress-related bone injury. These horses may have more than one focus of injury, and whole body examination may be justified.
- Intermittent lameness that cannot be reproduced in order to perform local analgesic techniques satisfactorily.
- Suspected thoracolumbar or pelvic region pain.
- Poor performance of ill-defined cause.
- Monitoring repair.

The examination should be as focused as possible. Obviously this is not always achievable and, with a hindlimb lameness which does not respond to local analgesic techniques, examination of the entire hindlimb and pelvic region may be justified. Whole body screening is time-consuming and often unrewarding and potentially exposes personnel to unnecessary levels of radiation. Even with a horse presenting with a history of poor performance, a comprehensive clinical examination, including ridden exercise, should be performed by an experienced clinician used to dealing with that type of sports horse. This usually allows a more targeted scintigraphic examination to be performed.

It is important to recognise the limitations of nuclear scintigraphy. While scintigraphy is very sensitive to stress-

Figure 1

Lateral bone phase images of the right front distal limb of a 10-year-old Warmblood dressage horse. Matrix size 256 x 256. The images were obtained with the gamma camera at variable distances from the foot; ***a)*** *0 cm,* ***b)*** *10 cm and* ***c)*** *20 cm. Note the inferior resolution in (b) and (c) compared to (a).*

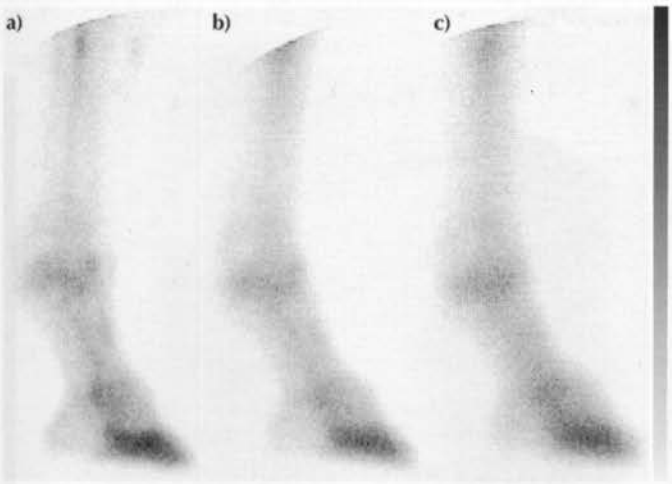

resulted bone injury, fractures and subchondral bone trauma, it is not necessarily a sensitive indicator of osteoarthritis (OA), except in joints such as the centrodistal (CD) and tarsometatarsal (TMT) joints, when there may be extensive involvement of subchondral bone even early in the disease process, or when there is active periarticular new bone formation, or advanced end-stage disease with subchondral bone involvement. With very low-grade lameness associated with low-grade joint disease, scintigraphy is often negative, especially if the horse is not in regular work. A horse may have obvious lameness associated with pain arising from the proximal or distal interphalangeal joints, with extensive periarticular osteophyte formation, with relatively normal RU. Osteochondrosis (OC) lesions of the trochlear ridges of the femur or the distal intermediate ridge of the tibia are often scintigraphically silent, whereas OC of the scapulohumeral joint is generally associated with IRU. It has previously been suggested that subchondral bone cysts (SBCs) or other osseous cyst-like lesions (OCLLs) may be scintigraphically silent. This may reflect failure to obtain sufficient counts to demonstrate the lesion or failure to obtain 2 views of the area. An SBC in the medial femoral condyle may be masked by uptake in the overlying lateral condyle and soft tissues unless sufficient counts are obtained. The medial femoral condyle is some distance from the gamma camera, is shielded by intervening muscle and bone, and therefore contributes substantially less radiation than the closer lateral condyle. In my experience, with good image quality, SBCs and other OCLLs are almost invariably associated with IRU. However, some OCLLs in the foot have had normal RU despite causing lameness. This may be related to the stage of cyst formation.

Following acute injury to bone, abnormal scintigraphic images are usually obtained within 12 h to 3 days; however, false negative results may be obtained occasionally. This is particularly true for ilial or acetabular fractures, when a positive result may not be apparent until 10–14 days after injury. Mild IRU may be shielded by the large overlying muscle mass. Therefore, if an ilial or acetabular fracture is suspected on clinical grounds, and a bone scan obtained within a few days of injury is negative, then the examination should be repeated after approximately 10 days.

Patient preparation is discussed in *Part I, Chapter 6*. A general purpose collimator is used for acquisition of images of the appendicular skeleton, head, neck and pelvic region, but superior quality images of the thoracolumbar region can be obtained using a high resolution collimator. The large overlying muscle mass results in scattered radiation and image quality is enhanced by reduction of scatter using the high resolution collimator (see *Part I, Chapter 5, Figure 1*). However, use of the high resolution collimator requires longer acquisition times in order to get a sufficient number of counts, since a higher proportion of scattered radiation is being removed. During earlier years of equine scintigraphy, most bone scans were obtained as static acquisitions but, with the development of motion correction software, superior quality images can be obtained using dynamic acquisitions and subsequent motion correction (see *Part I, Chapter 5*). Dynamic acquisition and motion correction is preferable for all images proximal to the metacarpophalangeal (MCP) and metatarsophalangeal (MTP) joints. Serious errors in interpretation of images of the sacroiliac (SI) joint region may occur without the use of motion correction[13].

Standardisation of position of the horse is useful to facilitate subsequent image analysis. For example, in order to accurately quantify differences between lateral images of the hocks, the hocks must be similarly positioned. Although post processing software often permits image inversion and rotation, if one image was obtained with the limb extended behind the body and the other with the limb extended forward, the 2 images cannot be mirrored. It is therefore preferable that images should be obtained with the limb underneath the body with the metacarpal region or metatarsal region in a vertical position. Standardisation of positioning is also helpful when a radiographic image is to be superimposed over a scintigraphic image to facilitate accurate anatomical localisation of a lesion identified scintigraphically.

When obtaining lateral images, it is essential to shield the contralateral limb from the gamma camera by holding a piece of lead rubber, at least 20 x 40 cm, between the limbs, or by using a free-standing lead sheet. When obtaining dorsal or cranial views of the forelimbs or plantar or caudal views of the hindlimbs, it is important to shield the hindlimbs and forelimbs, respectively, using a lead rubber screen with a minimum lead equivalent of 3 mm. The gamma camera must always be positioned as close to the limb as possible, but equidistant from both the left and right limbs for lateral views. For dorsal views of the carpus and more distal parts of the limb, or for plantar views of the tarsus and more distal parts of the limb, both limbs can usually be imaged simultaneously using a large FOV camera (500 mm diameter). However, cranial views of the left and right elbow and shoulder and caudal views of the stifle must be obtained separately. Care must be taken to position the camera

at a similar angle and distance from the limb for accurate comparisons between limbs. Increasing the distance between the subject and the camera results in loss of image resolution because more collimator holes become available to γ-ray penetration and, although the count rate stays the same, it is spread over a larger area of crystal surface (**Figure 1** and *Part I, Chapter 3, Figure 12*).

To obtain dorsal or plantar and lateral views of the distal extremities, it is necessary to either position the gamma camera below ground level, using a pit, or raise the horse onto a platform (see *Part I, Chapter 4*). Solar views of the front feet are obtained by positioning the gamma camera horizontally on the floor, and placing the foot to be examined on the camera, with the limb extended. The foot should be shielded with lead to mask radiation emanating from the more proximal parts of the limb. Two overlapping human lead thyroid protectors can be used for this purpose. The horse's head and neck should be held away from the limb being examined. To obtain solar views of a hind foot, the camera is positioned vertically, resting on the floor. The foot is held in the shoeing position, with the sole in contact with the camera. Supporting the toe on a wooden block or blocks helps to minimise movement.

Images can either be obtained over a set time, for example 2 mins for a static acquisition, or 35 2-sec frames for a dynamic acquisition, or a predetermined total number of counts can be acquired. It is important to recognise that an adequate number of counts must be obtained to acquire images which contain enough information for statistical significance. Ideally, a total count of at least 150,000–200,000 is required for detection of significant abnormalities in skeletally mature horses. Lower total counts result in lesions being missed. However, in skeletally immature horses a total count of 100,000–150,000 is usually adequate. When acquiring images using a preset acquisition time, it is essential to recognise when there is low RU in bone and to increase acquisition times accordingly. Low RU in bone results in images with poor contrast between soft tissues and bone and thus poor bone detail. It is a particular problem in old horses, in which there is reduced RU into bone[14]. In fat horses, more radiopharmaceutical in the thick mass of overlying soft tissues and increased scattered radiation reduce image contrast (**Figure 2**). The increased distance between bone and the gamma camera also results in poor contrast between bone and soft tissues. Poor RU into bone is also a problem in horses with 'cold limb' syndrome (see *Part I, Chapter 5*), when a variable proportion of the distal limbs may have poor uptake, either unilaterally or bilaterally (**Figure 3**). Although many modern software programmes allow normalisation of images so that images of the left and right limbs can be matched up, if there are vast differences in RU, image interpretation can still be severely confounded. If this is recognised during image acquisition then it may be preferable to markedly increase the scan time in the cold limb, to obtain more similar count rates in each limb, but this should be noted and recorded.

Focal areas of IRU are sometimes seen throughout a lame or a nonlame limb[15] (**Figure 4**). This may confound interpretation. A diffuse decrease in RU in lame limbs has also been described, possibly attributable to a compensatory increase in uptake in the sound limb due to uneven loading[16]. If there is a proximal lesion with intense IRU, the more distal parts of the limb may be cold[17,18], possibly due to reduced weightbearing (**Figure 5**). However, intense IRU in the foot is sometimes associated with

Figure 2

Dorsal bone phase image of the carpi of an overweight 8-year-old Warmblood of 672 kg bwt. Matrix size 256 x 256. Note the poor contrast between the bone and soft tissues because of the large amount of radiopharmaceutical in the soft tissues. There is mild IRU associated with a clinically quiescent exostosis on the medial aspect of the left third metacarpal bone.

generalised reduction in uptake in the more proximal parts of the limb (**Figure 6**). It has been suggested that asymmetrical RU throughout forelimbs may reflect vascular asymmetry attributable to pain or increased weightbearing[19]. However, in a prospective study of 202 horses undergoing routine scintigraphic examination of the forelimbs, there was no relationship between RU in the distal part of the limb and the lame limb[14].

WHICH IMAGES ARE NECESSARY?

The number of images obtained is dictated by the clinical presentation of the horse. If pain has been localised to the foot, it is useful to obtain dorsal vascular phase images, dorsal and lateral pool phase images and dorsal, lateral and solar bone phase images. 'Survey' images of the forelimbs should include dorsal and lateral images of the fetlocks and feet, dorsal and lateral views of the carpi, and lateral views of both the elbows and shoulders. In a young horse susceptible to stress-related bone injury, lateral views of the scapulae should be included. If abnormalities of either the elbow or shoulder regions are identified, cranial views may give additional information. The views described above should between them also include the long bones. In a horse with forelimb lameness unaffected by comprehensive local analgesic techniques, examination of the neck and cranial thoracic vertebrae, cranial ribs and sternum may also be indicated. 'Survey' images of the hindlimbs should

Figure 3

a) *Dorsal bone phase images of the distal aspect of the forelimbs of a 9-year-old Warmblood showjumper. Matrix size 256 x 256. There is poor RU throughout the distal aspect of the right forelimb and distal to the metacarpophalangeal joint in the left forelimb. This is due to inadequate blood flow to the distal parts of the limbs.* ***b)*** *Dorsal and lateral pool phase images and dorsal bone phase images of the distal aspect of the forelimbs of a 6-year-old Warmblood dressage horse. Matrix size 256 x 256. There is poor RU unilaterally in the left forelimb in both the pool and bone phase images. The pool phase images of the left forelimb resemble vascular phase images.*

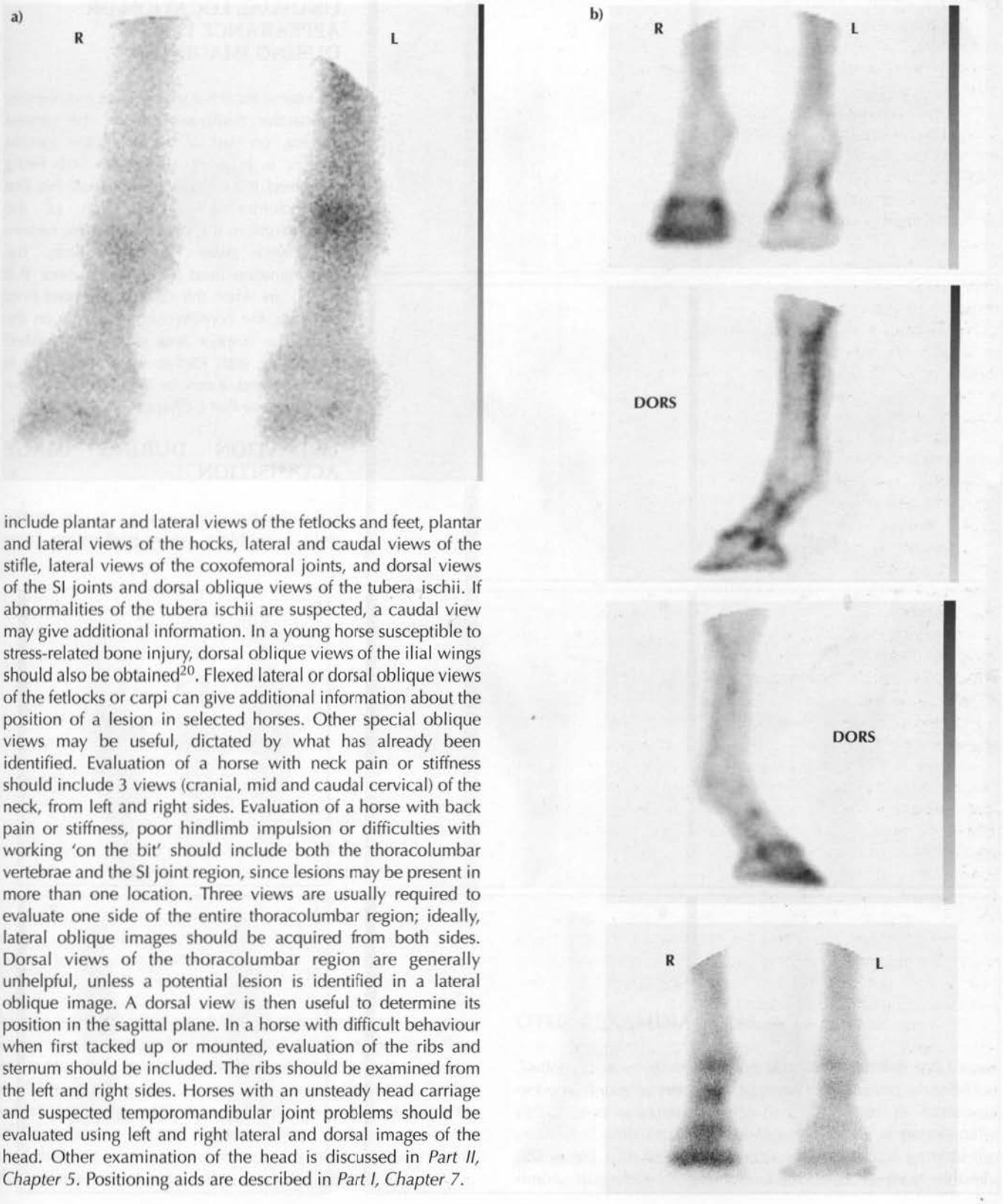

include plantar and lateral views of the fetlocks and feet, plantar and lateral views of the hocks, lateral and caudal views of the stifle, lateral views of the coxofemoral joints, and dorsal views of the SI joints and dorsal oblique views of the tubera ischii. If abnormalities of the tubera ischii are suspected, a caudal view may give additional information. In a young horse susceptible to stress-related bone injury, dorsal oblique views of the ilial wings should also be obtained[20]. Flexed lateral or dorsal oblique views of the fetlocks or carpi can give additional information about the position of a lesion in selected horses. Other special oblique views may be useful, dictated by what has already been identified. Evaluation of a horse with neck pain or stiffness should include 3 views (cranial, mid and caudal cervical) of the neck, from left and right sides. Evaluation of a horse with back pain or stiffness, poor hindlimb impulsion or difficulties with working 'on the bit' should include both the thoracolumbar vertebrae and the SI joint region, since lesions may be present in more than one location. Three views are usually required to evaluate one side of the entire thoracolumbar region; ideally, lateral oblique images should be acquired from both sides. Dorsal views of the thoracolumbar region are generally unhelpful, unless a potential lesion is identified in a lateral oblique image. A dorsal view is then useful to determine its position in the sagittal plane. In a horse with difficult behaviour when first tacked up or mounted, evaluation of the ribs and sternum should be included. The ribs should be examined from the left and right sides. Horses with an unsteady head carriage and suspected temporomandibular joint problems should be evaluated using left and right lateral and dorsal images of the head. Other examination of the head is discussed in *Part II, Chapter 5*. Positioning aids are described in *Part I, Chapter 7*.

Figure 4

Bone phase images of both hindlimbs of a horse with right hindlimb lameness. Matrix size 256 x 256. The images have been normalised. Note the IRU throughout the epiphyseal and metaphyseal regions of many bones of the right hindlimb from the stifle distally. This confounds interpretation. There is no indication of the site of a possible pathological lesion. The horse had a tear of the lateral meniscus of the femorotibial joint.

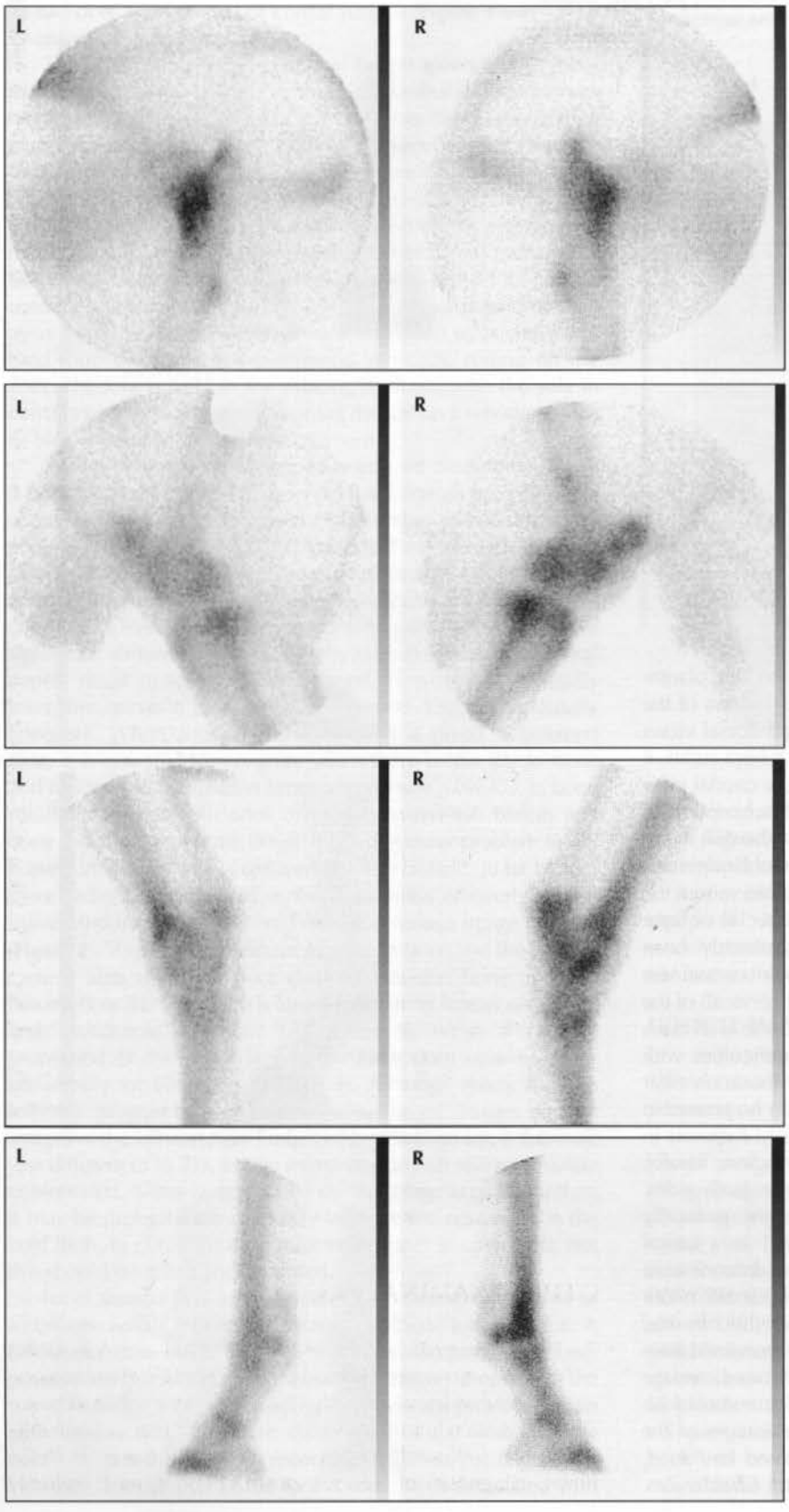

WHAT TO DO IF A HOT SPOT OF UNUSUAL LOCATION OR APPEARANCE IS SEEN DURING IMAGING

An intense focal hot spot may represent either radioactive contamination on the gamma camera, on part of the pit if the gamma camera is in a pit, or on the limb being examined. It is important to eliminate this, first by determining the location of the contamination. If it persists when the camera is moved away from the limb, the contamination must be on the camera. If it disappears when the camera is moved from the limb, the contamination must be on the limb. The suspect area should be washed thoroughly with Radiac wash[a]. If a foot is contaminated, it may be necessary to remove the shoe (see *Part I, Chapter 6*).

URINATION DURING IMAGE ACQUISITION

Urination during image acquisition is usually only a problem when performing large

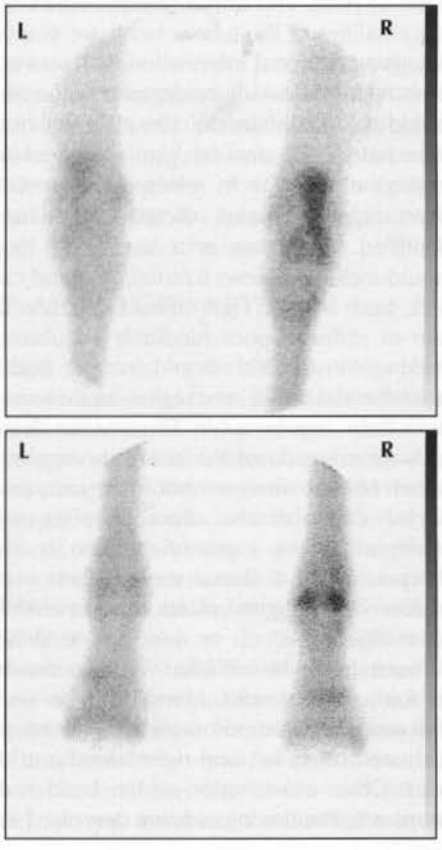

Figure 5

Lateral bone phase images of the shoulder and carpi of a 2-year-old Thoroughbred with right forelimb lameness. Matrix size 256 x 256. There is intense focal IRU in the right humeral tubercles. Note the generalised reduction in RU in the carpus of the lame right forelimb compared to the left.

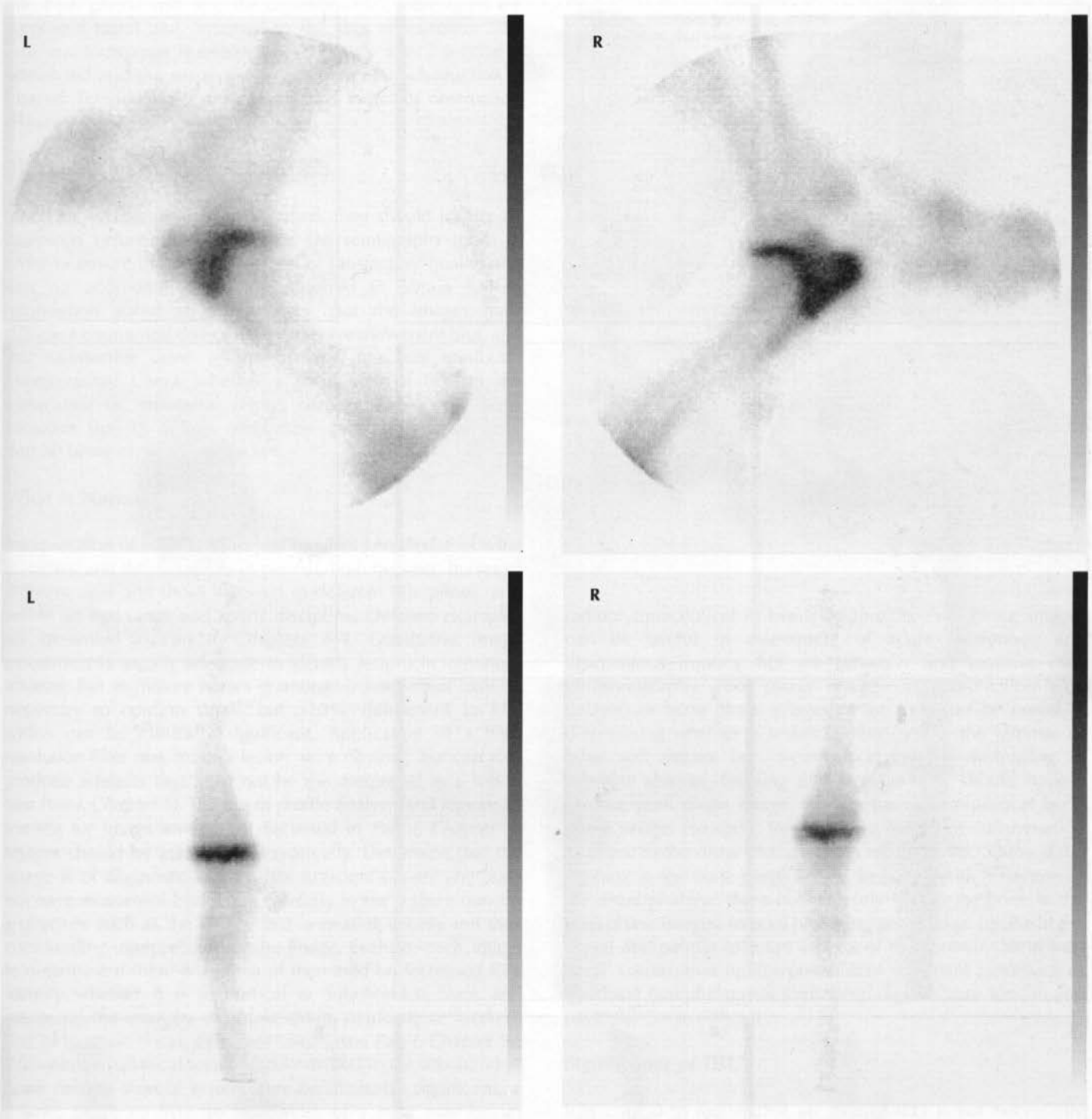

lengthy studies, often requiring repeated sedation, or when examining the hindlimbs of fillies and mares, especially if they are in season. A bucket in which to catch urine must always be available together with a mop and bucket containing Radiac wash solution. Every effort must be made to avoid contamination of the camera or pit, and if contamination of these areas or the lead shielding occurs, everything must be carefully washed with Radiac wash before proceeding (see *Part I, Chapter 12*).

OTHER EXAMINATIONS

To determine whether infection is present in either soft tissues or bone, it may be necessary to perform a labelled white blood cell scan or a leucoscan (see *Part II, Chapter 6*). Lameness associated with recurrent soft tissue swelling is occasionally associated with venous obstruction. In the distal parts of the limbs, diagnosis of venous obstruction is most reliably

Figure 6

Bone phase images of both forelimbs of a Grand Prix showjumper. There is focal intense IRU in the lateral aspect of the distal phalanx of the left forelimb (arrow) associated with a nondisplaced, incomplete, articular fracture of the distal phalanx. Note the generalised reduction in RU in the elbow and shoulder regions of the lame left forelimb compared to the right.

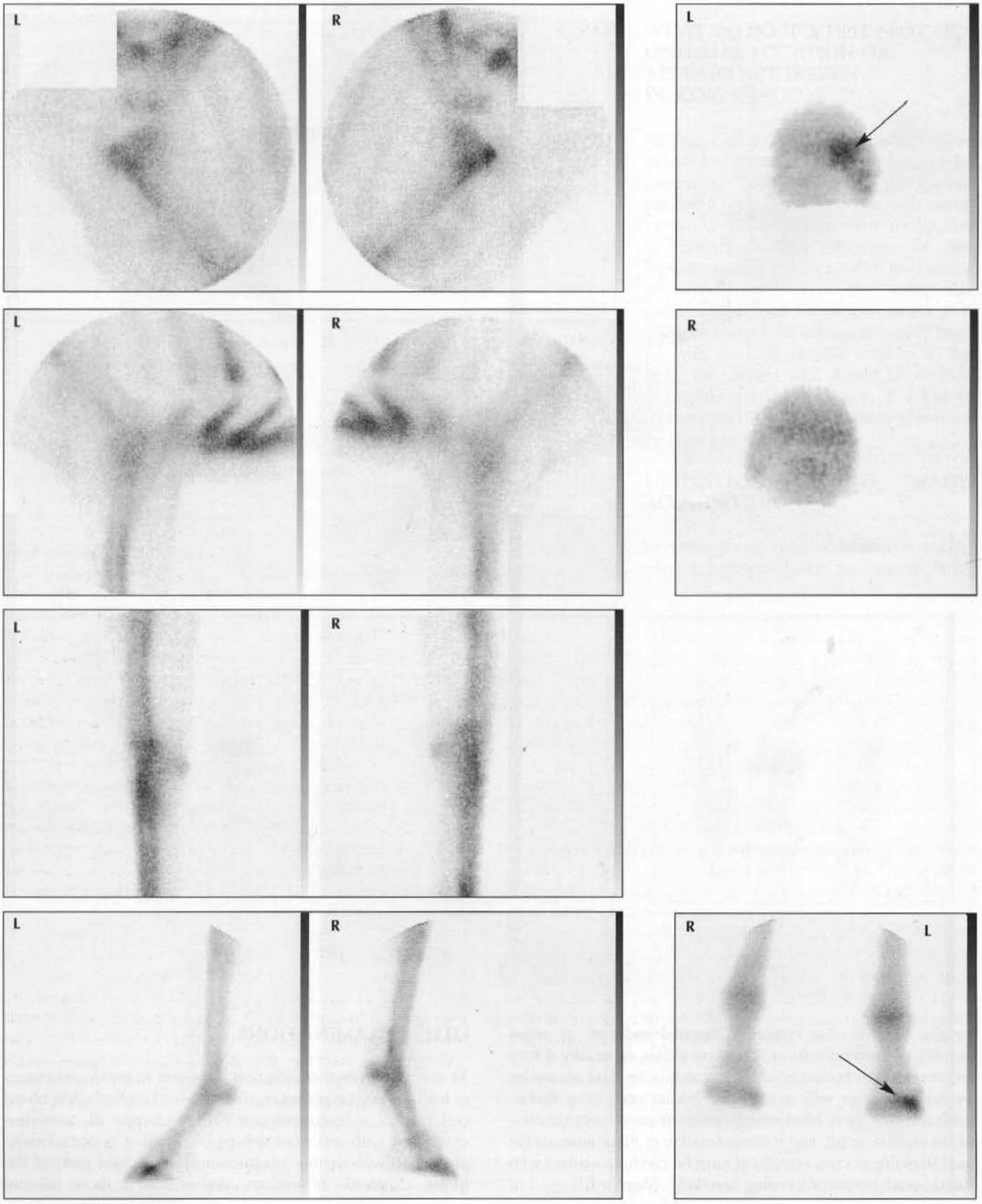

achieved using ultrasonography and Doppler ultrasonography; however, vessels proximal to the antebrachium and crus are inaccessible. Further information may be obtained by injecting ^{99m}Tc macroaggregated albumin (MAA) (1 MBq/100 kg bwt) into a peripheral vein (e.g. the cephalic vein); tourniquets are preplaced distal and proximal to the sites of injection. The proximal tourniquet is released immediately after injection is completed and the suspected region of venous obstruction is imaged. Termination of flow in a vessel indicates obstruction (**Figure 7**).

Figure 7

Lateral vascular phase image of the left axilla region after injection of ^{99m}Tc MAA into the left cephalic vein. Note the blunt-ended vessel indicating venous obstruction (A). The horse had a history of recurrent, acute onset, severe left forelimb lameness induced by work, associated with the development of extensive soft tissue swelling in the antebrachium that was exquisitely painful.

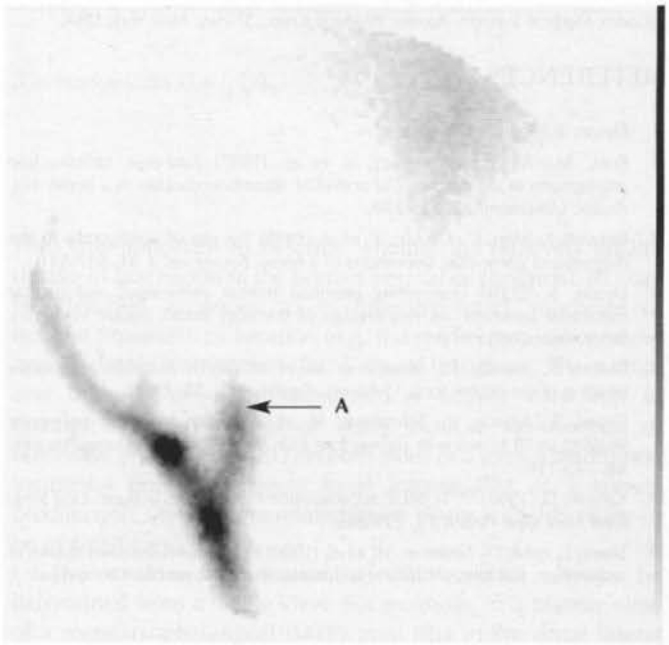

EVALUATION OF THE IMAGES

Once the images have been acquired, they should ideally be examined before the horse leaves the scintigraphy room in order to ensure that the images are of satisfactory quality and that no additional views are required to obtain further information about an area. Check that the images have sufficient counts and do not have excessive movement blur, and that radioactive urine in the bladder does not confound interpretation. Check whether a focal area of IRU in the metacarpal or metatarsal region corresponds with a bony exostosis (splint). Splints often have focal IRU indefinitely, despite being clinically quiescent.

What is Normal

Interpretation of what is abnormal requires knowledge of what is normal and the variability in normal, both between horses of different ages and those involved in different disciplines, and within an age range and sports discipline. Detailed examples are presented in *Part II, Chapters 1–4*. Qualitative image assessment is usually adequate to identify lesions in immature athletes, but in mature horses quantitative assessment may be necessary to confirm small, but >10%, differences in RU, which can be clinically significant. Application of a high resolution filter may make a lesion more obvious, but can also produce artefacts that must not be misinterpreted as a lesion (see *Part I, Chapter 5*). The use of profile analysis and regions of interest for image analysis is discussed in *Part I, Chapter 5*. Images should be assessed systematically. Determine that the image is of diagnostic quality, has sufficient counts and does not have movement blur. Look carefully to see if there may be a structure such as the kidney that is stealing counts and thus confounding interpretation of the image. Evaluate each image to determine if there is an area of increased or decreased RU, identify whether it is in cortical or subchondral bone and categorise the intensity of uptake (mild, moderate or marked) and its location (focal, diffuse or linear) (see *Part I, Chapter 9*). Whereas a small focal area of moderate IRU in the subchondral bone on one side of a joint may be clinically significant, a diffuse, moderate IRU on both sides of a joint may be an incidental finding. Comparison of images of contralateral sites is helpful, especially when evaluating IRU of uncertain significance, unless the horse is bilaterally lame.

Pool Phase Images

Pool phase images obtained distal to the carpus or tarsus can yield useful information, but further proximally are usually unrewarding, due to the normal high quantity of radiopharmaceutical in overlying muscle. Pool phase images can be useful in assessment of acute tendonous and ligamentous injuries, but are generally less sensitive than ultrasonography. Pool phase images, in combination with delayed or bone phase images of the foot, can be useful in determining whether a lesion is restricted to the laminar or other soft tissues, but interpretation can be misleading. A subsolar abscess, bruising and laminar tears should have a positive pool phase image, but a negative or equivocal bone phase image. However, long-standing soft tissue inflammation adjacent to the distal phalanx often results in IRU in the distal phalanx in the bone phase image. In horses with a fracture of the distal phalanx, there is often early IRU in the bone in the pool phase images. In pool phase images, intense uptake at the dorsal and palmar (plantar) aspects of the coronary band may 'steal' counts, making interpretation of important areas such as the distal interphalangeal joint, deep digital flexor tendon and navicular bursa difficult.

Significance of IRU

It is critical to realise that an area of IRU is not necessarily associated with pathological bone modelling, nor does it necessarily equate with pain causing lameness. It is also necessary to recognise that pathological changes may be present bilaterally; therefore, left versus right symmetry of a bone scan does not necessarily reflect normality, but may be the result of bilateral injury and lameness. False negative results, i.e. failure to identify an existing lesion, may be due to poor image quality, failure to obtain appropriate views, failure to allow sufficient time after injury to allow bone turnover to

increase, or misinterpretation of images. A negative bone scan may also reflect a primary soft tissue lesion, for example a meniscal tear or proximal suspensory desmitis, conditions which are often not associated with IRU.

MANUFACTURER'S ADDRESS

[a]Biodex Medical Systems, Atomic Products Corp., Shirley, New York, USA.

REFERENCES

1. Dyson, S. Unpublished data.
2. Ross, M., Maxson, A., Stacy, V. *et al.* (1997) First-pass radionuclide angiography in the diagnosis of aortoiliac thromboembolism in a horse. *Vet. Radiol. Ultrasound* **38**, 226-230.
3. Boswell, J., Marr, C., Cauvin, E. *et al.* (1999) The use of scintigraphy in the diagnosis of aortic-iliac thrombosis in a horse. *Equine vet. J.* **31**, 537-541.
4. Dyson, S. (2001) Unravelling proximal palmar metacarpal and plantar metatarsal lameness. In: *Proceedings of the 40th British Equine Veterinary Association Congress*. p 115.
5. Dyson, S., Murray, R., Schramme, M. *et al.* (2003) Magnetic resonance imaging of the equine foot: 15 horses. *Equine vet. J.* **35**, 18-26.
6. Dyson, S., Murray, R., Schramme, M. *et al.* (2002) Magnetic resonance imaging in 18 horses with palmar foot pain. *Proc. Am. Ass. equine Practnrs.* **48**, 145-154.
7. Kanishi, D. (1993) ^{99m}Tc-MDP accumulation mechanisms in bone. *Oral Surg. Oral Med. Oral Pathol.* **75**, 239-246.
8. Shani, J., Amir, D., Soskelne, W. *et al.* (1990) Correlations between uptake of technetium, calcium, phosphate and mineralisation in rat tibial bone repair. *J. Nucl. Med.* **31**, 2011-2014.
9. Castronovo, F. and Strauss, H. (1988) Dual tracer resorption and apposition in a rat fracture model. *Nucl. Med. Biol.* **15**, 181-185.
10. Schwartz, Z., Shani, J., Soskolne, W. *et al.* (1993) Uptake and biodistribution of technetium-99m-MD^{32}P during rat tibial bone repair. *J. Nucl. Med.* **34**, 194-108.
11. Okamoto, Y. (1995) Accumulation of technetium-99m methylene diphosphonate. Conditions affecting adsorption to hydroxyapatite. *Oral Surg. Oral Med. Oral Pathol.* **80**, 115-119.
12. Christin, R., Gazit, D., Ulmansky, M. *et al.* (1988) ^{99m}Tc-MDP uptake and histological changes during rat bone marrow regeneration. *Nucl. Med. Biol.* **15**, 469-476.
13. Dyson, S., Murray, R., Branch, M. *et al.* (2003) The sacroiliac joints: evaluation using nuclear scintigraphy. Part I: The normal horse. *Equine vet. J.* **35**, 226-232.
14. Dyson, S., Lakhani, K., Wood, J. *et al.* (2001) Factors influencing blood flow in the equine digit and their effect on uptake of ^{99m}technetium methylene diphosphonate into bone. *Equine vet. J.* **33**, 591-598.
15. Dyson, S. Unpublished data.
16. Pilsworth, R. (1996) Scintigraphic probe counting: 3. Artefacts. *Equine vet. Educ.* **8**, 230-243.
17. Pilsworth, R. (1996) Scintigraphic probe counting: 2. Interpretation of scan results. *Equine vet. Educ.* **8**, 103-112.
18. Ross, M. and Stacy, V. (2002) Nuclear medicine. In: *Diagnosis and Management of Lameness in the Horse*, Eds: M. Ross and S. Dyson, W.B. Saunders, Philadelphia. pp 119-212.
19. Ehrlich, P., Dohoo, I., O'Callaghan, M. *et al.* (1999) Results of bone scintigraphy in racing Standardbred horses: 64 cases (1992–1994). *J. Am. vet. med. Ass.* **215**, 982-991.
20. Hornof, W., Stover, S., Koblik, P. *et al.* (1996) Oblique views of the ilium and the scintigraphic appearance of stress fractures of the ilium. *Equine vet. J.* **8**, 356-359.

Chapter 9

IMAGE DESCRIPTION AND INTERPRETATION IN MUSCULOSKELETAL SCINTIGRAPHY

SUE J. DYSON and MARK J. MARTINELLI
Centre for Equine Studies, Animal Health Trust, Lanwades Park, Kentford, Newmarket CB8 7UU, UK.
California Equine Orthopedics, Encinitas, California 92404, USA.

Scintigraphic images, just like radiographic images, should be viewed critically and as objectively as possible. As with any imaging modality, knowledge of anatomy is an essential prerequisite. In order to communicate findings it is essential to have a unified method of image description. Image interpretation involves knowledge of both the principles of the formation of scintigraphic images and factors that can influence their appearance, and also experience of what findings can be seen as incidental abnormalities and how these may vary according to the age, discipline and work history of the horse. It is critical to appreciate that increased radiopharmaceutical uptake (IRU) or activity, while reflecting abnormal bone turnover or increased bone blood supply, is not necessarily synonymous with pain and thus does not necessarily reflect the anatomical source of pain causing lameness. Focal intense (also referred to in this text as marked) IRU may be seen in the nonlame limb of a unilaterally lame horse or in the lame limb in a site removed from that with pain. It is crucial that scintigraphic images are interpreted in the light of all other available clinical information, particularly when possible the response to local analgesia.

IMAGE DESCRIPTION

Unlike radiographs, a scintigraphic image is displayed and labelled as the camera sees the limb. Therefore, in dorsal views of the forelimbs the left forelimb is displayed on the right, whereas in plantar views of hindlimbs the left hindlimb is displayed on the left. Radiographic views describe the direction of the x-ray beam through the subject; from where it enters to where it exits the subject. This is not appropriate for scintigraphic images, which are formed by gamma radiation being acquired by the gamma camera from a specific direction, e.g. lateral, medial, dorsal, cranial, plantar or caudal. The description of the image should therefore refer to the position of the camera relative to the limb and the area being examined, the type of image (vascular, pool or bone [delayed] phase), and should also describe the radiopharmaceutical uptake (RU) or activity. From a given amount of uptake or activity in bone, the number of gamma rays detected by the camera is influenced by many factors, such as the proximity of the bone being examined to the gamma camera, the thickness of overlying soft tissues and the thickness of bone through which the gamma rays are being emitted. Some areas have greater RU than others in normal horses. For example, the epiphyseal regions of long bones have greater uptake than the metaphyseal and diaphyseal regions. Thus it is important to describe whether the relatively greater uptake in one region of the bone is normal or abnormal. RU can be classified according to its intensity (mild, moderate or marked [intense]), its location (e.g. the medial femoral condyle) and its distribution pattern (focal, linear or diffuse). The pattern and intensity of radiopharmaceutical activity can help to determine whether it is of likely clinical significance or otherwise. Mild diffuse IRU on both sides of a joint is a common incidental finding, whereas focal intense IRU at a known predilection site of stress-related bone injury is highly likely to be of significance.

The anatomical location of IRU cannot always be determined from a single view. For example, in a plantar view of a metatarsophalangeal (MTP) joint IRU in the distal lateral aspect of the third metatarsal bone (MtIII) could genuinely arise from the bone, but could also arise from the lateral proximal sesamoid bone (PSB). Differentiation is possible only by reference to a lateral view, and in some instances a flexed lateral view. In a dorsal or lateral view of a carpus it may be difficult to determine in which bone IRU is localised. Use of flexed lateral and flexed dorsal views may help to determine that what had appeared to be a single region of IRU in fact represented intense IRU in the third carpal bone and mild, focal IRU in the opposing subchondral bone of the radial carpal bone. Ideally, at least 2 different views of each area examined should be obtained whenever possible. In areas such as the cervical and thoracolumbar regions, obtaining images from both the left and right sides may help to determine if a lesion is one sided, or if IRU is evident from one side but not the other. In the thoracolumbar region a dorsal view may also help to determine if a lesion is to the left or right of the midline, although dorsal views of this area are otherwise of limited diagnostic value. It is therefore important that the images are evaluated as soon as possible after image acquisition, preferably before the horse leaves the room, so that additional views can be obtained if necessary.

A typical description of a scintigraphic image (**Figure 1**) may therefore read as follows:

Plantar bone phase image of the left and right hocks (left is to the left). Mild diffuse RU in the tuber calcanei (normal). Moderate, focal IRU in the subchondral bone of the lateral aspect of the tarsometatarsal and centrodistal joints (abnormal).

In some instances, accurate anatomical localisation is not possible from examination of the scintigraphic image alone. In these circumstances, co-registration and then superimposition of the scintigraphic image on a similarly positioned

Figure 1

Plantar bone phase image of the left and right hocks. Matrix size 256 x 256. Mild diffuse RU in the left and right tuber calcanei (normal). Moderate focal IRU in the subchondral bone of the lateral aspect of the centrodistal and tarsometatarsal joints in the left hock (abnormal).

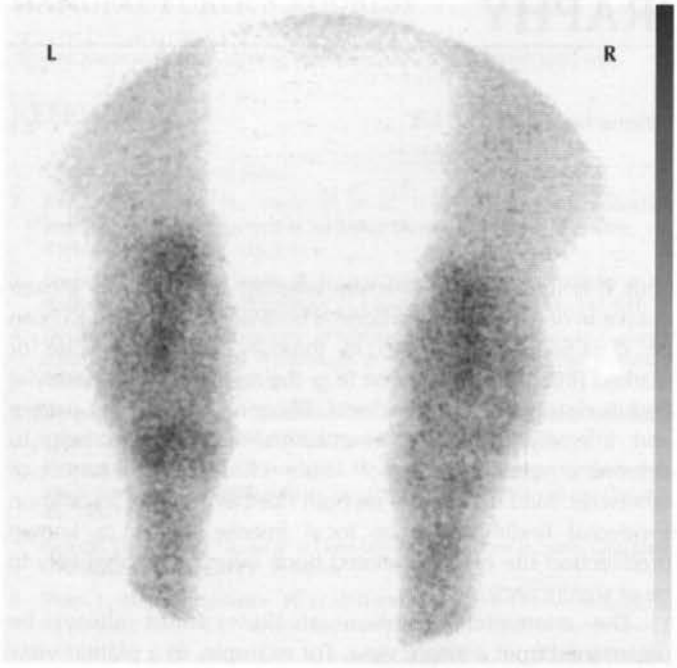

radiographic image may facilitate identification. Accurate anatomical localisation may be crucial for determining what additional clinical investigation needs to be performed. The IRU in the horse illustrated in **Figure 2** was determined by superimposition of scintigraphic and radiographic images to involve the sustentaculum of the fibular tarsal bone. Skyline radiographic views revealed significant modelling changes that were not evident in standard radiographic projections, and subtle focal mineralisation within the tarsal sheath. Abnormalities of the deep digital flexor tendon within the tarsal sheath were also identified ultrasonographically.

A specific region of interest (ROI) within an image can also be described by the mean number of counts per pixel within the ROI, thus giving more objective information about the radiopharmaceutical activity, and by drawing identical ROIs in contralateral sites accurate comparisons can be made between limbs. Similarly, ROIs can be drawn around the site of a suspected lesion and at a removed site within the same or a different bone so that ratios of mean counts per pixel can be calculated and comparisons made with the contralateral limb, or with known ratios in normal horses.

IMAGE INTERPRETATION

Before an image can be interpreted as normal or otherwise it must be determined that it is of adequate quality, i.e. there is an adequate number of counts, there is no movement blur and there are no artefacts created by, for example, urine splashing of the foot or limb, or urine in the bladder superimposed over the sacroiliac joint region or coxofemoral joint (see *Part I, Chapter 10*). In a mature horse there should ideally be at least 200,000 counts/image, although with a small area being

Figure 2

Lateral bone phase image of the left hock of an 8-year-old Icelandic pony with lameness alleviated by tibial and fibular nerve blocks. Matrix size 256 x 256. There is moderate abnormal focal IRU in the plantar aspect of the hock (A). Superimposition of a lateromedial radiographic view determined that the region of IRU coincided with the sustentaculum of the fibular tarsal bone. A skyline radiographic view revealed modelling of the sustentaculum tali and ill-defined mineralisation in the overlying soft tissues. Enlargement of the deep digital flexor tendon with ill-defined hypoechoic regions were identified by ultrasonographic examination.

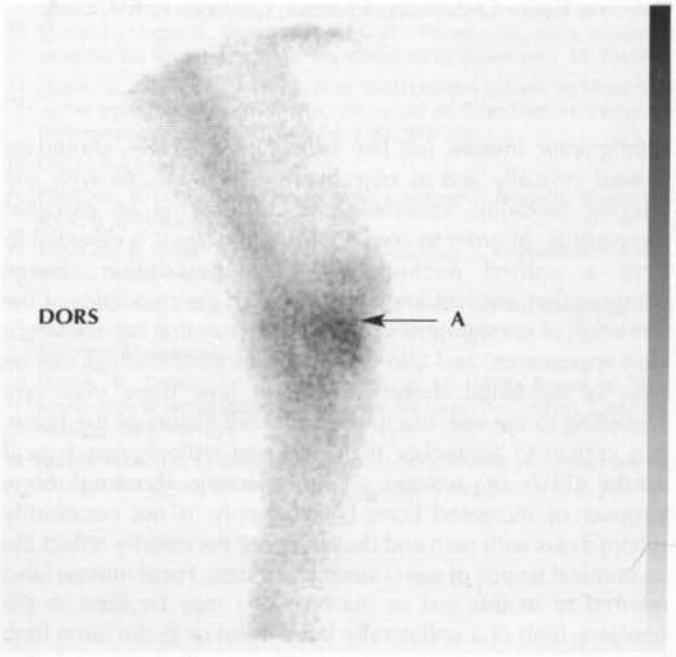

examined, such as a single solar view of a foot, a lower total count (e.g. 75,000) is acceptable. Lesions other than fractures are often associated with less RU than fractures and their identification in the region of a joint where there is already a fairly high normal activity requires higher total counts for meaningful comparisons to be made between limbs. A 10% difference in an ROI between 2 images that have total counts of only 100,000 is less likely to be of clinical significance than if the total counts are approximately 200,000. It is important to recognise that motion correction cannot totally compensate for excessive motion and repeat acquisition may be necessary if the edges of a structure are blurred.

Pattern of Radiopharmaceutical Uptake Throughout the Limb

It is helpful to display the images in a logical anatomical sequence and so that images of similar views of each limb can be viewed in close sequence for ease of comparison (see *Part I, Chapter 8, Figures 4 and 6*). If all images are displayed from proximally to distally in a limb it is easier to see the overall pattern of radiopharmaceutical distribution throughout each limb.

It is also important to review the overall pattern of radiopharmaceutical activity throughout the limb. Poor perfusion of one or more distal limbs will result in generalised reduced activity throughout the limb, the so-called 'cold limb' (see *Part I, Chapter 8, Figure 3*). If this problem is bilateral, the low counts obtained, unless image acquisition time is markedly increased, may result in lesions being missed. If the problem is

unilateral and image acquisition time is not increased in the cold limb to reach a similar total count to the contralateral limb, image interpretation becomes difficult. Some computer software allows normalisation of the images, but if the discrepancy in counts is large, normalisation cannot compensate.

There is sometimes generalised increase in radiopharmaceutical activity throughout the lame limb, especially in the subchondral bone of the joints, the so-called 'warm limb' (see *Part I, Chapter 8, Figure 4*), and it is important to recognise this before suggesting that there is significant IRU in a particular joint, when in fact all joints in the limb are similarly affected. If there is an area of marked IRU in the proximal part of a limb there may be reduced uptake throughout the more distal part of the limb compared to the contralateral limb. The reason for this commonly recognised feature is not known. There is also a phenomenon described as 'coning' in which the most intense site of IRU is at the site of the lesion, but less intense IRU continues further proximally or distally from the primary lesion.

Colour Tables

Many of the software programmes currently available offer the options of displaying images in a variety of different colour tables. Colour, while probably more striking to the client, has the potential to mislead and subtle changes may be overlooked or areas may have apparently enhanced contrast and thus give rise to false positive results. Black and white images are therefore preferred for image interpretation.

Anatomical Localisation

Determine anatomically where a region of IRU is located. This often requires 2 views. Is it in bone or the soft tissues? Intense RU in a *calcinosis circumscripta* lesion on the lateral aspect of the stifle may be misinterpreted as IRU in the proximal tibia in a lateral view (**Figure 3**); discrimination may only be possible using a caudal view. If IRU is in bone, is it confined to the cortex and subcortical bone or is it within the medulla? Enostosis-like lesions are associated with intense IRU within the medulla, whereas stress-related bone injury usually involves one or more cortices. Is there any soft tissue structure that attaches in the region that might result in an entheseous reaction? For example, moderate IRU in the proximoplantar aspect of MtIII may reflect entheseous damage of the proximal aspect of the suspensory ligament (SL). However, it might also reflect stress-related bone injury. It is also important to evaluate the shape of the bone because new bone formation may alter the bone contour, e.g. with spondylosis of a vertebral body in the thoracic region. The bone may also be altered in shape because of a displaced fracture. When assessing an area of apparent IRU it is important to be aware of the age and work history of the horse; uptake in subchondral bone is normally much more intense in immature athletes than mature horses. An immature horse has marked RU in the physes of the long bones. A mature horse which has been rested for a prolonged period may have normal radiopharmaceutical distribution despite the presence of a bony lesion.

Normal Variation

It is crucial to be aware that there is considerable variation in RU even in horses of comparable age; thus, reference to a variety of normal images of a region (see *Part II*) is invaluable. Generally, but not invariably, nonsignificant increases in RU tend to be bilaterally symmetrical, e.g. marked focal RU in the proximodorsal aspect of the proximal phalanges, which is normally cosidered to be an incidental finding in this type of horse (**Figure 6c**). It is also important to consider why there is relatively greater RU in certain sites. For example, the most mobile joints in the neck are the synovial articulations between the fifth and sixth and sixth and seventh cervical vertebrae. As a result of this, many mature horses develop modelling changes of these articulations and it is therefore not surprising that there is greater RU in these bones than in the more cranial vertebrae. This is also highlighted because the cranial thoracic articulations situated immediately caudad are shielded by the large attenuating muscle mass of the shoulder region (see *Part II, Chapter 4, Figure 20d*). There is always greater RU in the lateral condyle of the femur and the lateral aspect of the distal hock and proximal metatarsal region and the lateral condyle of MtIII, presumably reflecting increased loading at these sites compared to medially. Structures situated very superficially, such as the tubera sacrale, with minimal overlying soft tissues, have negligible attenuation of γ-rays and thus may appear to have marked but normal RU (see *Part II, Chapter 4, Figure 21b*). A structure such as a tuber coxae is both superficial and situated at the end of the ilium, so there is also some summation of activity from the underlying bone.

Breed and Use Variations

Normal patterns of RU are influenced by age, breed and use and are illustrated in *Part II, Chapters 1–4*. There appears to be greater variability of uptake in immature competition and

Figure 3

Lateral bone phase image of the right stifle of a 7-year-old Thoroughbred. Matrix size 256 x 256. There is marked focal IRU apparently in the proximocaudal aspect of the tibia. However, a caudal view showed that this IRU was in the soft tissues lateral to the tibia, coincident with a palpable mass, confirmed radiographically to be calcinosis circumscripta.

Figure 4

a) *Lateral bone phase image of the left hock of a 9-year-old Warmblood showjumper. Matrix size 256 x 256. There is moderate abnormal focal IRU in the dorsal aspect of the subchondral bone of the central and third tarsal bones (A). Note also the normal mild focal RU in the tuber calcanei (B). There was radiographic evidence of osteoarthritis of the centrodistal joint.* ***b)*** *Lateral view of the left hock of an 8-year-old Irish Draught cross Thoroughbred mare used for general purposes. Matrix size 256 x 256. There is marked focal abnormal IRU associated with the dorsal aspect of the subchondral bone of the talocalcaneal-centroquatral (proximal intertarsal) joint (A). There is also moderate focal abnormal IRU on the dorsal and plantar aspects of the tarsocrural joint (B). Lameness was substantially improved by either fibular and tibial nerve blocks or intra-articular analgesia of the tarsocrural joint. There was radiographic evidence of osteoarthritis of the talocalcaneal-centroquatral joint.* ***c)*** *Lateral bone phase image of the left hock of a 7-year-old Irish Sports Horse gelding used for general purposes. Matrix size 256 x 256. There is marked focal linear IRU associated with the subchondral bone of the centrodistal joint. Lameness was improved by fibular and tibial nerve blocks. There was radiographic evidence of marked narrowing of the tarsometatarsal joint space, probably reflecting effective fusion. The centrodistal joint space was narrowed but still clearly evident. There was smoothly outlined periarticular new bone involving both joints.* ***d)*** *Lateral bone phase image of the left hock of a 9-year-old Pony Club horse with acute onset severe left hindlimb lameness, partially improved by tibial and fibular nerve blocks. Matrix size 256 x 256. There is marked diffuse abnormal IRU in the central and third tarsal bones and the proximoplantar aspect of the third metatarsal bone. No significant radiological abnormality was detected at this stage, but within 2 months the horse had developed advanced osteoarthritis of the centrodistal and tarsometatarsal joints with severe, unremitting pain.*

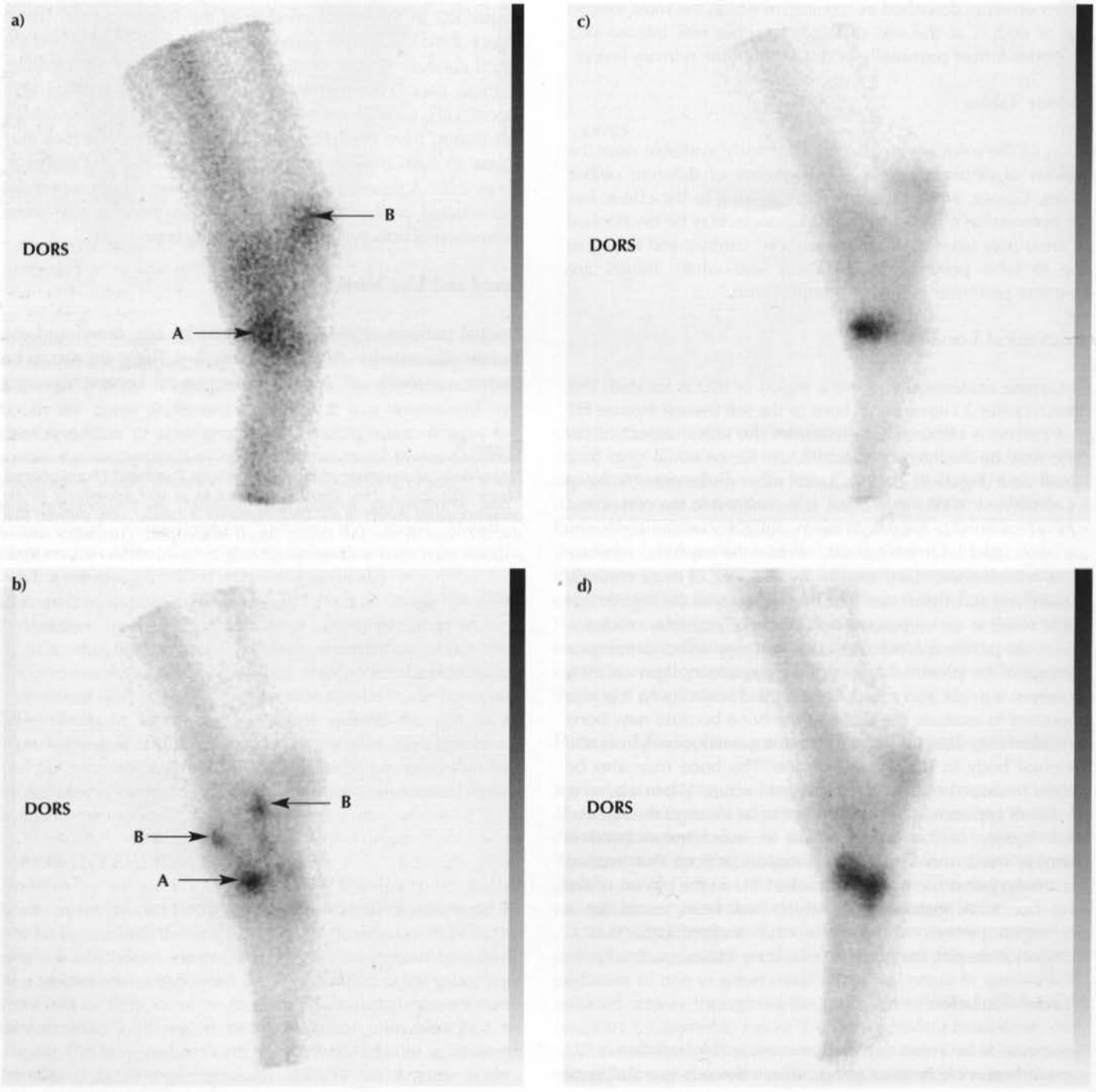

pleasure horses compared to immature Thoroughbred and Standardbred horses. However, these variations tend to be bilaterally symmetrical in any individual horse, assuming there is similar blood flow to each limb. Misinterpretation is therefore most likely in a bilaterally lame horse. Various lesions occur with different frequency in horses involved in different disciplines. Thus, interpretation of images is facilitated by knowledge of what lesions are common in any particular discipline[1] (see *Part II, Chapters 1–4*). In Standardbreds, for example, there may be several regions of IRU, one reflecting the site of primary injury and the others reflecting secondary injuries as the result of an altered way of moving. Such compensatory lesions may result in persistent lameness after the primary source of pain has been blocked. It is less common in Thoroughbred racehorses to have more than one region of IRU of clinical significance. Within a single breed and discipline it is important to recognise that local factors such as training methods and work surfaces may influence bone stress and injury occurrence and thus patterns of RU may vary.

Patient to Camera Distance

It is important to recognise that the camera's spatial resolution decreases with distance from the horse, so the further a site of radioactivity is from the gamma camera, the more blurring there will be in the image. Thus if the gamma camera is further away from one limb than another it may confound interpretation. Perceived radioactivity in an area is also influenced by the overlying tissues. Mild IRU in the medial femoral condyle may be unapparent in a lateral view, particularly if the total count is low, because of the large tissue mass between the source of radioactivity and the gamma camera, and the superimposition of gamma radiation from the lateral condyle. Historically, it was suggested that subchondral bone cysts in the medial femoral condyle were scintigraphically silent, but this was probably because an inadequate number of counts were acquired. In our experience, such bone cysts are usually associated with moderate focal IRU. Profound muscle atrophy, especially in the pelvic region, may cause higher count rates from underlying bone because there is less muscle mass to attenuate γ-rays; thus the bones may be perceived as having greater radiopharmaceutical activity than the contralateral, more normally muscled, side.

Duration of Injury

When considering the significance of a region of IRU it is important to relate the time of image acquisition to the time of onset of clinical signs. Stress-related bone injury usually results in immediate increased radiopharmaceutical activity because increased bone modelling precedes the development of a stress fracture. It would be anticipated that the level of activity would then progressively decline over the following 2 to 3 months. However, false negative results may be obtained for traumatic fractures of the ilium, particularly if around the acetabulum, if imaging is performed within 7 to 10 days of injury, in part due to shielding and attenuation of gamma rays by the overlying muscle mass and, presumably, a delay in intense osteoblastic activity developing.

A horse with chronic lameness associated with osteoarthritis may have only mild IRU in the subchondral bone of the affected joint. Horses with what we currently perceive as the same disease process may have different patterns of RU. For example, abnormal radiopharmaceutical activity associated with osteoarthritis of the centrodistal and tarsometatarsal joints is sometimes in a focal area, sometimes linear, parallel with the articulations or sometimes more diffuse. This pattern of uptake and its intensity is not necessarily correlated with either the extent of radiographic abnormalities or the degree of lameness (**Figures 1 and 4**). A variety of injuries or disease can affect a joint, each resulting in IRU, but of variable size, patterns, intensity and site (**Figures 1 and 3–5**).

Coincidental Regions of IRU

Knowledge of what lesions frequently have prolonged IRU, although with no related pain or lameness, is essential. Exostoses involving the second or fourth metacarpal bones or the proximolateral aspect of the third metatarsal bone, even if apparently long-standing and quiescent, often have focal moderate to intense IRU (see *Part II, Chapter 4, Figure 8bi*). The separate centres of ossification that are the summits of the cranial thoracic dorsal spinous processes (the withers) always have marked, focal, normal RU. Enostosis-like lesions in the long bones that have focal marked IRU are often not associated with lameness, although occasionally are.

As with reading radiographs, interpretation of scintigraphic images is not always a clear-cut situation and there is overlap between clinically normal horses and those with lameness. However, the intensity of radiopharmaceutical activity is sometimes, but not always, a reflection of likely clinical significance. For example, IRU is frequently seen in the lateral condyle of MtIII in young Thoroughbreds in training. There is a spectrum of uptake reflecting variable degrees of stress-related bone injury seen in clinically normal horses and those with subchondral bone trauma causing lameness. However, using ratios of counts in ROIs in the lateral condyle versus the mid-diaphyseal region of MtIII, no clinically normal horse had a ratio of greater than 3:1[2]. Thus, quantitative examination of images may be of value. This is particularly the situation in bilaterally lame horses, when meaningful comparisons cannot be made between the 2 limbs if lameness is associated with similar injuries in both.

Vascular and Pool Phase Images

Vascular images demonstrate blood flow to a region and can be useful to indicate if perfusion to the distal aspect of both forelimbs is similar. If there is asymmetry it is likely that RU into bone will also be asymmetrical[3]. Vascular images can also be used to demonstrate arterial obstructions, for example due to a thrombus in the aorta or iliac arteries (see *Part II, Chapter 6*).

Interpretation of pool phase images is less straightforward than bone or delayed phase images for a number of reasons. Although it is generally accepted that pool or soft tissue phase images principally reflect uptake in the soft tissues within the first 30 mins after injection of the radiopharmaceutical, there is in fact very rapid uptake into bone (**Figures 6a and 6c**). In the presence of infection in bone or a fracture there is almost immediate uptake into the injured bone. The relative uptake in the soft tissues versus bone is also time-dependent and, unless images of the left and right limbs are obtained

Figure 5

a) *Lateral bone phase image of the left hock of a 7-year-old Warmblood dressage horse with back pain associated with sacroiliac joint disease and low grade left hindlimb lameness. Matrix size 256 x 256.There is moderate focal abnormal IRU in the middle of the proximal row of tarsal bones. There was no detectable radiological abnormality. The horse was humanely destroyed for unrelated reasons. Magnetic resonance imaging demonstrated increased signal in the interosseous ligament between the central and third tarsal bones in T1- and T2-weighted images and abnormal bright signal in fat-suppressed images in the central tarsal bone at the ligament's insertion. Note also the mild diffuse normal RU in the hock region compared to the diaphyseal regions of the tibia and third metatarsal bone.* ***b)*** *Lateral bone phase image of the right hock of a 7-year-old riding horse. Matrix size 256 x 256. There is marked focal IRU in the proximal row of tarsal bones. This is in a similar position to the region of IRU in (a), but is more widespread. The horse was severely lame, but no radiological abnormality was detected. Lameness was substantially improved by fibular and tibial nerve blocks or by intra-articular analgesia of the tarsometatarsal joint, but showed no response to intra-articular medication.*

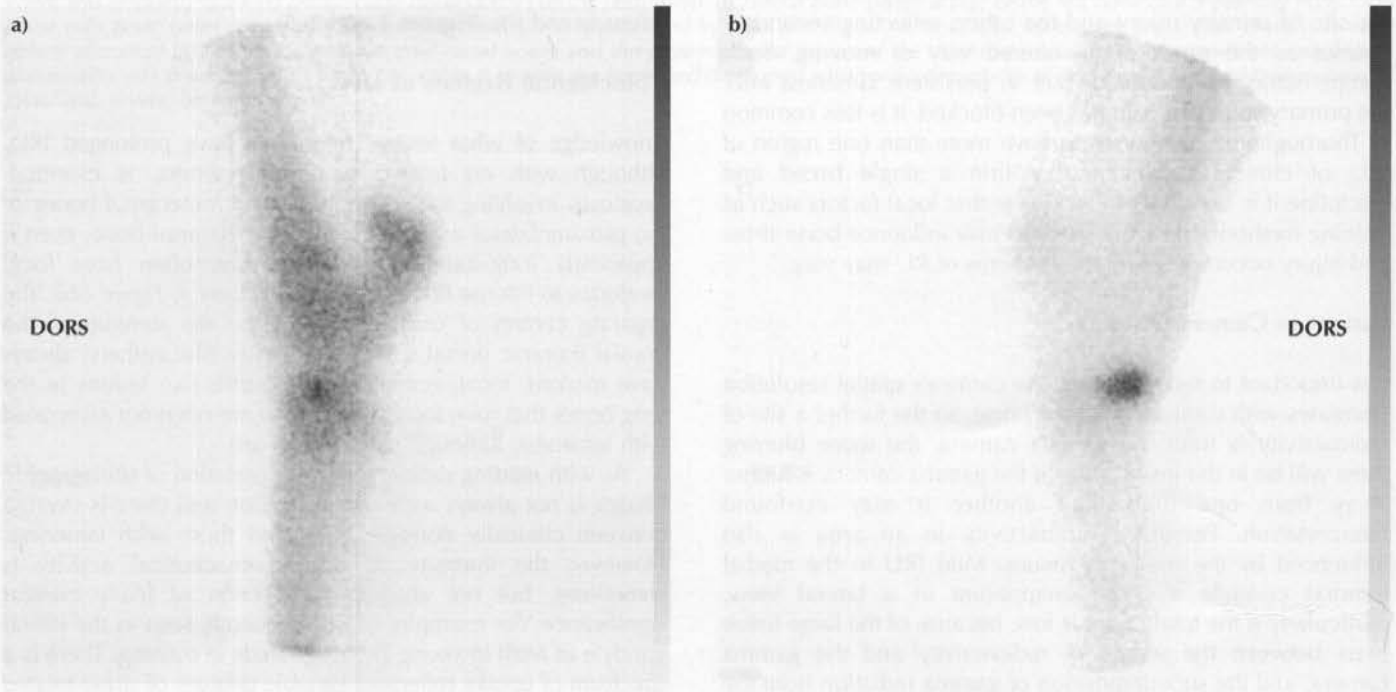

simultaneously, there will almost invariably be left-right asymmetry (**Figures 6a and 6b**). There is also delayed presence of radiopharmaceutical in and around major vascular plexi, which may mask uptake into local soft tissues. Although with acute tendonous or ligamentous injuries there may be associated IRU, in more chronic injuries RU is often normal, but this does not preclude the structure being the source of pain causing lameness. Paradoxically, abnormal IRU may be seen in muscle in bone phase images following either local fibre tearing or in some horses with recurrent exertional rhabdomyolysis. In the latter horses, muscle streaking of IRU is seen in several affected muscles, whereas in horses with a focal muscle injury the IRU tends to be focal and mild. IRU has also been seen unilaterally in the hamstring muscles of horses with unrelated lameness[4]. Based on imaging one horse on 2 occasions with IRU associated with a single episode of exertional rhabdomyolysis, activity may return to normal within 72 h[5]. However, some horses experiencing recurrent low grade exertional rhabdomyolysis each time they are exercised have persistent IRU[6].

False Positive Results

False positive results may be the result of over-interpretation of normal findings or misinterpretation of artefacts (see also *Part I, Chapter 10*). The foot is a common region for false positive results. Although many clinically normal horses or those with lameness unrelated to foot pain have similar RU throughout the distal phalanx and the navicular bone, mild to marked IRU in the region of the navicular bone and/or the region of insertion of the DDFT can be seen in horses without foot pain[4]. One horse had 130% IRU in the navicular bone compared to the peripheral regions of the distal phalanx in the lame limb and 150% IRU in the nonlame limb and *post mortem* examination revealed widespread histological changes in the navicular bone of the lame limb only[6]. Generalised IRU is often seen in the region of insertion of the DDFT on the distal phalanx in solar views of horses with and without foot pain[7]. Horses with insertional lesions of the DDFT identified using magnetic resonance imaging have tended to have focal IRU at part of the DDFT attachment rather than more generalised uptake in the insertional region[6]. IRU in a palmar process of the distal phalanx is a relatively common, apparently incidental finding.

False Negative Results

False negative results occur frequently for a variety of different reasons. These include a lesion which does not provoke much increased bone activity. Soft tissue lesions within the stifle involving, for example, the cruciate or meniscal ligaments or the meniscal cartilages, are often scintigraphically silent, although sometimes are associated with a mild but generalised IRU throughout the stifle region. Chronic proximal suspensory

Figure 6

a) *Lateral pool phase image of the distal aspect of the left forelimb of an 8-year-old Thoroughbred event horse with right forelimb lameness acquired 3–4 mins after injection of radiopharmaceutical. Matrix size 128 x128. There is normal intense RU at the vascular plexi proximal to the coronary band (A); moderate focal early bone uptake on the proximodorsal aspect of the proximal phalanx (B) and the dorsal aspect of the metacarpophalangeal joint (C); and mild linear normal RU in the vessels in the palmar aspect of the metacarpal and pastern regions (D).* ***b)*** *Lateral pool phase image of the distal aspect of the right forelimb of the same horse as (a), acquired approximately 2 mins later. Note the more intense RU in the foot, proximal phalanx and fetlock regions compared to (a) and that the palmar vessels are now barely apparent. There is abnormal focal mild IRU at the insertion of the deep digital flexor tendon (DDFT) (A). An insertional lesion of the DDFT with adhesion to the distal sesamoidean impar ligament was detected using magnetic resonance imaging.* ***c)*** *Lateral bone phase image of the distal aspect of the left forelimb; the same limb as (a). There is moderate focal RU in the proximodorsal aspect of the proximal phalanx, which is a common incidental finding in the sports shorse (A). There is normal mild focal RU close to the articular margin of the proximal phalanx (B) and associated with the proximal interphalangeal joint (C).*

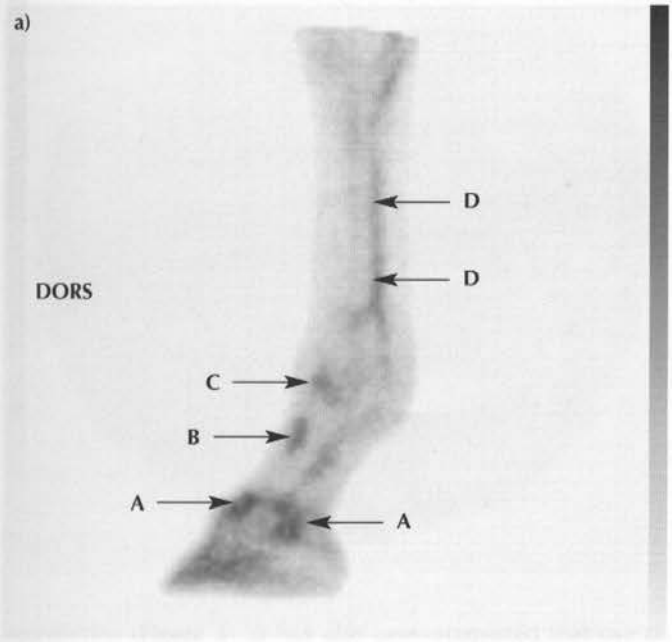

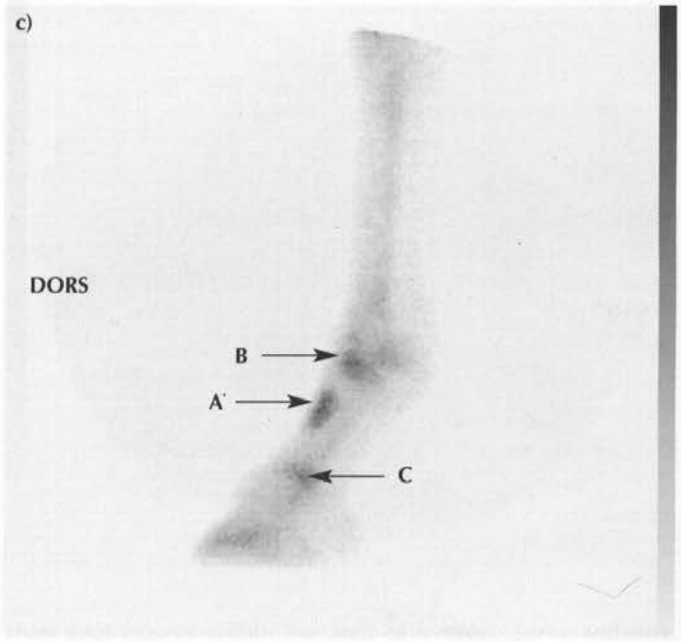

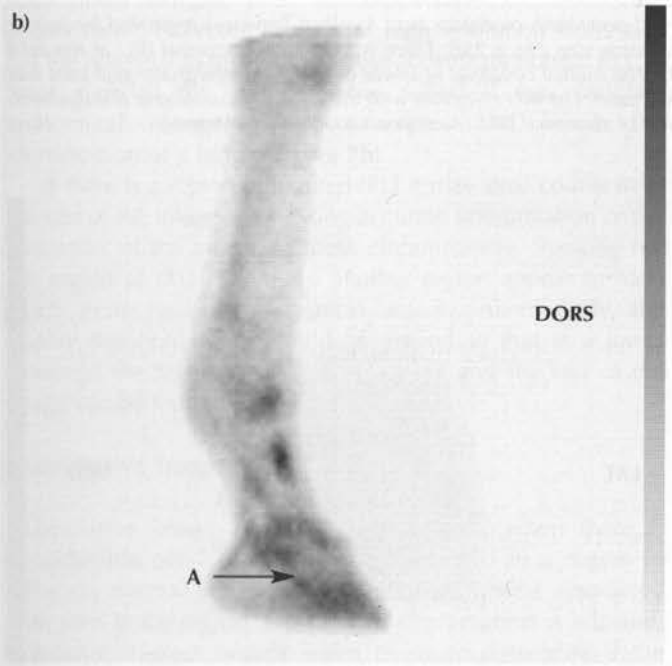

desmitis is frequently not associated with IRU in pool phase images. False negative results may be the result of shielding by muscle. For example, a fracture of the first thoracic vertebra may be missed because of the dense overlying shoulder musculature and the scapulae. Some horses with back pain associated with impinging dorsal spinous processes have negligible IRU, although pain is removed by infiltration of local anaesthetic solution around the affected spinous processes (**Figure 7**). Osteochondrosis lesions in some locations are not detectable scintigraphically. Horses with end-stage navicular disease may have normal RU in the navicular bone. Some osseous cyst-like lesions are scintigraphically silent in the distal phalanx despite being the cause of lameness. This probably relates to the stage of development of the cyst and involvement of surrounding bone or lack thereof.

Degree of Radiopharmaceutical Uptake and Lesion Types

The degree of RU reflects the extent of bone modelling, which itself relates to the nature of the pathological process and, to an extent, its chronicity. With intense IRU, the surrounding tissues appear to have much less radiopharmaceutical activity than normal because the high count density of the hotspot dominates the colour scale of the image. Such a pattern is typical of, but not exclusive to, a fracture and can be seen in association with a very actively developing osseous cyst-like lesion or in some joints with rapidly developing osteoarthritis (**Figure 4d**).

Image Modification

Application of a high resolution filter to an image sometimes accentuates a region of abnormal IRU which facilitates its

Figure 7

a) *Right lateral oblique bone phase image of the mid and caudal thoracic region. Matrix size 256 x 256. The kidney has been masked out. There is mild IRU in the dorsal spinous processes of the 12th to 16th thoracic vertebrae. There was radiographic evidence of mild impingement of the dorsal spinous processes of the 15th and 16th thoracic vertebrae only and infiltration of local anaesthetic solution around the summits of these 2 dorsal spinous processes eliminated this horse's severe bucking behaviour.* ***b)*** *The same image as (a) after application of a high resolution filter. Although appearing slightly blurred, the outline of the dorsal spinous processes is easier to see.*

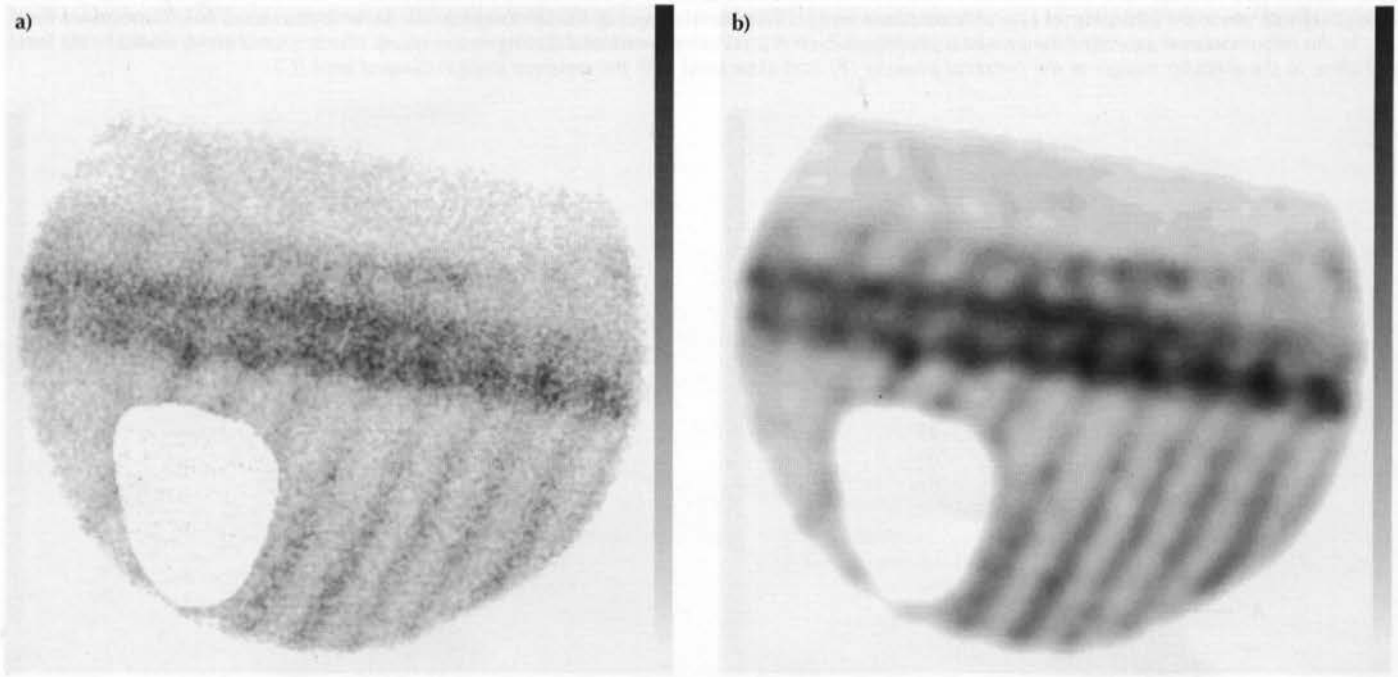

Figure 8

a) *Solar bone phase scintigraphic image of the right front foot of a 10-year-old pony with moderate right forelimb lameness improved by palmar (abaxial sesamoid) nerve blocks. The image has been zoomed (magnified). Matrix size 256 x 256. There is mild focal abnormal IRU at the axial junction of the medial palmar process and the body of the distal phalanx (A). The medial collateral ligament of the distal interphalangeal joint was poorly defined when examined ultrasonographically at the level of the coronary band. The IRU coincides with the region of insertion of this ligament.* ***b)*** *The same image as (a) after application of a high resolution filter. The region of abnormal IRU (A) appears much more intense.*

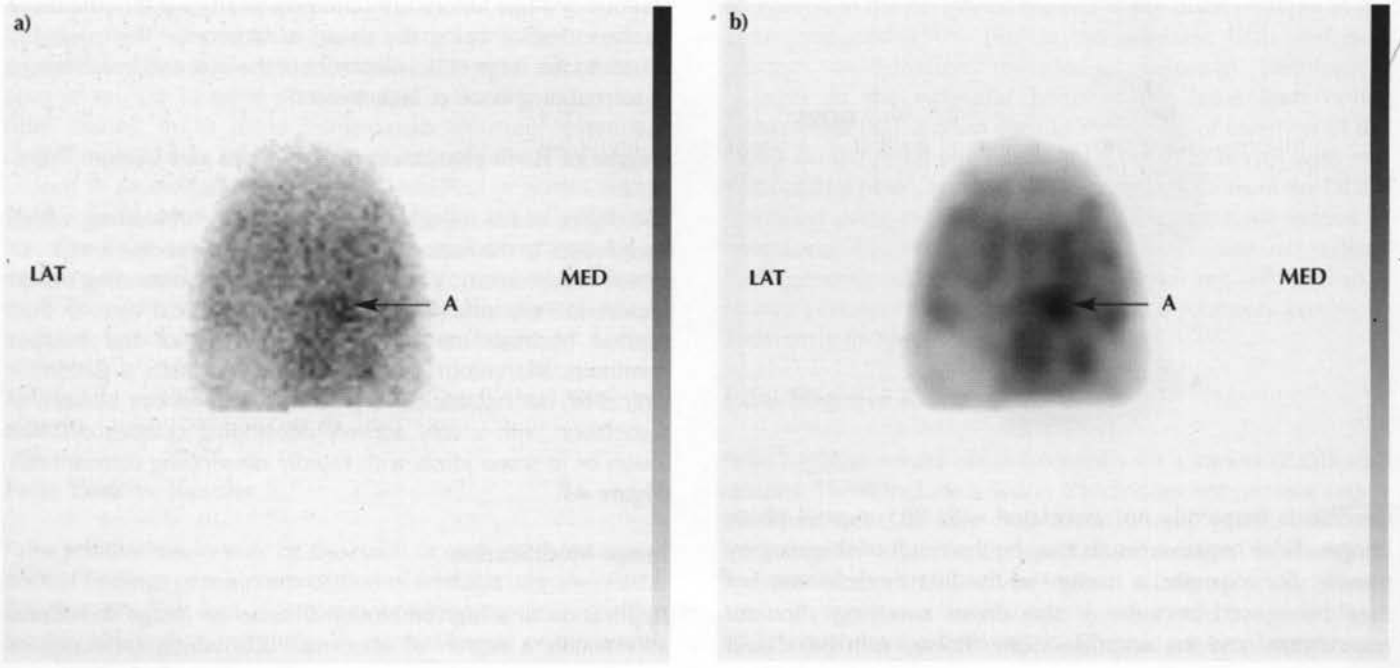

Figure 9

Solar images of the front feet of a 10-year-old Grand Prix showjumper with bilateral forelimb lameness associated with palmar foot pain. The images have been co-registered and identical ROIs drawn on both. Mean counts/pixel for each ROI was recorded: Left front; 1 = 38, 2 = 37, 3 = 29, 4 = 30, 5 = 30, 6 = 46. Right front; 1 = 39, 2 = 38, 3 = 34, 4 = 33, 5 = 34, 6 = 47. The ratio of mean counts/pixel in region 1, the navicular bone area, for the left and right forelimbs was 90%; for normalised images the ratio was 88%. Mean counts/pixel for region 1 was compared to the mean for regions 3, 4 and 5 and was 128% in the left fore and 115% in the right fore. The focal region with greatest IRU in the navicular bones, region 6, was also compared to the mean for regions 3, 4 and 5 and was 155% in the left fore and 140% in the right fore. The horse had multiple radiolucent zones along the distal border of each navicular bone, but these had not changed since purchase 2 years previously and no other radiological abnormality was detected. Magnetic resonance imaging revealed abnormal signal in both navicular bones as the only abnormality.

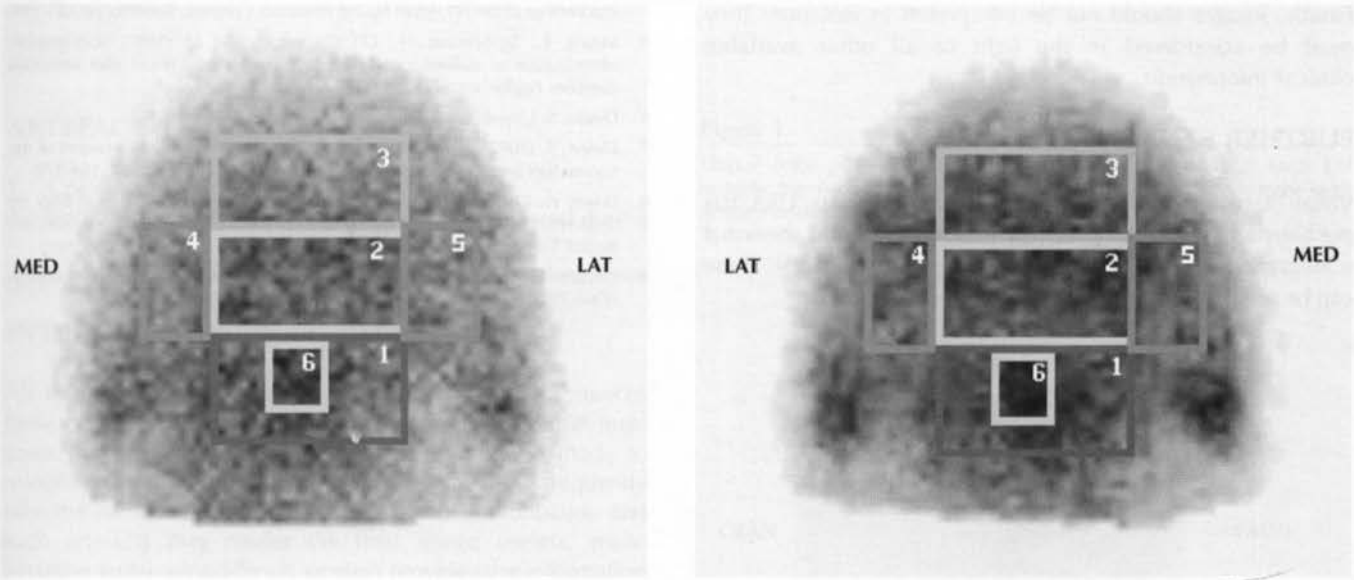

recognition (**Figure 8**). It has also been suggested that use of such filters can be used to compensate for low count acquisitions[8]. However, the use of high resolution filters also has the potential to mislead and over-accentuate normal RU. In areas such as the thoracolumbar region it may facilitate anatomical recognition of structures and hence the identification of a lesion (**Figure 7b**).

If there is a region of marked IRU it may steal counts from the rest of the image, prohibiting accurate interpretation of the remainder of the image. In these circumstances, masking out the region of IRU may make another region appear to have much more radiopharmaceutical activity. Alternatively, the display threshold scale should be altered so that at a lower threshold the region of IRU is burnt out and the rest of the image can be read.

Quantitative Image Analysis

Quantitative image analysis is most useful when there is considerable overlap with the degree of RU in a region in clinically normal horses and those with lameness associated with pain in the region, especially if the lameness is bilateral. It is also of great benefit when trying to determine if the degree of difference between left and right sides is great enough to potentially reflect clinical significance. The simplest methods include ROI and profile analysis. Obviously, ROIs can be drawn freehand on the left and right limbs, but precise sizing and location is not always easy. For this reason, mean counts/pixel should be evaluated rather than total counts within the area of interest. Some software programmes permit image inversion (mirroring) and co-registration so that left and right images can be precisely aligned. An ROI drawn on one image is then automatically drawn at precisely the same location on the contralateral limb. The software usually calculates the total number of counts in the ROI and the number of counts/pixel; it may also indicate the minimum and maximum counts/pixel and the standard deviation. Advanced software may also calculate the relative counts/pixel in the left and right images and express this as a percentage both before and after normalising the images (**Figure 9**). ROI analysis can be used to calculate ratios of radiopharmaceutical activity in an area compared with a reference area which is unlikely to change much. For example, the RU in facet joints in the thoracolumbar region and a rib have been compared[7].

In dorsal or plantar views a profile of variable width can be drawn across each limb to give graphic representations of radiopharmaceutical activity, which can be reasonably accurate provided that the horse was standing squarely during image acquisition and the camera was tangential to the limbs and not obliquely positioned. By moving the profile upwards or downwards, a comparison can be made between the relative radiopharmaceutical activity in the region of a postulated lesion and elsewhere in the limb. If radiopharmaceutical activity is similarly increased in the lame limb at a site removed from the postulated lesion, the IRU may be a generalised phenomenon rather than reflecting a genuine lesion.

CONCLUSIONS

Image interpretation is both an art and science. Experience of the normal uptake patterns for various types, work histories, disciplines and ages of horses and their variations is invaluable. It is hoped that the reference images in *Part II* of this book will provide a sound foundation. Scintigraphic images reflect a dynamic process and can be influenced by many factors, and knowledge of these is also important. Finally, images should not be interpreted in isolation; they must be considered in the light of all other available clinical information.

FURTHER STUDY

Vivian Stacey at the New Bolton Centre, Pennsylvania, USA, has put together a large group of very useful normal and abnormal scintigraphic images on a website for free access study. These can be seen at *http://caltest.vet.upenn.edu/nucmed*

REFERENCES

1. Twardock, A. (2001) Equine bone scintigraphic uptake patterns related to age, breed and occupation. *Vet. Clin. N. Am.* **17**, 75-94.
2. Shepherd, M.C. and Pilsworth, R.C. (1997) Stress reactions to the plantarolateral condyles of MTIII in UK Thoroughbreds: 26 cases. *Proc. Am. Ass. equine Practnrs.* **43**, pp 128-131.
3. Dyson, S., Lakhani, K. and Wood, J. (2001) Factors influencing blood flow in the equine digit and their effect on bone uptake of 99^{m} technetium methylene diphosphonate into bone. *Equine vet. J.* **33**, 591-598.
4. Ross, M. (2001) Hindlimb lameness in the Standardbred racehorse. In: *Proceedings of the 7th World Equine Veterinary Congress*, Sorrento. pp 185-190.
5. Morris, E., Seeherman, H., O'Callaghan, M. *et al.* (1991) Scintigraphic identification of skeletal muscle damage in horses 24 hours after strenuous exercise. *Equine vet. J.* **23**, 347-352.
6. Dyson, S. Unpublished data.
7. Dyson, S. (2002) Subjective and quantitative scintigraphic assessment of the equine foot and its relationship with foot pain. *Equine vet. J.* **34**, 164-170.
8. Eksell, P., Carlsson, S., Lord, P. *et al.* (2000) Effects of a digital filter on detectability of a phantom lesion in a scintigram of the equine tarsus. *Vet. Radiol. Ultrasound* **41**, 365-370.
9. Ueltschi, G. (2001) Radiologie und scintigraphie der wirbelsaule. In: *Proceedings of the 7th Geneva Congress of Equine Medicine and Surgery*. pp 47-51.

Chapter 10

ARTEFACTS AND NONSKELETAL UPTAKE ENCOUNTERED IN SKELETAL SCINTIGRAPHY

MARCUS J. HEAD
Rossdale & Partners, Beaufort Cottage Stables, High Street, Newmarket, Suffolk CB8 8JS, UK.

ARTEFACT

1. A product of human art and workmanship.
2. *Biol. etc.* A feature not naturally present, introduced during preparation or investigation.

The Oxford English Reference Dictionary, Oxford English Press 1996

INTRODUCTION

All imaging modalities produce artefacts. In some instances these can be manipulated and may aid diagnosis, but in most cases they are an annoyance and efforts must be made to minimise their effect. In skeletal scintigraphy, these frequently take the form of nonskeletal localisation of radionuclide and such artefacts may render the final image useless, make accurate assessment difficult, or even provide false information leading to misdiagnosis. Fortunately, most artefacts attributable to the hardware of the camera, collimator or computer are easily recognisable and many can be eliminated with routine quality control measures (see *Part I, Chapter 3*). The aim of this chapter is to provide a brief overview of the commonly encountered artefacts that occur during skeletal scintigraphy because of biological phenomena. This should enable their recognition and allow for speedier, more accurate and, ultimately, more satisfying scintigraphy.

SOFT TISSUE UPTAKE

Approximately 70% of an intravenous dose of ^{99m}Tc-methylene diphosphonate (Tc-MDP) and ^{99m}Tc-pertechnetate is excreted through the urinary tract within 4 h of injection[1]. Therefore, the bladder and kidneys feature on delayed phase images of the skeleton. Although activity associted with the kidneys and bladder is physiological, not artefactual, superimposition of this activity over skeletal sites in the acquired images can lead to potential diagnostic errors. In horses, the presence of a large, urine-filled bladder interferes with imaging of the pelvis. It is usually straightforward to distinguish between bladder activity and bone uptake by the pattern and shape of the region of radiopharmaceutical uptake (RU) (**Figure 1**). Comparison of tangential views and use of oblique views of the pelvis will demonstrate that the artefact extends beyond the boundaries of the normal bone outline. Masking such areas is possible with modern software and should be undertaken to ensure that subtle areas of skeletal increased radiopharmaceutical uptake (IRU) are not missed because of the intensity of uptake in the bladder. However, if

Figure 1

Dorsal bone phase image of the pelvis. There is marked, focal RU outside the boundaries of the pelvic bones (arrow) consistent with activity in the bladder.

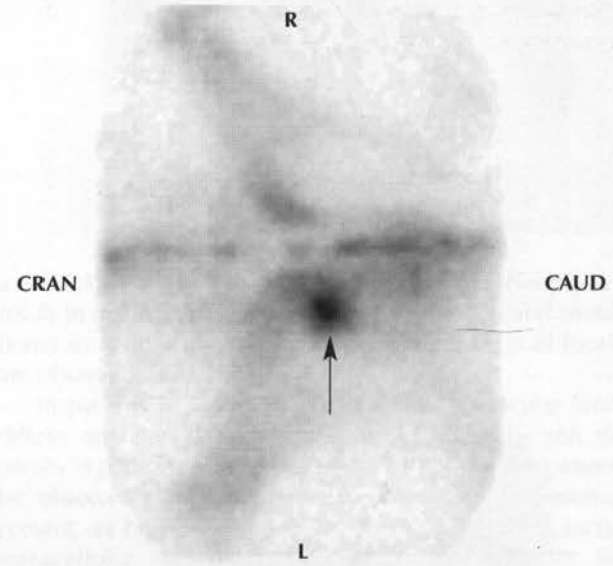

Figure 2

Right lateral bone phase image of the caudal thoracic spine. There is marked RU within the right kidney (arrow). This can obscure lesions in the caudal ribs or thoracic spine.

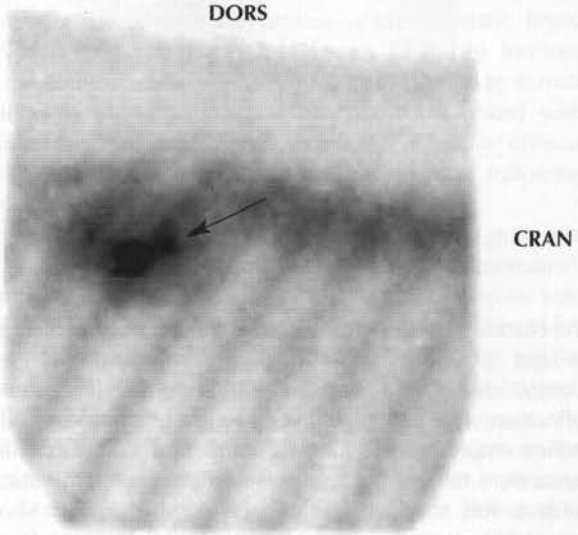

Figure 3

a) Caudal bone phase image of the pelvis. There are several linear regions of moderate IRU caused by uptake into damaged muscles (arrows). b) Lateral view of the right coxofemoral joint of the same horse as in (a). Note the moderate linear IRU in the caudal musculature.

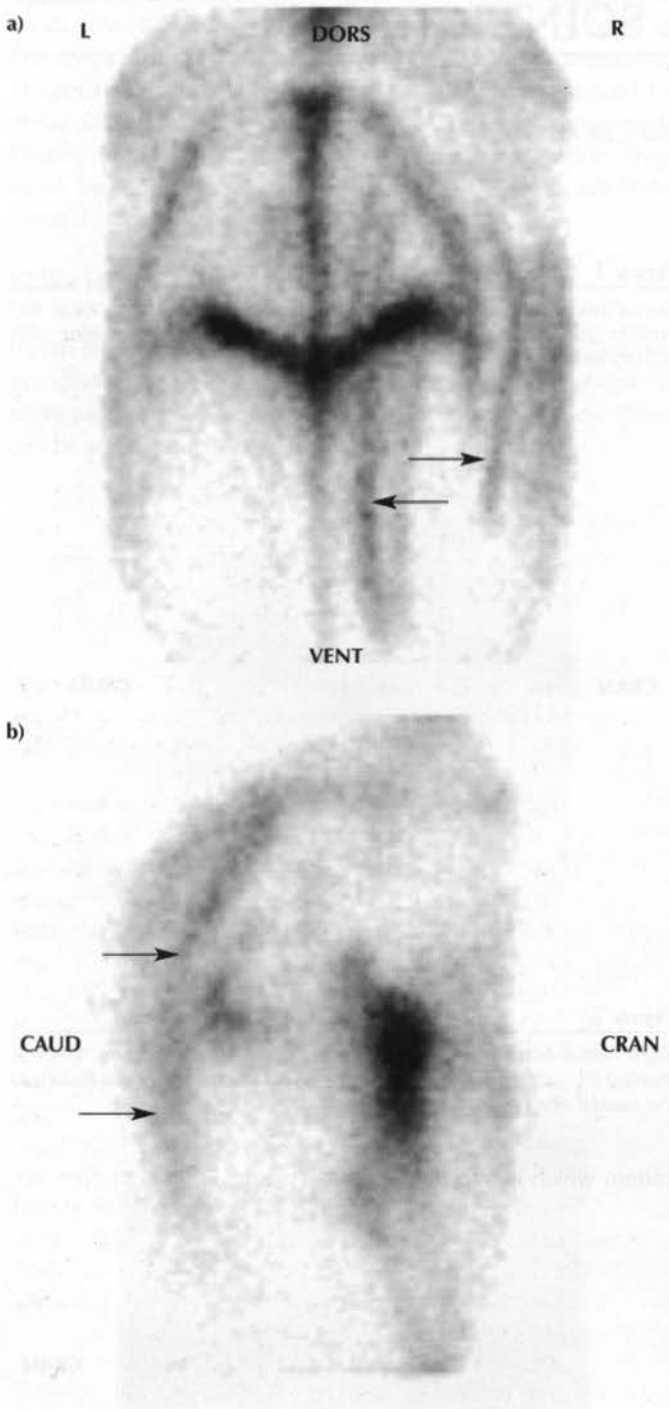

Figure 4

Left lateral bone phase image of the mid cervical region. There is a small, focal, intense area of apparent IRU within the ventral soft tissues of the neck (arrow) consistent with extravascular deposition of radiopharmaceutical during injection.

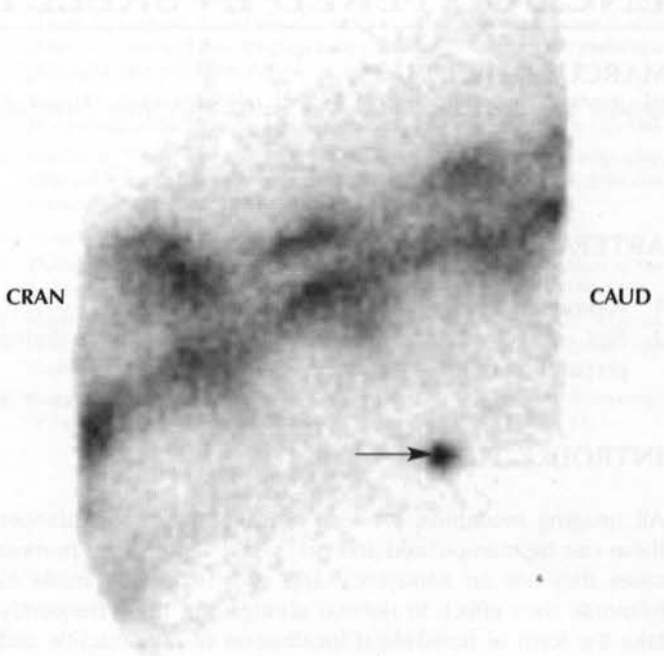

Figure 5

Right lateral bone phase image of the cranial cervical region. There is a small, focal, mild area of IRU in the soft tissues ventral to the first and second cervical vertebrae (arrow) caused by localisation of dissociated pertechnetate in the thyroid gland.

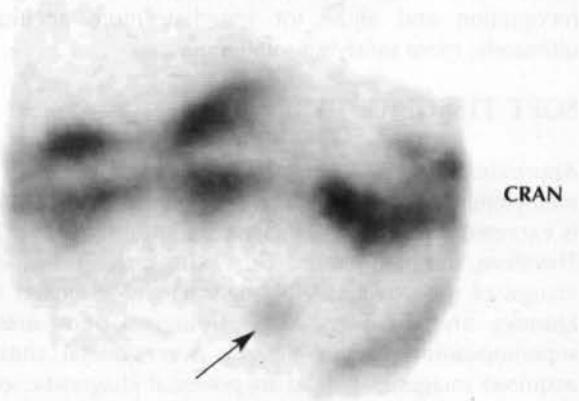

the bladder is superimposed over the area of interest, masking is not possible and image interpretation is seriously confounded. Image acquisition should be repeated after urination. The use of diuretics to hasten bladder filling and hence emptying is routine in many clinics. Occasionally, this procedure means that the horse enters the examination room with a full bladder. If this occurs, the animal should be returned to its stable immediately and allowed to urinate.

Localisation in the kidneys is easily recognised and, again, careful comparison of tangential views and the use of oblique views mean that this is not a significant problem. Heterogeneous uptake by the kidneys is frequently seen. Focal areas of IRU develop within the kidney and may underlie a rib. Areas of IRU in the caudal ribs should be assessed carefully in order to rule out renal uptake (**Figure 2**). Count stealing by the kidney can confound interpretation of

Figure 6

Artefacts created by fibular and tibial blocks. Matrix sizes 256 x 256. ***a)*** *Caudal and* ***b)*** *lateral views of the left tarsus and tibia of a 19-year-old Peruvian Paso gelding, obtained 48 h after performing 2 fibular and tibial nerve blocks. There is marked linear IRU associated with iatrogenic damage to the soft tissues adjacent to the tibia.* ***c)*** *Lateral view of left tibia of a 6-year-old Quarter Horse gelding, 24 h after fibular and tibial nerve blocks. There is marked linear IRU associated with the soft tissues lateral to the left tibia. Note the margin of the IRU extends beyond the margin of the cranial tibia, confirming it is not in bone. This could also be confirmed on a caudal view.* (a,b: Courtesy of Anne Bahr, Texas A&M University, USA. c: Courtesy of John Graham, University of Florida, Gainesville, USA.)

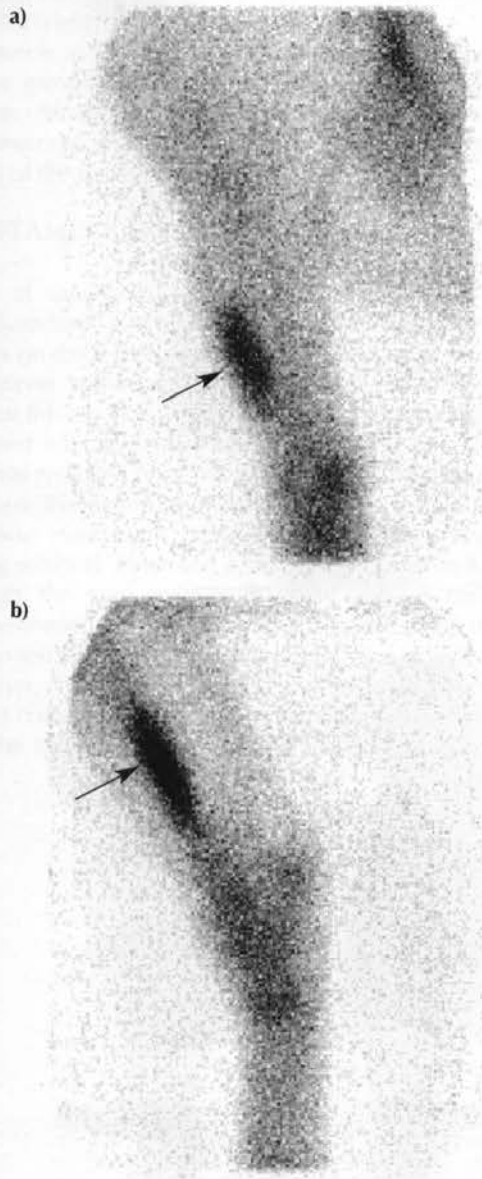

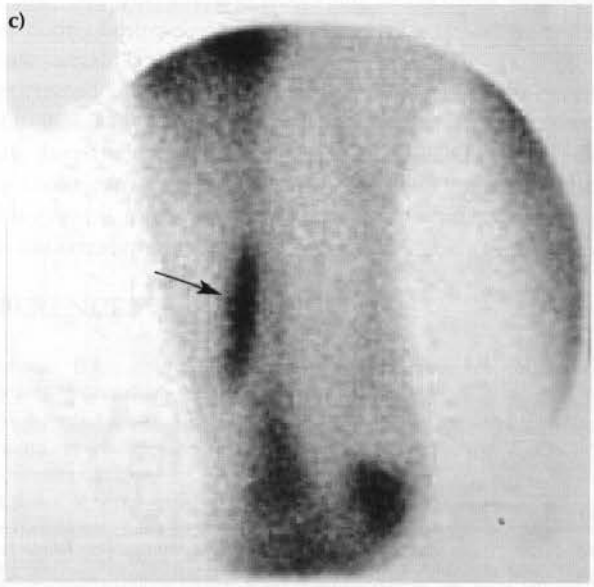

images of the caudal thoracic and cranial lumbar vertebrae and masking the kidney (see *Part I, Chapters 5 and 9*) facilitates accurate image interpretation.

In people, uptake by the mammary gland and pregnant uterus has been described[1], but this does not appear to be a problem in equine patients.

Calcification of soft tissues could be expected to result in nonskeletal deposition of radionuclide. This is certainly the case in small animals (e.g. *calcinosis cutis* in hyperadrenocorticism) and man (idiopathic pulmonary ossification, hyperparathyroidism)[1], but this phenomenon has not been observed by the author. *Calcinosis circumscripta* results in intense, focal IRU usually lateral to the stifle joint. It is generally readily differentiated as being outside the joint on a caudal view (see *Part I, Chapter 9, Figure 2*). Neoplasia may result in metastatic or dystrophic mineralisation and should be borne in mind if unusual single or multiple areas of focal IRU are observed.

In patients with poor renal and/or cardiovascular function, diffuse retention of bone tracers throughout the soft tissues results in poor bone to soft tissue contrast. A similar pattern will be observed in areas where large amounts of oedema are present, as bone tracers tend to accumulate in the increased extracellular fluid. Bone phase images of older horses commonly suffer from poor soft tissue/bone demarcation. ^{99m}Tc-MDP has a mild affinity for collagen and may localise in areas of scar tissue[1]. Rhabdomyolysis may cause localisation of radionuclide within muscle tissue. This is most commonly seen affecting the gluteal, *semitendinosus*, *semimembranosus* and *biceps femoris* muscles and produces a characteristic linear pattern which is often symmetrical (**Figures 3a and b**). In cases seen by the author, uptake within muscle has returned to normal on subsequent examinations and has not been linked with irreversible damage. This feature has been used in clinical practice in man to monitor heart muscle necrosis following myocardial infarction.

Even perfect intravenous injection technique may not prevent a small amount of extravasation of radiopharmaceutical. This results in an intense, focal area of IRU over the jugular vein (**Figure 4**). This can be a particular problem during studies of the cervical vertebrae. The author does not routinely place jugular catheters, but this is mandatory if the neck is to be imaged. Alternatively, a lead shield should be held over the injection site during image acquisition. Localisation of bone tracers in the lymph nodes may also occur following extravascular injection.

Poor labelling of the bone agent results in the presence of free pertechnetate and leads to a general increase in soft tissue

Figure 7

Lateral bone phase image of the left carpal region of a 9-year-old horse. There is moderate apparent IRU in the muscles caudal to the forearm (A) at the site of an ulnar nerve block carried out twice within 48 h of the scan. This horse had a nondisplaced radial fracture (B), the lameness from which was abolished by median and ulnar nerve block initially, and by median block only when the perineural analgesia was repeated one component at a time on the subsequent day. Matrix size 128x128.

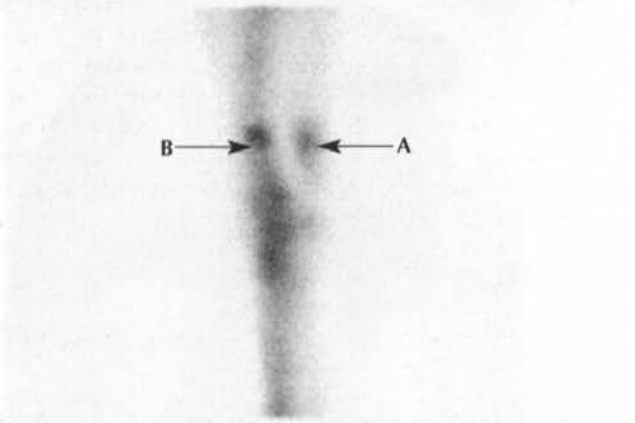

Figure 8

Dorsal bone phase image of the caudal pelvic region. The horse had a chronic right hindlimb lameness and associated disuse atrophy of the muscles over the right quarter. There is a general increase in counts recorded over all of the bones in the right hemipelvis due to reduced soft tissue attenuation.

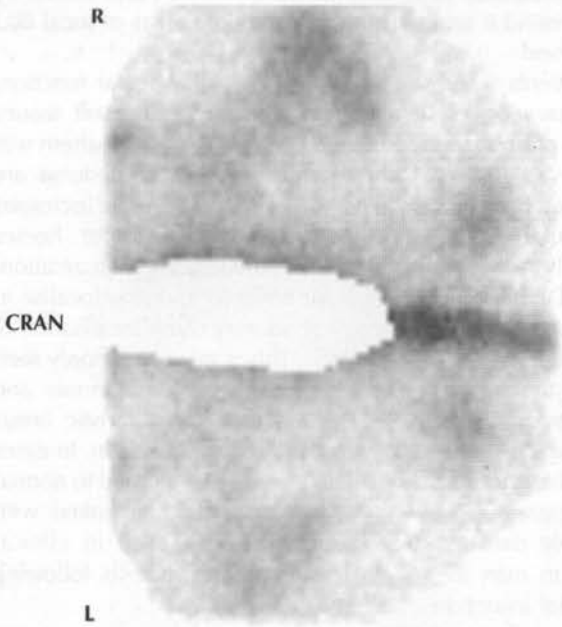

activity throughout the body[2]. Pertechnetate concentrates particularly in the thyroid and salivary glands (**Figure 5**). This artefact affects the overall quality of the image and it is important to recognise because it indicates technical problems with the generation of the labelled radiopharmaceutical.

Occasionally, mild, focal areas of IRU are seen in the soft tissues at the site of nerve blocks performed some time previously (particularly proximal limb regional blocks such as the fibular [peroneal] and tibial nerve blocks) (**Figure 6**). The

Figure 9

a) *Lateral bone phase image of the distal aspect of the left hindlimb. There is urine contamination of the solar surface of the hoof (arrows).* ***b)*** *Plantar bone phase image of the hocks. There are areas of intense, linear IRU on the skin surface caused by urine contamination (arrows). Note also the IRU in the left centrodistal joint (A) and the right second metatarsal bone (B).*

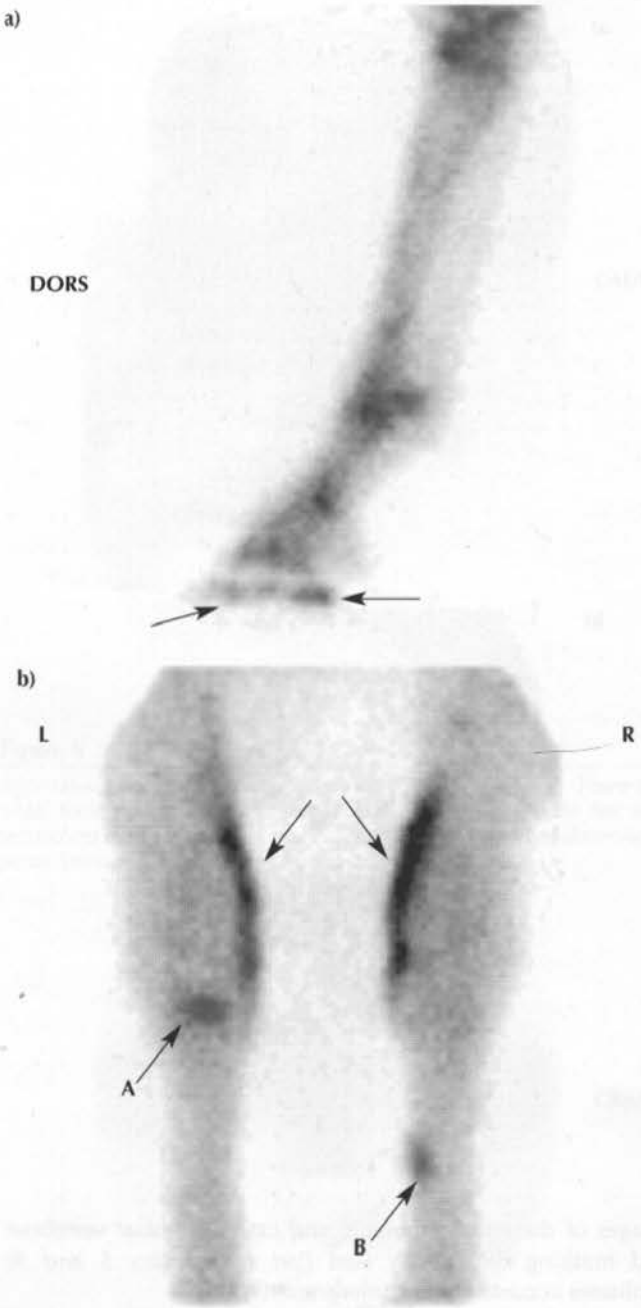

mechanism is probably due to local circulatory disturbances, muscle damage or direct binding to specific drugs. Investigations into this phenomenon have produced conflicting results[4-6]. Accumulation of bone markers at the site of recent injections is a relatively common finding, usually associated with the use of regional (perineural) anaesthesia[3] (**Figure 7**). Recommendations for the time to allow between nerve blocking and scintigraphic examination vary between clinicians. It is the author's view that nerve

blocks produce little effect on the distribution of radionuclide even if only a few days elapse between injection and examination. These artefacts can easily be accounted for if the complete history of the patient is known. In the author's opinion, recent regional anaesthesia is not a contraindication for bone scintigraphy. Other injections into muscle may produce abnormal soft tissue IRU[1], and this should be borne in mind when unusual patterns are seen.

Muscle atrophy results in an increase in the counts recorded by the gamma camera as a result of less attenuation by soft tissues. Atrophy due to a unilateral lameness results in asymmetrical images. This is most commonly seen on dorsal views of the pelvis (**Figure 8**).

CONTAMINATION

Areas of superficial, intense radiopharmaceutical localisation are characteristic of urine contamination. This most commonly occurs on the feet (**Figure 9a**), and measures to protect the feet of patients subsequent to injection of radionuclide help to prevent this artefact. Patients at the author's clinic have their feet wrapped with industrial tape immediately prior to injection, which is removed once the horse has left the stable, but before it enters the examination room. Gloves should be worn to minimise inadvertent contamination of the operator's hands during removal. However, a horse which box-walks may wear through the tape, with subsequent risk of contamination. Contamination on the palmar/plantar aspect of the shoe is easily recognised and can be masked out after image acquisition. However, if the horse is unshod and the solar aspect of the foot itself is contaminated, or there is urine trapped between the shoe and the sole, vigorous scrubbing of the foot is required and image acquisition must be repeated. Most clinics use boots or bandages on the distal limbs to promote radionuclide distribution and apply them several hours prior to injection. These should be left in place to protect the distal limbs from urine splashing and removed prior to image acquisition. Unfortunately, some patients urinate in the examination room and this may contaminate floors and equipment. Mares and fillies during oestrous sometimes represent a challenge and may urinate small amounts frequently, especially as they are manoeuvred into position (**Figure 9b**). Fortunately, urine contamination is easily recognised and, in cases where there is doubt, the patient should be cleaned and re-examined. Although inconvenient from an imaging point of view, the main concern in this event is safety and elimination of the radioactive residue from the environment (see *Part I, Chapter 12*).

REFERENCES

1. Lamb, C.R. (1990) Non-skeletal distribution of bone-seeking radiopharmaceuticals. *Vet. Radiol.* **31**, 246-253.
2. Daniel, G.B., Poteet, B. and Kowalsky, R.D. (1996) Image artifacts and quality control. In: *Handbook of Veterinary Nuclear Medicine*, North Carolina State University. pp 36-44.
3. Allhands, R.V., Twardock, A.R. and Boero, M.J. (1987) Uptake of ^{99m}Tc-MDP in muscle associated with a peripheral nerve block. *Vet. Radiol.* **28**, 181-184.
4. Gaughan, E.M., Wallace, R.J. and Kallfelz, F.A. (1990) Local anesthetics and nuclear medical bone images of the equine forelimb, *Vet. Surg.* **19**, 131-135.
5. Trout, D.R., Hornof, W.J., Liskey, C.C. *et al.* (1991) The effects of regional perineural anaesthesia on soft tissue and bone phase scintigraphy in the horse. *Vet. Radiol.* **32**, 140-144.
6. Trout, D.R., Hornof, W.J. and Fisher, P.E. (1991) The effects of intra-articular anaesthesia on soft tissue and bone phase scintigraphy in the horse. *Vet. Radiol.* **32**, 251-255.

Chapter 11

ELECTRONIC TRANSMISSION OF IMAGES

MARK J. MARTINELLI
California Equine Orthopedics, Encinitas, California 92404, USA.

In the 1990s, computer use for business and personal affairs increased dramatically. With the development of the internet, it became much more common to share information with others located at some distance. In human medicine, this enhanced communication has become known as 'telemedicine'. It is officially defined as communication and collaborative care enabled by multiple technologies. More simply stated, the goal of telemedicine is for specialists to aid in the diagnosis and treatment of patients not physically in their presence, via technological advancements. In practical terms, telemedicine can take many forms. It can mean taking radiographs in one location and then transmitting them electronically to specialists in large urban centres for interpretation. In another application, videoconferencing can put a virtual stethoscope or otóscope into the hands of experts from around the world, enabling remote diagnostic capabilities.

In veterinary medicine, most telemedicine revolves around diagnostic imaging. In this application, images must be acquired in, or converted into, digital information for transmission across network lines. Digitisation of the imaging modalities has become easier as a result of improved technologies. In equine scintigraphy, the new computer acquisition packages all function purely in the digital realm. This makes the electronic transfer of scintigraphic images especially germane.

This chapter describes image capture and their transmission by e-mail, which is as much as most readers will want or need to know. There is then a more detailed discussion of the mechanics of e-mail and file transfer protocol transmissions.

CAPTURE OF THE IMAGES

Most computer systems currently utilised for acquiring images in nuclear scintigraphy run a dedicated programme, producing raw data files that can be read only by that system. In order to facilitate transmission of images between individuals, it is imperative to convert the dedicated image format into a more universally read format. Depending on the scintigraphy software utilised, this may be accomplished in one of several ways. There may be a 'Save as' command within the programme that allows the user to choose the file format. Alternatively, many imaging programmes have an 'Export' function that accomplishes the same task.

In most systems, the images to be captured must be displayed individually. Using the print menu that enables you to print a hard copy of an image, there is usually an option either to export the file to a floppy disk or to capture the image and save it to an internal file so that the saved images can then be transferred *en masse* to a floppy disk. Each image needs a name so that it can be easily identified. The simplest method is to identify it by the name of the horse and then to number the images sequentially, or to also identify the area that the image depicts. There will be a choice of file format for the images.

CHOICE OF FILE FORMAT

The primary considerations for choice of format for sending and sharing images are 'universality' and 'file size compatible with interpretation'. The JPEG and TIFF (see *Glossary*) formats are most likely to be openable and readable by colleagues at another site, using almost any computer and image-handling programme. Most image capture systems enable this operation to be carried out simply by responding to the 'Save as' option in the 'Save' window.

Obviously, the more information recorded, the bigger the file. This has implications for sending images to a remote location as e-mail attachments. Some systems cannot handle overlarge or multiple attached files, and large files may take a long time to download or upload via the internet.

Table 1 gives an idea of the file size resulting from a typical monochrome scintigraphic image in different formats (matrix size 256 x 256). For comparison, a typical 2-page word processor document may be 20 Kb.

When viewed on a computer screen, there is little or no discernable difference in image quality between the above options, suggesting that there is little point in using a format that produces a larger file. It is therefore preferable to save files as JPEG or TIFF files.

Once the scintigraphic images are saved in a universal format, such as TIFF or JPEG, they can be transmitted to another location for viewing. There are several ways in which to accomplish this.

TRANSMISSION OF THE IMAGES

Files can simply be attached to an e-mail and then transferred electronically following the standard protocol for your internet service provider (ISP) and your computer's e-mail system. Alternatively, files of images can be sent using file transmission

Table 1: File sizes resulting from a typical monochrome scintigraphic image in different formats (matrix size 256 x 256)

Type of file	File size
Bitmap	193 Kb
TIFF	70 Kb
JPEG 'High'	25 Kb
JPEG 'Low'	12 Kb

protocol (FTP - see below). It is also possible to share bone scan images simply by posting them onto a website. For practices that host their own website, an area can be designated for posting bone scans for veterinarians or clients to access via their own computer. The pages should be password protected so only those with a right to view the images can sign on. One software system (Hermes) does allow for such access. The viewing workstation functions as a server on the internet so images can be viewed remotely.

This is as much as most of us want or need to know. The following discussion considers in more detail the logistics of e-mail and FTP transmissions and explains why problems are sometimes encountered.

E-MAIL

Viewing of the images by a recipient is sometimes difficult or impossible. In order to understand why there might be a problem with the transmission or encoding process, it is important to know more about the mechanics of e-mail. Once you hit the 'Send and Receive' button on your e-mail programme, an SMTP (simple mail transport protocol) server collects your outgoing message and transmits it, while a POP (post office protocol) server receives your incoming messages and stores them until they are collected by the addressee. In most instances these two aspects of the e-mail equation, the transmitter (SMTP server) and receiver (POP server) will be part of the same computer system, either within an institutional network or as part of your ISP network.

The protocols for SMTP and POP are fixed standards and use a system called ASCII (American Standard Code for Information Interchange) to encode e-mails. Neither cares what the content of the message is, but will ignore anything that is not in ASCII. ASCII is a set of characters that allow no special formatting like different fonts, bold, underlined or italic text. All the characters used in e-mail messages are ASCII characters. This character set enables rapid transmission of text from one place to another because the 'standard ASCII set' is comprised only of the characters 0–127. Computers, on the other hand, use a byte as their basic information packet. A byte can have 256 values (0–255). Consequently, if you sent a non-ASCII file via e-mail, it will come out garbled. Therefore, all e-mail messages are encoded in some way so that no number is greater than 127. These codes, however, may not be the same in all computers, and files containing these characters may not be displayed or converted properly by another ASCII programme. Because e-mail transmissions are limited to ASCII characters, graphics files and documents with non-ASCII characters created in word processors, spreadsheet or database programmes must be sent as attachments.

Attachments

To send graphics files, word processor files, programmes and other files which consist of characters which are more complex than the simple ones in the ASCII set, the file must be 'attached' to the e-mail message. In this way, the characters in the files are temporarily turned into ASCII characters. This temporary change is referred to as 'encoding' the file. When the file arrives at its destination it is 'decoded', reassembling the file into the original characters and character sequences.

The e-mail software used to send and receive e-mail handles the encoding and decoding of files. Different e-mail packages use different encoding/decoding methods and the user is generally not aware of the process unless the method that is used to encode the file is incompatible with the decoding method of the recipient's e-mail package. The three most popular encoding methods, in order of popularity, are UUEncode, Mime and BinHex.

It is important to know what method your e-mail software uses if you intend to send or receive any e-mail file attachments. The encoding method used when the file is attached to a message and sent must be the same method used to decode the file when it arrives at its destination, otherwise it will be unreadable.

It is sometimes advantageous to reduce file size prior to sending it as an attachment. There are numerous methods for reducing the size of a file so that it does not take up as much storage space on the hard disk, or can be transmitted more easily. Compressed files are files that have been temporarily shrunk by a special utility programme, many of which are freely available for both the PC and Macintosh (Mac). Frequently, compressed files are bundled together and archived so that groups of files can be transferred as one file.

An archive file is a file that contains other files; i.e. it is a bundle of files packaged together. Groups of files that belong together are archived because it is easier to move one bundled file from one place to another than it is to transfer many individual files, one at a time. Archiving programmes are also available, as freeware or for a nominal fee, that will work on either the PC or the Mac. Archived files are usually distinguished by their file extension. The most common are .zip, .arc, .lzh and .arj for PCs and .sit for Mac. Each requires a different utility to extract the individual files.

FILE TRANSFER PROTOCOL

File transfer protocol (FTP), a standard internet protocol, is the simplest way to exchange files between computers on the Internet, although it is not as common as sending e-mail attachments. FTP is an application protocol that uses the internet's TCP/IP protocols. Once the process is learned, it is much easier to transfer large files in this manner. For instance, FTP is commonly used to transfer web page files from their creator to the computer that acts as their server for everyone on the internet. It is also commonly used to download programmes and other files to your computer from other servers.

Basic FTP support is usually provided as part of a suite of programmes that come with TCP/IP. However, there are several FTP client programmes with a graphical user interface that are available as freeware and must be downloaded from the internet. Files can be transferred between a pair of machines with the FTP command, given that:

1. The machine you are using, the 'local host machine', has FTP and is somehow attached to the internet.
2. The machine you are attaching to, the 'remote host machine', is running FTP and is also attached to the internet.
3. You know the internet node name, also known as domain name, of the remote host machine. You may also use the remote host machine's internet IP address.

Most FTP programmes have detailed setup instructions for configuring the network connections.

SUMMARY

Save files as JPEGs or TIFFs. Send them as attachments to a covering e-mail, following standard protocol for your ISP and your computer's e-mail system.

GLOSSARY

There are many file formats that are used for images, but some are more useful and universally acceptable than others. The most compatible file formats for transmission across different platforms and operating systems are TIFF and JPEG. Other formats that the reader may encounter are BMP, MTF, GIF, PICT and EPS.

TIFF (Tagged Image File Format): This is a machine- and system-independent image standard, meaning it can be used on a Mac or PC. For this reason, it is a good choice for scientific applications and quantitative analysis. These files are labelled with '*.tif'.

JPEG (Joint Photographic Expert Group): Graphic file format created by this group of expert photographers from 2 international bodies. One of the notable aspects of this format is the high compression ratios that can be achieved without image degradation. Although JPEG employs significant data loss in compression, it does so by utilising an existing property of human vision where minute changes in colour are less noticeable than changes in brightness. Compression ratios can reach 10 or 20:1. It is also a good choice for compatibility between the Mac and PC. The suffix for these files is '*.jpg'.

BMP (Bitmap): This is a file format that is most commonly used in many PC applications, especially within the Windows operating system. Files created within these applications will automatically display the '*.bmp' suffix.

MTF (Metafile, Windows Metafile): This is another PC format that is exclusive to the Windows platform.

GIF (Graphics Interchange Format): A graphic file format originally developed by Compuserve for use on the internet. It supports colour image files and employs a patented lossless compression algorithm labelled LZW (Lempel-Ziv Welch). This relies on identifying a group of pixels of the same colour rather than listing each individual pixel. Images are labelled with '*.gif'.

PICT (Picture Format): This graphic file format is native to the Macintosh system. It is an object-oriented graphic format that relies more on the colour of each pixel than on the actual pixel value. Images are usually tagged with '*.pct'.

EPS (Encapsulated PostScript): A standard format for a drawing, image or complete page layout, allowing it to be placed in other documents. Exclusive to this file format, the header contains a low resolution preview of the file. The file suffix is '*.eps'.

FURTHER READING

Pfaffenberger, B. (1997) *Webster's New World Dictionary of Computer Terms*, 6th edn., Simon and Schuster, New York.

Hutchinson, T. (1997) *Dictionary of Computing, Multimedia, and The Internet*, Helicon Publishing Ltd., Oxford.

Chapter 12

RADIATION SAFETY

ROB C. PILSWORTH and KAREN GOLDSTONE
Rossdale & Partners, Beaufort Cottage Stables, High Street, Newmarket, Suffolk CB8 8JS, UK.
East Anglian Radiation Protection Services, Addenbrookes Hospital, Cambridge, Cambridgeshire CB2 2QQ, UK.

Nuclear medical studies involve the use of radioactive isotopes which are defined as open sources, i.e. the isotope is in a form that could potentially contaminate the environment, and is not sealed within any form of safety apparatus. Most of these solutions of isotopes visibly resemble water, have no smell, and therefore present real risks of inadvertent contamination.

For this reason, it is paramount that careful evaluation of the handling of these isotopes is made prior to the commencement of scintigraphic work, and that regular monitoring of dose rates received by staff and the degree of environmental contamination is carried out using suitable detectors and monitors.

In the UK, these activities are governed by several different sets of legislation. Under the Radioactive Substances Act of 1993, the Environment Agency issues licences both for keeping and using isotopes (the Registration) and for the accumulation and disposal of radioactive waste (the Authorisation). These licences are held separately from each other and both must be obtained. Once licensed, the work in practices for scintigraphy is governed by the Ionising Radiation Regulations 1999, an approved Code of Practice and guidance notes for which are available from the Health and Safety Executive[1]. The British Veterinary Association also publishes a résumé of these regulations and specific veterinary guidance notes[2], which are much more easily understood and are directly applicable to the horse. Obviously, scintigraphy is carried out worldwide, and other countries will have other sets of rules and regulations. It is not, therefore, the role of this chapter to go into great detail on the situation in the UK. However, the guiding principles of radiation safety, which would enable the UK's regulations to be obeyed, lead naturally to sound, safe working practices, and will form a sensible foundation for scintigraphic work elsewhere. It is worth stressing, however, that in certain countries the regulations are even more restrictive than in the UK, and prior assessment of these regulations is vital in order to avoid the risk of prosecution.

GENERAL PRINCIPLES

Radiation dose is affected by three main factors:

1. **Time** - of duration of exposure.
2. **Distance** - as a result of the inverse square law, doubling the distance between a point source and a worker results in a 4-fold reduction in the dose received.
3. **Shielding** - involving the use of screening with substances which have great powers of absorption of radiation, resulting, for instance, for ^{99m}Tc, in a 10-fold reduction of dose per mm shielding in the case of lead.

No other factors are involved, and if each of these is considered in turn for the whole process of performing scintigraphy, and steps taken to ensure that the dose reduction achieved is the maximum practical, then actual doses received are extremely small. However, clinics which use thermoluminescent dose meters or film badges for personal monitoring in radiography, worn beneath the lead aprons, will be used to getting film badge readings of 0 mSv (see below). This will not be the case once scintigraphic examinations are carried out on a regular basis, and staff are naturally alarmed when their normal radiation monitoring badge reading becomes higher. It is up to us as clinicians to ensure that all staff understand fully the risks involved of working with radiation, have a good grasp of the relative levels of exposure which may lead to damage, and use the principles of radiation protection at every stage to keep these doses as low as reasonably achievable; the ALARA principle. To do this, regular staff training is absolutely vital.

The most logical way to assess radiation safety in the context of scintigraphy is to go through each step of the process involved in the scintigraphic examination of the horse, look at the potential sources of radiation exposure, examine the potential risk if no safety measures were instituted, describe those safety measures, and make an assessment of the likely dose received using good working practices.

The theoretical dose risk in each case has been derived from the published dose constants for ^{99m}Tc[3]. The actual dose rates received following protection measures were measured using a commercial dose rate meter (Mini Instruments Minirad 1000 dose rate meter)[a] calibrated for detection of γ-rays.

UNITS FOR MEASUREMENT OF RADIATION

The standard SI unit for an absorbed dose of radiation is the Gray (Gy). However, because different types of radiation have different degrees of ability to damage tissue and, indeed, tissues have different sensitivities to radiation, the concepts of equivalent and effective doses were introduced. The equivalent dose is defined as the absorbed dose in Grays multiplied by a radiation-weighting factor. This weighting factor is a direct consequence of the ability of the radiation to produce cellular and tissue damage. For instance, the weighting factor for alpha particles is 20, making them extremely dangerous dose for dose compared with γ-rays. Fortunately for us, the weighting factor for γ-rays is 1 so the equivalent dose, expressed in Sieverts (Sv), is exactly the same as the absorbed dose in Grays. The effective dose in Sieverts used in the remainder of this chapter takes into account

Table 1: Radiation received from various environmental sources

Source	Equivalent dose
Chest x-rays (posterior-anterior and lateral)	0.02–0.05 mSv
Annual background radiation (London)	2.6 mSv/year
Annual background radiation (Cornwall)	7.8 mSv/year
Cosmic rays (air couriers)	5 mSv/year

differing tissue and organ sensitivity. The normal subunit we will employ is the milli-Sievert (mSv) or micro-Sievert (μSv). **Table 1** puts these figures into clinical context.

STEP 1: ELUTION, LABELLING AND CALIBRATION OF ISOTOPE

If at all possible, radiopharmaceutical should be received ready-labelled from a hospital radiopharmacy. Although this may be expensive and inconvenient, it removes altogether one of the major sources of ionising radiation hazard in the process of scintigraphy, in that no handling of open vials is necessary on site. Most human hospitals that have a radiopharmacy are very helpful and cooperative in the preparation of isotope doses for equine patients and, if distance and cost are not logistically impossible, this avenue should be pursued vigorously. If, however, a local supply of ready-labelled pharmaceuticals is not available, it then becomes essential to take receipt of a ^{99m}Tc generator from a commercial supply company. These generators are completely encased in radiation shielding and in themselves present little risk. Nevertheless, a system of safe housekeeping should be set up in advance of receiving the first generator, which will require the following steps:

1. (i) The radiopharmacy area must be adequately labelled, locked, and not accessible to other members of staff or the public. It should include eye wash bottles and a sink for decontamination and washing in case of accidents.
   (ii) The bench area should have a smooth, impervious, easily cleanable surface which should be coated with absorbent bench coat. This allows spillages to be dealt with by removing this coat and storing it in a safe area to allow disposal following adequate natural decay (60 h or 10 half lives is usually sufficient). The edges of the bench should be sealed and gaps and cracks in the surface should be avoided.
   (iii) Arrangements should be made for safe delivery of the generator into a specified lockable location on each occasion.
   (iv) Before elution of the isotope, the radiopharmacist must put on disposable gloves, a suitable overall, facemask including eye protectors and disposable overshoes. In this way, any spillage, splashing or inadvertent spraying of isotope can be dealt with by removal of protective clothing rather than by decontamination of affected skin.
   (v) A radiopharmacy preparation area has to be in place that includes either sufficient brickwork to protect the legs below the bench, lead shielding (at least 2 mm of lead) and a lead glass observation panel, behind which work which involves movement of unshielded vials can be carried out (**Figure 1**).

Figure 1

Drawing up measured doses of isotope for calibration behind the lead glass observation window. (Courtesy of A. Nelson, Rainbow Equine Clinic, Malton, UK.)

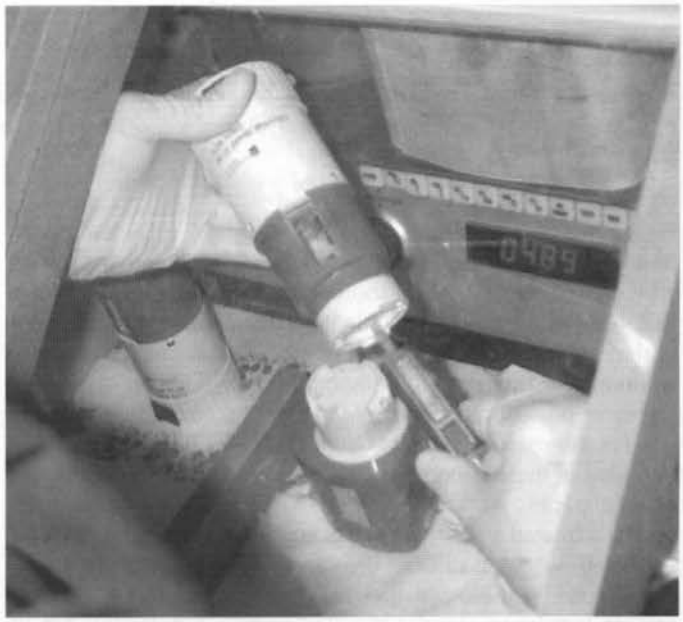

2. Handling tongs must be employed to move the vial from the elution chamber of the generator to the calibration equipment and from the calibration area to a safe lead storage pot. The vial must otherwise always be held in a lead pot of sufficient thickness to eliminate significant radiation leakage.
3. These movements should obviously be carried out rapidly to shorten the time during which the unshielded vial has the potential to irradiate the radiopharmacist. Once the dose required for labelling has been calculated, it is drawn up in a syringe held within a lead syringe shield. The size of the syringe should be as large as is practical in relation to the dose. For instance, to prepare a dose of 2 ml, a 10 ml lead shielded syringe should be used. This moves the fingers significantly further away than when using a 2 ml syringe, and results in an approximately 4-fold reduction of dose to the extremities.
4. Once whatever pharmaceutical is to be used has been labelled with technetium, it should be placed within a lead pot with a closely fitting lid. The lid should be sealed onto the pot with tape and a prescription label written out indicating the amount of activity present at the time of preparation, which pharmaceutical has been used, the date and the name of the radiopharmacist responsible for preparation. In the UK, this information must be recorded and kept for a minimum of 2 years.

Theoretical Potential Dose

Handling an unshielded flask of 5 GBq technetium held with the fingertips, a dose rate to the hand of 385 mSv/h might be received. Once placed within a glass injection vial but unshielded, a dose rate to the body, 100 cm away, of 0.12 mSv/h would result.

Measured Dose Rates Following Protection Measures

Actual dose rates recorded at the mouth of the elution chamber in a hospital radiopharmacy varied between 20–100 μSv/h. The dose rate at the orifice of a lead injection vial containing 5 GBq is 200 μSv/h. At the plunger end of a lead-shielded 10 ml syringe holding the same dose in 3 ml, a radiation level of 1–2 mSv/h was recorded. Ambient levels in a radiopharmacy bench area of approximately 10 μSv/h have been recorded in the hospital setting, with an average body dose of 3 μSv/session recorded[4]. Using the lead shielding described, in conjunction with long handling tongs and a lead glass observation panel, the actual doses involved in preparation of isotope are therefore kept extremely low.

STEP 2: DRAWING UP OF ISOTOPE AND INJECTION OF THE HORSE

1. The isotope should be kept contained within the lead storage vial and, immediately prior to injection, a perforated injection cap exchanged for the normal cap. This allows needle entry into the glass vial without undue exposure of fingers.
2. A syringe size should be selected which is approximately 4 times the required dose. In most cases, this will be a 10 ml syringe. The syringe should be encased in a lead or tungsten syringe shield (**Figure 2**).
3. Full protective overalls, disposable gloves and overshoes should be worn by both the person injecting the horse and the handler holding the horse.
4. A finger extremity monitor should be worn by the operative injecting the horse, on the same hand used to draw up the dose (**Figure 2**).
5. If possible, the horse should have an intravenous catheter placed prior to injection of isotope. This can be left *in situ* and flushed with heparin saline, so that further injections of diuretic and sedative prior to scintigraphy can be carried out through the same catheter, which can then be removed. Where clipping of the neck is not acceptable because of possible adverse effects on other management aspects, precluding the use of a catheter, great care should be taken during injection so that inadvertent injection of attendant personnel does not occur. If there is any potential difficulty in this respect, the horse should be sedated prior to handling and injection of the isotope.

Theoretical Potential Dose

An unshielded 5 ml syringe containing 5 GBq technetium would give a dose rate to the fingers of approximately 1770 mSv/h, and would exceed the annual dose limit in the UK in less than half an hour. This is obviously a high dose and can be reduced significantly by fitting a syringe shield. However, in the long axis of the syringe there is still effectively little barrier between the isotope and the fingertips. For this reason, extremity monitors are essential, and handling of the isotopes should be as rapid as possible to minimise exposure time. Under UK law, the legal limit for annual radiation exposure to the extremity is significantly higher than that for whole body (500 mSv vs. 20 mSv, respectively).

Figure 2

Drawing up an equine dose through a perforated vial cap. Note the extremity dose monitor on the wrist, in line with the unshielded port of the syringe, the syringe shield, and the protective gloves and overalls.

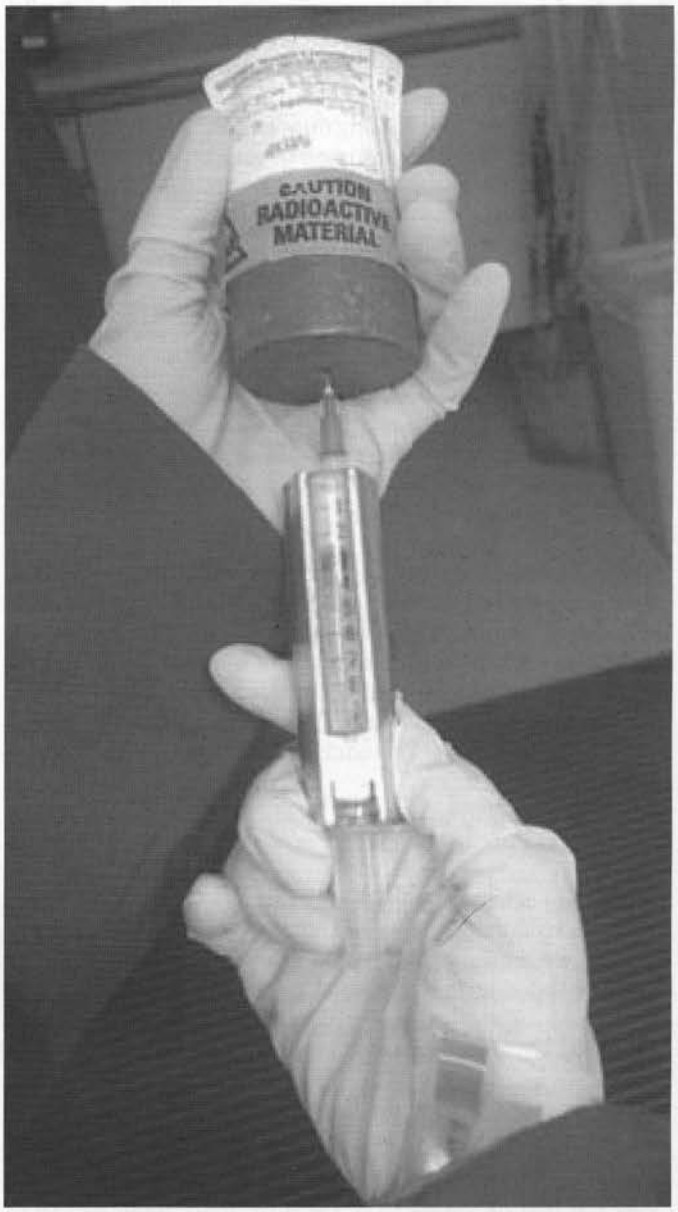

Measured Dose Rates Following Protection Measures

A shielded 10 ml syringe containing 5 GBq technetium in 3 ml gives recorded dose rates of:

1. At the clinician's body level, 20 μSv/h.
2. At the surface of the lead syringe casing, 30 μSv/h; 200 μSv/h at the lead glass window.
3. At the plunger of the syringe, between 1–2 mSv/h.

Obviously, in practice these syringes are handled for seconds, not hours, and experience of injecting 3 x 5 GBq on a daily basis gives extremity monitor readings of approximately 0.2–0.4 mSv/month. No body dose readings have been registered on the injector's whole body monitor.

STEP 3: DISTRIBUTION AND CLEARANCE OF THE ISOTOPE

During this period, the horse contains the whole of the injected dose. In the case of bone scanning, this will be gradually adsorbed into the skeleton, or excreted in urine. The urine pool on the stable floor presents one of the most significant risks of exposure because a) it is not shielded in any way, b) there is no attenuation of the γ-rays passing through soft tissues, in contrast to that portion of the dose adsorbed by the skeleton and c) from one-third to half of the injected dose is voided in the urine.

For this reason, the horse's stable should be regarded as a controlled area and the door adequately marked with the following information:

1. The radiation trefoil marker and the words 'Controlled area, radioactive material'.
2. The telephone number of the responsible party in case of an emergency.
3. A statement to the effect that the horse in the stable is radioactive, entry should be kept to a minimum, and overshoes and overalls must be worn.

The horse should not be groomed and no droppings or contaminated bedding removed until 10 half lives (60 h) from injection of isotope. It may be possible to negotiate with the regulatory authority on the removal of bedding from the box before this time, as long as the contaminated bedding is stored in a demarcated location on site, and is safely contained and suitably labelled as radioactive until decay has been completed for 60 h.

Theoretical Potential Dose

The average activity administered to the horse is 5 GBq ^{99m}Tc. Assuming half of this is excreted, with no decay, a urine pool of 2.5 GBq would result. This would give a radiation dose rate at 30 cm of approximately 1.3 mSv/h.

Measured Dose Rates Following Protection Measures

By eliminating access to the stable, the potential dose can be avoided altogether. However, the horse must be retrieved for the actual examination, and measured dose rates at this time, following 2–3 h of decay, are as follows:

1. At the urine pool, 0.5–1 mSv/h.
2. At 30 cm from the urine pool, 200–400 μSv/h.
3. At the stable door at injection, 20 μSv/h.
4. At the stable door 3 h after injection, 5 μSv/h.

The actual doses received by staff can be kept very small by ensuring rapid entry and exit to the stable and by using radiation signs to keep staff away from the stable doors.

STEP 4: THE SCINTIGRAPHIC EXAMINATION

During this process, it is unavoidable that staff will be in close proximity to a horse which carries significant levels of radioactivity. All 3 of the primary tenets of radiation dose reduction, time, distance and shielding, can be employed during this process to limit that dose under the ALARA principle. The following steps will ensure this:

1. The person restraining the horse for the examination should constantly be reminded to increase his or her distance from the horse's head once the horse is stationary.
2. A lead apron should be worn by the horse handler. Although γ-rays will not be halted by 0.25–0.35 mm of lead equivalent, the dose received will nevertheless be significantly reduced by approximately 50%. As long as a reduction is reasonably achievable it should be pursued; the wearing of a lead apron is therefore both sensible and advisable.
3. Consideration should be given to manufacturing a lead blanket for the horse to wear. Because of the weight of lead rubber, workers cannot normally be expected to wear more than 0.35 mm of lead equivalent. However, a 0.5 mm lead equivalent material will result in 60–70% reduction of γ-ray emission. The horse is certainly strong enough to wear this kind of protection. If a lead rug is made, it has to be manufactured in interlocking sections as the weight of the complete rug is too great to allow manual fitting to the horse (**Figures 3 and 4**).
4. All personnel in the room containing the horse should stand as far away from the horse as is practically possible, thereby reducing the dose received.
5. Dose monitoring badges should be worn by all members of staff and the room should be considered a 'strictly controlled' area. In the UK, this has important legal ramifications once the room is classified as such. In other countries, specific guidance should be sought on any regulations contingent upon a room containing a source giving rise to an ambient radiation dose rate of more than 7.5 μSv/h.
6. Contingency plans should be in force for the possibility of the horse urinating during the examination. A bucket on a handle containing a lining layer of at least 3 cm of wood shavings or cat litter to prevent splashback is ideal. Should the horse urinate on the floor, then the room should be cleared and an absorbent material (cat litter is ideal) sprinkled on the urine pool. This should be allowed to soak up the urine and then be swept up and bagged for storage to allow adequate decay. The surface of the floor should then be decontaminated using a cationic detergent solution specifically recommended for the job. All workers should wear disposable gloves, overshoes and overalls while performing decontamination work.
7. A contamination level at which work can continue following decontamination should be established, taking advice from trained authorities (in the UK this will be the Radiation Protection Advisor). Bear in mind that the gamma camera itself may detect contamination if it is not dealt with satisfactorily; this will result in the presence of artefacts on the images.

Theoretical Potential Dose

This is very difficult to calculate, as there are so many variables. Of the 5 GBq injected dose, approximately 2.5–3.0 GBq will remain in the horse. However, this will have decayed for 3 h, which results in a 25% fall in activity. It will also be distributed throughout the horse, the majority being in the skeleton.

Figure 3

The lead rug in place on a patient. Each panel can be removed individually for scintigraphic examination and replaced immediately following this procedure.

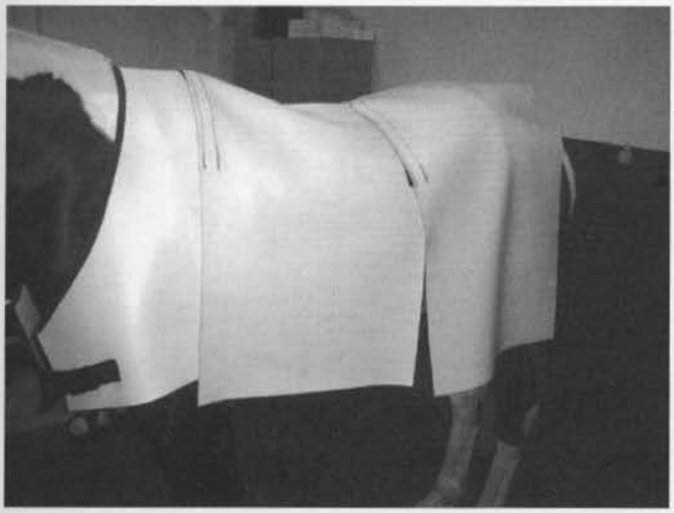

Figure 4

Right lateral view of thoracolumbar spine and right kidney. Matrix size 256 x 256. The lead rug has been placed over the cranial two-thirds of the field of view. The effect of 0.5 mm lead equivalent on staff doses received is clearly demonstrated.

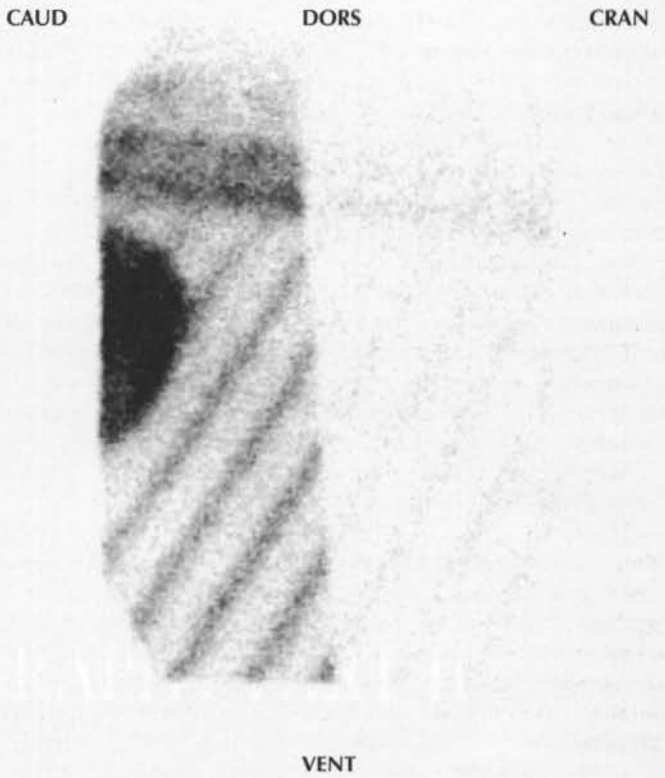

The half value layer for soft tissue is approximately that of water (4 cm), so the soft tissues of the horse result in significant dose absorption. Actual measured values without protection measures are therefore used here.

A horse injected with 5 GBq of activity and scanned 3 h from injection will typically have surface readings of 50–70 μSv/h. At 30 cm from the horse, this falls to 15 μSv/h. This is also the dose rate measured at the body of a handler when no lead gown or lead rug on the horse is used.

Measured Dose Rates Following Protection Measures

Actual measurements around a 500 kg horse injected with 5 GBq technetium and scanned 3 h later were as follows:

1. Horse skin surface, over rump, 50 μSv/h.
2. Horse skin surface, over rump, horse wearing 0.5 mm lead equivalent rug,15 μSv/h.
3. At handler's body surface, no lead gown or rug, 15 μSv/h.
4. At handler's body surface, no lead gown, horse wearing lead rug,10 μSv/h.
5. At handler's body surface, horse wearing lead rug, handler also wearing 0.25 mm lead equivalent apron, 2.5 μSv/h.

Using the principles of time (rapid and efficient scanning, and rotation of four staff members), distance (constantly being aware of avoiding proximity to the horse) and shielding (lead aprons for both horse and staff member) doses actually recorded by staff film badge readings range from 0.0–0.2 mSv/month in the author's clinic, scanning approximately 55 horses/month, rotated between 4 staff. This gives an actual dose/scan (based on 0.1–0.2 mSv/13 scans) of 7–15 μSv/scan. Actual measurements with an electronic personal dose meter (Siemens EPD)[b], which gives a direct reading, are in accord with this, with readings of 6–10 μSv/scan. In the UK, the dose level which would require a worker to be classified as a radiation worker is 6 mSv *per annum*; one groom would have to hold 500–1000 horses for scintigraphy for this to occur. In a clinic large enough to carry out this number of scans, it should be possible to ensure this does not occur by sensible staff rotation.

This introduces another method of dose reduction, that of 'dose sharing'. Regulations in the UK make it very clear that dose sharing must **never** be used to dilute unacceptably high dose levels so that they do not breach safety limits. Legislation requires that doses must be restricted by: first, using engineering controls, design and safety features; second, using systems of work; and third, using personal protective equipment. It does, however, make sense, having put in place all of the above steps, to rotate staff evenly so that the very small residual dose which cannot be reduced further is spread evenly between several workers, ensuring even lower personal doses.

STEP 5: FOLLOWING SCINTIGRAPHY

Waste Disposal

Contaminated needles, syringes and gloves can be stored for sufficient decay to allow disposal in the normal waste routes. A simple rolling system of storage bags marked with the days of the week will ensure a full seven days of decay, with no possibility of inadvertent earlier disposal. Bags should be checked with a monitor before disposal to establish that activity is negligible.

Horse Waste

The stable should not be entered for cleaning until 60 h after injection, according to the UK guidelines. Many clinics have emptied waste earlier than this, and stored it elsewhere until ultimate disposal from the site at a much later time. Detailed guidance on this should be sought from the regulatory authority in each country concerned.

The Horse

Experimental data shows that the horse falls below the level classified as a controlled area (7.5 μSv/h) by 24 h following injection. Further work-up, such as lameness investigation or radiography, should therefore be delayed until that time. It would seem realistic to allow these patients home at the total remaining activity permissible for a human to use public transport in the UK (0.5 GBq), which would also take 24 h (4 half lives) However, the possibility of contamination must also be considered. There will be great individual variation in this between countries; again, detailed individual guidance should be sought on this.

CONTAMINATION DETECTION

As the radioactive substances we use are invisible and have no smell, it is vital that monitoring for possible contamination is performed on a regular basis. This monitoring should include all sites in which isotope is handled and the hands and feet of workers who have been handling horses for nuclear medical studies. To do this, the purchase of a suitable contamination detector (Mini 900 Ratemeter, Type 44A probe)[a] is essential. These detectors are extremely sensitive, usually calibrated in counts/sec, and give alarming levels of noise for a very small amount of radioactivity. They therefore tend to alarm staff who are used to images of a Geiger counter in televised drama productions. My own view is that it is essential also to purchase a radiation dose meter[a], which will measure the radiation dose arising from the radioactive levels in the horse or in any contamination. This helps to allay staff fears when they see how small these doses are. This is also vital following accidental spillage or urination, in establishing a safe level of background radiation at which to restart work in the room.

In the UK, these instruments have to be tested and their performance checked annually. A hospital department of Medical Physics or your Radiation Protection Adviser will be able to help. The record of the test must be kept for two years. As a routine, the bench area should be inspected for contamination and the reading recorded, on a daily basis. Similarly, hands and feet of all personnel should be checked before and after injecting the horse and before and after scintigraphic examinations. Any contamination should be removed using standard cationic detergent solutions (Decon 90)[c] until radioactive levels return to a maximum of twice background and no more activity can be removed.

ENVIRONMENTAL MONITORING

These instruments should also be used to carry out regular (at least every two months) environmental monitoring of areas such as the muckheap and the horses' stables, so that radiation levels in these areas can be recorded. Again, these records should be kept for a minimum of two years under UK legislation.

MANUFACTURERS' ADDRESSES

[a]St Gobain Crystals and Detectors UK Ltd.,Burnham-on-Crouch, Essex, UK.
[b]Siemens Environmental Systems Ltd., Poole, Dorset, UK.
[c]Decon Laboratories, Hove, East Sussex, UK.

REFERENCES

1. Anon (1999) *Approved Code of Practice and Guidance Notes. Work with Ionising Radiation. Ionising Radiation Regulations 1999*, HSE Books, Sudbury, UK.
2. Anon (2002) *Veterinary Guidance Notes for the Ionising Radiation Regulations 1999*, BVA Publications, London, UK.
3. Anon (2002) *Radiation Protection Dosimetry: Radionuclide and Radiation Protection Data Handbook*, Nuclear Technology Publishing, Ashford, Kent, UK.
4. Barber, R.W. Unpublished data.

FURTHER READING

1. Huda, W. and Boutcher, S. (1989) Should nuclear technologists wear lead aprons? *J. Nuc. med. Technol.* **17**, 6-11.
2. Neuwirth, L. and Romine, C. (2000) Ancillary equipment to increase quality and reduce radiation exposure in the equine nuclear medicine laboratory. *Vet. Rad. Ultrasound* **41**, 470-475.
3. Widmer, W.R., Shaw, S.M. and Thrall, D.E. (1996) Effects of low-level exposure to ionising radiation: current concepts and concerns for veterinary workers. *Vet. Rad. Ultrasound* **37**, 227-239.

EQUINE SCINTIGRAPHY PART II

FIGURE LAYOUT *for* PART II

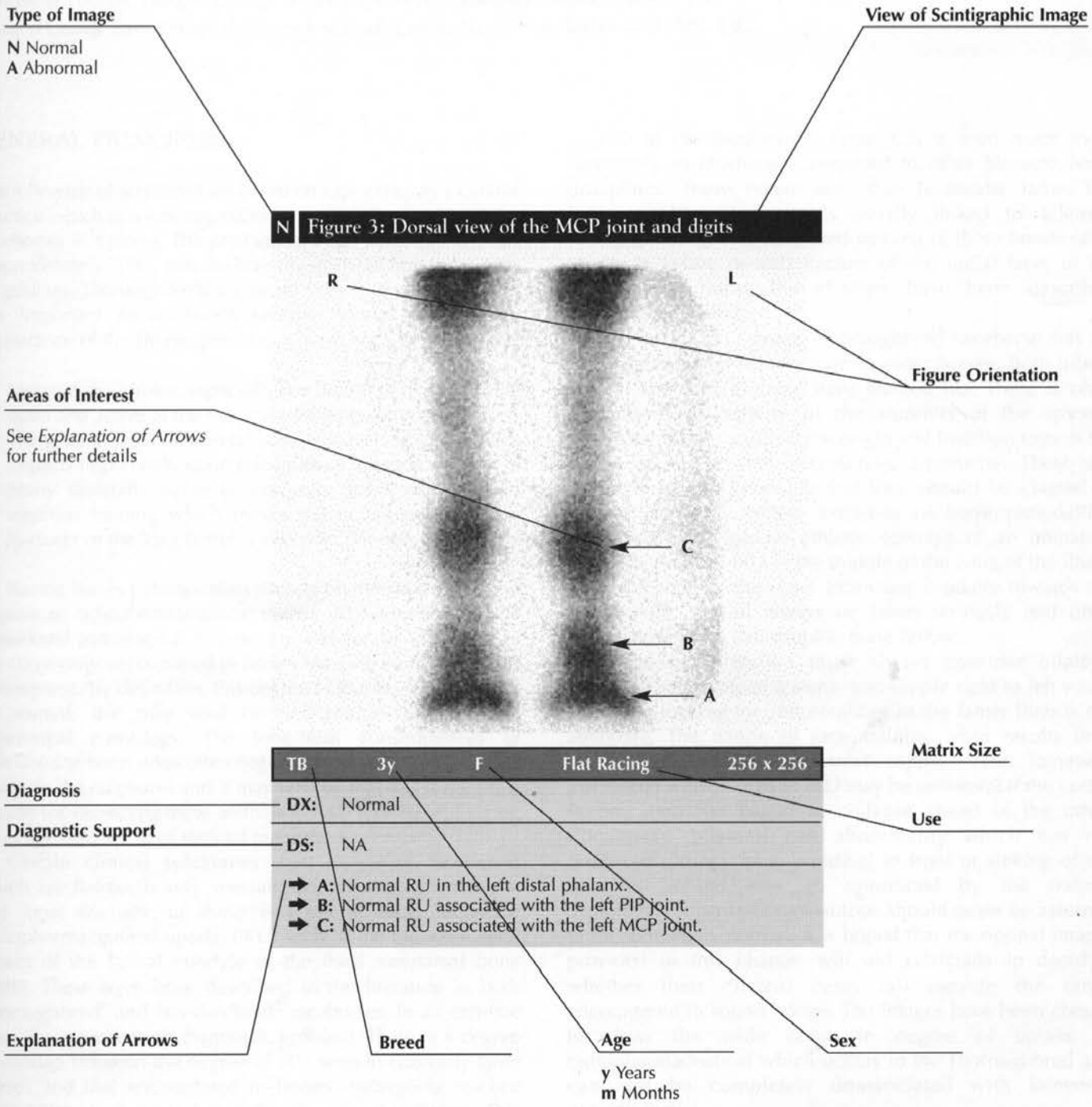

See page 12 for a full explanation of Terms and Abbreviations.

Chapter 1

THE EUROPEAN THOROUGHBRED

MIKE C. SHEPHERD and JOSIE MEEHAN
Rossdale & Partners, Beaufort Cottage Stables, High Street, Newmarket, Suffolk CB8 8JS, UK.
Beaufort Cottage Equine Hospital, Cotton End Road, Exning, Newmarket, Suffolk CB8 7NN, UK.

GENERAL PRINCIPLES

The following observations are based on experience in a clinical practice which services approximately 1000 Thoroughbred flat racehorses in training. The predominant age range is 2–3 years (approximately 70%), and the majority (65%) of horses are colts or geldings. Thoroughbreds are raced from 2 years of age. This has important repercussions for the normal scintigraphic appearance of the Thoroughbred racehorse because:

- Many of the physes, especially the distal radial physes, are open and active at the time race training commences.
- The general level of skeletal bone turnover is high and this impacts importantly upon principles of interpretation.
- Many skeletally naïve or immature specimens undergo vigorous training which makes the occurrence of stress fractures of the long bones a likely occurrence.

Racing horses put enormous stresses on their skeletons, and degrees of radiopharmaceutical uptake (RU) which would be considered pathological in older competition or sports horses are commonly encountered in horses showing no clinical signs of lameness. By definition, this degree of RU has to be classed as normal, but may well be undesirable and indicate subclinical pathology. The long-term consequences of subchondral bone stress often begin to show at 4, 5 and 6 years of age in the racehorse and it may well be that this is the price we pay for subjecting these animals to hard training and racing at an age below that of skeletal maturity.

Certain clinical syndromes exist in young racehorses which are linked to very special scintigraphic appearances. The most dramatic of these is areas of focal increased radiopharmaceutical uptake (IRU) seen in the plantarolateral aspect of the lateral condyle of the third metatarsal bone (MtIII). These have been described in the literature in both Thoroughbred[1] and Standardbred[2] racehorses. In an extreme case, these present no diagnostic problem. There is a degree of overlap between the degree of IRU seen in clinically lame horses and that encountered in horses undergoing marked remodelling in that site but in the absence of lameness. This was investigated in a small study in our clinic[1] and, although there was significant overlap between lame horses and normal horses, no normal horse showed a ratio of counts greater than 3:1 in the lateral condyle compared to the metaphysis of MtIII. In other words, any horse with a 3-fold increase in RU in the lateral condyle of MtIII compared with the metaphyseal region is likely to be undergoing pathological change in that site.

IRU in the third carpal bone (C3) is seen much more commonly in racehorses compared to other pleasure horse disciplines. These horses are often bilaterally lame. The increased bone turnover is usually linked to sclerosis radiographically, and continued training of these horses often results in fissure or slab fracture of the radial facet of the third carpal bone. The changes have been described histopathologically[3].

The pelvis in a young Thoroughbred racehorse has far more innate bone activity than in older horses. Both tubera sacrale and tubera coxae have marked RU. There is often associated RU activity in the summits of the spinous processes of the sacrum at the origin and insertion sites of the dorsal sacroiliac and sacrosciatic ligaments. These are encountered so commonly that they should be classed as normal, but may reflect extremes of bone remodelling consequent to vigorous athletic exercise of an immature skeleton. Areas of IRU in the middle of the wing of the ilium, or in the shaft of the ilium extending caudally towards the acetabulum, should **always** be taken seriously and often reflect impending catastrophic bone failure.

Image interpretation must always consider bilateral lameness and bilateral lesions, and simple right to left visual screening looking for abnormalities in the lamer limb is not adequate. The nature of race training often results in a bilateral distribution of stress injuries. The lameness associated with an area of IRU may be unilateral if the cortex in one limb has begun to collapse ahead of the other. Conversely, bilateral gait abnormality which has not produced distinct 'head nodding' in front or sinking of the quarters behind may go unnoticed by the trainer. Symmetrical distribution of isotope should never be assumed to be completely normal. It is hoped that the normal images provided in this chapter will aid clinicians in deciding whether their clinical cases fall outside the range encountered in sound horses. The images have been chosen to show the wide range in degree of uptake of radiopharmaceutical which occurs in the Thoroughbred and can still be completely unassociated with lameness or pathology.

SPECIFIC STRESS FRACTURES

A flat racehorse is often skeletally naïve when entering training and immature in terms of physeal closure and bone structure. Training involves repetitive cyclical loading; therefore, there is a high incidence of spontaneous fatigue injury and stress fracture. Just as the parts of a car often fail in

a predictable manner dependent upon their design, racehorse bone tends to fail in a predictable manner dependent upon foci of concentration of loading of the forces involved in locomotion. Stress fracture predilection sites therefore occur[4,5], which can aid in visual screening of scintigraphic images[6]. Although, in theory, stress fractures could occur anywhere in the long bones, the common predilection sites are as follows:

Third Metacarpal Bone (McIII)

- Mid to proximal third dorsal cortex.
- Proximal palmar cortex.
- Transverse stress fracture (associated with cortical fracture of the palmar cortex and a transverse periosteal reaction approximately 3–4 cm above the metacarpophalangeal joint surface).

Humerus

- Proximocaudal cortex immediately distal to the humeral head.
- Distal cranial and caudal cortex just proximal to the elbow joint.

Tibia

- Proximolateral cortex approximately 7 cm from the femorotibial joint surface.
- Mid diaphyseal region, characterised by endosteal new bone.
- Distal third caudal cortex endosteal reaction, often accompanied by fracture line seen on a caudocranial radiographic view.

Ilium

- Mid ilial wing (dorsal to the sacroiliac joint).
- Ilial shaft.

Spine

- Laminae of the facet joints of the lumbar vertebrae.

ENOSTOSIS-LIKE REACTIONS

Enostosis-like lesions (ELLs) appear scintigraphically as focal areas of intense IRU. They have previously been described as possible bone infarcts[7]. They are relatively common in Thoroughbreds and can be encountered as incidental findings not associated with lameness[8]. They are poorly understood, but may mimic endosteal stress fractures in the tibia both scintigraphically and radiographically.

PHYSEAL UPTAKE

The radial physis remains open in many 2-year-olds; therefore, there is often an intense transverse band of RU. However, despite radiographic closure in the later part of the 2-year-old year, many horses have a unilateral or bilateral area of RU in the region of the radial physis at 3–5 years of age. This is often normal and is not linked to lameness or apparent pathology. A similar region of IRU is often seen in the tibial crest, again associated with late physeal closure which is also normal. The masking of these physeal areas of RU in post image acquisition processing is desirable to avoid the effects of count stealing and allow visualisation of areas of mild IRU in their vicinity. Acquisition times also have to be altered if count stealing is suspected so that sufficient counts per pixel are acquired in the remainder of the field of view (see *Part I, Chapter 5*).

REFERENCES

1. Shepherd, M.C. and Pilsworth, R.C. (1997) Stress reactions in the plantarolateral condyles of the third metatarsal bone in UK Thoroughbreds: 26 cases. *Proc. Am. Ass. equine Practnrs.* **43**, 128-131.
2. Ross, M.W., Nolan, P.M., Palmer, J.A. *et al.* (1991) The importance of the metatarsophalangeal joint in Standardbred lameness. *Proc. Am. Ass. equine Practnrs.* **37**, 741-756.
3. Young, A., O'Brien, T. and Pool, R. (1988) Exercise related sclerosis in the third carpal bone of the racing Thoroughbred. *Proc. Am. Ass. equine Practnrs.* **34**, 339-346.
4. Mackey, V.S., Trout, D.R., Meagher, D.M. *et al.* (1987) Stress fractures of the humerus, radius and tibia in horses. *Vet. Radiol.* **28**, 26-31.
5. Pilsworth, R.C. and Webbon, P.M. (1988) The use of radionuclide bone scanning in the diagnosis of tibial stress fractures: a review of five cases. *Equine vet. J., Suppl.* **6**, 60-65.
6. Pilsworth, R. and Shepherd, M. (1997) Stress fractures. In: *Current Therapy in Equine Medicine 4*, Ed: N.E. Robinson, W.B. Saunders Co., Philadelphia. pp 104-111.
7. Rantanen, N.W., Rose, J., Grisel, G.R. *et al.* (1994) Apparent bone marrow infarcts in Thoroughbred racehorses. *J. equine vet. Sci.* **14**, 126-127.
8. Ramzan, P. (2002) Equine enostosis-like lesions: 12 cases. *Equine vet. Educ.* **14**, 143-148.

NORMAL HORSES

N Figure 1: Solar view of the RF foot

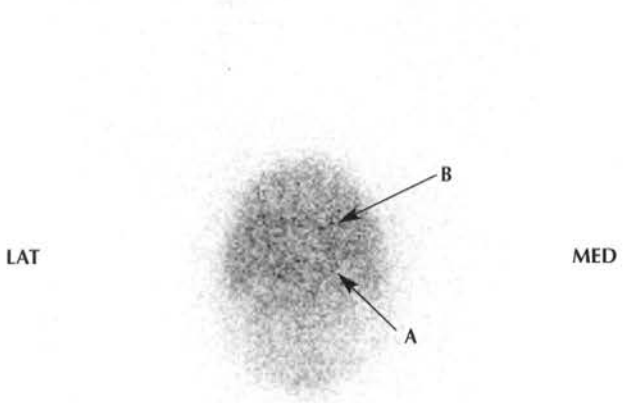

TB	3y	G	Flat Racing	256 x 256
DX:	Normal			
DS:	NA			

➔ **A:** Normal RU in the navicular bone.
➔ **B:** Region of insertion of the deep digital flexor tendon on the distal phalanx.

N Figure 2: Lateral view of the right MCP joint and digit

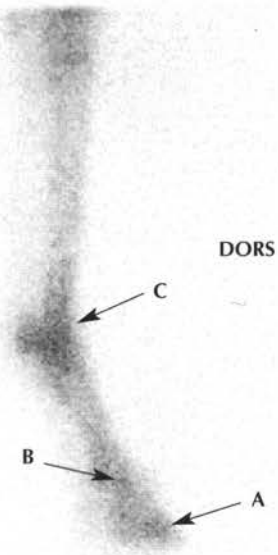

TB	2y	F	Flat Racing	256 x 256
DX:	Normal			
DS:	NA			

➔ **A:** Normal RU in the distal phalanx.
➔ **B:** Normal RU associated with the PIP joint.
➔ **C:** Normal RU associated with the MCP joint.

N Figure 3: Dorsal view of the MCP joints and digits

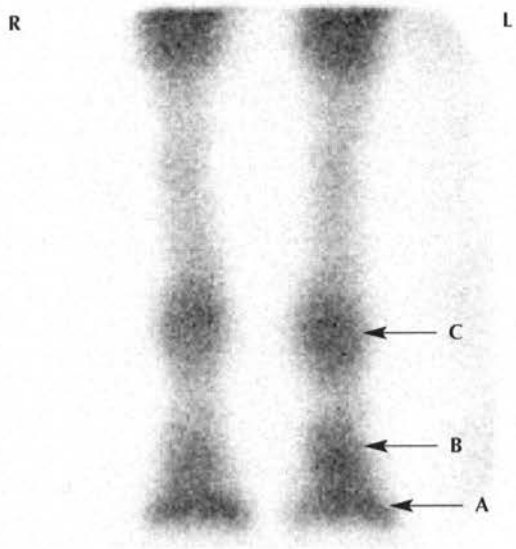

TB	3y	F	Flat Racing	256 x 256
DX:	Normal			
DS:	NA			

➔ **A:** Normal RU in the left distal phalanx.
➔ **B:** Normal RU associated with the left PIP joint.
➔ **C:** Normal RU associated with the left MCP joint.

N Figure 4: Dorsal view of the MCP joints and digits

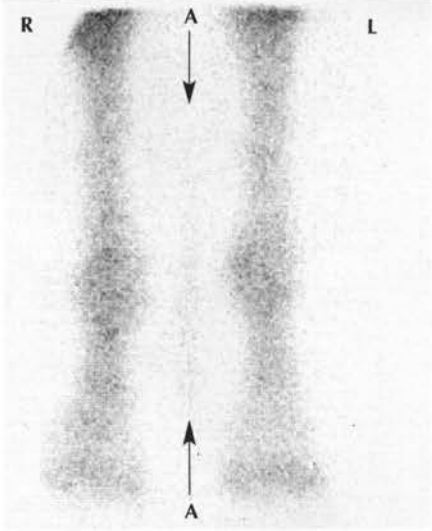

TB	2y	F	Flat Racing	256 x 256
DX:	Normal			
DS:	NA			

➔ **A:** Note the band of radioactivity between the forelimbs, the result of unguarded γ-rays in the gap between the lead leg shields
Note: Slight asymmetry in RU in the left and right limbs. This is not uncommon.

N Figure 5: Lateral view of the right carpus

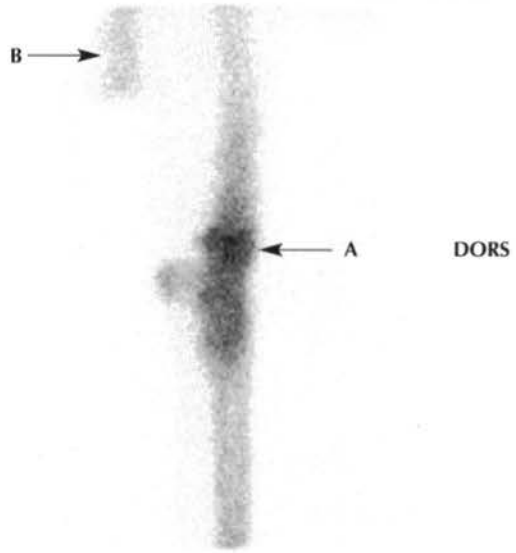

TB	3y	F	Flat Racing	128 x 128
DX:	Normal			
DS:	NA			

➡ **A:** The distal radial physis has normal RU, less than a 2-year-old. Compare with Figure 6.
➡ **B:** Left radius proximal to lead leg shield.

N Figure 6: Lateral view of the right carpus

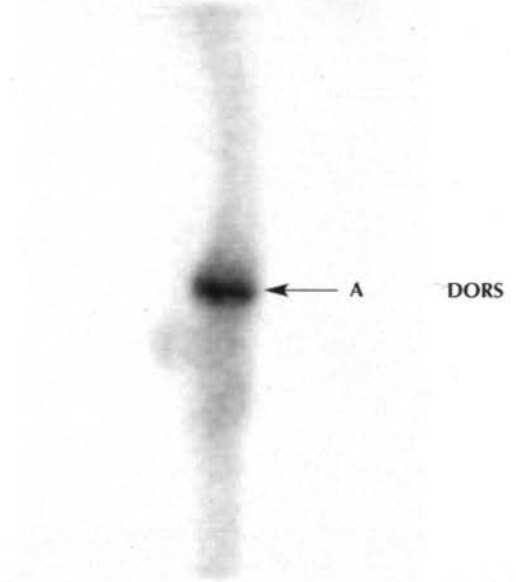

TB	2y	F	Flat Racing	128 x 128
DX:	Normal			
DS:	NA			

➡ **A:** Normal intense RU in the distal radial physis in a skeletally immature horse.

N Figure 7: Dorsal view of the carpi

TB	3y	F	Flat Racing	256 x 256
DX:	Normal			
DS:	NA			

➡ **A:** Normal RU associated with the distal radial physes.

N Figure 8: Lateral view of the left radius

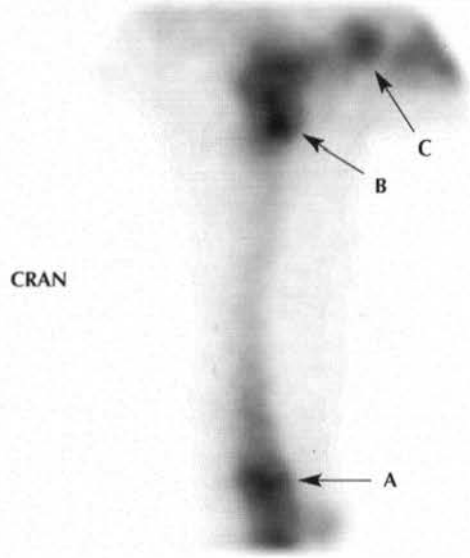

TB	3y	F	Flat Racing	128 x 128
DX:	Normal			
DS:	NA			

➡ **A:** Normal RU in the distal radial physis.
➡ **B:** Normal RU in the proximal aspect of the radius.
➡ **C:** Normal RU in the olecranon of the ulna.

N Figure 9: Lateral view of the left humerus, elbow and shoulder

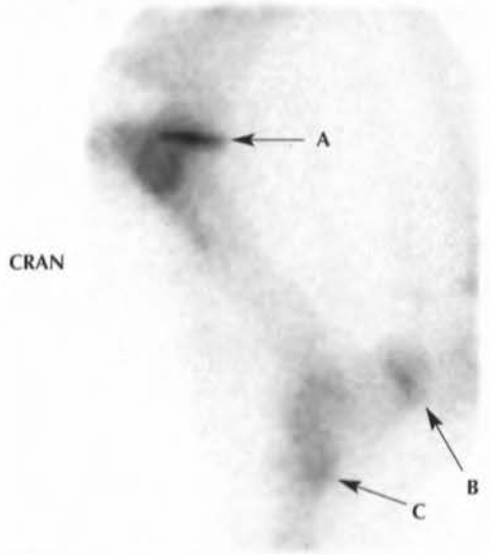

TB	2y	C	Flat Racing	128 x 128
DX:	Normal			
DS:	NA			

➔ **A:** Normal RU in the proximal humeral physis.
➔ **B:** Normal RU in the physis of the olecranon.
➔ **C:** Normal RU in the proximal caudal aspect of the radius.

N Figure 10: Lateral view of the left humerus, elbow and shoulder

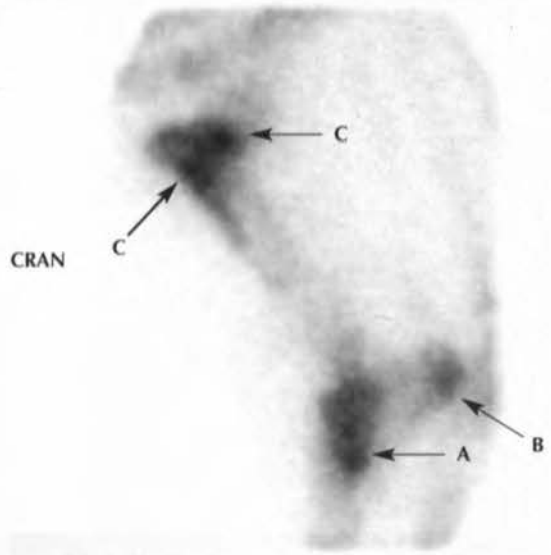

TB	3y	G	Flat Racing	128 x 128
DX:	Normal			
DS:	NA			

➔ **A:** Normal RU in the proximal caudal aspect of the radius.
➔ **B:** Normal RU in the olecranon.
➔ **C:** Normal RU in the proximal aspect of the humerus.

N Figure 11: Lateral view of the left scapula and shoulder

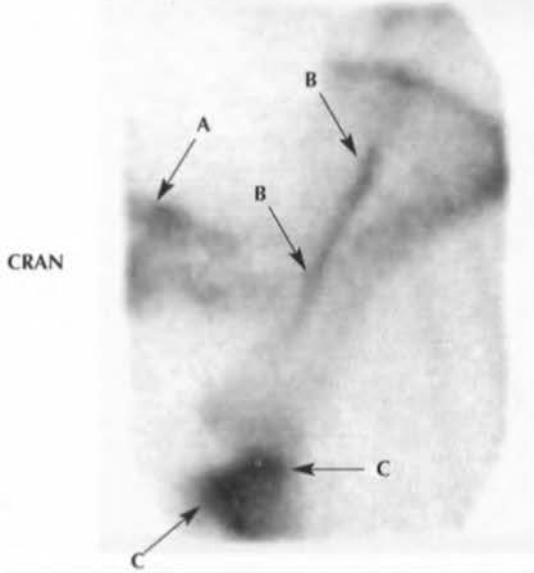

TB	3y	C	Flat Racing	128 x 128
DX:	Normal			
DS:	NA			

➔ **A:** Normal RU in the caudal cervical vertebrae.
➔ **B:** Normal RU in the spine of the scapula.
➔ **C:** Normal RU in the proximal aspect of the humerus.

N Figure 12: Lateral view of the right MTP joint and digit

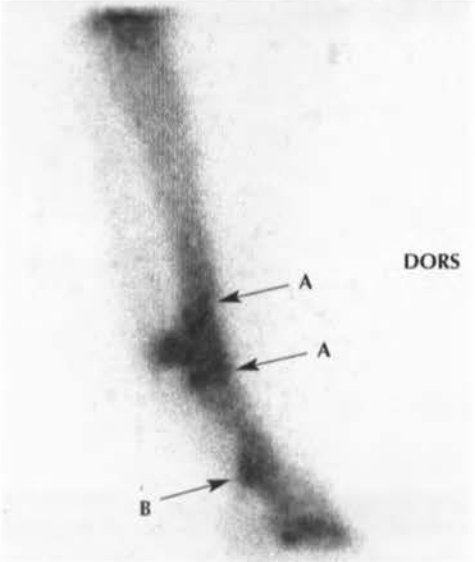

TB	2y	F	Flat Racing	256 x 256
DX:	Normal			
DS:	NA			

➔ **A:** Normal RU in the subchondral bone of the distal aspect of MtIII and the proximal aspect of the proximal phalanx.
➔ **B:** Normal RU in the plantar aspect of the PIP joint.

N Figure 13: Plantar view of the MTP joints and digits

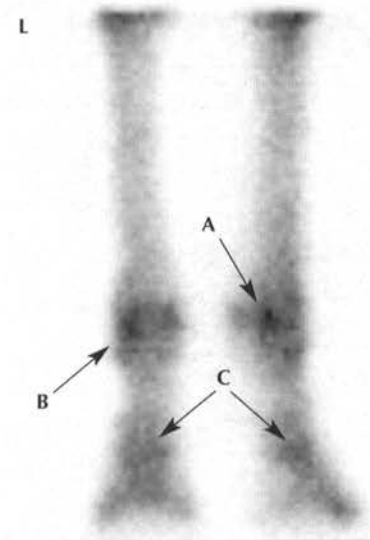

TB	3y	F	Flat Racing	128 x 128

DX: Normal

DS: NA

➔ **A:** Note the asymmetrical appearance of the distal aspect of the RH limb due to 'toe out' conformation. This rotation also gives the appearance of the lateral PSB being more axial than normal.
➔ **B:** Normal RU in the left lateral PSB.
➔ **C:** Normal RU in the PIP joints.

N Figure 14: Lateral view of the left tarsus

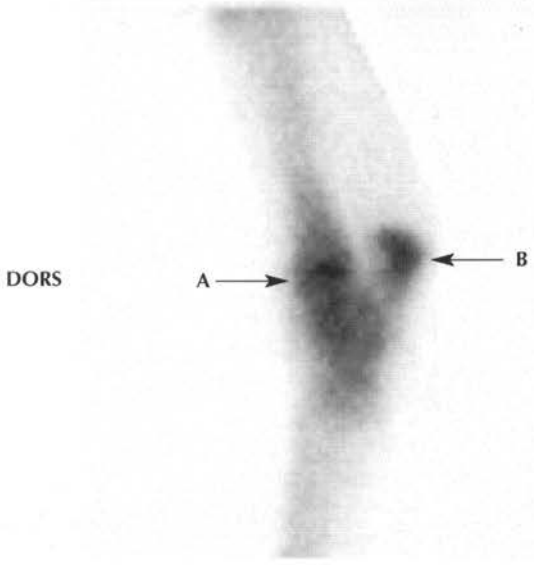

TB	3y	C	Flat Racing	128 x 128

DX: Normal

DS: NA

➔ **A:** Normal RU in the distal tibial physis.
➔ **B:** Normal RU in the tuber calcanei.

N Figure 15: Plantar view of the tarsi

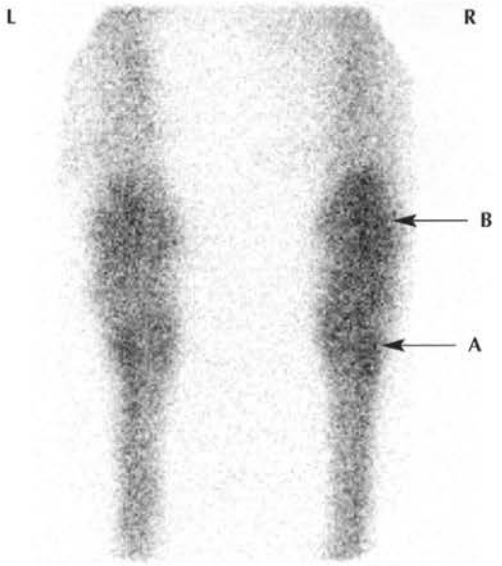

TB	3y	C	Flat Racing	256 x 256

DX: Normal

DS: NA

➔ **A:** Normal RU in the proximal lateral aspect of the metatarsal region.
➔ **B:** Normal RU in the tuber calcanei.

N Figure 16: Caudal view of the left tibia

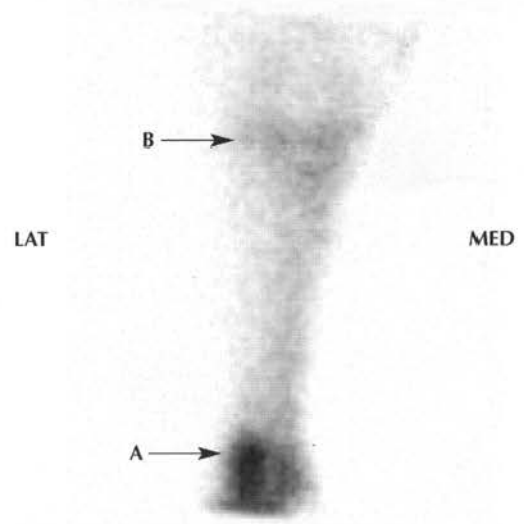

TB	2y	F	Flat Racing	128 x 128

DX: Normal

DS: NA

➔ **A:** Normal RU in the tuber calcanei.
➔ **B:** Normal RU in the proximal aspect of the tibia.
Note: Poor quality image, which is an unavoidable consequence of the distance between the bone and the gamma camera in this view.

N Figure 17: Lateral view of the left tibia

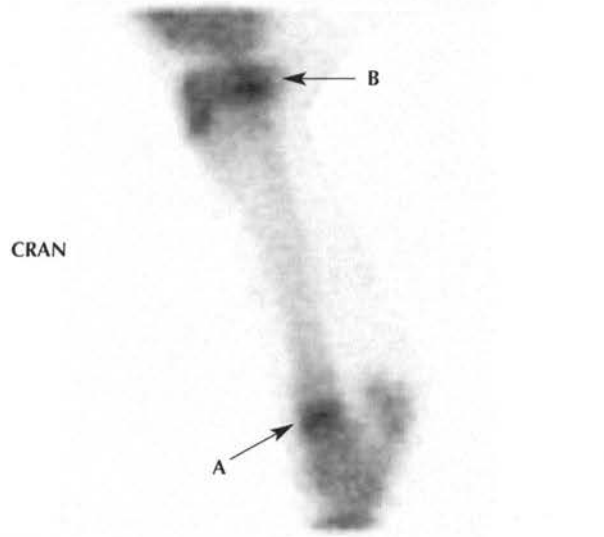

TB	2y	C	Flat Racing	128 x 128

DX: Normal

DS: NA

- **A:** Normal RU in the distal tibial physis.
- **B:** Normal RU in the proximal tibia. Note that it is common for the proximal caudal aspect of the tibia to have the greatest degree of activity.

N Figure 18: Lateral view of the left stifle

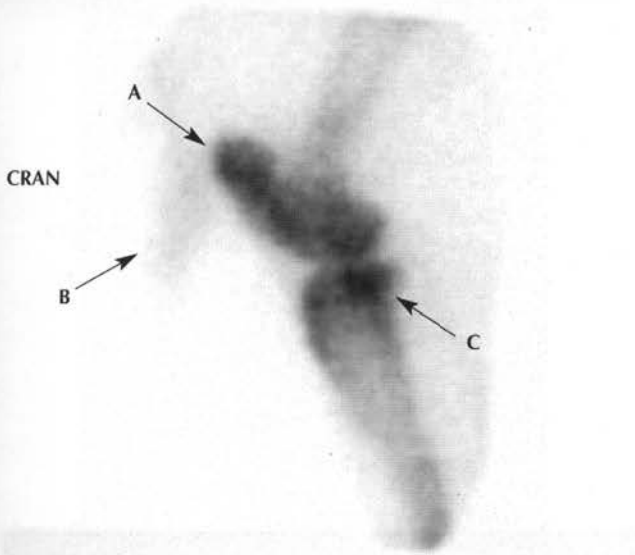

TB	7y	G	Flat Racing	128 x 128

DX: Normal

DS: NA

- **A:** Normal RU in the patella.
- **B:** Residual activity in the penis.
- **C:** Normal RU in the proximal aspect of the tibia.

N Figure 19: Lateral view of the left stifle

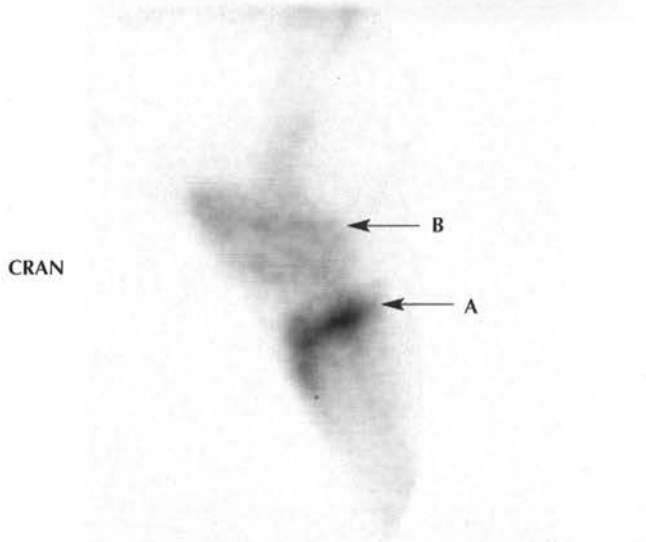

TB	2y	F	Flat Racing	128 x 128

DX: Normal

DS: NA

- **A:** Normal RU in the proximal tibial physis.
- **B:** Normal RU in the distal femoral physis.

N Figure 20: Lateral view of the left coxofemoral (CF) joint

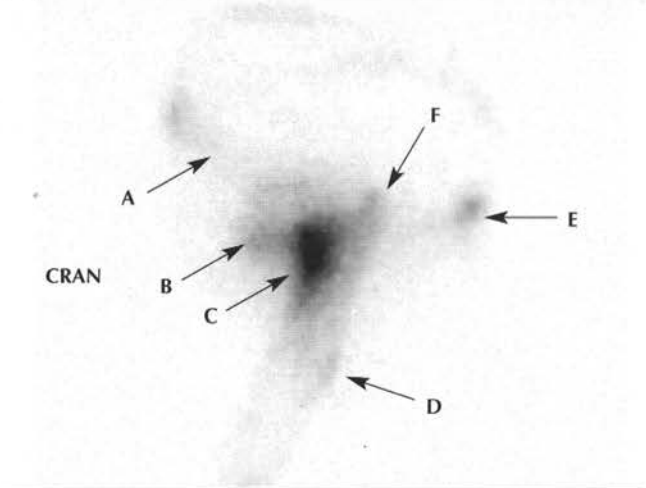

TB	4y	G	Flat Racing	128 x 128

DX: Normal

DS: NA

- **A:** Normal RU in the left ilial shaft.
- **B:** Normal radiopharmaceutical activity in the bladder.
- **C:** Normal RU in the proximal aspect of the femur in the region of the CF joint.
- **D:** Normal RU in the third trochanter of the femur.
- **E:** Normal RU in the left tuber ischii.
- **F:** Normal RU in the greater trochanter of the femur.

N Figure 21: Dorsal 45° lateral oblique view of the left ilium

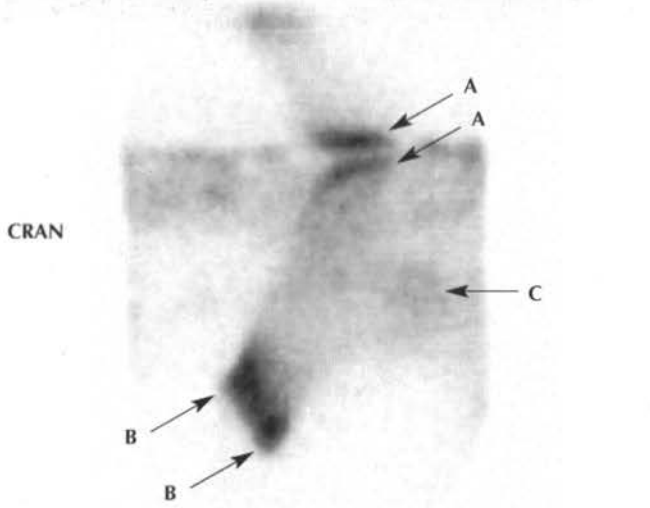

TB	2y	F	Flat Racing	128 x 128

DX: Normal

DS: NA

- **A:** Normal RU in the left and right tubera sacrale.
- **B:** Normal RU in the left tuber coxae. Note the focal region of slightly greater RU at the caudal aspect of the tuber coxae is normal.
- **C:** Radiopharmaceutical activity in the bladder making the contour of the ilial shaft poorly defined.

N Figure 22: Dorsal 45° lateral oblique view of the left ilium

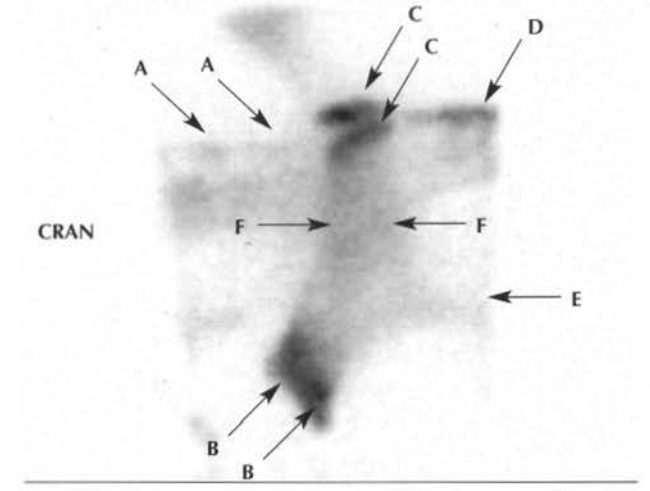

TB	3y	F	Flat Racing	128 x 128

DX: Normal

DS: NA

- **A:** Normal RU in the DSPs of the lumbar vertebrae.
- **B:** Normal RU in the left tuber coxae.
- **C:** Normal RU in both left and right tubera sacrale.
- **D:** Normal RU in the DSPs of the sacral vertebrae.
- **E:** Poorly defined band of RU in the ilial shaft.
- **F:** Region of sacroiliac joint.

N Figure 23: Dorsal view of the pelvis

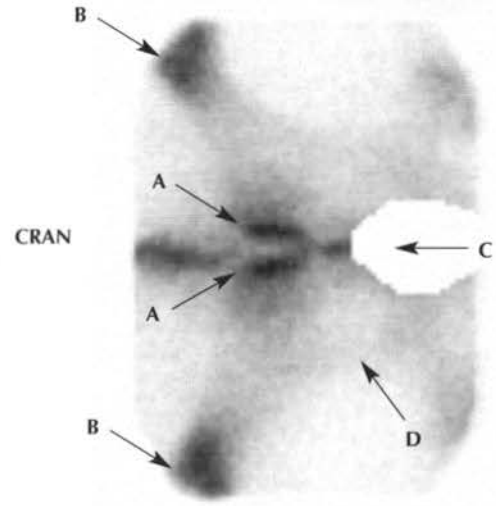

TB	4y	C	Flat Racing	128 x 128

DX: Normal

DS: NA

- **A:** Normal RU in the left and right tubera sacrale.
- **B:** Normal RU in the left and right tubera coxae.
- **C:** Region of the bladder masked.
- **D:** Normal RU in the ilial shaft.

N Figure 24: Dorsal view of the pelvis

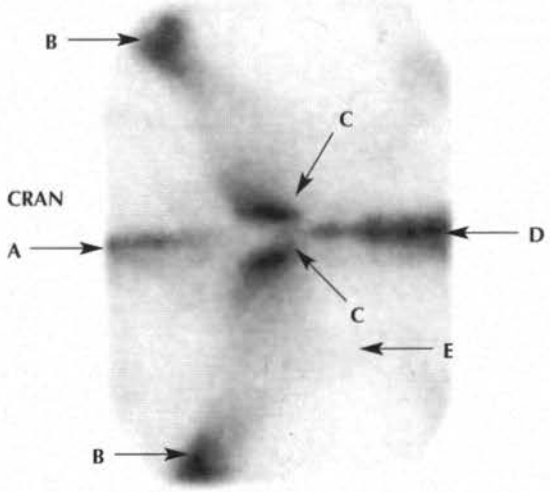

TB	3y	F	Flat Racing	128 x 128

DX: Normal

DS: NA

- **A:** Normal RU in the DSPs of the lumbar vertebrae.
- **B:** Normal RU in the left and right tubera coxae.
- **C:** Normal RU in the left and right tubera sacrale.
- **D:** Normal RU in the DSPs of the sacrum.
- **E:** Normal RU in the ilial shaft.

N Figure 25: Dorsal view of the caudal aspect of the pelvis

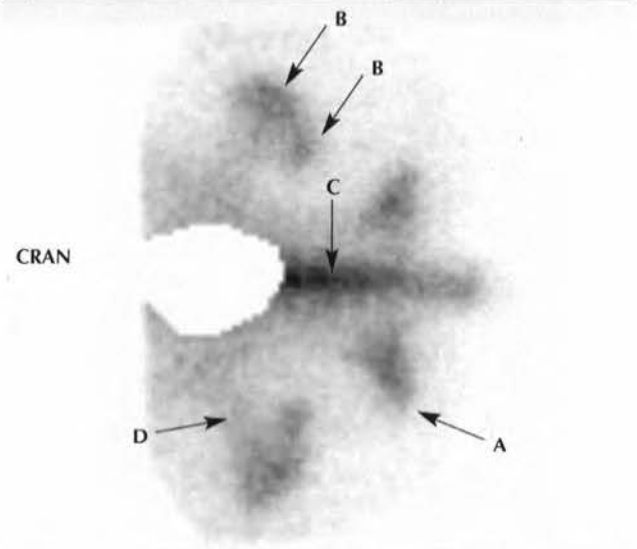

TB	4y	C	Flat Racing	128 x 128

DX: Normal

DS: NA

- **A:** Normal RU in the left tuber ischii.
- **B:** Normal RU in the greater and lesser trochanter of the right femur.
- **C:** Normal RU in the DSPs of the sacrum.
- **D:** Normal RU in the region of the CF joint.

N Figure 26: Dorsal view of the caudal aspect of the pelvis

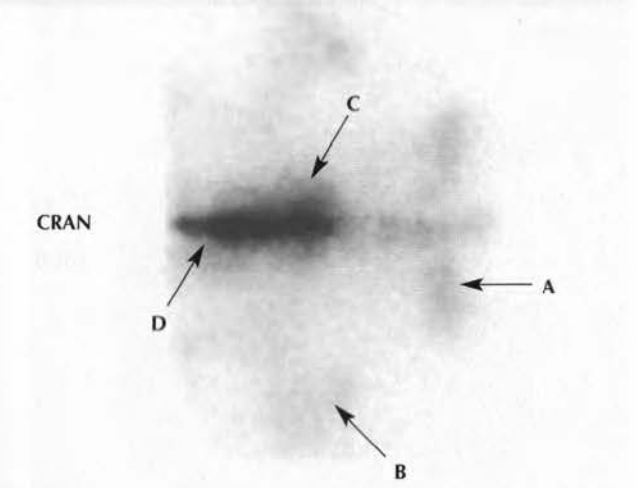

TB	2y	F	Flat Racing	128 x 128

DX: Normal

DS: NA

- **A:** Normal RU in the left tuber ischii.
- **B:** Normal RU in the greater trochanter of the left femur.
- **C:** Radiopharmaceutical activity in the bladder.
- **D:** Normal RU in the sacrum and bladder superimposed, not to be confused with a lesion.

N Figure 27: Left lateral view of the caudal aspect of the head and the cranial cervical vertebrae

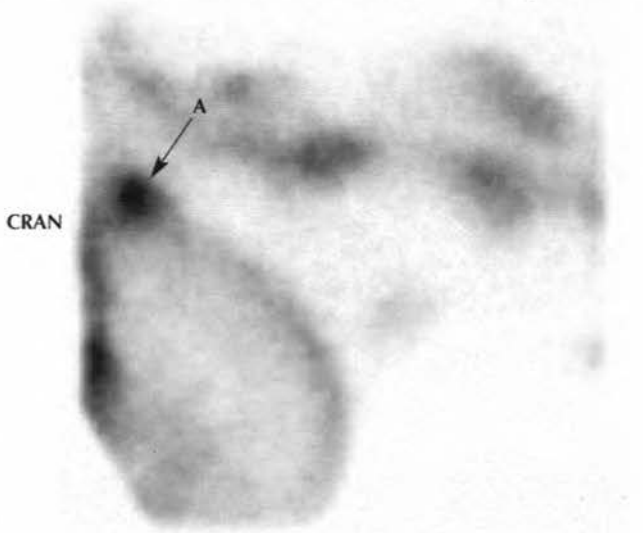

TB	2y	F	Flat Racing	128 x 128

DX: Normal

DS: NA

- **A:** Normal RU in the temporomandibular joint.

N Figure 28: Left lateral view of the mid cervical vertebrae

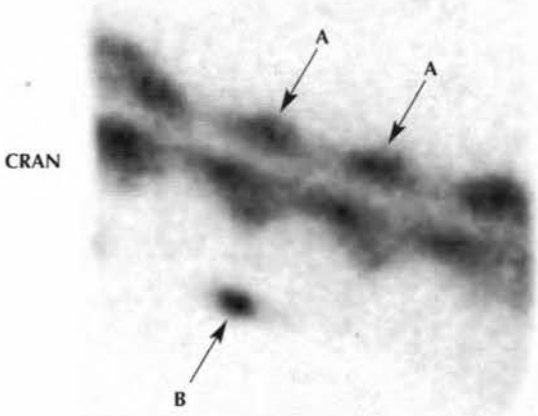

TB	2y	F	Flat Racing	128 x 128

DX: Normal

DS: NA

- **A:** Normal RU in the cervical vertebrae.
- **B:** Perivascular radioactivity associated with a 'leak' during injection.

N **Figure 29: Left lateral view of the caudal cervical vertebrae**

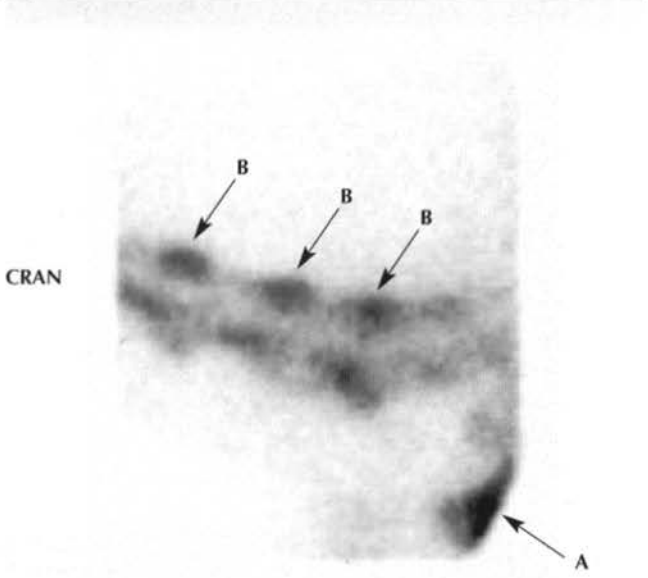

TB	2y	F	Flat Racing	128 x 128
DX:	Normal			
DS:	NA			

➔ **A:** Normal RU in the proximal aspect of the humerus.
➔ **B:** Normal RU in the cervical vertebrae.

N **Figure 30: Dorsal view of the cranial aspect of the thoracic spine**

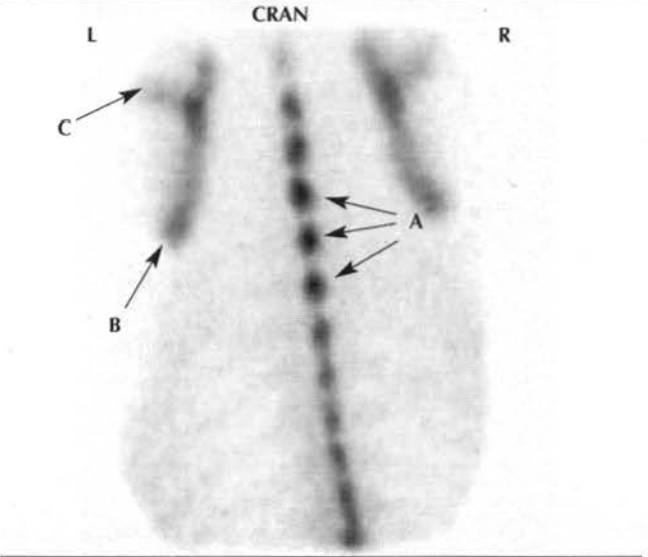

TB	2y	F	Flat Racing	128 x 128
DX:	Normal			
DS:	NA			

➔ **A:** Normal RU in the DSPs of the cranial thoracic vertebrae.
➔ **B:** Normal RU in the dorsal margin of the left scapula.
➔ **C:** Normal RU in the spine of the left scapula.

N **Figure 31: Dorsal 60° lateral oblique view of the cranial thoracic region**

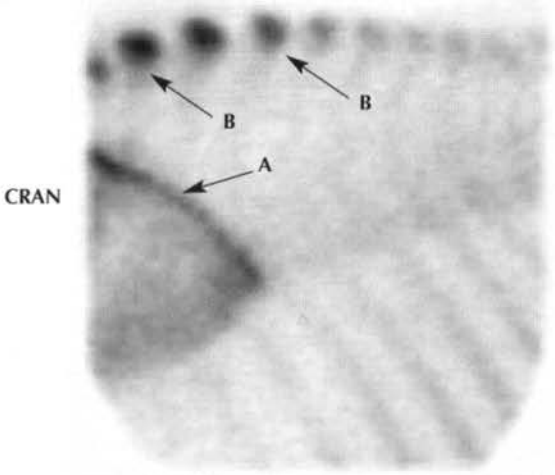

TB	3y	C	Flat Racing	128 x 128
DX:	Normal			
DS:	NA			

➔ **A:** Normal RU in the proximal aspect of the left scapula.
➔ **B:** Focal, intense normal RU in the summits of the cranial thoracic DSPs.

N **Figure 32: Dorsal 60° lateral oblique view of the mid to caudal aspect of the thoracic spine**

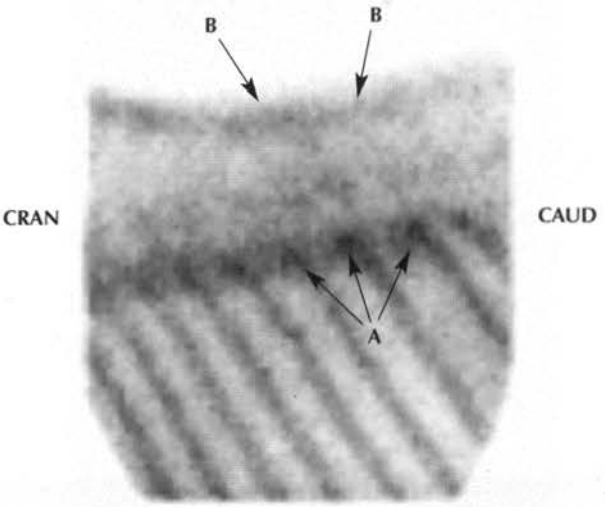

TB	3y	F	Flat Racing	128 x 128
DX:	Normal			
DS:	NA			

➔ **A:** Normal RU in the region of the costovertebral articulations.
➔ **B:** Normal RU in the summits of the DSPs in the mid to caudal thoracic vertebrae.

N Figure 33: Left lateral view of the sternum

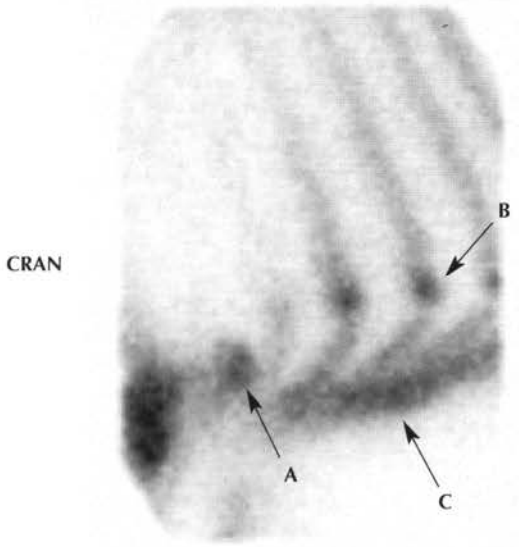

TB	4y	G	Flat Racing	128 x 128

DX: Normal

DS: NA

- **A:** Normal RU in the left olecranon.
- **B:** Normal RU at the costochondral junction.
- **C:** Normal RU in the sternum.

N Figure 34: Left dorsal 60° lateral oblique view of the caudal thoracic and cranial lumbar vertebrae

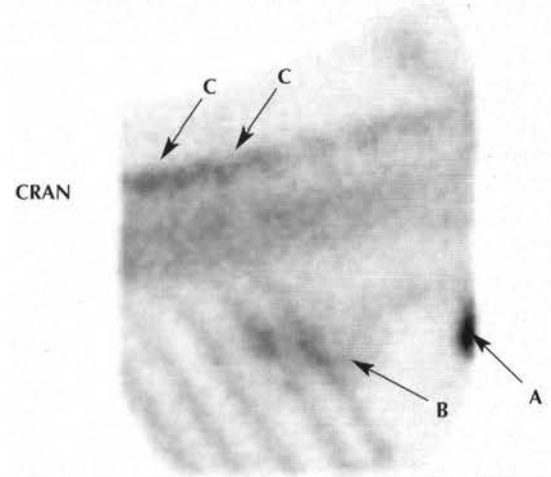

TB	3y	C	Flat Racing	128 x 128

DX: Normal

DS: NA

- **A:** Normal intense RU in the left tuber coxae.
- **B:** Normal moderate RU in the left kidney.
- **C:** Normal RU in the summits of the DSPs of the caudal thoracic vertebrae.

Note: Reduction in image quality compared to Figure 32 due to the overlying thick lumbar musculature.

N Figure 35: Right dorsal 60° lateral oblique view of the caudal thoracic and lumbar vertebrae

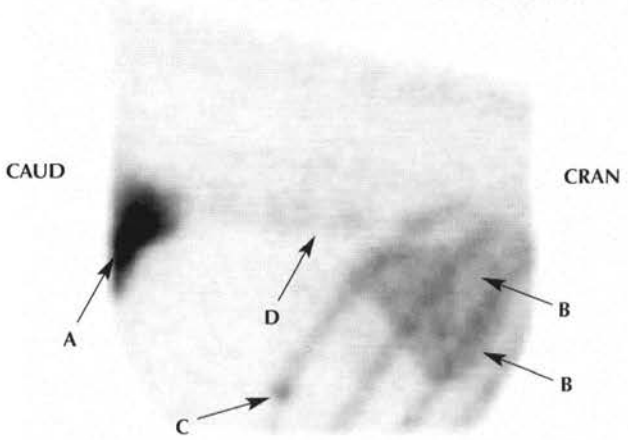

TB	3y	C	Flat Racing	128 x 128

DX: Normal

DS: NA

- **A:** Intense, normal RU in the right tuber coxae. Note how this dominates the image, a result of count capture.
- **B:** Normal RU in the right kidney.
- **C:** Normal RU in the costochondral junction of rib 18.
- **D:** Normal RU in the lumbar vertebrae.

N Figure 36: Dorsal view of the thoracolumbar region

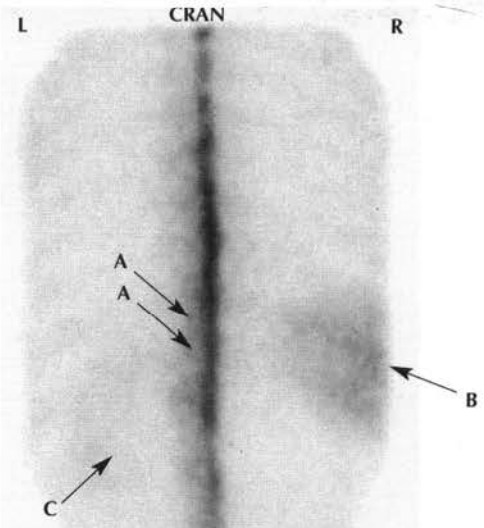

TB	3y	F	Flat Racing	128 x 128

DX: Normal

DS: NA

- **A:** Normal RU in the caudal thoracic DSPs.
- **B:** Normal RU in the right kidney.
- **C:** Normal RU in the left kidney.

Note: This view is seldom useful in clinical asessment of the spine in the Thoroughbred.

ABNORMAL HORSES

A **Figure 1: Lateral view of the distal aspect of the LF (a) and dorsal view of both forelimbs (b)**

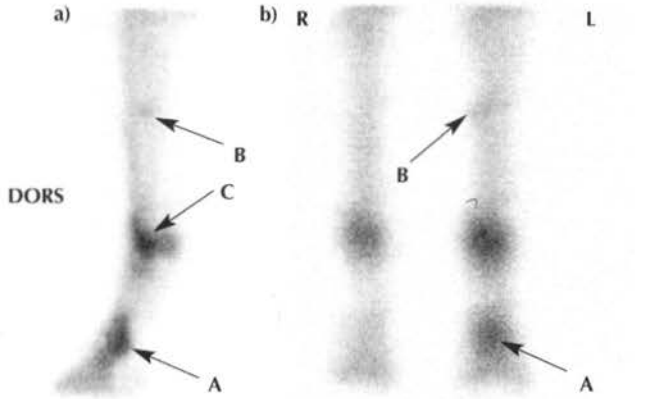

TB	3y	F	Flat Racing	128 x 128

DX: Active OCLL in the distal lateral condyle of the proximal phalanx.

DS: Radiography: Small OCLL with surrounding sclerosis in the distal lateral condyle of the proximal phalanx.

➡ **A:** Moderate, relatively focal IRU in the distal palmar aspect of the proximal phalanx of the LF.
➡ **B:** Mild, focal IRU in the mid diaphysis of the left McII.
➡ **C:** Mild, focal IRU in the palmar distal aspect of the left McIII.
Note: The generalised IRU in the left distal forelimb when compared to the right at sites away from the primary pathology. This is a relatively common finding.

A **Figure 2: Lateral view of the distal aspect of the RF**

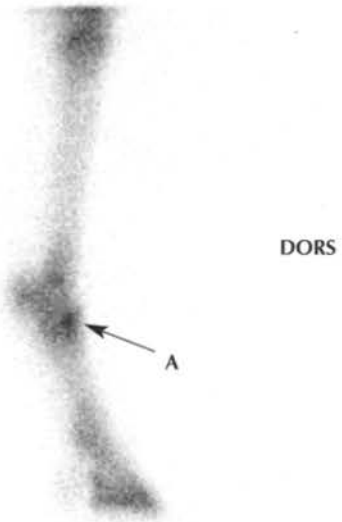

TB	3y	C	Flat Racing	256 x 256

DX: Short, incomplete sagittal fracture of the proximal aspect of the proximal phalanx.

DS: Radiography: Linear lucency mid sagittal proximal aspect of proximal phalanx, with periosteal reaction on the dorsoproximal aspect of the proximal phalanx.

➡ **A:** Moderate focal IRU associated with the dorsoproximal aspect of the proximal phalanx.

A **Figure 3: Lateral view of the distal aspect of the RF (a) and dorsal views of both forelimbs (b)**

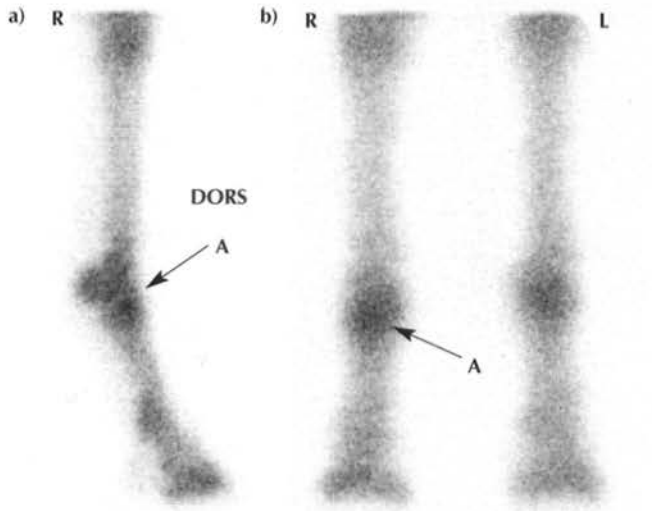

TB	3y	C	Flat Racing	256 x 256

DX: Bone injury of the proximal aspect of the proximal phalanx without radiographic signs of fracture.

DS: Site confirmed by diagnostic analgesia. Radiography: NAD.

➡ **A:** Moderate, focal IRU in the dorsoproximal aspect of the right proximal phalanx.

A **Figure 4: Lateral (a) and palmar (b) views of the distal RF**

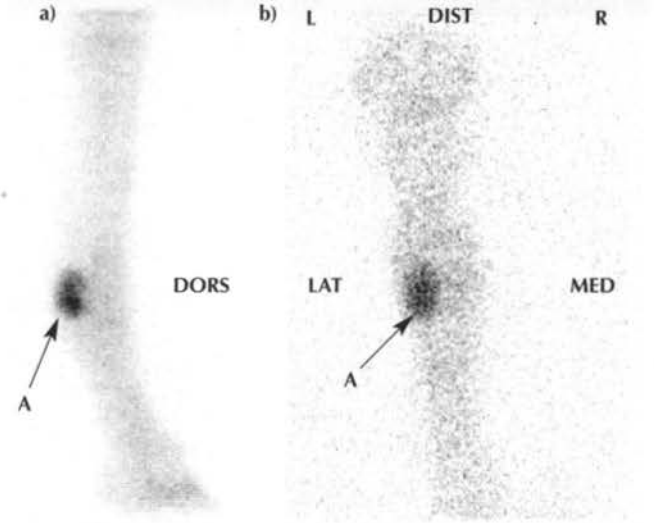

TB	3y	F	Flat Racing	256 x 256

DX: Injury to the lateral PSB.

DS: Radiography: Lucent changes in the mid body of the lateral PSB. No obvious fracture line was seen.

➡ **A:** Marked, focal IRU in the lateral PSB.
Note: The poor image quality in the solar view, a consequence of the distance from the PSB to the camera. This view is used only to localise the lesion mediolaterally.

A **Figure 5: Lateral view of the distal aspect of the LF (a) and dorsal views of both forelimbs (b)**

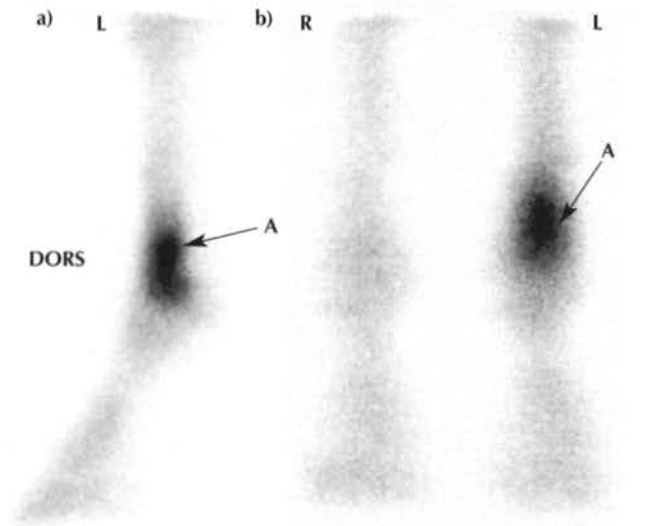

TB	-	G	Flat Racing	256 x 256
DX:	Distal palmar McIII stress fracture			
DS:	Radiography: Linear, horizontal radiolucent line through the distal palmar aspect of the McIII cortex with abundant periosteal new bone.			
➡ **A:**	Marked, focal IRU in the distal palmar aspect of the left McIII.			

A **Figure 6: Lateral view of the distal aspect of the LF (a) and dorsal view of both forelimbs (b)**

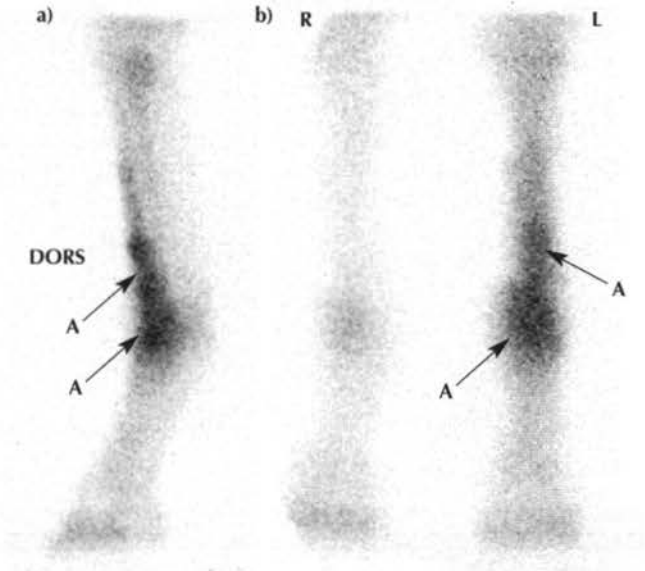

TB	3y	C	Flat Racing	256 x 256
DX:	Bone injury to dorsal distal aspect of McIII.			
DS:	Site confirmed by local analgesia. Radiography: NAD.			
➡ **A:**	Diffuse, marked IRU in the distal McIII and MCP joint.			

A **Figure 7: Lateral view of the left metacarpal region (a) and dorsal view of both forelimbs (b)**

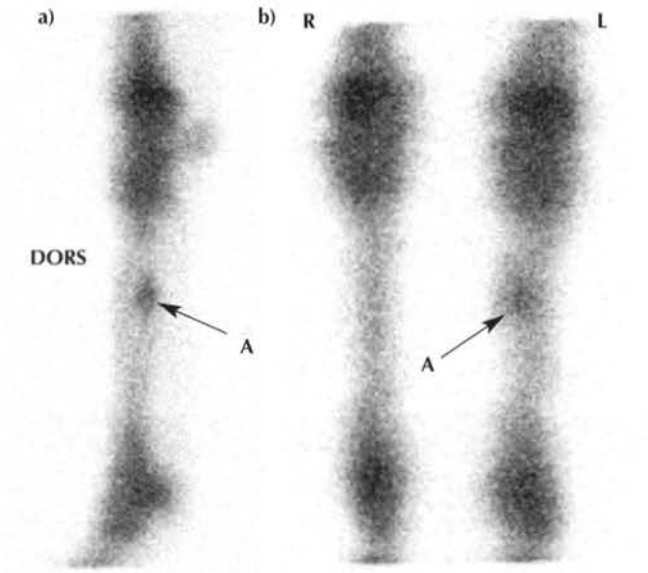

TB	3y	F	Flat Racing	256 x 256
DX:	Chronic fracture of the left McII.			
DS:	Radiography: Lytic line through the mid diaphysis of McII with an associated callus.			
➡ **A:**	Moderate, focal IRU in the mid McII.			

A **Figure 8: Lateral view of the distal aspect of the LF**

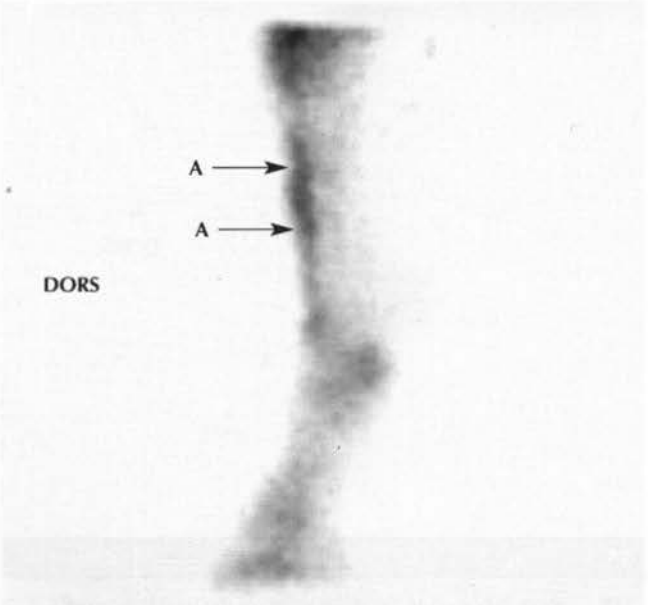

TB	3y	C	Flat Racing	128 x 128
DX:	Dorsal metacarpal periostitis (sore shins).			
DS:	Clinical signs: marked pain on palpation of dorsal McIII			
➡ **A:**	Moderate linear diffuse IRU in the dorsal aspect of McIII.			

A Figure 9a: Lateral view of the RF fetlock pool phase (4 mins)

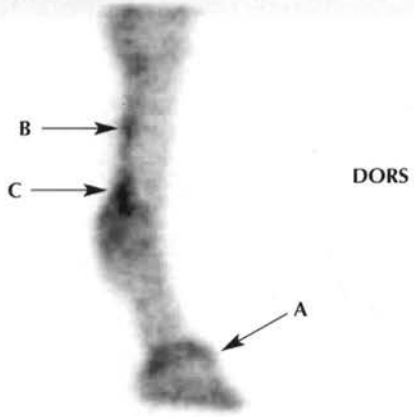

TB	4y	F	Flat Racing	128 x 128

DX: Distal branch suspensory desmitis in association with apical PSB disruption.

DS: Regional analgesia: sound to lateral 2 point block. Radiography: irregularities on the abaxial surface of the sesamoid. Ultrasonography: periligamentar fibrosis, increased size and decreased echogenicity of the distal lateral suspensory ligament.

➔ **A:** Coronary activity.
➔ **B:** Vascular plexis activity.
➔ **C:** IRU associated with the distal suspensory branch (note proximal to the position of the PSB).

A Figure 9b: Lateral bone phase image of the RF fetlock

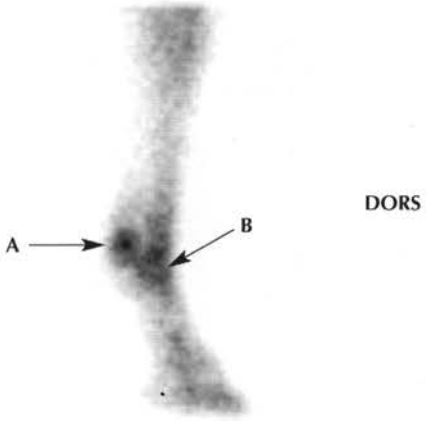

TB	4y	F	Flat Racing	128 x 128

DX: Distal branch suspensory desmitis in association with sesamoid disruption.

DS: *Details as for Figure 9a.*

➔ **A:** Moderate and focal IRU in the apical PSB.
➔ **B:** Mild IRU in the MCP joint.

A Figure 9c: Solar view of the distal RF

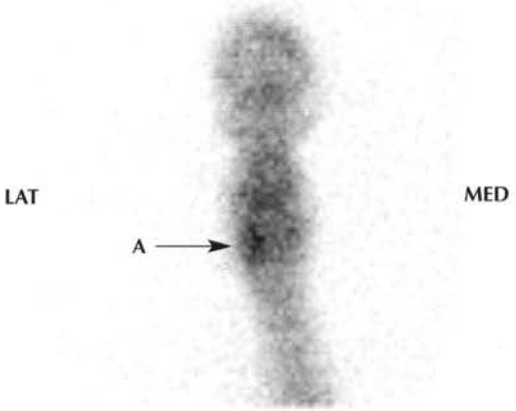

TB	4y	F	Flat Racing	128 x 128

DX: Distal branch suspensory desmitis in association with sesamoid disruption.

DS: *Details as for Figure 9a.*

➔ **A:** IRU associated with the lateral sesamoid.
Note: The solar view is used to replace the palmar view, which is impractical because of camera placement in the forelimb.

A Figure 10ab: Lateral view of the RF (a) and LF (b) fetlocks

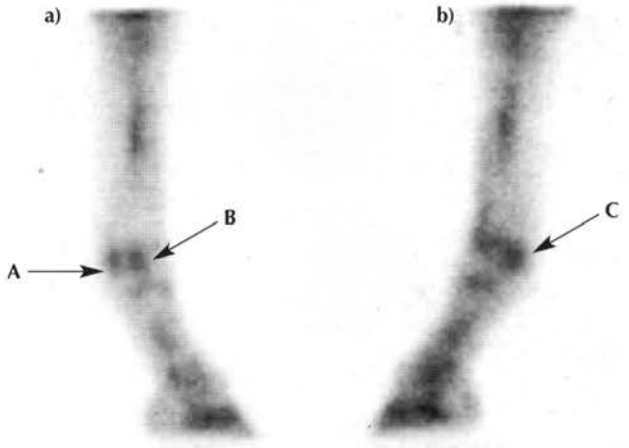

TB	3y	F	Flat Racing	256 x 256

DX: Subchondral bone injury to the medial condyle of right McIII.

DS: Regional analgesia: lameness localised to the right MCP joint. Radiography: NAD.

➔ **A:** Proximal sesamoid bone RF.
➔ **B:** IRU in the subchondral bone of the distal McIII.
➔ **C:** Proximal sesamoid bone LF.

A **Figure 10c: Dorsopalmar view of left and right fetlock**

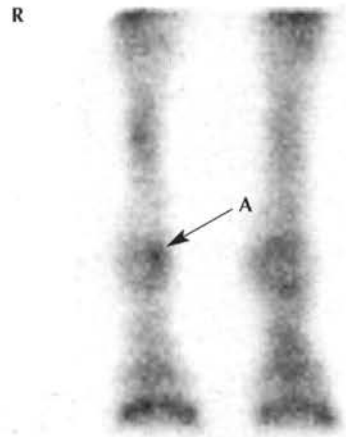

TB	3y	F	Flat Racing	256 x 256

DX: Subchondral bone injury to the medial condyle of right McIII.

DS: *Details as for Figure 10ab.*

➡ **A:** IRU in the medial condyle of McIII.
Note: The RF on the dorsopalmar view shows reduced uptake thoughout the limb compared to the LF, except in the medial condyle (lame leg/cool leg hot lesion syndrome). This is also apparent in the set time acquisition of the lateral view (see Figure 10ab).

A **Figure 10d: Solar view of the RF fetlock**

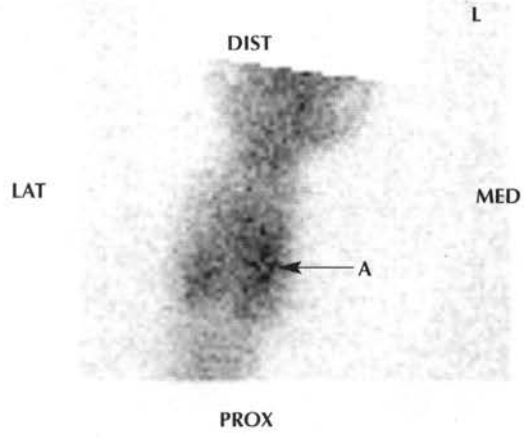

TB	3y	F	Flat Racing	256 x 256

DX: Subchondral bone injury to the medial condyle of McIII.

DS: *Details as for Figure 10ab.*

➡ **A:** IRU associated with the medial condyle.
Note: The image quality of the fetlock joint is poor due to the distance from the flexed fetlock joint to the camera. This view is used merely to confirm which condyle is affected, which cannot be done from the lateral view only.

A **Figure 11: Lateral view of the right carpus (a) and a dorsal view of both carpi (b)**

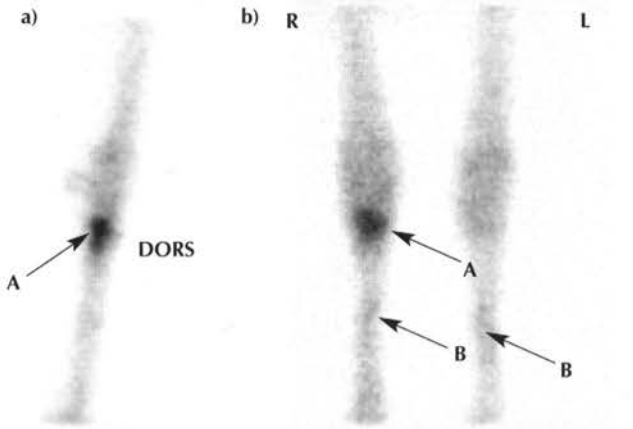

TB	5y	C	Flat Racing	128 x 128

DX: Avulsion fracture at the origin of the SL from the proximopalmar aspect of McIII.

DS: Radiography: Crescentic lucency with surrounding sclerosis on the proximal palmar aspect of McIII. Ultrasonography: SL enlarged and of heterogeneous echogenicity.

➡ **A:** Marked, focal IRU in the proximal palmar aspect of McIII.
➡ **B:** Mild, diffuse linear IRU in the dorsal aspect of mid McIII typical of dorsal metacarpal periostitis (sore shins).
Note: The triangular shape of the zone of IRU is typical of this condition.

A **Figure 12: Lateral view of the right carpus**

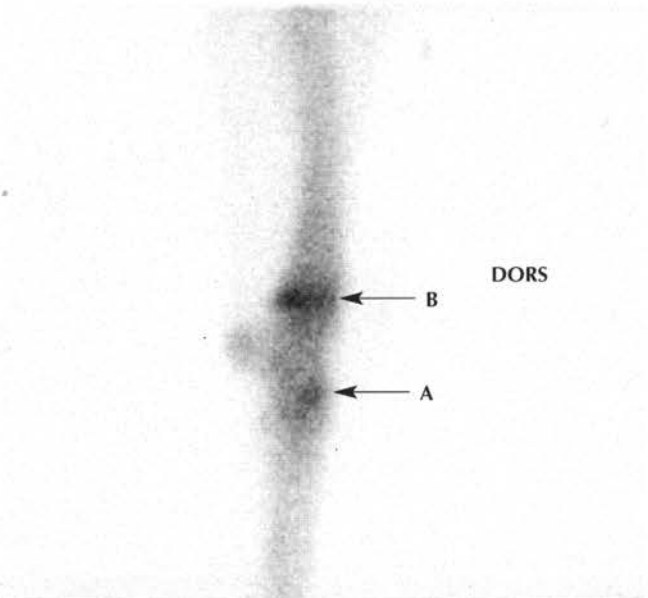

TB	2y	C	Flat Racing	256 x 256

DX: Stress (nonadaptive) remodelling of C3.

DS: Radiography: Sclerosis of the radial facet of both C3s.

➡ **A:** Moderate, focal IRU in the distal row of carpal bones.
➡ **B:** Normal intense RU in the distal radial physis

A **Figure 13: Lateral view of the right carpus**

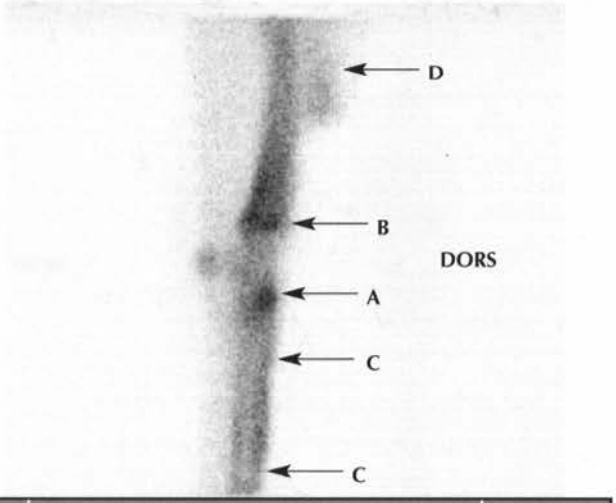

TB	3y	F	Flat Racing	256 x 256

DX: Stress (nonadaptive) remodelling of C3.

DS: Radiography: Moderate sclerosis of the radial facet of the right C3. Regional analgaesia: right fore lameness rendered sound by intra-articular analgesia of middle carpal joint.

- ➡ **A:** Moderate, focal IRU in the distal row of carpal bones.
- ➡ **B:** Normal RU in the distal radial physis.
- ➡ **C:** Diffuse linear IRU in the dorsal aspect of McIII.
- ➡ **D:** Background radioactivity due to inadequate shielding of the contralateral limb.

A **Figure 14: Dorsal view of both carpi**

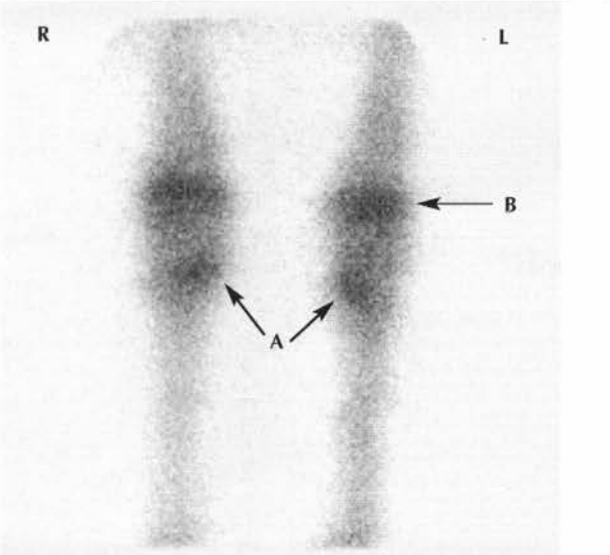

TB	2y	C	Flat Racing	256 x 256

DX: Stress (nonadaptive) remodelling of C3.

DS: Radiography: Sclerosis within the radial facet of both C3s.

- ➡ **A:** Moderate, focal IRU in the distal row of carpal bones of both forelimbs. The medial position of the IRU confirms the abnormal uptake to be associated with the radial facet of C3s.
- ➡ **B:** Normal RU in the distal radial physis.

A **Figure 15: Dorsal view of both carpi and metacarpal regions**

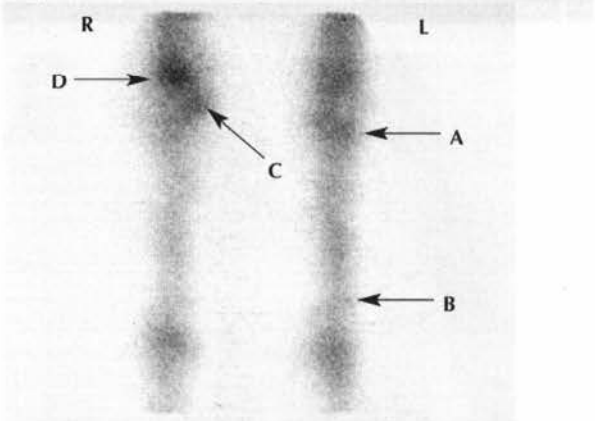

TB	3y	C	Flat Racing	256 x 256

DX: Multiple areas of bone injury detected scintigraphically throughout majority of skeleton.

DS: Radiography: Sclerosis C3. Osteoarthritis of the ABC joint.

- ➡ **A:** Moderate, focal IRU in the distal row of carpal bones of the left carpus.
- ➡ **B:** Moderate, focal IRU in the distal aspect of McIV. Note that this is much less marked than when imaged from the lateral aspect (see Figure 16).
- ➡ **C:** Moderate, focal IRU in the medial aspect of the right carpus in the RC bone.
- ➡ **D:** Moderate, focal, diffuse IRU in the distal aspect of the radius at the ABC joint.

A **Figure 16: Lateral view of the left carpus**

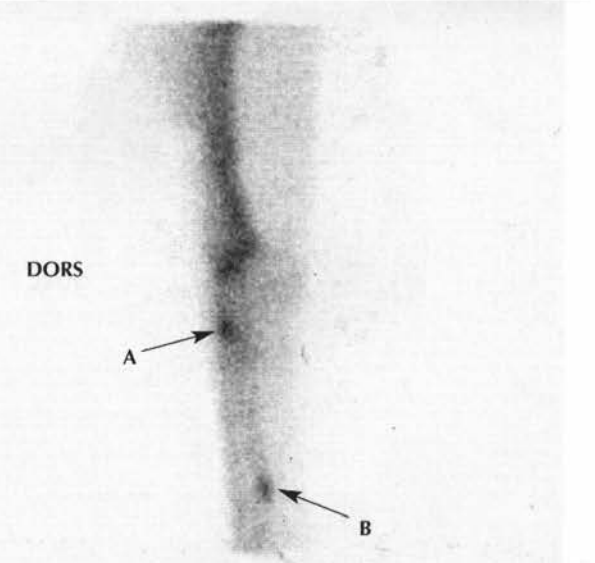

TB	3y	C	Flat Racing	256 x 256

DX: Stress (nonadaptive) remodelling of C3.

DS: Radiography: Sclerosis in C3.

- ➡ **A:** Focal, intense IRU in the distal row of carpal bones.
- ➡ **B:** Moderate, focal IRU in the distal aspect of McIV.

Note: The normal diffuse, linear RU in the caudal radius.

A **Figure 17: Lateral view of the right carpus (a) and dorsal view of both carpi (b)**

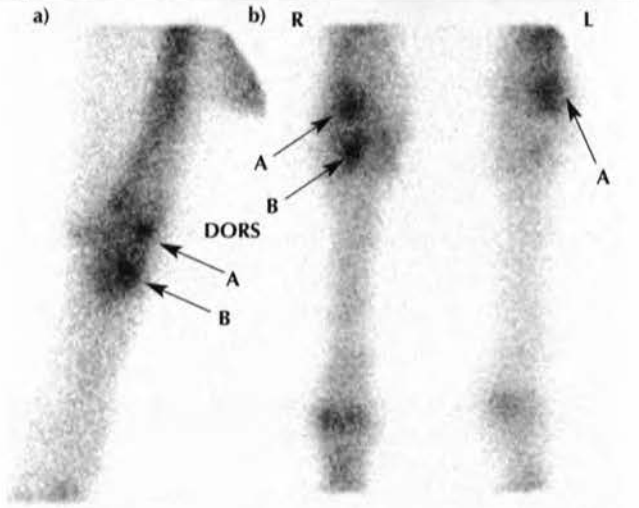

TB	4y	C	Flat Racing	256 x 256
DX:	Entheseophyte formation right RC bone.			
DS:	Radiography: Periosteal new bone formation on the dorsal aspect of the right RC bone.			
➡ **A:** Moderate, focal IRU in the lateral aspect of the distal radius of both left and right forelimbs. ➡ **B:** Moderate, focal IRU associated with the right RC bone.				

A **Figure 18: Lateral view of the right carpus**

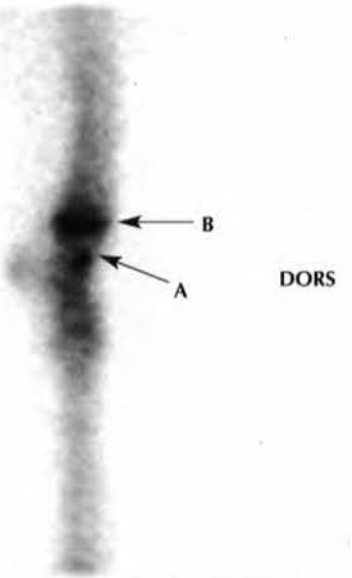

TB	3y	F	Flat Racing	128 x 128
DX:	Chip fracture of the distal radius.			
DS:	Radiography: Active new bone formation on the distal dorsolateral aspect of the radius, with 'chip' fracture pathology.			
➡ **A:** Moderate, focal IRU in the distal dorsal aspect of the radius. ➡ **B:** Normal RU in the distal radial physis.				

A **Figure 19: Dorsal view of both carpi**

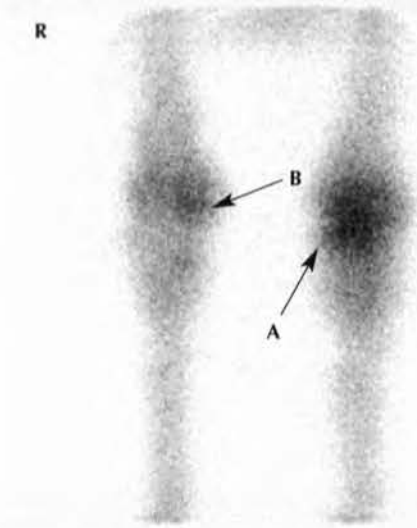

TB	3y	F	Flat Racing	256 x 256
DX:	Distal radial chip fracture.			
DS:	Radiography: Displaced osteochondral chip fracture in the distal aspect of the left radius.			
➡ **A:** Moderate, focal IRU in the distal medial aspect of the left radius and in the adjacent RC and IC bones. ➡ **B:** Moderate, focal IRU in the distal aspect of the right radius.				

A **Figure 20: Lateral view of the left carpus**

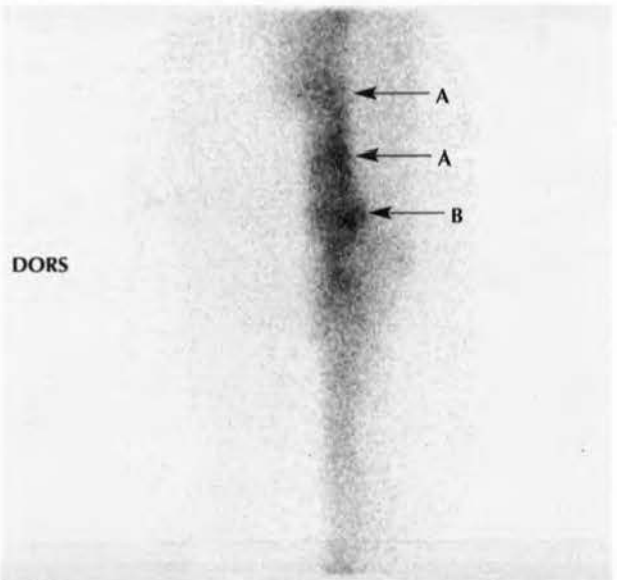

TB	2y	F	Flat Racing	256 x 256
DX:	Stress-related bone injury of the radius.			
DS:	No further investigation performed.			
➡ **A:** Mild, diffuse IRU in both the distal diaphyseal and metaphyseal regions of the radius. ➡ **B:** Normal RU in the caudal aspect of the distal radial physis.				

A Figure 21: Lateral view of the left carpus

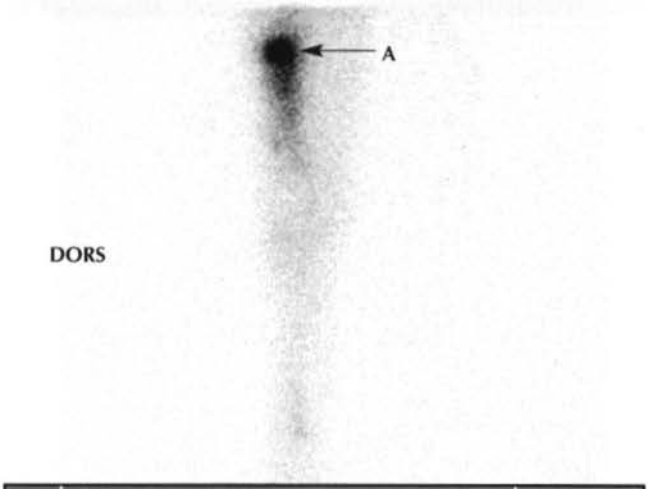

TB	4y	G	Flat Racing	256 x 256

DX: ELL in the distal aspect of the left radius.

DS: Radiography: Oval area of marked sclerosis in the distal one-third of the radius.

➡ **A:** Marked, focal IRU in the middle one-third of the radius. Note that this lesion was an incidental finding of no clinical significance in a sound limb.

Note: Poor quality of image due to count stealing by this 'hot' lesion. The enostosis should be masked out and the look-up tables recalibrated to examine the remaining sites in the limb.

A Figure 22: Lateral view of the right elbow joint

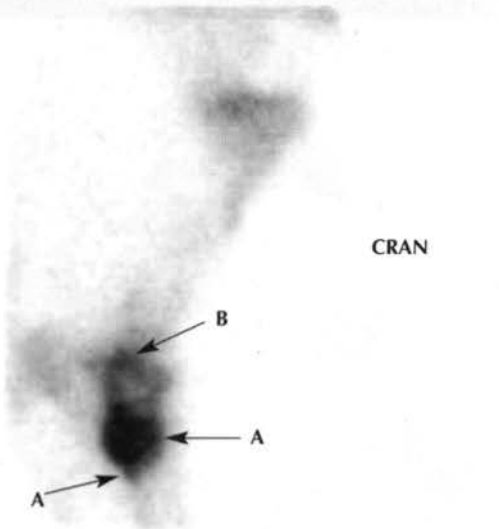

TB	8y	F	Flat Racing	128 x 128

DX: OCLL in the proximal radius and osteoarthritis of the elbow joint.

DS: Radiography: OCLL in the proximolateral aspect of the radius. Marked periarticular osteophytes around the lateral and medial aspects of the elbow joint.

➡ **A:** Marked focal IRU in the proximal radius.
➡ **B:** Mild, diffuse IRU in the distal humerus.

A Figure 23: Lateral view of the left shoulder and elbow regions

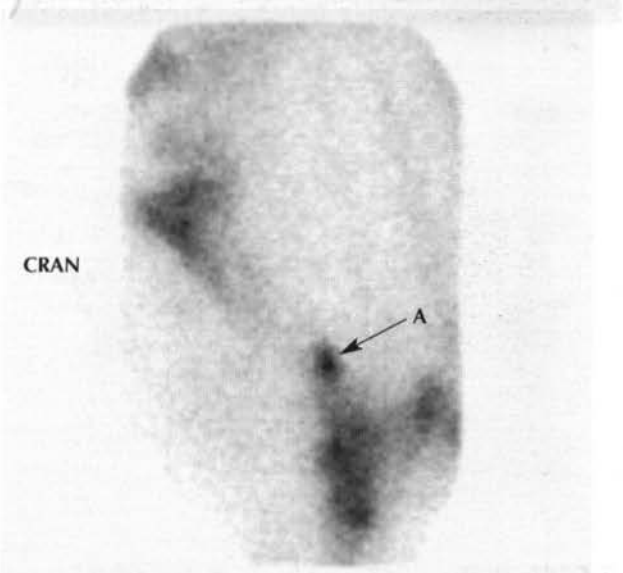

TB	3y	C	Flat Racing	128 x 128

DX: Humeral stress fracture.

DS: Radiography: Slightly irregular endosteal margin of the caudal cortex of the distal humerus. Sclerosis in same site on craniocaudal view.

➡ **A:** Marked, focal IRU in the caudal, distal aspect of the humerus.

A Figure 24: Lateral view of the left humerus

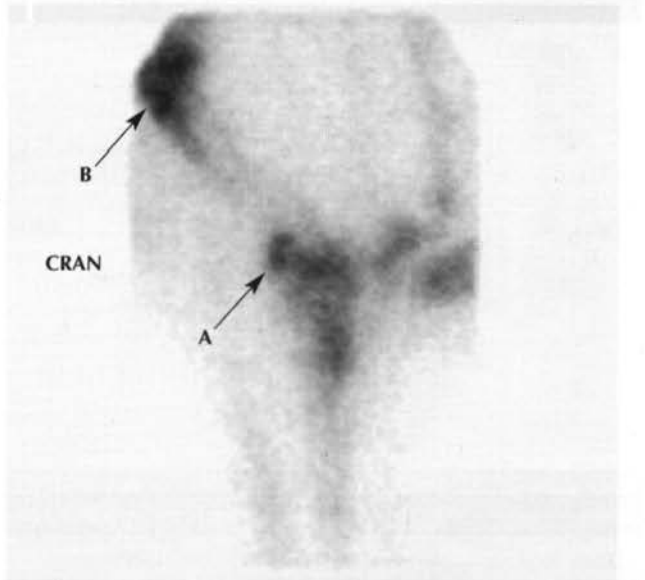

TB	3y	C	Flat Racing	128 x 128

DX: Distal humeral stress fracture.

DS: Radiography: Proliferative periosteal callus on distal cranial aspect of the humerus.

➡ **A:** Moderate, focal IRU in the cranial distal aspect of the humerus.
➡ **B:** Normal RU in the proximal humerus.

A **Figure 25: Lateral view of the right humerus and elbow regions**

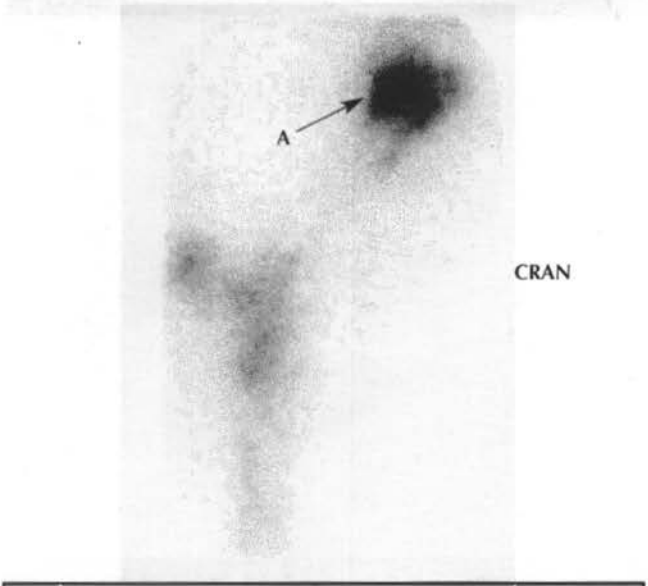

TB	3y	G	Flat Racing	128 x 128

DX: Proximal humeral stress fracture.

DS: Radiography: Periosteal new bone formation on the proximal caudal aspect of the humerus.

➡ **A:** Marked, focal IRU in the proximal caudal aspect of the humerus.

A **Figure 26: Lateral view of the left scapula and shoulder**

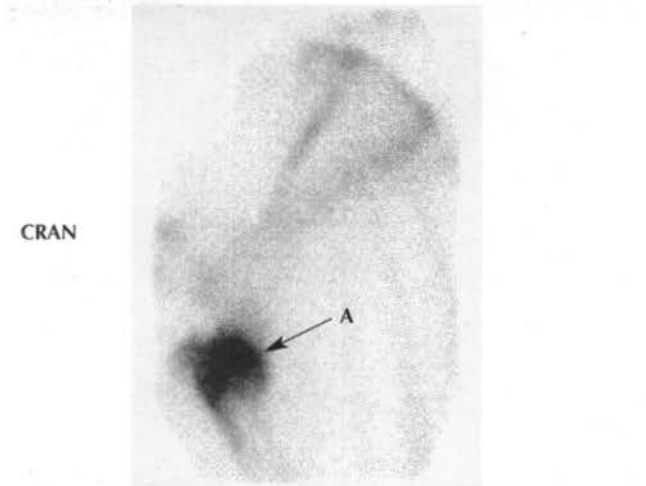

TB	2y	F	Flat Racing	128 x 128

DX: Proximal humeral physeal abscess.

DS: Radiography: Lysis around the physis; periosteal new bone caudal humeral head. Haematology and biochemistry changes consistent with infection.
Response to treatment: Radiographic and clinical improvement with 4 weeks of antimicrobial therapy.

➡ **A:** Marked, focal IRU in the proximal humeral epiphysis. Note that this is more proximal than the normal position of a humeral stress fracture.

A **Figure 27: Lateral view of the left scapula**

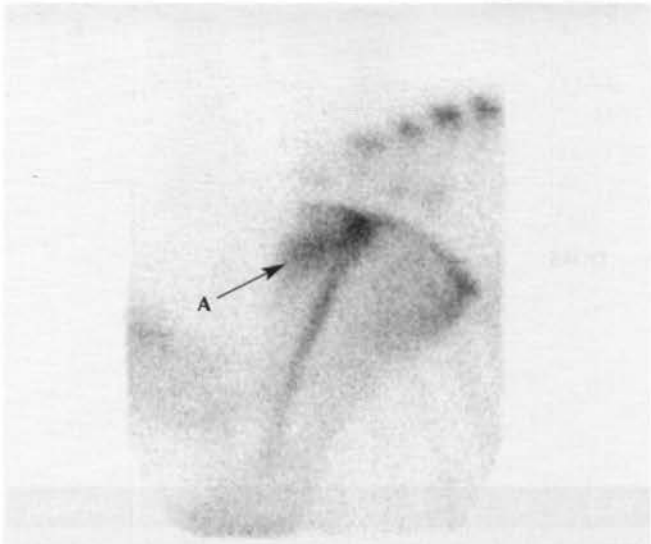

TB	2y	C	Flat Racing	256 x 256

DX: Traumatic fracture of the proximal aspect of the scapula.

DS: History of fall. Clinical signs: Reduced protraction of the limb at the walk. Radiography: Displaced fracture of the cranial proximal aspect of the scapula.

➡ **A:** Moderate, focal IRU in an oblique line in the cranial proximal aspect of the scapula.

A **Figure 28: Lateral view of the distal aspect of the LH (a) and plantar view of both hindlimbs (b)**

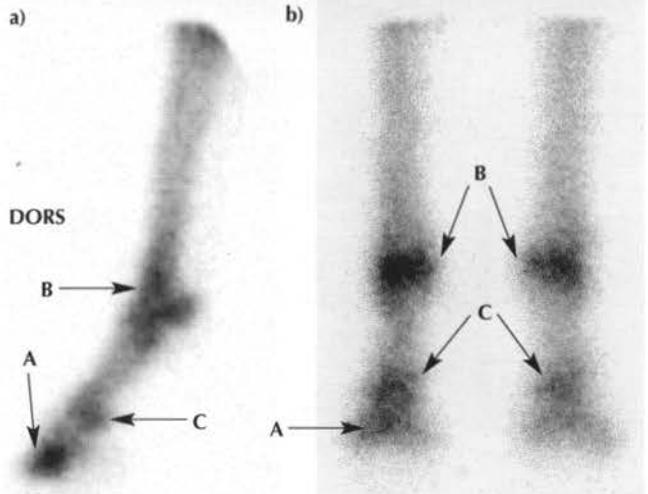

TB	1y	C	Flat Racing	128 x 128

DX: Intra-articular fracture of the distal phalanx.

DS: Radiography: Displaced intra-articular fracture of the left distal phalanx.

➡ **A:** Marked, focal IRU in the entire distal phalanx.
➡ **B:** Normal RU in the fetlock region.
➡ **C:** Normal RU associated with the PIP joint.
Note: Generalised increase IRU in the entire distal left hindlimb.

A **Figure 29: Lateral view of the distal aspect of the RH (a) and plantar view of both hindlimbs (b)**

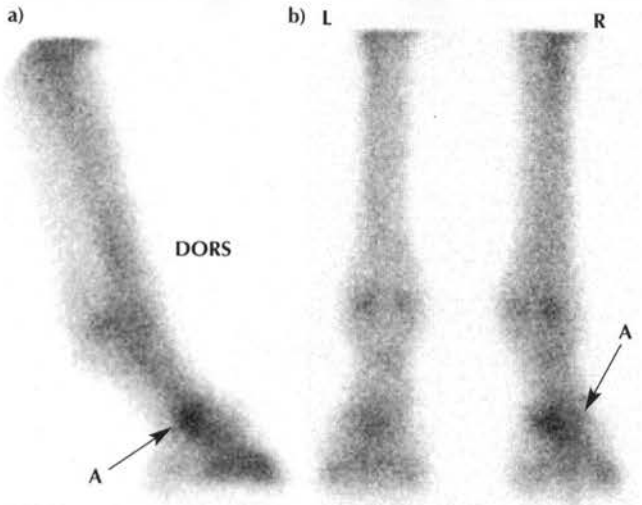

TB	7y	G	Flat Racing	128 x 128
DX:	Osteoarthritis of the right hind PIP joint.			
DS:	Radiography: Periarticular osteophyte formation.			
➡ **A:**	Moderate, focal IRU associated with the plantar aspect of the PIP joint.			

A **Figure 30: Lateral view of the distal aspect of the RH**

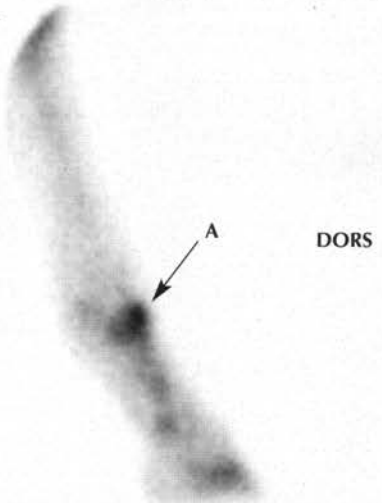

TB	3y	C	Flat Racing	128 x 128
DX:	Stress fracture of the proximal phalanx.			
DS:	Radiography: Periosteal new bone formation on the proximodorsal aspect of the proximal phalanx. No fracture line was seen.			
➡ **A:**	Intense, focal IRU in the proximal dorsal aspect of the proximal phalanx.			

A **Figure 31: Lateral view of the distal aspect of the LH (a) and RH (b) and plantar view of both hindlimbs (c)**

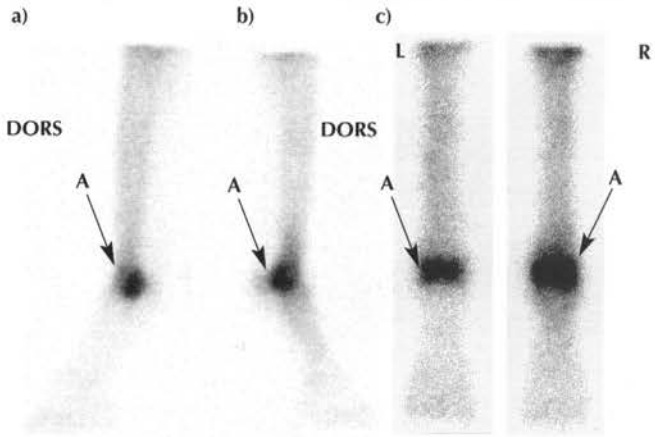

TB	3y	C	Flat Racing	256 x 256
DX:	Stress-related bone injury in the distal plantar aspect of MtIII, LH and RH.			
DS:	Radiography: Sclerosis in the distal plantarolateral aspect of each MtIII.			
➡ **A:**	Intense, focal IRU in the plantar distal aspect of each MtIII.			

A **Figure 32: Lateral view of the distal aspect of the LH (a) and plantar view of both hindlimbs (b)**

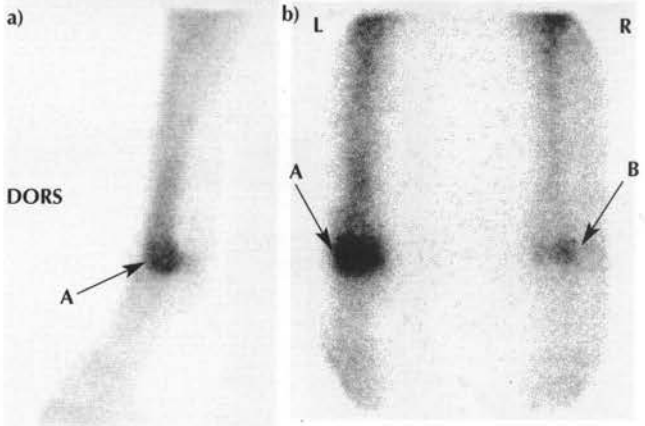

TB	4y	C	Flat Racing	256 x 256
DX:	Stress-related bone injury of the plantar aspect of the lateral condyle of MtIII of the LH.			
DS:	Regional analgesia: Plantar metatarsal and lateral plantar nerve blocks abolished the lameness. Radiography: Radiolucent area in the plantar aspect of the lateral condyle of MtIII, LH.			
➡ **A:**	Marked, focal IRU in the subchondral bone of the plantarodistal aspect of MtIII. Note that the plantar view confirmed the lateral position of the region of IRU and that the lateral view shows it to be not derived from the PSB.			
➡ **B:**	Less marked IRU in the identical site in the right hindlimb.			

A Figure 33: Lateral view of the distal aspect of the RH

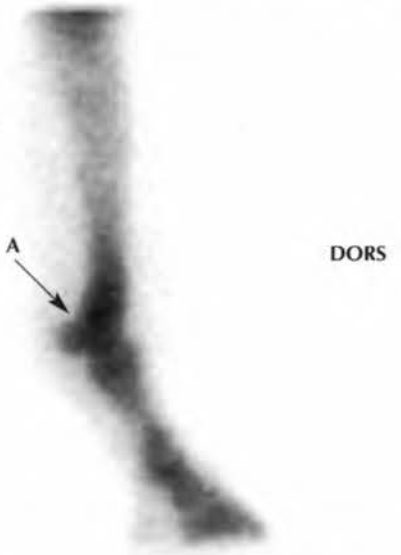

TB	3y	F	Flat Racing	128 x 128
DX:	Stress-related bone injury of the distal aspect of MtIII.			
DS:	Local analgesia: Intra-articular analgesia of the right MTP joint abolished the lameness. Radiography: NAD.			
➡ **A:**	Intense, diffuse IRU in the distal aspect of MtIII.			

A Figure 34: Plantar view of the distal aspect of both hindlimbs

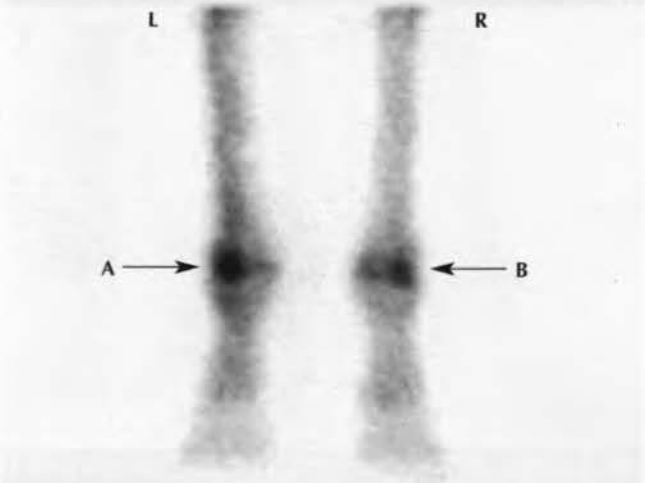

TB	5y	C	Flat Racing	128 x 128
DX:	Stress-related bone injury of the plantar aspect of the lateral condyle of MtIII, LH and RH.			
DS:	Clinical signs: Bilateral hindlimb lameness. Response to regional analgesia.			
➡ **A:**	Intense, focal IRU in the distal lateral aspect of the left MtIII.			
➡ **B:**	Moderate, focal IRU in the distal lateral aspect of the right MtIII. Note that a lateral view was required to rule out IRU in the lateral PSB.			

A Figure 35: Lateral view of the distal aspect of the RH

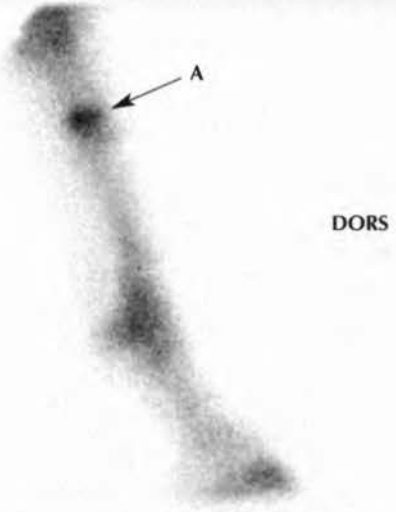

TB	3y	C	Flat Racing	256 x 256
DX:	ELL in the proximal aspect of MtIII.			
DS:	Radiography: Circular area of endosteal sclerosis in the proximal aspect of MtIII.			
➡ **A:**	Marked, focal IRU in the proximal aspect of MtIII.			
Note:	In this horse, diagnostic analgesia confirmed this lesion as the source of lameness. These lesions can, however, be seen unassociated with lameness (see Figure 21).			

A Figure 36: Lateral view of the distal aspect of the LH

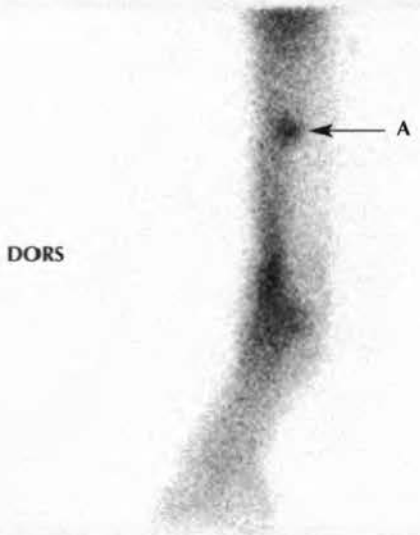

TB	5y	G	Flat Racing	256 x 256
DX:	Active periostitis MtII, 'splint'.			
DS:	Radiography: Periosteal new bone mid diaphysis of MtII. No evidence of a fracture line.			
➡ **A:**	Moderate, focal IRU in the region of MtII and MtIV. The plantar view confirmed that the region of IRU was in MtII.			
Note:	These can be found unassociated with lameness.			

A Figure 37: Lateral view of the distal aspect of the RH

TB	3y	C	Flat Racing	256 x 256
DX:	Stress-related bone injury of the proximal dorsal aspect of MtIII (sore shins).			
DS:	Not performed.			
➡ **A:**	Moderate, focal, linear IRU in the proximal dorsal aspect of MtIII. This can be an incidental finding.			

A Figure 38: Lateral view of the left hock (a) and a plantar view of both hocks (b)

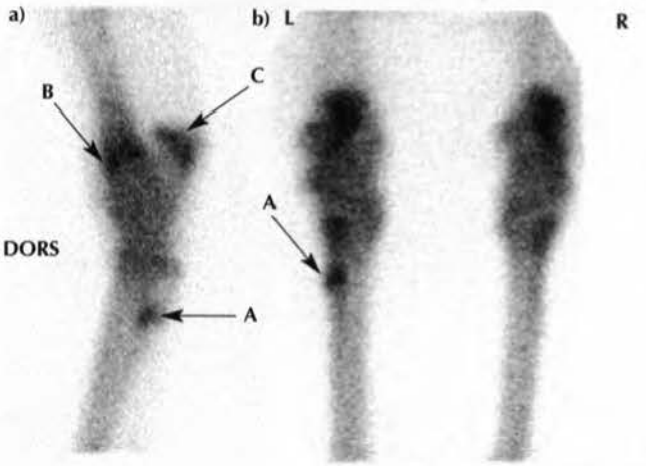

TB	2y	C	Flat Racing	256 x 256
DX:	Chronic non-union fracture of the proximal aspect of MtIV.			
DS:	Regional analgesia: rendered sound by lateral 'subtarsal' block, no improvement to 6 point block bone above the fetlock. Radiography: Fracture line and active periosteal new bone formation 9 months after injury.			
➡ **A:**	Moderate, focal IRU in the proximal aspect of MtIV.			
➡ **B:**	Distal tibial physis (normal).			
➡ **C:**	Calcaneal physis (normal).			

A Figure 39: Lateral view of the left hock

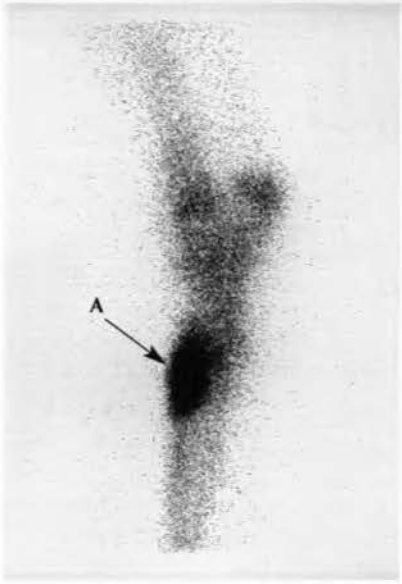

TB	5y	G	Flat Racing	128 x 128
DX:	Sequestrum formation following trauma.			
DS:	Radiography: Periostitis and focal bone lysis typical of sequestrum formation.			
➡ **A:**	Intense, focal IRU in the proximal dorsal aspect of MtIII.			

A Figure 40: Lateral view of the left hock

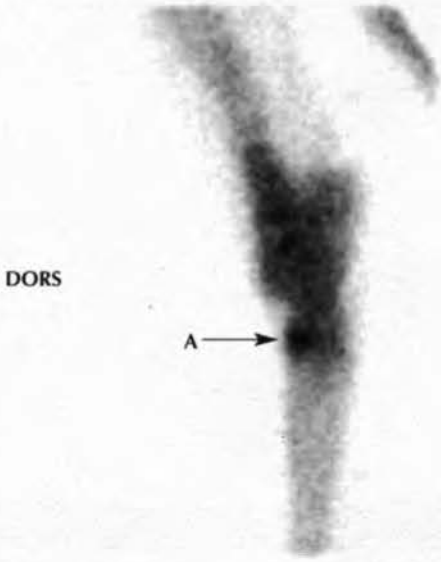

TB	3y	C	Flat Racing	128 x 128
DX:	Slab fracture of T3.			
DS:	Radiography: Periosteal new bone dorsal aspect of T3. Vertical lucent line dorsolateral aspect of T3.			
➡ **A:**	Intense, focal IRU in the dorsal aspect of T3.			

A **Figure 41: Plantar views of both hocks (a) and lateral view of the right hock (b)**

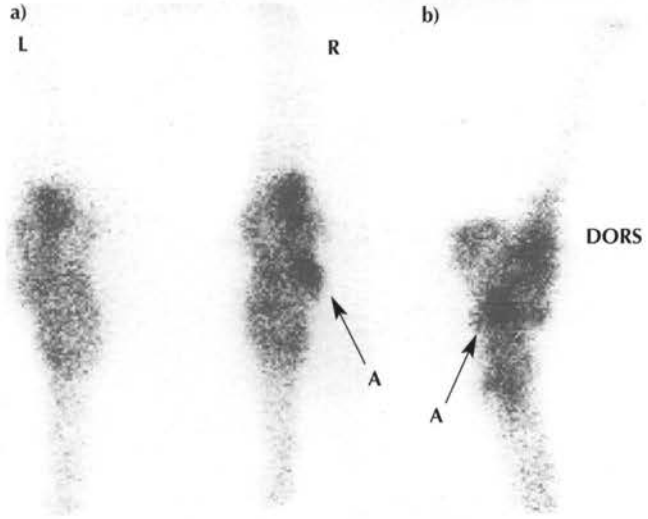

TB	4y	G	Flat Racing	128 x 128
DX:	Desmitis and entheseopathy short lateral collateral ligament of the TC joint.			
DS:	Radiography: Entheseophyte formation lateral talus.			
➡ **A:**	Moderate, focal IRU lateral talus at the site of insertion of the short lateral collateral ligament.			

A **Figure 42: Lateral view of the left tibia**

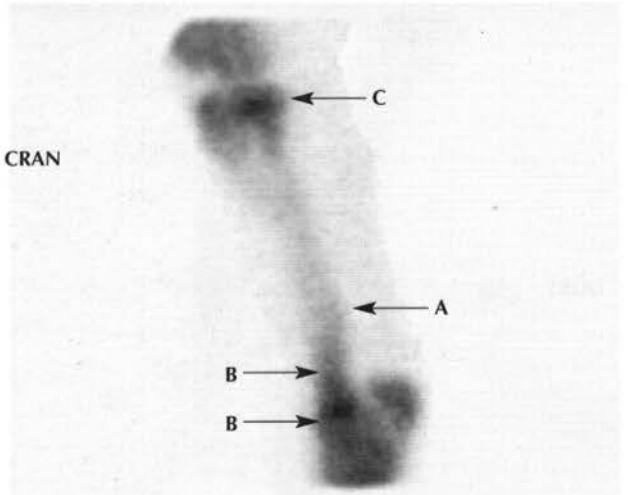

TB	4y	C	Flat Racing	128 x 128
DX:	Stress fracture of the distal aspect of the tibia.			
DS:	Radiography: Mild sclerosis of the cortex of the distal tibia.			
➡ **A:**	Mild, focal IRU in the caudal cortex of the distal tibia at the junction of the proximal two-thirds and distal one-third.			
➡ **B:**	Normal RU in the distal tibial epiphysis and metaphyseal region.			
➡ **C:**	Normal RU in the proximal aspect of the tibia.			
Note:	These stress fractures in the distal one-third of the tibia often have relatively mild IRU.			

A **Figure 43: Lateral view of the left hock**

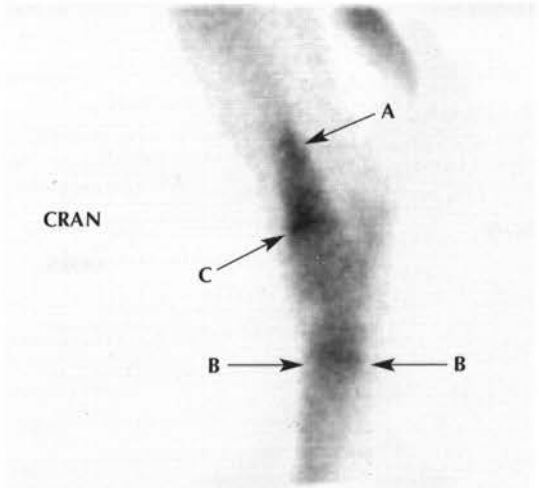

TB	4y	C	Flat Racing	128 x 128
DX:	Distal tibial stress fracture.			
DS:	Radiography: Vertical lucent line mid distal caudal cortex of tibia (caudocranial view). Marked endosteal sclerosis in the same site (lateromedial view).			
➡ **A:**	Moderate, focal IRU in distal diaphyseal region of the tibia.			
➡ **B:**	Mild, focal linear IRU in the region of the TMT joint.			
➡ **C:**	Normal diffuse, intense RU in the epiphyseal regions of the tibia.			

A **Figure 44: Lateral view of the right tibia**

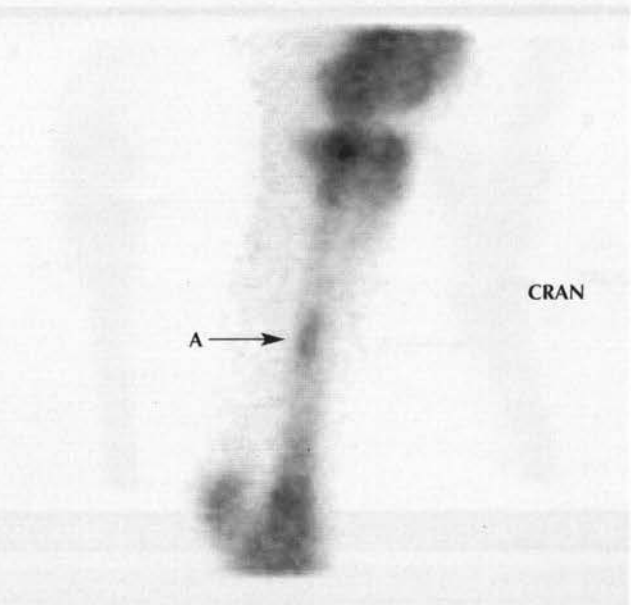

TB	3y	C	Flat Racing	128 x 128
DX:	Mid diaphyseal tibial stress fracture.			
DS:	Radiography: Endosteal callus in the mid diaphysis of the tibia.			
➡ **A:**	Mild, focal IRU in the mid diaphysis of the tibia.			

A **Figure 45: Lateral view of the right tibia**

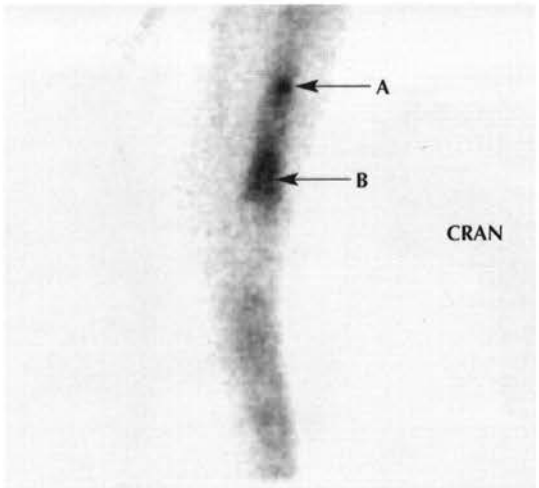

TB	3y	F	Flat Racing	128 x 128

DX: Mid diaphyseal tibial stress fracture.

DS: Radiography: Endosteal callus associated with the mid diaphysis of the tibia.

➡ **A:** Marked, focal IRU in the mid diaphysis of the tibia (abnormal).
➡ **B:** Marked, diffuse RU in the distal aspect of the tibia (normal).
Note: The site of uptake rather than its intensity indicates the site of injury, emphasising the importance of knowledge of normal regions of RU.

A **Figure 46: Lateral view of the left stifle**

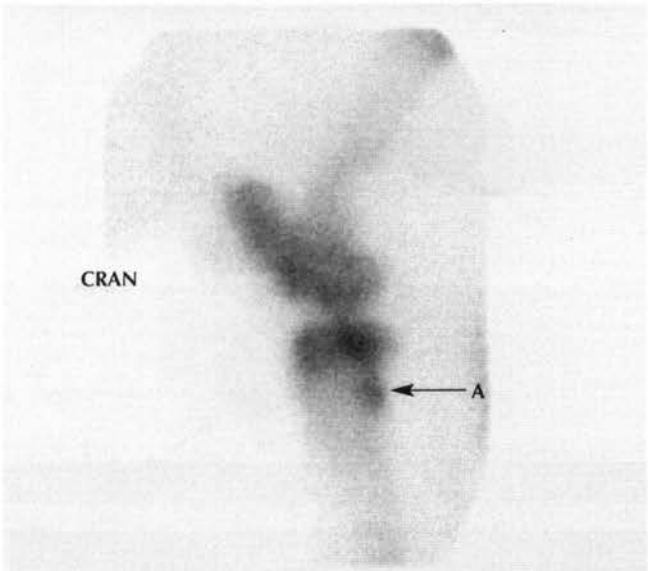

TB	3y	G	Flat Racing	256 x 256

DX: Proximal tibial stress fracture.

DS: Radiography: Periosteal new bone proximolateral cortex of the tibia.

➡ **A:** Moderate, focal IRU in the caudal proximal aspect of the tibia.

A **Figure 47: Lateral view of the right stifle**

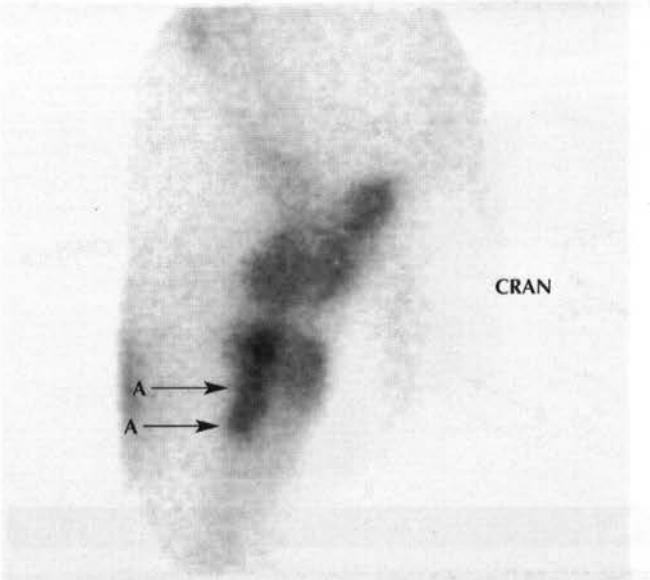

TB	4y	G	Flat Racing	128 x 128

DX: Proximal tibial stress fracture.

DS: Radiography: Marked periosteal new bone formation on the proximal caudolateral aspect of the tibia.

➡ **A:** Moderate, diffuse IRU in the proximal caudal aspect of the tibia.

A **Figure 48: Lateral view of the left (a) and right (b) stifles**

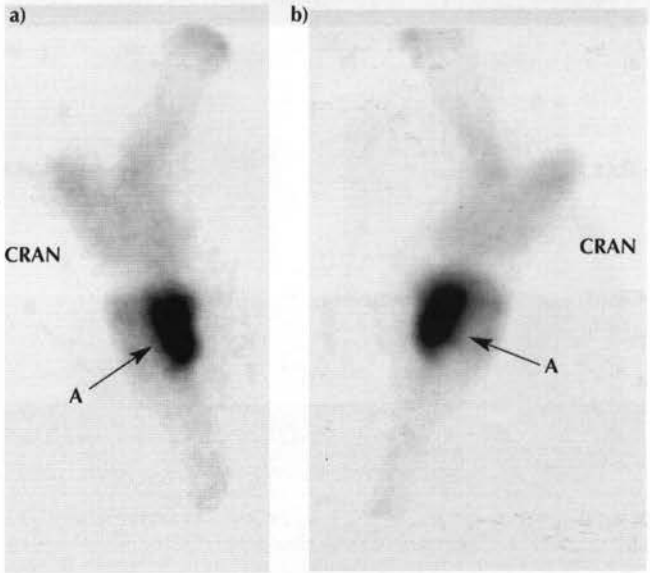

TB	4y	C	Flat Racing	128 x 128

DX: Bilateral proximal tibial stress fractures.

DS: Radiography: Abundant callus formation caudolateral cortex of the proximal aspect of both tibias.

➡ **A:** Marked, diffuse IRU in the proximal caudal aspect of both left and right tibias.

A Figure 49: Dorsal view of the pelvis

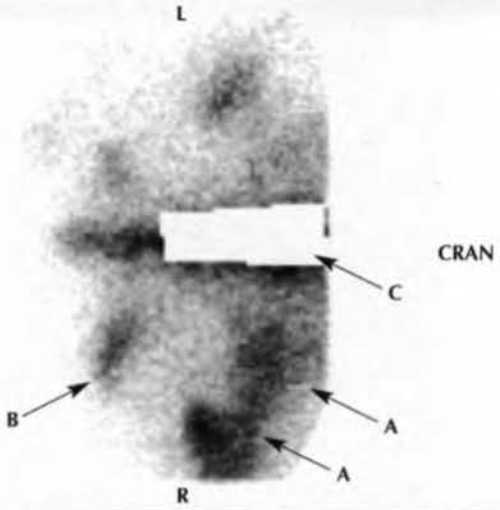

TB	2y	F	Flat Racing	128 x 128

DX: Bone injury (probable fracture) of the right acetabulum.

DS: History of fall and clinical signs.

- **A:** Moderate, focal IRU in the right CFJ.
- **B:** Mild, focal IRU in the right tuber ischii.
- **C:** Area masked to avoid count capture by radioactivity in the bladder.

Note: The left CFJ shows the normal relatively photopenic appearance of this site

A Figure 50: Lateral (a) and caudodorsal (b) views of the caudal pelvis

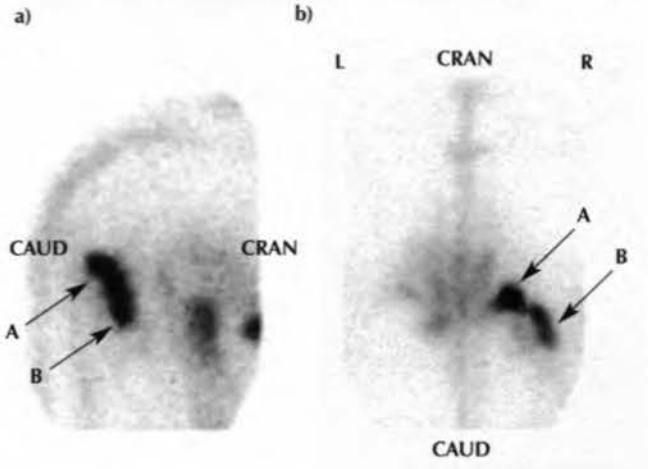

TB	11y	F	Flat Racing	128 x 128

DX: Displaced fracture of the tuber ischii.

DS: Ultrasonography: Ventral displacement of the entire tuber ischii.

- **A:** Intense, focal IRU in the parent bone of the right tuber ischii.
- **B:** Moderate, focal IRU in the ventrally displaced fragment detached from the right tuber ischii.

A Figure 51: Lateral (a) and dorsal (b) views of the caudal pelvis

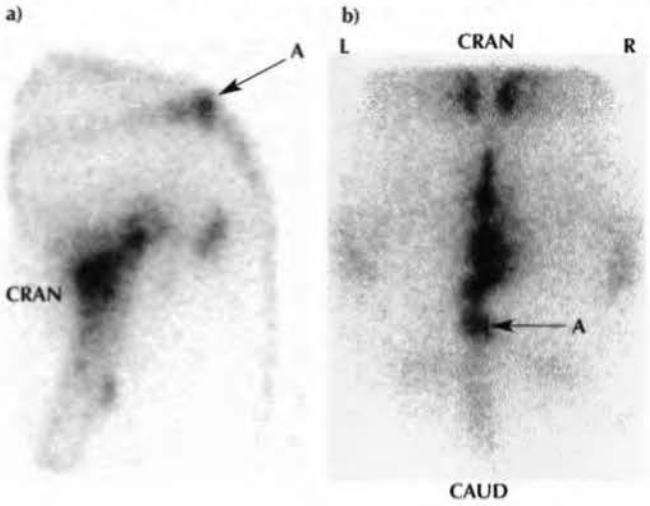

TB	2y	C	Flat Racing	128 x 128

DX: Displaced fracture of the first coccygeal vertebra.

DS: Radiography: Subluxation of the first coccygeal vertebra, with associated damage to the vertebral body.

- **A:** Moderate, focal IRU in the region of the first coccygeal vertebra.

A Figure 52: Dorsolateral oblique view of the right ilium

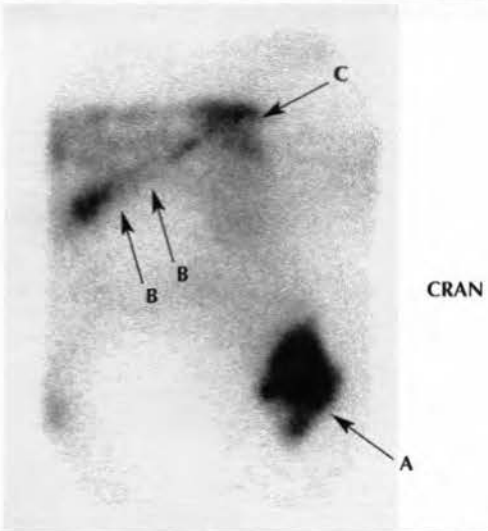

TB	6y	G	Flat Racing	128 x 128

DX: Ventrally displaced fracture of the right tuber coxae.

DS: Clinical examination. Ultrasonography: Ventrally displaced fracture of the right tuber coxae.

- **A:** Intense, irregular IRU in the right tuber coxae.
- **B:** Moderate, focal, linear IRU associated with the gluteal musculature.
- **C:** Left tuber sacrale.

A Figure 53: Dorsal 45° lateral oblique view of the right ilium

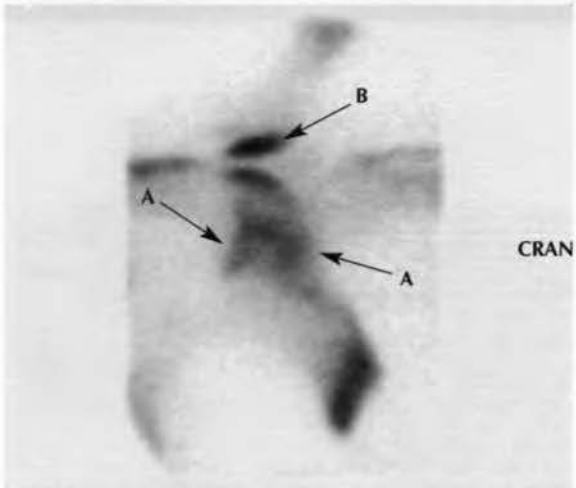

TB	2y	C	Flat Racing	128 x 128

DX: Ilial wing stress fracture.

DS: Clinical signs: pain on deep palpation of the right ilial musculature. Ultrasonography: Disruption of the dorsal surface of the right ilial wing.

➡ **A:** Moderate, focal IRU in a band extending from the cranial to the caudal margins of the ilial wing.
➡ **B:** Note that the contralateral tuber sacrale commonly shows apparent IRU when imaged in this plane because of summation of counts.

A Figure 54: Dorsal 45° lateral oblique view of the right ilium

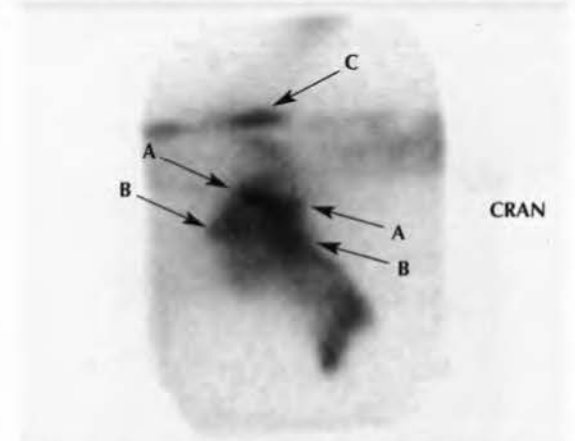

TB	3y	C	Flat Racing	128 x 128

DX: Ilial wing stress fracture.

DS: Ultrasonography: Step-like disruption of the dorsal surface of the ilium. Irregular hyperechogenic material suggestive of callus.

➡ **A:** Marked, focal IRU in a band extending from the cranial to the caudal margins of the ilial wing.
➡ **B:** Moderate, diffuse IRU in the area surrounding the fracture, associated with the area of 'honeycomb' callus on the surface of the ilium.
➡ **C:** Normal RU in the contralateral tuber sacrale.

A Figure 55: Dorsal view of the cranial pelvis

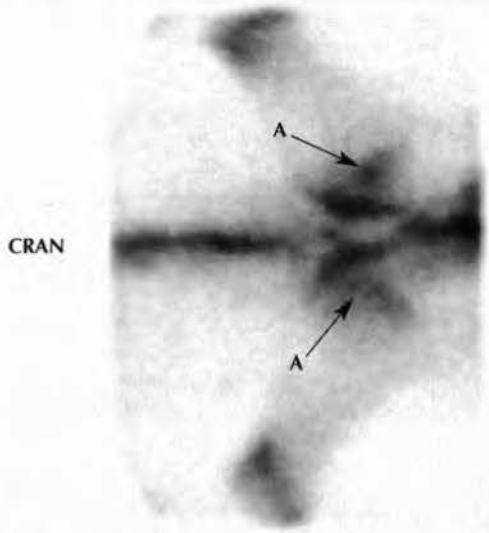

TB	8y	G	Flat Racing	128 x 128

DX: Bilateral ilial wing stress fractures.

DS: Ultrasonography: Bilateral disruption of the dorsal surface of the ilium, with surface irregularities typical of 'honeycomb' callus.

➡ **A:** Moderate, linear, focal IRU in both ilial wings.

A Figure 56: Dorsal 45° lateral oblique views of both left (a) and right (b) ilial wings

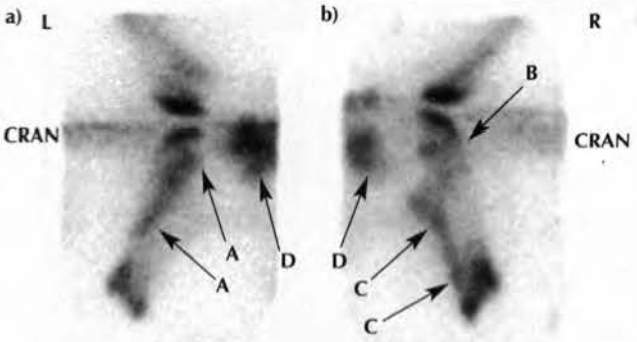

TB	3y	F	Flat Racing	128 x 128

DX: Bilateral ilial wing stress fractures.

DS: Clinical signs.

➡ **A:** Moderate, focal, linear IRU extending obliquely from the caudal to cranial aspects of the left ilial wing.
➡ **B:** Mild, poorly defined IRU in the cranial aspect of the right ilial wing.
➡ **C:** Moderate, linear IRU in the caudal margin of the right ilial wing.
➡ **D:** Bladder activity.
Note: Although not dramatic in terms of degree of IRU, these fractures often originate on the caudal cortex and propagate to the cranial cortex more laterally. These fractures have a high risk of becoming complete and displaced.

A **Figure 57: Dorsal 45° lateral oblique view of the right ilium**

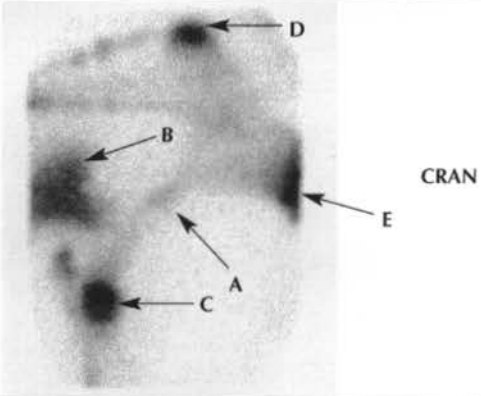

TB	3y	F	Flat Racing	128 x 128

DX: Ilial shaft stress fracture.

DS: Clinical signs: Intense guarding of pelvic musculature on right side with deep palpation. Local analgesia: No improvement to distal limb nerve blocks. Ultrasonography: NAD.

➡ **A:** Mild, focal IRU in the mid shaft of the right ilium.
➡ **B:** Radioactivity in the bladder.
➡ **C:** Normal RU associated with the proximal femur in the region of the CF joint.
➡ **D:** Normal RU in the tuber sacrale.
➡ **E:** Normal RU in the tuber coxae.
Note: These ilial shaft fractures often have relatively mild IRU compared with the normal sites of RU in this region. Masking B, C, D and E would have have enhanced this image significantly.

A **Figure 58: Dorsal 60° lateral oblique view of the left thoracolumbar region**

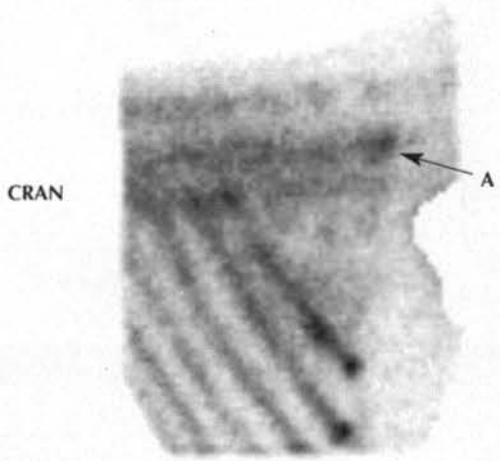

TB	2y	C	Flat Racing	128 x 128

DX: Lumbar vertebral laminar stress fracture.

DS: Clinical signs: Stiff action at the walk, mimicking tying-up. Reduced performance at fast exercise. No obvious lameness at the trot.

➡ **A:** Moderate, focal IRU associated with the dorsal laminar region of the 4th lumbar vertebra.

A **Figure 59: Dorsal 60° lateral left oblique views of the thoracolumbar (a) and lumbar (b) regions**

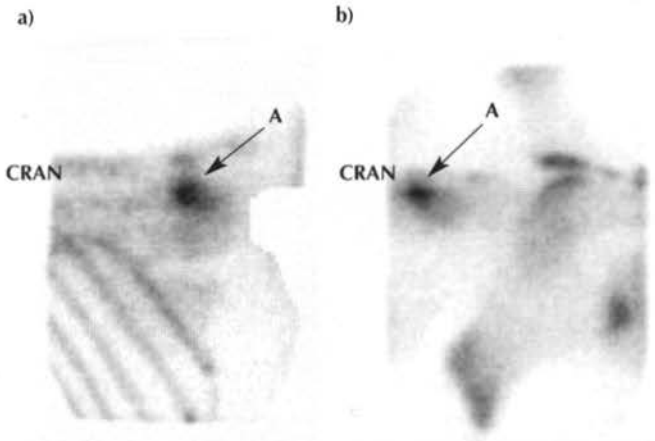

TB	3y	F	Flat Racing	128 x 128

DX: Lumbar vertebral laminar stress fracture.

DS: Clinical signs: Pain and lumbar muscle spasm on spinal manipulation. No lameness, but stiff gait at walk and trot.

➡ **A:** Intense, focal IRU in the dorsal aspect of the 3rd and 4th lumbar vertebrae.

A **Figure 60: Dorsal 60° lateral left oblique view of the caudal thoracic region**

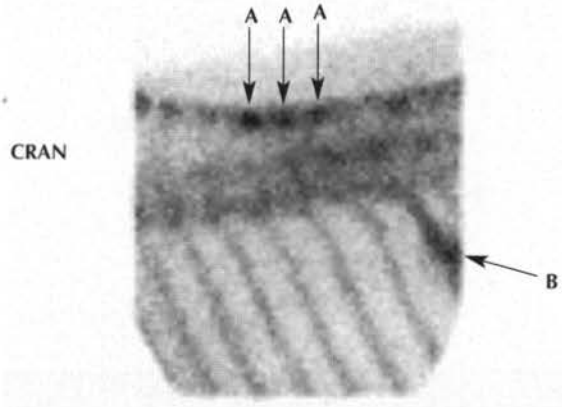

TB	3y	C	Flat Racing	128 x 128

DX: Impinging thoracic DSPs.

DS: Radiography: Impingement of the DSPs in the mid thoracic region with radiolucent and sclerotic regions in the cortical and subcortical bone at the points of apposition.

➡ **A:** Three areas of moderate, focal IRU in the summits of adjacent DSPs.
➡ **B:** Apparent IRU in a rib overlying the kidney (incidental finding).

A **Figure 61: Dorsal 60° lateral left oblique view of the mid thoracic region**

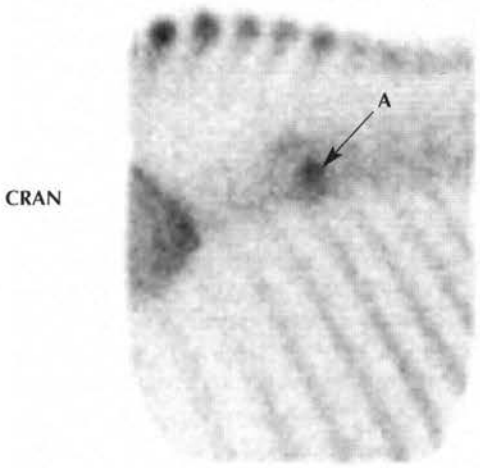

TB	3y	C	Flat Racing	128 x 128
DX:	Fracture of the base of the 9th thoracic DSP.			
DS:	Radiography: Transverse fracture through the ventral aspect of the 9th thoracic DSP.			
➡ **A:**	Marked, focal IRU in the 9th thoracic vertebra.			

A **Figure 62: Dorsal view of the caudal thoracic region**

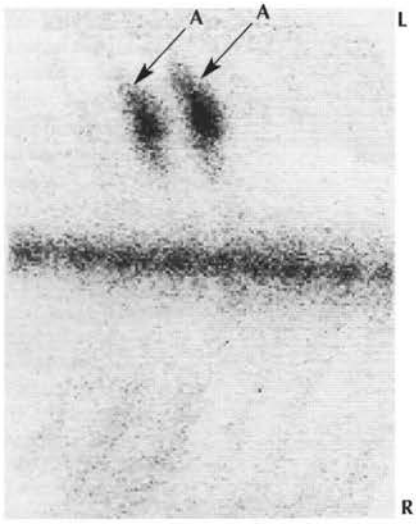

TB	2y	C	Flat Racing	128 x 128
DX:	Rib fracture.			
DS:	Ultrasonography: Step-like disruption of rib surface and periosteal new bone formation on the surface of the ribs.			
➡ **A:**	Marked, focal IRU in the left 16th and 17th ribs.			

A **Figure 63: Dorsal view of the caudal pelvis**

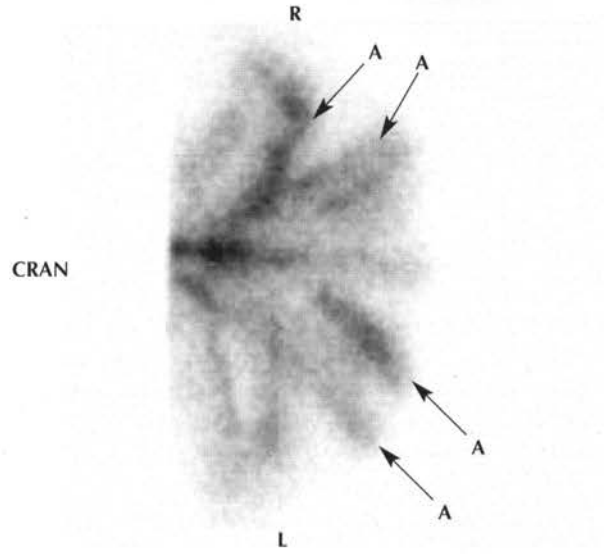

TB	2y	F	Flat Racing	128 x 128
DX:	Recurrent rhabdomyolysis.			
DS:	Blood biochemistry: Markedly elevated serum creatine kinase and aspartoaminotransferase.			
➡ **A:**	Multiple mild, moderate and marked linear areas of IRU in the muscles.			

A **Figure 64: Lateral view of the left thorax caudal to the scapula**

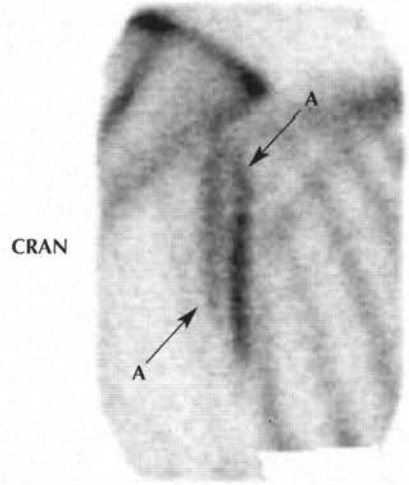

TB	2y	F	Flat Racing	128 x 128
DX:	IRU in the triceps muscle.			
DS:	Significance of finding unknown.			
➡ **A:**	Bands of moderate and intense focal IRU in the muscle mass caudal to the left scapula.			

Chapter 2

THE AMERICAN THOROUGHBRED

MARK J. MARTINELLI and RICK M. ARTHUR
California Equine Orthopedics, Encinitas, California 92404, USA.
311E Grandview Avenue, Sierra Madre, California 91024, USA.

The interpretation and significance of lesions of Thoroughbred racehorses is different from that for sport horses. Nuclear scintigraphy in North America developed as a diagnostic tool for the detection of stress fractures in long bones and stress remodelling. It became obvious that nuclear scintigraphy was ideally suited for detecting occult lesions in elite athletes before they became more serious injuries. Occult musculoskeletal lesions are usually classified as those that are not readily evident radiographically, but are still capable of causing catastrophic injury. In racehorses that show subtle or

Table 1: Location and frequency of IRUs associated with stress-related bone lesions in Thoroughbred racehorses in North America

	Location	Frequency†	Tendency to become a complete fracture with continued exercise (unstable)
Scapula:	Neck	Very uncommon	Yes
	Blade	Rare	No
Humerus:	Proximal caudal	Common	Yes
	Distal cranial/medial	Common	No
	Distal caudal	Relatively uncommon	Yes
Radius:	Mid shaft (intramedullary)	Common	No
Carpus:	Lateral distal radius	Common	Yes
	Third carpal bone	Common	No
	Radial carpal bone	Common	Yes
McIII:	Proximal palmar	Common	Yes*
	Mid shaft	Uncommon	Yes
	Dorsal cortex	Very common	No
	Distal transverse	Rare	Yes
	Medial distal palmar	Very common	No
	Lateral distal palmar	Common	Yes
Proximal sesamoid bones		Rare	Yes
Proximal phalanx (forelimb): Proximal dorsal		Common	Yes
Middle phalanx (forelimb)		Very rare	No
Distal phalanx (forelimb)		Uncommon	No
Navicular bone		Uncommon	No
Pelvis:	Ilium (tuber sacrale to tuber coxae)	Common	Yes
	Ilium (shaft)	Rare	Yes
Femur:	Distal caudal	Rare	No
Patella		Rare	No
Tibia:	Proximal caudal	Common	No
	Mid shaft lateral	Very common	Yes
	Distal medial	Relatively uncommon	Yes
Tarsus:	Central tarsal	Common	No
	Third tarsal bone	Uncommon	No
MtIII:	Intramedullary	Rare	No
	Medial distal plantar	Relatively uncommon	No
	Lateral distal plantar	Common	No
Proximal phalanx (hindlimb): Proximal dorsal		Relatively uncommon	Yes
Middle phalanx (hindlimb)		Very rare	No
Distal phalanx (hindlimb)		Rare	No
Cervical vertebrae		Relatively uncommon	No
Lumbosacral vertebrae		Relatively uncommon	No
Thoracic vertebrae (including withers)		Very rare	No
Coccygeal vertebrae		Very rare	No

*Fractures are most often an avulsion type, although diffuse IRUs are common. †The frequency of distribution of these lesions in terms of percentages of scintigraphy cases examined has been described elsewhere and compared to lesion frequency in both the sports horse and Standardbred[1].

intermittent signs of lameness, nuclear scintigraphy is an invaluable diagnostic tool. Because of the skeletal immaturity of many Thoroughbred racehorses, it is relatively easy to detect increased radiopharmaceutical uptake (IRU) compared with older sport horses. However, it is important to determine the clinical significance of any area of IRU. It is necessary to determine whether the lesion could have serious catastrophic consequences and whether the horse should be taken out of work completely or just have the training reduced in intensity. Trainers and owners want to know what the prognosis is for future racing soundness and what the convalescent period needs to be for proper healing to occur. Nuclear scintigraphy is useful to monitor the healing of injuries, especially stress fractures in the long bones. Once the radiopharmaceutical distribution has returned to normal, it is usually safe to say that remodelling has subsided and the horse can resume training.

Thoroughbred and Standardbred racehorses are both plagued by stress remodelling injuries, but Thoroughbreds have more lesions at risk of becoming complete fractures (**Table 1**). This difference is probably because of the faster speed at which Thoroughbreds race and may also be associated with different training methods, Thoroughbreds doing fewer miles than Standardbreds at faster speeds. Lesion distribution and frequency has been compared between the Thoroughbred and Standardbred and approximate percentages of occurrence at the predeliction sites are documented elsewhere[1].

There are several notable differences between the North American and European racing industries which result in a different distribution of musculoskeletal injuries[2]. In the USA, Thoroughbreds are trained on dirt tracks on a racetrack daily, whereas in the UK, uphill turf or all-weather gallops are often used, which are straight or gently curving to either the right or the left. There are more hindlimb and pelvic injuries in the UK compared to the USA. In contrast, the racetracks in the USA are built as an oval, with some turns tighter and more banked than others. Horses invariably race and train in the same direction. This places more stress on the forelimbs, especially the right forelimb. As in the UK, the prize money structure in the USA favours the racing of 2- and 3-year-olds rather than older horses, thereby predisposing to a mismatch of training intensity in relation to the maturity of the horse and, therefore, the frequent occurrence of stress fractures.

Table 1 lists the location and frequency of stress-related bone lesions in Thoroughbreds racing in North America. Data on the frequency of occurrence of these lesions have been described in a survey of over 400 scintigraphic examinations carried out in a racetrack clinic in California[3]. While all the fractures listed represent some level of significance to the racing industry, whether it be humane, practical or financial, two specific fractures deserve more attention. In the authors' opinion, humeral stress fractures represent the greatest risk of catastrophic injury to a Thoroughbred racehorse, especially those involving the proximal caudal cortex of the humerus. These lesions are relatively common in young racehorses, especially those that have just returned to training following a break of 2–4 months for an unrelated problem such as colic surgery or arthroscopy. These lesions are at high risk of becoming a complete and catastrophic fracture leading to humane destruction of the horse. Mid-shaft tibial stress fractures are also relatively common and are at risk of becoming complete fractures.

REFERENCES

1. Twardock, A.R. (2001) Equine bone scintigraphic uptake patterns related to age, breed and occupation. *Vet. Clin. N. Am.: Equine Pract.* **17**, 75-94.
2. Stover, S., Ardans, A., Read, D. *et al.* (1993) Patterns of stress fractures associated with complete bone fractures in racehorses. *Proc. Am. Ass. equine Practnrs.* **39**, 131-132.
3. Arthur, R. and Constantinide, B. (1995) Results of 428 nuclear scintigraphic examinations of the musculoskeletal system at a Thoroughbred racetrack. *Proc. Am. Ass. equine Practnrs.* **41**, 85-87.

Chapter 3

THE STANDARDBRED

MICHAEL W. ROSS
New Bolton Centre, 382 West Street Road, Kennett Square, Pennsylvania 19348-1692, USA.

SPECIAL INDICATIONS FOR SCINTIGRAPHY

Scintigraphic examination in the Standardbred (SB) racehorse is an enormously useful clinical tool in lameness diagnosis. Identification of primary and compensatory sites of abnormal bone modelling and correlation of these findings with clinical signs is critical in establishing accurate diagnoses and recommending appropriate clinical management. Scintigraphic examination is recommended for SBs in which pain causing lameness is localised to a region, but negative findings have been obtained using imaging modalities such as radiography and ultrasonography; lame SBs in which lameness has not been localised or in which the lower limb has been ruled out; SBs with high-speed lameness not amenable to the use of diagnostic analgesia at low speeds; and SBs with poor performance in which scintigraphic examination is part of comprehensive sports medicine evaluation. Scintigraphic examination is most useful when lameness has been localised, as the clinical relevance of findings has then been established, but since lameness is the leading cause of poor performance, scintigraphic examination is often rewarding even when localising signs are absent.

A common and important clinical sign of high-speed lameness is 'being on a line' (or 'hanging'). A SB is on a line when the driver has to pull harder on either rein in order to keep the horse moving straight during training or racing. Standardbred racehorses most often move away from a source of pain and, therefore, a horse on the right line is most often lame on the right side (horse bears away or hangs from right-sided pain). Occasionally, paradoxically, a SB will bear away from medially located pain and be on an unexpected line. This most often occurs in SBs with medially located right forelimb lameness such as pain associated with the middle carpal joint, medial distal third metacarpal bone (McIII), or medial aspect of the distal phalanx. In SBs on a line, diagnostic analgesia can be a time-consuming and confusing task and most practitioners find solving these lamenesses frustrating. Scintigraphic examination can provide extremely valuable information and is specifically indicated in this type of situation. Most often, scintigraphic examination reveals that these SBs have complex rather than straightforward or single sources of pain. Numerous sites of abnormal bone modelling and potential sources of pain explain why attempts to treat individual joints or regions and to block single sites have failed.

Delayed or bone phase imaging is the mainstay of SB scintigraphic imaging. However, flow and pool phase images are indicated in certain conditions. Flow phase images (first-pass) are used to assess shape of the terminal aorta and its branches and blood flow. Aortoiliac thromboembolism is a rare cause of hindlimb lameness in the SB racehorse. Flow and pool phase images are combined with delayed images in SBs with suspected front foot lameness.

Pool phase images are indicated when soft tissue injury in the metacarpal or metatarsal regions is suspected, or in horses with front foot lameness. Upper limb soft tissue imaging is not useful, because there is early radiopharmaceutical uptake (RU) into bone and accumulation of radiopharmaceutical in the kidneys and bladder, the latter causing pronounced background radiation and count stealing (see *Part I, Chapters 8 and 9*). Damaged skeletal muscle, widespread, generalised rhabdomyolysis or localised, individual muscle injury, is evident in delayed (bone phase) images and there is no need to evaluate upper limbs during the pool phase.

While musculoskeletal imaging is most important, there are occasional indications for internal organ imaging such as renal and liver function studies (see *Part II, Chapter 6*), lung perfusion studies (see *Part II, Chapter 7*) (to evaluate horses with exercise-induced pulmonary hemorrhage or suspected abscessation), or brain imaging. White cell imaging is rarely used to evaluate the bones and surrounding soft tissue for the presence of infection.

CONTRAINDICATIONS FOR SCINTIGRAPHY

There are few specific contraindications for scintigraphy other than economic considerations and potential negative drug interactions. Horses with laminitis or other severe lameness may not stand still for long enough to obtain adequate images. Using nerve blocks to enable severely lame horses to walk to scintigraphy and to stand still is usually contraindicated because of the possible risks of increased weightbearing. Since horses with stress-related subchondral or cortical bone injury are ideal candidates for scintigraphic examination, a bone scan is indicated in most instances; however, in horses with acute fractures resulting from known trauma, scintigraphic examination should be delayed for a minimum of 5–7 days, since there is a lag phase in bone modelling and a false negative scan may result. This is of particular importance in horses with pelvic fractures, in which other factors such as shielding from overlying skeletal muscle, distance, high background radiation levels from urine retention in the bladder and motion reduce image quality.

During cold weather or when ambient temperature drops abruptly, delayed images of the distal extremities may appear similar to pool phase images, a phenomenon presumed to be related to effective but normal shunting of blood away from the periphery. Upper limb and axial skeleton images appear normal. In the SB and any other horse, this phenomenon causes poor image quality and it is mandatory to repeat the scan on the

following day after exercising the horse and warming the extremities. Artefacts from persistence of radiopharmaceutical in vessels and soft tissues can lead to erroneous diagnoses.

Scintigraphic examination is rarely indicated when a known problem exists unless there is need to assess other limbs for the presence of compensatory lameness. Scintigraphic examination is useful in young horses to screen for presence of certain manifestations of osteochondrosis, such as *osteochondritis dissecans* (OCD) of the scapulohumeral joint and osseous cyst-like lesions (OCLLs) of the medial femoral condyle, but physeal activity precludes identification of subtle modelling around other sites of OCD. Therefore, scintigraphy is not sensitive as a survey tool for all OCD. While physeal activity precludes evaluation of many subtle areas of increased radiopharmaceutical uptake (IRU) and reduces sensitivity of imaging in weanlings to late yearlings, identification of severe lameness such as that associated with pelvic fractures is still possible.

NORMAL SCINTIGRAPHIC VIEWS AND VARIATIONS

The number and position of scintigraphic views depends on the specific area of interest, whether lameness has been localised, if flow and pool phase images are indicated, or if scintigraphic examination is part of comprehensive sports medicine evaluation. The mainstay of scintigraphic imaging of the SB and all sport horses is obtaining delayed (bone phase) images, but in some horses flow and pool phase images are obtained. I rely heavily on ultrasonographic examination in a SB with known or suspected soft tissue injury and it would be unusual for me to rely solely on results of pool phase images for several reasons. In the SB, as in all breeds, early bone uptake of radiopharmaceutical complicates interpretation of flow and pool phase images. In most instances, IRU seen in pool phase images represents early bone uptake that becomes progressively more apparent as imaging progresses. In my opinion, sensitivity of pool phase images is low, primarily because persistence of radiopharmaceutical in digital vessels 'steals' counts away from potential lesions in nearby soft tissues. For instance, a focal lesion in the suspensory ligament or superficial digital flexor tendon may be obscured by normal activity seen in the digital vessels, activity that persists well into the pool phase and beyond (**Figures 1–3, Normals**). I have been disappointed that pool phase images are often negative or equivocal in horses with chronic suspensory desmitis or superficial digital flexor tendonitis, and feel that, unless the lesion is acute (days to a few weeks old), sensitivity of pool phase scintigraphic images is poor.

In pool phase images, normal areas of RU such as those seen at the coronary band and distal aspect of the distal phalanx must be differentiated from authentic soft tissue accumulation of radiopharmaceutical. Similarly, when abnormal areas are apparent, it is important to differentiate early bone uptake of radiopharmaceutical from soft tissue accumulation (**Figure 15, Abnormals**). In most instances, progressive increased uptake from pool to bone phase images occurs, indicating that early IRU was indeed caused by early bone accumulation of radiopharmaceutical rather than pooling in the surrounding soft tissue structures.

Normal bone phase images, normal variations, some common artefacts and other normal findings are shown in **Figures 1–32, Normals**. To improve diagnostic accuracy, a minimum of two views of each body part should be taken, since numerous views help mitigate factors such as distance, shielding and motion. A phenomenon in normal horses associated with poor bone uptake of radiopharmaceutical and poor quality bone scans, that occurs most frequently in large breed and older horses, occurs occasionally in the SB racehorse when scanning in cold weather or when there is an abrupt drop in ambient temperature (**Figure 29, Normals**). A minimum of 20 bone phase images should be taken of the appendicular skeleton and a minimum of 8 bone phase images taken of the axial skeleton for initial screening (**Figures 30 and 31, Normals**).

ABNORMAL SCINTIGRAPHIC FINDINGS IN THE STANDARDBRED

The top 10 lameness conditions and various manifestations of these common problems have recently been reviewed[1]. The scintigraphic characteristics of these conditions and other less common findings are shown in **Figures 1–51, Abnormals**.

1. Front foot lameness
2. Carpal lameness and proximal metacarpal region
3. Metatarsophalangeal (MTP) joint lameness
4. Distal hock joint pain and other tarsal lameness
5. Suspensory desmitis - forelimb and hindlimb
6. Metacarpophalangeal (MCP) joint lameness
7. Splint bone disease
8. Stifle joint lameness
9. Rhabdomyolysis, muscle soreness
10. Other soft tissue lameness, curb, SDF tendonitis
11. Other stress related bone injuries and unusual conditions

When examining the images which follow, certain important points should be borne in mind, with particular relevance to the SB racehorse, as outlined below.

- IRU associated with severe bone pathology commences very early in pool phase images and can often be seen within 2 mins of radiopharmaceutical injection. When these sites are re-examined at bone phase, the intense IRU confirms that this is, in fact, early bone uptake rather than increased bloodflow or soft tissue injury.
- Almost all SB racehorses show mild IRU on the lateral aspect of the hindlimb when compared to the medial aspect, indicating that there is a continuum of increased IRU progressing from normal to abnormal. It is sometimes difficult to be categorical on the significance of IRU in this site without recourse to diagnostic analgesia.
- Because of anticlockwise racing, IRU often involves the lateral aspect of the left distal phalanx and the medial aspect of the right distal phalanx. Lesions involving the medial aspect of the distal phalanx will be missed if only a lateral view is taken, and can also be difficult to see on a plantar or palmar view. Only the solar view of the distal phalanx ensures complete evaluation of this bone.
- As in the TB racehorse, enostosis-like lesions (ELLs) can be encountered as incidental findings. They can also be definitively linked to lameness, in some horses, by use of

regional analgesia. Often, in horses with multiple ELLs, the lameness appears to be linked to the ELL with the most marked IRU on the bone scan. It may well be that these lesions can be present for a period of time without producing pain, but the more advanced they become, the more likely they are to be associated with lameness. In some horses, lameness associated with ELLs can return with return to training, following complete resolution with rest. In most horses, however, rest alone results in a return to normality.

DISTAL EXTREMITY

- Pool phase images in this site tend to be dominated by activity in the blood vessels which leads to count stealing. This makes identification of subtle lesions in the soft tissues difficult (see **Figure 1, Normals**).
- In the normal racing SB, the medial aspect of the forelimb tends to have greater blood flow than the lateral aspect. This shows in both pool and bone phase images (see **Figure 2, Normals**).
- Mild IRU of the navicular bone is often seen in the SB racehorse, particularly the 2-year-old, unassociated with lameness.

METACARPOPHALANGEAL (MCP) JOINT

- Mild diffuse RU is a normal finding in the MCP joints of the SB racehorse (see **Figure 4, Normals**).
- In the MCP joint, focal IRU in the distal metacarpal bone is the most common scintigraphic abnormality seen in the SB racehorse. This focal IRU is termed 'nonadaptive remodelling' (stress reaction) of the distal aspect of McIII. In contrast to the hindlimb, these focal areas of IRU are most often seen on the medial condyle. Use of a flexed lateral view helps to separate the PSBs from the condyles of the McIII and to distinguish between the proximal phalanx and McIII. Comparison of flexed medial and flexed lateral views or use of a flexed dorsal view permit accurate localisation of IRU in the medial or lateral condyle of McIII.

  As in similar lesions in the hindlimb on the lateral condyle, these lesions can be radiographically silent. Eventually, with continued training, subchondral sclerosis is seen. Bone necrosis will eventually lead to focal areas of lysis, seen as radiolucency on flexed dorsopalmar oblique projections. Eventual narrowing of the medial joint space is also often seen, indicative of substantial cartilage damage. When these radiographic signs are observed, the prognosis is significantly worse for these horses returning to full athletic function.

THE CARPUS AND METACARPUS

- Focal IRU in the carpus is often limited to the medial aspect, involving distal radial carpal bone and radial fossa of the third carpal bone (C3). The use of the flexed dorsal image allows clear identification of the exact site of the focal IRU in this situation.
- One of the most common findings in the SB racehorse is bilateral marked focal IRU in C3. These areas of IRU are often rectangular in shape, sited in the position of C3. On radiography, either intense sclerosis, incomplete fracture or complete sagittal fracture through the radial facet are often identified. It should be noted, however, that sensitivity of the bone scan in differentiating between dense sclerosis, subchondral bone change and small or large fracture fragmentation is not good and there is considerable overlap in scintigraphic appearance (**Figure 18, Abnormals**).
- In SBs with proximal metatarsal or metacarpal stress reaction or avulsion fracture of the suspensory origin, the area of focal IRU is often triangular in shape, especially on the lateral view (**Figures 13 and 14, Abnormals**).
- Note that mild IRU of McII and the medial aspect of the middle carpal joint is a common scintigraphic finding in the SB, as these horses apparently preferentially load the medial aspect of the forelimb. There is poor specificity in relation to IRU of the small metacarpal bones. Many SB racehorses will show pain on palpation of a bony exostosis of McII but show little IRU on bone scan, while in others, focal, marked IRU does not appear to be accompanied by clinical signs of pain or lameness associated with the site. In the hindlimb, focal IRU most often involves the lateral aspect of the limb and exostoses are more commonly seen on MtIV.
- Focal IRU in the dorsal cortex of McIII is a rare finding in the SB racehorse. In contrast, this scintigraphic abnormality is relatively common in the TB racehorse, particularly in the North American training situation. When it is seen in the SB, it is normally encountered in 2-year-old 'pacers', which have reached advanced race training.

THE SHOULDER

- The scapulohumeral joint in the SB racehorse is usually only imaged laterally, since stress-related injury of this region is extremely unusual. This is in contrast to the situation in the TB racehorse, where humeral stress fracture is one of the more common findings, especially following a return to training after a lay-off.

METATARSOPHALANGEAL (MTP) JOINT

- Focal IRU in the distal plantarolateral aspect of MtIII is one of the most common scintigraphic abnormalities of the MTP joint, and one of the most common and important abnormalities in the SB racehorse. When no radiographic abnormality is seen in this site, these injuries are termed stress reactions, and are thought to be a loading adaptation mismatch leading to subchondral bone sclerosis. Continued training of affected horses often results in necrosis of the subchondral bone. In this situation, IRU is even more intense on scintigraphic examination and subtle subchondral lucencies begin to appear on radiographs. The flexed plantarodorsal oblique projection of the distal condyle or the proximoplantarolateral distal dorsomedial projection are the best views to demonstrate these subtle radiolucencies in the middle of the condyle. When radiographic signs are evident, the prognosis for return to full athletic function is poor and, although these horses will often continue to race, the condition is usually performance-limiting. The pain experienced from this condition appears to be more intense at high speed, which may account for diminishing race performances. Note that, to determine the exact site of focal IRU in the MTP joint, a flexed lateral and a plantar image are

vital. The flexed lateral image moves the PSBs away from the bone surface in order to allow clear differentiation of the site of IRU.

- Focal IRU on the plantar proximolateral aspect of the proximal phalanx may be an incidental finding involving remodelling of that site but also can be associated with OCD fragmentation, as this is a predilection site for this condition. There is controversy over whether these plantar OCD fragments produce clinical pain. This author's view is that on some occasions they do and that the lameness may only be seen at high speed.
- Mild to moderate IRU of the lateral aspect of the MTP joint is a common incidental finding in the SB racehorse. Any IRU on the **medial aspect** of the MTP joint should be taken seriously, as this is almost always linked to pathology.

THE TARSUS

- On a plantar view of the tarsus, there is usually mild IRU in the proximal lateral aspect of MtIV and the lateral aspect of the TMT joint (see **Figure 17, Normals**). These are usually of no clinical relevance. However, these sites are close to common predilection sites for injury in the SB, e.g. osteoarthritis of the TMT joint or stress reaction in the proximal MtIII at the suspensory ligament origin. Careful scrutiny of this site is therefore essential.
- Focal IRU in the site of the TMT joint is the most common abnormal finding in the tarsus of the SB racehorse. The shape of the IRU is often approximately rectangular, corresponding to the anatomical shape of the TMT joint and its subchondral bone. Note that stress-related subchondral bone injury can lead to eventual fracture of the T3, and these fractures are almost always situated on the lateral aspect of the tarsus. These are best seen on a dorsomedial-plantarolateral oblique radiographic view. Scintigraphy is not particularly sensitive at differentiating between profound osteoarthritis of the TMT joint and fracture of T3 (see **Figures 34 and 35, Abnormals**).

THE STIFLE

- In scintigraphic images of the stifle, the proximity of the distal femoral physis and proximal tibial physis often introduces count capture, which reduces the contrast of the remainder of the view (see **Figure 45, Abnormals**).
- In the stifle joint, there is normally greater RU on the **lateral** aspect of the distal femur and proximal tibia when compared to the medial aspect. Any IRU on the **medial** aspect of the joint is an abnormal finding and can be linked to OCLLs in the medial femoral condyle, or osteoarthritis of the MFT joint. This is the most common scintigraphic abnormality in the SB racehorse stifle. Because these medially-situated lesions are not visible on lateral projections, a caudal view of the stifle is mandatory. Because the camera is at such a distance to the bone in this situation, image quality is poor but nevertheless of clinical use (see **Figure 43, Abnormals**).
- The tibia is usually not imaged separately in the SB racehorse, as the proximal half is evaluated on the stifle view and the distal half on views of the tarsus. As the tibia is a relatively rare site for stress-related bone injury in the SB, in contrast to the situation in the TB racehorse, these views normally suffice.

COXOFEMORAL (CF) JOINT

- RU in the CF joint is always intense on lateral projections because of summation of counts from the femur and pelvis. In contrast, RU in the CF joint on the dorsal view usually appears low, due to distance and attenuation by overlying muscle. This leads to possible confusion in the interpretation of images and focal IRU in this site on **lateral** images should not be overinterpreted as pathological. **Injuries** to the pelvis in the region at the CF joint often have relatively low levels of IRU. These can take over a week from injury to be significant enough to be seen on the dorsal view.

SPINE

- It is rare to encounter IRU in the thoracolumbar spine in the SB. Dorsal spinous process impingement does not appear to be a common finding, in contrast to the TB racehorse.
- Scintigraphic examination of the cervical spine is usually unrewarding in the SB racehorse and should not be performed routinely. In horses with neurological disease or obvious cervical pain, lateral images from both right and left should be obtained from the atlanto-occipital joint to the cranial thoracic area, including the neck base and scapula.

REFERENCES

1. Mitchell, J.B., Mitchell, J.M., Nolan, P.M. *et al.* (2003) The North American Standardbred. In: *Diagnosis and Management of Lameness in the Horse*, Eds: M.W. Ross and S.J. Dyson, W.B. Saunders Co., Philadelphia. pp 895-912.

NORMAL HORSES

N **Figure 1: Lateral and dorsal flow and pool phase images of the distal forelimbs**

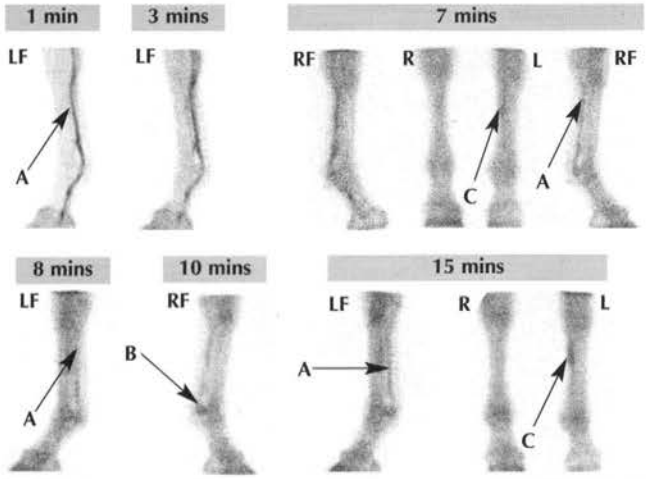

SB	3y	G	Trotter	128 x 128

DX: Normal

DS: NA

➔ **A:** Radiopharmaceutical in the metacarpal and digital veins. This can lead to count capture and reduced perception of mild IRU in the vicinity (see *Part I, Chapter 5*)
➔ **B:** Early bone uptake into PSB.
➔ **C:** Early bone IRU associated with exostosis of McII.

N **Figure 2: Dorsal flow phase image of the distal forelimbs**

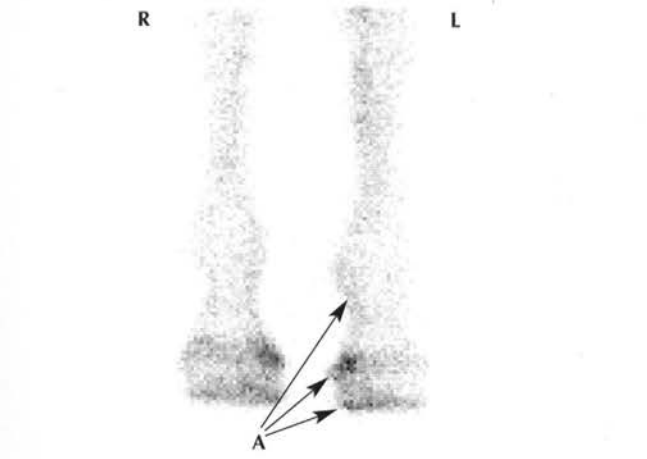

SB	3y	G	Trotter	128 x 128

DX: Normal

DS: NA

➔ **A:** Note the apparently greater degree of blood flow in the medial aspect of the coronary band and distal phalanx. RU persists in these regions well into pool phase. This is a normal finding in the SB racehorse.
Note: Composite (32, 2-sec/frame images) images.

N **Figure 3: Plantar pool phase image of the distal hindlimbs**

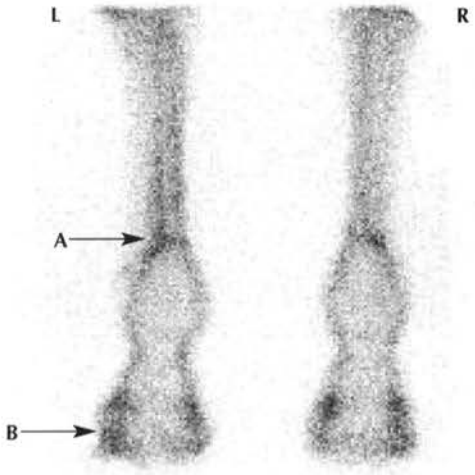

SB	2y	C	Pacer	128 x 128

DX: Normal

DS: NA

➔ **A:** Normal flow in plantar distal metatarsus.
➔ **B:** Normal flow in distal phalanx. The distribution of isotope between medial and lateral is more even in the hindlimbs.
Note: 1 min after radiopharmaceutical injection.

N **Figure 4: Lateral (a) and dorsal (b) bone phase images of the distal forelimbs**

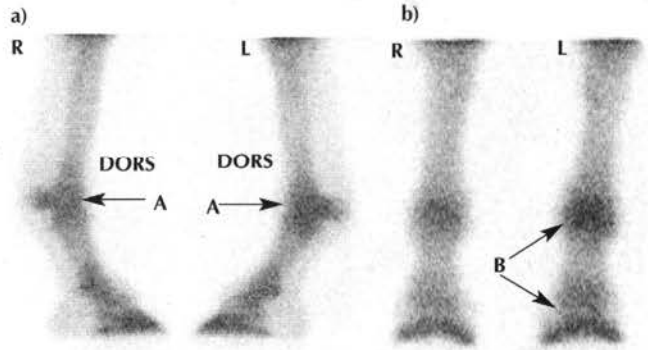

SB	3y	F	Trotter	200 x 200

DX: Normal

DS: NA

➔ **A:** Mild diffuse RU in the fetlock joint region (normal).
➔ **B:** Mild diffuse RU distal extremity LF (not clinically significant).

N Figure 5: Bone phase solar images of RF (a) and LF (b) feet

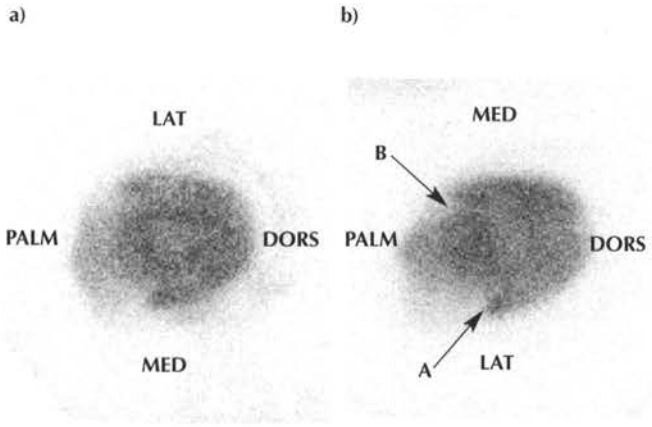

SB	3y	C	Trotter	200 x 200
DX:	Normal			
DS:	NA			

➡ **A:** Mild IRU in the palmar process.
➡ **B:** Mild IRU in the navicular bone. These findings in the LF are common and often unassociated with lameness in the SB.

N Figure 6a: Flexed lateral bone phase image of the distal LF

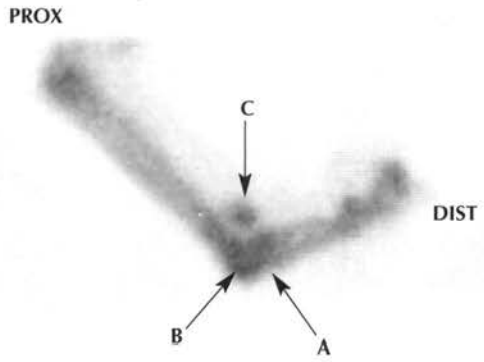

SB	2y	C	Trotter	200 x 200
DX:	Normal			
DS:	NA			

➡ **A:** Proximal phalanx.
➡ **B:** Distal lateral McIII.
➡ **C:** PSB.
Note: This special view is useful in differentiating IRU in the separate components of the joint.

N Figure 6b: Flexed medial bone phase image of the distal LF

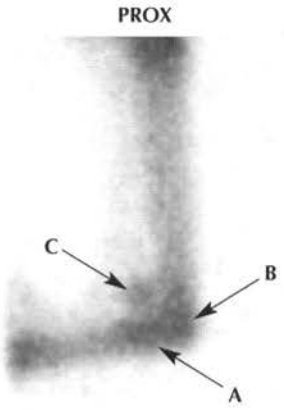

SB	2y	F	Trotter	200 x 200
DX:	Normal			
DS:	NA			

➡ **A:** Proximal phalanx.
➡ **B:** Distal medial McIII (a very common site for nonadaptive stress remodelling).
➡ **C:** PSB.
Note: This special view is useful in differentiating IRU in the separate components of the joint.

N Figure 6c: Flexed dorsal bone phase image of the distal LF

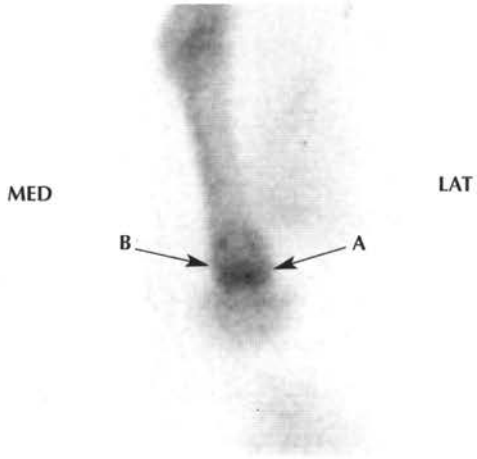

SB	2y	C	Trotter	200 x 200
DX:	Normal			
DS:	NA			

➡ **A:** Lateral distal McIII.
➡ **B:** Medial distal McIII.
Note: RU in both condyles in this normal horse is symmetrical. In horses affected by stress remodelling there will be marked asymmetry of RU.

N **Figure 7a: Lateral bone phase images of right (i) and left (ii) carpi**

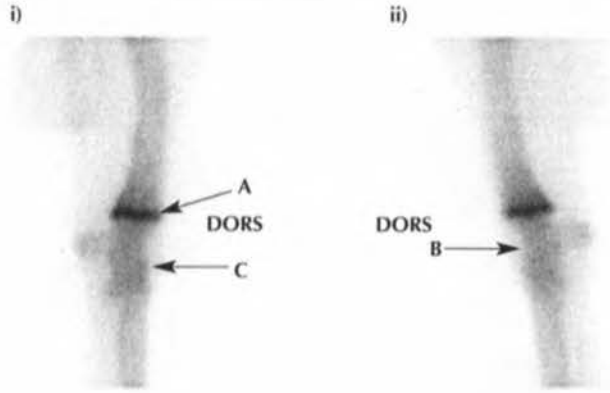

SB	2y	C	Trotter	200 x 200
DX:	Normal			
DS:	NA			

➔ **A:** Distal radial physis. This should be masked out for closer inspection of the remainder of the carpus (see *Part I, Chapter 5*) because of count capture.
➔ **B:** Relatively uniform RU throughout the carpal bones in a normal horse.
➔ **C:** Mild IRU in C3 within normal range for SB racehorse.

N **Figure 7b: Dorsal bone phase images of both carpi**

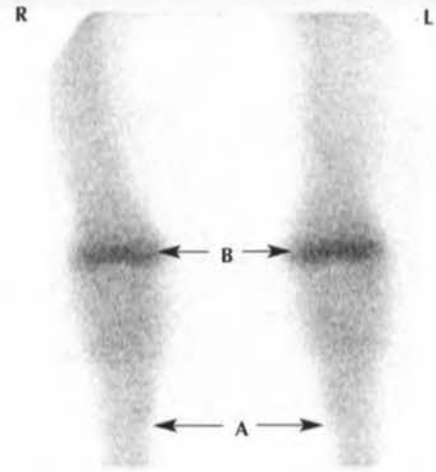

SB	2y	C	Trotter	200 x 200
DX:	Normal			
DS:	NA			

➔ **A:** Both carpi being imaged in the same field of view allows direct comparison for symmetry or otherwise of RU.
➔ **B:** Distal radial physis (normal) that leads to count capture or stealing. Acquisition time may need to be increased if set counts are used. Masking the physis will aid in image interpretation.

N **Figure 8: Flexed lateral bone phase image of the left carpus**

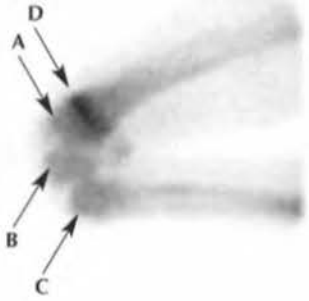

SB	2y	F	Trotter	200 x 200
DX:	Normal			
DS:	NA			

➔ **A:** Distal radial epiphysis.
➔ **B:** Radial carpal bone.
➔ **C:** Third carpal bone.
➔ **D:** Distal radial physis.
Note: Flexed lateral view allows clear differentiation of the composite bones of the carpus.

N **Figure 9: Lateral bone phase images of the right (a) and left (b) upper forelimbs**

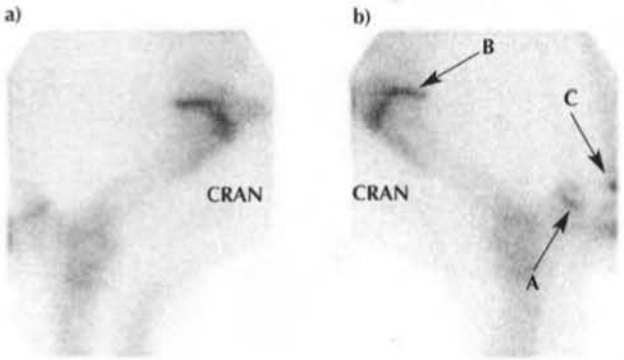

SB	2y	C	Trotter	200 x 200
DX:	Normal			
DS:	NA			

➔ **A:** RU in the physis of the olecranon.
➔ **B:** RU in the proximal humeral physis. Note that stress injuries to the humerus often occur in this site (except in the SB, in which they are rare), but should not be confused with normal physeal uptake.
➔ **C:** RU in the costochondral junction.

N Figure 10a: Lateral bone phase images of the right (i) and left (ii) upper forelimbs

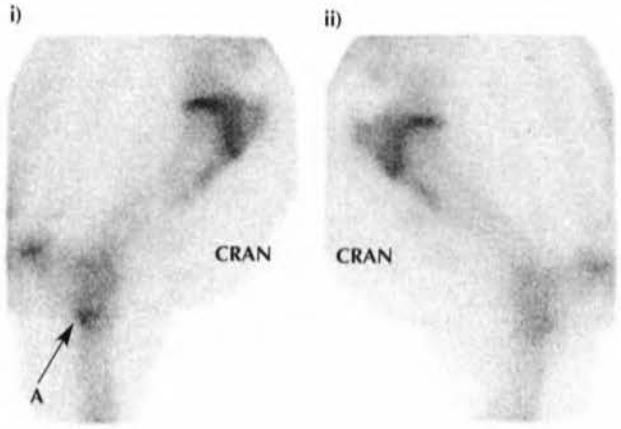

SB	2y	F	Trotter	200 x 200
DX:	Normal			
DS:	NA			

➔ **A:** Focal RU in the proximal radial tuberosity.
Note: This is more prominent in the RF than the LF in this image. Uptake is commonly asymmetrical in this site, but both LF and RF fall within the normal range in this case.

N Figure 10b: Lateral bone phase image of the upper LF

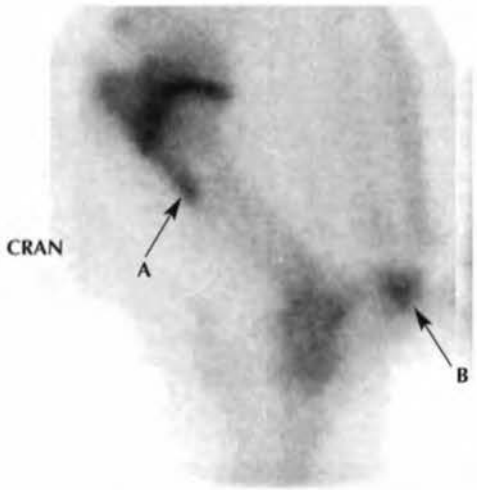

SB	2y	C	Trotter	200 x 200
DX:	Normal			
DS:	NA			

➔ **A:** RU in the deltoid tuberosity (normal).
➔ **B:** RU in the proximal olecranon (normal).

N Figure 11: Cranial bone phase images of the right (a) and left (b) upper forelimbs

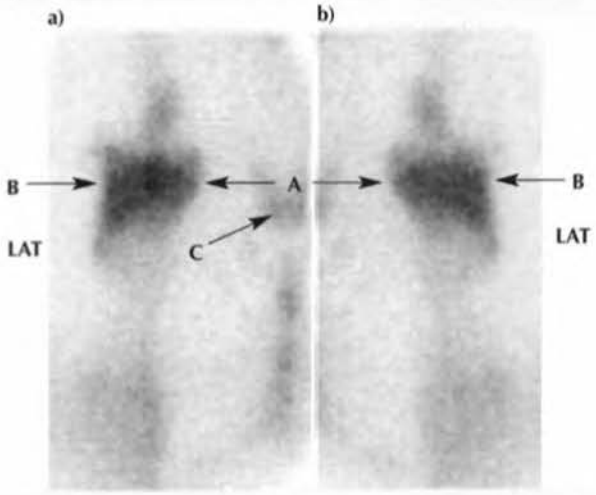

SB	2y	C	Trotter	200 x 200
DX:	Normal			
DS:	NA			

➔ **A:** Medial SH joint.
➔ **B:** Lateral SH joint.
➔ **C:** Sternum. Note that this view is not routinely acquired in the SB, as stress-related bone injury to the humerus is rare. It should, however, be routinely employed in the racing TB.

N Figure 12: Lateral bone phase images of the right (a) and left (b) shoulder regions

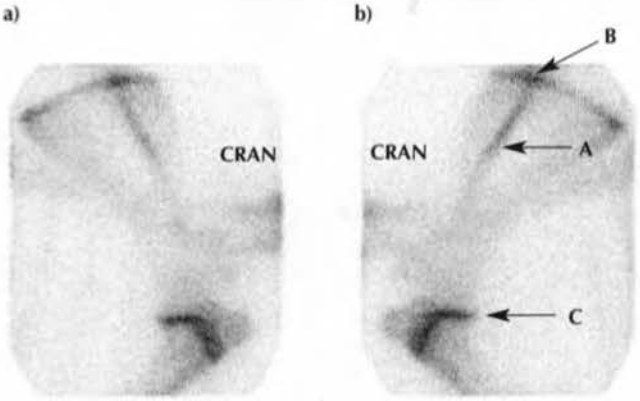

SB	3y	C	Trotter	200 x 200
DX:	Normal			
DS:	NA			

➔ **A:** Scapular spine.
➔ **B:** Normal RU at the junction of the scapular spine and border of the bone.
➔ **C:** Normal RU in the proximal humeral physis.

N Figure 13: Lateral bone phase images of the right (a) and left (b) distal hindlimbs

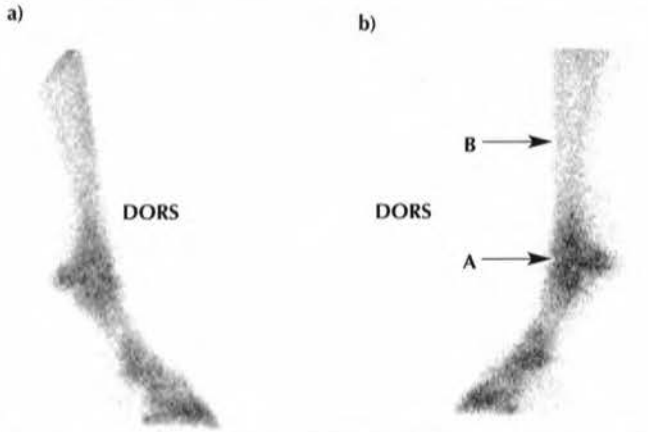

SB	2y	C	Trotter	200 x 200
DX:	Normal			
DS:	NA			

➔ **A:** Metaphyseal and epiphyseal regions.
➔ **B:** Diaphyseal region.
Note: Normal greater RU in the metaphyseal and epiphyseal regions of the long bones than in the diaphyseal region. Also note asymmetry of uptake throughout the distal extremity with that in the LH being greater than in the RH. This is of no clinical significance.

N Figure 14: Lateral LH (a), RH (b) and plantar (c) bone phase images of the distal hindlimbs

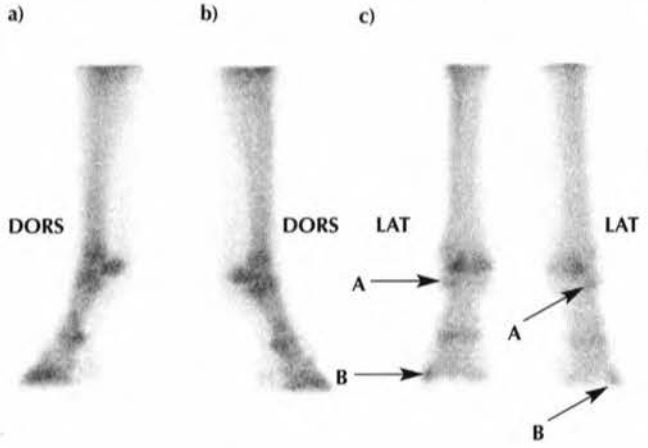

SB	2y	C	Pacer	200 x 200
DX:	Normal			
DS:	NA			

➔ **A:** Mild RU proximolateral proximal phalanx (can be seen in conjunction with large abaxial plantar osteochondral fragments).
➔ **B:** Small focal RU in lateral aspect of the distal phalanx (a common normal finding).

N Figure 15: Flexed medial bone phase image of the distal LH

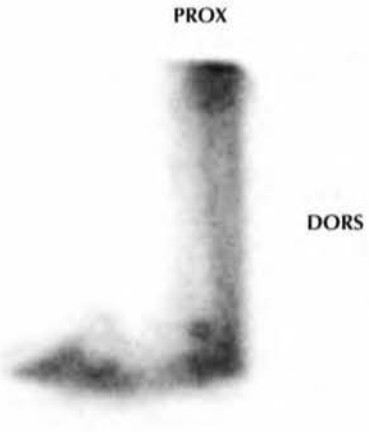

SB	2y	C	Trotter	200 x 200
DX:	Normal			
DS:	NA			

Note: The flexed medial view is achieved by extending the leg behind the horse and placing the medial aspect of the fetlock against the gamma camera. This view is vital to examine this site adequately.

N Figure 16: Lateral images of the right (a) and left (b) tarsal regions

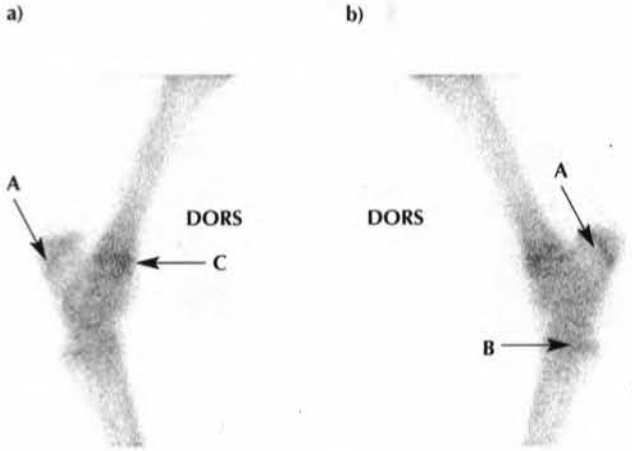

SB	2y	C	Trotter	200 x 200
DX:	Normal			
DS:	NA			

➔ **A:** Mild RU in the calcaneal physis (normal in a 2-year-old).
➔ **B:** Mild IRU in the TMT joint (of no clinical relevance).
➔ **C:** RU in the distal tibial physis. This can persist until over 3 years of age.

N Figure 17: Lateral RH (a), LH (b) and plantar (c) bone phase images of the tarsal regions

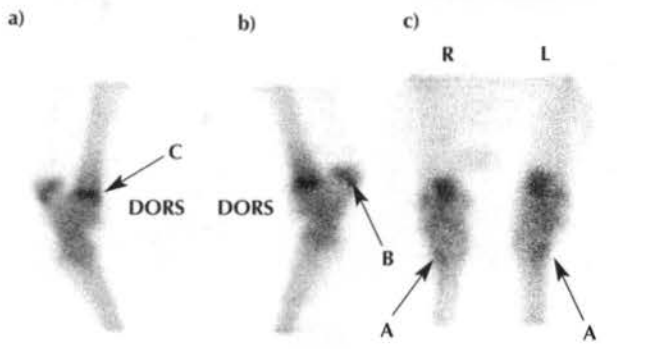

SB	2y	-	Pacer	200 x 200

DX: Normal

DS: NA

➔ **A:** RU in the proximal lateral aspect of MtIV and lateral aspect of the TMT joint. This RU is normal and should not be mistaken for that associated with osteoarthritis of the TMT joint, suspensory ligament origin lesions, or lesions of the proximal aspect of MtIV.
➔ **B:** Calcaneal physis (RU in this site confirms the horse is aged 2 years or less).
➔ **C:** RU in the distal tibial physis (persists to well over 3 years of age).

N Figure 18: Flexed lateral RH (a) and medial LH (b) bone phase images of the tarsal regions

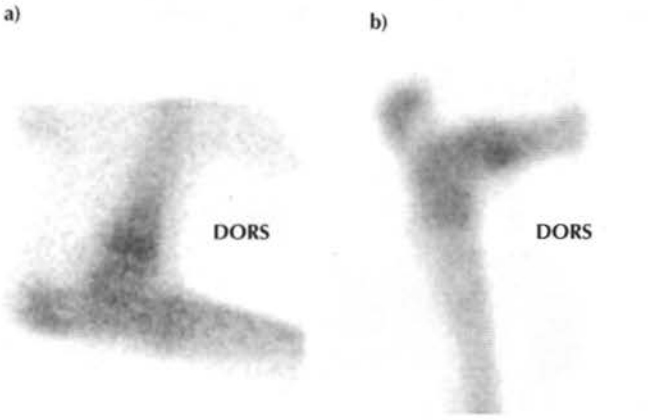

SB	2y	F	Trotter	200 x 200

DX: Normal

DS: NA

Note: These views are used to differentiate the bone of origin of lesions involving the distal tibia and talus in the SB. These would include, for instance, subchondral bone trauma of the distal tibia or sagittal fracture of the talus. These views are difficult to obtain and often affected by motion.

N Figure 19: Lateral bone phase images of the right (a) and left (b) stifle regions

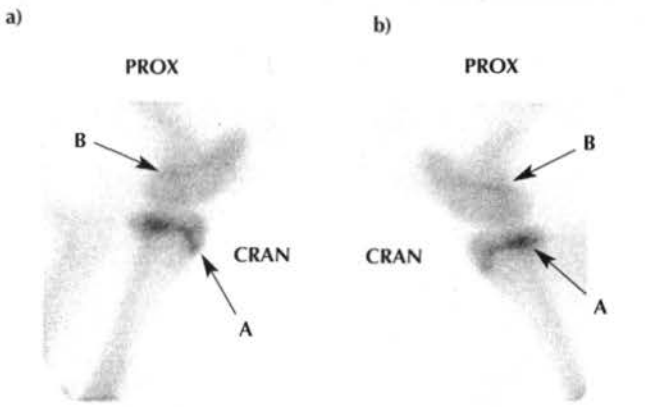

SB	2y	C	Pacer	200 x 200

DX: Normal

DS: NA

➔ **A:** Marked RU in the proximal tibial physis.
➔ **B:** Mild linear RU in the distal femoral physis.
Note: Count stealing by these sites can mask lesions of the stifle, making the caudal view essential to evaluate the medial aspect of the stifle joint.

N Figure 20: Lateral right (a), left (b) and caudal (c) bone phase images of the stifle regions

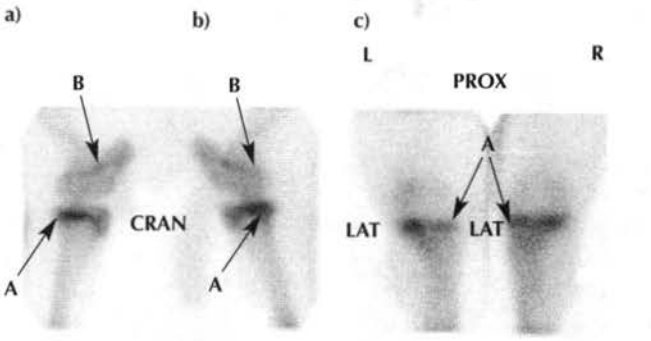

SB	2y	C	Pacer	200 x 200

DX: Normal

DS: NA

➔ **A:** Marked RU in the proximal tibial physis.
➔ **B:** Mild linear RU in the distal femoral physis.
Note: These areas should be masked out to examine the stifle joint itself for mild IRU associated with OCLLs of the distal femur or OA of the medial femorotibial joint. Count stealing can obscure these lesions (see *Part 1, Chapter 5*).

N Figure 21a: Lateral images of right (i) and left (ii) stifle regions and proximal tibiae

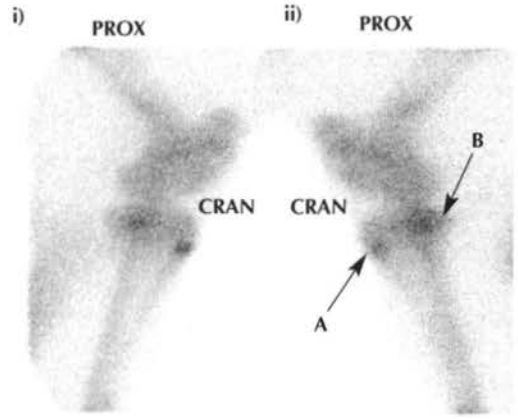

SB	3y	C	Pacer	200 x 200
DX:	Normal			
DS:	NA			

➡ **A:** Residual activity in the cranial proximal tibial physis.
➡ **B:** Apparent IRU associated with superimposition of proximal fibula and tibial physis.
Note: This gives a bilobed appearance to the proximal tibia on lateral views, which is normal.

N Figure 21b: Caudal images of left (i) and right (ii) stifle regions and proximal tibiae

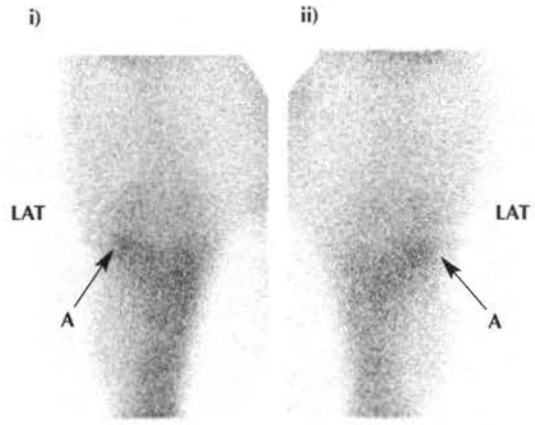

SB	3y	C	Pacer	200 x 200
DX:	Normal			
DS:	NA			

➡ **A:** RU in the lateral FT joint is often greater than in the medial FT in a caudal view.
Note: This is normal, and should not be confused with pathology. Any IRU in the medial femorotibial joint in the SB can indicate early OA, as this is a common predilection site.

N Figure 22a: Lateral bone phase images of the right (i) and left (ii) stifle regions

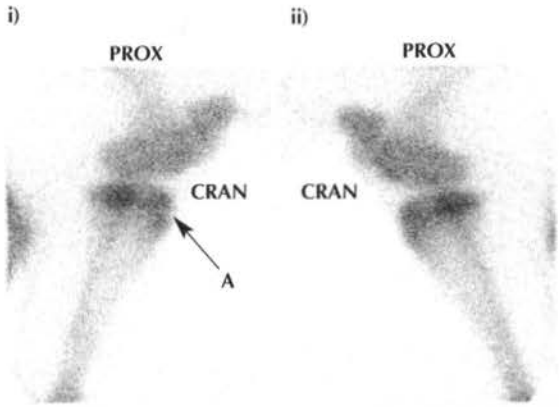

SB	4y	M	Pacer	200 x 200
DX:	Normal			
DS:	NA			

➡ **A:** Normal bilobed appearance of the proximal tibia (see Figure 21a).

N Figure 22b: Caudal bone phase images of the left (i) and right (ii) stifle regions

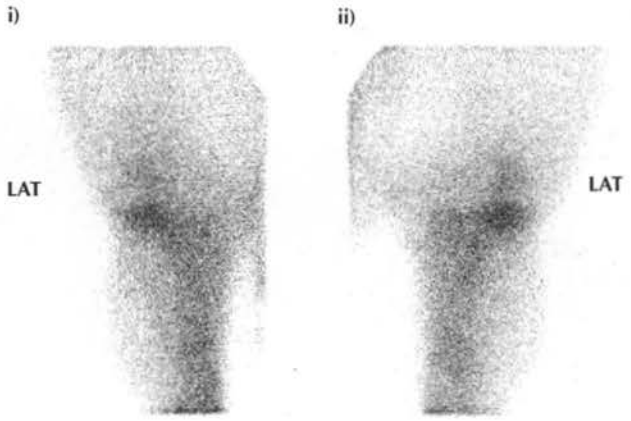

SB	4y	M	Pacer	200 x 200
DX:	Normal			
DS:	NA			

Note : Normal disparity in RU between medial and lateral FT joints.

N **Figure 23: Lateral bone phase images of the right (a) and left (b) coxofemoral and pelvic regions**

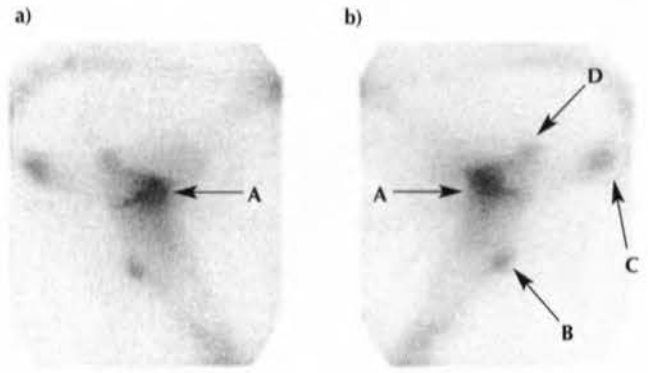

SB	3y	C	Trotter	200 x 200
DX:	Normal			
DS:	NA			

➡ **A:** Marked intense RU associated with CF joint (normal).
➡ **B:** Third trochanter.
➡ **C:** Tuber ischii.
➡ **D:** Greater trochanter of femur.
Note: IRU associated with enthesopathy or fracture of the 3rd trochanter and tuber ischii are rare findings in the SB.

N **Figure 25: Lateral (a) and caudal (b) bone phase images of the right coxofemoral and pelvic regions**

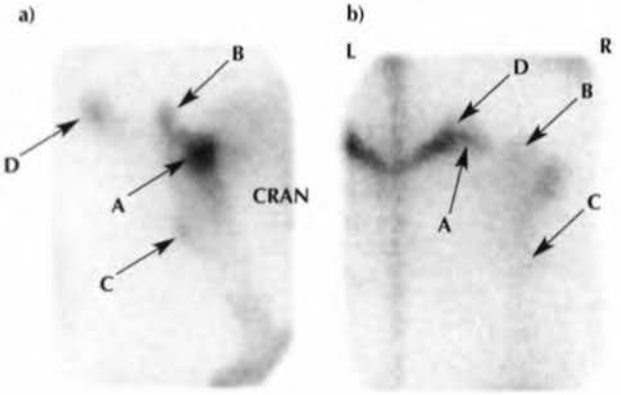

SB	5y	G	Pacer	200 x 200
DX:	Normal			
DS:	NA			

➡ **A:** CF joint.
➡ **B:** Greater trochanter of the femur
➡ **C:** Third trochanter of the femur
➡ **D:** Tuber ischii
Note: The caudal view is used to define injury of the tuber ischii, greater trochanter or 3rd trochanter further.

N **Figure 24: Dorsal transverse (a), right hemipelvic (b) and left hemipelvic (c) bone phase images**

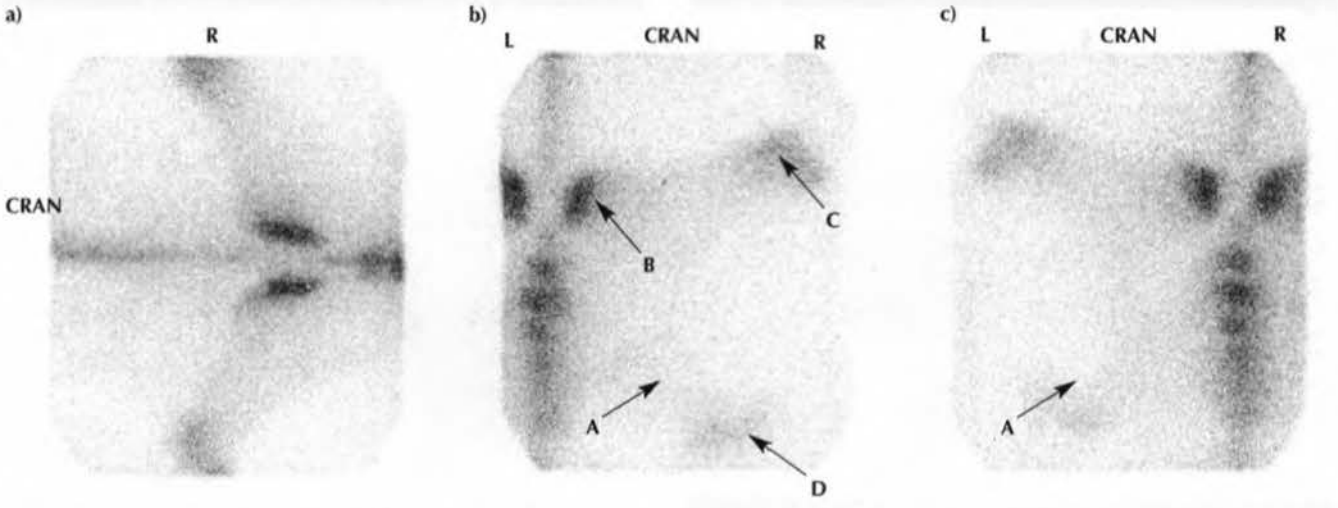

SB	3y	C	Trotter	200 x 200
DX:	Normal			
DS:	NA			

➡ **A:** CF joint (usually relatively photopenic in the normal horse).
➡ **B:** Tuber sacrale.
➡ **C:** Tuber coxae.
➡ **D:** Greater trochanter.
Note: These views are routinely acquired in addition to the lateral view of the CF joint in the SB.

N **Figure 26: Right lateral oblique bone phase images of the thoracolumbar region**

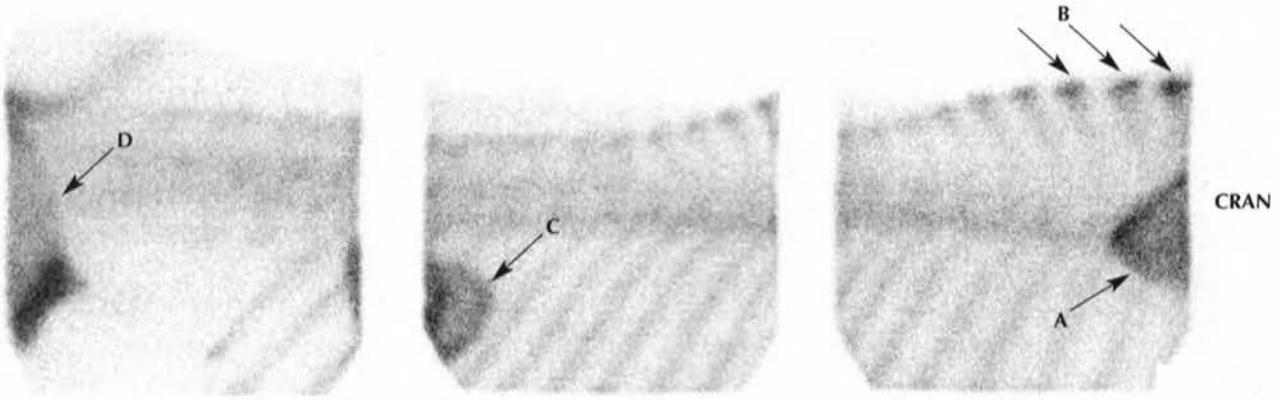

SB	3y	C	Trotter	200 x 200
DX:	Normal			
DS:	NA			

➡ **A:** Scapula.
➡ **B:** Summits of the DSPs of the cranial thoracic vertebrae.
➡ **C:** Right kidney.
➡ **D:** Ilium.

N **Figure 27: Left lateral dorsal oblique bone phase images of the thoracolumbar region**

SB	3y	C	Trotter	200 x 200
DX:	Normal			
DS:	NA			

➡ **A:** Left kidney. Note that the left kidney is more caudal and located further from the camera, appearing fainter in the left lateral image.

N Figure 28a: Right lateral bone phase images of the cervical vertebrae

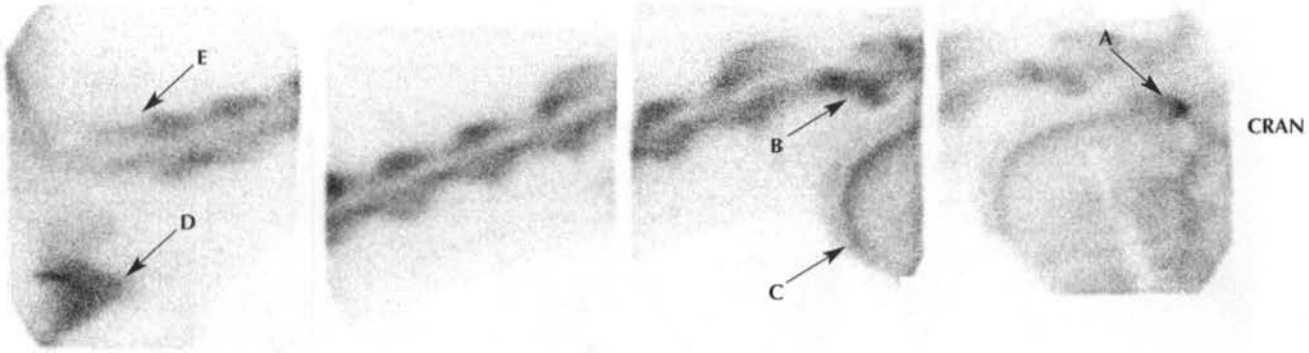

SB	3y	C	Pacer	200 x 200
DX:	Normal			
DS:	NA			

- **A:** Temporomandibular joint.
- **B:** Dens of C2.
- **C:** Mandible.
- **D:** Proximal humerus.
- **E:** Abrupt attenuation of radioactivity in the most caudal neck region due to muscle shielding. This results in apparent enhancement of RU in C6 and C7.

N Figure 28b: Left lateral bone phase images of the cervical vertebrae

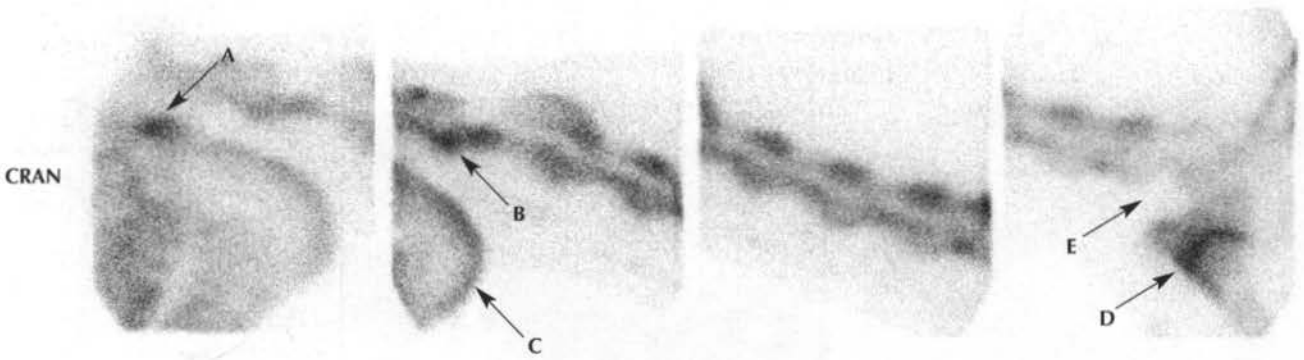

SB	3y	C	Pacer	200 x 200
DX:	Normal			
DS:	NA			

- **A:** Temporomandibular joint.
- **B:** Dens of C2.
- **C:** Mandible.
- **D:** Proximal humerus.
- **E:** Abrupt attenuation of radioactivity in the most caudal neck region due to muscle shielding. This results in apparent enhancement of RU in C6 and C7.

N Figure 29: Lateral bone phase images of the distal hindlimbs; initial images (a) and 24 h later (b)

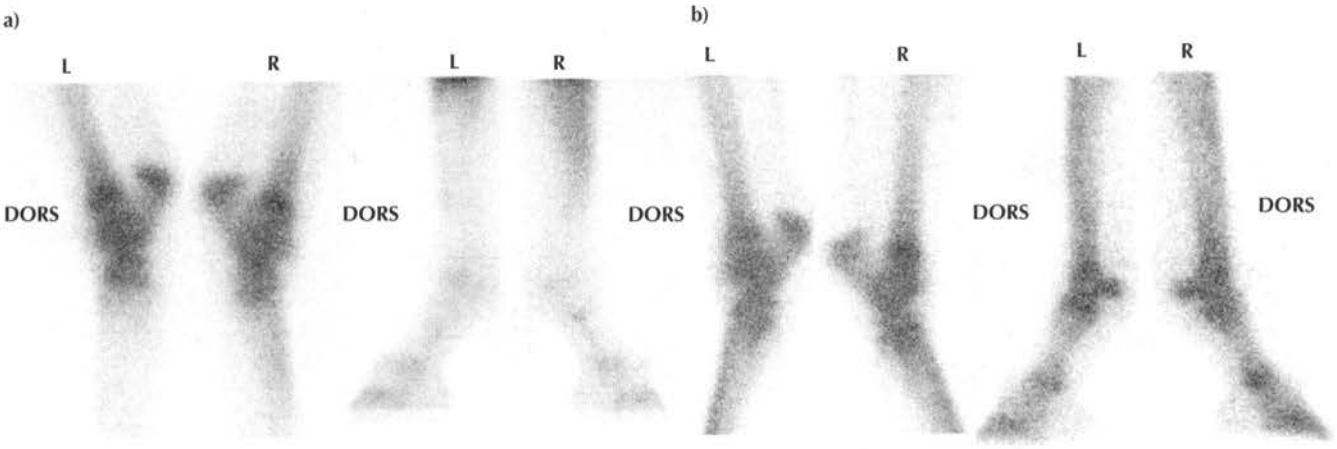

SB	3y	G	Pacer	200 x 200
DX:	Normal			
DS:	NA			
Note:	Poor quality bone uptake in the original images (a) and additional images taken 24 h later, after the application of a blanket and leg wraps and re-injection of ^{99m}Tc-HDP (rescan, b). In (a), note poor quality uptake in bones distal to the tarsi, whereas in the rescan images (b), normal uptake can be seen.			

N Figure 30: Caudal, dorsal and lateral bone phase images of the stifle regions and axial skeleton

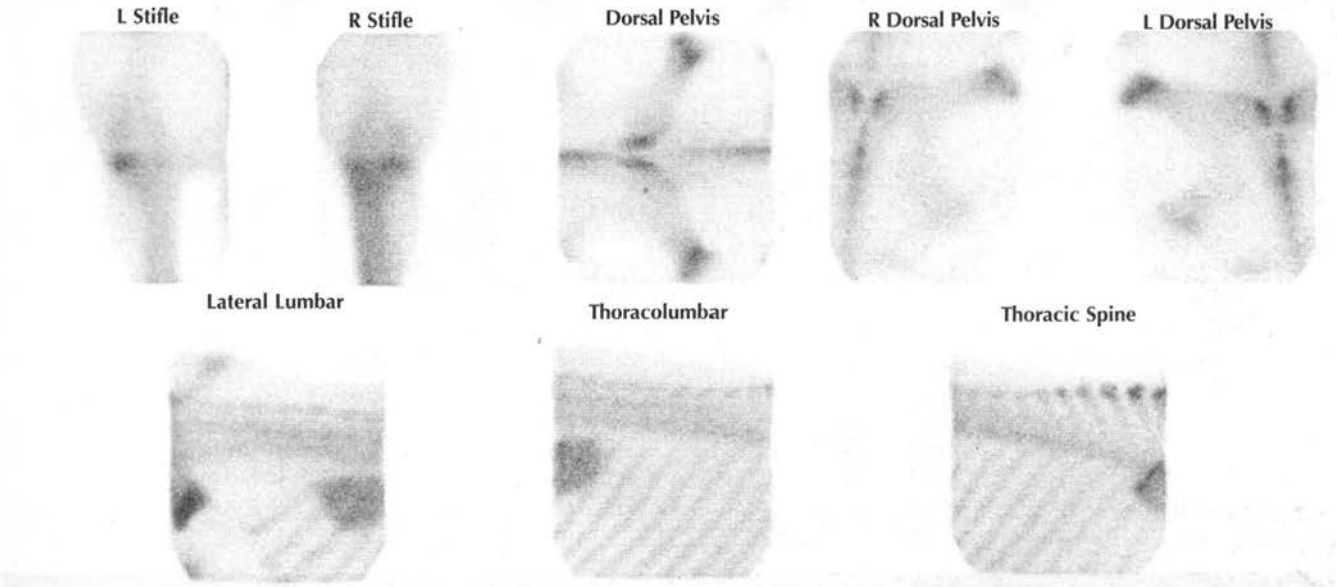

SB	2y	C	Trotter	200 x 200
DX:	Normal			
DS:	NA			
Note:	A minimum of 8 additional bone phase images of the stifle region and axial skeleton should be taken when assessing a SB for poor performance or a known high-speed lameness that is not localised to a particular limb.			

N Figure 31: Lateral (a), dorsal (b) and plantar (c) bone phase images of the fore- and hindlimbs

SB	2y	C	Trotter	200 x 200
DX:	Normal			
DS:	NA			
Note:	A minimum number of 20 bone phase images of the limbs should be taken for screening when performing a comprehensive sports medicine evaluation for a SB with poor performance or known high-speed lameness not localised to a particular limb. Additional views (see previous figures) should be taken to evaluate individual portions of the limbs more carefully.			

N Figure 32: Flow phase image of the terminal aorta and branches

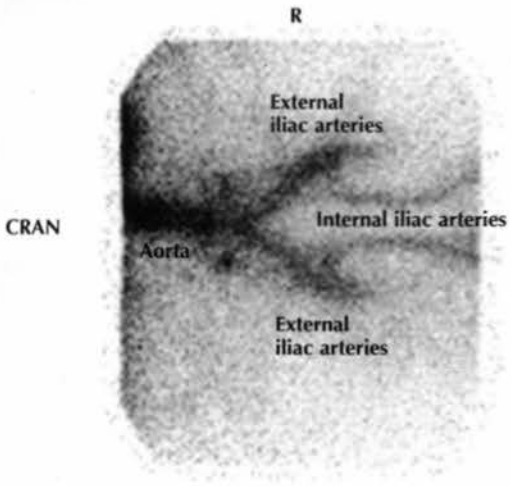

SB	3y	C	Pacer	128 x 128
DX:	Normal (see Figure 53, Abnormals, for abnormal SB).			
DS:	NA			
Note:	The terminal aorta divides in a V-shaped pattern into left and right external iliac arteries. The paired internal iliac arteries can be seen coursing caudally.			

ABNORMAL HORSES

A Figure 1: Solar bone phase view of the LF foot

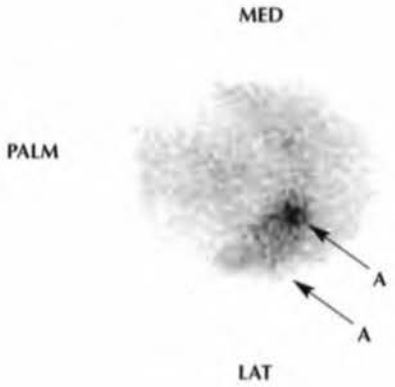

SB	4y	S	Pacer	200 x 200
DX:	Stress (nonadaptive) remodelling of the subchondral bone of the distal phalanx.			
DS:	Diagnostic analgesia: LF lameness abolished with palmar digital perineural analgesia. Radiography: narrowing of the lateral aspect of the DIP joint.			
➡ **A:**	Focal, intense IRU in the lateral aspect of the distal phalanx.			

A Figure 2: Lateral (a), dorsal (b) and solar (c) bone phase images of the distal LF

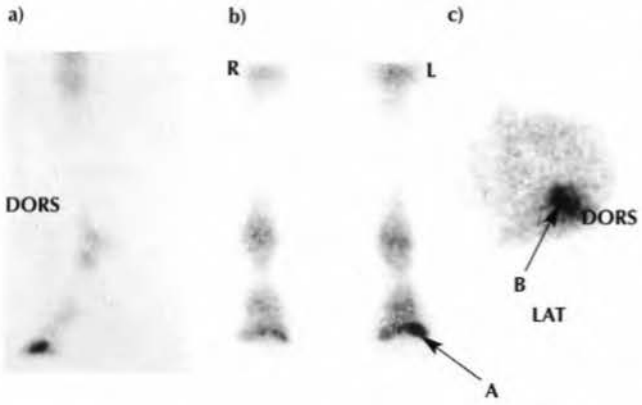

SB	3y	F	Trotter	200 x 200
DX:	Stress fracture of the lateral aspect of the distal phalanx in the LF.			
DS:	Diagnostic analgesia: LF lameness abolished with palmar digital block. Radiography: incomplete fracture of lateral aspect of the LF distal phalanx.			
➡ **A:**	Marked focal IRU in the lateral distal phalanx seen on the dorsal view.			
➡ **B:**	Marked focal IRU in the lateral aspect of the distal phalanx seen on the solar view.			

A Figure 3: Lateral bone phase image of the distal LH

SB	5y	G	Pacer	200 x 200
DX:	Abnormal modelling and degeneration of the LH navicular bone.			
DS:	Perineural analgesia: pronounced LH lameness abolished with plantar digital block. Radiography: extensive cavitation of navicular bone seen on the dorsoproximal-plantarodistal radiographic projection.			
➡ **A:**	Marked focal IRU in the navicular bone.			
Note:	Poor overall bone uptake in this limb more closely resembles a pool phase image.			

A Figure 4: Lateral LF (a), dorsal (b) and solar LF (c) bone phase images of the distal forelimbs

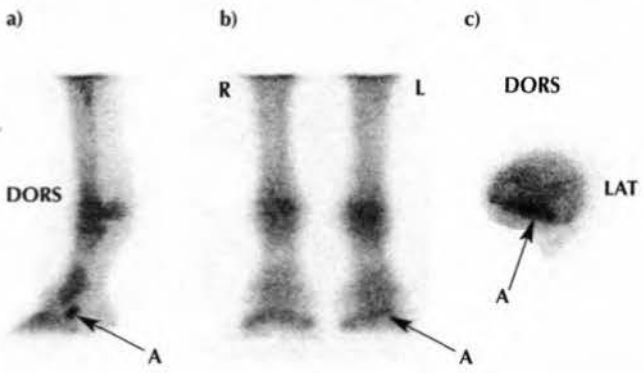

SB	4y	G	Pacer	200 x 200
DX:	Abnormal modelling of the LF navicular bone.			
DS:	Perineural analgesia: LF lameness abolished by palmar digital block. Radiography: sclerosis of the medullary cavity of the navicular bone seen in a palmaroproximal-palmarodistal oblique radiographic view.			
➡ **A:**	Marked focal IRU in LF navicular bone is evident in all views.			

A Figure 5: Lateral RF (a), LF (b) and dorsal (c) images of the distal forelimbs

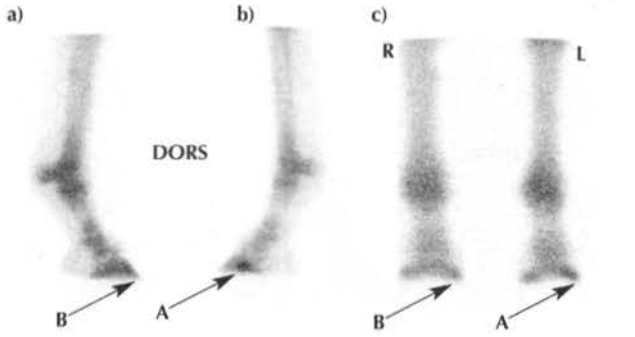

SB	3y	C	Trotter	200 x 200

DX: Stress (nonadaptive) remodelling of the subchondral bone of the distal phalanx.

DS: Diagnostic analgesia: LF lameness abolished by palmar digital nerve block. Radiography: NAD.

➡ **A:** IRU in the lateral LF distal phalanx involving the lateral subchondral region. This pattern of uptake is common in the SB showing forelimb lameness abolished with palmar digital block, and reflects stress remodelling in the distal phalanx.
➡ **B:** IRU in the RF medial distal phalanx involving the dorsal medial and laminar regions of the distal phalanx.

A Figure 6: Lateral RF (a), LF (b) and dorsal (c) bone phase images of the distal forelimbs

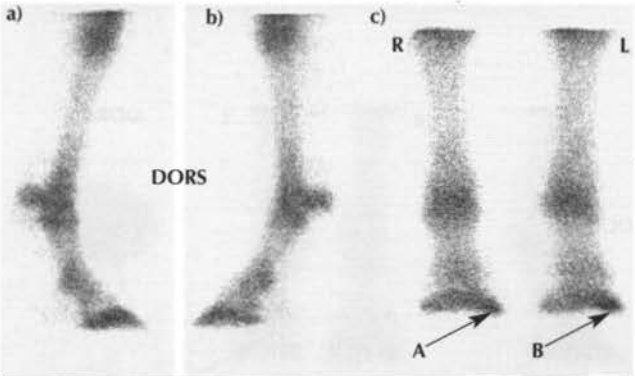

SB	2y	C	Pacer	200 x 200

DX: Stress remodelling of the distal phalanx as a suspected cause of high-speed lameness.

DS: NA

➡ **A:** Marked focal IRU in the medial aspect of the distal phalanx of the RF.
➡ **B:** Marked focal IRU in the lateral aspect of the distal phalanx of the LF.
Note: The similar distribution of IRU in the distal phalanx and distal phalanx fractures suggests that these fractures may be stress-related bone injuries rather than single-event episodes. Anticlockwise racing and fast training may influence the sites of occurrence.

A Figure 7: Lateral (a) and dorsal (b) bone phase images of the distal LF

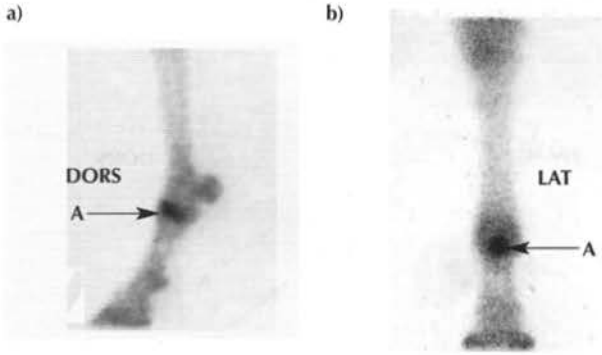

SB	2y	F	Pacer	200 x 200

DX: Short, incomplete mid sagittal fracture of proximal phalanx.

DS: Perineural analgesia: rendered sound by palmar digital block. Radiography: short mid sagittal fracture proximal aspect of proximal phalanx.

➡ **A:** Marked focal IRU in the proximal mid sagittal region of the proximal phalanx.
Note: Pain from lesions more proximal to a nerve block can be abolished by diffusion of local anaesthetic solution after injection. It is a regular occurrence that the pain from proximal phalanx fractures can be abolished by both palmar digital and abaxial sesamoid blocks.

A Figure 8: Lateral LF (a), dorsal (b), flexed dorsal LF (c) and flexed lateral LF (d) bone phase images of the distal forelimbs

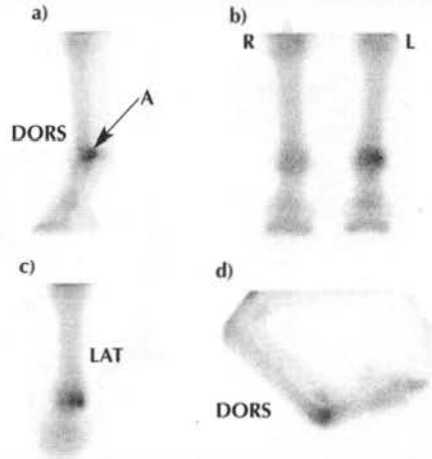

SB	5y	S	Pacer	200 x 200

DX: Nonadaptive remodelling of the distal aspect of McIII; osteoarthritis of the MCP joint.

DS: Clinical signs: severe LF lameness, positive response to lower limb flexion. Diagnostic analgesia: partial improvement to intra-articular analgesia of the MCP joint. Radiography: subchondral sclerosis with associated focal radiolucency in McIII.

➡ **A:** Marked focal IRU in the distal condyles of McIII.

A Figure 9a: Lateral RF 3 min (i), dorsal 11 min (ii) and lateral RF 13 min (iii) pool phase images of the distal forelimbs

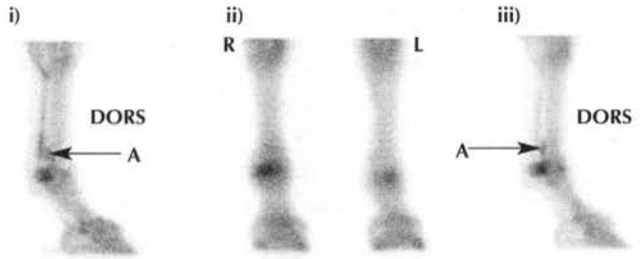

SB	4y	S	Trotter	128 x 128

DX: Severe osteoarthritis of the right MCP joint.

DS: Clinical signs: severe RF lameness. Pain on flexion of the RF MCP joint. Diagnostic analgesia: partial improvement with intra-articular analgesia of the RF MCP joint. Lameness completely abolished by low palmar (4-point) perineural analgesia. Radiography: severe periarticular new bone, irregularity of joint margin and subchondral sclerosis typical of marked osteoarthritis.

➔ **A:** Pooling in the palmar pouch of the MCP joint.
Note: IRU in the proximal palmar or plantar pouch extending proximally on Mc(Mt)III is an ominous scintigraphic finding in horses with severe osteoarthritis. These horses rarely recover athletic function.

A Figure 9b: Lateral RF (i), dorsal (ii) and flexed lateral RF (iii) bone phase images of the distal forelimbs

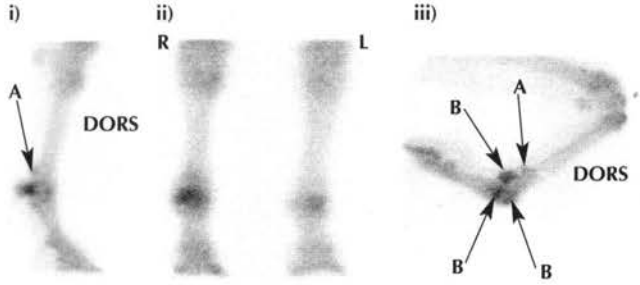

SB	4y	S	Trotter	200 x 200

DX: Severe osteoarthritis of the right MCP joint.

DS: *Details as for Figure 9a.*

➔ **A:** IRU persists well into bone phase.
➔ **B:** Marked IRU in all 3 components of the MCP joint.
Note: IRU of the proximal palmar or plantar pouch extending proximally on Mc(Mt)III is an ominous scintigraphic finding in horses with severe osteoarthritis. These horses rarely recover athletic function.

A Figure 10: Lateral RF (a), dorsal (b) and flexed lateral RF (c) bone phase images of the distal forelimbs

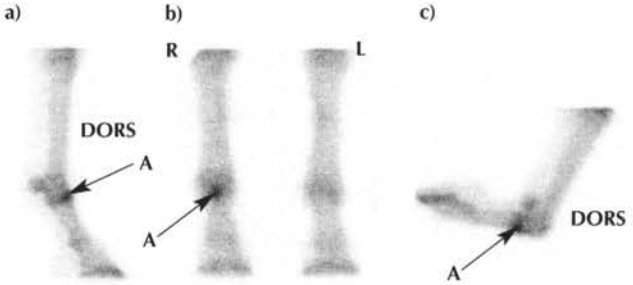

SB	3y	F	Pacer	200 x 200

DX: Short, incomplete mid sagittal fracture of the right proximal phalanx.

DS: Clinical signs: pain on palpation dorsoproximal aspect of proximal phalanx, RF lameness. Radiography: short, mid sagittal fracture.

➔ **A:** Focal, moderate to marked IRU in dorsal and axial aspects of proximal phalanx.
Note: Flexed view (c) is used to differentiate proximal phalanx from distal McIII.

A Figure 11: Lateral bone phase image of the distal LF

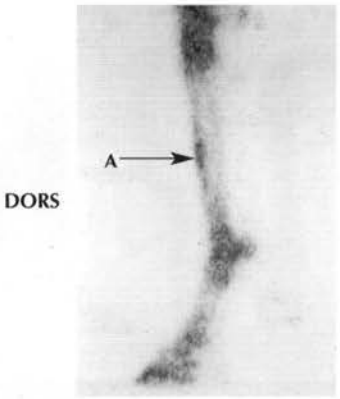

SB	2y	F	Pacer	200 x 200

DX: Periostitis (bucked shins).

DS: Clinical signs: mild LF lameness. Pain on palpation of the dorsal cortex of McIII. Perineural analgesia: lameness abolished with high palmar analgesia. Radiography: remodelling of the dorsal cortex; no obvious cortical fracture.

➔ **A:** Focal, mild to moderate linear IRU involving the dorsal cortex of McIII.
Note: This scintigraphic lesion is rare in the SB racehorse and is usually seen only in the forelimb of pacers, generally 2-year-olds in advanced training.

A **Figure 12: Dorsal bone phase images of both carpal regions**

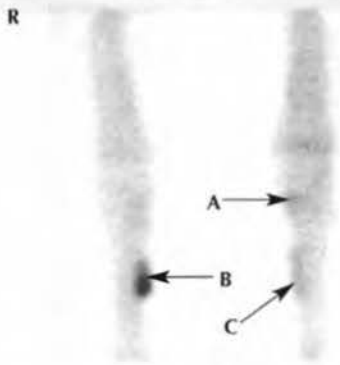

SB	3y	F	Pacer	200 x 200

DX: Active splint exostosis in RF and coexistence of IRU associated with splint exostosis and medial aspect of middle carpal joint in LF.

DS: Clinical signs: pain on palpation of a splint exostosis involving right McII. Radiography: periosteal new bone proliferation on McII on both forelimbs and sclerosis of the C3 in left carpus.

➡ **A:** Mild diffuse IRU in medial aspect of the LF middle carpal joint.
➡ **B:** Marked focal IRU in McII, RF.
➡ **C:** Mild focal IRU in McII, LF.
Note: Some SB racehorses can have painful 'splints' without substantial IRU, while in others marked IRU is not accompanied by clinical signs of pain or lameness.

A **Figure 13a: Dorsal 10 min (i) and lateral LF 12 min (ii) pool phase images of the distal forelimbs**

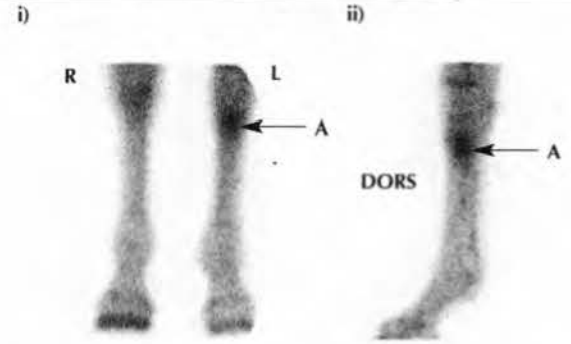

SB	2y	F	Trotter	128 x 128

DX: Avulsion fracture of the proximal palmar aspect of McIII.

DS: Clinical examination: pain on palpation of proximal palmar aspect McIII. Perineural analgesia: LF lameness abolished by both middle carpal intra-articular analgesia and high palmar (subcarpal) block. Radiography: avulsion fracture McIII. Ultrasonography: irregularity and step defect palmar surface McIII.

➡ **A:** Marked focal IRU in the proximal aspect of McIII.
Note: Intense uptake in pool phase images often reflects early bone uptake rather than genuine soft tissue pooling.

A **Figure 13b: Lateral LF (i) and dorsal (ii) bone phase images of both carpi**

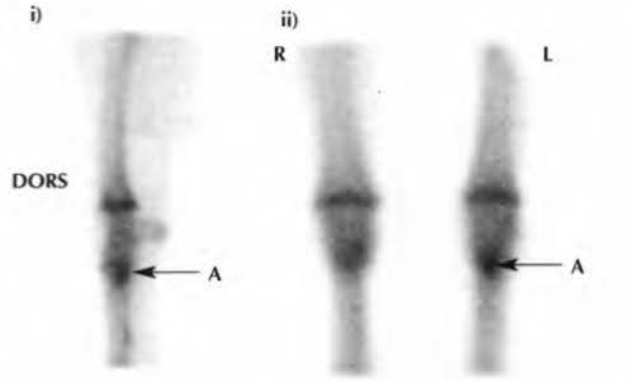

SB	2y	F	Trotter	200 x 200

DX: Avulsion fracture of the proximal palmar aspect of McIII.

DS: *Details as for Figure 13a.*

➡ **A:** Marked focal IRU associated with proximal palmar aspect of McIII, indicative of stress fracture, avulsion fracture or stress reaction.
Note: Triangular appearance of the region of IRU in the lateral view is commonly seen in horses with stress reaction and avulsion fracture.

A **Figure 14: Dorsolateral (a), lateral RF (b) and flexed lateral RF (c) bone phase images of the carpal regions**

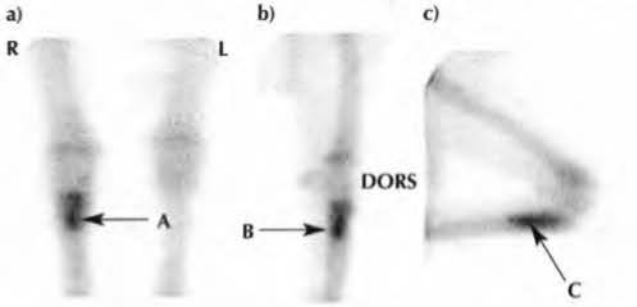

SB	4y	G	Pacer	200 x 200

DX: Longitudinal fracture of proximal palmar cortex McIII.

DS: Regional analgesia: pronounced RF lameness abolished with high palmar analgesia, significantly improved with intra-articular analgesia of the middle carpal joint. Radiography: longitudinal fracture of the proximal palmar aspect of McIII.

➡ **A:** Marked focal IRU in the proximal McIII.
➡ **B:** IRU is approximately triangular in pattern but extends further distally in McIII compared to Figure 13a,b. This infers that the injury extends further distally than the origin of the suspensory ligament alone.
➡ **C:** Use of the flexed view confirms that all IRU is associated with McIII, not carpal bones.

A **Figure 15ab: Lateral (a) and dorsal (b) pool phase images (2 mins) of the distal forelimbs**

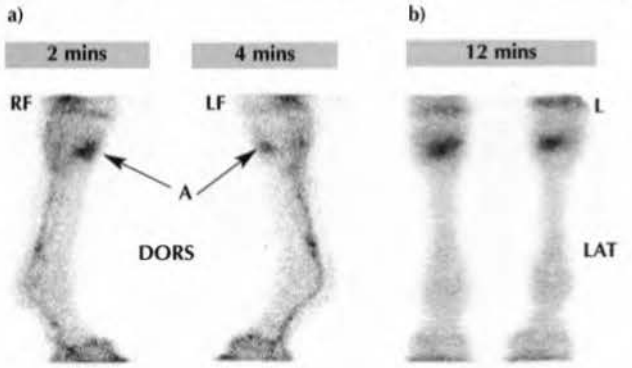

SB	2y	F	Trotter	128 x 128

DX: Incomplete fracture of the 3rd carpal bone.

DS: Diagnostic analgesia: lameness abolished by intra-articular analgesia MC joint. Radiography: sclerosis of the radial facet of C3 with incomplete linear lucency.

➡ **A:** Very early IRU in C3 at 2 mins.

Note: Although the lameness was seen in the right foreleg following C3 fracture, a focal area of marked IRU is also present in the radial facet of the contralateral limb. This is commonly the case, associated with mild bilateral lameness. Completion of a fracture through the radial facet results in severe acute onset lameness, but the scintigraphic appearance of the 2 limbs is often relatively similar, at least initially.

A **Figure 15cd: Lateral (c) and dorsal (d) bone phase images of both carpi**

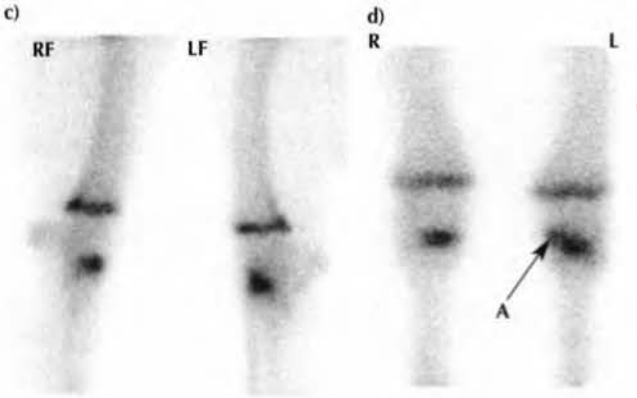

SB	2y	F	Trotter	200 x 200

DX: Incomplete fracture of the 3rd carpal bone.

DS: *Details as for Figure 15a,b.*

➡ **A:** On these standing, weightbearing, dorsal images, separating the exact site of IRU in the carpus is difficult. Compare with Figure 15e.

A **Figure 15e: Flexed dorsal bone phase images of right (i) and left (ii) carpi**

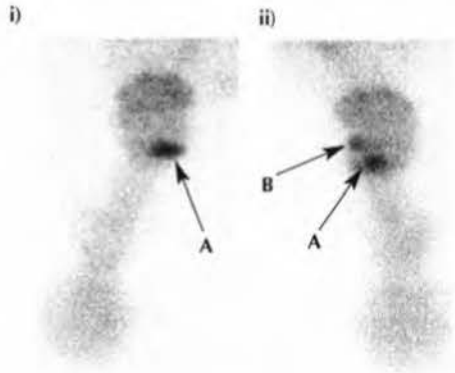

SB	2y	F	Trotter	200 x 200

DX: Incomplete fracture of the 3rd carpal bone.

DS: *Details as for Figure 15a,b.*

➡ **A:** IRU in the radial facet of 3rd carpal bone seen in this dorsal flexed view.

➡ **B:** IRU in distal radial carpal bone. This illustrates the usefulness of the flexed dorsal view in separating the exact site of IRU in the carpus.

A **Figure 16: Lateral RF (a), LF (b) and dorsal (c) bone phase images of the carpal regions**

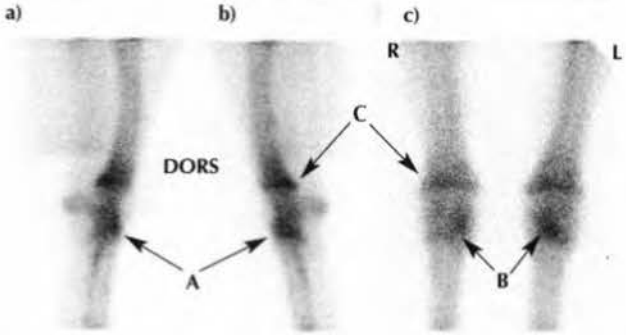

SB	4y	S	Trotter	200 x 200

DX: Stress (nonadaptive) remodelling and osteochondral fragmentation in middle carpal joint.

DS: Clinical signs: bilateral forelimb lameness. Middle carpal joint effusion. Radiography: osteochondral fragmentation of the radial and 3rd carpal bones. Sclerosis with associated focal radiolucency in C3.

➡ **A:** Moderate focal IRU in the dorsal aspect of the middle carpal joint in both forelimbs.

➡ **B:** Moderate focal IRU associated with medial aspect of the middle carpal joint in both forelimbs. Note that this pattern differs from simple involvement of C3 alone.

➡ **C:** RU in the distal radial physis (normal).

A Figure 17: Dorsal bone phase images of both carpi

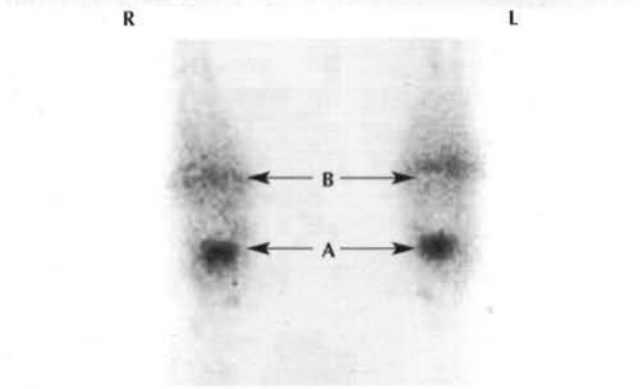

SB	2y	F	Trotter	200 x 200

DX: Sagittal slab fracture right C3, sclerosis left C3.

DS: RF lameness abolished by middle carpal joint intra-articular analgesia. Radiography: sagittal slab fracture of the radial facet of C3 in the RF. Marked sclerosis of the same site in the LF.

➡ **A:** Marked focal IRU in C3.
➡ **B:** Mild normal RU in the distal radial physis.
Note: Rectangular shape of the IRU in the dorsal view closely correlates with anatomical outline of C3. Note also that scintigraphy shows poor sensitivity in discriminating between marked sclerosis, minor fragmentation and marked sagittal fractures.

A Figure 18: Dorsal bone phase images of both carpi

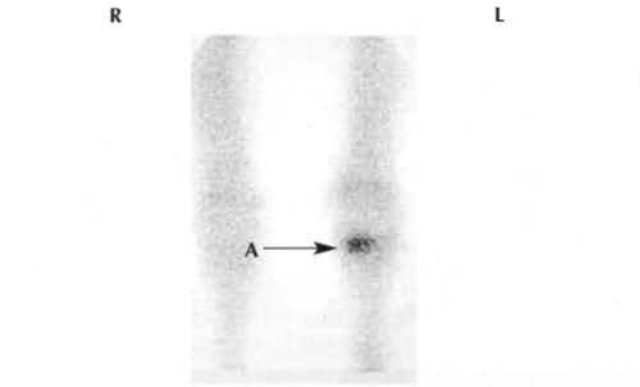

SB	3y	-	Pacer	200 x 200

DX: Stress (nonadaptive) remodelling of left 3rd carpal bone.

DS: LF high-speed lameness; horse on a left line during speed work. Diagnostic analgesia: lameness abolished by middle carpal joint intra-articular analgesia. Radiography: marked sclerosis of C3.

➡ **A:** Marked focal IRU in left 3rd carpal bone.
Note: The rectangular shape of the zone of IRU corresponds to the anatomical shape of C3, in this horse confined to the radial facet.

A Figure 19: Lateral LF (a) and dorsal (b) bone phase images of the carpal regions

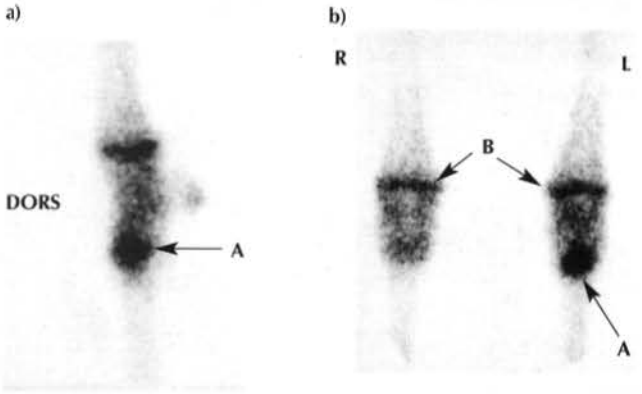

SB	3y	G	Pacer	200 x 200

DX: Dorsomedial articular fracture of proximal aspect of McIII.

DS: Clinical examination: pain on palpation of proximal dorsomedial aspect of McIII. Diagnostic analgesia: lameness abolished by intra-articular analgesia middle carpal joint. Radiography: fracture and bony proliferation of dorsoproximal aspect McIII.

➡ **A:** Marked focal IRU proximal left McIII.
➡ **B:** Moderate linear IRU in the distal radial physis (normal).

A Figure 20: Lateral RF (a) and LF (b), and cranial RF (c) and LF (d) bone phase images of the brachial regions

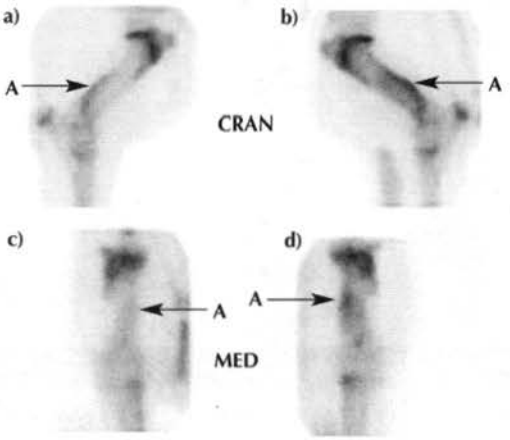

SB	2y	C	Pacer	200 x 200

DX: Humeral stress fractures.

DS: Severe LF lameness, negative to perineural and intra-articular analgesia. Radiography: endosteal and periosteal thickening of the caudal humeral cortices.

➡ **A:** Bilateral, moderate, diffuse, linear IRU in the caudomedial humeral cortices.
Note: This lesion is extremely rare in the SB in contrast to the TB racehorse.

A Figure 21: Lateral bone phase image of the left mid thoracic region

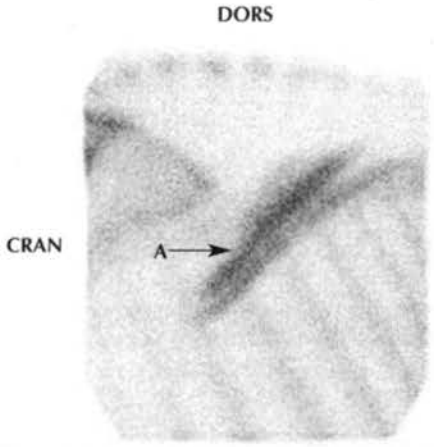

SB	3y	C	Pacer	200 x 200

DX: Focal muscle uptake in left *latissimus dorsi*.

DS: NA

➔ **A:** Moderate linear IRU in the *latissimus dorsi*.
Note: Forelimb muscle IRU is unusual to rare, and is probably an incidental finding.

A Figure 22: Plantar (a) and solar LH (b) bone phase images of the distal hindlimbs

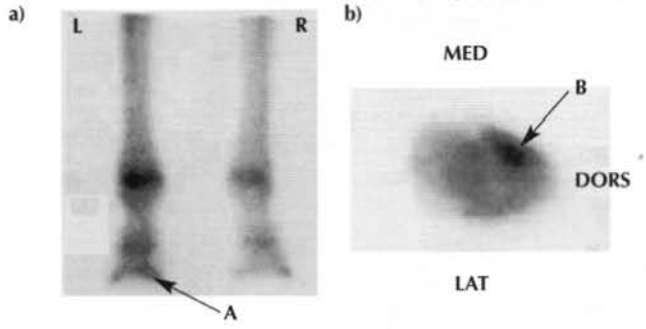

SB	4y	G	Pacer	200 x 200

DX: Stress fracture of the medial plantar process of the LH distal phalanx.

DS: LH lameness. Diagnostic analgesia: lameness abolished by plantar digital block. Radiography: stress fracture of medial plantar process of the distal phalanx.

➔ **A:** Mild IRU in the medial aspect of the distal phalanx.
➔ **B:** Marked focal IRU in the medial plantar process of the distal phalanx.
Note: Lesions on the medial aspect of a limb can go completely unnoticed if only a lateral view is taken. This lesion only shows well on the solar view, which was triggered by the abnormal finding of IRU on the medial aspect of the distal phalanx on the plantar view.

A Figure 23: Lateral LH (a), flexed lateral LH (b) and plantar (c) bone phase images of the distal hindlimbs

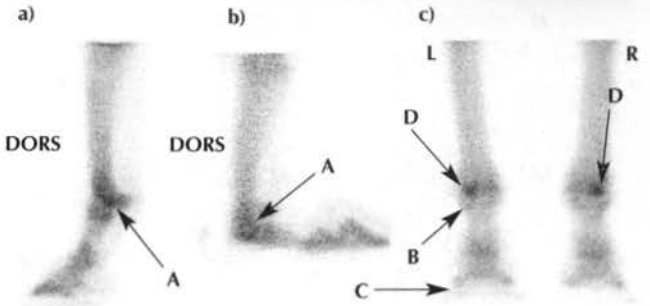

SB	3y	F	Trotter	200 x 200

DX: Nonadaptive remodelling of the distal aspect of MtIII.

DS: LH lameness localised to MTP joint by diagnostic analgesia (low plantar block).

➔ **A:** Moderate IRU distal MtIII.
➔ **B:** Mild focal IRU in the proximal lateral aspect of the proximal phalanx. This IRU is of no clinical significance and is common in SB racehorses.
➔ **C:** Mild IRU in the lateral aspect of the distal phalanx. This IRU is of no clinical significance and is common in SB racehorses.
➔ **D:** IRU in the plantarolateral condyle. Note that this has to be differentiated from IRU in the PSB by using the lateral and flexed lateral views.
Note: The flexed lateral view is essential for the SB racehorse with suspected MTP joint lameness.

A Figure 24: Lateral (a) and plantar (b) bone phase images of the left MTP joint

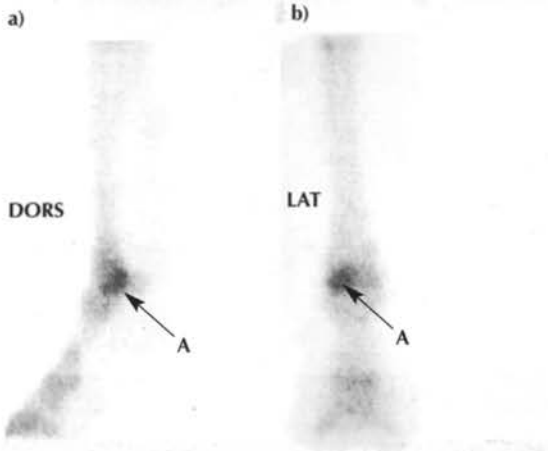

SB	3y	C	Pacer	200 x 200

DX: Subchondral bone damage caused by nonadaptive remodelling of distal plantarolateral aspect of MtIII.

DS: Diagnostic analgesia: LH lameness abolished by low plantar analgesia. Radiography: xeroradiographs revealed sclerosis of distal plantar aspect of MtIII, with associated small radiolucency centrally.

➔ **A:** Focal, moderate IRU in the plantarolateral condyle of MtIII.

A **Figure 25: Plantar (a) and flexed lateral (b) bone phase images of the distal LH**

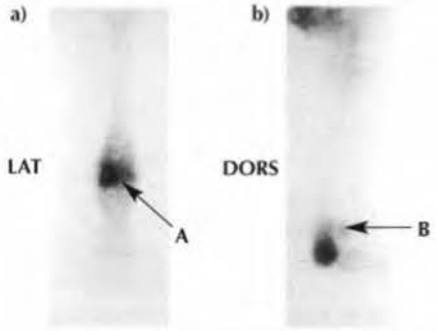

SB	4y	G	Trotter	200 x 200

DX: Advanced subchondral bone damage as a result of nonadaptive remodelling of the distal, plantarolateral aspect of the MtIII.

DS: Diagnostic analgesia: LH lameness abolished with low plantar analgesia. Radiography: sclerosis of lateral condyle with central radiolucency.

➡ **A:** Focal IRU in plantarolateral aspect of the condyle.
➡ **B:** The PSB is clearly separated from the region of IRU in the flexed view.
Note: When radiolucency is seen in the site of these stress reactions, considerable subchondral bone damage has invariably occurred, with bone necrosis and often eventual cavitation. The prognosis in these horses is guarded to poor.

A **Figure 26: Flexed lateral bone phase image of the distal LH**

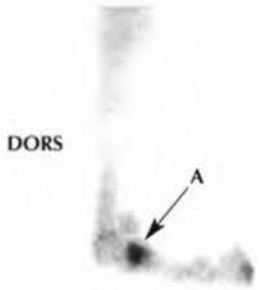

SB	2y	C	Pacer	-

DX: Mid sagittal fracture of the LH proximal phalanx.

DS: Regional analgesia: LH lameness abolished by intra-articular analgesia of the MTP joint. Radiography: short radiolucency extending from the sagittal groove. No evidence of periosteal reaction on dorsoproximal aspect of the distal phalanx seen on the lateromedial projection.

➡ **A:** Marked focal IRU in the plantaroproximal aspect of the proximal phalanx.
Note: This flexed view is useful in confirming the true location of IRU. The position of this lesion may explain the lack of periosteal new bone on the dorsal surface of the proximal phalanx on radiography. This injury is unusual; most sagittal fractures of the proximal phalanx have periosteal callus dorsally.

A **Figure 27: Plantar (a) and flexed lateral LH (b) bone phase images of the distal hindlimbs**

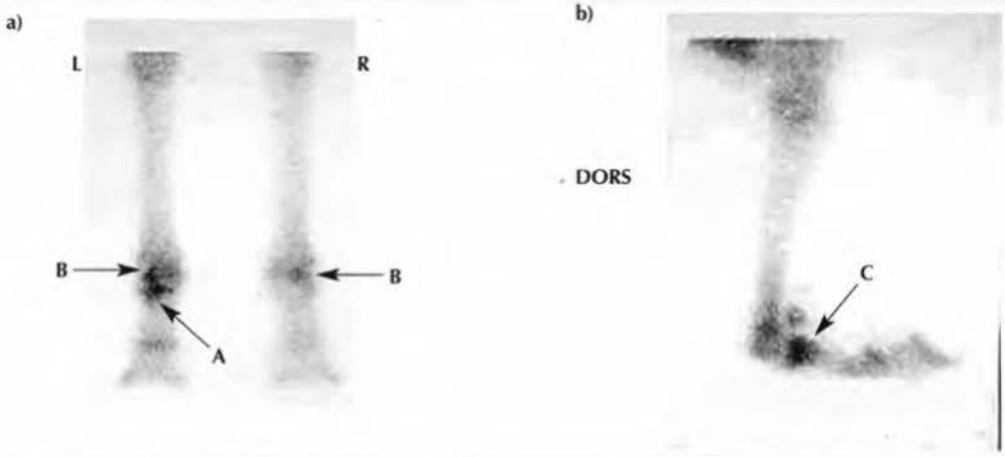

SB	2y	C	Pacer	200 x 200

DX: Mid sagittal fracture of LH proximal phalanx.

DS: Clinical examination: positive response to lower limb flexion. Diagnostic analgesia: LH lameness abolished by low plantar analgesia. Radiography: radiolucency extending distally from the sagittal groove of the proximal phalanx.

➡ **A:** Focal moderate IRU in the axial aspect of the proximal phalanx. Note that, in this plantar view, the lesion is further from the camera than in forelimb proximal phalanx fractures, and does not show as clearly as in those horses.
➡ **B:** Mild to moderate focal IRU in distal plantarolateral aspect of McIII.
➡ **C:** Flexed lateral view clearly shows IRU to involve the proximal phalanx (especially the plantar aspect). This is an important use of the flexed lateral view to demonstrate not only that IRU is in the proximal phalanx rather than distal MtIII, but also that it is in the plantar rather than dorsal aspect. This differentiates the injury from a dorsal frontal fracture.

A Figure 28: Lateral images of the distal LH (a) and RH (b)

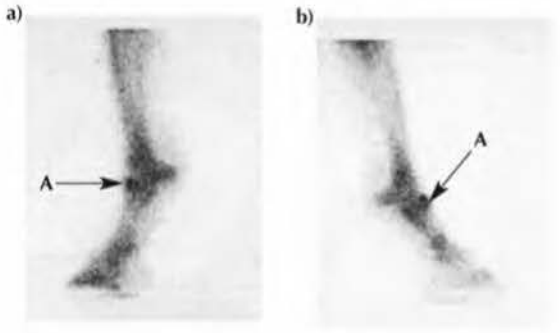

SB	3y	C	Trotter	200 x 200

DX: Bilateral dorsal frontal fracture of the hind proximal phalanges.

DS: Diagnostic analgesia: primary RH lameness switching to LH lameness following intra-articular analgesia of the right MTP joint. Radiography: lucency in the frontal plane of the dorsal proximal phalanx associated with periosteal new bone.

➡ **A:** Focal moderate IRU in the proximodorsal aspect of the proximal phalanx bilaterally.
Note: This injury is much more common in the RH in the SB, but is occasionally seen in both limbs or unilaterally in the LH.

A Figure 29: Lateral (a) and plantar (b) bone phase images of the distal LH

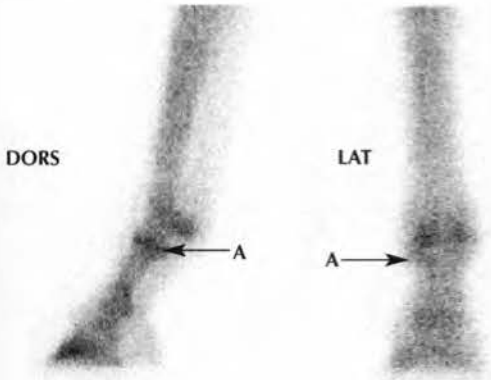

SB	3y	F	Pacer	200 x 200

DX: Plantar process OCD in the LH.

DS: Lameness seen only at high speed and not sufficiently pronounced to perform diagnostic analgesia. Radiography: plantar process OCD with fragmentation of the plantar process.

➡ **A:** Focal mild IRU involving proximolateral aspect of the proximal phalanx seen on both lateral and plantar views.
Note: It is not possible categorically to link radiographic and scintigraphic findings with the lameness in the horse.

A Figure 30: Lateral (a) and plantar (b) bone phase images of the distal RH

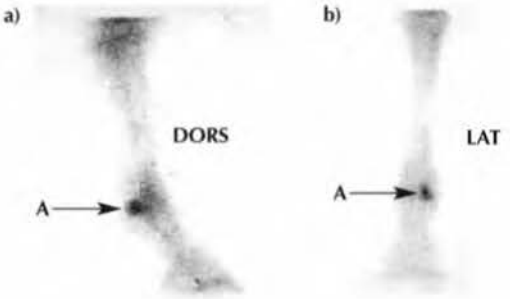

SB	3y	G	Pacer	200 x 200

DX: Lateral sesamoiditis RH.

DS: Diagnostic analgesia: RH lameness localised to the MTP joint by low plantar block. Radiography: mild sclerosis of the lateral PSB.

➡ **A:** Focal moderate IRU in the lateral PSB.
Note: On the plantar view, the intensity and site of IRU could be confused with a stress remodelling lesion of MtIII. The lateral and, more especially, flexed lateral views are essential to discriminate the true site of RU.

A Figure 31: Plantar bone phase image of the distal hindlimbs

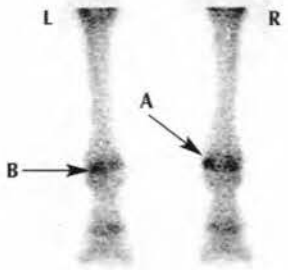

SB	3y	C	Pacer	200 x 200

DX: Medial RH sesamoiditis/bony fragmentation.

DS: Regional analgesia: RH lameness localised to MTP joint by low plantar analgesia. Radiography: sesamoiditis and fragmentation of the abaxial sesamoid surface. Ultrasonography: insertional desmitis of the medial branch of the suspensory ligament and bony fragmentation.

➡ **A:** Moderate IRU in medial aspect of the right MTP joint.
➡ **B:** Moderate IRU on plantarolateral aspect of the left MTP joint.
Note: RU on the lateral aspect of this joint is normal in the SB racehorse (see Figure 24). Any IRU on the medial aspect is likely to be linked to pathology. IRU on the medial aspect can be missed if only a lateral view is acquired.

A **Figure 32: Lateral LH (a) and plantar (b) bone phase images of the tarsal regions**

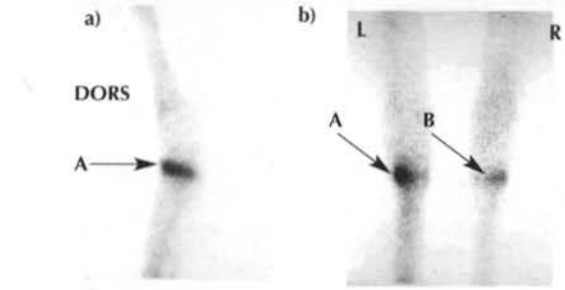

SB	2y	F	Trotter	200 x 200

DX: Nonadaptive remodelling of the TMT joint; early osteoarthritis.

DS: Diagnostic analgesia: LH lameness partially improved by TMT joint intra-articular analgesia. Radiography: mild radiographic changes in both TMT and CD joints, consisting of osteophyte formation and mild subchondral lucency.

➡ **A:** Marked focal IRU in the TMT joint, consistent with osteoarthritis.
➡ **B:** Mild IRU involving lateral aspect of the right TMT joint.
Note: Count stealing results in poor definition of both the remainder of the LH and the RH. Note also that these lesions are primarily located on the lateral aspect of the joint to begin with, although the whole joint may eventually be involved (IRU in this site is the most common abnormal scintigraphic finding in the SB tarsus).

A **Figure 33: Lateral RH (a), LH (b) and plantar (c) bone phaase images of both tarsal regions**

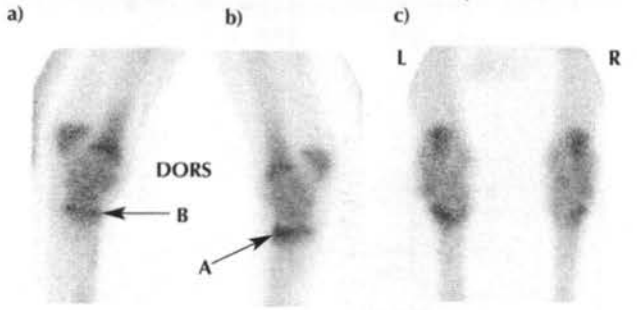

SB	3y	C	Trotter	200 x 200

DX: Frontal slab fracture of the 3rd tarsal bone (LH) and osteoarthritis of the tarsometatarsal joint (RH).

DS: Clinical signs: poor racing performance, 'hiking' behind, bilateral hindlimb lameness, left worse than right. Radiography: T3 slab fracture LH and OA of TMT joint RH.

➡ **A:** Marked IRU in dorsal aspect of the TMT joint in the LH.
➡ **B:** Mild linear IRU in the TMT of the RH.
Note: In SBs with slab fracture and advanced osteoarthritis, the intensity is greater on the dorsal aspect of the joint. In low grade early osteoarthritis, a more typical appearance is the linear band of IRU seen in the RH.

A **Figure 34: Lateral bone phase image of the right tarsal region**

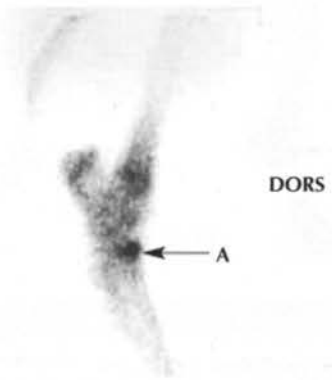

SB	4y	S	Trotter	200 x 200

DX: Osteoarthritis of the right CD joint.

DS: Diagnostic analgesia: severe RH lameness, not improved by TC or TMT joint intra-articular analgesia. Radiography: extensive subchondral lysis of central tarsal bone and T3.

➡ **A:** Marked focal IRU involving dorsal aspect of the distal tarsus.
Note: The degree of IRU seen in these SBs would usually be consistent with fracture or advanced active osteoarthritis of the CD joint.

A **Figure 35: Lateral bone phase image of the right tarsal region**

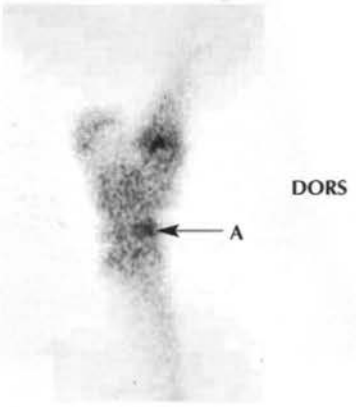

SB	3y	C	Pacer	200 x 200

DX: Fracture of the central tarsal bone.

DS: Diagnostic analgesia: RH lameness abolished by intra-articular analgesia of the TC joint. Radiography: central tarsal bone fracture.

➡ **A:** Moderate focal IRU in the central tarsal bone.
Note: IRU in this horse is located more proximally than in Figure 34, which involved T3 and the TMT joint.

A **Figure 36: Lateral LH (a) and plantar (b) bone phase images of the tarsal regions**

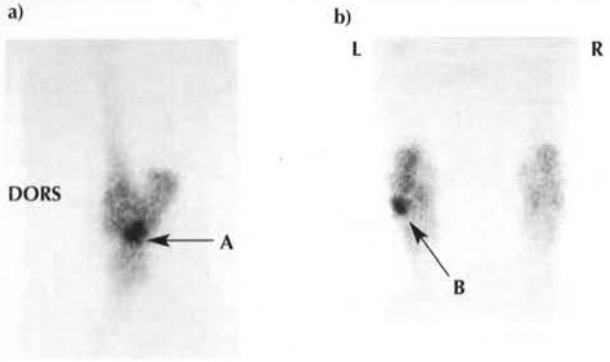

SB	5y	G	Pacer	200 x 200

DX: Enthesopathy of the lateral collateral ligament of the TC joint.

DS: Clinical signs: mild TC effusion, subtle periarticular swelling of the TC joint. Diagnostic analgesia: LH lameness (2/5) 75–80% improved with intra-articular analgesia of the TC joint. Radiography: periosteal new bone on lateral aspect of the calcaneus.

➔ **A:** Marked focal IRU in the distal aspect of calcaneus.
➔ **B:** The plantar view clearly demarcates this IRU to involve the lateral aspect of the calcaneus, differentiating it from the talocalcaneal articulation or distal plantar aspect of talus.

A **Figure 37: Lateral LH (a), plantar (b) and flexed lateral LH (c) bone phase images of the tarsal regions**

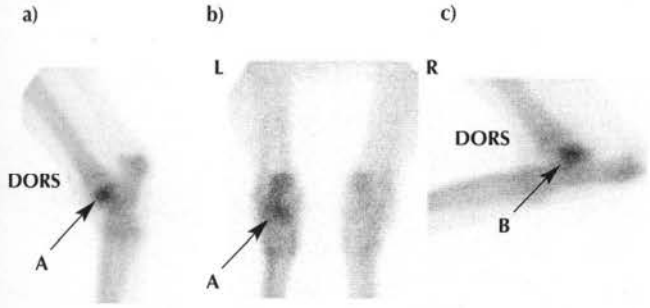

SB	8y	G	Pacer	200 x 200

DX: Sagittal fracture of the left talus.

DS: Clinical signs: mild TC effusion. Diagnostic analgesia: LH lameness abolished by intra-articular analgesia of the TC joint. Radiography: incomplete sagittal fracture of the talus.

➔ **A:** Focal moderate IRU in the TC joint seen on the lateral and plantar images.
➔ **B:** The flexed lateral view allows discrimination in the site of IRU between the distal tibia and the talus.

A **Figure 38: Lateral pool phase (a) and bone phase (b) images of the left tarsal region**

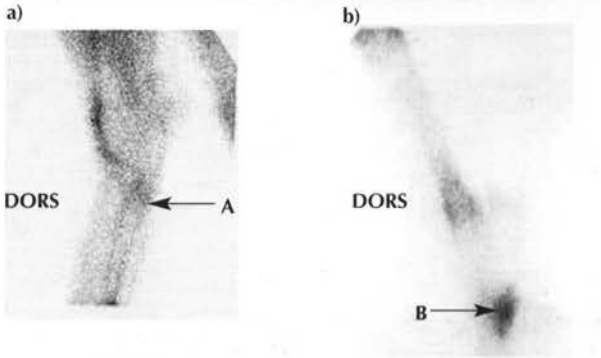

SB	5y	G	Pacer	*See Note*

DX: Avulsion fracture of the proximal plantar aspect of MtIII associated with PSD.

DS: Clinical signs: LH lameness; mild swelling of the proximal plantar metatarsal region of the LH. Ultrasonography: enlargement, irregularity in outline and hypoechogenicity of the proximal suspensory ligament.

➔ **A:** Pooling of radiopharmaceutical in the proximal plantar metatarsal region consistent with active PSD.
➔ **B:** Marked focal IRU in an approximately triangular outline.
Note: Differential diagnosis of this scintigraphic appearance includes avulsion fracture of proximal MtIII, longitudinal fracture or stress reaction in MtIII. Matrix sizes: 128 x 128 (a); 200 x 200 (b).

A **Figure 39: Lateral RH bone phase image of the tarsal region**

SB	2y	C	Trotter	200 x 200

DX: Exostosis of right MtIV.

DS: Clinical signs: mild RH lameness with painful exostosis on abaxial aspect of MtIV. Radiography: mild bony proliferation in proximal MtIV.

➔ **A:** Focal IRU in proximal MtIV.

A **Figure 40: Lateral (a) and caudal (b) bone phase images of the right stifle region**

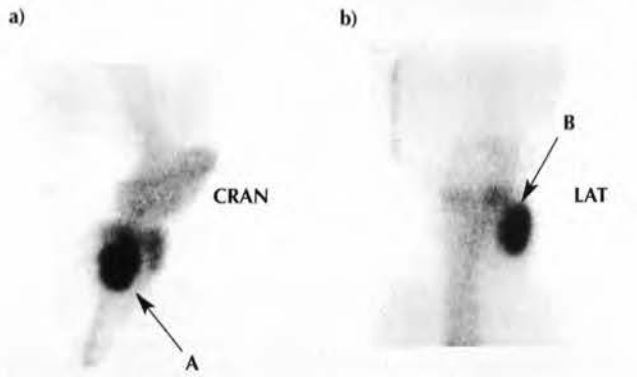

SB	3y	C	Pacer	200 x 200

DX: *Calcinosis circumscripta* of the stifle region as an incidental finding.

DS: NA

➡ **A:** Marked focal IRU apparently associated with the proximal tibia.
➡ **B:** In the caudal view, the zone of intense IRU is clearly outside the margins of the tibia. This was associated with *calcinosis circumscripta* of no clinical significance.

A **Figure 41: Lateral (a) and caudal (b) bone phase images of the right stifle region**

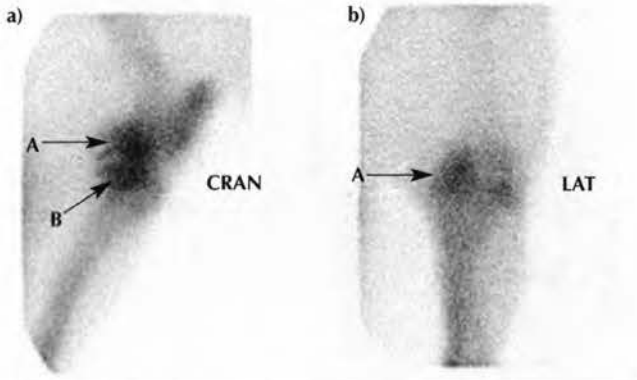

SB	6y	M	Pacer	200 x 200

DX: Osteoarthritis of the MFT joint.

DS: Clinical signs: MFT effusion, RH lameness (3/5). Radiography: severe narrowing of the MFT joint space.

➡ **A:** Focal, moderate IRU in distal femur.
➡ **B:** Focal IRU in proximal tibia.
Note: These scintigraphic signs are pathognomonic for osteoarthritis of the MFT joint. This is the most common scintigraphic abnormality of the SB stifle. Note also that the caudal view is essential for appreciation of this condition in many horses. This degree of IRU would be associated with pathology likely to end the horse's athletic career.

A **Figure 42: Lateral (a) and caudal (b) bone phase images of the left stifle region**

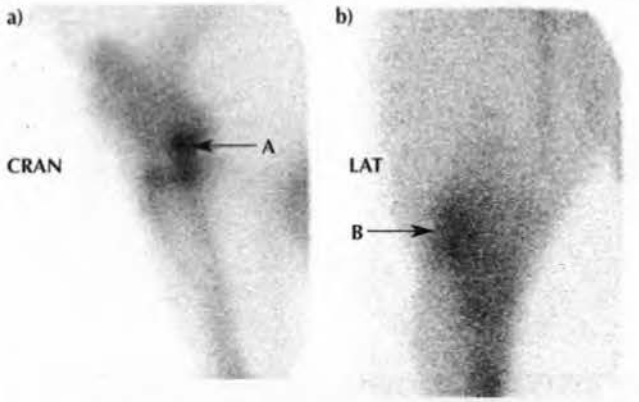

SB	7y	M	Pacer	200 x 200

DX: Osteoarthritis of the LFT joint.

DS: Clinical signs: mild effusion of the LFT joint, severe LH lameness. Diagnostic analgesia: moderate (50%) improvement with intra-articular analgesia of all 3 compartments of the left stifle joint.

➡ **A:** Focal, moderate IRU in distal lateral femur.
➡ **B:** Diffuse, moderate IRU in proximal lateral tibia.
Note: Osteoarthritis of the LFT joint is an unusual scintigraphic finding in the SB racehorse.

A **Figure 43: Lateral (a) and caudal (b) bone phase images of the right stifle region**

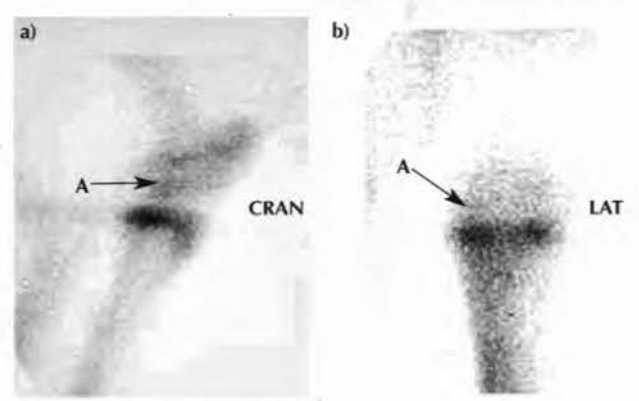

SB	2y	F	Pacer	200 x 200

DX: OCCL of the distal medial femoral condyle.

DS: Clinical signs: RH lameness. Diagnostic analgesia: Lameness significantly improved (75%) to MFT analgesia. Radiography: evidence of an OCCL.

➡ **A:** Very mild IRU in the medial femoral condyle is swamped by the normal intense RU in the proximal tibial physis. Count stealing by the physis obscures RU in an OCCL that was clearly evident radiographically. Masking of the physis would reveal moderate IRU in the medial femoral condyle.

A Figure 44: Lateral (a) and caudal (b) bone phase images of the left crus

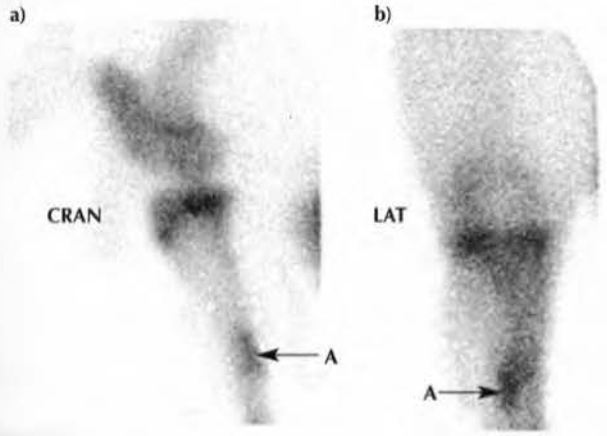

SB	2y	C	Pacer	200 x 200

DX: Caudolateral tibial stress fracture.

DS: Diagnostic analgesia: negative to perineural and intra-articular blocks.

➡ **A:** Focal, moderate IRU in the caudolateral tibial cortex.
Note: It is essential to obtain 2 views to differentiate cortical from intramedullary IRU and to distinguish IRU associated with iatrogenic damage from nerve blocks.

A Figure 45: Lateral bone phase images of the left (a) and right (b) tibiae

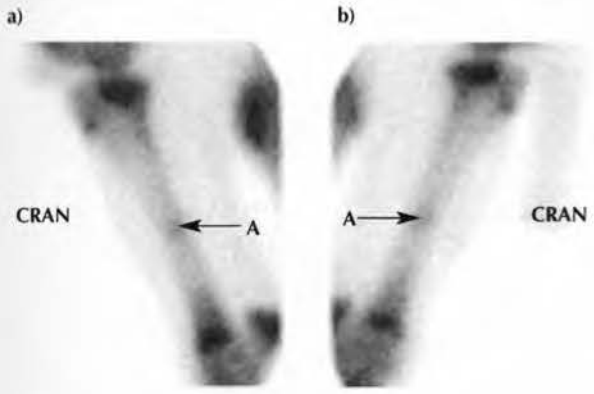

SB	3y	C	Trotter	200 x 200

DX: Bilateral tibial stress fractures.

DS: High-speed lameness not amenable to nerve blocks at the walk and trot. No clinical signs to confirm the seat of pain. Radiography: proliferative new bone on the caudal and caudolateral tibial cortices.

➡ **A:** Mild, diffuse IRU left and right caudal tibia.
Note: This type of stress fracture is relatively rare in the SB compared to the TB racehorse but, like in the TB, there is only mild IRU.

A Figure 46: Lateral RH (a) and LH (b) and caudal (c) bone phase images of the crus

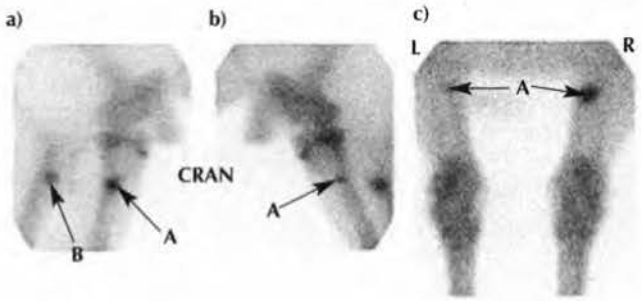

SB	3y	C	Pacer	200 x 200

DX: ELLs of the tibia.

DS: Clinical signs: high-speed RH lameness, no obvious seat of pain on clinical examination. Diagnostic analgesia: no response to perineural and intra-articular analgesia. Radiography: intramedullary sclerosis on caudocranial and lateromedial projections in the mid endosteum.

➡ **A:** Focal, moderate IRU in the right and left tibiae.
➡ **B:** Activity seen in the left tibia, which was unshielded during acquisition of the image of the RH.
Note: ELLs are a relatively unusual finding in the SB. They may be unilateral or bilateral, associated with lameness or an incidental finding.

A Figure 47: Lateral bone phase image of the right coxofemoral region

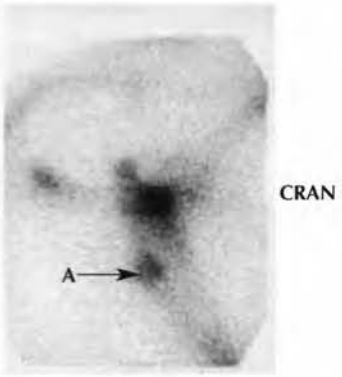

SB	4y	G	Trotter	200 x 200

DX: Enthesopathy of the right 3rd trochanter.

DS: Diagnostic analgesia: no response to any perineural and intra-articular analgesia. Clinical signs: RH lameness (coincidental LF lameness from osteoarthritis DIP joint).

➡ **A:** Marked, focal IRU in the great trochanter.
Note: This lesion is rare in the SB racehorse and, in this horse, may have been the result of compensatory loading owing to the forelimb lameness. IRU is more commonly seen following a fall or the horse becoming cast.

A **Figure 48: Lateral RH (a) and LH (b), left (c) and right (d) hemipelvic, and cranial (e) and caudal (f) transverse pelvic bone phase images of the pelvic region**

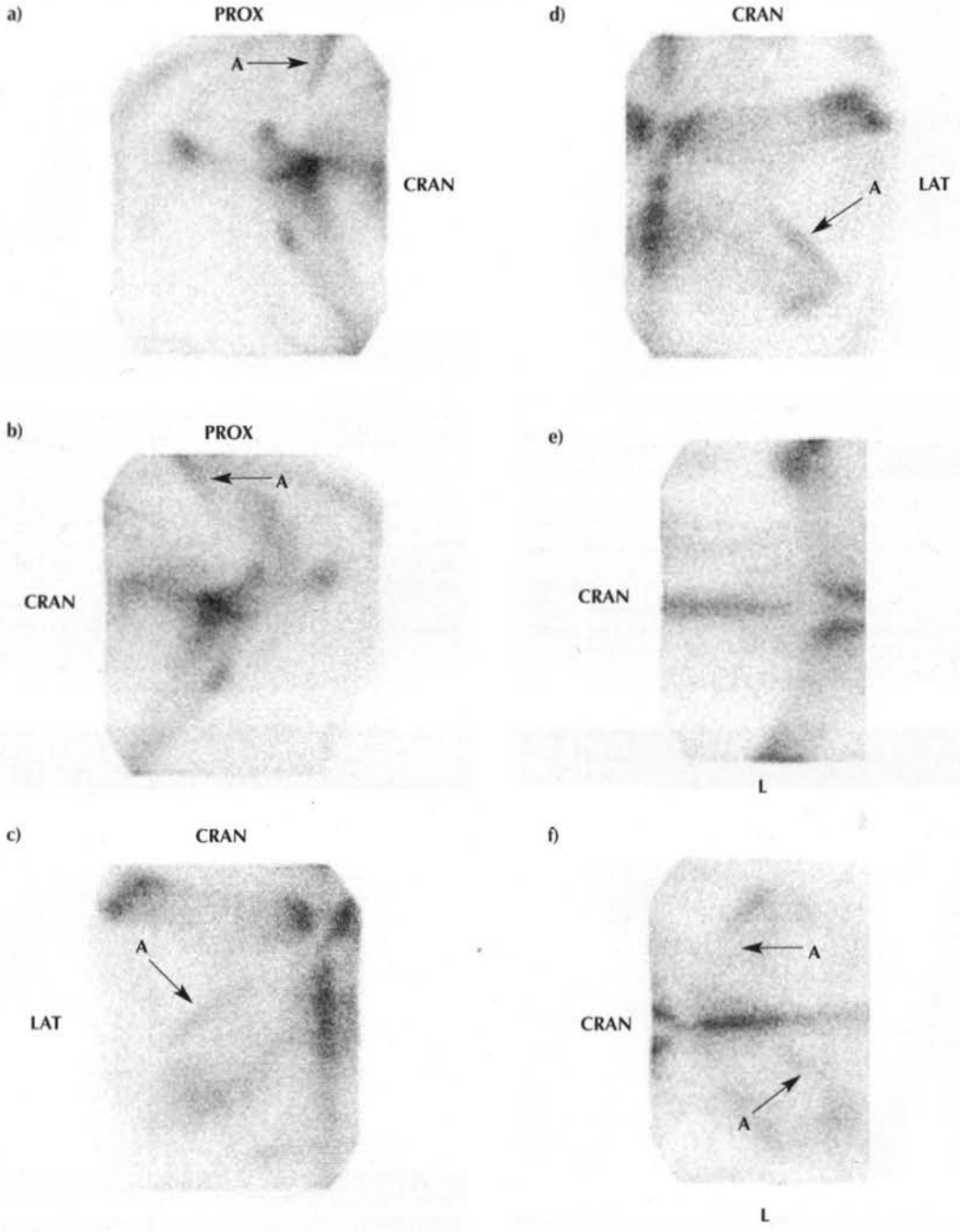

SB	3y	F	Trotter	200 x 200
DX:	Generalised rhabdomyolysis.			
DS:	NA			
➡ **A:** Diffuse, mild, linear IRU in the gluteal musculature. **Note:** This appearance is typical of rhabdomyolysis, which can be confirmed by measuring plasma creatine kinase and aspartate aminotransferase levels. This condition can be linked to high-speed lameness and poor performance.				

A Figure 49: Lateral bone phase image of the left thigh

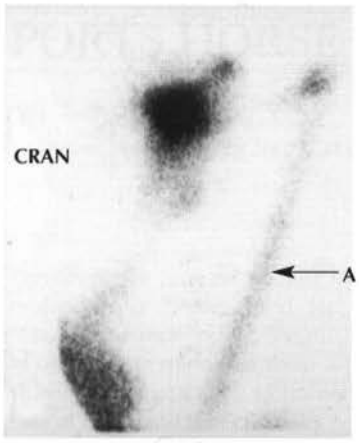

SB	2y	C	Pacer	200 x 200
DX:	Localised linear IRU in *semitendinosus* muscle.			
DS:	LH lameness linked to dorsal frontal fracture of proximal phalanx.			
➔ **A:**	Mild, focal linear IRU extending from the tuber ischii down to the level of the stifle (*semitendinosus* muscle). This was thought to be an incidental or compensatory finding.			
Note:	Windowing of this image has deliberately been adjusted to accentuate this mild uptake, resulting in saturation at the CF joint.			

A Figure 50: Dorsal bone phase image of the right hemipelvis

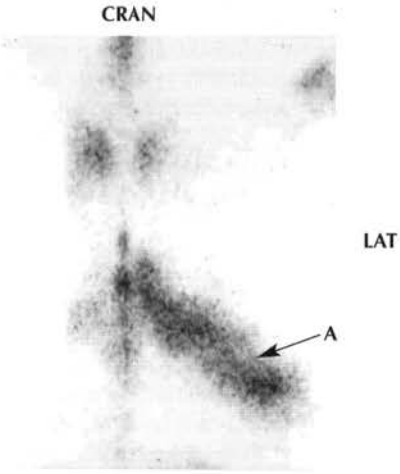

SB	2y	G	Pacer	200 x 200
DX:	Localised IRU in the gluteal muscles.			
DS:	NA			
➔ **A:**	Diffuse, moderate, linear IRU in the right gluteal musculature.			
Note:	This scintigraphic finding occurred in association with a cortical fracture of MtIII of the same leg. IRU in individual skeletal muscles in the ipsilateral lame leg is a relatively common finding in the SB racehorse.			

A Figure 51: Vascular phase image of the terminal aorta and branches

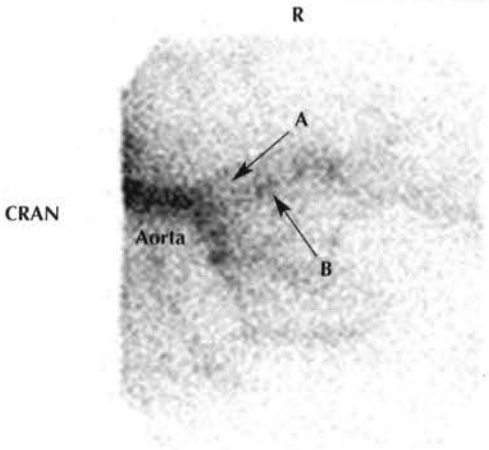

SB	5y	G	Pacer	128 x 128
DX:	Aortoiliac thromboembolism.			
DS:	Severe intermittent RH lameness. Prolonged saphenous vein filling time. Rectal examination: abnormal findings. Ultrasonography: abnormal changes in blood flow. Quantitative deficit in scintigraphic flow study.			
➔ **A:**	The normal V-shaped configuration of the external iliac arteries is lost.			
➔ **B:**	The internal iliac arteries are no longer seen.			

Chapter 4

THE SPORTS HORSE

SUE J. DYSON
Centre for Equine Studies, Animal Health Trust, Lanwades Park, Kentford, Newmarket, Suffolk CB8 7UU, UK.

This chapter considers the use of nuclear scintigraphy for orthopaedic evaluation of horses used for showjumping, dressage, eventing, endurance riding, hunting and pleasure riding. It should be borne in mind that there are relatively few studies that have systematically examined patterns of radiopharmaceutical uptake (RU) in clinically normal horses in maximum work. This chapter is based on both published and unpublished data related to clinically normal horses evaluated at the Animal Health Trust between January 1998 and December 2001, a review of the literature and experiences with the clinical evaluation and scintigraphic examination of approximately 1800 sports horses presented with lameness or poor performance. There are no marked differences in the normal appearance in horses used for these different sports disciplines, but there are some differences in the incidence of different conditions causing lameness or poor performance.

There are no special indications for scintigraphic examination over and above those discussed in *Part I, Chapter 8*. There is a natural tendency to focus on abnormalities, but even a negative scintigraphic examination can be helpful, since it excludes many potential diagnoses. For example, if a horse with hindlimb lameness is potentially dangerous to nerve block, has no localising clinical signs and scintigraphic examination of the limb is negative, there is a high probability that pain is associated with either proximal suspensory desmitis or stifle pain, so that subsequent local analgesic techniques can be targeted specifically to these areas.

When considering nuclear scintigraphic examination it is important to recognise when scintigraphy is unlikely to be helpful. Most horses that present with hindlimb or fore- and hindlimb ataxia do not have scintigraphic abnormalities, unless ataxia is associated with either a traumatically induced bone injury of the cervical or thoracolumbar vertebrae, or associated with active osteoarthritis (OA) of the synovial articulations of the caudal cervical vertebrae. Horses with very low-grade lameness often have no detectable scintigraphic abnormalities, especially if the horse has been rested. Horses with subtle poor performance problems often have no detectable scintigraphic abnormalities and whole body examinations searching for a potential cause are time-consuming, expensive, result in unnecessary exposure of staff to radiation and are often frustrating, since incidental abnormalities may be identified which serve only to confuse the picture. Whole body examinations should be resisted whenever possible. Recent skin or soft tissue trauma, resulting in localised increased blood supply, results in diffuse increased radiopharmaceutical uptake (IRU) which confounds interpretation.

Image description and interpretation is described in *Part I, Chapter 9*, but in sports horses in particular there are many pitfalls of interpretation. It is quite common to find regions of IRU unrelated to lameness. RU in solar views of the distal phalanx is often asymmetrical from medial to lateral and this may reflect foot imbalance, or the way in which the foot is loaded (**Figure 6d, Normals**). Horses with low heel conformation tend to have IRU in the region of the navicular bone[1]. Quantitative analysis of solar images of the foot may facilitate interpretation[1]. There is frequently a diffuse area of IRU in the region of insertion of the deep digital flexor tendon on the distal phalanx in solar images (**Figure 6b, Normals**). Intense focal uptake of radiopharmaceutical is often seen on the dorsoproximal aspect of the proximal phalanx in both forelimbs, both hindlimbs, or all 4 limbs (**Figure 5d, Normals**). Although such areas of IRU have previously been incriminated as potential causes of pain resulting in lameness[2,3], the frequency of their occurrence, the occurrence in several limbs simultaneously and the lack of correlation with the response to local analgesic techniques[4] makes it unlikely that they should be considered of clinical significance. Quiescent exostoses (splints) involving the second (McII and MtII), third (McIII and MtIII) and fourth (McIV and MtIV) metacarpal and metatarsal bones frequently have marked focal IRU (**Figures 7b, 8b[i] and 15d[i], Normals**). Focal areas of IRU are often seen in the diaphyses of long bones, especially McIII and MtIII, associated with enostosis-like lesions identified radiographically that are clinically silent (**Figures 8d[i-iii], Normals**). These focal areas of IRU may hide other lesions associated with lameness, and images should be reassessed after masking out these areas (see *Part I, Chapter 5*). There is often IRU in the lateral aspect of the distal hock and proximal metatarsal region seen in plantar views of the hocks[5]. This presumably reflects the loading patterns of the bones. Focal areas of IRU have been seen in the distal diaphysis of the tibia unilaterally, unassociated with lameness. Uptake in the stifle region varies hugely between horses; while the majority have a region of relatively IRU in the proximal caudal aspect of the tibia in lateral views, in some horses there is greater uptake in the tibial crest region and in others all regions of the stifle have similar uptake of the radiopharmaceutical (**Figures 16a–c, Normals**). *Calcinosis circumscripta*, while not common, is associated with intense focal IRU on the lateral aspect of the femorotibial (FT) joint. There is frequently relatively IRU in the summits of the dorsal spinous processes in the mid to caudal thoracic region either associated or unassociated with radiographic evidence of impingement, whereas in other horses there is uniform uptake in the summits of the dorsal spinous processes despite radiographic evidence of impingement (**Figure 18b, Normals**). There is often rather poor correlation with scintigraphic and clinical findings and the response to local infiltration with local

anaesthetic solution, emphasising the dangers of scintigraphic interpretation in isolation. RU in the sacroiliac joint region is influenced by age and, to a lesser extent, by breed and work discipline[6]. Movement and superimposition of the bladder both make image interpretation of this area impossible.

False negative scintigraphic results can occur, i.e. a lesion causing lameness may be present, but not detectable scintigraphically. This applies to many soft tissue injuries such as cruciate ligament or meniscal cartilage injuries, proximal suspensory desmitis without insertional fibre involvement, low grade osteoarthritis (OA), especially in high motion joints, chronic osteochondrosis lesions, and some osseous cyst-like lesions.

The atlas of images that follows cannot be completely comprehensive, but attempts in the first section (Normals) to show a spectrum of the different patterns of radiopharmaceutical activity encountered in clinically normal horses. In some regions there are huge differences between horses, but generally activity is bilaterally symmetrical in any individual horse, assuming blood flow is similar. Sports horses range enormously in age, conformation and degree of muscle development and these factors, together with recent work history, influence scintigraphic images. In the second section (Abnormals), some of the more common abnormalities are illustrated. It is considered vitally important to interpret the scintigraphic images in the light of all the clinical information available. Interpretation of images in isolation can, in my experience, be highly misleading.

REFERENCES

1. Dyson, S. (2002) Subjective and quantitative scintigraphic assessment of the equine foot and its relationship with hoof pain. *Equine vet. J.* **24**, 164-170.
2. Metcalf, M., Forrest, L. and Sellett, L. (1990) Scintigraphic pattern of ^{99m}Tc-MDP uptake in exercise induced proximal phalangeal trauma in horses. *Vet. Radiol.* **31**, 17-21.
3. Ehrlich, P., Seeherman, H., Callaghan, M. *et al.* (1998) Results of bone phase scintigraphy in horses used for show jumping, hunting or eventing : 141 cases (1988–1994). *J. Am. vet. med. Ass.* **213**, 1460-1467.
4. Dyson, S. Unpublished data.
5. Murray, R. and Dyson, S. Unpublished data.
6. Dyson, S., Murray, R., Branch, M. *et al.* (2003) The sacroiliac joints: evaluation using nuclear scintigraphy Part I: the normal horse. *Equine vet. J.* **35**, 226-232.

NORMAL HORSES

N **Figure 1a: Dorsal summed blood flow image of the distal forelimbs**

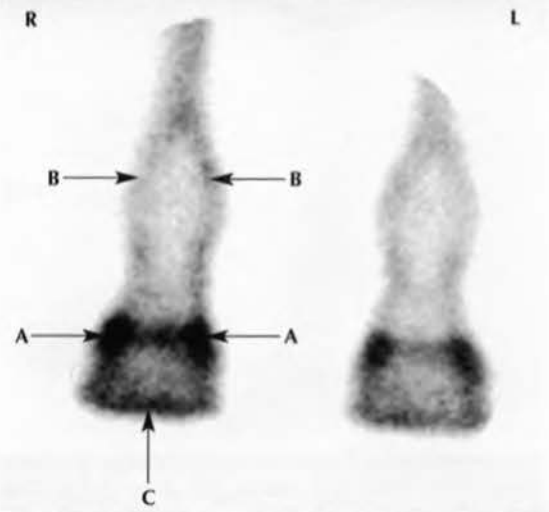

Irish TB	13y	G	Dressage & Am. Showjumping	128 x 128

DX: Normal

DS: NA

➔ **A:** Normal, focal, intense radiopharmaceutical activity at the medial and lateral aspects of the coronary band.
➔ **B:** Mild diffuse radiopharmaceutical activity in the digital vessels.
➔ **C:** Moderate activity in the region of the sole.

N **Figure 1b: Dorsal summed blood flow image of the distal forelimbs**

WB	7y	G	Dressage	128 x 128

DX: Normal

DS: NA

Note: In this normal horse there is less blood flow to the left forelimb. This may influence subsequent radiopharmaceutical activity in pool (see Figure 2b) and bone phase images.

N **Figure 2a: Dorsal pool phase image of the distal forelimbs obtained approximately 5 min after injection**

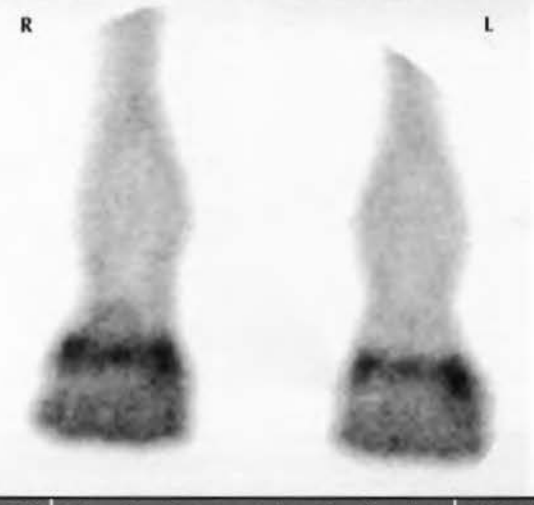

Irish TB	13y	G	Dressage & Am. Showjumping	128 x 128

DX: Normal

DS: NA

Note: The same horse as Figure 1a. Normal, focal, intense radiopharmaceutical activity persists associated with the coronary vasculature, which can mask radiopharmaceutical activity elsewhere. Radiopharmaceutical is less apparent in the digital vessels compared to Figure 1a.

N **Figure 2b: Dorsal pool phase image of the distal forelimbs**

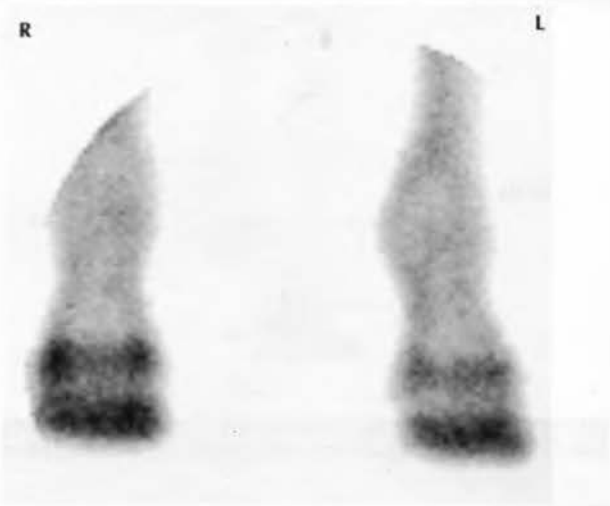

WB	7y	G	Dressage	128 x 128

DX: Normal

DS: NA

Note: The same horse as Figure 1b. Asymmetrical blood flow to the forelimbs has resulted in reduced radiopharmaceutical activity in the left forelimb (on the right); RU in the laminae in the solar region is more obvious than in Figure 2a.

N **Figure 3a: Lateral pool phase images of the distal LF obtained approximately 8 mins after injection**

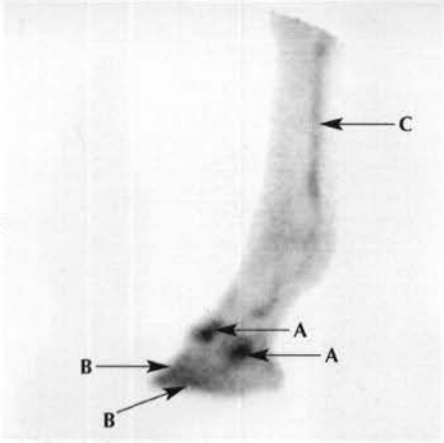

Irish TB	13y	G	Dressage & Am. Showjumping	128 x 128

DX: Normal

DS: NA

- ➔ **A:** Normal, focal, intense radiopharmaceutical activity persists at the coronary band.
- ➔ **B:** Mild radiopharmaceutical activity is seen in the dorsal and solar laminae.
- ➔ **C:** Mild radiopharmaceutical activity is still apparent in the digital vessels.

Note: Same horse as Figures 1a and 2a.

N **Figure 3b: Lateral pool phase image of the distal LF obtained approximately 8 mins after injection**

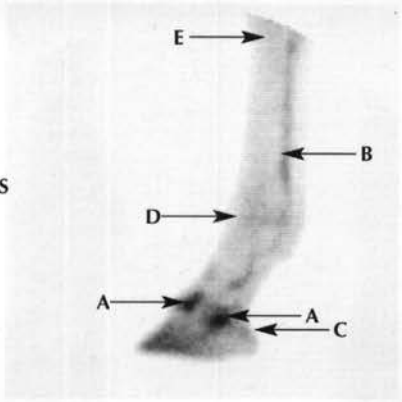

WB	9y	G	Dressage (Prix St George)	128 x 128

DX: Normal

DS: NA

- ➔ **A:** Normal radiopharmaceutical activity in the coronary band region is less intense than in Figure 3a.
- ➔ **B:** Activity remains more obvious in the digital vessels.
- ➔ **C:** Activity remains more obvious in vessels in the palmar aspect of the foot.
- ➔ **D:** Radiopharmaceutical activity in the soft tissues, or early uptake into bone is more obvious in the fetlock region.
- ➔ **E:** Radiopharmaceutical activity in the soft tissues, or early uptake into bone, is more obvious in the carpal region.

N **Figure 3c: Lateral pool phase image of the distal RF obtained approximately 11 mins after injection**

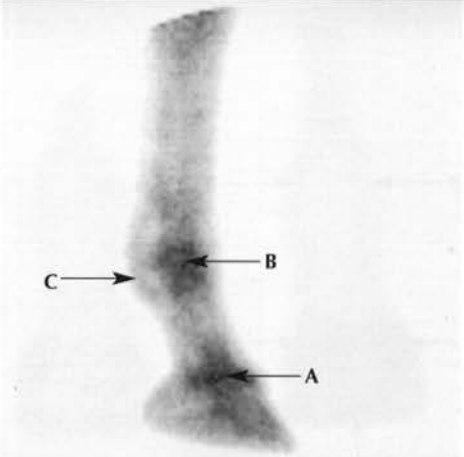

WB	9y	G	Dressage (Prix St George)	128 x 128

DX: Normal

DS: NA

- ➔ **A:** Normal radiopharmaceutical activity is more diffuse just proximal to the coronary band compared to Figure 3b.
- ➔ **B:** More intense activity associated with the fetlock region.
- ➔ **C:** Greater radiopharmaceutical activity in some of the soft tissues in the palmar aspect of the limb, but not in the superficial digital flexor tendon.

Note: Same horse as Figure 3b.

N **Figure 4a: Dorsal bone phase image of the distal forelimbs**

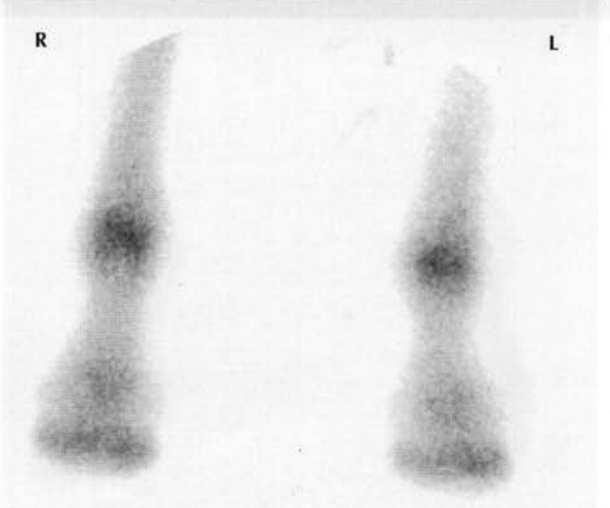

AxW	16y	M	General Purpose	256 x 256

DX: Normal

DS: NA

Note: Normal, moderate, diffuse radiopharmaceutical activity in the fetlock region; radiopharmaceutical activity associated with the proximal interphalangeal joint region and the distal aspect of the foot is greater than in the metacarpal and proximal pastern regions. Compare with Figure 4b.

N **Figure 4b: Dorsal bone phase image of the distal forelimbs**

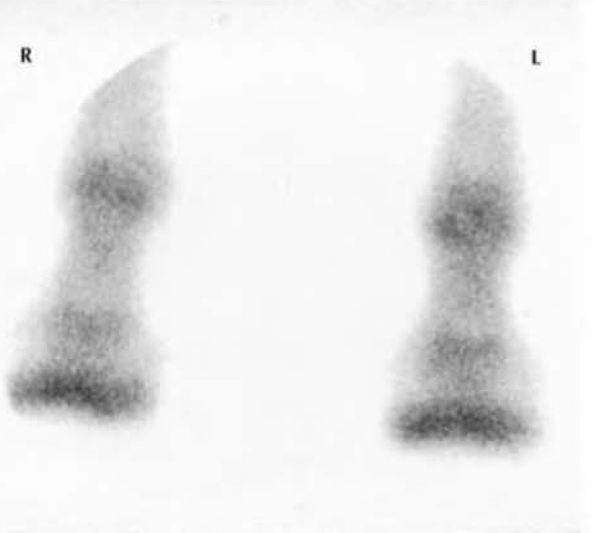

IDx	5y	G	General Purpose	256 x 256
DX:	Normal			
DS:	NA			
Note:	Normal, moderate, diffuse RU in the distal phalanx is greater than that in the fetlock and pastern regions. Compare with Figure 4a. (In this broad-chested horse, the most lateral aspect of the right front foot is beyond the margin of the 500 mm FOV gamma camera).			

N **Figure 4c: Dorsal bone phase image of the distal forelimbs**

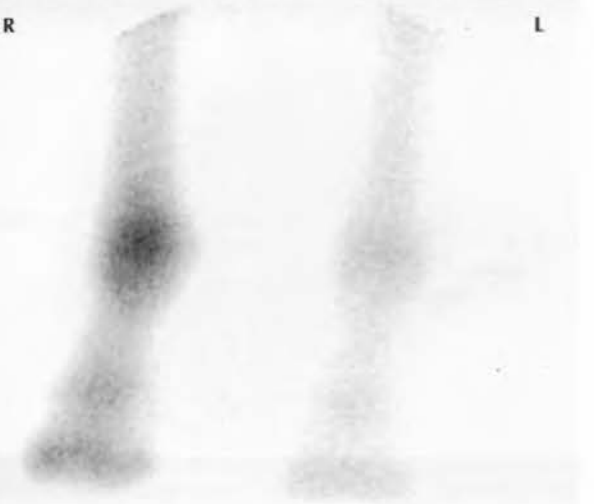

TBx	9y	G	Pony Club Activities	256 x 256
DX:	Normal			
DS:	NA			
Note:	Normal RU in the right forelimb, but markedly reduced RU in the left forelimb, associated with reduced distal limb blood flow at the time of injection; an example of the cold limb syndrome.			

N **Figure 5a: Lateral bone phase image of the distal LF**

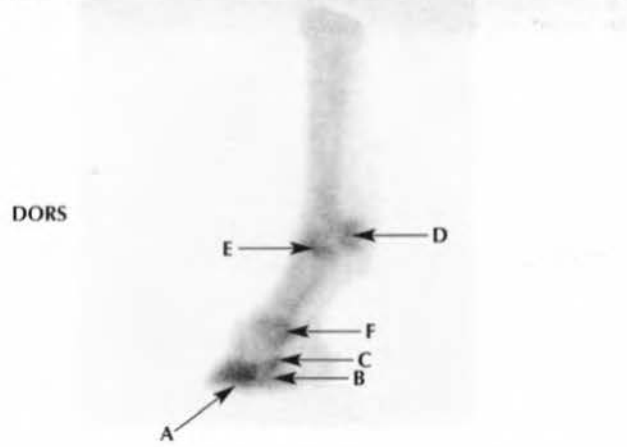

IDx	5y	G	General Purpose	256 x 256
DX:	Normal			
DS:	NA			
	➡ **A:** Moderate, diffuse RU in the body of the distal phalanx. ➡ **B:** Less RU in the palmar processes. ➡ **C:** Less RU in the ossified cartilages of the foot. ➡ **D:** Mild, diffuse RU in the proximal sesamoid bones. ➡ **E:** Mild, diffuse RU in the subchondral bone of the MCP joint. ➡ **F:** Mild, diffuse RU in the palmar aspect of the PIP joint.			
Note:	Compare this normal distribution with other variants in Figures 5b–d.			

N **Figure 5b: Lateral bone phase image of the distal LF**

DWB	5y	G	Dressage	256 x 256
DX:	Normal			
DS:	NA			
Note:	Mild, diffuse RU in the distal phalanx and the palmar aspect of the PIP joint, with greater RU in the subchondral bone of the distal McIII and the proximal phalanx and in the proximal sesamoid bones. Compare this normal distribution with Figures 5a, c and d.			

N Figure 5c: Lateral bone phase image of the distal LF

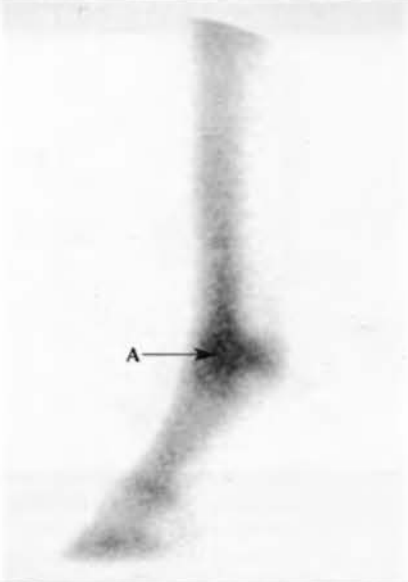

TBx	9y	G	Eventing (Int.)	256 x 256
DX:	Normal			
DS:	NA			
➡ **A:**	Relatively greater RU in the distal aspect of the McIII compared to elsewhere. Compare this normal distribution with Figures 5a, b and d.			

N Figure 5d: Lateral bone phase image of the distal LF

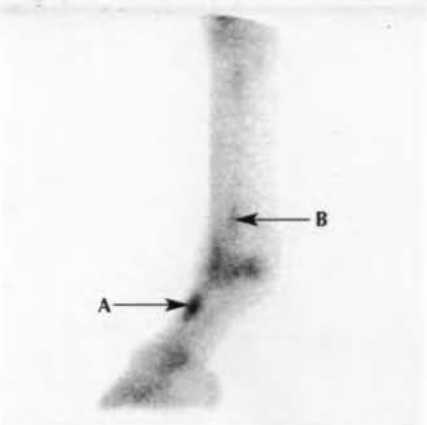

Irish TB	9y	G	Hunting & Am. Competition	256 x 256
DX:	Normal			
DS:	NA			
➡ **A:**	Intense, focal, normal RU in the proximal dorsal aspect of the proximal phalanx. Symmetrical uptake was seen in the contralateral forelimb and is often seen in all 4 limbs. Although such findings have previously been attributed to stress-induced bone injury in horses that jump, this pattern of radiopharmaceutical activity is a relatively frequent finding in normal horses from a variety of disciplines.			
➡ **B:**	Mild IRU seen in the distal palmar aspect of the third metacarpal bone, compared to Figures 5a–c.			

N Figure 6a: Solar bone phase image of the RF foot

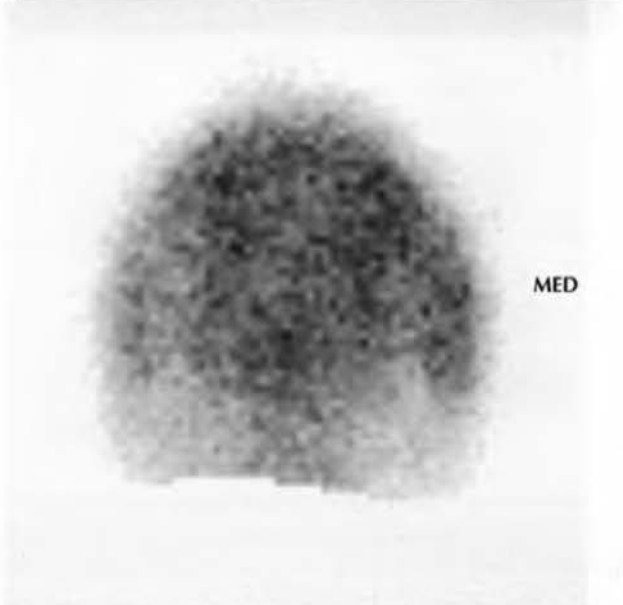

DWB	8y	G	Dressage	128 x 128
DX:	Normal			
DS:	NA			
Note:	Relatively uniform normal RU throughout the distal phalanx and the navicular bone. Compare with Figures 6b–e.			

N Figure 6b: Solar bone phase image of the RF foot

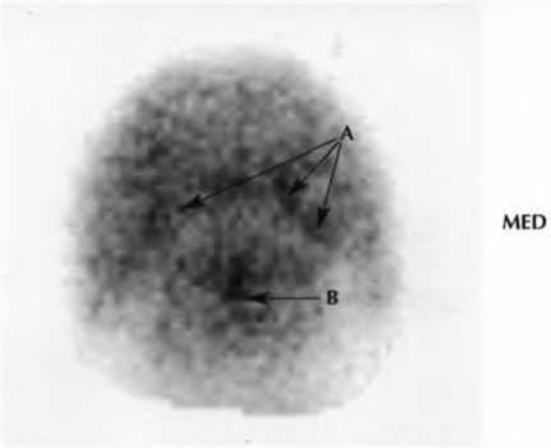

TB	7y	G	Am. Competition	128 x 128
DX:	Normal			
DS:	NA			
➡ **A:**	Relatively greater RU in the region of insertion of the deep digital flexor tendon compared to the rest of both the distal phalanx and navicular bone.			
➡ **B:**	Relatively greater RU also in the centre of the navicular bone.			
Note:	This pattern of RU is most often seen in horses with low heels, but can also be seen in those with more normally conformed feet, that are currently free from lameness. Compare with Figures 6a and c–e.			

N Figure 6c: Solar bone phase image of the RF foot

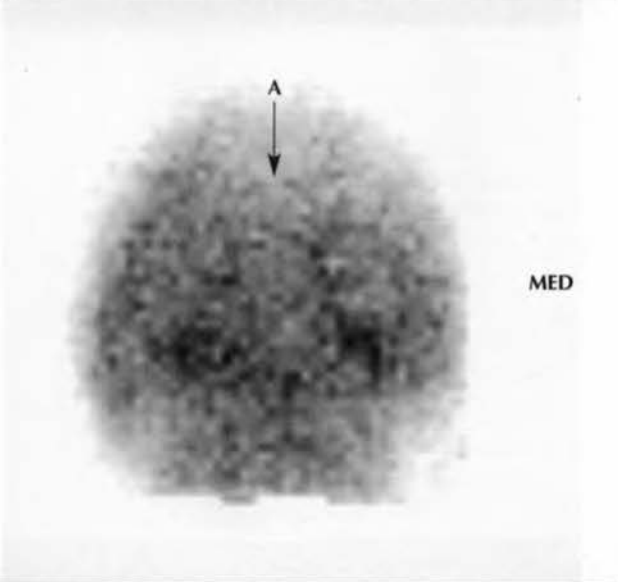

DanWB	5y	S	Dressage	128 x 128
DX:	Normal			
DS:	NA			
➡ **A:**	Relatively reduced RU in the toe region of the distal phalanx because this bone had a large crena. Compare with Figures 6a, b, d and e.			

N Figure 6d: Solar bone phase image of the RF foot

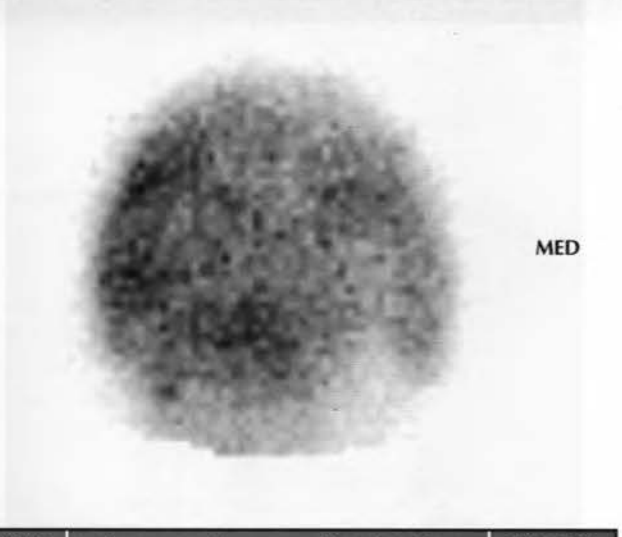

BWB	5y	S	Showjumping	128 x 128
DX:	Normal			
DS:	NA			
Note:	There is diffusely more RU on the lateral side of the distal phalanx and navicular bone compared with medially. Such asymmetry is often seen in horses with chronic foot imbalance, or abnormalities of conformation resulting in uneven loading of the foot. Compare with Figures 6a–c.			

N Figure 6e: Solar bone phase image of the RF foot

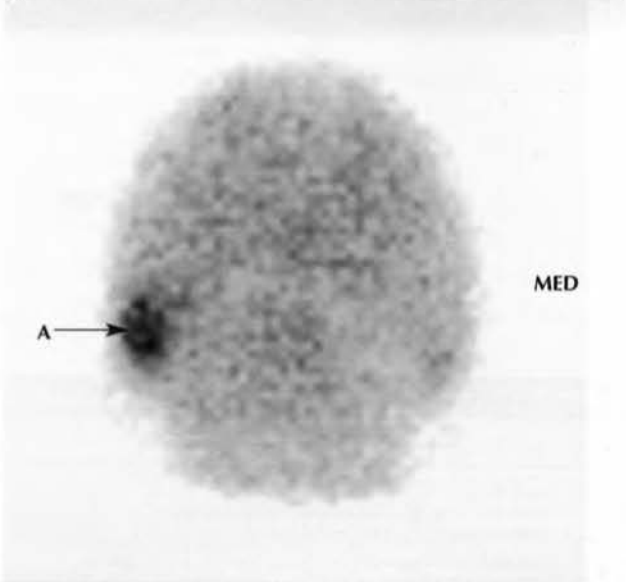

TBxCB	7y	G	General Purpose & Am. Competition	256 x 256
DX:	Normal			
DS:	NA			
➡ **A:**	Focal, moderate IRU in the lateral palmar process of the distal phalanx. This is seen not infrequently as an incidental finding.			

N Figure 7a: Lateral bone phase image of the right radius, carpus and metacarpal region

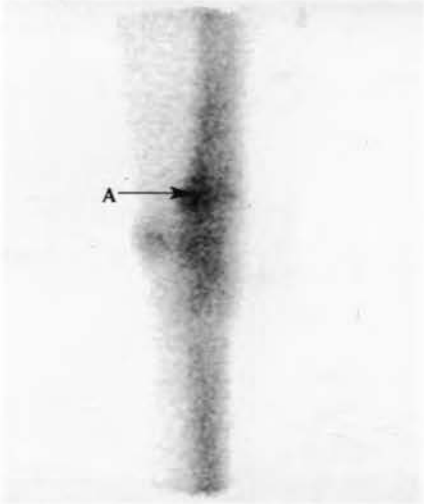

DWB	5y	G	Dressage	256 x 256
DX:	Normal			
DS:	NA			
➡ **A:**	Relatively greater RU in the caudal distal aspect of the radius compared with elsewhere, and in the carpal region relative to the rest of the radius and the metacarpal region. Compare this normal pattern with Figures 7b and c.			

N **Figure 7b: Lateral bone phase image of the right radius, carpal and metacarpal regions**

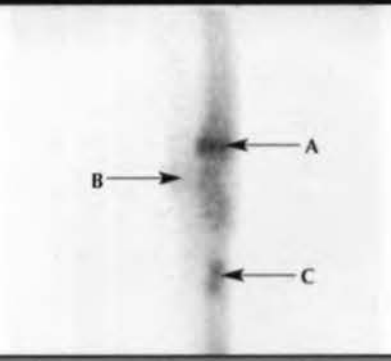

DWB	5y	S	Dressage	256 x 256

DX: Normal

DS: NA

- **A:** There is relatively IRU in the cranial to caudal aspects of the physeal region of the distal aspect of the radius compared to elsewhere.
- **B:** There is reduced radiopharmaceutical activity in the accessory carpal bone compared with elsewhere in the carpus.
- **C:** Note also the region of IRU in the metacarpal region associated with a large, long-standing, apparently quiescent bony exostosis (splint). Splints frequently have increased radiopharmaceutical activity while not being associated with pain.

Note: The same horse as Figure 8b.

N **Figure 7c: Lateral bone phase image of the right radius, carpus and metacarpal regions**

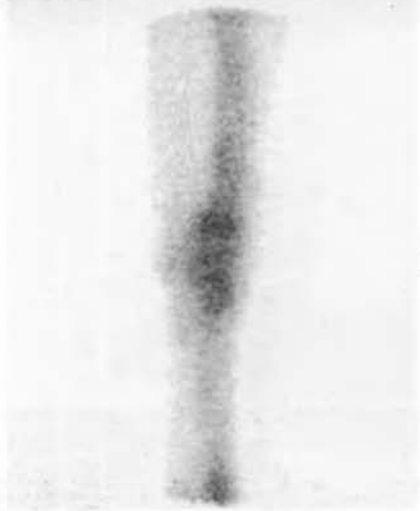

Cob	7y	G	General Purpose	256 x 256

DX: Normal

DS: NA

Note: RU in the carpus and distal aspects of the radius and McIII is similar, but greater than elsewhere. Compare with other normal patterns of radiopharmaceutical activity in younger horses in Figures 7a and b.

N **Figure 8a: Dorsal bone phase image of the carpi**

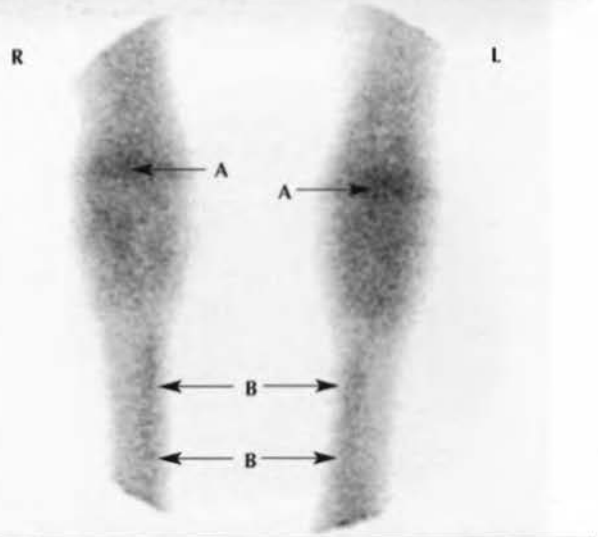

DWB	5y	S	Dressage	256 x 256

DX: Normal

DS: NA

- **A:** Normal, moderate RU in the physeal region of the distal radii (L>R), compared with elsewhere.
- **B:** Note also the greater RU in the medial aspect of the third metacarpal bones, compared with laterally. Compare with Figures 8b and c.

N **Figure 8b(i): Dorsal bone phase image of the distal radii, carpi and metacarpal regions**

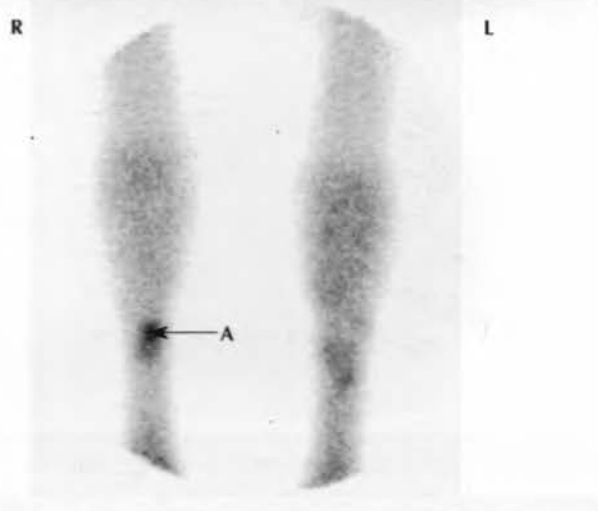

DWB	5y	S	Dressage	256 x 256

DX: Normal

DS: NA

- **A:** Focal, intense IRU in the right McII, corresponding with a long-standing, apparently quiescent splint, unassociated with pain.

Note: The same horse as Figure 7b.

N Figure 8b(ii): Dorsal bone phase image of the distal radii, carpi and metacarpal regions

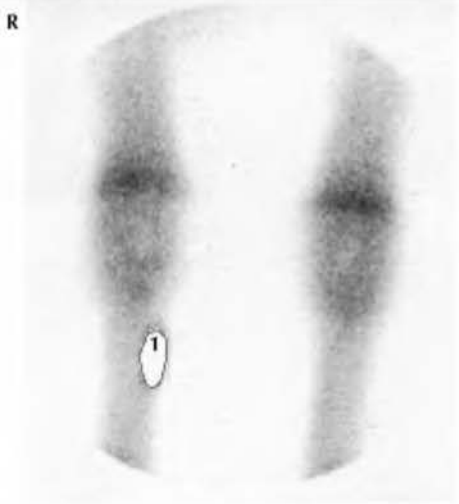

DWB	5y	S	Dressage	256 x 256

DX: Normal

DS: NA

Note: The same horse as Figure 8b(i). After masking out the splint (1), a more normal pattern of RU is seen elsewhere. There is normal greater mild diffuse linear RU in the physeal region of the distal radii. Compare with Figure 8c.

N Figure 8c: Dorsal bone phase image of the carpi

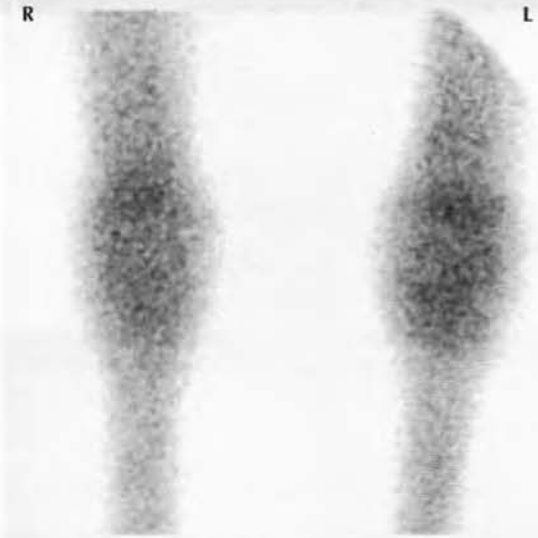

Cob	7y	G	General Purpose	256 x 256

DX: Normal

DS: NA

Note: There is diffuse mild greater RU in the carpi compared with the radii and metacarpal regions. Compare with Figures 8a and b.

N Figure 8d(i): Dorsal bone phase image of the carpi and metacarpal regions

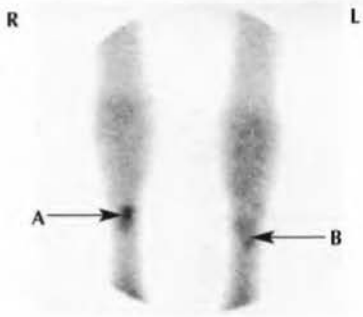

DWB	9y	M	Showjumping	256 x 256

DX: Normal

DS: NA

➔ **A:** Focal intense IRU in the proximal medial aspect of the right McIII, associated with a well-circumscribed area of increased radiopacity proximal to the nutrient foramen of the McIII, typical of an ELL. Compare with Figure 8d(iii).

➔ **B:** Mild, diffuse IRU in the proximal aspect of the left McIII. Compare with Figure 8d(ii).

Note: ELLs have been associated with lameness, but are frequently an incidental finding of no significance, as in this horse. The intense IRU seen in the right McIII should not be confused with IRU associated with a palmar cortical fatigue fracture. Although most stress fractures are sited more proximally, a few occur proximal to the nutrient foramen.

N Figure 8d(ii): Lateral bone phase image of the left carpus and metacarpal region

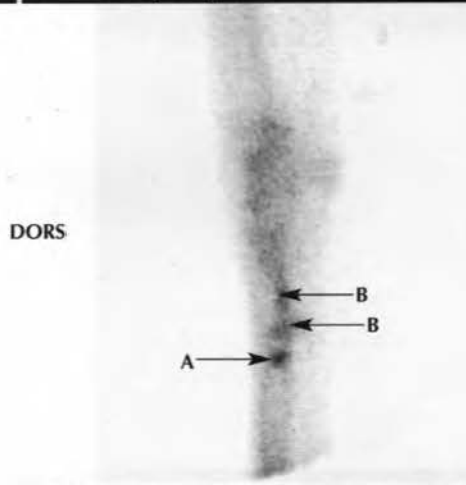

DWB	9y	M	Showjumping	256 x 256

DX: Normal

DS: NA

➔ **A:** Moderate focal IRU in the mid metacarpal region.

➔ **B:** Two regions of mild focal IRU further proximally. Compare with Figure 8d(i).

Note: The same horse as Figures 8d(i) and d(iii). Each of these areas of IRU was associated with a well-circumscribed region of increased radiopacity consistent with an ELL.

N **Figure 8d(iii): Lateral bone phase image of the right carpus and metacarpal region**

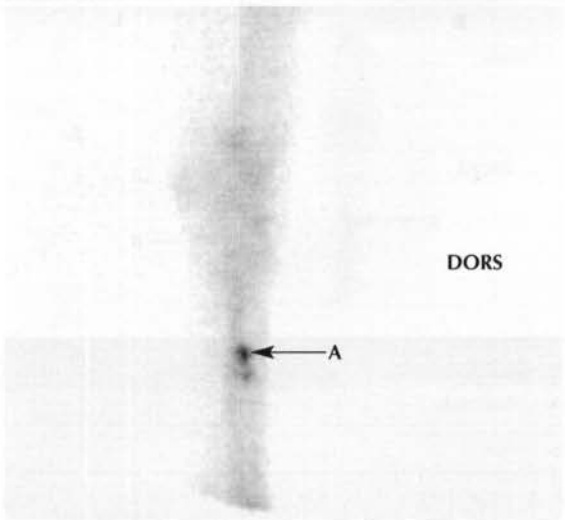

DWB	9y	M	Showjumping	256 x 256

DX: Normal

DS: NA

➔ **A:** The same horse as Figures 8d(i) and d(ii). Note the focal intense IRU in the McIII dorsal to the palmar cortex associated with an ELL. There is relatively reduced radiopharmaceutical activity elsewhere. Compare with Figure 8d(i).

N **Figure 9a(ii): Lateral bone phase image of the left elbow region and sternum**

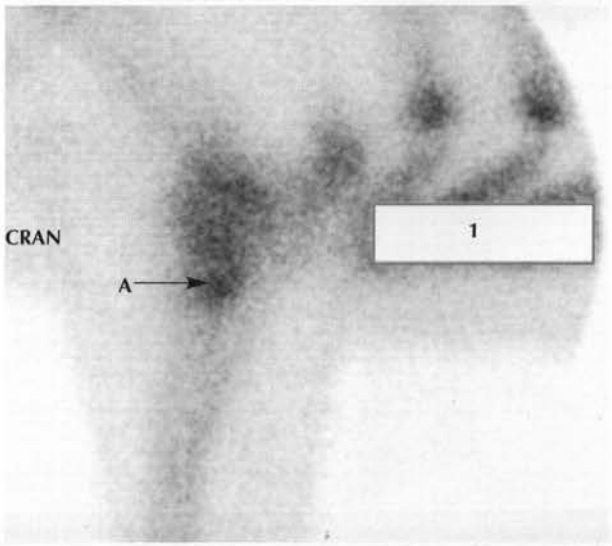

DWB	5y	S	Dressage	256 x 256

DX: Normal

DS: NA

➔ **A:** After masking out the sternum (1), a focal, more intense region of RU is seen in the subchondral bone of the proximal aspect of the radius.

N **Figure 9a(i): Lateral bone phase image of the left elbow region and sternum**

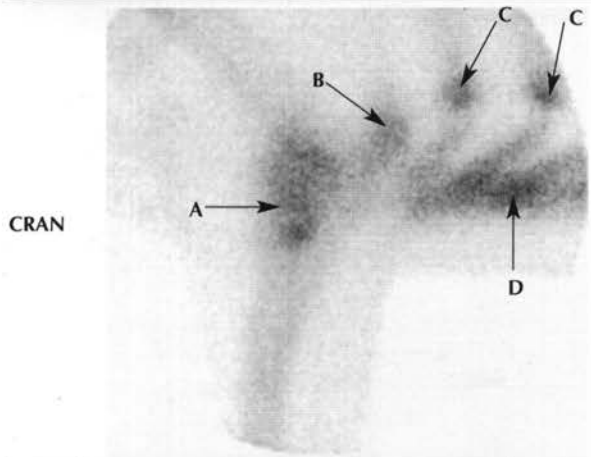

DWB	5y	S	Dressage	256 x 256

DX: Normal

DS: NA

➔ **A:** Diffuse RU in the region of the elbow joint.
➔ **B:** Diffuse RU in the proximal aspect of the olecranon, compared to the radius and humerus.
➔ **C:** Focal RU at the costochondral junctions.
➔ **D:** Diffuse RU in the sternum.
Note: Compare this normal radiopharmaceutical activity with Figure 9b.

N **Figure 9b: Lateral bone phase image of the left elbow region and sternum**

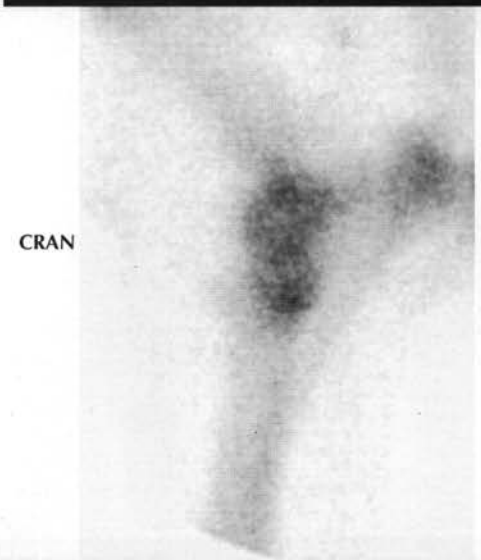

TB	11y	G	Eventing (Adv.)	256 x 256

DX: Normal

DS: NA

Note: Relatively greater RU in the distal humerus and proximal radius compared with Figure 9a. This is a normal pattern of radiopharmaceutical activity.

N **Figure 10a(i): Lateral bone phase image of the caudal neck region and right shoulder**

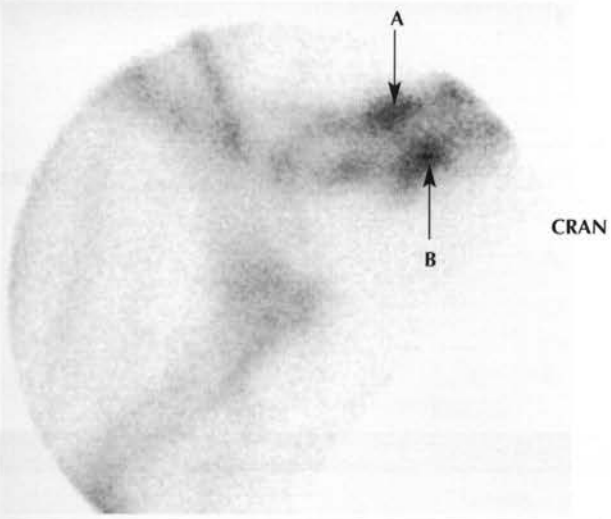

AxW	16y	M	Am. Competition	256 x 256

DX: Normal

DS: NA

➡ **A:** Relatively intense, normal RU in the vertebral arch of the 7th cervical vertebra.
➡ **B:** Relatively intense, normal RU in the vertebral body of the 7th cervical vertebra.

N **Figure 10a(ii): Lateral bone phase image of the caudal neck region and right shoulder**

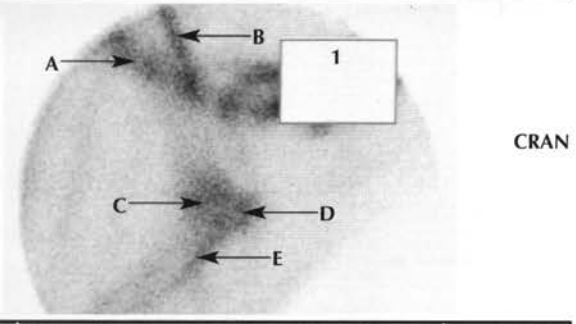

AxW	16y	M	Am. Competition	256 x 256

DX: Normal

DS: NA

➡ **A:** Greater radiopharmaceutical activity in the caudal aspect than elsewhere in the scapula.
➡ **B:** Greater radiopharmaceutical activity in the scapular spine than elsewhere in the scapula.
➡ **C:** Greater radiopharmaceutical activity in the humeral head than elsewhere in the humerus.
➡ **D:** Greater radiopharmaceutical activity in the tubercles than elsewhere in the humerus.
➡ **E:** Greater radiopharmaceutical activity in the deltoid tuberosity than elsewhere in the humerus.
Note: After masking out the 7th cervical vertebra (1), the shoulder region is better defined. Compare this normal pattern of radiopharmaceutical activity with Figures 10b and c.

N **Figure 10b: Lateral bone phase image of the right shoulder region**

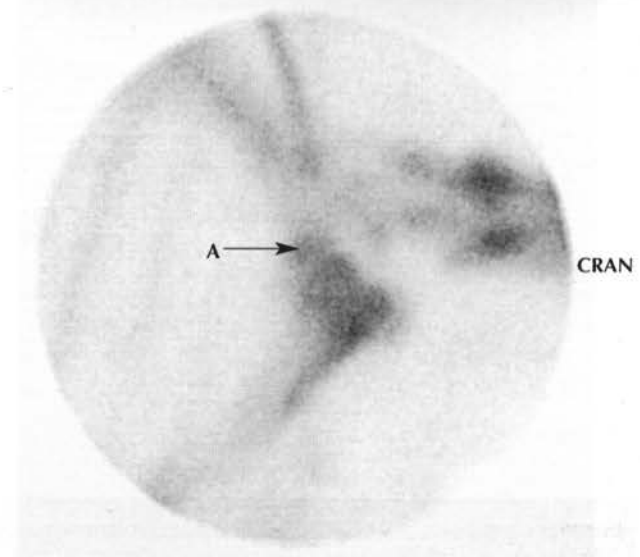

TBx	9y	G	Eventing (Int.)	256 x 256

DX: Normal

DS: NA

➡ **A:** Note the normal IRU in the distal scapula compared with Figures 10a and c.

N **Figure 10c: Lateral bone phase image of the right shoulder region**

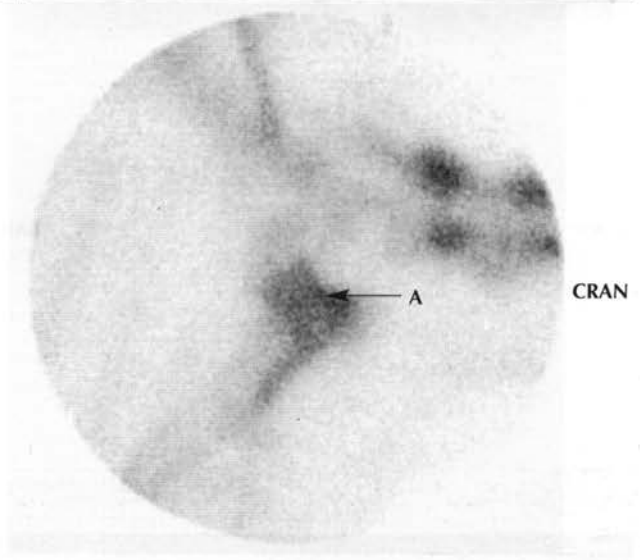

TBx	9y	G	National Hunt Racing	256 x 256

DX: Normal

DS: NA

➡ **A:** Note the normal but relatively greater RU in the cranial aspect of the humeral head compared with Figures 10a and b.

N **Figure 11a: Lateral bone phase image of the right scapula**

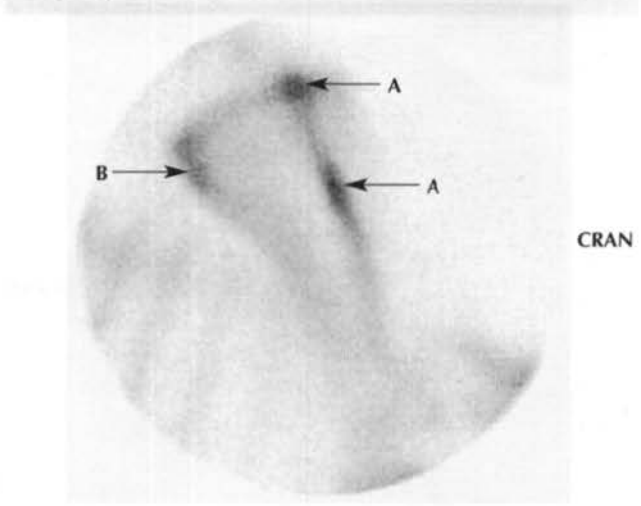

DWB	5y	S	Dressage	256 x 256

DX: Normal

DS: NA

➔ **A:** Normal, focal, intense RU in the proximal and mid aspects of the scapular spine relative to the rest of the bone.
➔ **B:** Mild RU in the caudal angle of the scapula relative to the rest of the bone.
Note: Compare with Figures 11b and c.

N **Figure 11b: Lateral bone phase image of the right scapula**

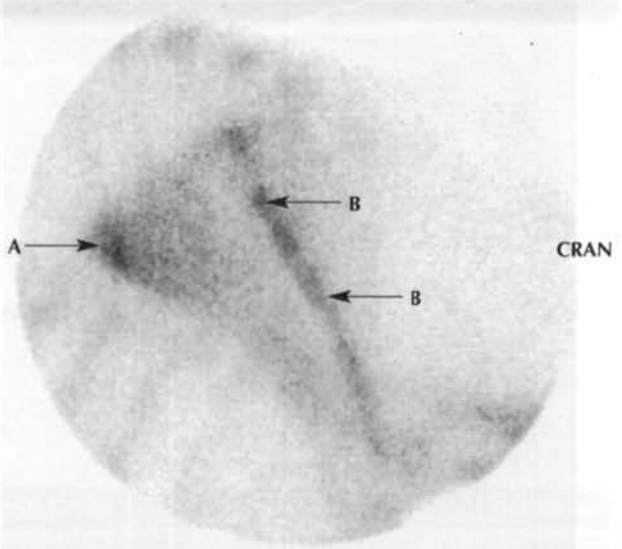

IDxTB	8y	G	Am. Competition	256 x 256

DX: Normal

DS: NA

➔ **A:** Normal, moderate, focal RU in the caudal angle of the scapula.
➔ **B:** Diffuse RU associated with the scapular spine.
Note: Compare with Figures 11a and c.

N **Figure 11c: Lateral bone phase image of the right scapula**

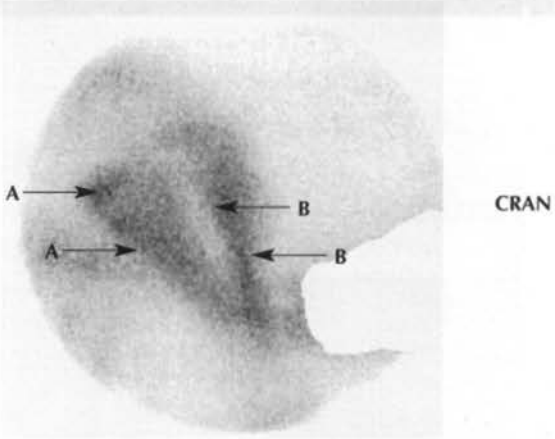

Han.	14y	G	Dressage (Prix St George)	256 x 256

DX: Normal

DS: NA

➔ **A:** Greater radiopharmaceutical activity associated with the caudal aspect of the bone.
➔ **B:** Greater radiopharmaceutical activity associated with the scapular spine.
Note: The caudal cervical vertebrae have been masked out. There is greater diffuse radiopharmaceutical activity in the soft tissues compared with Figures 11a and b. The outline of the scapula is therefore less clear.

N **Figure 12a: Plantar bone phase image of the distal aspect of the hindlimbs**

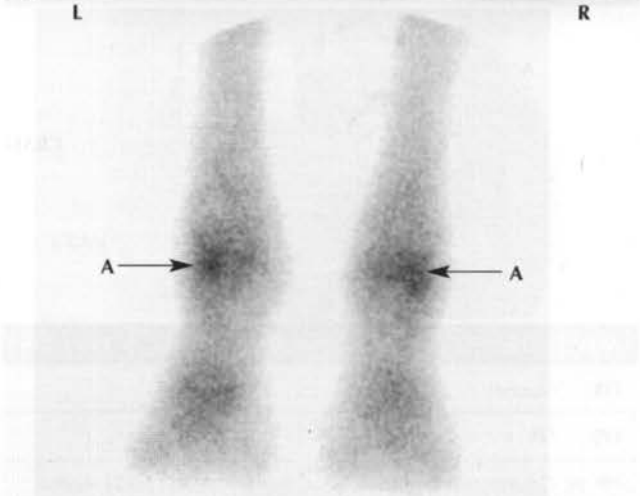

Irish SH	9y	G	Showjumping	256 x 256

DX: Normal

DS: NA

➔ **A:** Normal, focal, moderate RU in the distal lateral aspect of the MtIII and/or lateral proximal sesamoid bone.
Note: Compare with Figures 12b and 13a–c. Many normal horses stand slightly toe-out behind, which positions the lateral plantar aspect of the hind fetlocks closest to the camera.

N **Figure 12b: Plantar bone phase image of the distal aspect of the hindlimbs**

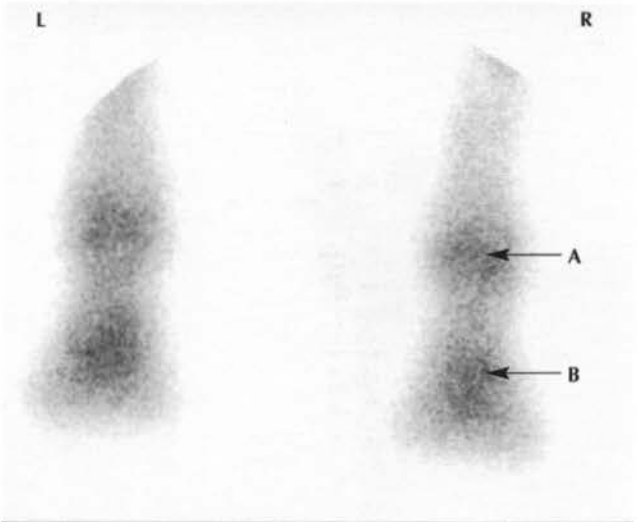

TB	8y	G	Am. Competition	256 x 256

DX: Normal

DS: NA

➔ **A:** Normal, diffuse, moderate greater RU associated with the MTP joint compared with elsewhere.
➔ **B:** Normal, diffuse, moderate greater RU associated with the PIP joint compared with elsewhere.

N **Figure 13b: Lateral bone phase image of the distal aspect of the LH**

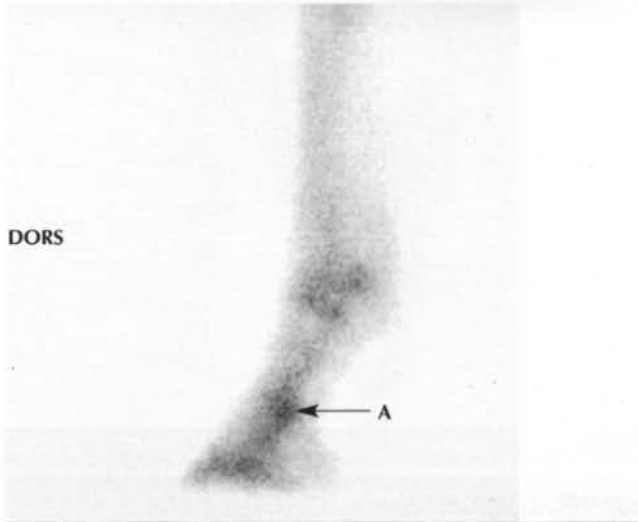

TB	8y	G	Am. Competition	256 x 256

DX: Normal

DS: NA

➔ **A:** Normal, moderate, focal RU in the plantar aspect of the PIP joint, with mild RU in the MTP and PIP joints and the distal phalanx compared with elsewhere.
Note: The same horse as Figure 12b. Compare with Figures 13a and c.

N **Figure 13a: Lateral bone phase image of the distal aspect of the LH**

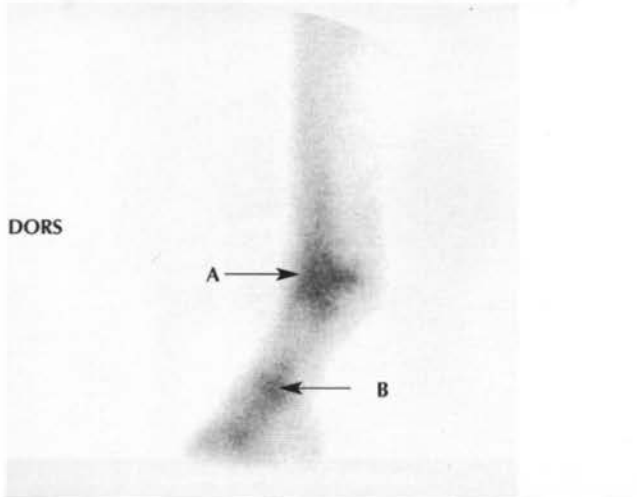

Irish SH	9y	G	Showjumping	256 x 256

DX: Normal

DS: NA

➔ **A:** Normal, moderate, diffuse RU associated with the subchondral bone of the distal aspect of the MtIII and the proximal aspect of the proximal phalanx and in the proximal sesamoid bones.
➔ **B:** Mild, diffuse RU associated with the PIP joint.
Note: The same horse as Figure 12a.

N **Figure 13c: Lateral bone phase image of the distal aspect of the LH**

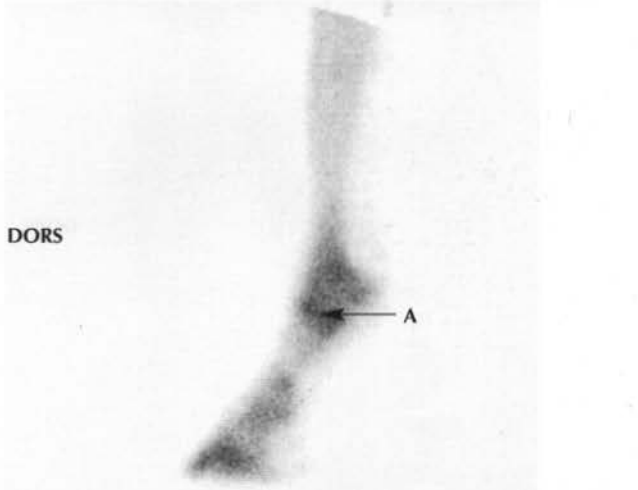

TB	6y	G	Eventing (Int.)	256 x 256

DX: Normal

DS: NA

➔ **A:** Normal, moderate, focal RU in the proximal subchondral bone of the proximal phalanx. Radiopharmaceutical activity is greater in the MTP joint and distal phalanx compared with elsewhere. Compare with Figures 13a and b.

N Figure 14a: Lateral bone phase image of the right hock

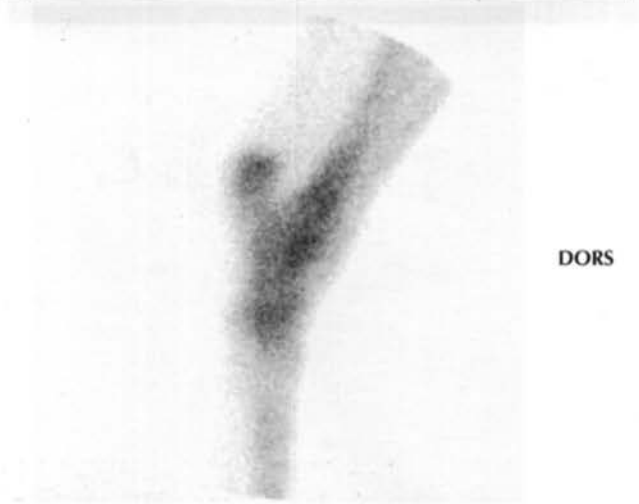

TB	10y	G	Hunting & Am. Competition	256 x 256

DX: Normal

DS: NA

Note: Normal, diffuse, mild increased radiopharmaceutical activity associated with the entire hock region compared with the tibial diaphysis and the metatarsal region. Radiopharmaceutical activity is slightly greater in the dorsal aspect of the talus, compared with elsewhere in the hock. Compare with Figures 14b and c.

N Figure 14b: Lateral bone phase image of the right hock

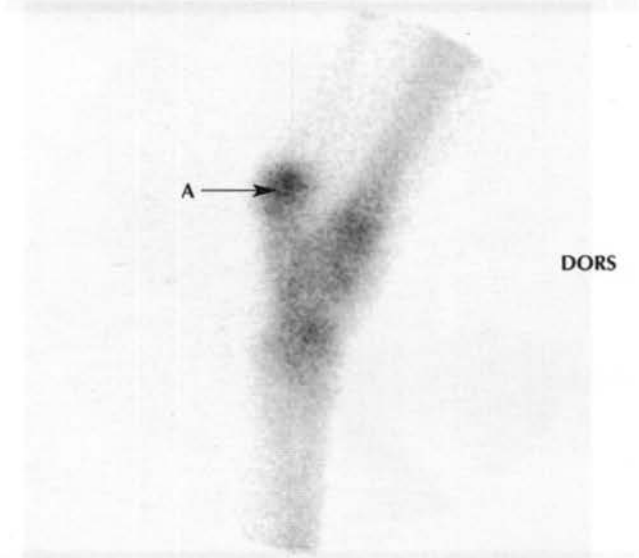

TB	10y	G	Eventing (Adv.)	256 x 256

DX: Normal

DS: NA

➔ **A:** Normal mild, diffuse RU associated with the entire hock region, with normal moderate focal greater RU in the tuber calcanei. Compare with Figures 14a and c.

N Figure 14c: Lateral bone phase image of the right hock

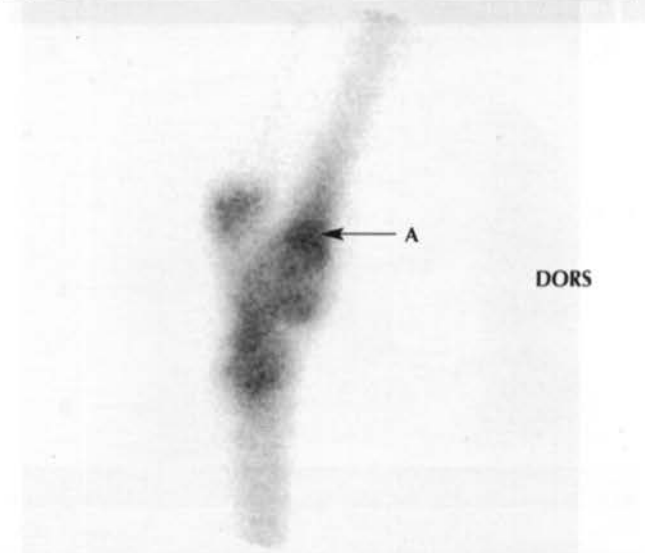

TB	6y	G	Eventing (Int.)	256 x 256

DX: Normal

DS: NA

➔ **A:** Normal, mild, diffuse RU associated with the entire hock region, with normal greater moderate focal RU in the subchondral bone of the distal tibia. Compare with Figures 14a and b.

N Figure 15a: Plantar bone phase image of both hocks

TB	10y	G	Hunting & Am. Competition	256 x 256

DX: Normal

DS: NA

Note: Normal, mild, diffuse greater RU in the entire hock region. Activity appears greatest in the tubera calcanei, which tend to be positioned closest to the gamma camera. Many horses stand toe-out, so the tuber calcanei may appear more medially positioned than expected because of rotation of the limb. The same horse as Figure 14a. Compare with Figures 15b and c.

N Figure 15b: Plantar bone phase image of both hocks

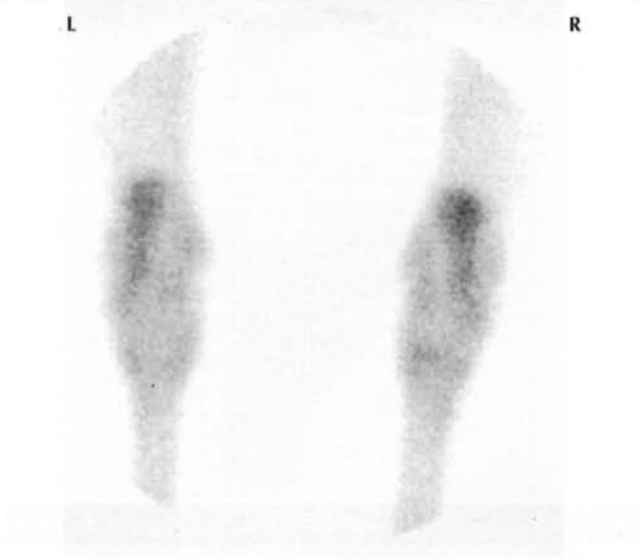

TB	10y	G	Eventing (Adv.)	256 x 256

DX: Normal

DS: NA

Note: Normal, mild, diffuse RU in the entire hock region, which is slightly greater in the tubera calcanei. The same horse as Figure 14b. Compare with Figures 15a and c.

N Figure 15c: Plantar bone phase image of both hocks

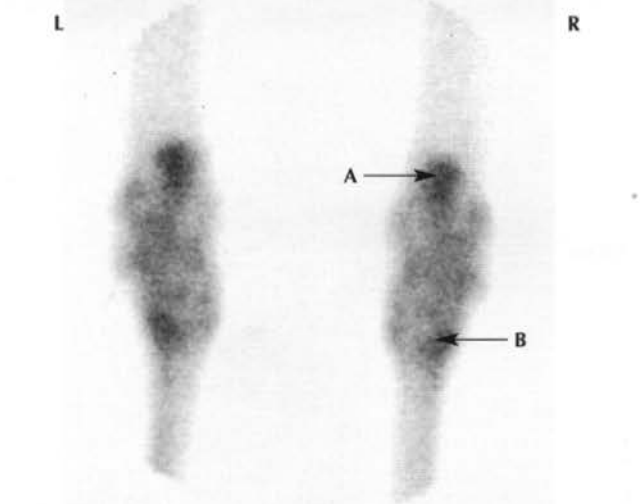

TB	6y	G	Eventing (Int.)	256 x 256

DX: Normal

DS: NA

➡ **A:** Normal, mild, diffuse greater RU in the entire hock region, with normal moderate focal RU in each tuber calcanei.
➡ **B:** Normal moderate focal RU in the distal lateral aspect of each hock/proximal metatarsal region.
Note: The same horse as Figure 14c. Compare with Figures 15a and b.

N Figure 15d(i): Plantar bone phase image of both hocks

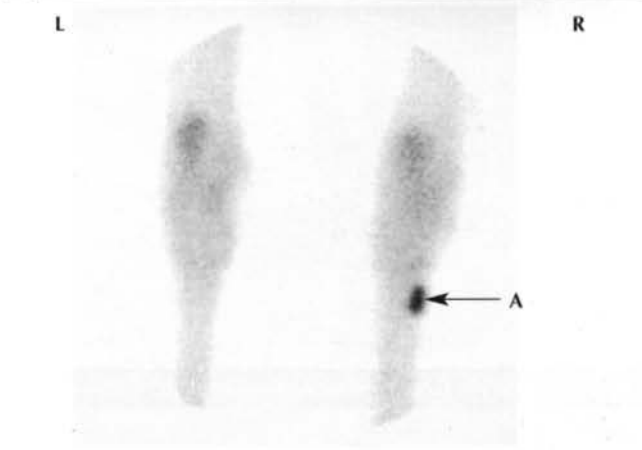

IDxTB	12y	G	Showjumping & Eventing	256 x 256

DX: Normal

DS: NA

➡ **A:** Normal focal intense IRU associated with a large exostosis (a splint) involving the right 4th and 3rd metatarsal bones. The exostosis was long-standing, cold and apparently inactive. However, typically such exostoses have focal intense IRU.
Note: Relatively, the rest of the hock region has reduced radiopharmaceutical activity. Compare with Figures 15d(ii) and d(iii).

N Figure 15d(ii): Plantar bone phase image of both hocks

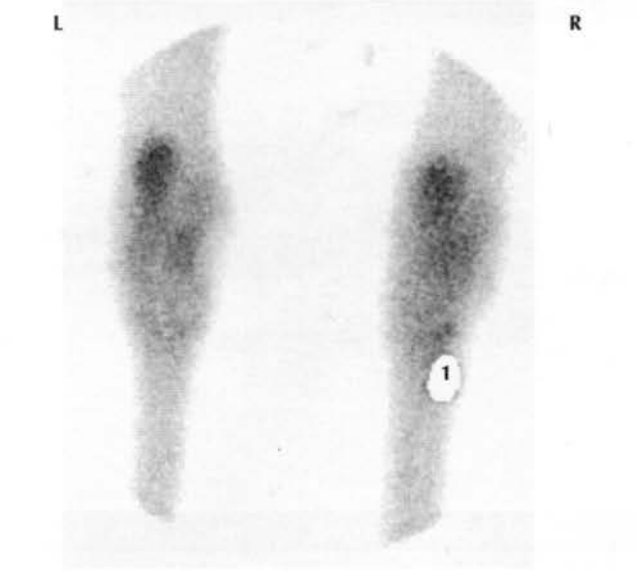

IDxTB	12y	G	Showjumping & Eventing	256 x 256

DX: Normal

DS: NA

Note: The same image as Figure 15d(i) after masking out the splint (1). A more normal pattern of radiopharmaceutical activity is now seen in the hock region.

N **Figure 15d(iii): Lateral bone phase image of the right hock**

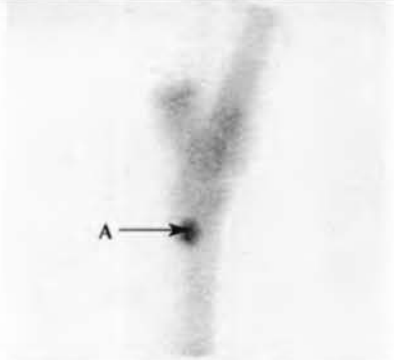

IDxTB	12y	G	Eventing & Showjumping	256 x 256

DX: Normal

DS: NA

➔ **A:** Focal, intense IRU associated with the bony exostosis on the MtIII and MtIV that results in apparently reduced radiopharmaceutical activity elsewhere in the hock region.

Note: Same horse as in Figures 15d(i) and d(ii). This focal intense IRU should not be confused with that due to enthesopathy of the suspensory ligament, or a primary stress-induced injury of the MtIII. In the plantar view, the area of IRU is sited more laterally than IRU associated with these injuries (see Abnormals, Figures 11 and 12). The results of scintigraphic examination must always be correlated with those of clinical examination; this horse had an obvious lateral splint.

N **Figure 16b: Lateral bone phase image of the left stifle**

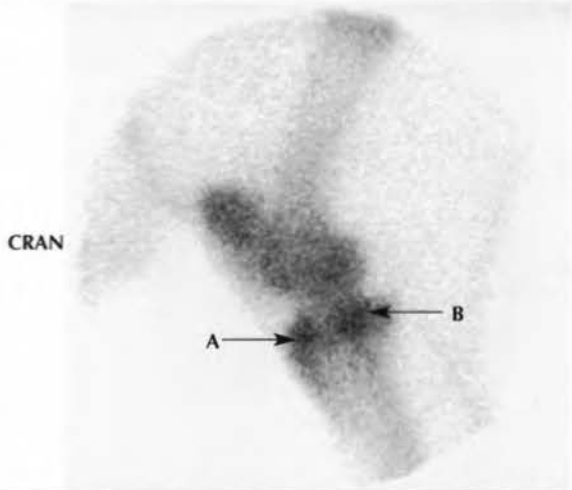

DWB	8y	S	Showjumping (International)	256 x 256

DX: Normal

DS: NA

➔ **A:** Normal focal, moderate RU in the cranial aspect of the tibial plateau.

➔ **B:** Normal focal, moderate RU in the caudal aspect of the tibial plateau.

Note: Normal, diffuse, mild greater RU associated with the entire stifle region than elsewhere. Compare with Figures 16a and c.

N **Figure 16a: Lateral bone phase image of the left stifle**

Han.x	11y	M	Am. Competition	256 x 256

DX: Normal

DS: NA

Note: Normal, mild, diffuse greater RU associated with the stifle joint compared to elsewhere. Compare with Figures 16b and c.

N **Figure 16c: Lateral bone phase image of the left stifle**

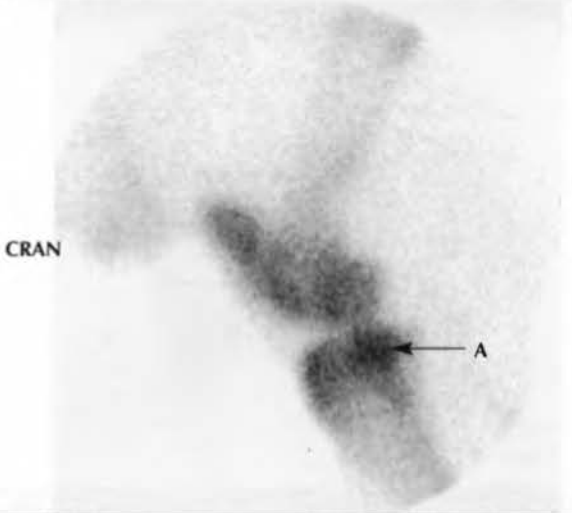

TB	8y	G	Eventing (Int.)	256 x 256

DX: Normal

DS: NA

➔ **A:** Greater focal moderate normal RU in the caudal aspect of the tibial plateau.

Note: Normal, mild, diffuse RU associated with the entire stifle region. Compare with Figures 16a and b. Sometimes there is focal, moderate greater RU in only the cranial aspect of the tibial plateau.

N Figure 16d: Caudal bone phase image of the left stifle

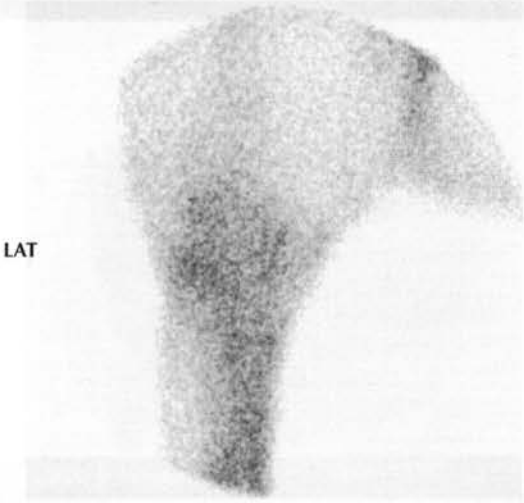

TB	7y	G	Dressage (Med.)	256 x 256

DX: Normal

DS: NA

Note: Normal radiopharmaceutical activity acquired over a 2 min acquisition resulting in only 120,656 counts; definition of the bones is rather poor because of the low total count caused by the distance between the gamma camera and the bones, and the overlying soft tissues having a shielding effect. Compare with Figure 16e.

N Figure 16e: Caudal bone phase image of the left stifle

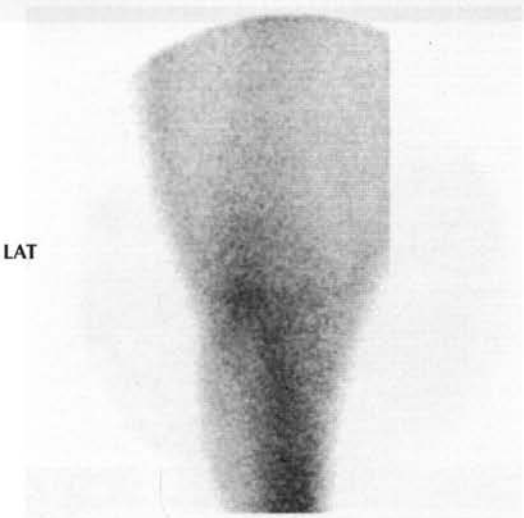

Trak.	7y	G	Dressage	256 x 256

DX: Normal

DS: NA

Note: Acquired over 3 min to achieve a total count of 373,671. There is generalised increased radiopharmaceutical activity compared with Figure 16d, but the shielding effect of muscle and the distance from the camera still results in poor definition of the bones and stifle joint.

N Figure 17a: Lateral bone phase image of the left CF joint

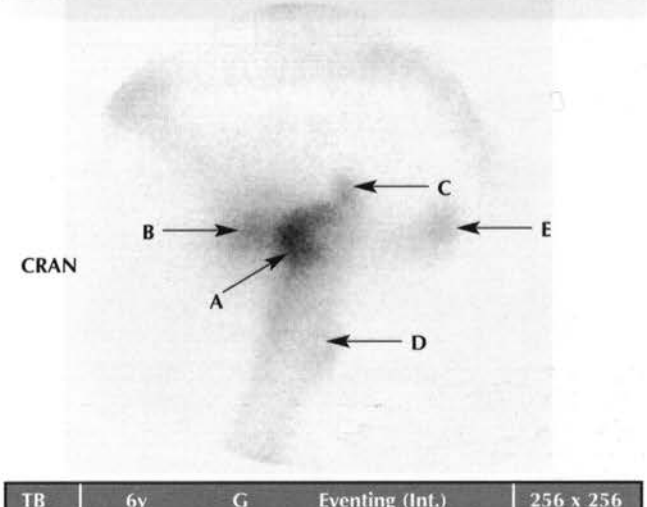

TB	6y	G	Eventing (Int.)	256 x 256

DX: Normal

DS: NA

➡ **A:** Normal, moderate, focal radiopharmaceutical activity in the region of the femoral head superimposed on the acetabulum.
➡ **B:** Mild activity in the pubis.
➡ **C:** Mild activity in the greater trochanter of the femur.
➡ **D:** Mild activity in the third trochanter of the femur.
➡ **E:** Mild activity in the ischium.
Note: Compare with Figure 17b.

N Figure 17b: Lateral bone phase image of the left CF joint

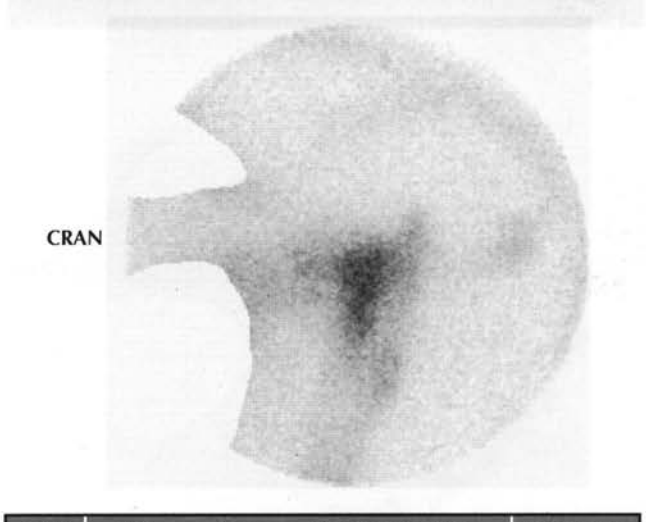

BWB	10y	M	Am. Competition	256 x 256

DX: Normal

DS: NA

Note: The distribution of radiopharmaceutical activity in the bones is similar to Figure 17a, but there is relatively greater activity in the soft tissues of this bigger-muscled, fatter horse; therefore, definition of the bone margins is less clear. Radioactivity in the bladder can confound interpretation if the bladder is superimposed.

N **Figure 18a(i): Right lateral oblique bone phase image of the cranial thoracic vertebrae (T2–T12)**

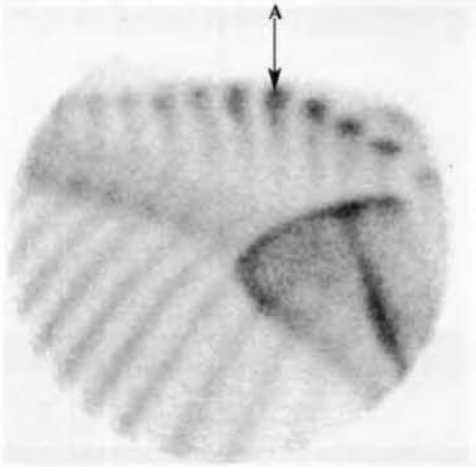

GWB	6y	S	Dressage	256 x 256

DX: Normal

DS: NA

➔ **A:** Summit of the DSP of T6.
Note: Normal, moderate, focal greater RU associated with the summits of theDSPs of the 3rd to 8th thoracic vertebrae. This and the intense radiopharmaceutical activity in focal regions of the scapula result in rather poor definition of the vertebral bodies and facet joints. Compare with Figure 18a(ii).

N **Figure 18a(ii): Right lateral oblique bone phase image of the cranial thoracic vertebrae (T2–T12)**

GWB	6y	S	Dressage	256 x 256

DX: Normal

DS: NA

Note: The summits of the DSPs of T3–T6 and the scapula have been masked out (1). There is now much better definition of the more ventral aspects of the DSPs, vertebral bodies and ribs compared with Figure 18a(i).

N **Figure 18b(i): Right lateral oblique bone phase image of the caudal thoracic vertebrae (T10–L1)**

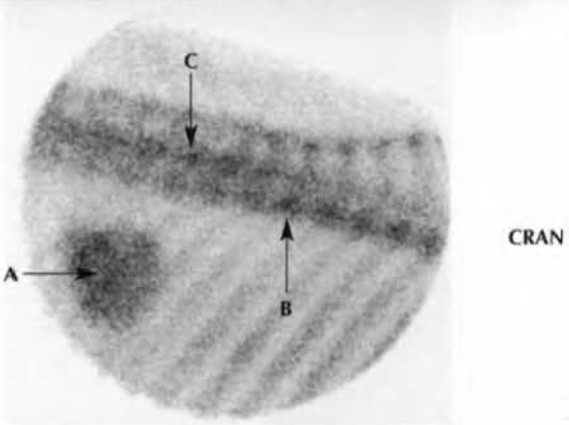

GWB	6y	S	Dressage	256 x 256

DX: Normal

DS: NA

➔ **A:** Moderate, normal radiopharmaceutical activity associated with the kidney.
➔ **B:** Radiopharmaceutical activity associated with the vertebral bodies tends normally to be greatest in the mid thoracic region.
➔ **C:** Activity associated with the facet joints increases in the caudal thoracic region.
Note: Spacing of the DSPs and mild increased radiopharmaceutical activity in the summits of the DSPs.

N **Figure 18b(ii): Right lateral oblique bone phase image of the caudal thoracic vertebrae (T10–L1)**

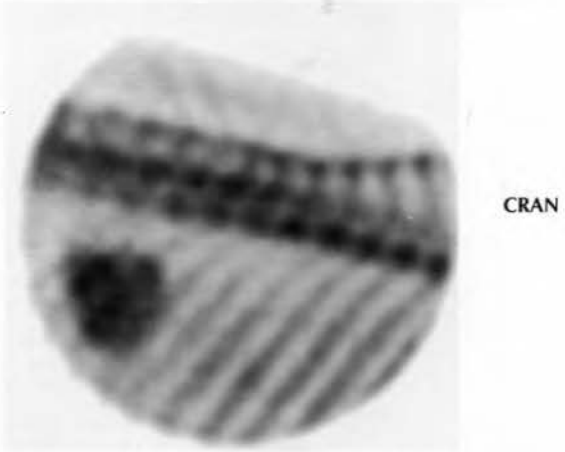

GWB	6y	S	Dressage	256 x 256

DX: Normal

DS: NA

Note: The same image as Figure 18b(i) after application of a high resolution filter. This smoothes the image and makes anatomical resolution easier.

N Figure 18c(i): Right lateral oblique bone phase image of the caudal thoracic and lumbar vertebrae

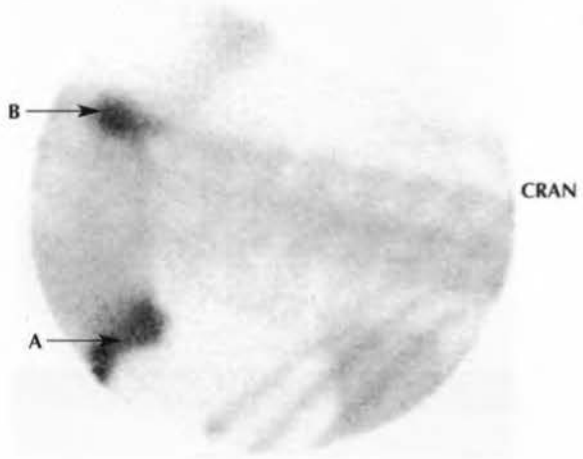

GWB	6y	S	Dressage	256 x 256

DX: Normal

DS: NA

➔ **A:** Normal, focal, intense RU associated with the right tuber coxae.
➔ **B:** Normal, focal, intense RU associated with the tuber sacrale.
Note: This results in rather poor definition of the vertebrae and ribs.

N Figure 18c(ii): Right lateral oblique bone phase image of the caudal thoracic and lumbar vertebrae

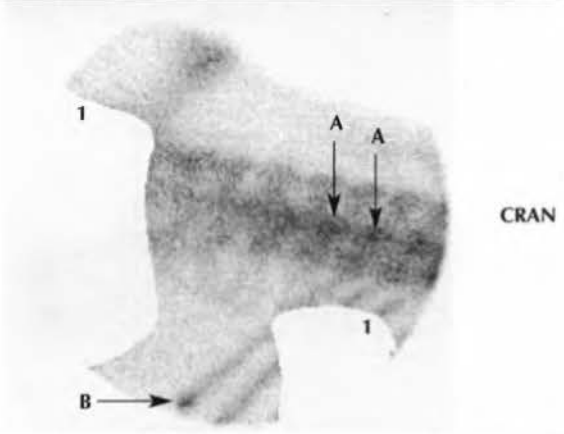

GWB	6y	S	Dressage	256 x 256

DX: Normal

DS: NA

➔ **A:** Radiopharmaceutical activity associated with the facet joints is normally greatest at the thoracolumbar junction and declines caudally.
➔ **B:** Normal mild focal greater RU at the most distal aspect of the 18th rib.
Note: The same image as Figure 18c(i) after masking out the tubera coxae and sacrale and the kidney (1). Note the improved definition of the thoracolumbar vertebrae and the ribs.

N Figure 19a: Right lateral bone phase images of the thoracic vertebrae (T11–L1)

Irish SH	7y	G	Eventing	256 x 256

DX: Normal

DS: NA

Note: Normal, focal, moderate radiopharmaceutical activity associated with the kidney, more intense where the kidney and ribs are superimposed. Compare with Figures 18b(i) and b(ii). This results in rather poor definition of the vertebrae.

N Figure 19b: Right lateral bone phase images of the thoracic vertebrae (T11–L1)

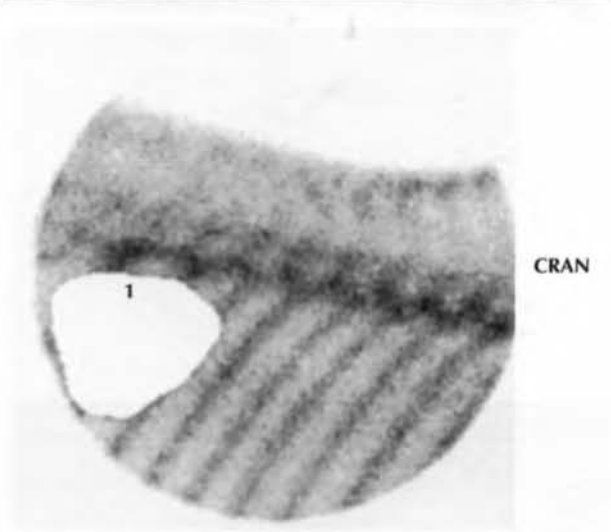

Irish SH	7y	G	Eventing	256 x 256

DX: Normal

DS: NA

Note: The same image as Figure 19a after masking out the kidney (1). Definition of the vertebrae is much improved compared with Figure 19a.

N **Figure 20a(i): Left lateral bone phase image of the cranial cervical vertebrae (C1–C3) and caudal aspect of the head**

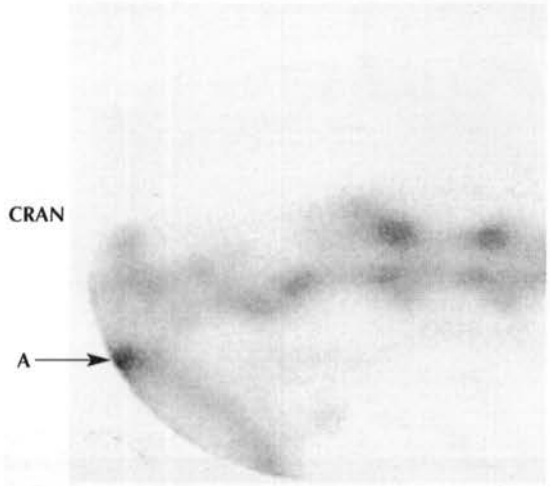

GWB	6y	S	Dressage	256 x 256
DX:	Normal			
DS:	NA			
➔ **A:**	Normal, focal, intense radiopharmaceutical activity associated with the left temporomandibular joint. This makes definition of the cervical vertebrae rather poor. Compare with Figures 20a(ii) and b.			

N **Figure 20b: Left lateral bone phase image of the cranial cervical vertebrae**

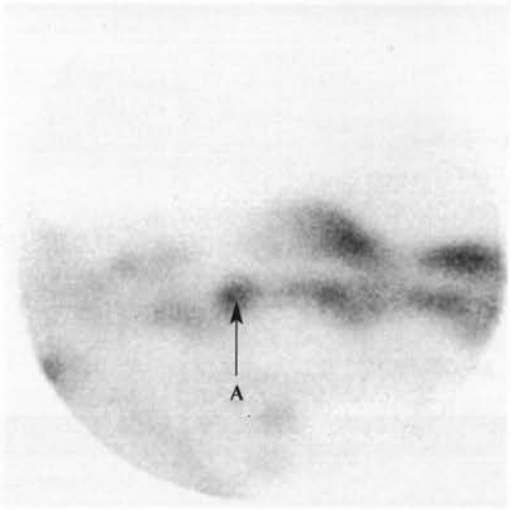

IDxTB	15y	G	Am. Competition	256 x 256
DX:	Normal			
DS:	NA			
➔ **A:**	Normal, moderate IRU associated with the odontoid peg of the 2nd cervical vertebra (the axis). Compare with Figure 20a(ii).			

N **Figure 20a(ii): Left lateral bone phase image of the cranial cervical vertebrae (C1–C3) and caudal aspect of the head**

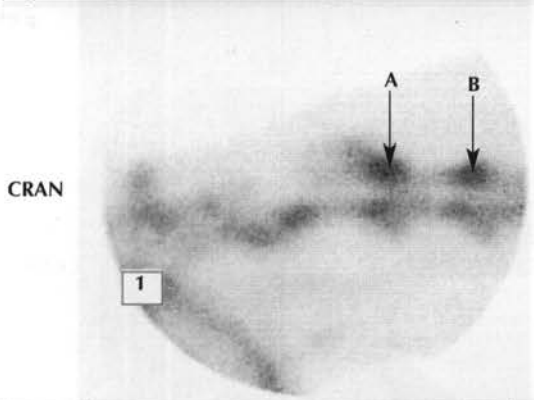

GWB	6y	S	Dressage	256 x 256
DX:	Normal			
DS:	NA			
➔ **A:**	Normal, moderate increased radiopharmaceutical activity associated with the dorsal aspect of the 2nd cervical vertebra compared to ventrally.			
➔ **B:**	Normal, moderate increased radiopharmaceutical activity associated with the dorsal aspect of the 3rd cervical vertebra compared to ventrally.			
Note:	The same image as Figure 20a(i) after masking out the temporomandibular joint (1). There is much better definition of the soft tissues of the neck and the cervical vertebrae. Compare also with Figure 20b.			

N **Figure 20c: Left lateral bone phase image of the mid to caudal cervical vertebrae (C3–C7)**

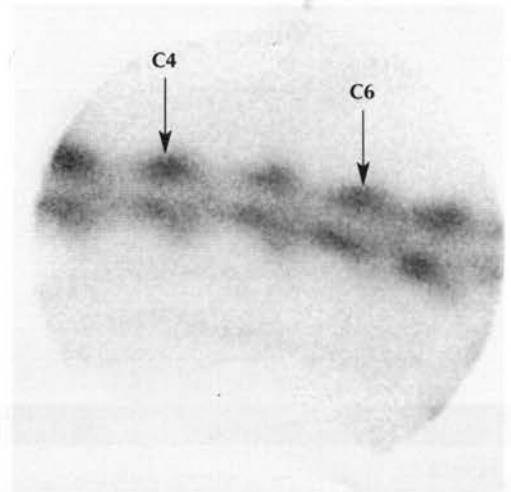

GWB	6y	S	Dressage	256 x 256
DX:	Normal			
DS:	NA			
Note:	Normal, relatively less RU in the 4th to 6th vertebrae compared to more cranially or caudally.			

N Figure 20d: Left lateral bone phase image of the caudal cervical (C5–C7) and cranial thoracic vertebrae

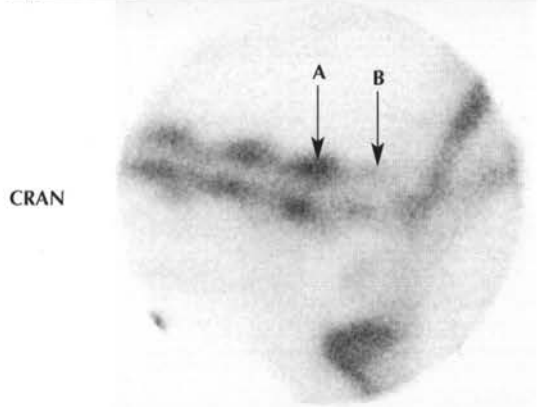

GWB	6y	S	Dressage	256 x 256

DX: Normal

DS: NA

- **A:** Normal, moderate, focal greater radiopharmaceutical activity associated with the dorsal aspect and vertebral body of the 7th cervical vertebrae.
- **B:** Apparently normal reduced radiopharmaceutical activity associated with the 1st thoracic vertebra compared to the cervical vertebrae, in part due to the thickness of the overlying soft tissues.

Note: The scapula is superimposed over the more caudal thoracic vertebrae.

N Figure 21a: Dorsal bone phase image of the pelvic region

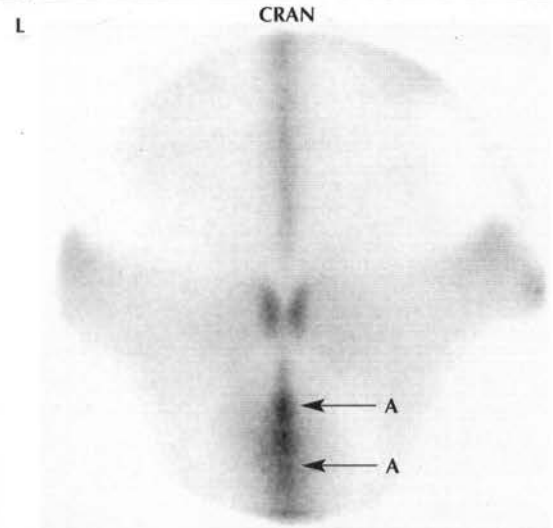

GWB	6y	S	Dressage	256 x 256

DX: Normal

DS: NA

- **A:** Region of normal, moderate, diffuse IRU caudally due to superimposition of radioactivity in the bladder over the sacrococcygeal spine. This results in apparently reduced radiopharmaceutical activity elsewhere in the pelvic region. Compare with Figure 21b.

N Figure 21b: Dorsal bone phase image of the pelvic region

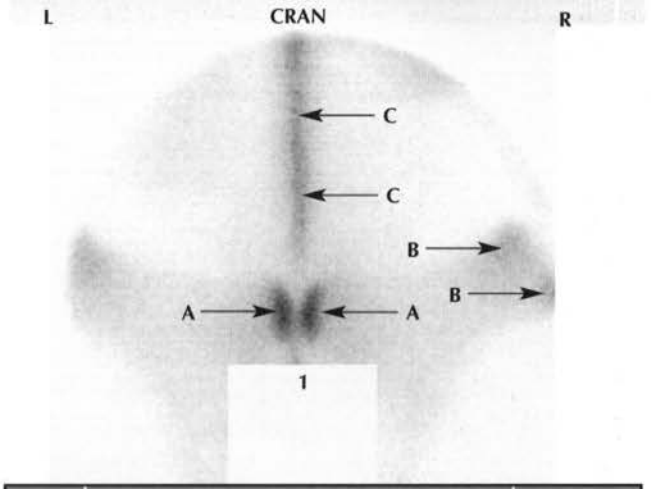

GWB	6y	S	Dressage	256 x 256

DX: Normal

DS: NA

- **A:** Normal, moderate, focal RU associated with the superficially positioned tubera sacrale.
- **B:** Normal, mild, focal radiopharmaceutical activity associated with the right tuber coxae.
- **C:** Normal, mild, focal radiopharmaceutical activity associated with the lumbar vertebrae.

Note: The same image as Figure 21a after masking out the bladder (1).

N Figure 21c: Dorsal bone phase image of the pelvis after masking out the bladder and caudal sacrum

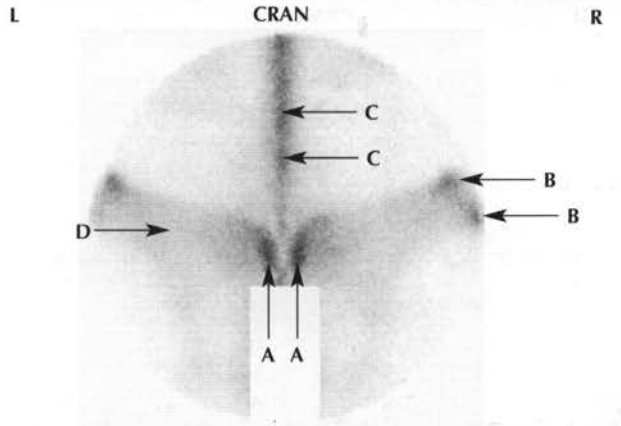

Conn.xA	10y	G	Showjumping (International)	256 x 256

DX: Normal

DS: NA

- **A:** Normal, moderate, focal RU associated with the superficially located tubera sacrale.
- **B:** Normal, moderate, focal RU associated with the right tuber coxae.
- **C:** Normal, moderate, focal RU associated with the lumbar vertebrae.
- **D:** Normal, mild, diffuse RU associated with the sacroiliac joint regions.

N **Figure 22a: Caudal oblique bone phase image of the tubera ischii**

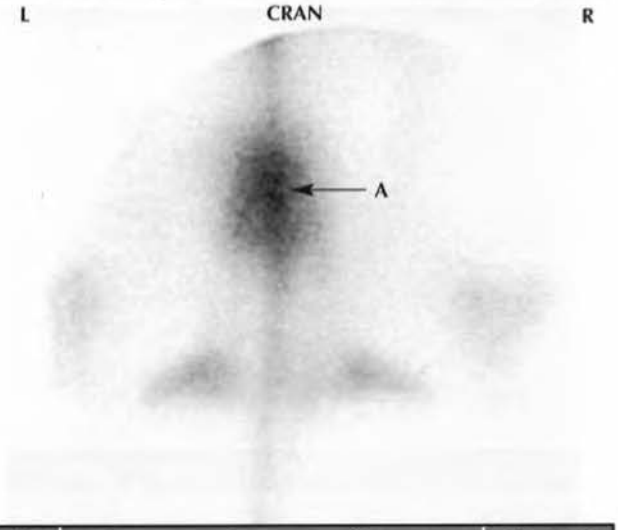

GWB	6y	S	Dressage	256 x 256

DX: Normal

DS: NA

➔ **A:** Normal, intense RU associated with radioactivity in the bladder, resulting in apparently relatively reduced radiopharmaceutical activity elsewhere in the pelvis. Compare with Figure 22b.

N **Figure 22b: Caudal oblique bone phase image of the tubera ischii**

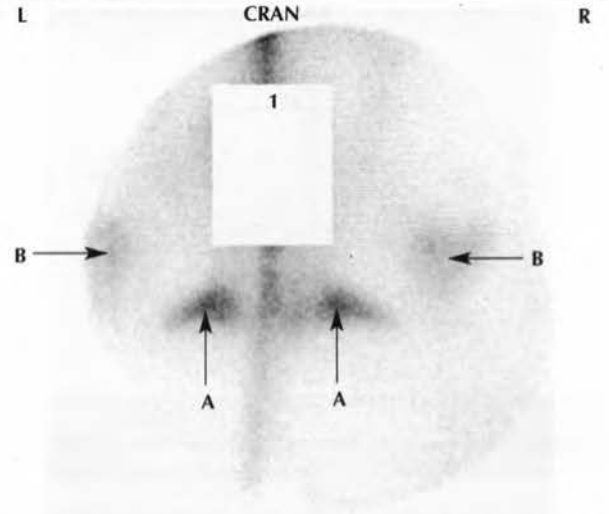

GWB	6y	S	Dressage	256 x 256

DX: Normal

DS: NA

➔ **A:** The left and right tubera ischii are now clearly defined.
➔ **B:** Mild radiopharmaceutical activity is also seen associated with the left and right CF joints.
Note: The same image as Figure 22a after masking the bladder (1).

N **Figure 23a: Dorsal bone phase image of the head**

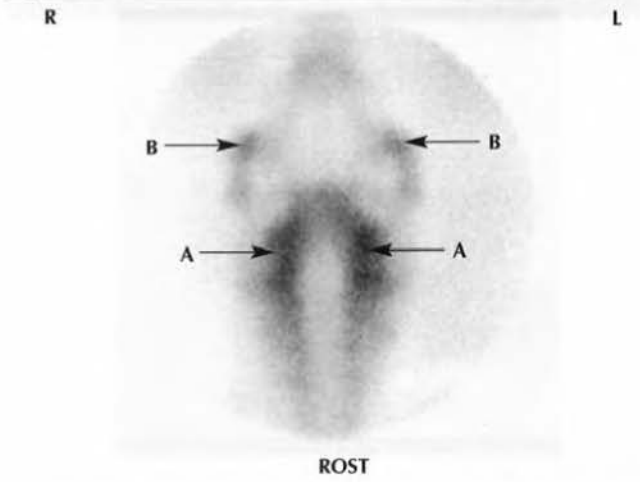

GWB	6y	S	Dressage	256 x 256

DX: Normal

DS: NA

➔ **A:** Moderate, normal, diffuse increased radiopharmaceutical activity associated with the caudal aspect of the tooth arcades.
➔ **B:** Normal, mild, focal radiopharmaceutical activity associated with the left and right temporomandibular joints, which are symmetrical. Compare with Figure 23b.

N **Figure 23b: Left lateral bone phase image of the head**

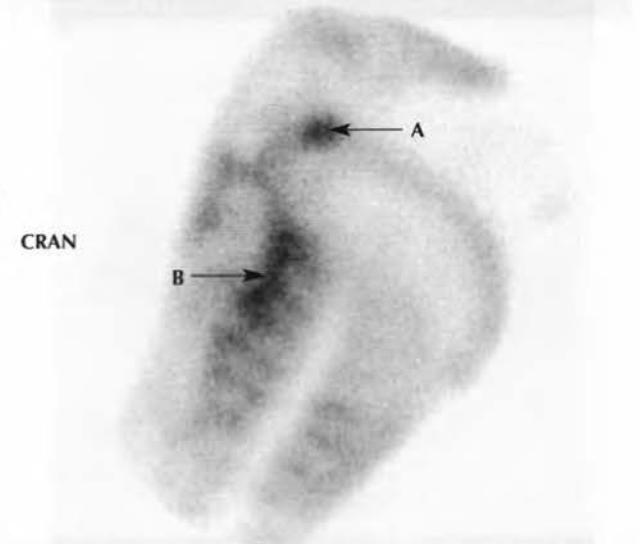

GWB	6y	S	Dressage	256 x 256

DX: Normal

DS: NA

➔ **A:** Normal, focal, intense greater RU associated with the temporomandibular joint.
➔ **B:** Normal, diffuse, intense RU associated with the caudal aspect of the upper tooth arcade.

ABNORMAL HORSES

A Figure 1a: Solar (palmar) bone phase image of the LF foot

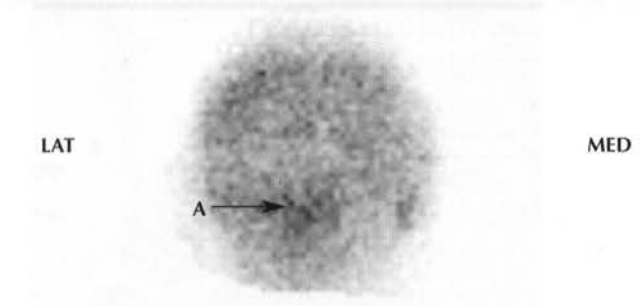

Irish	6y	G	Showjumping	128 x 128

DX: Navicular disease.

DS: Results of local analgesia: perineural analgesia of the palmar digital nerves or intrathecal analgesia of the navicular bursa eliminated lameness; intra-articular analgesia of the DIP joint resulted in 60% improvement in lameness. Radiography and ultrasonography: negative results. Magnetic resonance imaging: abnormal bright signal in navicular bone in fat-suppressed images.

Mild bilateral forelimb lameness, LF>RF.
➔ **A:** Mild, focal IRU in the navicular bone. Radiopharmaceutical activity in the navicular bone 113% more than the peripheral regions of the distal phalanx; radiopharmaceutical activity in focal region 132% more than the peripheral regions of the distal phalanx.
Note: Image acquired as 256 x 256 and then zoomed.

A Figure 1b: Solar bone phase image of the LF foot

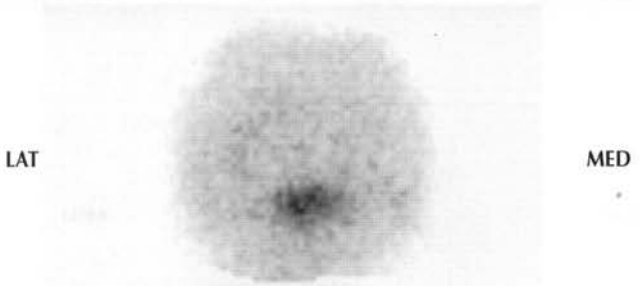

TBx	10y	G	Eventing	128 x 128

DX: Navicular disease.

DS: Results of local analgesia: perineural analgesia of the palmar digital nerves resulted in mild improvement in lameness; lameness eliminated by palmar (abaxial sesamoid) nerve blocks; moderate improvement in lameness within 5 mins of intra-articular analgesia of the DIP joint. Radiography: subtle, poorly defined radiolucent zone in the centre of the navicular bone seen in dorsoproximal-palmarodistal oblique views only; no abnormality detected in palmaroproximal-palmarodistal oblique views. Magnetic resonance imaging: large cavity in centre of navicular bone penetrating the flexor cortex, with evidence of fluid accumulation in the bone and some mineralisation. Irregular surface of the opposing surface of the deep digital flexor tendon.

Severe LF lameness.
Note: Intense, focal, abnormal IRU in the centre of the navicular bone, with relatively reduced RU in the distal phalanx.

A Figure 1c: Solar bone phase image of the LF foot

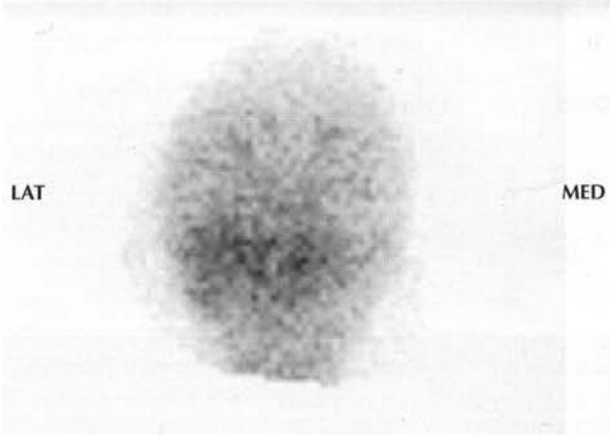

DWB	9y	G	Dressage (Prix St George)	128 x 128

DX: Navicular disease.

DS: Results of local analgesia: perineural analgesia of the palmar digital nerves of left and right forelimbs abolished lameness and greatly improved action. Intrathecal analgesia of the navicular bursa of the left forelimb alleviated left forelimb lameness and resulted in obvious right forelimb lameness. Radiography: no significant radiological abnormality detected.

Loss of action.
Note: Moderate, diffuse, abnormal IRU throughout navicular bone.

A Figure 2a: Lateral pool phase image of the RF foot

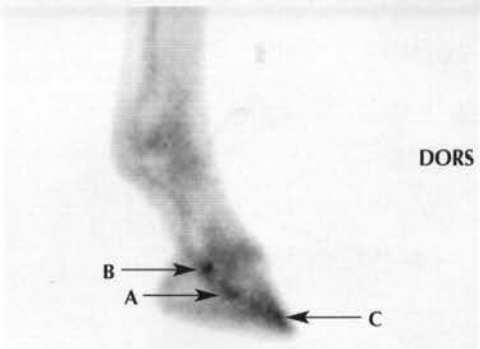

DWB	6y	G	General Purpose & Am. Dressage	128 x 128

DX: Deep digital flexor tendonitis.

DS: Results of local analgesia: lameness substantially improved by perineural analgesia of the palmar digital nerves, by intra-articular analgesia of the DIP joint, or by intrathecal analgesia of the navicular bursa. Radiography and ultrasonography: negative. Magnetic resonance imaging: severe lesions in the DDFT proximal to the navicular bone and at its insertion.

Moderately severe RF lameness.
➔ **A:** Moderate, focal, abnormal IRU in the region of the deep digital flexor tendon.
➔ **B:** Normal radiopharmaceutical activity associated with a vascular plexus at the coronary band.
➔ **C:** Normal radiopharmaceutical activity associated with a vascular plexus at the toe region.

A **Figure 2b: Lateral (i) and solar (palmar) (ii) bone phase image bone phase images of the LF foot**

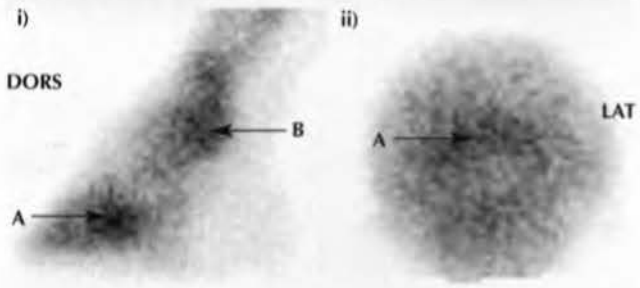

TB	6y	G	Eventing (Int.)	128 x 128

DX: Deep digital flexor tendonitis.

DS: Results of local analgesia: lameness improved substantially by perineural analgesia of the palmar digital nerves, or by intra-articular analgesia of the DIP joint. Radiography and ultrasonography: negative. Magnetic resonance imaging: moderate lesions in the DDFT proximal to the navicular bone and at the insertion. Normal signal in the distal phalanx.

Sudden onset LF lameness. Variable degree (mild to moderately severe) of LF lameness.
➔ **A:** Mild, focal, abnormal IRU in the region of insertion of the deep digital flexor tendon. Similar activity could be associated with subchondral bone trauma.
➔ **B:** Mild radiopharmaceutical activity in the palmar aspect of the PIP joint in the lateral view is a normal finding.

A **Figure 3: Solar bone phase image of the RH foot**

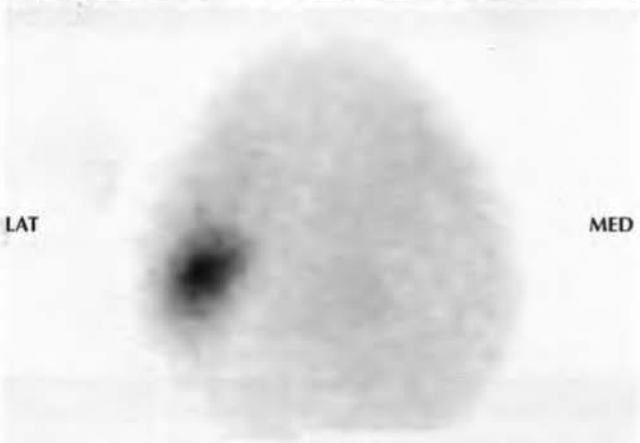

AxWxTB	12y	M	Endurance Riding	128 x 128

DX: Fracture of the lateral plantar process of the distal phalanx.

DS: Radiography: nondisplaced, nonarticular fracture of the distal phalanx. Follow-up radiography: healed fracture.

Sudden onset RH lameness after completion of 150 mile ride; sound within 24 h, but limb sometimes favoured when turning.
Note: Intense, focal, abnormal IRU in the lateral plantar process of the distal phalanx, with apparently reduced radiopharmaceutical activity elsewhere in the distal phalanx and navicular bone.

A **Figure 4: Dorsal (a) and lateral (b) bone phase images of the RF foot and fetlock**

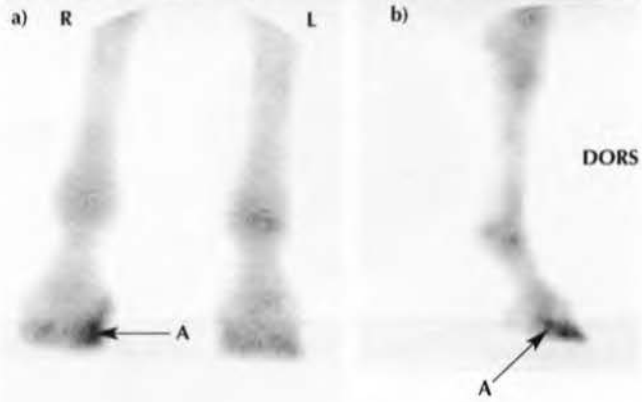

Conn.	5y	M	Native Showing	256 x 256

DX: Fracture of the base of the medial cartilage of the foot.

DS: Results of local analgesia: lameness abolished by perineural analgesia of the palmar (abaxial sesamoid) nerves, but unaffected by perineural analgesia of the palmar digital nerves, or by intra-articular analgesia of the DIP joint. Radiography: fracture at the junction of the ossified medial cartilage of the foot with the distal phalanx.

RF lameness.
➔ **A:** Moderate, focal, abnormal IRU in the medial, palmar aspect of the RF distal phalanx.

A **Figure 5: Solar bone phase image of the RF foot**

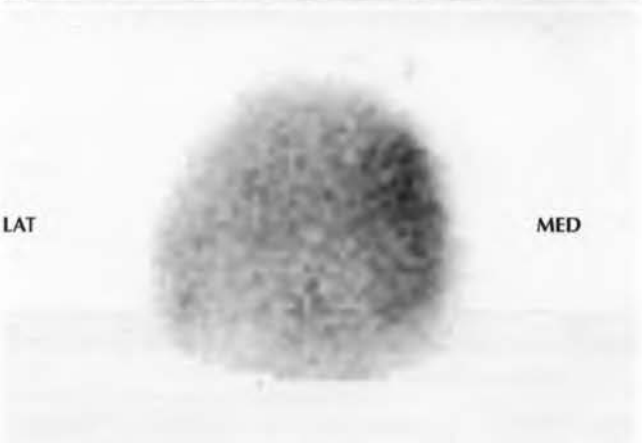

Pony	15y	G	Eventing	128 x 128

DX: Bone trauma.

DS: Results of local analgesia: lameness improved about 60% by perineural analgesia of the palmar digital nerves and abolished by palmar (abaxial sesamoid) nerve blocks. Lameness not altered by intra-articular analgesia of either the DIP or PIP joints. Radiography: negative. Follow-up scintigraphic examination: normal.

Sudden onset RF lameness.
Note: Moderate, diffuse, abnormal IRU in the medial aspect of the distal phalanx.

A **Figure 6: Solar bone phase image of the RF foot**

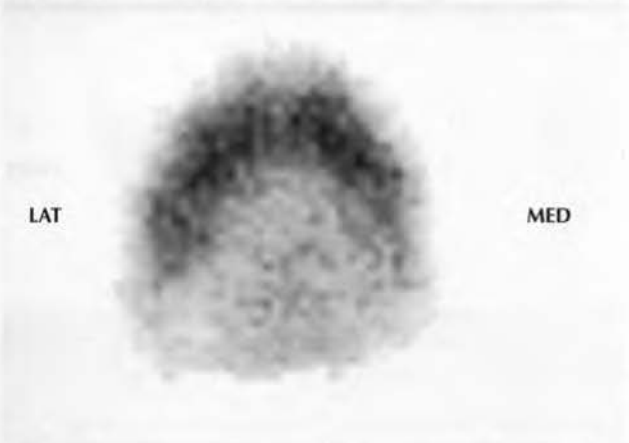

Welsh(A)	6y	M	Driving & Showing	128 x 128

DX: Laminitis.

DS: Results of local analgesia: lameness not altered by palmar digital nerve blocks, but eliminated by perineural analgesia of the palmar (abaxial sesamoid) nerves. Slightly improved by intra-articular analgesia of the DIP joint. Radiography: increased dorsal hoof wall thickness. Response to treatment.

Sudden onset lameness, RF>>LF; no increase in digital pulse amplitudes and no reaction to hoof testers.
Note: Image acquired as 256 x 256 and zoomed. Moderate, diffuse, abnormal IRU around solar margin of distal phalanx.

A **Figure 7: Lateral bone phase image of the LF foot**

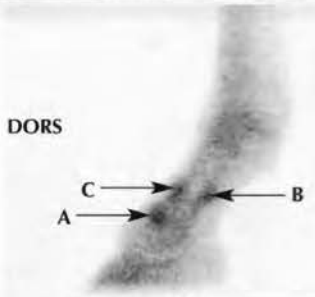

WB	14y	G	Dressage	256 x 256

DX: Osteoarthritis of the PIP joint. Desmitis of the middle distal sesamoidean ligament(s).

DS: Results of local analgesia: lameness not altered by palmar digital nerve blocks, but eliminated by perineural analgesia of the palmar (abaxial sesamoid) nerves. Partial improvement following intra-articular analgesia of the PIP joint. Radiography: periarticular new bone formation on the dorsal aspect of the PIP joint. New bone on the 3rd quarter of the palmar aspect of the proximal phalanx. Ultrasonography: lateral distal sesamoidean ligament enlarged and diffusely hypoechoic distally; new bone formation on the palmar aspect of the proximal phalanx at its insertion.

Bilateral forelimb lameness, LF>>RF.
➔ **A:** Moderate, focal, abnormal IRU on dorsal aspect of PIP joint.
➔ **B:** Mild, focal, abnormal IRU on palmar aspect of proximal phalanx.
➔ **C:** Mild, focal, normal IRU on dorsal aspect of proximal phalanx.

A **Figure 8: Plantar (a), left lateral (b) and right lateral (c) bone phase images of the hind fetlocks**

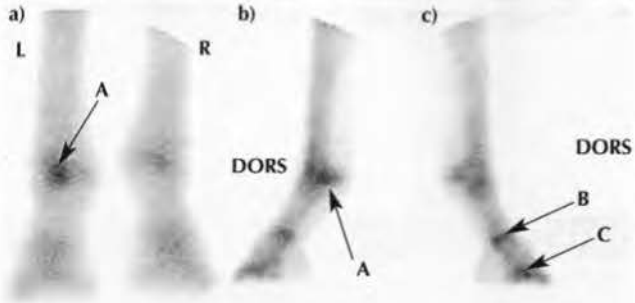

O	5y	M	Dressage	256 x 256

DX: Subchondral bone trauma of the lateral condyle of the MtIII.

DS: Results of local analgesia: plantar (abaxial sesamoid) nerve blocks resulted in marginal improvement in lameness. Lameness removed by perineural analgesia of the plantar and plantar metatarsal nerves (low 4-point block). Lameness improved 50% after intra-articular analgesia of the MTP joint. Radiography: negative. Ultrasonography: negative.

LH lameness.
➔ **A:** Moderate, focal, abnormal IRU in the plantar lateral condyle of the MtIII.
➔ **B:** Moderate, diffuse increased radiopharmaceutical activity in the region of the right PIP joint is normal.
➔ **C:** Moderate, diffuse increased radiopharmaceutical activity in the region of the right distal phalanx is normal.

A **Figure 9: Dorsal (a) and lateral (b) bone phase images of the carpi**

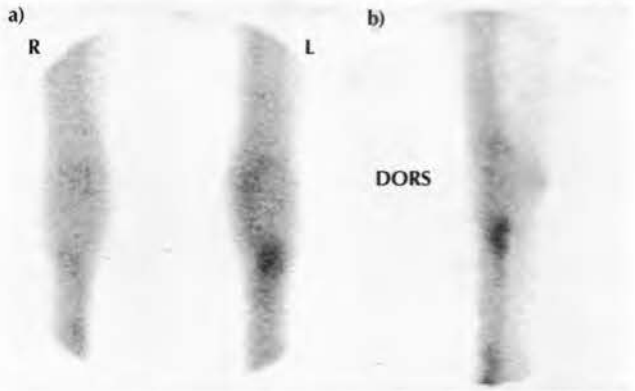

Han.	12y	G	Dressage	256 x 256

DX: Palmar cortical fatigue/stress fracture of the McIII.

DS: Characteristics and degree of lameness. Results of local analgesia: lameness abolished by perineural analgesia of the palmar metacarpal (subcarpal) nerves. Radiography: no detectable radiological abnormality. Ultrasonography: no detectable abnormality. Focal IRU in the proximopalmar aspect of the McIII in pool phase images; there is very early RU into bone in association with a fracture.

Sudden onset LF lameness.
Note: Intense, focal, abnormal IRU in the proximal palmar aspect of the McIII.

A **Figure 10ab: Dorsal (a) and lateral (b) pool phase images of the left carpus**

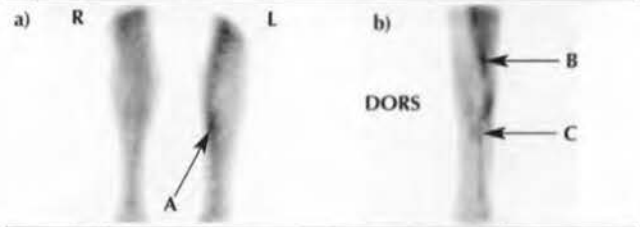

Am.TB	13y	G	Showjumping (Grand Prix)	128 x 128

DX: Proximal suspensory desmitis and enthesopathy.

DS: Characteristics and degree of lameness. Results of local analgesia: perineural analgesia of the palmar metacarpal (subcarpal) nerves resulted in substantial improvement in lameness. Lameness not altered by intra-articular analgesia of the middle carpal joint. Radiography: negative. Ultrasonography: diffuse reduction in echogenicity of the dorsal half of the suspensory ligament from 7 to 10 cm distal to the accessory carpal bone.

Sudden onset severe LF lameness of 2 weeks' duration.

➡ **A:** Focal, intense, abnormal IRU in the proximomedial aspect of the metacarpal region seen in the dorsal view only.

➡ **B:** Normal, intense, diffuse IRU in the caudal muscles of the antebrachium.

➡ **C:** Mild (compared with RF [not shown]) abnormal IRU in the proximopalmar aspect of the McIII in the lateral image.

Note: Many horses with proximal suspensory desmitis have normal RU in both pool and bone phase images; therefore, a negative result does not preclude proximal suspensory desmitis.

A **Figure 10cd: Dorsal (c) and lateral (d) bone phase images of the left carpus**

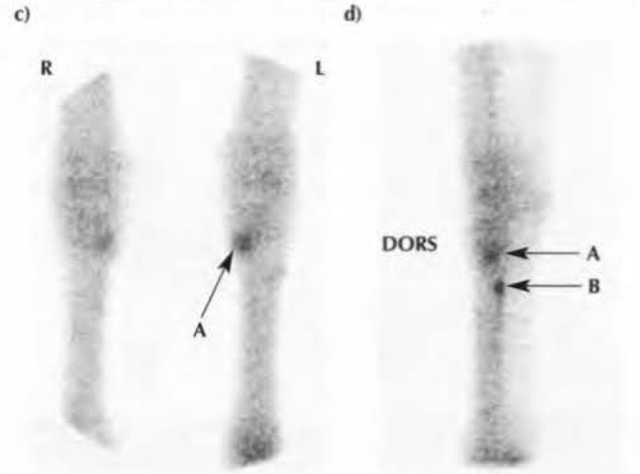

Am.TB	13y	G	Showjumping (Grand Prix)	256 x 256

DX: Proximal suspensory desmitis and enthesopathy.

DS: *Details as for Figure 10ab.*

➡ **A:** Focal mild IRU in the proximal medial aspect of the left McIII at the level of the carpometacarpal joint.

➡ **B:** Focal, intense, abnormal IRU in the proximal palmar aspect of the left McIII.

A **Figure 11: Plantar (a) and lateral (b) bone phase images of the right hock**

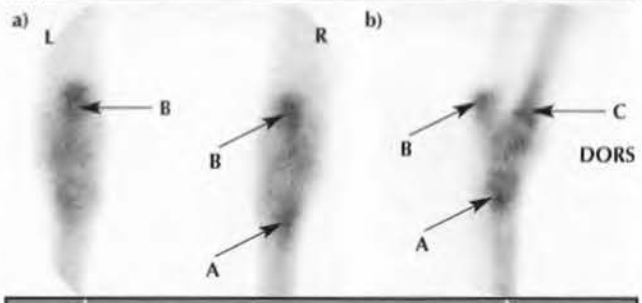

BWB	10y	G	Showjumping (Grand Prix)	256 x 256

DX: Proximal suspensory desmitis and enthesopathy.

DS: Results of local analgesia: lameness substantially improved by perineural analgesia of the deep branch of the lateral plantar nerve. Radiography: mild increased opacity of the proximolateral aspect of the MtIII (can be seen as an incidental finding). Ultrasonography: suspensory ligament enlarged and diffusely hypoechoic from 3 to 5 cm distal to the tarsometatarsal joint, with an almost anechoic lesion dorsomedially.

RH lameness.

➡ **A:** Moderate, focal, abnormal IRU in the proximal plantar and lateral aspect of the MtIII.

➡ **B:** Moderate, normal, diffuse increased radiopharmaceutical activity in the calcaneus.

➡ **C:** Moderate, normal, diffuse increased radiopharmaceutical activity in the distal tibia.

A **Figure 12: Plantar (a) and lateral (b) bone phase images of the left hock**

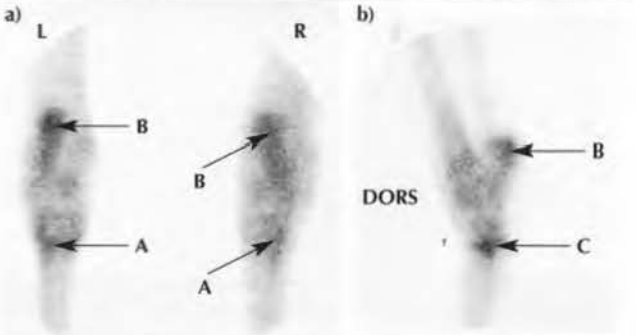

SF	9y	S	Showjumping (Grand Prix)	256 x 256

DX: Stress-related bone injury of the plantar aspect of the MtIII.

DS: Results of local analgesia: perineural analgesia of the plantar metatarsal (subtarsal) nerves eliminated lameness. No response to intra-articular analgesia of the tarsometatarsal joint. Radiography: negative. Ultrasonography: negative.

LH lameness.

➡ **A:** Mild, focal, normal IRU in the distal lateral aspect of the hocks and proximal metatarsal regions.

➡ **B:** Mild to moderate, normal, diffuse radiopharmaceutical activity associated with the calcaneus.

➡ **C:** Focal, intense, abnormal IRU in the proximal plantar aspect of the MtIII of the LH.

Note: Attenuation of activity by the soft tissue structures in the plantar view.

A Figure 13a: Lateral bone phase image of the left hock

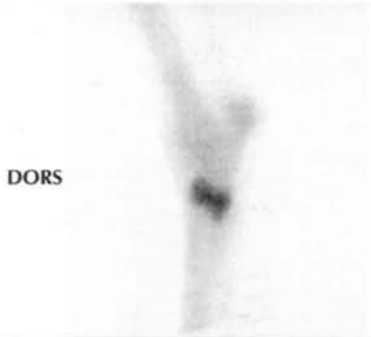

Welsh(D)	19y	G	Pony Club Activities	256 x 256

DX: Periarticular hock trauma/atypical osteoarthritis of the talocalcaneal-centroquatral (proximal intertarsal) CD and TMT joints.

DS: Results of local analgesia: no response to nerve blocks performed distal to the hock. Lameness substantially improved by perineural analgesia of the tibial and fibular nerves. No response to intra-articular analgesia of the TMT joint. Radiography: narrowing of the CD and TMT joints. Follow-up radiographs obtained 2 months later revealed extensive new bone on the dorsolateral aspect of the CD and TMT joints and the lateral aspect of the central and 3rd tarsal bones; there was also narrowing of the lateral aspect of the proximal intertarsal joint. Ultrasonography: negative.

Severe LH lameness.
Note: Intense, diffuse, abnormal IRU in the distal bones of the hock.

A Figure 13b: Plantar (i) and lateral (ii) bone phase images of the left hock

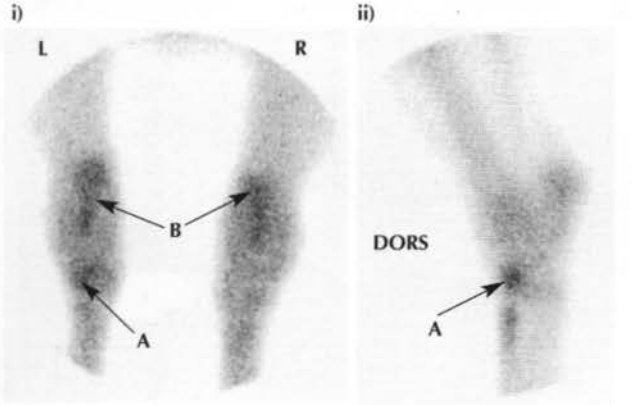

DWB	13y	G	Dressage (Adv.Med.)	256 x 256

DX: Osteoarthritis of the centrodistal and tarsometatarsal joints.

DS: Results of local analgesia: lameness substantially improved by intra-articular analgesia of the TMT joint. Radiography: mild periarticular osteophyte formation involving the CD and TMT joints.

LH lameness (and poor forelimb action).
➡ **A:** Mild, focal, abnormal IRU in the dorsal and lateral aspects of the central and 3rd tarsal bones.
➡ **B:** Normal, diffuse increased radiopharmaceutical activity in the calcanei.

A Figure 13c: Plantar (i) and lateral (ii) bone phase images of the left hock

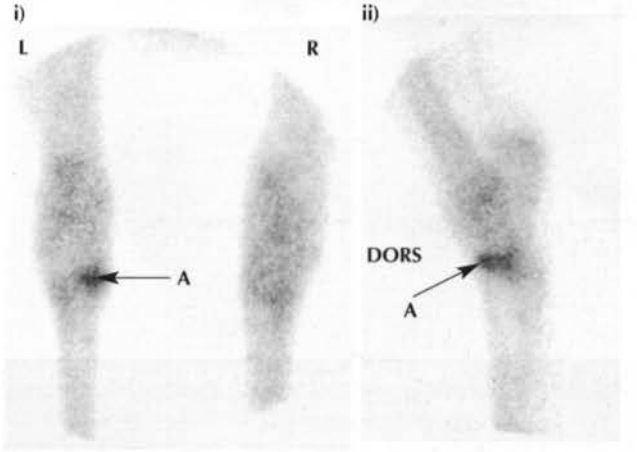

TBx	7y	G	Dressage & Showjumping	256 x 256

DX: Osteoarthritis of the centrodistal joint.

DS: Results of local analgesia: improved action after intra-articular analgesia of the CD joint. Positive response to intra-articular medication. Radiography: narrowing of the CD joint space and slight periarticular osteophyte formation.

Limited hindlimb impulsion.
➡ **A:** Moderate, linear, focal, abnormal IRU associated with the subchondral bone of the CD joint, especially medially.

A Figure 14a: Lateral bone phase images of the left (i) and right (ii) stifles

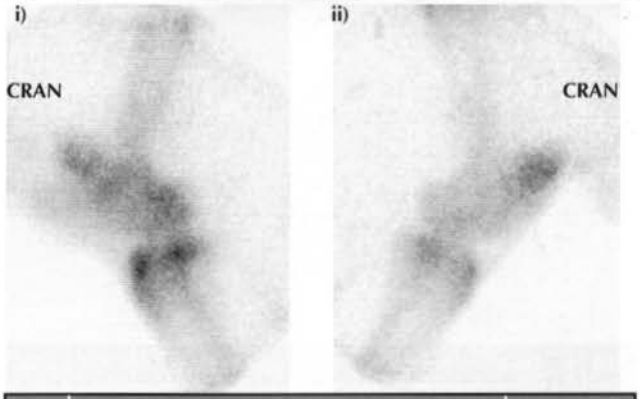

TB	8y	G	Eventing	256 x 256

DX: Nonspecific IRU in the left stifle; this is not uncommon in association with some intra-articular lesions.

DS: Results of local analgesia: intra-articular analgesia of the medial femorotibial joint resulted in marked improvement in lameness. Radiography: negative. Arthroscopy: fibrillation of the cranial ligament of the medial meniscus at its insertion, with softening of the underlying cartilage and subchondral bone.

LH lameness.
Note: The image of the right stifle has been rescaled to match the left. There is mild, generalised IRU in the left distal femur and proximal tibia.

A **Figure 14b: Lateral bone phase images of the left (i) and right (ii) stifles**

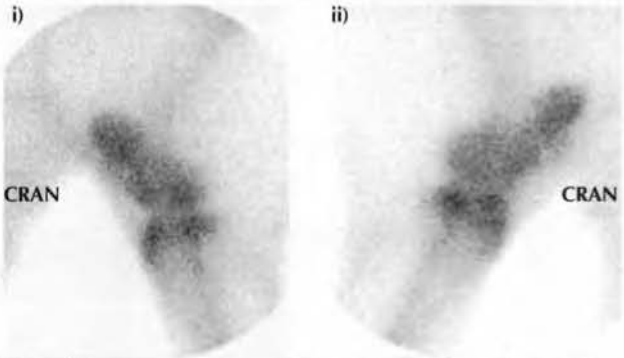

TBx	10y	G	Dressage, Showjumping & Eventing	256 x 256

DX: Nonspecific IRU in the right stifle.

DS: Results of local analgesia: lameness substantially improved by intra-articular analgesia of the medial and lateral femorotibial joints. Radiography: periarticular osteophyte formation on the medial and caudal aspects of the proximal tibia. Arthroscopy: *grade 3* tear of the medial meniscus; cranial ligament of the medial meniscus swollen and haemorrhagic; full thickness cartilage erosions on the distal femur; periarticular osteophyte formation.

RH lameness.
Note: The image of the left stifle has been rescaled to match the right. There is diffuse, mild, abnormal IRU in the right distal femur and moderate, diffuse IRU in the proximal tibia.

A **Figure 14c: Lateral bone phase image of the left stifle**

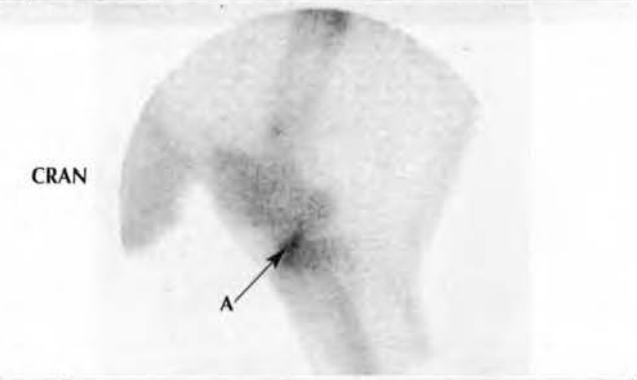

TB	10y	G	Eventing (Adv.)	256 x 256

DX: Nonspecific IRU.

DS: Results of local analgesia: lameness substantially improved after intra-articular analgesia of the medial and lateral femorotibial joints. Radiography: small osseous opacity immediately cranial to the intercondylar eminence of the tibia. Arthroscopy: tearing of the cranial meniscal ligament of the medial meniscus; vertical tear in the cranial meniscal ligament of the lateral meniscus; fibrillation of the lateral meniscus; synovial proliferation in the lateral femorotibial joint; modelling of the axial aspect of the lateral femoral condyle.

LH lameness.
➡ **A:** Focal, moderate, abnormal IRU in the cranioproximal aspect of the left tibia.

A **Figure 14d: Lateral bone phase image of the right stifle**

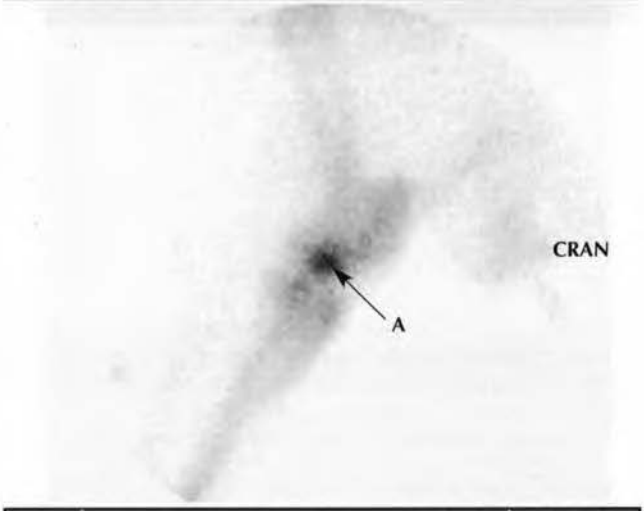

Pony	7y	G	Showing	256 x 256

DX: Subchondral bone cyst.

DS: Results of local analgesia: lameness eliminated by intra-articular analgesia of the medial femorotibial joint. Radiography: well-defined subchondral bone cyst in the medial femoral condyle.

Intermittent subtle RH lameness.
➡ **A:** Moderate, focal, abnormal IRU in the medial femoral condyle. See also *Part I, Chapter 5, Figure 15*.

A **Figure 15: Caudal oblique (a) and caudal (b) bone phase images of the tubera ischii**

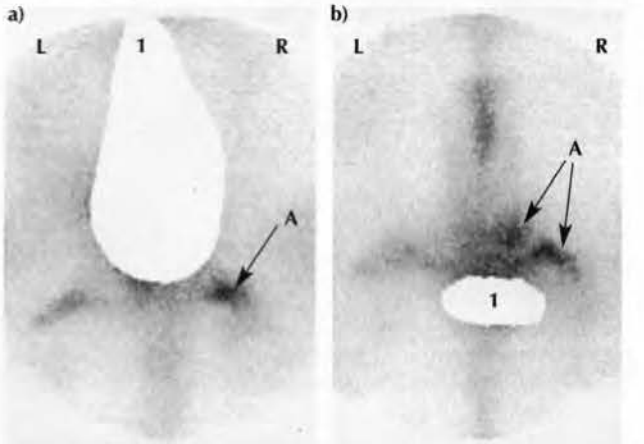

WB	16y	M	General Purpose	256 x 256

DX: Fracture of the tuber ischium.

DS: Clinical signs: mild atrophy of muscles around the right side of the tail head. Results of local analgesia: negative response to tibial and fibular nerve blocks and intra-articular analgesia of all 3 compartments of the stifle.

Mild RH lameness.
➡ **A:** Moderate, focal, abnormal IRU in the right tuber ischium. The right tuber ischium is also of abnormal shape.
Note: The region of the bladder has been masked out (1).

A Figure 16: Lateral bone phase image of the right CF joint

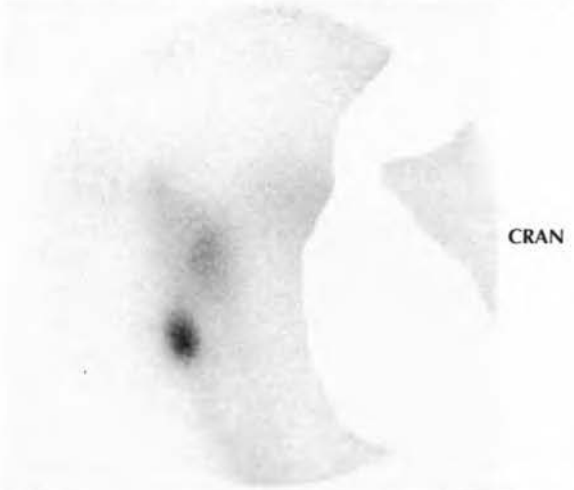

DWB	7y	G	Dressage (Med.)	256 x 256

DX: Fracture of the 3rd trochanter of the femur.

DS: Results of local analgesia: negative response to fibular and tibial nerve blocks and intra-articular analgesia of all 3 compartments of the stifle. Ultrasonography: no evidence of abnormality of the insertions of superficial gluteal and *tensor fascia latae* muscles.

Acute onset, severe RH lameness.
Note: Focal, intense, abnormal IRU in 3rd trochanter of the femur.

A Figure 17a: Right lateral bone phase image of the 9th to 18th thoracic vertabrae

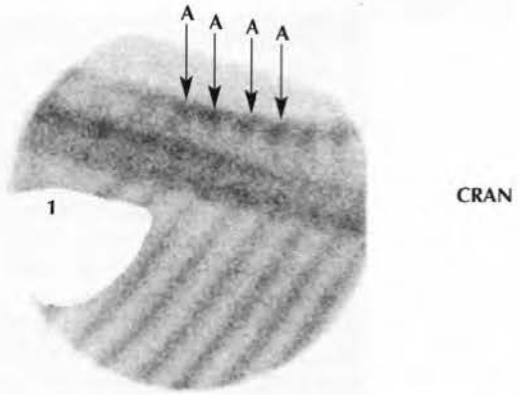

Brit.WB	5y	G	Dressage (Nov.)	256 x 256

DX: Nonspecific IRU in the summits of several thoracic DSPs; such activity can be associated with impingement, but can also be seen in horses with widely spaced DSPs.

DS: Radiography: impingement of the summits of the DSPs of the 12th and 13th thoracic vertebrae. Results of local analgesia: after infiltration of local anaesthetic solution around the 2 impinging DSPs, the horse worked easily on the bit, with a marked improvement in hindlimb impulsion.

Reluctant to work on the bit; poor hindlimb impulsion.
➡ **A:** Mild IRU in the summits of the 11th to 14th thoracic DSPs.
Note: The kidney has been masked out (1).

A Figure 17b: Right lateral bone phase image of the 10th thoracic to 2nd lumbar vertebrae

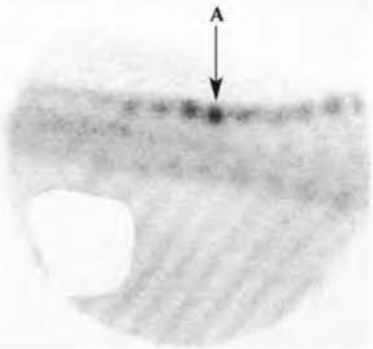

TB	8y	G	Eventing & Showjumping	256 x 256

DX: Impinging DSPs.

DS: Radiography: severe impingement and overriding of the DSPs of the 12th thoracic to 2nd lumbar vertebrae inclusive, with cortical sclerosis and subchondral lysis at points of apposition. Results of local analgesia: infiltration of local anaesthetic solution around the impinging DSPs produced markedly improved hindlimb impulsion and willingness to work.

Reluctant to jump; stiff.
➡ **A:** Intense, focal, abnormal IRU in the summit of the DSP of the 14th thoracic vertebra, with moderate focal IRU in the summits of adjacent DSPs.

A Figure 17c: Left lateral bone phase image of the 10th thoracic to 2nd lumbar vertebrae

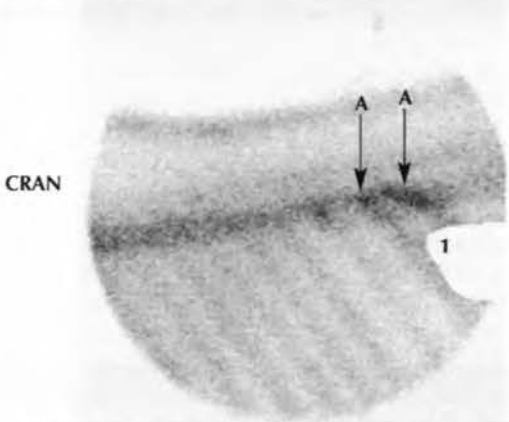

TBx	5y	G	Potential Dressage	256 x 256

DX: Osteoarthritis of the facet joints.

DS: Radiography: severe modelling of the articular facet joints with periarticular new bone and abnormal joint spaces. Ultrasonography: confirmed that the facet joints on both left and right sides were abnormal.

Back stiffness, limited hindlimb impulsion, reluctance to work and refusal to work on the bit.
➡ **A:** Moderate, focal, abnormal IRU in the facet joints between the 16th and 17th, and 17th and 18th, thoracic vertebrae.
Note: The kidney has been masked out (1).

A **Figure 17d: Right lateral bone phase image of the 9th to 18th thoracic vertebrae**

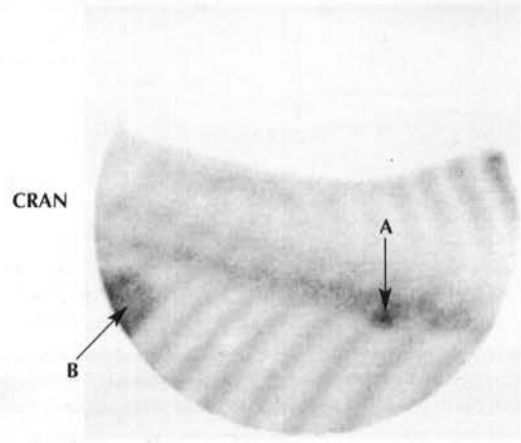

DWB	11y	G	Showjumping (Grand Prix)	256 x 256

DX: Spondylosis involving the 11th and 12th thoracic vertebrae.

DS: Radiography: large spondyles on the ventral aspect of the vertebral bodies of the 11th and 12th thoracic vertebrae.

Poor hindlimb impulsion and back stiffness.
➡ **A:** Intense, focal, abnormal IRU in the vertebral bodies of the 11th and 12th thoracic vertebrae. Note the more ventral location of the region of IRU compared to Figure 17c.
➡ **B:** Normal IRU in the kidney.

A **Figure 18: Dorsal bone phase image of the pelvic region**

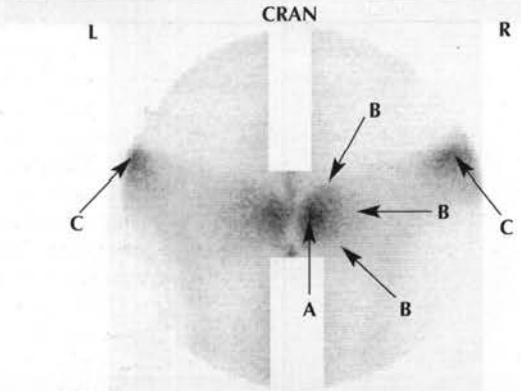

TB	7y	G	General Purpose & Am. Competition	256 x 256

DX: Sacroiliac joint disease.

DS: Results of local analgesia: vast improvement in clinical signs after infiltration of local anaesthetic solution in the sacroiliac joint regions. *Post mortem* examination: major modelling changes of the sacroiliac joints.

Poor hindlimb impulsion. Back stiffness. Reluctance to work.
➡ **A:** Normal, intense radiopharmaceutical activity in the right tuber sacrale.
➡ **B:** Clear definition between (A) and the sacroiliac joint region.
➡ **C:** Normal, moderate IRU in the tubera coxae.
Note: Abnormal asymmetry of RU in the left and right sides, with abnormal loss of definition between the tuber sacrale and sacroiliac joint regions on the left side.

A **Figure 19: Dorsal bone phase image of the pelvic region**

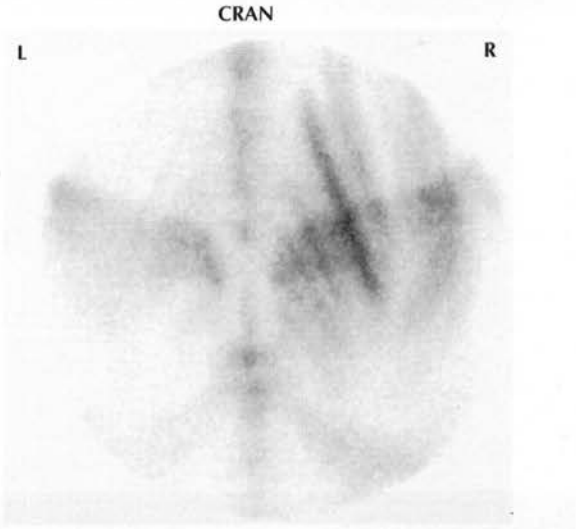

Pony	6y	M	Showjumping	256 x 256

DX: Recurrent exertional rhabdomyolysis.

DS: Elevated serum muscle enzyme activity: creatine kinase 220 iu/l; aspartoaminotransferase 1036 iu/l.

Poor performance.
Note: Moderate, diffuse (in streaks) IRU in the gluteal musculature, especially on the right side.

Chapter 5

THE HEAD

PETE H. L. RAMZAN
Rossdale & Partners, Beaufort Cottage Stables, High Street, Newmarket, Suffolk CB8 8JS, UK.

The increased availability of scintigraphic facilities in equine practice has coincided with a resurgence in interest in equine dentistry among veterinary surgeons. While understanding of the scintigraphic appearance of the equine head is limited in comparison to that of the limbs, the technique has found use in the investigation of a variety of conditions, notably dental sepsis[1]. Scintigraphy is now recognised as a valuable adjunct to other diagnostic aids, such as radiography and endoscopy, when dealing with diseases of the head.

Investigation of potential periapical dental sepsis is the predominant application of cranial scintigraphy in horses. Periapical infections of cheek teeth can necessitate surgical management in the form of tooth extraction or repulsion; this is often costly and complication rates are high. Unfortunately, due to superimposition of anatomical structures, radiographic examination of the head can prove an unreliable means of identifying affected teeth[2]. Unless there is supporting evidence, such as an obviously diseased or fractured clinical crown, there may be considerable uncertainty about which tooth, if any, should be removed and in such circumstances scintigraphy may be invaluable. While bone phase scintigraphic images typically have only moderate resolution, the sensitivity to increased bone metabolism is extremely useful for detecting lesions which may not be visible radiographically. Scintigraphy has been shown to have excellent sensitivity and moderate specificity for detecting dental disease in the horse[1]. When used in conjunction with radiography, a very high sensitivity and specificity for infection ensues. Scintigraphy, unlike computed tomography or magnetic resonance imaging, can be performed on a conscious animal and can add to the body of evidence regarding the site of infection.

Scintigraphic examination of the head may also be incorporated into the investigation of other conditions, such as headshaking and some neurological diseases[1]. Scintigraphy is used in order to identify any active bone lesion which might explain the clinical presentation; in the case of headshakers, this may include periapical dental sepsis or temporomandibular joint pathology. In practice, scintigraphy is frequently used as a last attempt to arrive at a diagnosis following the exhaustion of other routes of investigation. Scintigraphy can occasionally be useful in cases of neurological dysfunction following trauma if radiographic examination fails to detect fracture pathology and an accurate diagnosis or prognosis is required.

Most cranial scintigraphy in the horse is undertaken using the bone marker ^{99m}Tc-MDP. Typically, only bone-phase images are acquired; pool-phase acquisitions do not usually provide additional useful information and are seldom performed[1,3] (**Figure 1, Abnormals**). While ^{99m}Tc-MDP is the radiopharmaceutical of choice, there may be occasions when ^{99m}Tc-HMPAO-labelled leucocyte scans can detect infection in sites which have normal bone marker uptake[4]. They are, however, generally much less useful than ^{99m}Tc-MDP scans because of poor anatomical resolution and, due to cost, are unlikely to be used in anything other than the most involved cases. Brain imaging studies are used infrequently in equine medicine and are discussed further in *Part II, Chapter 6*.

Horses generally have to be more heavily sedated for acquisition of head images than for limb imaging because they have to tolerate having the gamma camera close to the head. It is important that nothing is placed between the head and camera that might attenuate radioactivity (e.g. hands or headcollar). A reduction in camera-patient movement can be achieved by resting the head on a supporting bracket attached to the camera (see *Part I, Chapter 7, Figure 2*). In order to obtain good quality images, a balance must be struck between the length of acquisitions and patient movement; this can be aided by the use of dynamic acquisitions and motion correction software. Typical scintigraphic views of the equine head include left and right lateral, dorsal and ventral images. Lateral views are easily acquired and, in most horses, the entire head is imaged in a single view. Dorsal views are best obtained with the camera slightly tilted to be parallel with the head, while the manner in which ventral views are acquired will depend on the type of camera mounting. Oblique views may be used to assist lesion localisation. On occasion, it may be helpful to place lead shielding between the maxillary and mandibular arcades when acquiring dorsal and/or ventral images. This eliminates superimposition and can be achieved by the use of a customised lead 'gag' or by placing a lead-gloved arm in the mouth using a full-mouth speculum. Image quality can also be enhanced when acquiring dorsal images by holding a lead shield under the head to attenuate γ-rays from the neck and chest. When focal increased radiopharmaceutical uptake (IRU) is observed in the region of a cheek tooth during cranial scintigraphy, it is important to mark its location accurately on the skin using a small lead marker so that subsequent radiographic examination can identify the correct tooth (**Figure 3, Abnormals**).

Normal patterns of ^{99m}Tc-MDP uptake in the equine head have been incompletely described[1,5]; however, it is clear that there are significant differences in scintigraphic appearance between age groups. Horses less than one year of age have activity which neatly outlines the main anatomical features of the skull (the maxillae, mandible and bony orbit); however, on lateral views, there is typically no uptake that might allow differentiation of the cheek teeth (**Figure 1, Normals**). Normal 2-year-old horses can have irregular scintigraphic activity, with areas of relatively greater radiopharmaceutical uptake (RU) over the apices of some cheek teeth, especially the caudal maxillary cheek teeth (**Figure 2, Normals**). The interproximal bone between the 2nd and 3rd

cheek teeth in all arcades may have increased activity and mandibular 'eruption cysts' are visible scintigraphically (**Figure 4, Normals**). The irregular scintigraphic appearance of 2- and 3-year-old horses is due to the active bone modelling that accompanies eruption of the cheek teeth (**Figures 2–5, Normals**).

Normal horses of 3 years of age typically have the most irregular scintigraphic uptake of all age groups (**Figures 3–5, Normals**). Combinations of focal areas of RU may be observed over the apices of various maxillary cheek teeth as well as in the interproximal bone adjacent to the 1st, 2nd and 3rd cheek teeth of all arcades. Although some of these areas of normal RU may be intense, they are usually bilaterally symmetrical. Scintigraphic activity associated with mandibular 'eruption cysts' also tends to be prominent in 3-year-old horses (**Figure 4, Normals**).

Focal activity over the apices of cheek teeth tends to taper off once the permanent dentition has erupted. Horses of 4 years of age may still have areas of greater RU over the apices of the 6th maxillary cheek teeth and mild activity in the region of mandibular eruption, but by 5 years of age the activity is usually quite uniform (**Figure 8, Normals**). Scintigraphic activity in horses aged 5–10 years often allows for extremely good differentiation of cheek teeth due to uptake in the alveolar and interproximal bone (**Figure 9, Normals**). Teeth appear as 'filling defects' with relatively less activity than surrounding bone and it is usually easy to distinguish the 4th maxillary cheek teeth, which have less reserve crown than adjacent teeth (**Figure 8, Normals**). After 10 years of age, this clear delineation of cheek teeth gradually disappears and is replaced by a diffuse pattern of activity corresponding to the diminishing depth of the alveolar sockets (**Figure 10, Normals**).

On lateral images, maxillary activity generally tends to be greater than mandibular activity for all age groups. Areas of relatively greater RU associated with the caudal mandibular cheek teeth are much less conspicuous than corresponding maxillary sites. A feature of many images, especially in horses over 5 years of age, is focal activity in the skull, associated with the ethmoturbinate region (**Figure 7, Normals**). This typically appears as an area of increased activity immediately caudal and axial to each maxillary arcade on dorsal images; it is visible on lateral images dorsal and caudal to the most caudal maxillary cheek tooth. Temporomandibular joints (TMJs) appear as intense focal areas of RU; currently there is no information on patterns of TMJ uptake associated with different oral/dental disorders. While synovial sepsis or trauma to TMJs can result in IRU[6,7], caution must be exercised when attributing significance to asymmetrical uptake in the absence of clinical signs.

It is clear that in the horse there are some specific patterns of scintigraphic activity associated with certain diseases. ^{99m}Tc-MDP uptake associated with periapical dental sepsis is typically focal and intense, with IRU located over the apical region (**Figures 1, 2, 4–6, Abnormals**). Sinusitis may be represented by a diffuse region of increased activity over the affected sinus[1] (**Figures 9–11 Abnormals**). Advanced periodontal disease has a characteristic appearance with intense, diffuse linear uptake along the affected arcades and little or no differentiation of dental structures (**Figures 7, 8, Abnormals**). Occasionally, intense IRU may be noted in horses with suture periostitis or exostoses, although these are evident clinically (**Figure 14, Abnormals**). Patterns of activity associated with other head-related pathology such as tumours, ethmoid haematomas and sinus cysts have not been described mainly because scintigraphy plays a minor role in their diagnosis.

When interpreting scintigraphic images of the head, it is important to consider any abnormal uptake in the light of all available clinical information. Typically, a horse undergoing scintigraphy of the head will already have had clinical, radiographic and endoscopic examinations and, in the case of dental sepsis, there will probably be a high index of suspicion over one or two cheek teeth before the scan is undertaken. Bearing in mind that animals less than 5 years of age may have areas of intense RU associated with erupting dentition, it may generally be assumed that unilateral regions of IRU are most likely to be significant. Quantitative analysis of scintigraphic images using region of interest count densities may assist in the diagnosis of dental disease if there is doubt upon subjective interpretation[1].

REFERENCES AND FURTHER READING

1. Weller, R., Livesey, L., Maierl, J. *et al.* (2001) Comparison of radiography and scintigraphy in the diagnosis of dental disorders in the horse. *Equine vet. J.* **33**, 49-58.
2. Gibbs, C. and Lane, J.G. (1987) Radiographic examination of the facial, nasal and paranasal sinus regions of the horse. *Equine vet. J.* **19**, 474-482.
3. Gayle, J.M., Redding, W.R., Vacek, J.R. *et al.* (1999) Diagnosis and surgical treatment of periapical infection of the third mandibular molar in five horses. *J. Am. vet. med. Ass.* **215**, 829-832.
4. Boswell, J.C., Schramme, M.C., Livesey, L.C. *et al.* (1999) Use of scintigraphy in the diagnosis of dental disease in four horses. *Equine vet. Educ.* **11**, 294-298.
5. Metcalf, M.R., Tate, L.P. and Sellett, L.C. (1989) Clinical use of ^{99m}Tc-MDP scintigraphy in the equine mandible and maxilla. *Vet. Radiol.* **30**, 80-87.
6. Weller, R., Cauvin, E.R., Bowen, I.M. and May, S.A. (1999) Comparison of radiography, scintigraphy and ultrasonography in the diagnosis of a case of temporomandibular joint arthropathy in a horse. *Vet. Rec.* **144**, 377-379.
7. Hoskinson, J.J. (2001) Equine nuclear scintigraphy: indications, uses and techniques. *Vet. Clin. N. Am.: Equine Pract.* **17**, 63-74.
8. Dixon, P.M. (1999) Dental Anatomy. In: *Equine Dentistry*, Eds: G.J. Baker and J. Easley, W.B. Saunders Co., Philadelphia. pp 3-28.

The descriptive dental nomenclature used in the figure legends within this chapter has been described fully elsewhere[8].

NORMAL HORSES

N Figure 1: Left lateral view of the head

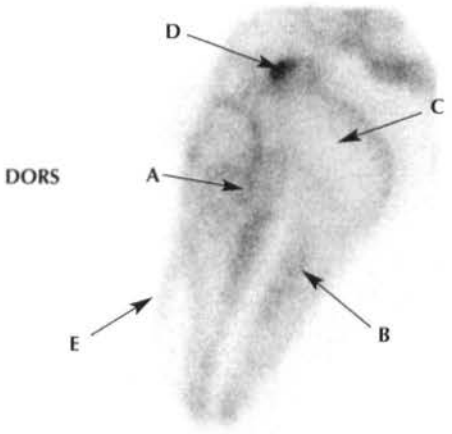

TB	6m	C	–	128 x 128
DX:	Normal			
DS:	NA			

➡ **A:** Maxilla.
➡ **B:** Mandible (horizontal ramus).
➡ **C:** Mandible (vertical ramus).
➡ **D:** Temporomandibular joint.
➡ **E:** Nasal bone.

N Figure 2: Left lateral view of the head

TB	2y	F	Flat Racing	128 x 128
DX:	Normal			
DS:	NA			

➡ **A:** Temporomandibular joint.

N Figure 3: Left lateral view of the head

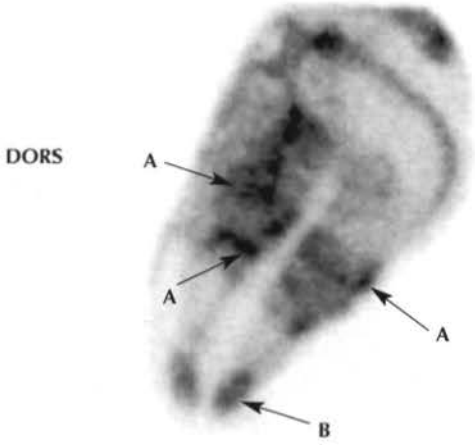

TB	3y	C	Flat Racing	128 x 128
DX:	Normal			
DS:	NA			

➡ **A:** Irregular uptake due to erupting dentition.
➡ **B:** Incisor uptake

N Figure 4: Right lateral view of the head

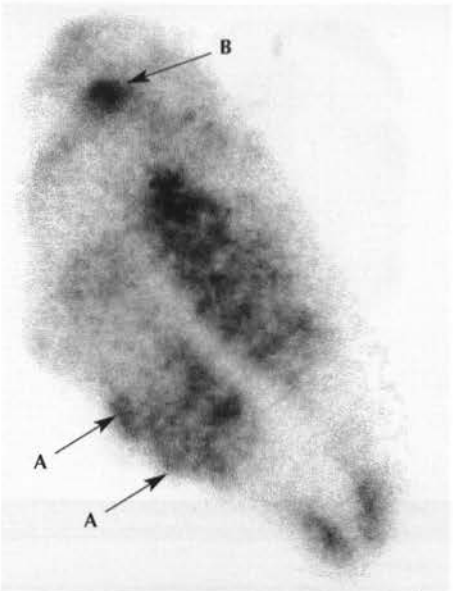

TB	3y	F	Flat Racing	128 x 128
DX:	Normal			
DS:	NA			

➡ **A:** Mandibular 'eruption cysts'.
➡ **B:** Temporomandibular joint.

N Figure 5: Dorsal view of the head

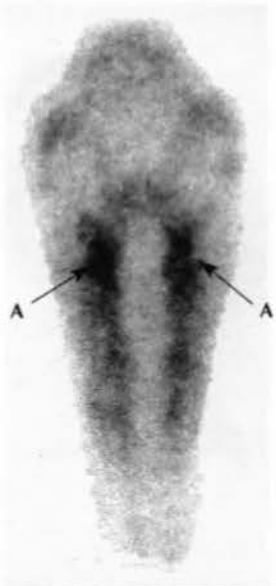

TB	3y	F	Flat Racing	128 x 128
DX:	Normal			
DS:	NA			
➔ **A:** Greater uptake through the caudal cheek teeth of the maxillary and mandibular arcades.				

N Figure 6: Right lateral view of the head

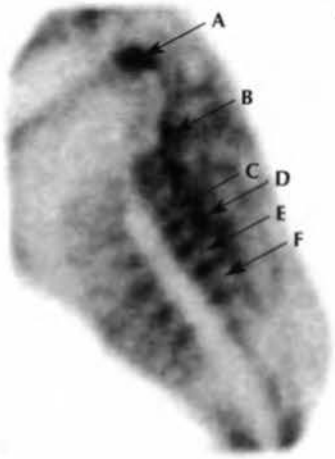

TB	4y	G	National Hunt Racing	128 x 128
DX:	Normal			
DS:	NA			
➔ **A:** Temporomandibular joint. ➔ **B:** Ethmoturbinate uptake. ➔ **C:** Cheek tooth 110. ➔ **D:** Cheek tooth 109. ➔ **E:** Cheek tooth 108. ➔ **F:** Cheek tooth 107.				

N Figure 7: Dorsal view of the head

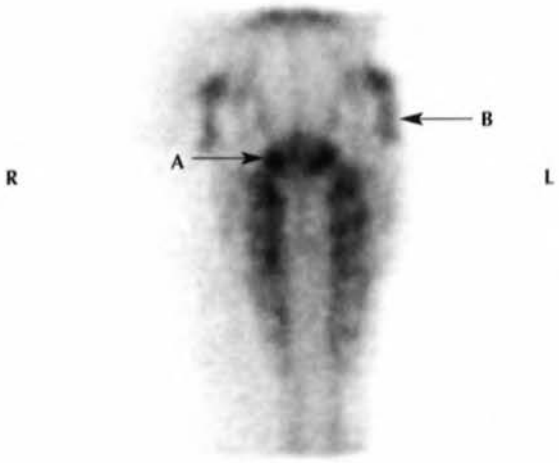

TB	4y	G	National Hunt Racing	128 x 128
DX:	Normal			
DS:	NA			
➔ **A:** Ethmoturbinate uptake. ➔ **B:** Zygomatic arch uptake.				

N Figure 8: Left lateral view of the head

TBx	5y	M	General Purpose	128 x 128
DX:	Normal			
DS:	NA			
➔ **A:** Maxillary 4th cheek tooth (tooth 209).				

N Figure 9: Right lateral view of the head

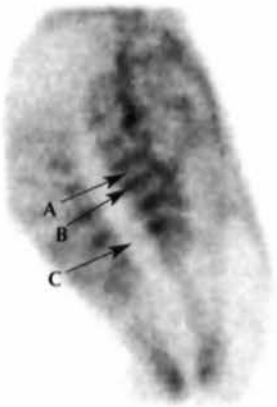

DORS

TBx	8y	M	General Purpose	128 x 128
DX:	Normal			
DS:	NA			

➔ **A:** Reserve crown of cheek tooth 109.
➔ **B:** Relatively greater RU in the surrounding bone.
➔ **C:** Clinical crowns of the cheek teeth characterised by lack of uptake.

N Figure 10: Left lateral view of the head

DORS

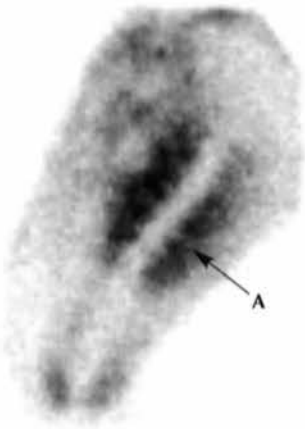

TB	15y	G	Eventing	128 x 128
DX:	Normal			
DS:	NA			

➔ **A:** Lack of definition of individual cheek teeth.

ABNORMAL HORSES

A Figure 1: Left lateral pool phase image of the head

DORS

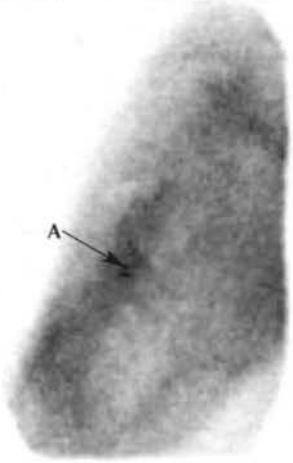

WB	4y	G	Dressage	128 x 128

DX: Periapical infection of tooth 209

DS: Head carriage problems. Small slab fracture of 209. Radiography confirmed periapical changes; however, concurrent infundibular caries of 208 created doubt over which tooth to extract. Scintigraphy confirmed 209 as the problem, and successful extraction was undertaken.

➡ **A:** Moderate diffuse IRU left maxillary arcade. Poor definition of affected tooth, demonstrating that bone phase images are more sensitive (see Figure 2).

A Figure 2: Left lateral bone phase image of the head

DORS

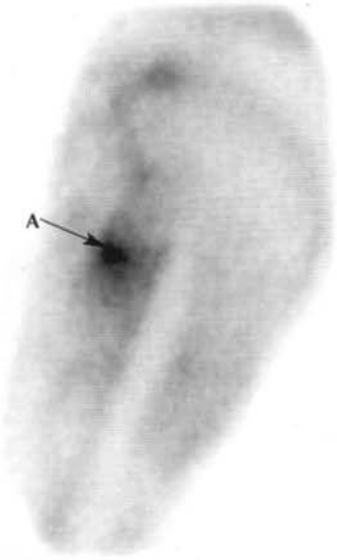

WB	4y	G	Dressage	128 x 128

DX: Periapical infection of tooth 209

DS: *Details as for Figure 1.*

➡ **A:** Marked IRU over apex of 209.
Note: Image resolution superior to pool phase image.

A Figure 3: Left lateral bone phase image of the head

DORS

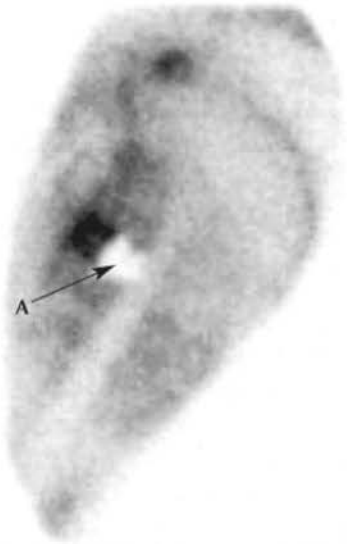

WB	4y	G	Dressage	128 x 128

DX: Periapical infection of tooth 209

DS: *Details as for Figure 1.*

➡ **A:** A lead marker has been positioned below the area of IRU to assist lesion localisation.

A Figure 4: Dorsal bone phase image of the head

R L

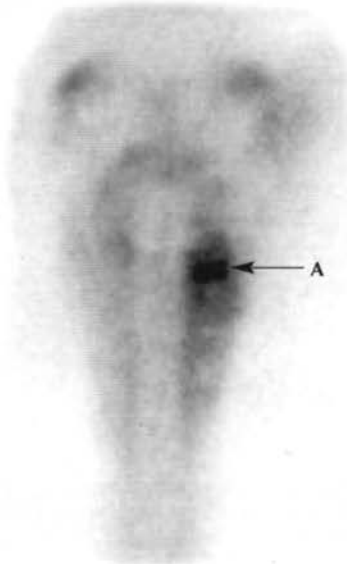

WB	4y	G	Dressage	128 x 128

DX: Periapical infection of tooth 209

DS: *Details as for Figure 1.*

➡ **A:** Marked IRU over apex of tooth 209.

A Figure 5: Dorsal view of the head

TB	3y	F	Flat Racing	128 x 128
DX:	Periapical infection of tooth 109.			
DS:	Small slab fracture of 109; no radiographic abnormalities. Abnormal head carriage at exercise. Periapical infection confirmed upon extraction of tooth 109.			
➡ **A:**	Moderate IRU over tooth 109.			

A Figure 6: Left lateral view of the head

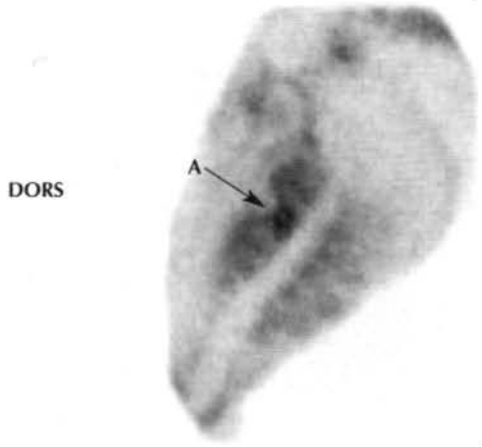

TB	11y	G	General Purpose	128 x 128
DX:	Periapical infection of tooth 209.			
DS:	History of abnormal head carriage. Radiographic/clinical examination revealed grossly diseased tooth 209 of longstanding appearance. Scintigraphy undertaken to determine presence of any current inflammation/infection. Tooth 209 subsequently extracted with partial resolution of clinical signs.			
➡ **A:**	Marked focal IRU around tooth 209.			

A Figure 7: Left lateral view of the head

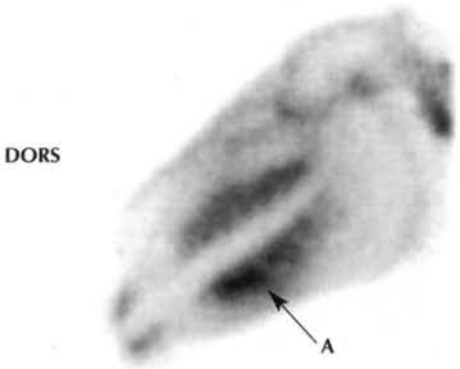

TBx	15y	M	General Purpose	128 x 128
DX:	Periodontal disease (mandibular arcades).			
DS:	Generalised periodontal disease of both mandibular arcades associated with left-sided wavemouth.			
➡ **A:**	Marked diffuse uptake left mandibular arcade with loss of definition of dental structures.			

A Figure 8: Ventral view of the head

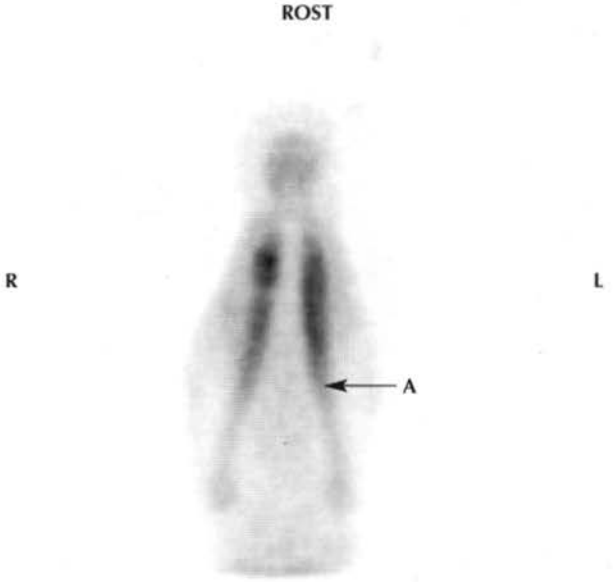

TBx	15y	M	General Purpose	128 x 128
DX:	Periodontal disease.			
DS:	*Details as for Figure 7.*			
➡ **A:**	Mandible.			

A Figure 9: Right lateral view of the head

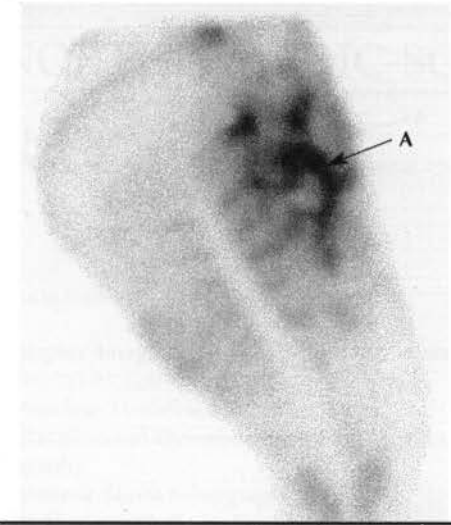

TB	4y	F	Flat Racing	128 x 128
DX:	Sinusitis.			
DS:	Chronic purulent right-sided nasal discharge with radiographic evidence of maxillary sinusitus. Scintigraphy used to eliminate dental origin sinusitis due to recurrent nature of problem.			
➡ **A:**	Marked irregular IRU associated with the right maxillary sinuses.			

A Figure 10: Left lateral view of the head

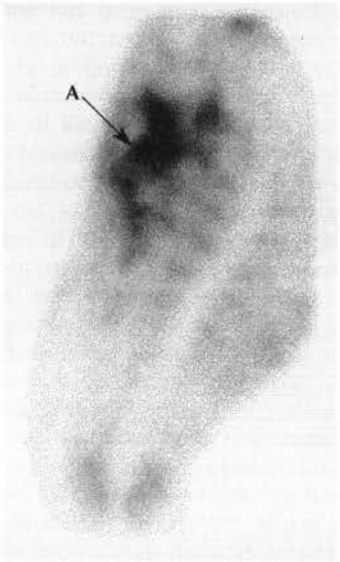

TB	4y	F	Flat Racing	128 x 128
DX:	Sinusitis.			
DS:	*Details as for Figure 9.*			
➡ **A:**	Marked irregular IRU associated with the maxillary sinuses.			
Note:	Pathology is actually right-sided, which illustrates the importance of acquiring dorsal images.			

A Figure 11: Dorsal view of the head

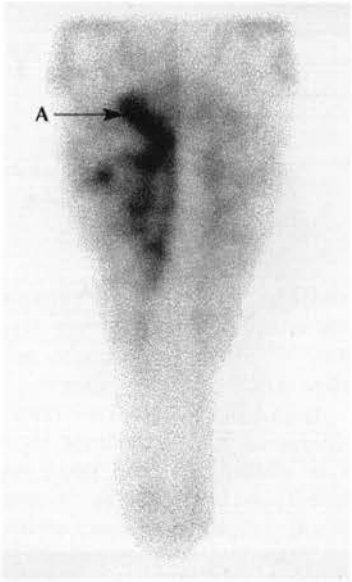

TB	4y	F	Flat Racing	128 x 128
DX:	Sinusitis.			
DS:	*Details as for Figure 9.*			
➡ **A:**	Marked IRU associated with the right maxillary sinuses.			
Note:	Dorsal image permits localisation of sinusitis to the right side.			

A Figure 12: Left lateral view of the head

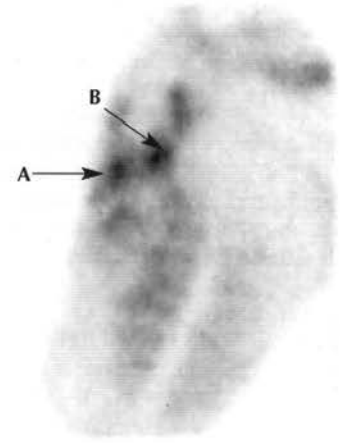

TB	12y	G	Eventing	128 x 128
DX:	Cranial trauma.			
DS:	Cranial trauma sustained during fall; horse presented with concussion, ataxia and left-sided epistaxis. Scintigraphy performed as, apart from obvious frontal depression, no radiographic abnormalities.			
➡ **A:**	Marked focal areas of IRU in frontal/lacrimal bones.			
➡ **B:**	Marked focal areas of IRU in bony orbit.			

A **Figure 13: Dorsal view of the head**

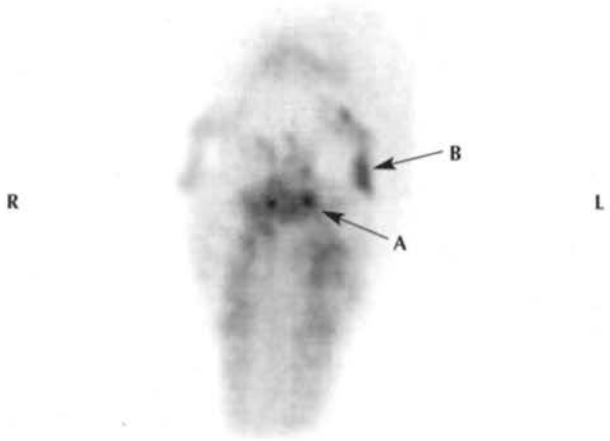

TB	12y	G	Eventing	128 x 128
DX:	Cranial trauma.			
DS:	*Details as for Figure 12.*			

➡ **A:** Marked IRU in frontal region. On this view, the uptake is impossible to distinguish from the ethmoturbinate region; a lateral view is required.
➡ **B:** Marked IRU in left zygomatic arch.

A **Figure 14: Left lateral view of the head**

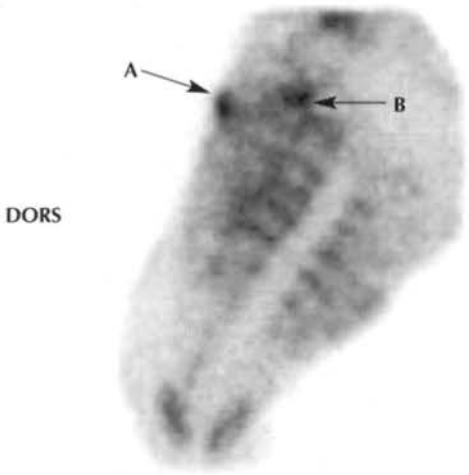

TB	7y	M	Flat Racing	128 x 128
DX:	Suture periostitis.			
DS:	NA.			

➡ **A:** Marked focal IRU associated with nasofrontal suture.
➡ **B:** Normal ethmoturbinate uptake.

Chapter 6

NONORTHOPAEDIC SCINTIGRAPHY

RUSSELL J. MALTON
Rossdale & Partners, Beaufort Cottage Equine Hospital, Cotton End Road, Exning, Newmarket, Suffolk CB8 7NN, UK.

The following topics are covered in this chapter:

1. **Scintigraphic Imaging of Infection and Inflammation** (Labelled White Cell Scans)
2. **Renal Nuclear Medicine Studies**
3. **Aortoiliacofemoral Thrombosis: First-Pass Radionuclide Angiography**
4. **Portosystemic Shunt Scintigraphy**
5. **Hepatic Nuclear Medicine Studies**
6. **Brain Scintigraphy**
7. **Uterine Clearance Scintigraphy**
8. **Radionuclide Angiocardiography**
9. **Gastric Emptying**
10. **Thyroid Scintigraphy**

Equine skeletal scintigraphy has become a major contributor to lameness diagnosis and is probably the most commonly performed scintigraphic imaging procedure in veterinary medicine[1]. Nonskeletal nuclear medicine studies in horses do not have a well established role in routine diagnostics. In contrast, in people and, to a lesser extent, small animals, nuclear medicine has been used extensively to investigate many of the internal organs both morphologically and functionally[1]. As a general rule, static studies provide morphological information about the size, shape and position of target organs or the presence of space-occupying lesions within them, whereas dynamic studies provide information about organ function through measurement of rates of accumulation and removal of radiopharmaceutical by the organ[2]. A number of the original morphological investigations have since been replaced by newer technologies such as ultrasonography, computed tomography (CT) and magnetic resonance imaging (MRI). Nuclear medicine technology has itself progressed and more advanced imaging techniques such as single photon emission computed tomography (SPECT) allow creation of 3-dimensional images of radiopharmaceutical uptake (RU) providing more precise information on location, size and extent of lesions[3]. Positron emission tomography (PET), along with newer radiopharmaceuticals, has further enhanced the diagnostic capabilities for quantification of organ function in people[4]. Application of these more advanced technologies in veterinary medicine has been limited, largely due to equipment costs. Application of these technological advancements for use in horses is also limited by patient size. This limits future potential for the newer 3-dimensional technologies whereby the gamma camera must be capable of rotating around the patient. Patient size also limits the amount of information which can be gained with conventional gamma camera studies; e.g. hepatic function studies using the gamma camera require simultaneous imaging of both the heart and liver, which cannot be achieved with even the largest field of view cameras. A number of the function studies also require complex mathematical analyses, including deconvolution analysis, which require specialist knowledge and input.

Clearances of specific radiopharmaceuticals from the circulation have been used successfully to evaluate renal function quantitatively in horses and have the advantage of not requiring a gamma camera. Radiopharmaceutical clearance studies to evaluate hepatic function have been carried out successfully in dogs.

The objective of this book is to provide a practical guideline on when, why and how to scan, and this chapter emphasises those nuclear medicine procedures which have current clinical diagnostic merit. Reference is made to the original procedures carried out in the horse and to some procedures which are used primarily for research. Current procedures carried out in other species which may have future practical relevance in equine diagnostics are included. Few, if any, of these nonskeletal nuclear medicine procedures are carried out as part of routine diagnostic evaluations and some of the original procedures carried out two decades ago never found favour as diagnostic aids. This is probably due to a combination of factors, including technical difficulties in carrying out and interpreting the information, provision of information of limited diagnostic value, and replacement by other technologies such as diagnostic ultrasound. Equipment costs, access to stable radiopharmaceuticals, and safety considerations and regulations may also have limited the popularity of these procedures.

The provision of accurate information on organ function and localising inflammation or infection are two areas where nuclear medicine studies may have further potential for the future[1].

SCINTIGRAPHIC IMAGING OF INFECTION AND INFLAMMATION

Introduction

Early detection and localisation of significant inflammation or infection in all species can prove difficult[5]. Early detection of the focus of infection helps guide more specific diagnostic procedures, such as arthrocentesis or biopsy, and allows more accurate decisions to be made regarding patient therapy. Monitoring the response to such therapy aids patient management and helps determine a prognosis. In the horse, the presence of infection or inflammation is usually identified through a combination of clinical examination, blood testing and diagnostic imaging procedures. Imaging options

including radiography and ultrasonography usually require gross morphological changes for localisation of a focus of inflammation or infection[6]. These changes are not specific for infection and in the early stages are unlikely to be detected. Increased bone turnover associated with orthopaedic infection may be detected by skeletal scintigraphy, but the presence of active inflammation cannot be determined[7]. In addition, the size of the horse poses significant limitations on detection of localised infection or inflammation within the abdomen or thorax[8].

Scintigraphic methods used to detect foci of inflammation rely on the radiolabelling of blood constituents which target and participate in the inflammatory process. The universal constituent used to date has been the leucocyte. Blood leucocytes migrate to and accumulate at sites of active inflammation where their primary role is to locate, phagocytose and destroy invading bacteria. Radiolabelling leucocytes without affecting cell viability and function has therefore allowed scintigraphic detection of sites of accumulation[6,9]. The procedure is not specific for detection of bacterial infection because many disease processes are associated with an inflammatory response, including neoplasia[5].

Gamma camera imaging for the detection of foci of inflammation or infection using radiolabelled white blood cells has been carried out in people for over 25 years[10].

Inflammatory conditions which have been imaged using labelled leucocyte scintigraphy include acute and chronic osteomyelitis, discospondylitis, intra-abdominal sepsis/abscesses, inflammatory bowel disease, acute and chronic pyelonephritis, myocardial inflammation following infarction, vascular graft infections, skeletal metastases and pyrexia of unknown origin (PUO)[9-13].

PUO presents a significant diagnostic challenge and, although labelled leucocyte scintigraphy appears to be the ideal method for investigation, it is not considered particularly useful, especially in previously well patients[10]. It is suggested that this is because many of these pyrexias are caused by noninfective pathology or nonpyogenic organisms. Pyrexia in patients with pre-existing medical conditions is considered more likely to have a pyogenic cause and labelled leucocyte scanning has greater indication[10]. With the development of newer technologies, labelled leucocyte scintigraphy has been outdated as a diagnostic tool for investigating a number of the above conditions in man. However, it remains important for imaging inflammatory bowel disease and musculoskeletal sepsis[10,14].

The two radiopharmaceuticals which can currently be used to radiolabel leucocytes are ^{111}Indium oxine (^{111}In-oxine) and ^{99m}Tc-hexamethylpropyleneamine oxine (^{99m}Tc-HMPAO). ^{111}In-oxine was the first to be used and has been used extensively in people, where it is still considered the agent of choice for identifying the site of infection when localising signs are lacking[14]. It is also the preferred radiopharmaceutical for localisation of intra-abdominal sepsis, because of its greater specificity in the delayed scan (24 h post injection)[6,14]. There is only one report in the literature of the use of ^{111}In-oxine to localise an intra-abdominal abscess in a horse[8]. In another study, an *in vitro* comparison was made between leucocytes labelled with either of the two radiopharmaceuticals to compare their labelling characteristics, viability and phagocytic function post labelling[6].

^{99m}Tc-HMPAO was originally developed for cerebral blood flow studies, as it is a lipophilic complex which can cross the blood brain barrier (see *Brain Scintigraphy*). It also has the ability to diffuse across the cell membrane at room temperature, where it becomes bound to intracellular receptors (as does ^{111}In-oxine). This makes it suitable for leucocyte labelling[9,10].

Although ^{99m}Tc-HMPAO is the radiopharmaceutical most commonly used in labelled leucocyte studies in the horse, reports in the literature of use of the technique are limited, making assessment of its validity as a routine diagnostic tool difficult[15]. One of the more successful reports involved a retrospective review of use of the technique for detection of orthopaedic infection as the cause of lameness in a series of 14 horses[7]. No false negative or false positive results were found and important information that affected patient management was provided in over 50% of the cases. Its use in the diagnosis of intra-abdominal abscesses in horses has also been reported[16]. Another study showed that the application of ^{99m}Tc-HMPAO-labelled leucocyte scintigraphy supported a diagnosis of ulcerative colitis and facilitated appropriate management in two horses with histories and clinical signs consistent with phenylbutazone toxicity. Limitations of this report include the presence of only one normal control animal in the study[17]. Recent studies have demonstrated abnormal RU in horses showing weight loss as a result of partial or complete small intestinal malabsorption. The observed pattern of uptake was considered suggestive of the presence of intestinal pathology, and indicative of its anatomical distribution. Specific pathology, prognosis or likely response to treatment could not be predicted[18,19]. A small study which aimed to determine the stability and biodistribution of ^{99m}Tc-HMPAO-labelled leucocytes in the horse also showed focal accumulation of radiolabelled leucocytes in the region of a confirmed septic digital tendon sheath[11].

Other radiolabelled products are used to image inflammation. A number of these are the focus of continued research and include ^{99m}Tc-human polyclonal immunoglobulin (^{99m}Tc-HIG), monoclonal anti-leucocyte antibodies, monoclonal antibodies to activated endothelium, ^{99m}Tc-Dextran, ^{99m}Tc-citrate, chemotactic peptides, ^{99m}Tc-interleukin-8 and ^{99m}Tc-ciprofloxacin (Infecton). The diagnostic value of several of these 'inflammation seeking' agents is affected by low target to background ratios[4,5].

Sulesomab (LeukoScan[a]; Immunomedics Inc., Morris Plains, New Jersey, USA) is a ^{99m}Tc-labelled murine antibody fragment for nuclear medicine imaging of activated granulocytes. Its primary potential use in people is to differentiate soft tissue infection from osteomyelitis and to diagnose equivocal appendicitis[20,21]. It is also used to locate sites of unusual infections, including endo- and pericarditis, pneumonia and infections of abdominal organs, particularly in patients with fever of unknown origin. Advantages over conventional leucocyte-tagged radiopharmaceuticals include ease of handling the antibody and elimination of handling blood[22].

[a]Although no work has been published on the use of LeukoScan, anecdotal evidence indicates that it is effective in identifying foci of infection in the horse and is simple to use (S.J. Dyson,personal communication).

A **Figure 1: Labelled leucocyte scan of the dorsal caudal pelvis obtained 75 mins (a) and 210 mins (b) post injection**

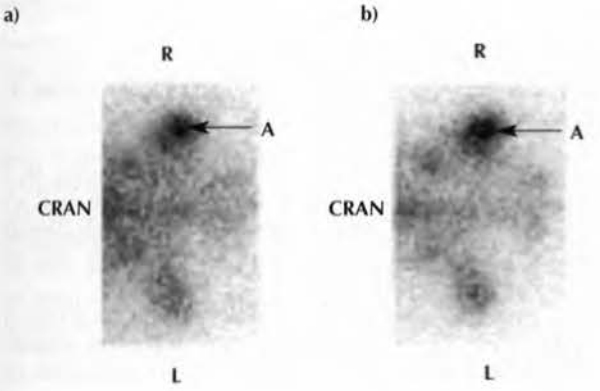

TB	3m	F	-	128 x 128

DX: Osteomyelitis of right femur/hip.

DS: Septic coxofemoral joint/radiographic evidence of osteomyelitis.

RH lameness with marked inflammatory blood profile.
➡ **A:** Intense IRU in right femur.
Note: Radiopharmaceutical: ^{99m}Tc-HMPAO.

A **Figure 2: Labelled leucocyte scan of the right lateral abdomen/pelvis obtained 75 mins (a) and 210 mins (b) post injection**

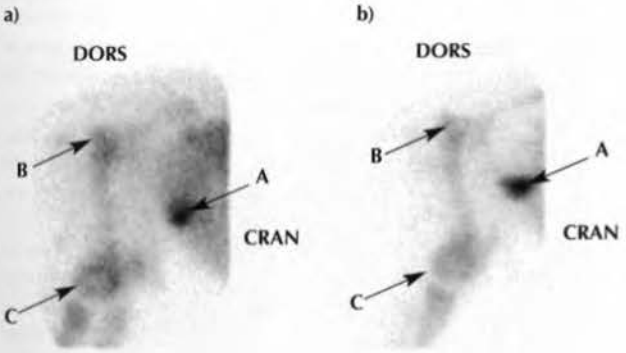

TB	3m	F	-	128 x 128

DX: Umbilical abscess.

DS: Septicaemia/osteomyelitis. Marked inflammatory blood profile and lameness.

➡ **A:** Intense IRU in caudal ventral abdomen.
➡ **B:** Greater trochanter of right femur.
➡ **C:** Right stifle.
Note: Radiopharmaceutical: ^{99m}Tc-HMPAO.

N **Figure 3a: Labelled leucocyte scan of the lateral distal LH obtained 60 mins post injection**

Shire	7y	G	-	128 x 128

DX: Normal

DS: NA

Note: Radiopharmaceutical: ^{99m}Tc-HMPAO.

A **Figure 3b: Labelled leucocyte scan of the lateral distal RH obtained 60 mins post injection**

Shire	7y	G	-	128 x 128

DX: Necrosis and inflammation of distal digital annular ligament with adhesions to underlying lateral branch of superficial digital flexor tendon. No bacteria seen on histopathology.

DS: Surgical exploration and resection. Histopathological findings.

➡ **A:** Focal IRU in plantar mid pastern region of RH.
Note: Radiopharmaceutical: ^{99m}Tc-HMPAO.

N **Figure 4: Labelled leucocyte scan of the right caudal abdomen obtained 60 mins post injection**

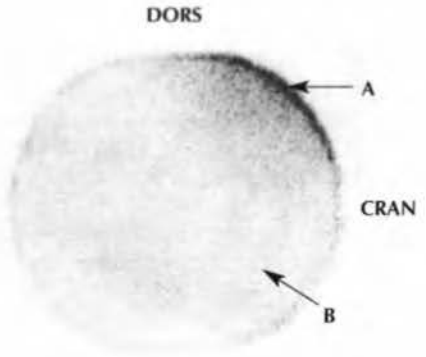

-	-	-	-	128 x 128
DX:	Normal			
DS:	NA			
➔ **A:** Caudal border of lung lobes. ➔ **B:** No areas of IRU. **Note:** Radiopharmaceutical: ^{99m}Tc-HMPAO.				

Studies in people have shown a comparative increase in sensitivity and specificity in the diagnosis of orthopaedic infection, but its sensitivity and specificity for the diagnosis of inflammatory bowel disease is questionable[23-26]. No reported case studies using this radiopharmaceutical in horses have been found in the literature.

Possible Indications for Labelled Leucocyte Scanning in the Horse

- Localisation of the site or sites of suspected sepsis in a septicaemic neonate or in a lame foal which has an inflammatory blood picture but in which neither clinical nor radiographic investigation has revealed a site of infection (**Figures 1 and 2**).
- To determine whether lesions identified on clinical examination or by other diagnostic techniques involve significant inflammation or sepsis, e.g. radiolucent or radiopaque areas (**Figures 3a and 3b**).
- Evaluation of post operative patients with pyrexia or persistent pain or swelling. The strongest indication is in orthopaedic patients with suspected sepsis of a healing fracture or the site of an orthopaedic implant. Bone scan is less likely to distinguish normal fracture healing from infection in such cases.
- Diagnosis of inflammatory bowel disease (**Figures 4–6**).
- To monitor progression or response to therapy of an identified inflammatory or septic condition.
- Investigation of pyrexia of unknown origin in patients with pre-existing medical conditions[10].

A **Figure 5: Labelled leucocyte scan of the right lateral abdomen obtained 60 mins post injection**

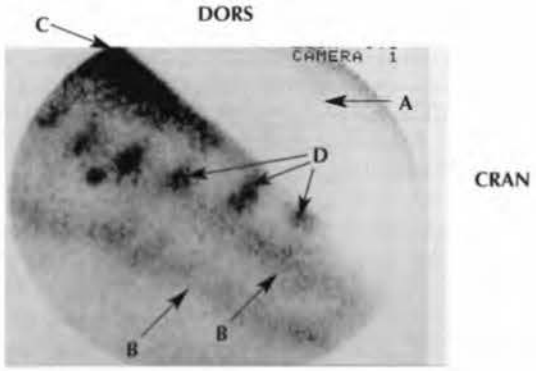

TB	1.5y	G	-	128 x 128
DX:	Lymphocytic plasmocytic colitis.			
DS:	Rectal biopsy. Ill-thrift, lethargy and recurrent colic.			
➔ **A:** Area of lungs shielded using computer software to enhance other areas of increased uptake. ➔ **B:** Linear IRU in region of large colon. ➔ **C:** Caudodorsal lungs. ➔ **D:** Ribs. **Note:** Radiopharmaceutical: ^{99m}Tc-HMPAO.				

A **Figure 6: Labelled leucocyte scan of the right lateral abdomen obtained 60 mins post injection**

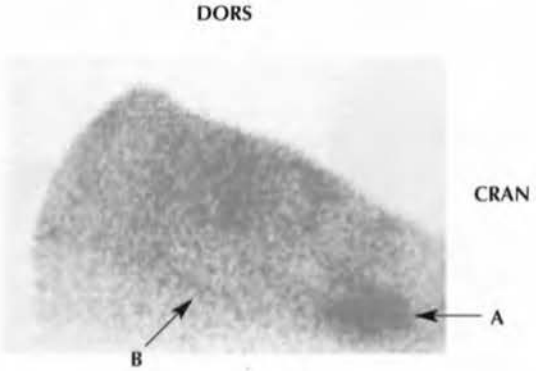

TB	18y	G	-	128 x 128
DX:	Eosinophilic colitis.			
DS:	Rectal biopsy.			
6 weeks diarrhoea, anorexia and recurrent colic. ➔ **A:** Focal IRU cranioventral abdomen. ➔ **B:** Generalised IRU in region of right ventral colon. **Note:** Radiopharmaceutical: ^{99m}Tc-HMPAO.				

Radiopharmaceuticals Used to Label Leucocytes

^{111}Indium-oxine (^{111}In-oxine) was the first radiopharmaceutical used in leucocyte-labelled studies in man, where it still plays an important role today. Only one study using this radiopharmaceutical in a horse has been documented in the literature[8].

^{99m}Tc-HMPAO was originally developed for cerebral blood flow studies in man and, due to its lipophilic nature, it was found to successfully label leucocytes. Although technetium has superior imaging characteristics, ^{111}In-oxine has advantages for imaging chronic inflammation and is therefore likely to remain more useful for labelled leucocyte studies in man[10]. ^{99m}Tc-HMPAO is, however, the most commonly used radiopharmaceutical for leucocyte labelled studies in the horse.

^{99m}Tc-HMPAO has the following advantages[5,6,9,10,13,14]:

- Technetium has superior imaging characteristics. The photon energy is more suited to gamma camera imaging resulting in greater spatial resolution. The higher photon flux eliminates the need for long acquisition times.
- More selective labelling of granulocytes than monocytes.
- Ability to label leucocytes in the presence of plasma, which inhibits premature leucocyte activation.
- Wide availability and relatively low cost of technetium allows higher initial activity to be used for labelling. This helps counter the poorer labelling efficiency of ^{99m}Tc-HMPAO.

The major potential disadvantage is excretion of ^{99m}Tc-complexes through the urinary tract and hepatobiliary excretion resulting in gastrointestinal uptake. In people, this may compromise diagnostic assessment of these body systems[14]. A small study investigating the application of labelled leucocytes for diagnosis of right dorsal colitis in two horses showed no discernable hepatic uptake, posing a question over the significance of hepatobiliary excretion for this procedure in horses. The reconstituted radiopharmaceutical is also unstable and must be labelled within 30 mins of reconstitution[5]. Various additives have been used to extend the shelf life of the technetium eluate[27].

^{111}In-oxine has a higher labelling efficiency and higher label retention. The longer half life (67 h) is considered an advantage for imaging chronic inflammation; however, neutrophils have an average circulation time of only 10–12 h, with the result that localisation of labelled leucocytes at the site of an inflammatory focus is completed by 24 h[6,10]. Further delayed imaging is therefore unlikely to provide additional information.

A major disadvantage of ^{111}In-oxine is the higher photon energy of the emissions requiring special collimators which often have poor spatial resolution. The low photon flux necessitates longer acquisition times, risking poor image quality due to patient movement[6]. The high cost per unit dose may limit the dosage used , further influencing image quality. The longer half life of ^{111}In-oxine also imposes a time delay for patient release[5].

Method for Carrying Out Labelled Leucocyte Scan

The following procedures are performed.

Blood Sampling

The jugular vein is clipped and prepared aseptically. At least 100 ml blood is collected into 60 ml syringes containing anticoagulant using a 19 gauge or larger bore needle or catheter (to minimise damage to the cells). The anticoagulant of choice is acid-citrate-dextrose (ACD) with a typical concentration of 1.5 parts ACD to 8.5 parts whole blood[27]. Commercial blood transfer bags containing CPDA-1 anticoagulant are a convenient source of the anticoagulant and are simple to use.

[b]*Separation of Leucocytes, Granulocytes or Neutrophils*[27]

The erythrocye fraction is allowed to sediment, as centrifugation of whole blood is not an efficient method for obtaining leucocytes. Erythrocyte sedimentation is usually rapid for equine blood. The leucocyte-rich, platelet-rich plasma is carefully removed and centrifuged at low speed to pellet the leucocytes. The platelet-rich supernatant is removed and centrifuged at high speed to leave cell-free plasma, which is used for washing the cells after labelling and for resuspending the cells for re-injection. Separation of neutrophils or granulocytes requires the use of isopycnic gradients and various methods for carrying out such procedures have been reported[27].

[b]*Radiolabelling of Cells*

For radiolabelling with ^{99m}Tc-HMPAO, the radiochemical is first produced according to manufacturer's recommendations (Ceretec; Amersham). Briefly, this involves addition of 5 ml sterile eluate containing a known radioactive dose from a ^{99}Mo/^{99m}Tc generator to a vial containing HMPAO, stannous chloride and sodium chloride. Radiochemical purity may be assessed using ascending chromatographic systems[6]. The cells for labelling are resuspended in either saline for labelling with the indium complex or plasma for ^{99m}Tc-HMPAO. The radiopharmaceutical is added to the cell suspension and incubated for a set period (up to 30 mins). Cell-free plasma is then added to the suspension to remove any unbound radionuclide and, after centrifugation, the supernatant is removed and the plug of cells resuspended in plasma for re-injection. For ^{99m}Tc-HMPAO, the incubation process is initiated within 20 mins of radiochemical formation. The labelling efficiency is determined by measuring the activity on the labelled cells and the activity remaining in the labelling medium.

Equation 1

$$\% \text{ Labelling efficiency} = \frac{\text{Radioactivity on cells}}{\text{Radioactivity on cells + radioactivity in labelling medium}} \times 100$$

A labelling efficiency of at least 50% with high cell viability is desirable.

[b]These procedures are normally carried out by a radiopharmacy department.

Reinjection and Scan

The horse should be catheterised for reinjection. (for scanning method see *Acquisition Details* below.)

Dosage

Optimal radioactivity doses for labelled leucocyte studies in the horse have not been validated and large dose ranges have been reported in the literature for ^{99m}Tc-HMPAO (1 to 10 MBq/kg bwt)[15].

Dosages of around 1.1 to 1.3 GBq (30–35 mCi) for the adult horse are likely to provide satisfactory count densities. The count densities achieved also depend somewhat on labelling efficiency and time of scan post injection.

For ^{111}In-oxine, radioactivity of 11.1 to 37 MBq (0.3 to 1.0 mCi) is typically used at the time of radiolabelling[5]. In the single equine study reported in the literature using ^{111}In-oxine, the dose used was not recorded.

N **Figure 7: Dorsal view of kidneys: gamma camera quantitative renal scintigraphy (prior to depth correction)**

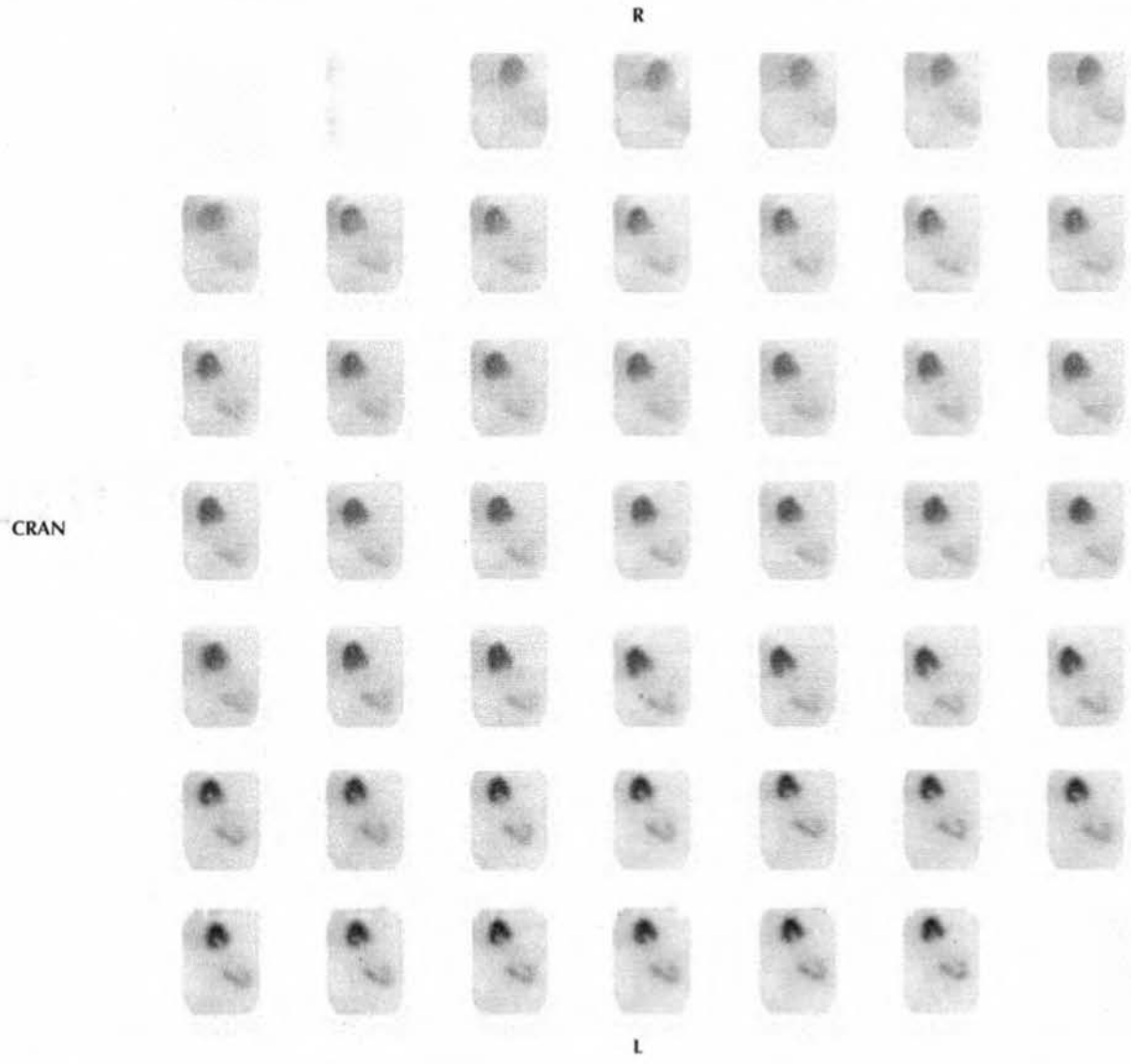

TB	4.5y	G	-	128 x 128
DX: Normal				
DS: NA				
Note: 60 x 5-sec frames started immediately prior to injection of radiopharmaceutical. Empty frames at the start of the study and those with excess movement have been removed. Radiopharmaceutical: ^{99m}Tc-DTPA.				

Acquisition Details

- Images are usually acquired at 1 and 4 h post injection. Delayed images may be obtained at 22 to 24 h.
- A low energy, parallel hole, general purpose or high resolution collimator is used for ^{99m}Tc-HMPAO studies. A medium energy collimator is necessary for ^{111}In-oxine.
- Static images may be obtained using a 128 x 128 or 256 x 256 matrix. Counts of 150,000 or greater are usually obtained for ^{99m}Tc-HMPAO.
- Dynamic frame mode acquisitions using a 128 x 128 matrix may be carried out when patient motion is a problem and correction software is available.

Interpretation of Images

In general terms, focal accumulation of radiolabelled leucocytes at sites where they are not 'normally' considered to accumulate is indication of an inflammatory focus.

The limited number of studies reported in both normal horses and those with confirmed disease imposes major limitations on our ability to interpret what is normal biodistribution and what is abnormal accumulation of radiolabelled leucocytes. This is most notable in evaluation of the abdomen and thorax.

In all species, varying degrees of 'normal distribution' have been characterised by uptake in the spleen, lungs, liver, bone marrow, gastrointestinal tract and urinary tract[13,15,17,28,29]. Removal of damaged leucocytes by the reticuloendothelial system is likely to account for some of the uptake in those organs. Uptake may be seen in the kidneys associated with excretion of ^{99m}Tc-complexes. Hepatobiliary excretion is associated with delayed gastrointestinal radiolabel activity, which has led to false positive diagnosis of inflammatory bowel disease in people[14,30]. Its significance has, however, been questioned in the horse[17].

RENAL NUCLEAR MEDICINE STUDIES

Introduction

A number of methods are used to investigate renal disease or dysfunction in horses in clinical practice, including physical and ultrasonographic examinations, serum biochemical analysis, urinalysis, and fractional and sulphanilate clearance testing. Serum biochemical analysis and urinalysis are the most commonly employed methods to evaluate renal disease; however, interpretation is subject to limited sensitivity and specificity. Both BUN and creatinine concentrations require a 75% decrease in functioning nephrons or in glomerular filtration rate (GFR) before levels rise above the normal range[31]. Many nonrenal factors can also alter BUN concentration independent of changes in renal function[31]. Urine specific gravity is subject to large normal variation and may be influenced by concurrent medication. Dilute urine may also be caused by abnormalities other than primary renal disease. The location of the kidneys limits physical examination and excess fat or intestinal gas may obstruct ultrasonographic evaluation[32].

Early detection of alterations in renal function or blood flow are necessary in order to implement therapeutic strategies which

N Figure 8: Dorsal view of kidneys: gamma camera quantitative renal scintigraphy (prior to depth correction)

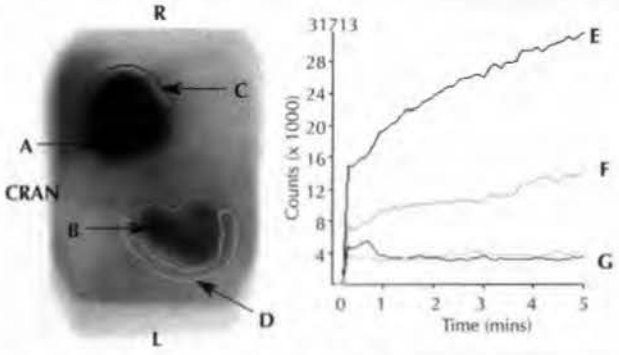

TB	4.5y	G	-	128 x 128

DX: Normal

DS: NA

- **A:** Summed image of right kidney with region of interest.
- **B:** Summed image of left kidney with region of interest.
- **C:** Background region of interest for right kidney.
- **D:** Background region of interest for left kidney.
- **E:** Time-activity curve for right kidney.
- **F:** Time-activity curve for left kidney.
- **G:** Time-activity curves for background regions of interest.

Note: 60 x 5-sec frames started immediately prior to injection of radiopharmaceutical.
Radiopharmaceutical: ^{99m}Tc-DTPA.

N Figure 9: Lateral view of right kidney: gamma camera quantitative renal scintigraphy (prior to depth correction)

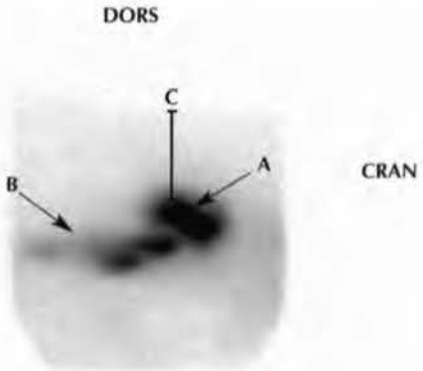

TB	4.5y	G	-	128 x 128

DX: Normal

DS: NA

- **A:** Right kidney.
- **B:** Ureter.
- **C:** Measurement for depth correction of right kidney.

Note: Summed dynamic or static acquisition following gamma camera quantitative renal scintigraphy.
Radiopharmaceutical: ^{99m}Tc-DTPA.

may prevent progression of renal disease and damage[33]. Two of the most reliable measures of renal function are GFR and effective renal plasma flow (ERPF) or effective renal blood flow (ERBF).

GFR is defined as the sum total of the filtration rates of each functioning nephron, which represents an index of functional renal mass[31]. Quantitative assessment of GFR relies on measurement of a substance which is freely filtered by the glomerulus and does not undergo synthesis, metabolism, secretion or reabsorption by the kidney. The substance must also not become bound to plasma proteins. Inulin clearance is the standard method for GFR measurement. This procedure requires constant and precise i.v. infusion of inulin, water loading, bladder catheterisation and sample collection over several hours, making it impractical in the clinical setting. Creatinine clearance may also be used to estimate GFR; however, prolonged urine collection is necessary and the procedure has not been validated in horses with renal disease[31]. Nuclear medicine studies have been developed which are less time-consuming, do not require urine collection and have been shown to correlate well with inulin clearance tests for assessment of GFR in a number of species, including horses[31,33,34].

^{99m}Tc-diethylenetriaminepentaacetic acid (^{99m}Tc-DTPA) has similar properties to inulin, making it a suitable radiopharmaceutical for GFR estimation. Measurement of radioactivity present in serial blood samples taken following i.v. administration allows construction of a plasma disappearance curve, from which the GFR can be calculated using a 2-compartment model[35]. The percentage of an injected dose of ^{99m}Tc-DTPA extracted by the kidneys within a 10 min period using a gamma camera has been shown to correlate well with inulin clearance in people, dogs and cats for estimation of GFR[36]. It also has the advantage of providing information on individual kidney function. This procedure in horses is less accurate because of difficulties in correcting for background activity and attenuation owing to various kidney depths. Movement of the patient within the study period also diminishes the accuracy of the procedure[34].

Any condition which results in marked hypotension and/or release of endogenous pressor agents can result in reduced renal blood flow, which may cause renal ischaemia and tubular damage and can lead to cortical necrosis and acute renal failure[33,37]. Quantitative measurements of renal blood flow, termed effective renal blood flow (ERBF) and effective renal plasma flow (ERPF), are considered good indicators of renal function[38]. Measurement of absolute renal blood flow and renal plasma flow requires general anaesthesia and catheterisation of the major renal blood vessels, invalidating it as a clinical procedure. Indirect estimations of ERPF and ERBF can be made by measuring plasma clearance of an inert substance which is almost completely extracted from the blood on its first pass through the kidneys[31,32,34]. Para-aminohippurate (PAH) clearance has been the accepted standard measurement for ERPF estimation. However, like inulin clearance, the procedure is technically demanding and impractical for clinical use. Radiopharmaceuticals have been developed which allow noninvasive and technically simple estimation of ERBF. ^{131}I-orthoiodohippuric acid (^{131}I-OIH) plasma clearance studies have been shown to correlate well with PAH clearances for estimation of ERBF in horses[33]. Because of the less than desirable imaging characteristics of ^{131}I-OIH, efforts have been made to develop a ^{99m}Tc agent to measure ERPF. A more recent study measuring ^{99m}Tc-mercaptoacetyltriglycine (^{99m}Tc-MAG_3) plasma clearance in horses showed that this might be a useful and clinically applicable radiopharmaceutical for estimation of ERBF[38]. ^{99m}Tc-ethylene dicysteine (^{99m}Tc-EC), a metabolite of the brain imaging agent ^{99m}Tc-ethylene cysteine dimer (^{99m}Tc-ECD), has shown lower plasma protein binding and higher renal clearance than ^{99m}Tc-MAG_3 in human and animal studies. ^{99m}Tc-EC may ultimately be a more suitable agent for renal clearance studies.

Direct scintigraphic imaging of the kidneys over a finite period following rapid i.v. injection of radiopharmaceutical can be used to estimate ERBF. As with GFR estimation, this technique is less accurate in the horse due to difficulties in correction for kidney depth and background activity.

Information on renal size, shape and location can be gained from images taken during and immediately after quantitative gamma camera studies using ^{99m}Tc-DTPA or ^{99m}Tc-MAG_3[39]. ^{99m}Tc-dimercaptosuccinic acid (^{99m}Tc-DMSA) and ^{99m}Tc-glucoheptonate (^{99m}Tc-GH) show some binding to tubular epithelial cells, which provides better morphological detail and allows calculation of relative renal function between left and right kidney. No published information on the use of renal morphology scintigraphy in horses has been found.

Glomerular Filtration Rate Measurement

Indications

- Identification of early alterations in renal function in order to prevent progression of renal disease and damage.
- Evaluation of response to therapy and as an aid to prognosis.
- Detection and monitoring of subclinical renal disease caused by nephrotoxic agents (e.g. aminoglycosides).

Radiopharmaceutical

^{99m}Tc-diethylenetriaminepentaacetic acid (DTPA) is used.

Dosage

Recommended dose is 111 to 148 MBq (3 to 4 mCi)[36]. Doses reported in the literature for plasma clearance and gamma camera percentage uptake studies vary from 3 to 30 mCi (111 to 1110 MBq)[33,34]. 3 mCi is plenty for plasma clearance studies because blood or plasma samples are counted in a well detector with a high efficiency, whereas 10 times the dose is necessary for the gamma camera because of its low efficiency.

For the gamma camera studies, inaccuracies in measuring the pre-injection dose may be introduced if the dosage is too high (recommended maximum dose in small animals is 148 MBq or 4 mCi)[36].

An advantage of using low dose radiopharmaceuticals is the relative safety for handling and monitoring horses undergoing treatment.

Techniques

Blood Clearance Method

Duplicate samples from the dose solution are diluted and stored to provide dose standards allowing calculation of total injected dose.

An accurate dose volume is injected as a bolus into the left jugular vein at time zero. Heparinised blood samples are then collected at accurately timed intervals up to 180 mins post injection. Recommended time intervals are 12, 40, 60, 120 and 180 mins. Samples are then centrifuged and 0.5 to 1.0 ml aliquots of plasma are pipetted into test tubes for counting in a scintillation well counter.

Radioactivity in counts per min or % injected dose per ml plasma is plotted against time, producing a plasma disappearance curve, and the GFR is calculated using a 2-compartment mathematical model[33,36]. Computer programmes are available to carry out such analyses.

Percentage Uptake (Gamma Camera Method)[36]

See **Figures 7–9**.

Acquisition Details

- A known small volume of the total dose (i.e. 1/10th) is precounted for several seconds at a distance of 60 cm from the centre of the gamma camera in order to calculate predose counts per min. The gamma camera will be overwhelmed because of dead time loss if the full dose is used. A matrix size of 64 x 64 is typically used.
- The camera is positioned 15 cm over the dorsum of the standing horse, centred over the thoracolumbar junction. Sedation should be avoided or minimised where possible, to avoid renal hypotension and a consequent reduction in GFR. If a small field of view camera is used, a diverging collimator may be necessary in order to view both kidneys.
- Acquisition starts immediately upon rapid injection of the ^{99m}Tc-DTPA. Multiple 5 to 15 sec frames are acquired for a minimum of 3 mins, using 64 x 64 or 128 x 128 matrices.
- Following the dynamic study, static lateral images of each kidney are obtained to allow measurement of kidney depth for depth correction. A 128 x 128 or 256 x 256 matrix is used.
- Post injection counts are taken of the empty syringe and catheter at a distrance of 60 cm from the camera and converted to counts per min (64 x 64 matrix).

GFR Calculation

- Frames are corrected for motion.
- Regions of interest are drawn over each kidney and around the lateral border of each kidney for background counts. Activity vs. time curves are created for each kidney and background ROI.
- Net kidney counts for each kidney from 1–3 mins post injection are calculated:
  Net kidney count = (kidney ROI cts) - (background ROI cts) x (No. pixels in kidney ROI/No. pixels in background ROI).
- Percent injected dose in each kidney is calculated:
  % Injected dose = net kidney cts/[(predose cts) - (post dose cts)] x 100.
- Correct % injected dose for depth using lateral images acquired of each kidney. Linear absorption coefficient in soft tissue is used for calculation (0.153/cm).
- Depth corrected % injected dose = % injected dose x $e^{(0.153 \times \text{kidney depth in cm})}$, where (e = base of natural logarithm).
- GFR can be calculated using the following regression equation[34]:
  GFR = 0.8257 (depth corrected % injected dose at 1 to 3 mins) + 66.
- Split kidney function can be expressed as a percentage of total depth corrected net counts or % injected dose. Individual kidney GFRs can also be calculated.

Interpretation

Plasma clearance studies carried out in clinically normal horses have revealed the following glomerular filtration rates (ml/min/kg): 1.47 ± 0.27[34]; 1.79 ± 0.18[31]; 1.93 ± 0.34[31].

A comparative % injected dose study (gamma camera) revealed a GFR of 1.55 ± 0.22[34].

The same study indicated that this method did not correlate significantly with the recognised standard inulin clearance and suggested that it may not be as reproducible as the plasma clearance method for GFR estimation. The plasma clearance method showed a correlation coefficient to inulin clearance of 0.66[34]. GFR estimations may be more reproducible in horses which have lost their functional renal reserve and in which the residual functional mass is constantly performing at its maximum. The accuracy of GFR estimation using ^{99m}Tc-DTPA also decreases when renal disease is severe and the GFR is very low. Other measures of renal function are of more use in these circumstances.

N Figure 10: Angiogram of the terminal aorta

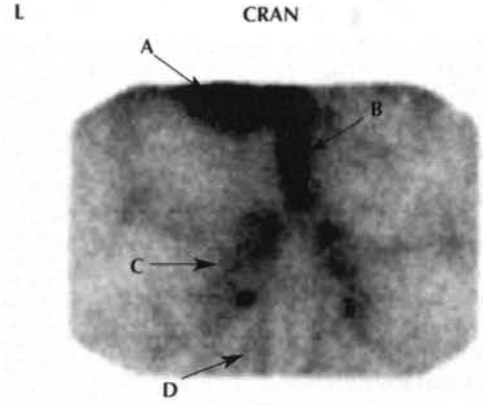

TB	7y	G	-	128 x 128
DX:	Normal			
DS:	NA			

➔ **A:** Left kidney.
➔ **B:** Terminal aorta.
➔ **C:** Left external iliac artery.
➔ **D:** Left internal iliac artery.
Note: Summed 45 x 2-sec frames started at time of injection of radiopharmaceutical.
Radiopharmaceutical: ^{99m}Tc-MDP.

N **Figure 11: Angiogram of the terminal aorta**

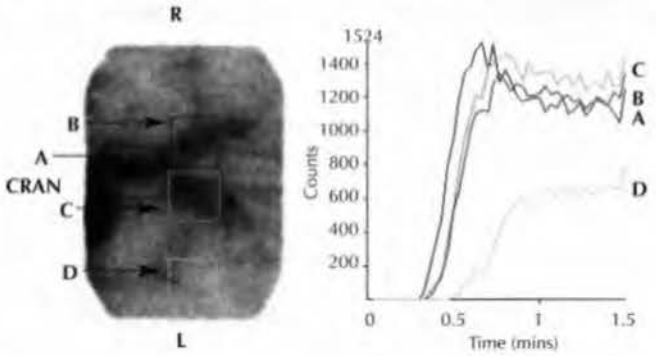

TB	7y	G	-	128 x 128

DX: Normal

DS: NA

- **A:** Terminal aorta region of interest and corresponding time-activity curve.
- **B:** Right external iliac artery region of interest and corresponding time-activity curve.
- **C:** Left external iliac artery region of interest and corresponding time-activity curve.
- **D:** Background region of interest.

Note: Summed 45 x 2-sec frames started at time of injection of radiopharmaceutical.
Radiopharmaceutical: ^{99m}Tc-MDP.

A **Figure 12: Angiogram of the terminal aorta**

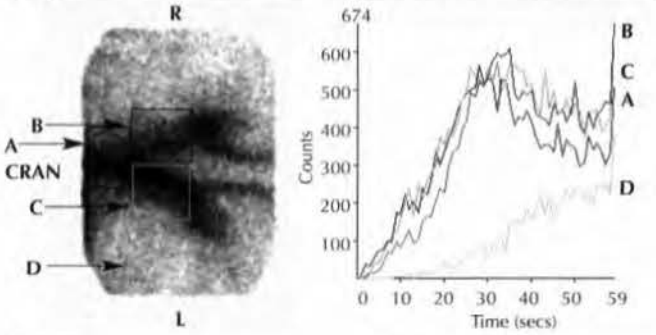

TBx	9y	M	-	128 x 128

DX: Apparent decreased flow through right external iliac artery. May be assessed quantitatively by comparison of area under the curve data which estimates total blood flow through the vessels.

DS: NA

- **A:** Terminal aorta region of interest and corresponding time-activity curve.
- **B:** Right external iliac artery region of interest and corresponding time-activity curve.
- **C:** Left external iliac artery region of interest and corresponding time-activity curve.
- **D:** Background region of interest.

Note: Summed 45 x 2-sec frames started at time of injection of radiopharmaceutical.
Radiopharmaceutical: ^{99m}Tc-MDP.

Effective Renal Blood Flow and Effective Renal Plasma Flow Measurement

Indications

- Quantification of renal function and, ideally, detection of early dysfunction.
- Monitoring response to therapy for primary or secondary renal dysfunction.
- Evaluation of the influence of certain medications on renal function in metabolically compromised horses.

Radiopharmaceuticals

- ^{131}I-orthoiodohippuran (^{131}I-OIH).
- ^{99m}Tc-mercaptoacetyltriglycine (^{99m}Tc-MAG$_3$).

Dosage

- ^{131}I-OIH: 11.25 to 14.8 MBq (300 to 400 μCi).
- ^{99m}Tc-MAG$_3$: 185 to 296 MBq (5 to 8 mCi).

Techniques

Blood Clearance Method

The same protocol is followed as that for ^{99m}Tc-DTPA. Sampling times are somewhat arbitrary and guidelines are therefore based on reported studies.

Sampling times for ^{131}I-OIH studies have been at 3 min intervals for 30 mins, then 5 min intervals for a further 30 mins[32].

Sampling times for ^{99m}Tc-MAG$_3$ have been at 5, 10, 15, 20, 30, 45, 60, 90, 120, 150 and 180 mins following injection[38].

Calculations are based on fitting a plasma disappearance curve which follows a logarithmic function and is analysed by a 2-compartment model[32,34].

Effective renal blood flow is calculated from effective renal plasma flow by the following equation:

ERBF = ERPF/(1 - PCV), where PCV = packed cell volume

Interpretation

Plasma clearance studies carried out in clinically normal horses have revealed the following ERBF or ERPF data for ^{131}I-IOH:

Mean ERBF 18.42 ± 1.57 (8 horses)[33]
Mean ERBF 10.75 (range 6.57–12.63; 6 horses)[32]
Mean ERPF 6.26 (range 4.33–6.80; 6 horses)[32]
Mean ERPF 8.24 ± 2.88[40].

A study using ^{99m}Tc-MAG$_3$ for estimation of ERPF in 10 clinically normal horses revealed a clearance rate (ml/min/kg) of mean (ERPF) 7.9 ± 1.5 (range 5.5-10.6)[38].

These results were shown to be repeatable in 3 horses. Evaluation of 2 horses with renal failure showed reduction in clearance rates. Clinical recovery in one horse was mirrored by improvement in the estimated clearance rate.

The radiopharmaceuticals used are not entirely removed from the blood on first pass through the kidneys, resulting in measurements which underestimate the true renal plasma flow. In addition, ^{99m}Tc-MAG$_3$ has higher protein binding capacity and a smaller volume of distribution than either ^{131}I-OIH or PAH, potentially further influencing the estimation of ERBF. ^{99m}Tc-MAG$_3$ studies in people, dogs and horses have, however, indicated similar results between the different agents used[36,38].

Percentage Uptake (Gamma Camera) Method

Quantitative scintigraphy has been shown to provide an adequate means of estimating effective renal plasma flow in dogs, but the technique has not been evaluated in horses[41]. As with the GFR studies using the gamma camera, correction for kidney depth and motion limits the accuracy of this technique in horses.

Summary

Measurement of glomerular riltration rate and effective renal blood flow by the method of plasma clearance of radiopharmaceuticals is a valid and potentially highly useful clinical tool for evaluation of renal function in horses. The procedure is noninvasive, simple to perform, safe and gives repeatably accurate estimations of renal function.

Although gamma camera percentage uptake of radiopharmaceutical methods for estimating GFR and ERBF are possible, technical difficulties, largely a result of patient size and motion, render this a less valid procedure.

AORTOILIACOFEMORAL THROMBOSIS: FIRST-PASS RADIONUCLIDE ANGIOGRAPHY

Introduction

Aortoiliacofemoral thrombosis is an uncommon condition in horses characterised by exercise-induced, mild to moderately severe, unilateral or bilateral hindlimb lameness which resolves or improves following cessation of exercise[41]. This is often preceded by a history of variable hindlimb stiffness and loss of performance. Occlusion of the terminal aorta and its major branches and embolism of the peripheral hindlimb vessels results in muscle ischaemia and pain. The severity of the lameness exhibited depends upon the extent of vascular occlusion[42-44]. There is a higher incidence of the condition in males and, although there is no particular breed predilection, it has been most commonly reported in racehorses. The exact aetiology of the condition is uncertain; however, damage to the intima of the affected blood vessels by mechanical factors is considered most likely[43,45].

Diagnosis of aortoiliacofemoral thrombosis is based on history, clinical presentation, pre- and post exercise muscle enzyme determination and rectal palpation combined with ultrasonography *per rectum*[41,42,46]. Ultrasonography has become the method of choice for obtaining a definitive diagnosis and monitoring response to treatment[45-47].

Doppler ultrasound techniques have also been used to determine the presence of thrombi beyond the level of the external iliac artery, and to determine blood flow at the level of the femoral artery in the inguinal region[48]. An additional diagnostic technique involves monitoring for the development of hypoxaemia in an affected limb by measuring the partial pressure of oxygen in blood taken from both saphenous veins before and after exercise[48]. Contrast arteriography has been advocated to diagnose the condition. However, it is invasive, requires general anaesthesia and is not considered necessary[42,46].

First-pass radionuclide angiography of the terminal aorta and branches is a simple, noninvasive method to provide qualitative information on blood vessel morphology and semiquantitative blood flow data in horses with suspected aortoiliacofemoral thrombosis[42,46].

Indications

- To assist in the diagnosis of hindlimb lameness thought to be associated with aortoiliacofemoral thrombosis. Can be used in conjunction with skeletal scintigraphy.
- Assessment of the severity of vascular occlusion by providing qualitative information on vessel morphology and semiquantitative information on blood flow.
- Repeat studies may help evaluate progression of the condition and document the response to therapy.

Radiopharmaceuticals

A variety of radiopharmaceuticals can potentially be used; however, the best images are obtained by using a radiopharmaceutical of high concentration (mBq/ml) which produces a tight bolus of activity[49].

- ^{99m}Tc-methylene diphosphonate (^{99m}Tc-MDP) or ^{99m}Tc-hydroxymethylene diphosphonate (^{99m}Tc-HDP). Use of these agents allows skeletal scintigraphy of the hindlimbs and pelvis to be carried out concurrently. This is especially valid when other diagnostic procedures have proved inconclusive. High background activity may adversely affect image quality if immediate repeat studies are necessary because of patient movement or malpositioning[42].
- ^{99m}Tc-diethylenetriaminepentaacetic acid (^{99m}Tc-DTPA) or ^{99m}Tc-sulphur colloid. These agents are rapidly cleared and are useful for multiple studies[42].
- ^{99m}Tc-pertechnetate ($^{99m}TcO_4^-$). Lower doses of radiopharmaceutical may be used, but high background activity precludes repeat studies[42].

Dosage

The dose for ^{99m}Tc-MDP or ^{99m}Tc-HDP is as for skeletal scintigraphy, 1 GBq/100 kg bwt.

Lower doses can be used for the other radiopharmaceuticals. Approximately 1 GBq per study is suggested.

Acquisition Details

- Images are obtained using a low energy, parallel hole general purpose or high resolution collimator.
- The camera is positioned level, and dorsal to the region of the terminal aorta. A 7 to 10 cm gap between the horse and camera is allowed, to prevent damage to the camera from sudden movement.

- A dynamic acquisition is started at the time of, or within 20 secs of, rapid administration of the radiopharmaceutical into the jugular vein; or when radioactivity is first seen on the persistence monitor. Using the latter technique, no frames are wasted by starting acquisition prematurely. Thirty to 45 x 2-sec frames or 60 to 90 x 1-sec frames are acquired, depending upon the time the acquisition is started following injection.
- A 64 x 64 or 128 x 128 matrix is used.

Analysis and Interpretation

- The frames in which filling of the vessels can be identified are summed and the images examined for vessel conformation and symmetry. In the normal patient, the 'V'-shaped bifurcation of the external iliac arteries, along with symmetrical linear caudal extension of the internal iliac arteries, should be seen (**Figure 10**). Significant deviation from this pattern should be interpreted as abnormal.
- Regions of interest are created over: 1) the terminal aorta; 2) the region including the right external and internal iliac arteries; 3) the region including the left external and internal iliac arteries and 4) a background region.

Time versus activity curves are created from the data from each ROI. An estimate of total blood volume for each ROI can be calculated from integrated area under the time versus activity curves. The mean and standard deviation values for each ROI can be compared[42] (**Figures 11 and 12**) (NB: computer software programmes are readily available to perform the analyses).

In horses in which the terminal aorta appears normal by palpation and ultrasonography, obstruction may be in the femoral artery. Blood flow in each femoral artery can be assessed by positioning the gamma camera lateral to the crus of the limb to be examined. Evaluation of venous obstruction is discussed briefly in *Part I, Chapter 8*.

PORTOSYSTEMIC SHUNT SCINTIGRAPHY

Introduction

Portosystemic shunts may be congenital or acquired, intra- or extrahepatic[50]. Although they occur as a common congenital disorder in dogs and, to a lesser degree, in cats, the prevalence of portosystemic shunts in horses is unknown[51,52]. There have been few reports of documented congenital extrahepatic portosystemic shunts in foals[51,53]. Clinical signs are often variable and nonspecific and serum biochemical tests to assess liver function are also nonspecific, making diagnosis difficult. Vague intermittent neurological signs such as blindness, ataxia and depression are the result of hepatic encephalopathy which, along with stunted growth, is caused by hepatocellular atrophy secondary to altered hepatic blood flow and hepatic insufficiency[50]. Other diagnostic procedures that may be of use include liver biopsy, ultrasonography, intraoperative portal angiography and scintigraphic flow studies of the liver. Histopathology usually shows nonspecific hepatocellular atrophy, necrosis, and fibrosis and biliary hyperplasia[50]. Conventional and colour-flow Doppler ultrasonography are highly accurate for diagnosing congenital portosystemic shunts in cats, but the greater size of the foal is likely to reduce the accuracy of this technique[54]. Portal angiography allows more specific diagnosis, but the procedure requires general anaesthesia and is invasive. Neither ultrasonography nor portal angiography provide quantitative data about the degree of shunting[55,56].

Portal blood flow is able to be detected and measured noninvasively using scintigraphic flow studies of the liver. This is achieved by means of measurement of radioactivity within the heart and liver following either i.v. or *per rectum* administration of radiopharmaceutical[56]. Two i.v. techniques using ^{99m}Tc-sulphur colloid have been described, including the use of one technique to specifically aid the diagnosis of a portosystemic shunt in a foal[51]. This technique involves analysing the first pass of ^{99m}Tc-sulphur colloid through the circulation to determine the relative contribution of hepatic arterial and portal venous blood flow to the total liver blood flow. An increased ratio of hepatic arterial blood flow to portal blood flow (hepatic perfusion index) is seen with portosystemic shunting. Other liver conditions, such as hepatitis, may alter this ratio, which decreases the specificity of this technique. The technique is also susceptible to errors in calculation and observer bias and its value as a screening test for portosystemic shunts in foals is questionable.

Per rectum administration of ^{99m}Tc-pertechnetate ($^{99m}TcO_4^-$) is considered a simple, inexpensive and effective means of diagnosing and quantifying portosystemic shunts in dogs and cats[57]. It has also been used successfully by this author to diagnose the condition in a foal. When administered in high concentration *per rectum*, a proportion of ^{99m}Tc-pertechnetate is rapidly absorbed across the colonic mucosa. A high concentration is necessary, as less than 15% of the initial dose undergoes rapid absorption via this route. Its normal transit through the portal vessels to the liver and, shortly thereafter, the heart, can be imaged by dynamic scintigraphic studies. The normal time delay between detection of the radiopharmaceutical in the liver and heart is related to patient size. ^{99m}Tc-pertechnetate is not actively taken up by the liver or heart and the study is therefore essentially a nuclear angiogram of the portal system. When portosystemic shunting is present, some of the administered radiopharmaceutical reaches the heart at the same time as, or before, it is detected in the liver. During the first pass of ^{99m}Tc-pertechnetate, the ratio of integrated heart to liver counts can be used to estimate the percentage of portal blood flow which has bypassed the liver through the shunt. This estimate is termed the 'shunt fraction' and its calculation in studies using *per rectum* ^{99m}Tc-pertechnetate in people, dogs and cats has been described[52,55,58,59]. Shunt fraction calculation has been shown to vary significantly between operators, posing questions over its reliability for comparative studies[60].

Indications

- This is a simple and inexpensive screening test for the presence of a portosystemic shunt and may be indicated in foals where more common causes of neurological abnormalities, such as trauma, vertebral body abscesses, brain abscesses, and meningitis, have been ruled out[51].
- Estimation of the degree of shunting by calculating the shunt fraction.
- Follow-up evaluation of surgical intervention by comparison of pre- and post operative shunt fraction calculations. The comparison may not be reliable because of interstudy variability[52,60].

Radiopharmaceutical

- ^{99m}Tc-pertechnetate ($^{99m}TcO_4^-$).

Dosage[45]

A dose rate of 37 to 74 MBq/kg has been used in small animals and is suggested as a guideline for dosage in foals. As less than 15% is initially absorbed through the colonic mucosa, the dose should be concentrated in 1 to 2 ml saline.

Method of Administration

- The foal is sedated and placed in left lateral recumbancy on a padded surface. The gamma camera is lowered to centre over the cranial abdomen on the right side. If a rectangular field of view camera is used, the long side of the camera is orientated parallel to the long axis of the vertebral column.
- A 12 French soft rubber catheter is inserted into the rectum and cautiously advanced a short distance into the caudal colon. The radiopharmaceutical is administered through the catheter via one limb of an attached 3-way stop cock. The catheter is immediately flushed with 10 to 15 ml of room air via the other limb of the stop-cock. Room air is used to avoid dilution of the radiopharmaceutical.

Acquisition Details

- A large field of view gamma camera fitted with a general purpose, low energy, parallel hole collimator is used.
- A dynamic acquisition is started immediately prior to administration of the radiopharmaceutical; 180 x 1-sec frames, or 90 x 2-sec frames are acquired using a 64 x 64 or a 128 x 128 matrix size.

Interpretation

A normal portoangiogram in people and dogs reveals uptake of radiopharmaceutical in the portal vessels approximately 10 to 22 secs following administration[55,57]. Liver uptake is subsequently seen and, after a further delay (portal hepatic transit time), uptake is recorded in the heart. This delay is approximately 12 secs in the dog[55,57]. The normal delay is likely to be slightly longer in the foal due to the larger size (**Figures 13a and 13b**).

When portosystemic shunts exist, radioactivity appears in the heart at the same time or prior to its appearance in the liver (**Figures 14a and 14b**).

Anatomical localisation of the heart and liver can be made prior to the study using ultrasonography. Lead markers can be placed for subsequent identification following the scan. Alternatively, the structures can be identified on composite images of the entire study.

For calculation of the 'shunt fraction', time-activity curves for ROIs drawn over the liver and heart are created from the data after the first appearance of the radiopharmaceutical in either organ. The arrival of the radiopharmaceutical is characterised by a doubling of the counts above background[52]. Integration of the curves over a time interval representing the normal liver-to-heart delay allows calculation of the shunt fraction[52,55].

Equation 2

$$\text{Shunt fraction} = \frac{\Sigma \text{ total heart counts}}{\Sigma \text{ total heart counts} + \Sigma \text{ total liver counts}} \times 100$$

Shunt fraction values in normal animals are less than 5%. This will increase as the time interval over which the calculation is made increases.

HEPATIC NUCLEAR MEDICINE STUDIES

Introduction

The diagnosis and evaluation of hepatic disorders in the horse relies on historical information, clinical signs, laboratory findings, ultrasonographic findings and results of liver biopsy. The clinical signs and laboratory findings are often nonspecific and variable because the liver performs multiple functions, and massive loss of hepatic mass usually has to occur before many of the laboratory parameters are altered[50]. Measures commonly used to assess hepatic function include serum bile acid concentration, serum bilirubin concentration and indirect tests of protein synthesis, carbohydrate metabolism and lipid metabolism. These measures can, to varying degrees, confirm decreased hepatic function; however, they do not specifically determine the degree of dysfunction[61]. Clearance of bromsulphalein (BSP) from the blood has been used to evaluate liver function. The plasma half-life of BSP is prolonged when greater than 50% of hepatic function is lost. Again, this does not provide accurate information on the degree of dysfunction and the test is prone to error if plasma concentration of albumin is markedly decreased or plasma bilirubin is markedly increased. Pharmaceutical grade BSP is also no longer commercially available[50].

Nuclear medicine studies have been used extensively in people to assess the liver and hepatobiliary system. It is considered the technique of choice for diagnosing acute cholecystitis and, in paediatrics, it assumes great importance in studying the aetiology of jaundice and many other disorders involving the liver and biliary tract, including cystic fibrosis and post liver transplantation management[62-65]. In animals, hepatic and hepatobiliary scintigraphy originally provided information on hepatic and biliary morphology and biliary kinetics[66-68]. A number of subsequent scintigraphic methods were used to quantify hepatic excretion of radiopharmaceutical, but none were able to measure hepatic uptake reliably[69].

Quantification of hepatocyte function requires measurement of the efficiency of uptake of a radiopharmaceutical which is taken up exclusively by the liver and excreted into the bile with minimal backflow into the blood. ^{99m}Tc-iminodiacetic acid derivatives fulfil these requirements. The higher molecular weight derivatives undergo less competitive inhibition in the presence of elevated serum bilirubin levels, resulting in less compensatory renal excretion[70]. This measure of hepatic extraction efficiency is termed the hepatic extraction fraction (HEF) and is defined as the proportion of radiopharmaceutical removed from the blood on each circulatory pass through the liver[61,69,70]. For

N **Figure 13a: Nuclear portoangiogram of the right abdomen and thorax**

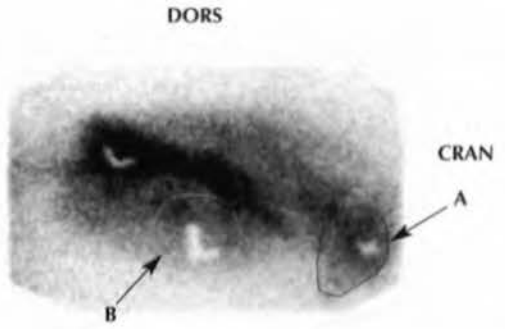

TBx	5m	C	-	128 x 128
DX:	Normal			
DS:	NA			

➔ **A:** Region of interest placed over heart.
➔ **B:** Region of interest placed over cranioventral liver.
Note: Summed 90 x 2-sec frames starting immediately prior to *per rectum* administration of radiopharmaceutical. Lead markers were placed over liver and heart, imaged ultrasonographically immediately prior to scanning. Radiopharmaceutical: ^{99m}Tc-pertechnetate.

N **Figure 13b: Time-activity curves from nuclear portoangiogram of the right abdomen and thorax**

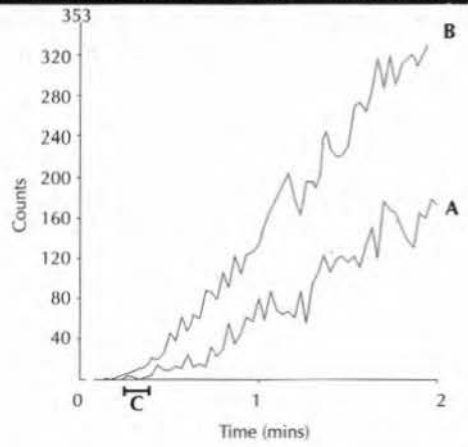

TBx	5m	C	-	128 x 128
DX:	Normal			
DS:	NA			

➔ **A:** Time-activity curve for heart ROI.
➔ **B:** Time-activity curve for liver ROI.
➔ **C:** Time delay between liver uptake and uptake in heart.
Note: Summed 90 x 2-sec frames starting immediately prior to *per rectum* administration of radiopharmaceutical. Radiopharmaceutical: ^{99m}Tc-pertechnetate.

A **Figure 14a: Nuclear portoangiogram of the right abdomen and thorax**

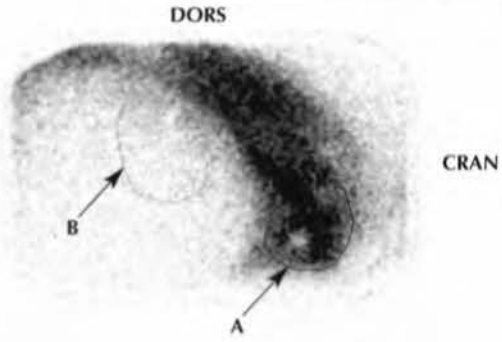

TBx	3m	C	-	128 x 128
DX:	Portocaval shunt.			
DS:	NA			

Stunted growth, neurological signs, blood profile indicating liver pathology.
➔ **A:** Region of interest placed over heart.
➔ **B:** Region of interest placed over region of presumed, normal location of liver (not visualised).
Note: Summed 90 x 2-sec frames starting immediately prior to *per rectum* administration of radiopharmaceutical. Lead markers were placed over liver and heart, imaged ultrasonographically immediately prior to scanning. Radiopharmaceutical: ^{99m}Tc-pertechnetate.

A **Figure 14b: Time-activity curves from nuclear portoangiogram of the right abdomen and thorax**

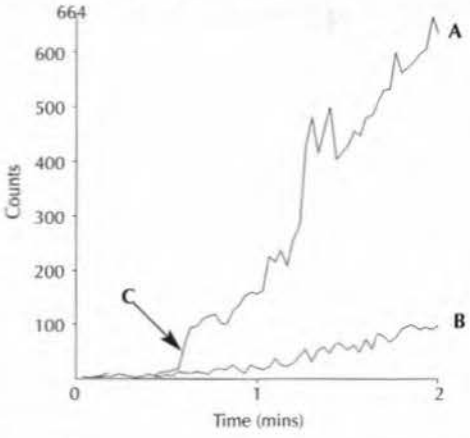

TBx	3m	C	-	128 x 128
DX:	Portocaval shunt.			
DS:	Stunted growth, neurological signs, blood profile indicating liver pathology.			

➔ **A:** Time-activity curve for heart ROI.
➔ **B:** Time-activity curve for liver ROI.
➔ **C:** Activity in heart precedes and greatly exceeds that in liver.
Note: Summed 90 x 2-sec frames starting immediately prior to *per rectum* administration of radiopharmaceutical. Radiopharmaceutical: ^{99m}Tc-pertechnetate.

direct measurement of HEF, the radiopharmaceutical must also be supplied to the liver as a single, discrete intravascular bolus[69,71]. Direct measurement from a peripheral i.v. injection is therefore not possible, as only 20% of the cardiac output is presented to the liver on each circulatory pass. The majority of the radiopharmaceutical is recirculated, producing a continually changing concentration to the hepatocytes[69,70]. Direct measurement therefore requires injection of the radiopharmaceutical into the hepatic artery or portal vein, which is invasive and clinically impractical.

Deconvolution analysis is a mathematical technique which transforms the data from an i.v. injection to simulate injection directly into the hepatic vessels[71]. This technique has been used to assess hepatocyte function in people, dogs and cats. In one study, it has been shown to correlate well with the direct measurement technique and with quantitative histopathology in dogs with experimentally-induced liver disease[69]. A similar study in cats with experimental cholangiohepatitis, however, showed no significant derangement of scintigraphic parameters despite the presence of severe multifocal histological abnormalities[72]. Deconvolutional analysis requires the creation of liver and heart time-activity curves to provide input data. This procedure is not possible in the horse, because the heart and liver cannot be included in the same field of view.

Plasma clearance of ^{99m}Tc-mebrofenin has been assessed in the dog as an alternative approach to quantifying hepatic function[61]. Plasma time-activity curves derived following i.v. injection of ^{99m}Tc-mebrofenin had kinetics of a 2-compartment model. The area under the curve data, integrated for 1 to 60 mins, was shown to correlate very highly with the first-pass hepatic extraction efficiency calculated following mesenteric injection of the radiopharmaceutical, both in normal dogs and those with decreased hepatic extraction efficiency as a result of experimentally-induced liver disease. Linear regression analysis was used to create a formula for calculating the hepatic extraction fraction from the integrated area under the curve data[61].

In another study in normal dogs and dogs with experimentally-induced liver damage, the area under normalised heart time-activity curves was used to calculate hepatic extraction and compared with direct measurement of hepatic extraction following mesenteric venous injection with ^{99m}Tc-mebrofenin. A good correlation was found between these methods, and a formula for calculating hepatic extraction was derived using linear regression analysis[73].

In summary, both 'hepatic extraction fraction', calculated by deconvolutional analysis, and 'hepatic excretion rate $T_{1/2}$' (time from maximum hepatic uptake to 1/2 maximum activity) have been shown in dogs to be good predictors of the severity of hepatocellular damage in toxin-induced liver disease[69]. The method for deconvolutional analysis is not technically possible in horses because the liver and heart cannot be imaged simultaneously. However, both plasma clearance of ^{99m}Tc-mebrofenin and the scintigraphically-derived heart time-activity curves have been shown to correlate well with direct measures of hepatic extraction in dogs. These procedures therefore have the potential in the horse to provide valuable information on hepatic function, but they must be validated before they are recommended for clinical application. Validation in the horse is likely to require multiple studies of both normal horses and those with known hepatic disease, documented with histopathological information from biopsy material and, where possible, necropsy.

Hepatic scintigraphy studies reported in the horse to date are scant. They include a morphological study comparing ^{99m}Tc-iminodiacetic acid derivatives and a study using ^{99m}Tc-disofenin to determine normal morphology of the liver and biliary tract of the adult horse, and to determine the effects of feeding on biliary kinetics[66,67].

Indications and parameters are consequently limited at present and the procedure is somewhat laborious, which restricts the use of hepatic imaging in the clinical setting.

Indications

- Evaluation of hepatic morphology.
- Measurement of biliary kinetics and hepatic excretion.
- Assessment of biliary tract patency.

Radiopharmaceuticals

- All studies in the horse are carried out using one of the ^{99m}Tc-iminodiacetic acid derivatives. These are extracted and excreted by the hepatocyte via a carrier-mediated organic anion pathway (similar to the clearance mechanism for bilirubin)[71]. ^{99m}Tc-mebrofenin and ^{99m}Tc-disofenin are the more commonly used radiopharmaceuticals in this group.
- ^{99m}Tc-sulphur colloid, used to evaluate hepatic morphology in other species, cannot be used. It is preferentially taken up by the active macrophage-monocyte system in the lungs of horses, which obscures liver visualisation[66,67].

Dosage

Recorded radioactivity doses in the horse are in the range of 2.6 to 3.3 MBq/kg (0.07 to 0.09 mCi/kg).

Acquisition Details[67,74]

- Multiple views may be obtained for evaluation of hepatic morphology. The right lateral view gives the best overall visualisation of the liver.
- A diverging collimator is typically used to allow inclusion of the whole liver.
- The acquisition starts 5 mins after injection of the radiopharmaceutical. Sixty-sec static images are acquired at 5 min intervals for 60 mins, then at 70, 80 and 90 mins post injection. Alternatively, fewer images may be acquired at 5, 10, 15, 30, 45, 60 and 90 mins post injection. 250,000 to 500,000 counts per acquisition are advised.
- Dynamic frame images may allow for motion correction.
- A 128 x 128 matrix is typically used.

Interpretation[67,74]

- Morphology: Maximum hepatic RU has usually occurred by 10 mins. Size, shape and homogenicity can be assessed visually.
- Biliary kinetics: Washout curves can be created for the liver and biliary tract using strategically placed regions of interest

and algorithms to correct for areas of superimposition of liver, biliary tract and duodenum. Various quantitative measures of bile flow can be calculated, including:

T_{max} = time from injection to peak activity.
T_{50} = time from injection to 50% of peak counts.
$T_{1/2}$ = time from T_{max} to 1/2 maximum activity.

BRAIN SCINTIGRAPHY

Introduction

Conventional radionuclide brain imaging was originally developed for the detection of intracranial neoplasms[75]. Interpretation relies upon exclusion of the injected radiopharmaceutical from the brain parenchyma by the blood-brain barrier in normal patients[75,76]. Disruption of the blood-brain barrier by intracranial lesions such as tumours, abscesses or cysts allows the radiopharmaceutical to localise in the brain substance. Scintigraphic detection of cerebrovascular and inflammatory brain diseases has also been recorded in the dog[75]. The mechanism of localisation is unknown, but it is thought to involve diffusion rather than active transport[75].

Conventional radionuclide brain imaging to detect space-occupying lesions in people and small animals has largely been superceded through the development and widespread use of computed tomography and magnetic resonance imaging, which provide greater spatial resolution and usually do not rely on disruption of the blood-brain barrier[4,75]. Although this technology is applicable to the equine patient, access to the equipment is still somewhat limited and, therefore, planar scintigraphy is more relevant, although far from routine.

Newer instrumentation, including single photon emission computed tomography (SPECT) and positron emission tomography (PET), has allowed advancement of nuclear medicine studies in brain imaging in people. The technology provides tomographic images which have superior spatial and contrast resolution providing more precise localisation of lesions[75]. In addition, newer radiopharmaceuticals have been produced which are able to cross the blood-brain barrier, allowing for measurement of cerebral blood flow and studies of focal and regional grey matter function and neuroreceptor function. ^{99m}Tc-HMPAO is considered the 'gold standard' for cerebral blood flow imaging and provides information in a number of conditions, including epilepsy and brain damage following head trauma[4].

Two-dimensional planar images are not able to detect subtle changes in regional brain uptake of radiopharmaceutical, limiting the use of conventional scintigraphy in cerebral blood flow studies.

SPECT and PET therefore provide functional information on the brain which cannot be achieved with CT or MRI. Unfortunately, cost and access to equipment limits the availability of this technology even to small animal medicine, regardless of the technical difficulties of size and handling of an anaesthetised adult equine patient. A retrospective analysis of 116 dogs and cats examined by planar brain scintigraphy with proven intracranial diseases concluded that brain scintigraphy has a high sensitivity and specificity for focal disease, including tumours[77]. Planar brain scintigraphy is not as sensitive for diffuse brain disease, but specificity for diffuse disease is good when detected[77]. The availability of conventional equipment and relatively low cost, along with the ability to carry out the procedure in a standing sedated patient, makes planar brain scintigraphy a reasonable option for evaluating the equine brain.

No reports of brain scintigraphy in the equine patient have been found in the literature, which probably reflects, in part, the limited number and types of conditions which affect the equine brain. Other than plain radiography, CT, MRI and angiography have been reported in the literature as ancillary techniques for evaluating suspected intracranial lesions[75].

Clinical signs seen with focal brain lesions include[78]:

- Seizures.
- Alterations in consciousness; i.e. depression, stupor, coma.
- Abnormalities of motor function; i.e. ataxia, hypermetria, intention tremor, hemiparesis, tetraparesis, tetraplegia.
- Abnormal pupil size or light reflexes.
- Blindness, menace response deficit.
- Strabismus.
- Facial paralysis.
- Dysphagia.

The most common cause of seizures in adult horses older than 1 year of age are brain trauma, hepatoencephalopathy and toxicity. Tumours, especially pituitary adenoma, may cause seizures and blindness in horses older than 7 years. Neonatal maladjustment syndrome, trauma and bacterial meningitis are

A **Figure 15: Brain scan DTPA images: left lateral (a), right lateral (b), dorsal (c) and caudodorsal (d) views**

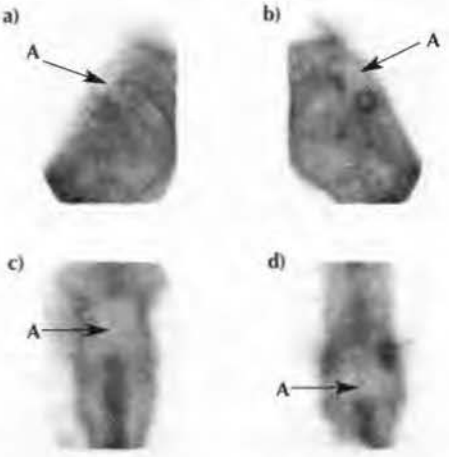

TBx	9y	G	-	128 x 128
DX:	Normal scan, as no significant RU within the calvarium to indicate disruption of the blood- brain barrier.			
DS:	NA			
➡ **A:** Region of calvarium free of significant RU. **Note:** 15 x 3-sec frames with automotion correction. Radiopharmaceutical: ^{99m}Tc-DTPA.				

the most common causes of seizures in young foals, and trauma is the most common cause in older foals. Cerebral abscesses occur rarely[79].

Indications

Planar scintigraphy is indicated for:

- Suspected intracranial space-occupying lesions; i.e. tumour, abscess.
- Seizures where extracranial causes have been ruled out.
- Further evaluation of head trauma with suspected brain injury.
- Unexplained behavioural changes with suspected intracranial aetiology.

Radiopharmaceuticals

Radiopharmaceuticals available for equine brain scintigraphy include:

- ^{99m}Tc-DTPA (diethylenetriaminepentaacetic acid), which is confined to the blood pool, does not pass the normal blood brain barrier and is cleared rapidly by the kidneys minimising background activity (**Figure 15**).
- ^{99m}Tc-GHA (glucoheptonate), which has similar properties to DTPA but is cleared more slowly from the blood pool. ^{99m}Tc-GHA provides good lesion:background contrast and was formerly the agent of choice, but is no longer available.
- ^{99m}Tc-pertechnetate; scans obtained are of poorer quality as a result of normal accumulation of this agent in choroids plexus and salivary glands, and slower blood clearance results in higher background activity.
- ^{99m}Tc-HMPAO, which is a lipophilic molecule which diffuses past the blood-brain barrier and is thought to be trapped in the intracellular compartment of the brain by its conversion to a hydrophilic compound. Distribution of this agent provides a map of cerebral blood flow; however, detection of filling defects in most cases requires high spatial and contrast resolution which cannot be achieved with planar scintigraphy (**Figure 16a and 16b**).
- ^{99m}Tc-L,L-ECD (complex of ^{99m}Tc with ethyl cysteinate dimer or ethylene dicysteine di-ethylester), which is a neutral, lipophilic complex which is thought to diffuse across cell membranes and becomes trapped following enzymatic conversion to a less lipophilic form. Like ^{99m}Tc-HMPAO, ^{99m}Tc-ECD provides a map of cerebral blood flow, but there are significant differences in regional distribution between the two radiopharmaceuticals which does not make direct comparison possible. As with ^{99m}Tc-HMPAO, planar scintigraphy imposes major limitations upon interpretation of normal and abnormal cerebral blood flow (**Figure 17a, 17b and 17c**).

Dosage

Radioactivity of the radiopharmaceuticals used with reported success are in the range of 2.8–3.7 GBq[76]. The dose range in all studies carried out in adult horses by this author is 3.0–4.5 GBq.

A **Figure 16a: Cerebral blood flow scans: left lateral (i), right lateral (ii) and zoomed dorsoventral (iii) views using HMPAO**

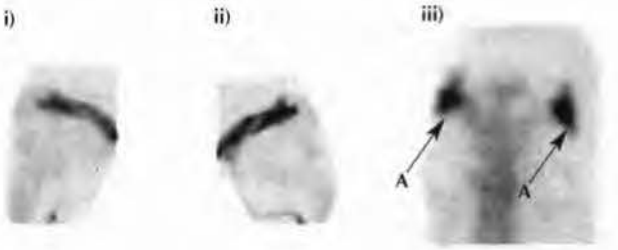

TBx	9y	G	-	128 x 128
DX:	Normal variability in cerebral blood flow detected by planar scintigraphy makes this procedure of questionable value for the detection of possible brain lesions.			
DS:	NA			
➔ **A:**	Marked salivary gland uptake, suggestive of poor radiopharmaceutical labelling.			
Note:	15 x 3-sec frames with automotion correction. Radiopharmaceutical: ^{99m}Tc-HMPAO.			

A **Figure 16b: Cerebral blood flow scans: left lateral (i), right lateral (ii) and zoomed dorsal (iii) views using HMPAO**

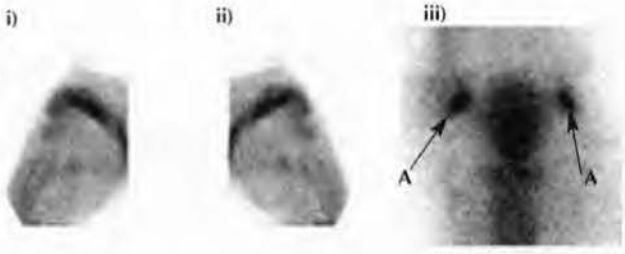

TBx	12y	M	-	128 x 128
DX:	Normal variability in cerebral blood flow detected by planar scintigraphy makes this procedure of questionable value for the detection of possible brain lesions.			
DS:	NA			
➔ **A:**	Marked salivary gland uptake, suggestive of poor radiopharmaceutical labelling.			
Note:	15 x 3-sec frames with automotion correction. Radiopharmaceutical: ^{99m}Tc-HMPAO.			

A **Figure 17a: Dorsal/frontal images of the head, with radioactive reference markers on the skin (i) and after computerised removal of markers (ii)**

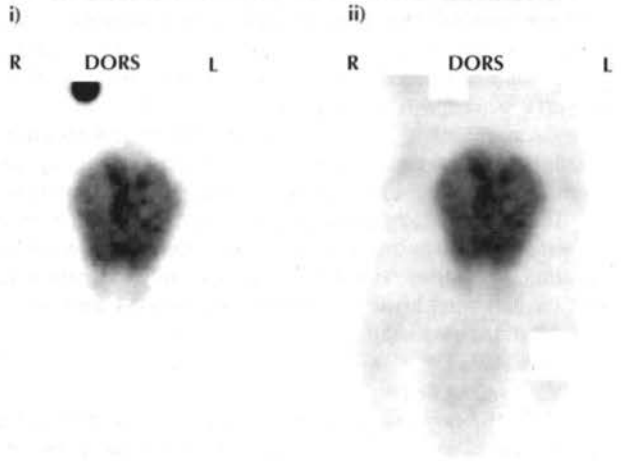

-	-	-	-	128 x 128

DX: Normal variability in cerebral blood flow detected by planar scintigraphy makes this procedure of questionable value for the detection of possible brain lesions.

DS: NA

Note: Scan of cerebral blood flow using ECD.
20 x 1-sec frames, summed with automotion correction.
Radiopharmaceutical: ^{99m}Tc-L,L-ECD (Neurolite).

A **Figure 17b: Left lateral images of the head, with radioactive reference markers on the skin (i) and after computerised removal of markers (ii)**

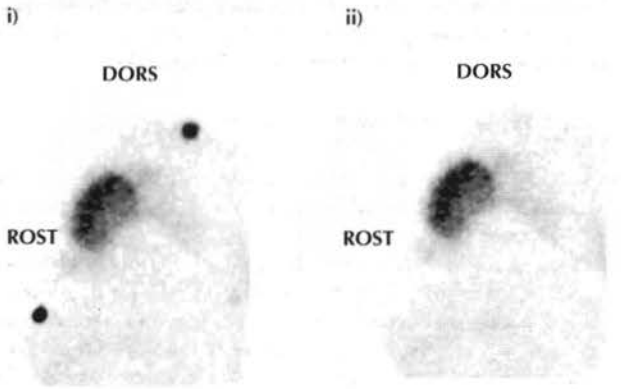

-	-	-	-	128 x 128

DX: Normal variability in cerebral blood flow detected by planar scintigraphy makes this procedure of questionable value for the detection of possible brain lesions.

DS: NA

Note: Scan of cerebral blood flow using ECD.
20 x 1-sec frames, summed with automotion correction.
Radiopharmaceutical: ^{99m}Tc-L,L-ECD (Neurolite).

A **Figure 17c: Right lateral images of the head, with radioactive reference markers on the skin (i) and after computerised removal of markers (ii)**

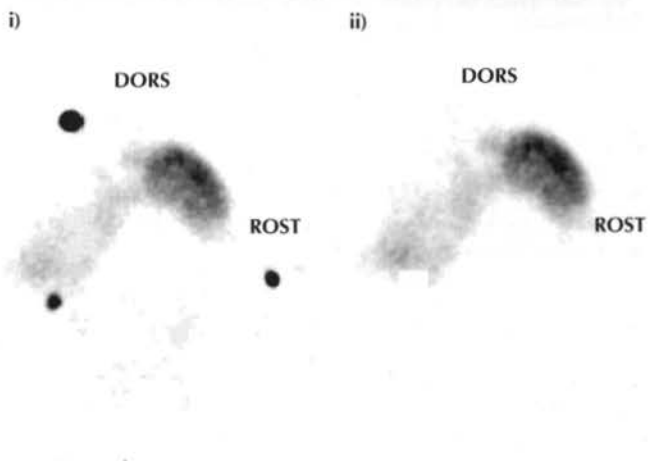

-	-	-	-	128 x 128

DX: Normal variability in cerebral blood flow detected by planar scintigraphy makes this procedure of questionable value for the detection of possible brain lesions.

DS: NA

Note: Scan of cerebral blood flow using ECD.
20 x 1-sec frames, summed with automotion correction.
Radiopharmaceutical: ^{99m}Tc-L,L-ECD (Neurolite).

Administration and Time of Scan

Jugular catheter placement is recommended for i.v. administration of the radiopharmaceutical.

DTPA scans are usually carried out between 1 and 2 h following administration because of rapid renal clearance of radiopharmaceutical.

Glucoheptonate scans (where this agent is available) are typically carried out 1 to 4 h post injection.

HMPAO scans for cerebral blood flow are typically carried out at 1 to 2 h post injection.

ECD scans for cerebral blood flow have been carried out 30 mins post injection.

Acquisition Details

- The scan may be performed with the horse under standing sedation or general anaesthesia. The level of sedation must be adequate to allow safe movement of the camera close to the head, while overdosing should be avoided to minimise movement during acquisition. Drugs which may lower the seizure threshold should be avoided. Blinkers are often useful for the more nervous patient. Providing a chin rest for the horse helps limit movement.
- Three standard views are normally obtained in a sedated animal; left lateral, right lateral and dorsal. A caudal view (behind the poll) is obtained in the anaesthetised animal and when considered safe in the sedated horse. The dorsal view is considered the most useful for evaluation of the

cerebral cortex[75]. Additional oblique views may be indicated to localise an identified lesion further.
- A large field of view gamma camera fitted with a low energy, general purpose or high resolution collimator is used.
- Static images maybe obtained using a 256 x 256 or 128 x 128 matrix. Images should be acquired to a preset number of counts, ideally a minimum of 250,000.
- Dynamic images of 20 or 30 three-sec frames using a 128 x 128 matrix may be acquired if motion correction is necessary. These are converted into static images.

Interpretation

DTPA and GH are normally excluded from the brain parenchyma, which contains background activity only (**Figure 15**). The tissues surrounding the calvarium usually retain marginal activity which helps to outline the brain and provide anatomical landmarks[75]. They may also obscure areas of the brain on certain views. Focal accumulation of radiopharmaceutical within the brain, which is repeatable on multiple views, constitutes a positive scan. Diffuse or poorly defined regions of RU are more difficult to interpret and artefacts need to be recognised to prevent a false positive diagnosis. Poor binding of ^{99m}Tc to the radiopharmaceutical results in free pertechnetate which accumulates in areas of the brain where DTPA and GH are excluded, and in the salivary glands, potentially resulting in a misdiagnosis[75]. Images with poor lesion:background ratios may be enhanced by background subtraction techniques. Focal RU within the brain indicates disruption of the blood-brain barrier and is not pathogonomic for neoplasia. Inflammatory lesions and acute cerebrovascular injury must also be considered as differential diagnoses[76].

Asymmetrical uptake of ^{99m}Tc-HMPAO or ^{99m}Tc-ECD as part of the cerebral blood flow study may be an indication of normal functional blood flow differences to regions of the brain at the time of the study. The difficulties involved in detection, localisation and interpretation of abnormalities in these blood flow studies limit their application in conventional brain scintigraphy[4].

Summary

Although clinical indications for equine brain imaging are few, planar brain scintigraphy should be considered when focal brain disease is suspected and:

- There is no access to MRI or CT.
- General anaesthesia is contraindicated or not desired.
- Financial constraints apply.

UTERINE CLEARANCE SCINTIGRAPHY

Introduction

Recurrent endometritis is a major cause of infertility and subfertility in the mare, resulting in significant economic losses to the equine industry[80]. Contamination of the uterus at the time of breeding causes endometritis and this must be cleared within 96 h to allow the embryo to survive[81]. The mechanisms responsible for resistance to endometritis include phagocytosis, local uterine antibody-mediated immunity and physical clearance of bacteria and inflammatory products[80,81]. Impaired uterine clearance during oestrus is considered to be a major cause of recurrent endometritis. Some older multiparous mares have dysfunctional mechanical clearance of inflammatory products during oestrus, making them susceptible to recurrent endometritis[81].

Scintigraphy can be used to evaluate mechanical clearance of the uterus and offers a simple, minimally invasive and potentially reliable means of diagnosing a delay in uterine clearance during oestrus. Studies have indicated that normal mares clear >50% of radiocolloid infused into the uterus within 2 h, whereas those susceptible to endometritis or with poor cervical dilatation show significantly reduced clearance[80,81].

Indication

Identification of delayed uterine clearance as a component of recurrent endometritis and consequent infertility or subfertility.

Radiopharmaceutical

^{99m}Tc-Albumin colloid (^{99m}Tc-μAA; 'Microlite' from El du Pont de Nemours & Co., Billerica, Massachusetts): this radiocolloid has been chosen because of its ease of preparation and higher target to background ratio compared with other radiocolloids[80]. The particle size range of the colloid is 100 nm to 5 μm (NB: this is not to be confused with ^{99m}Tc-MAA, which is a suspension with particle sizes between 10 and 100 μm and is used for lung perfusion studies).

Dosage

The recommended dose is 370 GBq ^{99m}Tc-μAA. No statistically significant difference in uterine clearance was noted with larger doses, and image quality was similar[80]. The radiocolloid is buffered to pH 7.0 in a total volume of 2 ml or less.

Time and Method of Administration

- Evaluation is advised during the physiological cyclic season and can be performed in mares from Day 3 of oestrus to 48 h after ovulation[80].
- The mare is restrained using light sedation (20 mg acetylpromazine maleate i.v. was used in the reported studies) and the camera is positioned laterally in contact with the mare's flank prior to infusion of the radiocolloid.
- The ^{99m}Tc-μAA is infused through the cervix into the uterine body via a sterile pipette with an attached 3-way stopcock and flushed with 10 ml saline.

Acquisition Details

- A large field of view gamma camera equipped with a low energy, general purpose, parallel hole collimator is used.
- Right lateral and left lateral images are acquired for 180 secs each at 0, 15, 30, 60, 12 and 240 mins after infusion.
- A 256 x 256 or 128 x 128 matrix may be used.
- Dynamic frame mode acquisitions may be obtained if motion correction is deemed necessary.

Analysis and Interpretation

Clearance of the radiocolloid from the uterus can be evaluated qualitatively on the sequential images obtained.

Region of interest (ROI) data of the uterus and a background (BKD) ROI for each image acquired allows calculation of net uterine counts (NUC):

NUC = (uterine ROI cts) - (BKD ROI cts x uterine ROI pix/ BKD ROI pixels)

Quantitative evaluation of uterine clearance involves analysis and linear regression of a time-activity curve generated from net uterine counts, corrected for physical decay and soft tissue attenuation, and normalised to the 100% dose. The geometric mean from right and left net uterine counts, corrected for physical decay, is an accepted standard for correction of soft tissue attenuation derived from gastric emptying studies in people[80].

Interpretation relates to the percentage of the initial dose remaining in the uterus over time. Reproductively normal mares clear >50% of infused ^{99m}Tc-μAA within 2 h of infusion[81].

RADIONUCLIDE ANGIOCARDIOGRAPHY

Nuclear medicine studies of the heart using single photon emission tomography (SPECT) are considered the most clinically rewarding of all nuclear medicine investigations carried out in people[4]. The main indication for these studies is ischaemic heart disease, which is not a recognised cardiac condition in the horse.

A method of performing first-pass radionuclide angiocardiography to measure left ventricular ejection fraction, as an index of cardiac performance, has been described in the horse[82]. Although the procedure has also been used to detect left-to-right cardiac shunts in horses, there are no recognised advantages over standard echocardiography. Therefore, it has not become a routine diagnostic procedure[83].

Both first-pass radionuclide angiocardiography and gated radionuclide ventriculography have been used in people to evaluate valvular incompetence, and studies in dogs have suggested potential clinical value in assessing the severity of mitral regurgitation and congestive heart failure[84,85]. With the development of simpler, more user-friendly software programmes, these techniques may ultimately have a proven role in the clinical assessment of horses with suspected congestive heart failure. ^{99m}Tc-MDP has been used as the radiopharmaceutical for first-pass radionuclide angiocardiography in horses and ^{99m}Tc-labelled red blood cells have been used for radionuclide ventriculography[86].

For details regarding techniques for first-pass radionuclide angiocardiography and radionuclide ventriculography[82,87], see the relevant references.

GASTRIC EMPTYING

Introduction

Gastric emptying can be measured using scintigraphy in horses. In people and small animals, this technique is used to document outflow obstructions and determine and monitor the response to medical or surgical treatment[88]. In horses, it has been used to evaluate the effects of prokinetic drugs[89]. Normal gastric peristalsis is biphasic, with contraction followed by relaxation of the pyloric sphincter resulting in the larger particles remaining in the cardia while the smaller particles and fluid empty rapidly. By this means, 75% of fluid should leave the stomach within 30 mins of ingestion while solid food remains considerably longer[90]. Simultaneous dual radionuclide acquisitions can be used to measure both solid and liquid phase gastric emptying.

Radiopharmaceuticals

- Solid phase: ^{99m}Tc-sulphur colloid.
- Liquid phase: ^{111}In-DTPA or ^{99m}Tc-DTPA.
- Dual phase: ^{99m}Tc-sulphur colloid and ^{111}In-DTPA.

Dosage and Administration

- ^{99m}Tc-SC: 370 MBq incorporated into egg albumin.
- ^{111}In-DTPA: 37 MBq in water.
- ^{99m}Tc-DTPA: 370 MBq in water.

Radiopharmaceuticals for liquid phase are administered by nasogastric tube. For dual phase studies, both radiopharmaceuticals can be administered by nasogastric tube or by feeding mixed with 1 g/kg grain.

Acquisition Details

- Following administration, right and left lateral images of the cranial abdomen are obtained immediately, at 15 mins, 30 mins and every 30 mins for 180 mins.
- A large field of view gamma camera fitted with a low energy, general purpose, parallel hole collimator is used.
- Sixty 1-second static acquisitions using a 128 x 128 matrix may be used. Longer acquisition times may be necessary when using ^{111}In-DTPA to achieve adequate counts. The photopeak needs to be reset to 174 and 247 keV when using ^{111}In-DTPA.

Analysis and Interpretation

Decay-corrected gastric region of interest against time curves are plotted using the geometric mean for correction of soft tissue attenuation between right and left sides. The curves are best fit by power exponential function to allow calculation of the rate of gastric emptying[88,89]. T_{50} = time required for 50% gastric emptying of the original radioactivity to occur.

Normal gastric emptying half-times in horses have not been recorded.

THYROID SCINTIGRAPHY

Introduction

Thyroid scintigraphy has been used in horses to assess cranial cervical masses which are suspected to involve thyroid carcinoma[91-94]. This is likely to be most useful when aspiration or biopsy findings are equivocal.

Although thyroid adenomas are common, thyroid carcinomas are uncommon in the horse. Clinical signs are

usually restricted to an enlargement of the craniolateral neck, but multiple skeletal metastases and respiratory tract metastases have been recorded. Work intolerance has also been recorded in a horse with thyroid carcinoma[92].

The diagnosis of thyroid carcinoma is based upon the anatomical location of the mass, serum T3 and T4 values, *in vitro* thyroid function tests, and biopsy or needle aspiration of the mass. The serum T3 and T4 values and thyroid function tests alone are not considered diagnostic for thyroid neoplasia[91]. Therefore, if aspiration or biopsy findings are equivocal, scintigraphy may prove useful[95].

Sodium ^{99m}Tc-pertechnetate and sodium [^{131}I]-iodide are the radiopharmaceuticals used for thyroid imaging. Both products are actively transported into the thyroid gland by the follicular thyroid cells. The uptake of ^{99m}Tc-pertechnetate by the thyroid gland is lower than that of ^{131}I-iodide, but the 6 h half-life of ^{99m}Tc allows a higher amount of radioactivity to be administered, which improves the target to nontarget ratio. In addition, the 8 day half-life of ^{131}I-iodide dictates prolonged isolation[92].

If the thyroid neoplasm is shown to concentrate radioactive iodine, radioactive iodine therapy may be an option[91].

Indications

- To determine the size and extent of suspected thyroid carcinoma.
- To assess for possible metastatic sites in the cervical region and thorax.

Radiopharmaceuticals

- Na $^{99m}TcO_4$ (sodium ^{99m} Tc-pertechnetate).
- $^{131}I^-$ (sodium iodide): half life is 8.04 days.

Dosage

- $^{99m}TcO_4^-$: 1.3 GBq (35 mCi).
- $^{131}I^-$: 18 MBq (500 μCi).

Acquisition Details

- $^{99m}TcO_4^-$ scans are carried out 30 mins following injection.
- $^{131}I^-$ scans are performed 24 h following injection.
- Three standard views are normally taken in the sedated animal; left lateral, right lateral and ventral.
- Static images may be obtained using a 256 x 256 or 128 x 128 matrix. Images should be acquired to a preset number of counts, ideally a minimum of 200,000 for $^{99m}TcO_4^-$. 50,000–100,000 counts may be adequate for ^{131}I because of the higher target to back-ground ratio.
- Dynamic images of 20 or 30 three-sec frames using a 128 x 128 matrix may be acquired if motion correction is necessary.
- The photopeak needs to be reset to 364 and 637 KeV when using $^{131}I^-$.

Interpretation

- An abnormal thyroid scintigram is likely to show heterogeneous RU throughout an enlarged lobe of the thyroid gland.
- If a mass arises from tissues other than the thyroid, both thyroid lobes should show normal size and RU.

ACKNOWLEDGEMENTS

The author would like to thank: J. Walmsley for supplying Figures 3a and 3b; N. Menzies-Gow for supplying Figures 4, 5 and 6; and D. Votion, H. Zreik, A. Seret, I. Origer, O. Jacqmot and Y. Bertrand for supplying Figures 17a, 17b and 17c.

REFERENCES

1. Weaver, M.P. (1995) Twenty years of equine scintigraphy - a coming of age? *Equine vet. J.* **27**, 163-165.
2. Kowalsky, R.J. (1996) Principles of radioactive decay, radioactivity, ^{99m}Tc generator and radiopharmacy. In: *Handbook of Veterinary Nuclear Medicine*, Eds: C.R. Berry and G.B. Daniel, North Carolina State University, Raleigh, North Carolina. pp 1-9.
3. Berry, C.R. (1996) Single photon emission computed tomography. In: *Handbook of Veterinary Nuclear Medicine*, Eds: C.R. Berry and G.B. Daniel, North Carolina State University, Raleigh, North Carolina. pp 45-48.
4. Britton, K.E. (1999) Diagnostic applications. In: *Textbook of Radiopharmacy*, 3rd edn., Ed: C.B. Sampson, Gordon and Breach Science, Amsterdam, The Netherlands. pp 337-367.
5. Hoskinson, J.J. and Tucker, R.L. (1996) Scintigraphic imaging of inflammation and infection. In: *Handbook of Veterinary Nuclear Medicine*, Eds: C.R. Berry and G.B. Daniel, North Carolina State University, Raleigh, North Carolina. pp 162-169.
6. Daniel, G.B., Tucker, R.L., Buckman, T. *et al.* (1992) *In vitro* comparison of equine granulocytes labeled with ^{99m}Tc-hexamethylpropyleneamine oxime or ^{111}In-oxine. *Am. J. vet. Res.* **53**, 871-875.
7. Long, C.D., Galuppo, L.D., Waters, N.K. *et al.* (2000) Scintigraphic detection of equine orthopedic infection using Tc-HMPAO labeled leukocytes in 14 horses. *Vet. Radiol. Ultrasound* **41**, 354-359.
8. Koblik, P.D., Lofstedt, J., Jakowski, R.M. *et al.* (1985) Use of ^{111}In-labeled autologous leukocytes to image an abdominal abscess. *J. Am. vet. med. Ass.* **186**, 1319-1322.
9. Tucker, R.L., Daniel G.B., Daniel, S.L. *et al.* (1992) *In vitro* evaluation of canine granulocytes labelled with ^{99m}Tc- hexamethylpropyleneamine oxime. *Vet. Radiol. Ultrasound* **33**, 241-246.
10. Peters, A.M. (1995) Imaging infection and inflammation in veterinary practice. *Equine vet. J.* **27**, 242-244.
11. Butson, R.J., Webbon, P.M. and Fairbairn, S.M. (1995) ^{99}Tc^{m}-HMPAO labeled leukocytes and their biodistribution in the horse: a preliminary investigation. *Equine vet. J.* **27**, 313-315.
12. Neuwirth, L., Kuperus, J.H., Calderwood-Mays, M. *et al.* (1995) Comparative study of indium-^{111} leukocytes and nephrosonography for detection of experimental pyelonephritis in dogs. *Vet. Radiol. Ultrasound* **36**, 253-258.
13. Roddie, M.E., Peters, A.M., Danpure, H.J. *et al.* (1988) Inflammation: imaging with Tc-^{99m} HMPAO-labeled leukocytes. *Radiol.* **166**, 767-772.
14. Mountford, P.J., Kettle, A.G., O'Doherty, M.J. *et al.* (1990) Comparison of ^{99m}Tc-HM-PAO leukocytes with Indium-^{111}-oxine leukocytes for localizing intraabdominal sepsis. *J. nucl. Med.* **31**, 311-315.
15. Ramzan, P.H.L. and McGladdery, A.J. (2003) The use of ^{99m}Tc-hexamethylpropyleneamine oxime (^{99m}-HMPAO) labelled leucocyte scintigraphy in equine medical investigations: 8 cases. *Equine vet. J.* (In press).
16. Lattimer, J.C., Reed, A.L. and Johnson, P.J. (1995) Preliminary results of ^{99m}Tc HMPAO labeled leucocyte scintigraphy in horses. *Vet. Radiol. Ultrasound* **36**, 363.
17. East, L.M., Trumble, T.N., Steyn. P.F. *et al.* (2000) The application of ^{99m}Tc-hexamethylpropyleneamine oxime (^{99m}Tc-HMPAO) labeled white blood cells for the diagnosis of right dorsal ulcerative colitis in two horses. *Vet. Radiol. Ultrasound* **41**, 360-364.
18. Weller, R. and Marr, C.M. (2000) Nuclear scintigraphy with ^{99m}Tc-HMPAO labelled leucocytes in the assessment of horses with malabsorption. *Vet. Radiol. Ultrasound* **41**, 564.
19. Menzies-Gow, N.J., Weller, R., Bowen, I.M. *et al.* (2003) Use of nuclear scintigraphy with ^{99m}Tc-HMPAO labeled leucocytes to assess equine small intestinal malabsorption. *Vet. Rec.* (In Press).
20. Ryan, P.J. (2002) Leukoscan for orthopaedic imaging in clinical practice. *Nucl. med. Commun.* **23**, 707-714.
21. Barron, B., Hanna, C., Passalaqua, A.M. *et al.* (1999) Rapid diagnostic

imaging of acute, nonclassic appendicitis by leukoscintigraphy with sulesomab, a technetium 99m-labeled antigranulocyte antibody Fab' fragment. *Surgery* **125**, 288-296.

22. Becker, W., Bair, J., Behr, T. *et al.* (1994) Detection of soft-tissue infections and osteomyelitis using a technetium-99m-labeled anti-granulocyte monoclonal antibody fragment. *J. nucl. Med.* **35**, 1436-1443.
23. Devillers, A., Garin, E., Polard, J.L. *et al.* (2000) Comparison of Tc-99m-labelled antileukocyte fragment Fab' and Tc-99m-HMPAO leukocyte scintigraphy in the diagnosis of bone and joint infections: a prospective study. *Nucl. med. Commun.* **21**, 747-753.
24. Hakki, S., Harwood, S.J., Morrissey, M.A. *et al.* (1997) Comparative study of monoclonal antibody scan in diagnosing orthopaedic infection. *Clin. Orthop.* **335**, 275-285.
25. Stokkel, M.P., Reigman, H.E. and Pauwels, E.K. (2002) Scintigraphic head-to-head comparison between 99m Tc-WBCs and 99m Tc-leukoscan in the evaluation of inflammatory bowel disease: a pilot study. *Eur. J. nucl. Med. mol. Imaging* **29**, 251-254.
26. Charron, M., Di Lorenzo, C., Kocoshis, S.A. *et al.* (2001) (99m)Tc antigranulocyte monoclonal antibody imaging for the detection and assessment of inflammatory bowel disease newly diagnosed by colonoscopy in children. *Pediatr. Radiol.* **31**, 796-800.
27. Ellis, B.L. and Sampson, C.B. (1999) Radiolabelling of blood cells-theory and practice. In: *Textbook of Radiopharmacy*, 3rd edn., Ed: C.B. Sampson, Gordon and Breach Science, Amsterdam, The Netherlands. pp 83-104.
28. Moon, M.L., Hinkle, G.N. and Krakowka, G.S. (1988) Scintigraphic imaging of technetium ^{99m}-labeled neutrophils in the dog. *Am. J. vet. Res.* **49**, 950-955.
29. Charron, M., Orenstein, S.R. and Bhargava, S. (1994) Detection of inflammatory bowel disease in pediatric patients with Technetium-^{99m}-HMPAO-labeled leukocytes. *J. nucl. Med.* **35**, 451-455.
30. Reynolds, J.H., Graham, D. and Smith, F.W. (1990) Imaging inflammation with ^{99}Tc-^{m} HMPAO labelled leucocytes. *Clin. Radiol.* **42**, 195-198.
31. Matthews, H.K., Andrews, F.M., Daniel, G.B. *et al.* (1992) Measuring renal function in horses. *Vet. Med.* **88**, 349-356.
32. Held, J.P. and Daniel, G.B. (1991) Use of nonimaging nuclear medicine techniques to assess the effect of flunixin meglumine on effective renal plasma flow and effective renal blood flow in healthy horses. *Am. J. vet. Res.* **52**, 1619-1621.
33. Matthews, H.K., Andrews, F.M., Daniel, G.B. *et al.* (1992) Comparison of standard and radionuclide methods for measurement of glomerular filtration rate and effective renal blood flow in female horses. *Am. J. vet. Res.* **53**, 1612-1616.
34. Walsh, D.M. and Royal, H.D. (1992) Evaluation of a single injection of ^{99m}Tc-labeled diethylenetriaminepentaacetic acid for measuring glomerular filtration rate in horses. *Am. J. vet. Res.* **53**, 776-780.
35. Barthez, P.Y., Hornof, W.J., Cowgill, L.D. *et al.* (1998) Comparison between the scintigraphic uptake and plasma clearance of ^{99m}Tc-diethylenetriaminepentacetic acid (DTPA) for the evaluation of the glomerular filtration rate in dogs. *Vet. Radiol. Ultrasound* **39**, 470-474.
36. Twardock, A.R., Krawiec, D.R. and Itkins, R.J. (1996) Renal imaging I: functional renal scintigraphy. In: *Handbook of Veterinary Nuclear Medicine*, Eds: C.R. Berry and G.B. Daniel, North Carolina State University, Raleigh, North Carolina. pp 122-130.
37. Divers, T.J., Whitlock, R.H., Byars, T.D. *et al.* (1987) Acute renal failure in six horses resulting from haemodynamic causes. *Equine vet. J.* **19**, 178-184.
38. Woods, P.R., Drost, W.T., Clarke, C.R. *et al.* (2000) Use of ^{99m}Tc-mercaptoacetyltriglycine to evaluate renal function in horses. *Vet. Radiol. Ultrasound* **41**, 85-88.
39. Twardock, A.R. (1996) Renal imaging II: morphology scintigraphy. In: *Handbook of Veterinary Nuclear Medicine*, Eds: C.R. Berry and G.B. Daniel, North Carolina State University, Raleigh, North Carolina. pp 131-132.
40. Hood, D.M., Amoss, M.S., Gremmel, S.M. *et al.* (1982) Renovascular nuclear medicine in the equine: a feasibility study. *Southwestern Vet.* **35**, 19-26.
41. Dyson, S.J. and Worth, L. (1997) Aortoiliacofemoral thrombosis. In: *Current Therapy in Equine Medicine 4*, Ed: N.E. Robinson, W.B. Saunders Co., Philadelphia. pp 267-268.
42. Ross, M.W., Maxson, A.D., Stacy, V.S. *et al.* (1997) First-pass radionuclide angiography in the diagnosis of aortoiliac thromboembolism in a horse. *Vet. Radiol. Ultrasound* **38**, 226-230.
43. Barrelet, A. (1993) Aorto-iliac thrombosis in a breeding stallion and an eventer mare. *Equine vet. Educ.* **5**, 86-89.
44. Stashak, T.S. (Ed.) (1987) The pelvis: thrombosis of the caudal aorta or iliac arteries. In: *Adams' Lameness in Horses*, 4th edn., Lea and Febiger, Philadelphia. pp 750-751.
45. Azzie, M.A.J. (1969) Aortic/iliac thrombosis of Thoroughbred horses. *Equine vet. J.* **1**, 113-116.
46. Boswell, J.C., Marr, C.M., Cauvin, E.R. *et al.* (1999) The use of scintigraphy in the diagnosis of aortic-iliac thrombosis in a horse. *Equine vet. J.* **31**, 537-541.
47. Edwards, G.B. and Allen, W.E. (1988) Aorto-iliac thrombosis in two horses: Clinical course of the disease and the use of real-time ultrasonography to confirm diagnosis. *Equine vet. J.* **20**, 384-387.
48. Rijkenhuizen, B.M. (1997) Aortoiliacfemoral thrombosis - new approach. In: *Proceedings of the 36th British Equine Veterinary Association Congress*, Equine Veterinary Journal Ltd., Newmarket. p 92.
49. Daniel, G.B., Wantshek, L., Bright R. *et al.* (1990) Diagnosis of aortic thromboembolism in two dogs with radionuclide angiography. *Vet. Radiol. Ultrasound* **31**, 182-185.
50. Barton, M.H. and Morris, D.D. (1998) Diseases of the liver. In: *Equine Internal Medicine*, Eds: S.M. Reed and W.M. Bayly, W.B. Saunders Co., Philadelphia. pp 707-738.
51. Buonanno, A.M., Carlson, G.P. and Kantrowitz, B. (1988) Clinical and diagnostic features of portosystemic shunt in a foal. *J. Am. vet. med. Ass.* **192**, 387-389.
52. Koblik, P.D. and Hornof, W.J. (1996) Portosystemic shunt imaging. In: *Handbook of Veterinary Nuclear Medicine*, Eds: C.R. Berry and G.B. Daniel, North Carolina State University, Raleigh, North Carolina. pp 97-105.
53. Lindsay, W.A., Ryder, J.K., Beck, K.A. *et al.* (1988) Hepatic encephalopathy caused by a portocaval shunt in a foal. *Vet. Med.* **83**, 798.
54. Lamb, C.R., Forster-van Hijfte, M.A., White, R.N. *et al.* (1996) Ultrasonographic diagnosis of congenital portosystemic shunt in 14 cats. *J. small anim. Pract.* **37**, 205-209.
55. Daniel, G.B., Bright, R., Monnet, E. *et al.* (1990) Comparison of per-rectal portal scintigraphy using ^{99m}Technetium pertechnetate to mesenteric injection of radioactive microspheres for quantification of portosystemic shunts in an experimental dog model. *Vet. Radiol. Ultrasound* **31**, 175-181.
56. McEvoy, F.J., Forster-van Hijfte, M.A. and White, R.N. (1998) Detection of portal blood flow using per-rectal ^{99m}Tc-pertechnetate scintigraphy in normal cats. *Vet. Radiol. Ultrasound* **39**, 234-237.
57. Daniel, G.B., Bright, R., Ollis, P. *et al.* (1991) Per-rectal portal scintigraphy using ^{99m}Technetium pertechnetate to diagnose portosystemic shunts in dogs and cats. *J. vet. int. Med.* **5**, 23-27.
58. Koblik, P.D., Komtebedde, J., Yen, C.-K. *et al.* (1990) Use of transcolonic ^{99m}technetium-pertechnetate as a screening test for portosystemic shunts in dogs. *J. Am. vet. med. Ass.* **196**, 925-930.
59. Shiomi, S., Kuroki, T., Kobayashi, K. *et al.* (1988) Portal circulation by technetium-^{99m}pertechnetate per-rectal portal scintigraphy. *J. nucl. Med.* **29**, 460-465.
60. Samii., V.F., Kyles, A.E., Long, C.D. *et al.* (2001) Evaluation of interoperator variance in shunt fraction calculation after transcolonic scintigraphy for diagnosis of portosystemic shunts in dogs and cats. *J. Am. vet. med. Ass.* **219**, 1116-1119.
61. Matwichuk, C.L., Daniel, G.B., DeNovo, R.C. *et al.* (2000) Evaluation of plasma time-activity curves of technetium-^{99m}-mebrofenin for measurement of hepatic function in dogs. *Vet. Radiol. Ultrasound* **41**, 78-84.
62. Chatziioannou, S.N., Moore, W.H., Ford, P.V. *et al.* (2000) Hepatobiliary scintigraphy is superior to abdominal ultrasonography in suspected acute cholecystitis. *Surgery* **127**, 609-613.
63. Nadel, H.R. (1996) Hepatobiliary scintigraphy in children. *Semin. nucl. Med.* **26**, 25-42.
64. Roca, I. and Ciofetta, G. (1998) Hepatobiliary scintigraphy in current pediatric practice. *Q. J. nucl. Med.* **42**, 113-118.
65. O'Connor, P.J., Southern, K.W., Bowler, I.M. *et al.* (1996) The role of scintigraphy in cystic fibrosis. *Hepatol.* **23**, 281-287.
66. Theodorakis, M.C., Bermudez, A.J., Manning J.P. *et al.* (1982) Liver scintigraphy in ponies. *Am. J. vet. Res.* **43**, 1561-1565.
67. Hornof, W.J. and Baker, D.G. (1986) Biliary kinetics of horses as determined by quantitative nuclear scintigraphy. *Vet. Radiol. Ultrasound* **27**, 85-88.
68. Boothe, H.W., Boothe, D.M., Komkov, A. *et al.* (1992) Use of hepatobiliary scintigraphy in the diagnosis of extrahepatic biliary obstruction in dogs and cats: 25 cases (1982-1989). *J. Am. vet. med. Ass.* **201**, 134-141.
69. Daniel G.B., De Novo, R., Schultze, A.E. *et al.* (1998) Validation of deconvolution analysis for measurement of hepatic function in dogs with toxic-induced liver disease. *Vet. Radiol. Ultrasound* **39**, 375-383.

70. Frier, M. (1999) Mechanisms of localisation of radiopharmaceuticals. In: *Textbook of Radiopharmacy*, 3rd edn., Ed: C.B. Sampson, Gordon and Breach Science, Amsterdam, The Netherlands. pp 283-290.

71. Bahr, A., Daniel, G.B., DeNovo, R. *et al.* (1996) Quantitative hepatobiliary scintigraphy with deconvolution analysis for the measurement of hepatic function in dogs. *Vet. Radiol. Ultrasound* **37**, 214-220.

72. Newell, S.M., Graham, J.P., Roberts, G.D. *et al.* (2001) Quantitative hepatobiliary scintigraphy in normal cats and in cats with experimental cholangiohepatitis. *Vet. Radiol. Ultrasound* **42**, 70-76.

73. Daniel, G.B., DeNovo, R., Bahr, A. *et al.* (2001) Evaluation of heart time-activity curves as a predictor of hepatic extraction of ^{99m}Tc-mebrofenin in dogs. *Vet. Radiol. Ultrasound* **42**, 162-168.

74. Daniel, G.B., Berry, C.B. and Newell, S. (1996) Hepatic scintigraphy. In: *Handbook of Veterinary Nuclear Medicine*, Eds: C.B. Berry and G.B. Daniel, North Carolina State University, Raleigh, North Carolina. pp 85-93.

75. Daniel, G.B., Twardock, A.R., Tucker, R.L. *et al.* (1992) Brain scintigraphy. *Prog. vet. Neurol.* **3**, 25-34.

76. Dykes, N.L. (1996) Conventional (planar) brain scintigraphy. In: *Handbook of Veterinary Nuclear Medicine*, Eds: C.R. Berry and G.B. Daniel, North Carolina State University, Raleigh, North Carolina. pp 133-137.

77. Dykes, N.L., Warnick, L.D., Summers, B.A. *et al.* (1994) Retrospective analysis of brain scintigraphy in 116 dogs and cats. *Vet. Radiol. Ultrasound* **35**, 59-65.

78. Reed, S.M. (1998) Cranial trauma. In: *Current Therapy in Equine Medicine* 2nd edn., Ed: N.E. Robinson, W.B. Saunders Co., Philadelphia. p 379.

79. Andrews, F.M. and Matthews, H.K. (1998) Seizures, narcolepsy and cataplexy. In: *Equine Internal Medicine*, Eds: S.M. Reed and W.M. Bayly, W.B. Saunders Co., Philadelphia. pp 451-457.

80. Neuwirth, L., LeBlanc, M.M., Mauragis, D. *et al.* (1995) Scintigraphic measurement of uterine clearance in mares. *Vet. Radiol. U ltrasound* **36**, 64-68.

81. LeBlanc, M.M., Neuwirth, L., Asbury, A.C. *et al.* (1994) Scintigraphic measurement of uterine clearance in normal mares and mares with recurrent endometritis. *Equine vet. J.* **26**, 109-113.

82. Koblik, P.D., Hornof, W.J., Rhode, E.A. *et al.* (1985) Left ventricular ejection fraction in the normal horse determined by first-pass nuclear angiocardiography. *Vet. Radiol. Ultrasound* **26**, 53-62.

83. Koblik, P.D. and Hornof, W.J. (1987) Use of first-pass nuclear angiocardiography to detect left-to-right cardiac shunts in the horse. *Vet. Radiol. Ultrasound* **28**, 177-180.

84. Daniel, G.B., Kerstetter, K.K., Sackman, J.E. *et al.* (1998) Quantitative assessment of surgically induced mitral regurgitation using radionuclide ventriculography and first pass radionuclide angiography. *Vet. Radiol. Ultrasound* **39**, 459-469.

85. Arrington, K., Bright, J.M. and Daniel, G.B. (2001) The use of gated radionuclide ventriculography as a non-invasive method of evaluating right ventricular function in dogs with experimentally induced congestive heart failure. *Vet. Radiol. Ultrasound* **42**, 62-69.

86. Koblik, P.D. and Hornof, W.J. (1985) Diagnostic radiology and nuclear cardiography. *Vet. Clin. N. Am.: Equine Pract.* **1**, 289-309.

87. Daniel, G.B. (1996) Myocardial imaging II: Functional scintigraphy. In: *Handbook of Veterinary Nuclear Medicine*, Eds: C.B. Berry and G.B. Daniel, Carolina State University, Raleigh, North Carolina. pp 115-121.

88. Berry, C.B., Hornof, W.J. and Steyn, P. (1996) Gastrointestinal scintigraphy. In: *Handbook of Veterinary Nuclear Medicine*, Eds: C.B. Berry and G.B. Daniel, North Carolina State University, Raleigh, North Carolina. pp 138-142.

89. Neuwirth, L., Merritt, A.M. and Lester, G. (1995) Dual-phase gastric emptying in horses. *Vet. Radiol. Ultrasound* **36**, 362.

90. Fenger, C.K., Bertone, A.L., Bertone, J.J. *et al.* (1998) Gastrointestinal motility and adynamic ileus. In: *Equine Internal Medicine*, Eds: S.K. Reed and W.M. Bayly, W.B. Saunders Co., Philadelphia. pp 207-215.

91. Joyce, J.R., Thompson, R.B., Kyzar, J.R. *et al.* (1976) Thyroid carcinoma in a Horse. *J. Am. vet. med. Ass.* **168**, 610-612.

92. Hillidge, C.J., Sanecki, R.K. and Theodorakis, M.C. (1982) Thyroid carcinoma in a horse. *J. Am. vet. med. Ass.* **181**, 711-714.

93. Held, J.P., Patton, C.S., Toal, R.L. *et al.* (1985) Work intolerance in a horse with thyroid carcinoma. *J. Am. vet. med. Ass.* **187**, 1044-1045.

94. Hovda, L.R., Shaftoe, S., Rose, M.L. *et al.* (1990) Mediastinal squamous cell carcinoma and thyroid carcinoma in an aged horse. *J. Am. vet. med. Ass.* **197**, 1187-1189.

95. Brawner, W.R. Jr. (1996) Thyroid and parathyroid imaging. In: *Handbook of Veterinary Nuclear Medicine*, Eds: C.B. Berry and G.B. Daniel, Carolina State University, Raleigh, North Carolina. pp 115-121.

Chapter 7

PULMONARY SCINTIGRAPHY

DOMINIQUE-MARIE VOTION and PIERRE LEKEUX
Department of Physiology, Faculty of Veterinary Medicine, University of Liège, Bat.B42 Sart Tilman, B-4000 Liège, Belgium.

THE CONTRIBUTION OF SCINTIGRAPHY TO THE INVESTIGATION OF LUNG FUNCTION

The current diagnostic approach to respiratory disorders is based on history, physical examination, endoscopy, radiography and thoracic ultrasonography. Pulmonary function testing in resting and exercising horses may also contribute to clinical evaluation of the horse's lung[1]. The aforementioned methods give vital information about the global respiratory function and structural characteristics of the respiratory tract. However, in some clinical situations these methods may lack sensitivity to detect regional abnormality and/or subclinical disease. Because scintigraphy can scrutinise regional lung function, this technique may reveal localised abnormalities. In addition, scintigraphy may be able to detect malfunction where conventional functional tests fail to do so[2,3] and, therefore, has a role to play in the early detection of respiratory problems, which is crucial for avoiding their exacerbation or preventing secondary complications.

Scintigraphic evaluation of lung ventilation, lung perfusion, the ventilation-perfusion relationship and alveolar-capillary barrier permeability have clear indications for the diagnosis and management of equine respiratory disorders. This chapter describes the general procedure for equine pulmonary scintigraphy and details the specific procedures necessary to perform those scintigraphic tests which are of clinical interest. Additionally, background information and research applications regarding clearance of the mucociliary apparatus, aerosol deposition in the respiratory tract and blood cellular elements are provided. New perspectives for equine pulmonary scintigraphy are also mentioned.

GENERAL PROCEDURE FOR EQUINE PULMONARY SCINTIGRAPHY

Horse Preparation

Sedation facilitates handling of the horse during the scintigraphic procedure and aids prevention of movement during image acquisition. However, the α_2-adrenergic agonists currently used as sedatives may affect respiratory function, especially in horses with chronic obstructive pulmonary disease (COPD), in which the mechanics of breathing may be altered[4]. Nevertheless, sedation of the horse may be an obligatory prerequisite for some scintigraphic procedures, such as ventilation studies, where difficult horses can cause background contamination by disconnecting from the tracer administration device during the inhalation procedure.

Radiopharmaceuticals

Most radiopharmaceuticals used for pulmonary scintigraphy are ^{99m}Tc-labelled compounds prepared by adding sodium pertechnetate [$Na^+(^{99m}TcO_4)^-$] to lyophilised reaction vials. In human medicine, adverse reactions to radiopharmaceuticals are rare[5]. The same radiopharmaceuticals are used in the veterinary field as for human medicine and dosages are usually simply adapted to the horse's weight. Adverse reactions associated with radiopharmaceuticals may not be excluded and precautions must be taken against untoward complications. However, the majority of the radiopharmaceuticals described in this chapter have been used repeatedly without undesirable clinical manifestation. The use, dose and administration route of the radiopharmaceuticals for equine lung scintigraphy are summarised in Table 1.

Image Acquisition

The horse's lungs are usually scanned from both sides. The large surface of the equine lungs necessitates the acquisition of at least two views (depending on the gamma camera field of view) per lung (i.e. one cranial and one caudal for each lung). When only two views are required to image one entire lung, the half views may be connected afterwards in single lateral left and right lung images using a specially devised computer programme. For that purpose, radioactive markers[a] should be stuck on the horse's left and right chest walls, at the intersection of both lung halves but outside the lung field (i.e. at the top level of the 10th rib), and image acquisition should be stopped after a defined time (e.g. 60 x 2 sec frames) rather than a fixed number of counts. Connection of half views requires correction for radioactive decay. The cranial and caudal aspects of the lung are of different sizes; therefore, if acquisition is performed for a set number of counts, acquisition times will be different. Therefore, in addition to correcting for the time elapsed between acquisition of the two views, it is necessary to correct for acquisition length for each view.

Dorsal views of the left and right lungs are useful to determine radiopharmaceutical distribution in each lung. This information is not easily obtainable from lateral images.

Image Post Processing

Although valid clinical information can be derived from half views, quantitative analysis (which is necessary to compare a

[a]A piece of felt with a drop of ^{99m}Tc applied to the horse's thorax using acrylic glue, or commercially available markers.

Table 1: Radiopharmaceuticals for equine lung imaging

Radiopharmaceutical	Study	Dose	Route of administration	Comments	Trade Name & Company (Nonexhaustive list‡)
^{67}Ga citrate	Imaging of infection	Not reported	i.v.	[+]: high sensitivity for identifying infection [–]: poor specificity, long physical half-life (3.3 days), poor quality images	Neoscan (Nycomed) ^{67}Ga (DuPont) ^{67}Ga (Tyco Healthcare)
^{111}In oxine-labelled WBC	Imaging of infection and inflammation	Depends on labelling procedure	i.v.	[+]: contrary to ^{99m}Tc, long physical half-life (2.8 days) enables follow-up over 6 h [–]: laborious labelling procedure, physical half-life requires long horse quarantine, poor quality images, potential leucocyte activation	^{111}In Oxine (Amersham Healthcare)
^{81m}Kr gas	Ventilation	1.8 l/min*	Inhalation	[+]: true ventilation data, on-line acquisition data, dual acquisition with ^{99m}Tc-MAA, high quality images, low radiation dose, easy to administer, no quarantine [–]: expensive, limited availability	KryptoScan (Tyco Healthcare)
	Perfusion	25 ml/min*†	Gas infusion	[+]: on-line acquisition data [–]: artefacts due to circulating activity, more time-consuming and expensive than the ^{99m}Tc-MAA method	
^{99m}Tc-antibody fragment	Imaging of infection and inflammation	4.5 MBq/kg bwt	i.v.	[+]: easy to prepare, no blood manipulation, no leucocyte activation [–]: low uptake of target cells, unspecific radioactivity extravasation	LeukoScan (Immunomedics)
^{99m}Tc-carbon clusters	Ventilation	Not reported	Inhalation	[+]: small hydrophobic particles, probably a better ventilation imaging agent than ^{99m}Tc-liquid aerosols [–]: might induce serious background contamination	Technegas (Tetley Medical)
^{99m}Tc-DTPA	Ventilation Alveolar clearance	7.4 MBq/kg bwt 7.4 MBq/kg bwt	Inhalation Inhalation	[–]: lung clearance [+]: detection of subclinical inflammation	CIS-DTPA (CIS) DTPA (Draximage) TechneScan DTPA (Tyco Healthcare) DTPA (Nycomed) Techneplex (Bracco)
^{99m}Tc-HMPAO -labelled WBC	Imaging of infection and inflammation	Depends on labelling procedure	i.v.	[+]: as opposed to ^{111}In, qualities linked to a ^{99m}Tc-labelled product [–]: laborious labelling procedure, potential leucocyte activation	Ceretec (Amersham Healthcare)
^{99m}Tc-MAA	Perfusion	1.11 MBq/kg bwt	i.v.	[+]: imaging of the whole lungs, the easiest method, images of exercising perfusion may be obtained	MAA (Draximage) MAA (Nycomed) Macrotec (Bracco) Pulmolite (CIS) TechneScan LyoMAA (Tyco Healthcare)
^{99m}Tc-Nanocolloid	Ventilation	7.4 MBq/kg bwt	Inhalation	[+]: no lung clearance, the less expensive technique for ventilation imaging	Venticoll (Nycomed)
^{99m}Tc-oxides	Alveolar clearance	Not reported	Inhalation	[+]: sharp starting point of the clearance curve [–]: possible premature oxidisation of the particles, might induce serious background contamination	Pertechnegas (Tetley Medical)
^{99m}Tc-RBC labelling kit	First pass blood flow, EIPH detection (?)	7 MBq/kg bwt	i.v.	[–]: usefulness not proven for EIPH detection and quantification	Ultratag (Tyco Healthcare)

*The elution rate suggested is for a generator containing approximately 925 MBq (25 mCi) of its parent isotope. †Elution of the generator with 5% dextrose in water. ‡Trade names and companies list may not be complete; in addition, owner of products may change over time.

subject or group of subjects from an objective point of view) requires connection of half views in a global image. Connection of half views requires the following steps to be performed for each lung:

1. Correct the pixels' value of half views for radioactive decay according to a reference time (e.g. time of the first image acquired).
2. Align cranial and caudal images using the radioactive marker as reference.
3. Generate a vertical cutting line passing through the centre of the radioactive reference marker.
4. Reject pixels in the half views caudal and cranial to the vertical line in the cranial and caudal views, respectively.
5. Combine the half views to create a composite image representing the lateral view of the whole lung (**Figure 1**).

The borders of the left and right lung images may be defined using computerised isocount lines that visually fit the lung edges. The isocount lines are generated by an isocontour

N Figure 1: Lateral views of the right lung

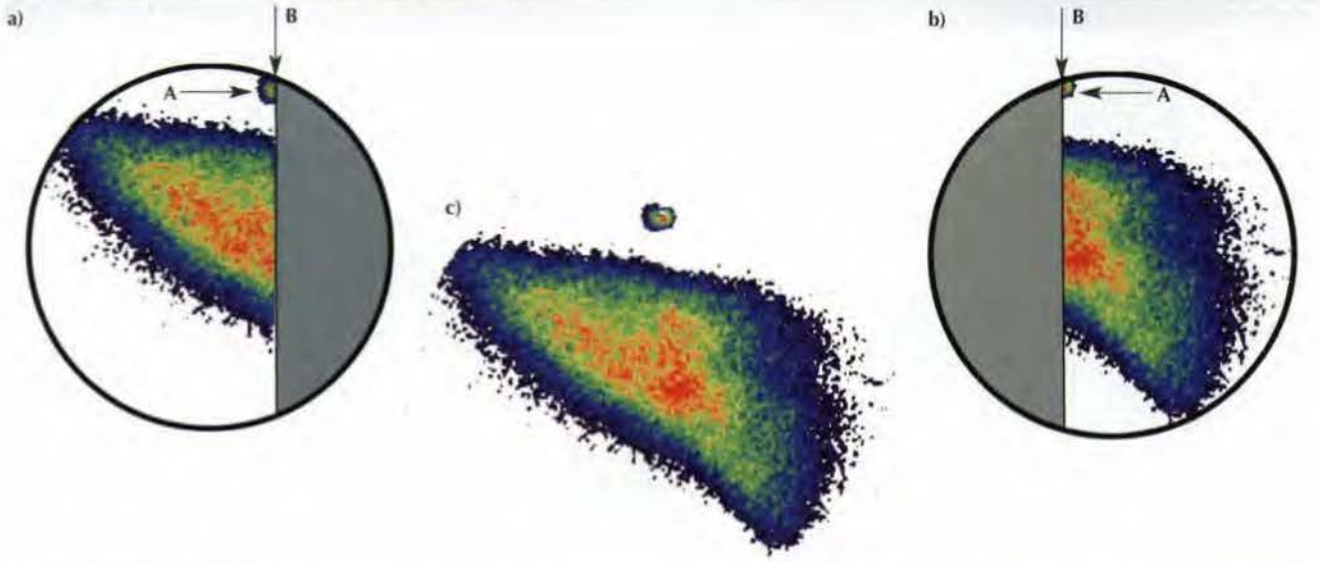

Right lung reconstruction	Half views (a) and (b) 128 x 128	Whole lung (c) 256 x 256

➡ **A:** The caudal (a) and cranial (b) half lateral views of the right lung are aligned using a radioactive marker stuck at the upper level of the 10th rib and seen on both images.
➡ **B:** A cutting line passing through the centre of the reference marker enables rejection of redundant pixels.
Note: Half views are added and the lateral view of the whole lung is obtained (c).

function that draws a line between pixels with a value equal to a definite percentage of the maximum pixel value found in the image. This percentage should not be chosen arbitrarily but should correspond to a rapid mean count decline per pixel. In addition, it should be set at a value sufficiently high (e.g. 10–12%) so as to exclude counts due to background.

Image Limitation

Planar scintigraphy provides 2-dimensional images of the 3-dimensional distribution of radiopharmaceuticals within the body. Pixels of a lateral view of the lung represent a column of tissue and the counts recorded originate from both lungs, with a much larger contribution from the lung closer to the gamma camera. Therefore, counts recorded in a specific region may emanate from any depth at that site, from either lung. In addition, patchy abnormalities involving only some portions of a lung may be masked, especially in the thicker parts of the lung. Image post processing is helpful to highlight regional dysfunction, and is required to extract quantitative information from a lung scan.

CLINICAL STUDIES

Procedure for Perfusion Scintigraphy

Background Information

Perfusion scintigraphy is much more easily performed than ventilation studies and can yield a lot of potentially useful clinical information concerning common conditions, such as COPD, abscesses, bronchitis and recovery or response to treatment (**Figure 2**). This technique can readily be performed in practice. It does not require a large field of view camera, as up to 4 images can be taken to cover the entire lung field. Useful clinical information can be derived from visual examination of the images alone (**Figure 2**) without the need to connect half or quarter views. Perfusion scintigraphy is therefore an excellent introduction to pulmonary scintigraphic studies.

Blood distribution through the ramifications of the pulmonary artery, called lung perfusion, may be assessed by scintigraphy. In a conscious, standing horse, pulmonary perfusion is distributed along a vertical gradient in which the perfusion increases from the dorsal to the ventral regions of the lung[6]. As in people, this gradient was originally attributed to gravitational effect in association with the balance between pulmonary arterial, pulmonary venous and alveolar pressures. However, the gravitational model failed to explain perfusion heterogeneity within horizontal (i.e. isogravitational) planes[7] and perfusion redistribution towards the dorsal lung region, whatever the animal's position (e.g. lateral, dorsal or ventral recumbency), in anaesthetised animals, including horses[8,9]. With the emergence of high-resolution technologies, new studies in several species provide evidence that the structure of the pulmonary arterial tree is the primary determinant of pulmonary perfusion distribution. Within this fixed structure, passive factors, including hydrostatic pressure and/or distension of pulmonary vessels as well as active local factors such as sheer stress or hypoxic vasoconstriction, determine regional flow[10].

Indications

The 3-dimensional distribution of pulmonary perfusion at rest and during exercise has been studied extensively in healthy horses using fluorescent microspheres[11]; however, the

A **Figure 2: Dorsal view of left and right lungs. Vascular perfusion study of a COPD case before (a) and after (b) treatment (*Figures courtesy of Robert Twardock*)**

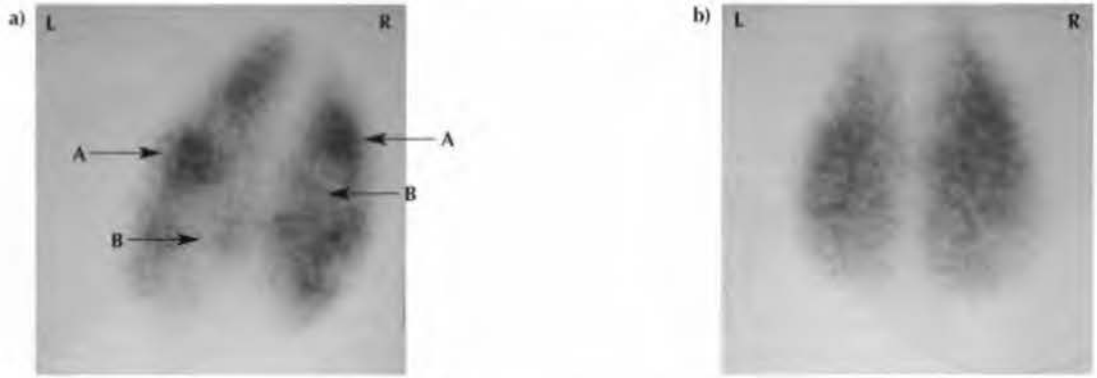

Shetland	9y	M	256 x 256

DX: Allergic bronchitis.

DS: Radiography: lungs within normal limits; slight concave appearance of diaphragm. Tracheal wash: no bacteria grown or abnormal cells seen. Second MAA scan 5 days after admission and first scan.

➔ **A:** Regions of greater, more normal perfusion.
➔ **B:** Photopenic regions low in or lacking perfusion.
Note: In contrast to skeletal scintigraphy, pathology in pulmonary perfusion scintigraphy is indicated by 'cold spots' indicating lack of or reduced perfusion and MAA deposition. Before treatment (a), MAA distribution is very nonuniform, 'patchy', showing regions of greater more normal perfusion (A) intermingled with photopenic regions low in or lacking perfusion (B). After treatment (b), MAA distribution is uniform, corresponding in intensity to the anatomical width and depth of the lungs seen from the dorsal view. Pony had been in respiratory distress for 1 week when first scanned.

technique requires euthanasia of the horse. In contrast, scintigraphy is minimally invasive and can be repeated on the same animals sequentially over time. However, scintigraphy has less spatial resolution than the fluorescent microsphere technique. Perfusion scintigraphy is indicated to:

- Aid in the diagnosis of an unknown disorder, to understand mechanisms of gas exchange impairment.
- Assess the extent of a known pulmonary disease, or to determine the severity of functional disturbance.
- Study modifications of perfusion induced by respiratory disorders.
- Determine factors influencing the perfusion distribution. Because of their tall lungs (around 45 cm along the gravitational axis in an average-sized horse vs. 30 cm in man), horses are considered to be a good model for studying the role of gravity.
- Follow the regional changes of perfusion induced by respiratory disorders, medication or anaesthesia.
- Evaluate the contribution of perfusion redistribution with exercise to the location of exercise-induced pulmonary haemorrhage (EIPH).

Procedure

Radiopharmaceutical

Perfusion studies can be performed with infused radioactive gases or the entrapped ^{99m}Tc-labelled particles technique.

Entrapped Radioactive Particles: The standard method for lung perfusion imaging uses ^{99m}Tc-labelled macroaggregates of human serum albumin (^{99m}Tc-MAA). Following injection into the jugular vein, these large radioactive particles (generally ranging from 10–90 µm in size) are completely trapped in the pulmonary vascular bed, reflecting the distribution of pulmonary blood flow. This multiple iatrogenic embolism occurs at the first pass through the pulmonary circulation and the radiopharmaceutical does not reach the systemic circulation. This procedure is safe, because the number of capillaries occluded by particles is very small compared to the total number of pulmonary vessels. Radiopharmaceutical administration does not affect pulmonary mechanics or gas exchange. The particles are eliminated from the lungs by metabolic degradation and phagocytosis. In man, the biological half-life is reported to be approximately 11 h and the effective intrapulmonary half-life 1–2 h. Radioactivity is released from the degraded particle and is progressively eliminated via the kidneys.

Radioactive Gases: The only gas suitable for perfusion scintigraphy in horses is ^{81m}Kr. The main indication for use of this gas is the potential to monitor on-line regional changes induced by specific conditions (e.g. position change in an anaesthetised horse).

Radiopharmaceutical Administration Procedure

The radiopharmaceuticals are administered through a catheter placed in the jugular vein.

Entrapped Radioactive Particles: The injectate must be homogenised by gently swirling the syringe prior to i.v. administration. Blood should not be drawn into the syringe; the radiopharmaceutical must be introduced directly into the bloodstream to avoid formation of clots. As pulmonary blood flow is influenced by changes in alveolar pressure associated with breathing, ^{99m}Tc-MAA must be injected over several breaths. Images may be obtained immediately afterwards. The resulting images show the average distribution of blood flow during inspiration and expiration.

^{81m}Krypton Gas: The ^{81m}Kr/^{81}Rb generator is eluted with dextrose in water and the solution containing dissolved ^{81m}Kr is continuously infused into the jugular vein following passage through a bacterial filter. Image acquisition starts once a steady-state count distribution is achieved[6].

Image Acquisition

With infused ^{81m}Kr, only perfusion of the caudal aspect of the lungs can be studied because of artefacts associated with radiopharmaceutical circulating in the right heart, superimposed on a lateral view of the cranial aspect of the lungs. On-line data acquisition gives real-time pulmonary perfusion images. With entrapped radioactive particles, cranial and caudal views of both lungs can be acquired. The images represent the perfusion at the moment of administration of the radioactive particles. Consequently, exercising perfusion may be studied through the administration of radioactive particles during the final step of an exercise test performed on a treadmill. The exercising images can be obtained after the horse has recovered from exercise.

Image Post Processing

The borders of the perfused lungs may be delineated with isocount lines. The number of pixels within these isocount lines determines the size (Sz) of the lung images. The variation in size (ΔSz), height (ΔHgt) and length (ΔLgt) of the perfusion images (see *Image Post Processing* in *Procedure for Ventilation Scintigraphy*) may be useful in the study of functional adaptations to specific conditions (e.g. exercise or hypoxaemia).

Regional distribution of pulmonary perfusion is particularly difficult to analyse on lateral images because the thickness of the lungs varies in the different parts of the perfusion image. Consequently, the recorded radioactivity depends not only on blood flow but also on the volume of the region considered. To interpret perfusion images, it may be necessary to create ratio images that adjust for the problem of volume. Depending on the objective of the study, several possibilities exist. For example, perfusion redistribution induced by exercise may be examined using exercising (Q_E) vs. resting (Q_R) perfusion ratio (Q_E/Q_R) images, whereas mechanisms of gas exchange impairment may be explored through the creation of ventilation to perfusion ratio (V/Q) images. The methodology to create ratio images is explained in the section *Procedure for the Study of the Ventilation-Perfusion Relationship*.

Interpretation of Functional Images

Pulmonary perfusion images look similar to ventilation images. Uneven radioactivity distribution may be observed in horses with pulmonary disease (**Figure 2**).

At exercise, an intense recruitment of pulmonary capillaries is observed, as shown by ΔSz, ΔHgt and ΔLgt of perfusion scans from rest to exercise[12] (see *Image Post Processing* in *Procedure for Ventilation Scintigraphy*). Moreover, analysis of Q_E/Q_R images indicates that this marked perfusion redistribution occurs in the dorsal region of the lungs (**Figure 3**). This feature of the physiological response of the equine lung to exercise may conceivably contribute to the location of bleeding sites in EIPH.

Procedure for Ventilation Scintigraphy

Background Information

Air distribution from conducting airways to parenchyma, called lung ventilation, may be studied by scintigraphy. In a conscious, standing horse, a vertical gradient of pulmonary ventilation exists; the dorsal lung region is therefore less ventilated than the lower region[6]. The ventilation distribution is determined by regional compliance and resistance, two factors that may be affected by respiratory disorders. During tidal breathing, the dorsal portion of the lung is less compliant, resulting in reduced regional ventilation. In addition, changes in pleural pressure are greater in the ventral and middle than the dorsal portion of the horse's lung, further contributing to the preferential distribution of ventilation to the ventral portion of the lung during inflation[13].

Indications

The potential applications of ventilation scintigraphy are to:

- Aid in the diagnosis of an unknown disorder, or to understand mechanisms of gas exchange impairment.
- Assess the extent of a known pulmonary disease, or to determine the severity of functional disturbance.
- Study modifications of ventilation induced by respiratory disorders.
- Follow the regional changes of ventilation after therapy, or during the clinical evolution of disease.
- Follow the regional changes of ventilation induced by anaesthesia.
- Define the topographical distribution of ventilation to serve as a baseline study in horses undergoing a pharmacological or an allergen provocation test.
- Study the topographical distribution of air over the inspiration phase of the respiratory cycle in order to determine the best moment for puff inhalation of drug to target specific site(s) within the lungs.

Procedure

Radiopharmaceuticals

Ventilation studies can be performed with radioactive gases or ^{99m}Tc-labelled aerosols.

Radioactive Gases: Of all radioactive gases used in human nuclear medicine, krypton-81m (^{81m}Kr) is the only one suitable for ventilation studies in horses. The other radioactive gases (e.g. Xenon-133 [^{133}Xe], Xenon-127 [^{127}Xe], Oxygen-15 [^{15}O] and Nitrogen-13 [^{13}N]) are not appropriate for equine

N Figure 3: Lateral views of the right lung

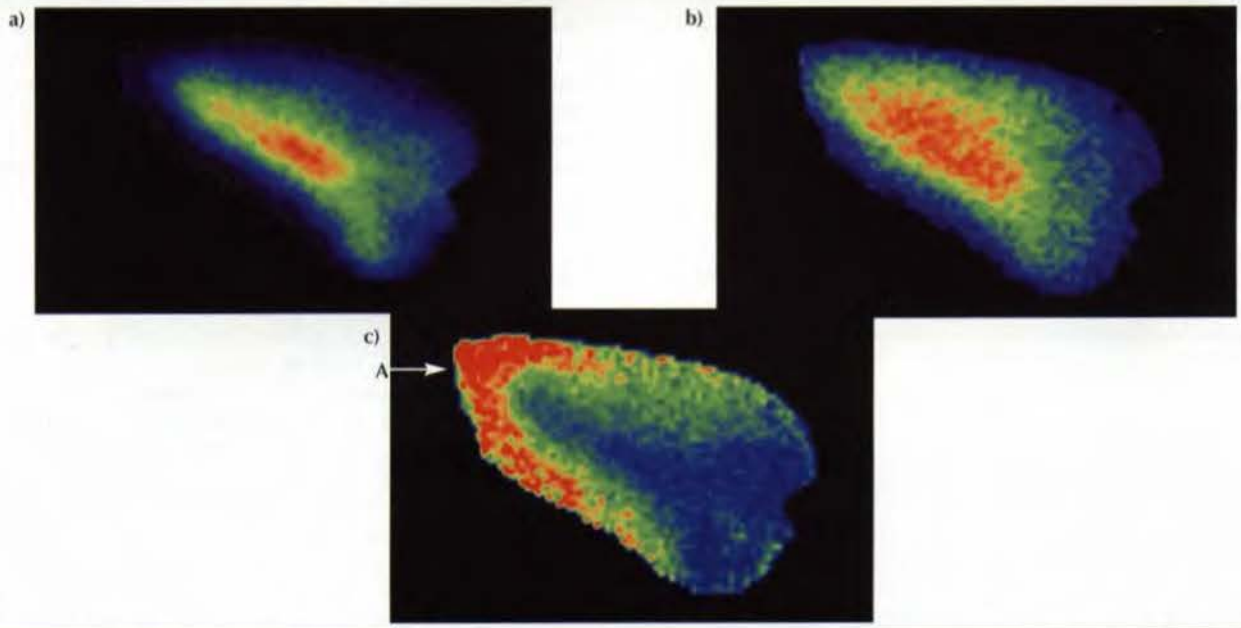

Perfusion redistribution induced by exercise | **128 x 128**

Exercise induces an intense recruitment of pulmonary capillaries as demonstrated by perfusion scans enlargement from rest (a) to exercise (b). The regional perfusion redistribution induced by exercise (c) was visualised by dividing the exercising (Q_E) by the resting (Q_R) perfusion image.

➡ **A:** The obtained computed ratio (Q_E/Q_R) image (c) demonstrated marked perfusion redistribution in the caudo-dorsal region of the lung.

N Figure 4: Administration of ventilation-imaging agents

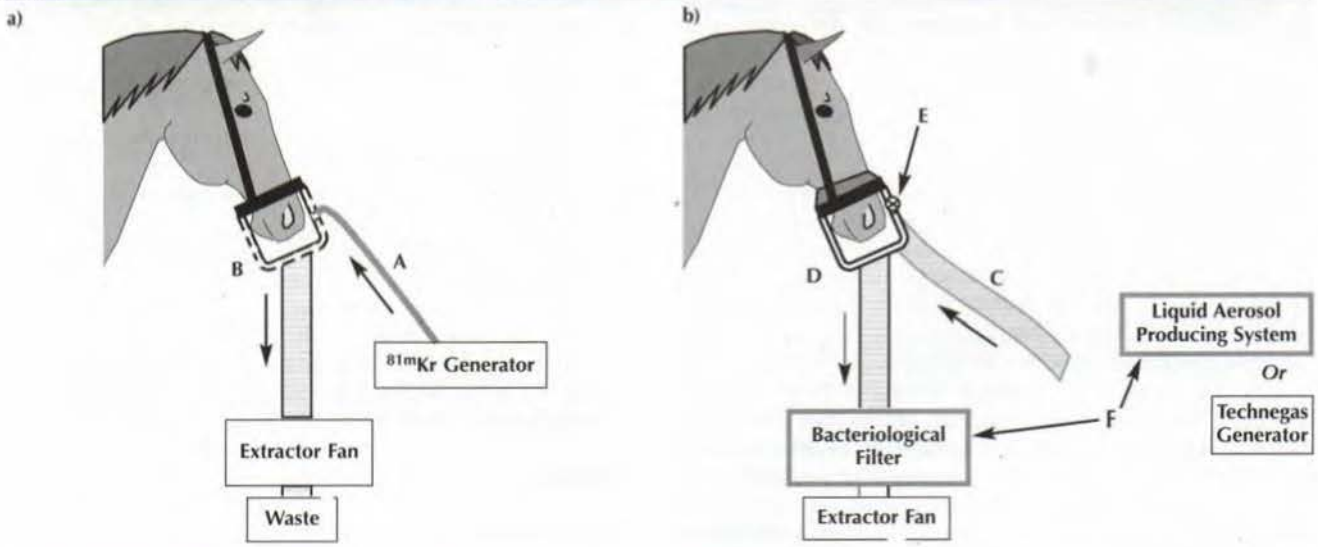

Administration of ventilation-imaging agents

➡ **A,B:** ^{81m}Kr gas eluted from its generator is delivered via narrow-bore tubing (**A**) into a loosely fitting face mask with many holes (**B**), which allows room air to enter freely during inspiration. An extractor fan connected to the mask directs expired gas to an open waste system where ^{81m}Kr, heavier than air, can decay.

➡ **C–F:** Liquid and solid radioactive aerosols are delivered via large-bore tubing (**C**) to a tightly attached face mask (**D**). Room air enters the system on demand via a one-way valve set on the mask (**E**). An extractor fan directs exhaled air to a bacteriological filter where undeposited radioactive particles are trapped. Filtered air freely leaves the system. The radioactive solution to be aerosolised by the aerosol-producing system, as well as the bacteriological filter, must be enclosed in lead shielding (**F**) to minimise radiation exposure.

N Figure 5: Lateral views of the left lung, delineated by a 12% isocount line

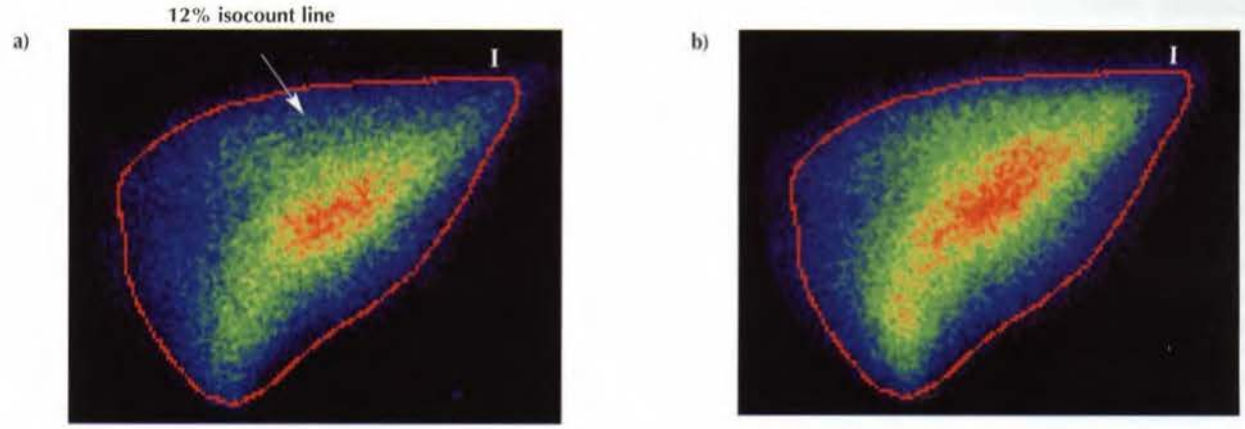

Delineation of the lung boundaries	256 x 256

When true ventilation images are not available (i.e. ^{81m}Kr ventilation scans), the lung boundaries of the ventilation scans may be delineated using isocount lines (I) drawn on the perfusion scans (a) and superimposed on the aerosol deposition images (b). In the perfusion scan shown, a 12% isocount line corresponded to an abrupt mean count decline per pixel.

N Figure 6: Lateral views of the left and right lungs

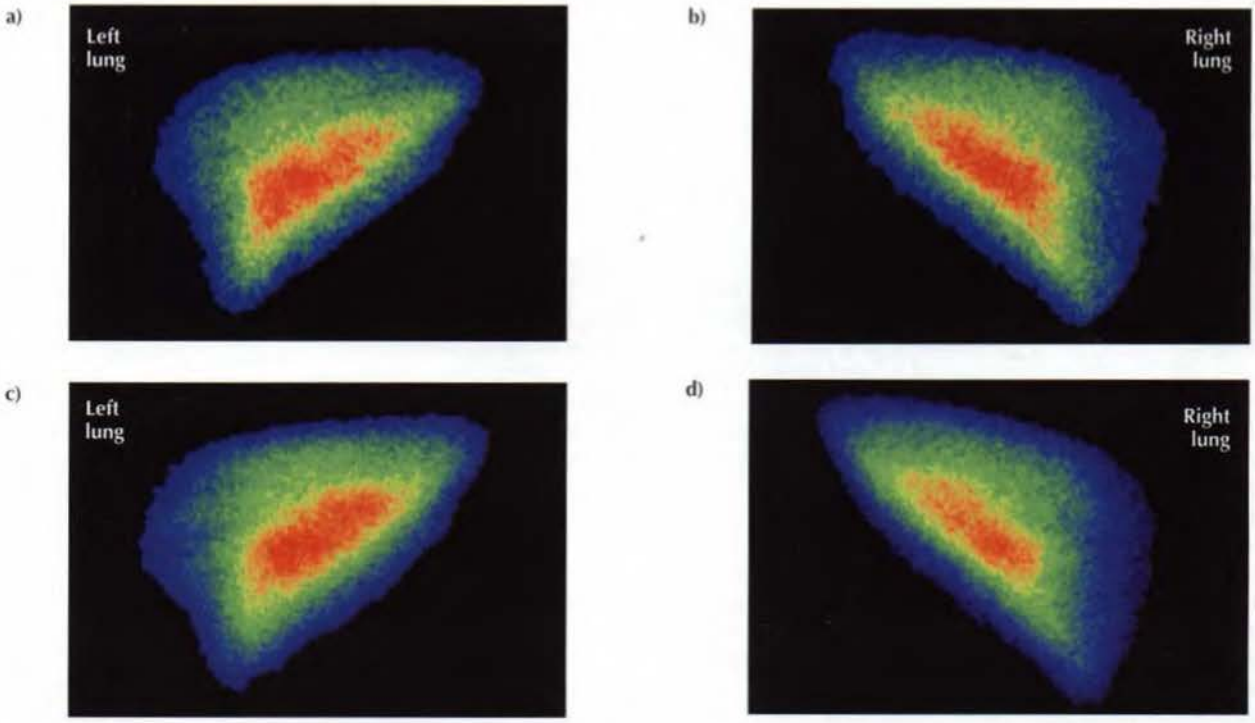

Ventilation and perfusion images in a healthy horse	256 x 256

The radioactivity distribution patterns within the ventilation (a,b) and perfusion (c,d) images are similar in healthy horses.

scintigraphy because of their physical properties (half-life and/or γ-energy emission). ^{81m}Kr is a noble gas that is chemically and physiologically inert; it decays by emitting a single 190 KeV γ-ray and therefore provides a clean spectrum for analysis which falls within the energy range considered most suitable for γ-imaging of large animals. In addition, the short half-life (13 sec) of ^{81m}Kr confers numerous advantages over ^{99m}Tc-labelled ventilation-imaging radiopharmaceuticals:

- Ventilation studies may be repeated without interference from any previous administration, so that ventilation changes induced by treatment (e.g. response to a bronchodilator) or experimental conditions can be monitored on-line.
- Dual isotope ventilation-perfusion scintigraphy (i.e. the perfusion is usually imaged with a ^{99m}Tc-labelled radiopharmaceutical) is possible, since the 140 KeV emission of ^{99m}Tc does not interfere with detection of the mono-energy peak of ^{81m}Kr.
- Its use is associated with a low radiation dose.
- There is no need for a system to collect exhaled gas because there is no risk of long-term environmental contamination.
- There is no need for quarantine of the horse after the procedure. In human nuclear medicine, the steady-state inhalation of ^{81m}Kr scintigraphy is considered to be the gold-standard method of studying regional ventilation of the lung[14]. Unfortunately, the short half-life (4.58 h) and high cost of a ^{81m}Kr generator limit its use in equine practice.

Radioactive Liquid Aerosols: Liquid ^{99m}Tc-labelled aerosols are used primarily to visualise the ventilated equine lung. An aerosol of ^{99m}Tc-diethylene-triamine-penta-acetic acid (^{99m}Tc-DTPA) is currently the most popular. However, ^{99m}Tc-DTPA is cleared from the lungs by passive diffusion through the intercellular junctions of the alveolar-capillary barrier. This property may be useful in the detection of subclinical respiratory problems (see *Procedure for the Scintigraphic Study of the Alveolar-Capillary Barrier*), but causes the radiopharmaceutical to redistribute from the lungs during the time required to acquire ventilation images (around 20–30 mins). A radiopharmaceutical such as albumin colloids, that does not diffuse out of the lungs and whose distribution activity therefore remains virtually static, is preferable.

During tidal breathing, deposition of inhaled aerosol takes place by impaction in the larger airways and by sedimentation in the lung periphery (i.e. smaller airways and alveoli), where it reflects regional ventilation. The relative amount of aerosol deposition in ventilated regions and conducting airways depends on the aerodynamic properties of the aerosol particles, airway characteristics and breathing pattern. Therefore, an aerosol deposition image may not truly represent an image of ventilation, as the deposition pattern is not only a function of ventilation. This weakness of the radioactive aerosol vs. ^{81m}Kr gas inhalation technique can be minimised by producing aerosol with aerodynamic properties that favour deposition by sedimentation (i.e. the aerosol produced should be monodisperse[b] and the aerosol particles should ideally have a mean aerodynamic diameter around 0.5 μm). Liquid ^{99m}Tc-labelled aerosols are less expensive and, because they are more readily available than ^{81m}Kr, they therefore constitute a first-class radiopharmaceutical for clinical ventilation imaging in horses. However, disadvantages include:

- Clumping of particles in the airways, producing hot-spot artefacts on the images.
- The colloid is exhaled.
- There is a high radiation dose during administration.
- Perfusion and ventilation studies cannot be performed simultaneously.
- It is not a gas and therefore does not show pure ventilation.

Radioactive Solid Aerosol: An ultrafine ^{99m}Tc-labelled carbon dry aerosol, Technegas, may be produced using a Technegas generator[15]. The size of the Technegas particles is below 0.2 μm[16], which is much smaller than the liquid aerosol particles usually produced. In addition, unlike liquid aerosols, which grow rapidly in size by absorption of water vapour within the conducting airways, Technegas particles are hydrophobic and do not enlarge. As Technegas behaves like a gas in its ability to penetrate the airways, but is retained within the lungs like an aerosol, it is often referred to as a 'pseudo-gas'. Technegas does not diffuse through the intercellular junctions of the alveolar-capillary barrier; therefore, the only limiting factor for image acquisition is the ^{99m}Tc half-life. The use of Technegas for equine lung studies has not been reported in the literature. Technegas has been used for ventilation imaging in cattle, where it appears more suitable for use in examination of ventilated parts of lungs than liquid ^{99m}Tc-labelled aerosol[17]. The main disadvantage of Technegas is the high cost of the generator. However, Technegas is a ^{99m}Tc-labelled radiopharmaceutical; therefore, it can be produced for several days using a ^{99}Mo/^{99m}Tc generator.

Radiopharmaceutical Generation and Administration Procedure

The techniques for dispensing ventilation-imaging agents are illustrated in **Figure 4**.

^{81m}Krypton Gas: ^{81m}Kr gas is eluted by air passing through a ^{81m}Kr/Rubidium-81 (^{81}Rb) generator. A flow rate of 1.5–2.0 l/min is considered to be optimal for elution efficiency. The radioactive tracer is delivered directly from the generator into a loosely fitting face mask worn by the horse, or to an intratracheal catheter. The length of the tube between the generator and face mask should be kept to a minimum to reduce losses due to radioactive decay. Images are acquired once a steady-state count distribution image is obtained. The rapid physical decay of ^{81m}Kr prevents equilibration between inspired and alveolar radioactive gas concentrations. As a consequence, the regional count rate is determined largely by the arrival of fresh ^{81m}Kr, i.e. the regional ventilation[18].

Radioactive Liquid Aerosols: Jet and ultrasonic nebulisers are used primarily to produce liquid aerosols of radiolabelled solutions. The size distribution of nebulised aerosol droplets is heterodisperse[c]. It would be preferable to produce monodisperse radioactive aerosols for ventilation imaging; a

[b]All the aerosol particles behave as if they are the same size. [c]The particles or droplets in the aerosol have a range of sizes.

spinning disc generator, condensation generator or vibrating generator might be used for making such monodisperse aerosols. The system generating the radioactive aerosol should, at least, produce an aerosol suspension with droplet size ranging from 0.5–2.0 µm, i.e. one that can potentially reach and be deposited in the alveoli. Droplets smaller than 0.1 µm in diameter may remain suspended and be exhaled without deposition.

The ^{99m}Tc-labelled aerosol is delivered for a few minutes to the horse through a flexible tube connected to a face mask sealed tightly around the horse's nose to prevent radioactive contamination of the examination room. A one-way valve set on the mask may ensure air supplementation during inspiration. Exhaled air must be vented through a filter mechanism in order to trap undeposited radioactive aerosol particles. After aerosol administration, the horse should continue to breathe through the system for a few breaths in order to filter out residual radioactivity. Imaging should start immediately after aerosol administration to avoid significant changes in the distribution pattern by mucociliary clearance or, for radiopharmaceuticals that are washed out of the lungs, alveolar clearance.

Technegas: To produce Technegas, sodium pertechnetate deposited in a graphite crucible is evaporated to dryness at 2550°C under an argon atmosphere in the Technegas generator. The resulting dry aerosol is a suspension of carbon clusters labelled with ^{99m}Tc.

The same delivery and collection system can be used for Technegas as for radioactive aerosol inhalation. The Technegas generator can simply be connected to the assembly instead of the liquid aerosol producing system. As opposed to liquid aerosols, the total radioactive dose to be administered is delivered in a few breaths. Therefore, accidental disconnection from the circuit would induce a more serious contamination of the background in comparison to radioactive liquid aerosols.

Image Acquisition

With the short-lived gas ^{81m}Kr, ventilation images are acquired during steady-state inhalation of the tracer, the horse being positioned with the thorax against the face of the gamma camera. Conversely, aerosol deposition images are acquired following the administration of the ventilation-imaging agent.

Half views of the lungs are acquired that may be connected by image post processing, requiring radioactive markers to be stuck on the horse's chest walls. These may be small radioactive sources emitting out of the ^{81m}Kr energy range (e.g. Americium-241 [^{241}Am]; 60 keV) or, when sodium pertechnetate is available, a drop of ^{99m}Tc-eluate absorbed on pieces of felt.

Image Post Processing

Following connection of half views, the lung borders may be defined. With ^{81m}Kr, isocount lines may delineate the lung boundaries and Sz of the lung images may be obtained. The dimensions of a drawn rectangle that includes the isocount line define the height (Hgt) and length (Lgt) of the lung images. The ΔSz, ΔHgt and ΔLgt may be observed under pathological conditions (e.g. bronchoconstriction) or experimental challenge.

On aerosol deposition images, isocount lines may not represent the lung boundaries if aerosol particles significantly impact in conducting airways before reaching ventilated alveoli. The comparison of the size of the aerosol deposition image vs. the true size, determined on a ^{81m}Kr ventilation scan, informs about the aerosol's ability to reach alveoli. When ^{81m}Kr gas is not available, the lung borders may be assumed by reference to pulmonary perfusion scans (presupposing that a) there is no perfusion defect and b) the perfused and ventilated areas are matched; **Figure 5**).

The equilibrium images for ^{81m}Kr mainly reflect the tidal space of the lung (i.e. including the anatomical dead space), whereas use of labelled aerosols allows visualisation of conducting airways in proportion to airway impaction. This airway impaction may be quantified by calculating a penetration index (PI). This parameter is obtained by calculating the ratio of radioactive counts emanating from the lungs in the peripheral region (ROI_{Per}; i.e. containing mainly lung parenchyma) to the central region (ROI_{Cen}; i.e. including the major bronchi). A high index indicates high peripheral deposition.

Interpretation of Functional Images

In healthy horses, ^{81m}Kr gas ventilation and small-sized aerosol deposition images have a uniform appearance throughout both lungs. The radioactivity distribution patterns are very similar to those found in perfusion images (**Figure 6**). Equine lung volume is not distributed equally between the left and right lungs; the right lung contains about 55% total lung volume and lung size is therefore higher for the right than the left lung. Despite its larger size, the activity recorded for the right lung is similar to that for the left[19], because the majority of counts recorded are from the more superficial parts of the lung.

Because of functional modifications (e.g. bronchoconstriction, airway inflammation, changes in the breathing pattern), pulmonary diseases alter the ventilation distribution. Since many factors may restrict aerosol particle penetration more significantly than ^{81m}Kr gas distribution to the lung periphery, aerosol deposition images might be more sensitive to functional disturbances than ^{81m}Kr ventilation scans. No comparative study has been reported in the literature. Lung disorders usually result in excessive aerosol deposition in ROI_{Cen} and poor tracer distribution in ROI_{Per} (**Figure 7**). Therefore, under pathological conditions, the aerosol deposition image does not permit measurement of regional ventilation on a quantitative basis. However, the severity of airflow obstruction is reflected by the degree of central impaction that may be measured by calculating the PI. The dimensions, PI and shape of the lung image are sensitive means of discriminating normal from abnormal lung function, as well as monitoring efficiency of a treatment and/or environmental management to restore normal function (**Figure 8**).

Procedure for the Study of the Ventilation-Perfusion Relationship

Background Information

In people, gradients in the ventilation and perfusion distributions generate a vertical gradient in the V/Q; V/Q is higher in the upper regions than in the lower regions. If gravity was the major factor determining V/Q distribution, a greater V/Q mismatch should result from these vertical

A **Figure 7: Lateral views of the left and right lungs**

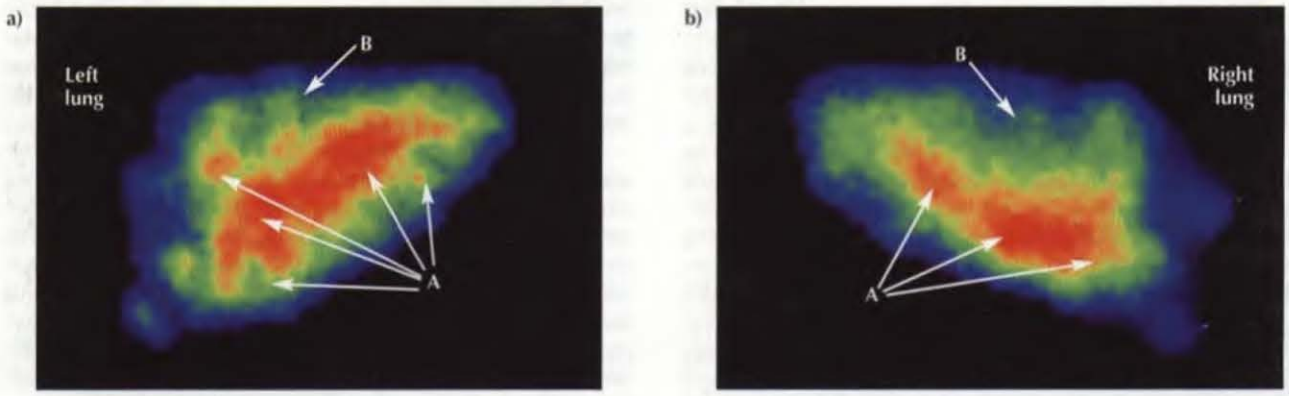

Ventilation images in a horse with COPD | 256 x 256

During exacerbation of COPD signs, lung secretions and bronchoconstriction impede aerosol particles from reaching the most peripheral part of the lungs. The ventilation-imaging agent impacts in large conducting airways, resulting in patchy aerosol dispersal within the airway (**A**) and poor alveolar distribution (**B**).

A **Figure 8: Lateral views of the left and right lungs**

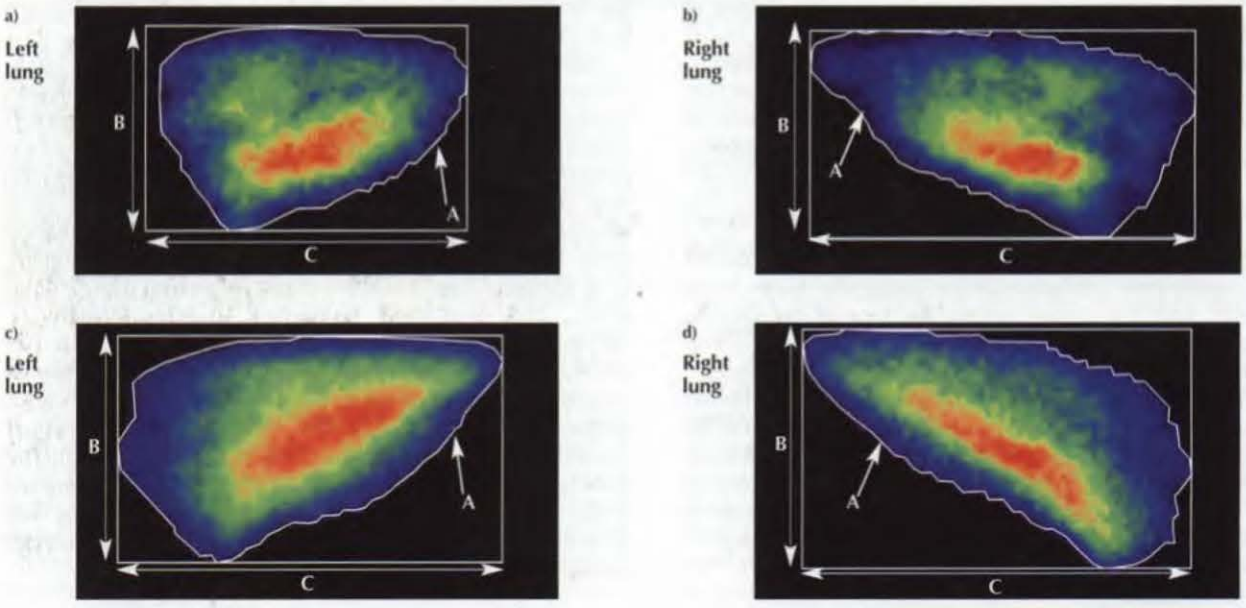

Scintigraphic assessment of ventilation improvement | 128 x 128

During clinical signs of COPD (a,b), functional modifications restrict the lung ventilation as reflected by the reduced dimensions of the ventilation images compared to images acquired following adequate management of the horse (i.e. during clinical remission of the disease obtained at pasture; c,d); ventilation improvement is mirrored by variations in size, height and length. The pattern of distribution is also much improved during remission.

- **A:** Size: ΔSz left lung +20.4%; ΔSz right lung +5.1%
- **B:** Height: ΔHgt left lung +12.5%; ΔHgt right lung +16.5%
- **C:** Length: ΔLgt left lung +21.3%; ΔHgt right lung +11.8%

Note: These figures are a comparison of a) with c) and b) with d).

gradients in horses compared to people, because of a larger lung height. Surprisingly, in a standing, unsedated horse, the ventilation and perfusion distributions are closely matched throughout the lung height[6], challenging the role of gravity in V/Q distribution.

The good match of ventilation and perfusion results in near optimal arterial oxygenation. Mismatching of ventilation and blood flow within diseased lungs is the most common cause of hypoxaemia.

Indications

The diagnostic possibilities of pulmonary scintigraphy are exploited to their full extent only when ventilation and perfusion scintigraphy are combined. Uses of scintigraphic analysis of the ventilation-perfusion relationship include:

- Aiding in the diagnosis of an unknown disorder, or to understand the mechanisms of gas exchange impairment.
- Assessing the extent of a known pulmonary disease or quantifying the degree of ventilation and perfusion mismatch.
- Following regional changes of the ventilation-perfusion relationship induced by respiratory disorders, medication or anaesthesia.
- Monitoring response to therapy.

Procedure

Radiopharmaceuticals

The radiopharmaceuticals, methods of administration, and their advantages and disadvantages for ventilation and perfusion scintigraphy have been detailed in the previous sections. Several combinations of radiopharmaceuticals are possible; the ventilation and perfusion images can be acquired:

- Alternately using ^{81m}Kr gas for both functional parameters.
- Simultaneously, ventilation being imaged with ^{81m}Kr gas and perfusion with ^{99m}Tc-MAA.
- Subsequently, using ^{99m}Tc-radiopharmaceuticals for both functions.

The last combination is the least expensive option in veterinary nuclear medicine because of the ease of access to a ^{99m}Tc-generator, but the disadvantages must also be considered.

Radiopharmaceutical Administration Procedure

When ventilation and perfusion images are imaged with ^{99m}Tc-radiopharmaceuticals, the aerosol deposition images should be acquired first. Because all the ^{99m}Tc-MAA particles injected for perfusion scintigraphy are lodged in the lungs, the total radioactivity trapped in the lung is known in advance. The distribution of radioactivity following nebulisation is difficult to predict because it depends on too many parameters (e.g. nebuliser efficiency, breathing pattern). As a result, the activity used for the perfusion study may be adjusted to achieve a high ratio between the perfusion and ventilation counts, thereby minimising artefacts due to residual activity of the study performed first.

Image Acquisition

When ventilation and perfusion are imaged with ^{81m}Kr, the main advantage is the absence of interference from the residual activity of one study to the next, but the study is limited to the caudal parts of the left and right lungs.

During steady-state inhalation of ^{81m}Kr gas and following administration of the ^{99m}Tc-radiopharmaceutical for perfusion imaging, images of ventilation and perfusion may be recorded concurrently using two different acquisition channels. The major benefit of dual isotope acquisition is the perfect matching between pixels of the ventilation and perfusion images. This is the method of choice.

When ventilation and perfusion images are both obtained with the use of ^{99m}Tc-radiopharmaceuticals, the decay-corrected residual radioactivity of the aerosol deposition image has to be removed by computed subtraction, taking into account time elapsed between acquisition of both images. Consequently, image acquisition times must be recorded. This subtraction assumes no significant redistribution of the radioactive aerosol.

Image Post Processing

For the creation of ratio images, the left and right lung images are treated separately. The following steps are performed sequentially:

- The computer programme exactly superimposes both lung images with the help of the radioactive marker stuck on the chest wall.
- Images are delineated by a line that includes isocount lines of the two images used to create the ratio image.
- The decay-corrected residual activity due to the first scintigraphic procedure is subtracted from the second set of images when necessary.
- The mean count per pixel of the numerator and denominator images are equalised.
- The individual value of each pixel in the numerator image is divided by the corresponding pixel value of the denominator image. From the pixels' value of the V/Q image obtained, functional information is provided, such as the regions hyper- (R_1), equally (R_2) and hypoventilated (R_3) in regard to perfusion. Additional parameters may be calculated in these regions, such as the sizes of R_1, R_2 and R_3 (Sz_{R1}, Sz_{R2} and Sz_{R3}, respectively), the regional mismatching factor (Ir_i) and the intraregional mismatching index (Lr_i). These last two parameters define the degree of mismatching between the ventilation and perfusion distributions within the region under study[19].

The following points should be noted:

- The radioactive marker used to connect half views of the lung may serve for image superimposition.
- If an area of the lung is unperfused or unventilated, it does not trap any radiopharmaceutical. If this area is situated in the peripheral part of the lung, it is not included within the isocontour line. The union of the ventilation and perfusion isocount lines enables the study of unventilated perfused area(s) and *vice versa*. Nonventilated and nonperfused

area(s) are excluded from the V/Q analysis when located in lung periphery. The shape of the lung image may provide this information.

- A correction factor (F_1) must be applied to the counts of the aerosol deposition image in order to subtract residual counts. F_1 is calculated as follows:

Equation 1

$F_1 = e^{-\lambda t}$ where $\lambda = {}^{99m}Tc$ decay constant
t = time elapsed between aerosol and perfusion image acquisitions

As λ is equal to $0.693/T_{1/2}$, where $T_{1/2}$ is the physical half-life, the corrective factor can be expressed by the following equation:

Equation 2

$F_1 = e^{-(0.693t/T_{1/2})}$

When performing the ventilation study with the ^{81m}Kr gas (the perfusion images being performed with either ^{81m}Kr or ^{99m}Tc-labelled particles), this correction is unnecessary.

- To adjust for the fact that different radioactive doses are present within the lungs after the ventilation and perfusion procedures, the mean pixel count of the ventilation image must be equalised to the mean of the perfusion scan. The corrective factor (F_2) to apply on the ventilation image is:

Equation 3

$F_2 = (Q^{Mean}/V^{Mean})$

with Q^{Mean} being calculated by summing the counts of individual pixels of the perfusion image and dividing the result by the number of pixels contained in the image. V^{Mean} is obtained in the same manner but concerns the corresponding ventilation image.

- The size of the different regions (Sz_{Ri}) is expressed as % of the total number of pixels defining the computed V/Q scan:

Equation 4

$Sz_{Ri} = R_{ipx}/Tot_{px}$
where R_{ipx} = number of pixels included in the region i
Tot_{px} = total number of pixels included within the line used to delineate the ventilation and perfusion images.

Ir_i is calculated by dividing the amount of counts of the ventilation image by the amount of counts of the perfusion image for all pixels defining the region. The factor Ir_i corresponds to the V/Q ratio of the region, so that $Ir_1>1$, $Ir_2 \approx 1$ and $Ir_3<1$. By definition, Ir_i calculated on the whole lung area equals 1. Lr_i expresses the variability of pixels V/Q within a region:

Equation 5

$Lr_i = (\Sigma V_j.Q_j)^2/(\Sigma V_j^2.\Sigma Q_j^2)$
where V_j and Q_j = activity of V and Q of each pixel (j) defining the region.

Lr_i extends from 0 (i.e. complete mismatching between V and Q) to 1 (i.e. complete matching between V and Q; V = Q anywhere in the region).

Interpretation of Functional Images

In healthy horses, the ventilation and perfusion distribution patterns are closely matched, as indicated by the Lr_i value calculated on the whole lung as well as in the different regions[19]. Scintigraphy performed on a group of horses clinically affected with COPD demonstrated that this parity is disrupted by the disease. This mismatch was correlated with the V/Q inadequacy evaluated by the alveolar-arterial difference in oxygen pressure ($AaDO_2$). This disparity between ventilation and perfusion distributions was still present after medical treatment, despite apparent clinical recovery. These observations suggest that functional impairment may require a longer period to resolve than clinical signs, and emphasises the importance of regional V/Q determination[2]. Scintigraphy performed in horses suffering from EIPH demonstrated significant reduction in ventilation and perfusion to the dorso-caudal lung fields, i.e. at the bleeding sites. The perfusion deficit was more pronounced than the ventilation change, resulting in high ventilation-perfusion ratio in those areas of the lung[20].

Procedure for the Scintigraphic Study of the Alveolar-Capillary Barrier

Background Information

Small hydrophilic compounds deposited in lung periphery diffuse passively through the tight intercellular junctions of the alveolar-capillary barrier. Because the junctions of the pulmonary vascular endothelium are larger than those of alveolar cells, the speed of clearance from lungs to blood is determined by alveolar epithelium permeability and, among other things, inversely related to the molecular weight of the hydrophilic molecule. Structural alterations of the alveolar junction, due to the inflammatory process that may accompany infectious and noninfectious respiratory diseases, accelerate the speed of clearance. *In vivo*, the permeability of the alveolar epithelium is evaluated by studying the passage through the alveolar-capillary barrier of radiolabelled hydrophilic solutes administered to the alveoli by nebulisation.

Indications

Scintigraphic measurement of the alveolar clearance rate allows quantification of alveolar epithelial damage. Although nonspecific, this quantitative information may be useful to:

- Follow both the time course and severity of lung injury.
- Monitor the repair process of the alveolar epithelium, e.g. following equine influenza, equine herpesvirus, bronchopneumonia.
- Improve management of horses with COPD.
- Evaluate response to therapy.
- Detect subclinical pulmonary disorders.
- Improve awareness of alveolar oedema formation and resolution.

Procedure

Radiopharmaceuticals

The integrity of the alveolar epithelial membrane can be assessed by measuring its permeability to ^{99m}Tc-DTPA or Pertechnegas.

^{99m}Tc-DTPA: DTPA is a chemically inert stable chelate, which is electrically neutral and easily labelled with ^{99m}Tc. DTPA has a molecular radius that enables slow passage through the tight junctions of the alveolar epithelium. Once in the interstitium, DTPA rapidly crosses the larger junctions of endothelial cells to reach the bloodstream. As ^{99m}Tc-DTPA concentration in the aerosol particles may influence the measured clearance, the aerosol preparation must be standardised with regard to the volume of eluate added to the lyophilised vial used to prepare ^{99m}Tc-DTPA.

Pertechnegas: Pertechnegas, a variant of Technegas, may also be produced using the Technegas generator and sodium pertechnetate. The vapour produced by the machine is a micro-aerosol mixture of ^{99m}Tc oxides. Immediately on contact with the water vapour of the respiratory tract, these oxides hydrolise and revert to pertechnetate ions. Unlike Technegas, pertechnetate quickly passes from alveoli to the blood compartment. This clearance is quicker than that of ^{99m}Tc-DTPA because it has a smaller molecular radius. The use of Pertechnegas for the study of alveolar clearance in equine lungs has not been reported in the literature. The compulsory nasal breathing of horses might induce a premature transformation of Pertechnegas into pertechnetate in the water-saturated nasal cavities, thereby inducing hygroscopic growth of the new-borne ions. This undesired increase in size might decrease the percentage of inhaled radioactivity that reaches alveoli in horses, in comparison to people.

Radiopharmaceutical Administration Procedure

The techniques for generating and dispensing ^{99m}Tc-DTPA and Pertechnegas are those described for ventilation imaging with radioactive liquid aerosols and Technegas, respectively. A potential advantage of Pertechnegas over the ^{99m}Tc-DTPA nebulised aerosol is that the radiopharmaceutical is completely inhaled within a few breaths. This might provide a sharpest start point of the clearance curve.

Image Acquisition

Images should be acquired as soon as possible following radiopharmaceutical administration; because the tracer is cleared rapidly, the study may focus on only one specific area of one lung. Dynamic acquisitions of this lung area are framed sequentially, continuously, using 30 sec acquisitions for at least 20 mins. Images in which the horse moves are rejected.

Image Post Processing

Measurement of alveolar epithelial clearance is influenced by mucociliary transport and bronchial clearance, since it is impossible to obtain exclusive deposition on alveolar surfaces, and the lung is a 3-dimensional organ where ciliated and respiratory epithelia overlap on a 2-dimensional view. The influence of these two clearance mechanisms may be minimised by restricting analysis to the ROI_{Per}. However, when the analysis is focused on the first 20 mins, the influence of counts emanating from conducting airways on alveolar clearance rate determination is minimal[21]. The correct delineation of the lung may be obtained by superimposition of the lung contour determined by a previous perfusion image.

Calculation of alveolar clearance necessitates the correction of each frame acquired for radioactive decay, taking, for example, the end of tracer administration as time 0 (T_0). The ROI of the lung to be analysed should be defined on a perfusion image and reported on all frames. From the ROI counts, an activity vs. time curve is generated. The coefficient of time or fraction cleared per unit time, estimated by fitting a monoexponential decay curve to the observed counts, measures the regional clearance rate (k). Results may also be expressed in half-time clearance from lung to blood ($T_{1/2} = \ln 2/k$). Correction for blood and tissue background activities is not necessary (i.e. radioactivity recirculates in pulmonary vasculature, or enters tissue spaces outside the lungs, but within the counting field of the gamma camera).

Interpretation of Functional Data

The clearance rate of inhaled hydrophilic aerosols from the lungs is a highly sensitive test that enables subclinical alteration of the alveolar epithelium barrier to be detected. For example, when stabled in a controlled environment (i.e. without allergens that potentially exacerbate clinical signs), horses prone to COPD showed a ^{99m}Tc-DTPA clearance rate intermediate between healthy and clinically-affected horses. The alveolar clearance measurement was a more sensitive indicator of lung damage than pulmonary function tests (i.e. mechanics of breathing and arterial gases measurement) that were not significantly modified by the ongoing subclinical inflammatory process[3]. Detection of subclinical diseases at an early stage is extremely useful for effective environmental and/or medical management, as well as for the prevention of clinical symptoms and/or irreversible structural deterioration.

EXPERIMENTAL STUDIES

Study of Mucociliary Function

Background Information

The mucociliary function, acting as a defence mechanism, may be studied via scintigraphic determination of mucociliary clearance. The tracheal mucociliary clearance is determined by imaging the migration of a small amount of radioactive insoluble particles deposited in the trachea. The distance moved over time measures the tracheal mucous transport (TMT) rate[22]. This rate should be measured in conscious, unsedated horses because it decreases with sedation[23]. Clinical studies have demonstrated impairment of the tracheal clearance mechanisms with respiratory diseases[24,25].

Bronchial mucociliary clearance (BMC) has never been studied in equids. Efficiency of mucociliary clearance in large airways may be assessed by determining the rate of removal of a radioactive aerosol of insoluble particles administered by nebulisation. The mean aerodynamic diameter of the aerosol droplets produced should be chosen to favour deposition in large conducting airways rather than alveoli.

Research Applications

A high degree of individual variation in TMT of the deposited particles has been demonstrated[26]. Therefore, interpretation of scintigraphic determination of TMT (and probably BMC) may be difficult. However, determination of TMT and BMC rates may be of value to:

- Determine the effects of disease or environmental pollutants on lung mucociliary clearance.
- Study the possible effect on the mucociliary function of pharmacological agents such as antibiotics and anti-inflammatory drugs.
- Assess the efficacy of mucolytics, expectorants or mucokinetics.
- Correlate the changes in biochemical and physical properties of lung secretions with clearance efficiency.

Study of Aerosol Deposition

Background Information

Treatment of equine respiratory disorders by inhalation of therapeutic aerosols is clinically efficient[27]. The inhalation route has several well-recognised advantages over other routes of drug administration[28]. The therapeutic efficacy of the inhaled drug is governed by aerosol characteristics (i.e. determined by its formulation and physicochemical properties and by the inhalation device), technique of administration and the disease itself (e.g. bronchoconstriction and mucus plugs may impede the drug from reaching its target). To optimise aerosol therapy, knowledge of the total and regional deposition, as well as an understanding of the factors affecting these depositions, is very important. Scintigraphy offers the opportunity to examine and quantify the distribution of radioactive aerosols within the respiratory tract.

The deposition of a therapeutic aerosol should be studied using the drug labelled with a suitable γ-emitter (ideally ^{99m}Tc). This drug labelling permits simultaneous correlation between its regional deposition and pulmonary function changes. However, chemical labelling of the drugs commonly used in the management of equine respiratory disorders is often impossible[29]. Drug deposition and clinical efficacy may be studied simultaneously by producing an aerosol made of a mixture of drug and radioactive components (e.g. ventilation imaging agents). However, the distribution of radioactivity may not represent the drug's distribution, since dissociation of the radioactive component from the drug may occur during both aerosolisation and passage within the conducting airways.

Aerosol deposition may also be studied with polystyrene and Teflon particles, since they are biologically inert, and they may be labelled with various radionuclides including ^{99m}Tc. The physical characteristics of the radioactive aerosol produced should mimic the properties of the aerosolised drug to be studied. Aerosol deposition studies can establish[30]:

- The quantity of drug released from an inhalation device.
- The quantity of the realised drug reaching the respiratory tract and its fractionation within different ROIs.
- The depth of aerosol penetration and/or the amount of aerosol restrained to large airways.
- The homogeneity of aerosol distribution within the different lung regions.
- The aerosol distribution outside the lungs (e.g. face mask, upper airways, filter).

Research Applications

Aerosol deposition studies provide information that aims to:

- Define the physicochemical characteristics required for an aerosolised drug to attain a specific lung location.
- Improve inhalation devices in their ability to efficiently deliver drugs to target site(s).
- Study the distribution of an aerosol bolus at specific moments during the inspiration phase of respiration in order to improve targeting of drug receptor sites.
- Investigate the effect of diseases on regional aerosol distribution.
- Ensure that the drug reaches the affected area.
- Investigate the benefit of opening airways with bronchodilators before administration of a therapeutic aerosol.
- Simultaneously assess drug deposition and clinical efficacy of a drug formulation and/or inhalation device.
- Discover the location of drug receptor sites.
- Recommend dosages for a particular delivery system.
- Understand interaction of the lungs with inert particles or pollutants.

Scintigraphic Studies with Radiolabelled Blood Cells

Background Information

Blood cells for equine pulmonary studies can be labelled with ^{99m}Tc or Indium-111 (^{111}In). With its 173 and 247 KeV γ-emissions, ^{111}In is appropriate for the scanning of large animals. However, its long physical half-life (2.8 days) restricts its use to experimental procedures. All blood cellular elements may potentially be labelled. Several efficient labelling strategies are reported in the literature for the subpopulation of white[31–35] and red[36] blood cells of horses. Pulmonary inflammation and infection may then be detected by scintigraphy. In addition, pulmonary recruitment and lung extravasation of white blood cells may be monitored continuously[33,35]. The usefulness of labelled red blood cells in detection and quantification of EIPH remains to be proven[36].

A new radiopharmaceutical that would label neutrophils *in vivo* might potentially be used for studying inflammatory cell recruitment in the lungs of horses with COPD[37]. This ^{99m}Tc-

anti-granulocyte monoclonal antibody Fab' fragment is directed against a surface glycoprotein, nonspecific cross-reacting antigen (NCA-90), present on neutrophils. The binding of this antibody fragment to granulocytes does not affect function of cells as *in vitro* leucocyte labelling procedures are reported to[38].

Research Applications

Study of inflammatory cell recruitment into the lung is of major importance, since these cells are postulated to damage the pulmonary tissue into which they migrate. Scintigraphy with labelled white blood cells may contribute to:

- Defining the pulmonary cell kinetics of subpopulations of white blood cells in horses undergoing a pharmacological or an allergen provocation test.
- Study of the potential correlation between lung inflammatory cell recruitment and pulmonary dysfunction.
- Identification of factors controlling neutrophil migration into the lung and thereby better understanding of the pathogenesis of inflammatory lung diseases, especially in horses with COPD.
- Investigation of the effect of pro- or anti-inflammatory drugs on inflammatory cell recruitment into the lung.
- Improvement of drug and/or environmental management of pulmonary inflammatory conditions.

The clinical applications of labelling of inflammatory cells are:

- Imaging of infection and/or inflammation (see *Part II, Chapter 6*).
- The investigation of intrathoracic infection in the foal suspected of being affected with *Rhodococcus equi* infection.

The labelling of red blood cells might be useful in the detection of exercise-induced pulmonary haemorrhage and to quantify the amount of haemorrhage. First-pass imaging with labelled red blood cells may be useful in imaging the blood vessels of the lung.

New Perspective for Equine Pulmonary Scintigraphy

Developments in the field of radiopharmacy have enlarged the spectrum of nuclear medicine to molecular imaging. Several target-specific agents are becoming available, such as antibodies and peptides that have affinity for a specific receptor. Radiolabelled monoclonal antibodies targeting endothelial adhesion molecules might be of interest to better understand factors controlling leucocyte migration in respiratory disease, as well as to assess novel anti-inflammatory strategies that would act by blocking the adhesion molecules, i.e. one of the primary steps in leucocyte recruitment from blood to inflammatory sites. Labelled cytokines (e.g. interleukin-8) and chemotactic peptides which target inflammation may also help to elucidate mechanisms involved in leucocyte recruitment. Radiolabelled peptides used in the detection of deep venous thrombosis may provide an interesting tool for EIPH detection and, perhaps, quantification.

ACKNOWLEDGEMENTS

The authors gratefully acknowledge the Fonds National de la Recherche Scientifique of Belgium for supporting this work, as well as Dr Van Erck and Mrs Leblond for their contribution to the manuscript.

REFERENCES

1. Ainsworth, D.M. and Biller, D.S. (1998) Respiratory system. In: *Equine Internal Medicine*, Eds: S.M. Reed and W.M. Bayly, W.B. Saunders Co., Philadelphia. pp 251-289.
2. Votion, D., Ghafir, Y., Vandenput, S. *et al.* (1999) Analysis of scintigraphical lung images before and after treatment of horses suffering from chronic pulmonary disease. *Vet. Rec.* **144**, 232-236.
3. Votion, D.M., Vandenput, S.N., Duvivier, D.H. *et al.* (1999) Alveolar clearance in horses with chronic obstructive pulmonary disease. *Am. J. vet. Res.* **60**, 495-500.
4. Broadstone, R.V., Gray, P.R., Robinson, N.E. *et al.* (1992) Effects of xylazine on airway function in ponies with recurrent airway obstruction. *Am. J. vet. Res.* **53**, 1813-1817.
5. Keeling, D.H. (1999) Adverse reactions and untoward events associated with the use of radiopharmaceuticals. In: *Textbook of Radiopharmacy: Theory and Practice*, 3rd edn., Gordon and Breach Science Publishers, Amsterdam. pp 431-446.
6. Amis, T.C., Pascoe, J.R. and Hornof, W. (1984) Topographical distribution of pulmonary ventilation and perfusion in the horse. *Am. J. vet. Res.* **45**, 1597-1601.
7. Hakim, T.S., Lisbona, R. and Dean, G.W. (1987) Gravity-independent inequality in pulmonary blood flow in humans. *J. appl. Physiol.* **63**, 1114-1121.
8. Dobson, A., Gleed, R.D., Meyer, R.E. *et al.* (1985) Changes in blood flow distribution in equine lungs induced by anaesthesia. *Q. J. expt. Physiol.* **70**, 283-297.
9. Jarvis, K.A., Steffey, E.P., Tyler, W.S. *et al.* (1992) Pulmonary blood flow distribution in anesthetized ponies. *J. appl. Physiol.* **72**, 1173-1178.
10. Glenny, R.W. (1998) Blood flow distribution in the lung. *Chest* **114**, 8S-16S.
11. Erickson, H.H., Bernard, S.L., Glenny, R.W. *et al.* (1999) Effect of furosemide on pulmonary blood flow distribution in resting and exercising horses. *J. appl. Physiol.* **86**, 2034-2043.
12. Harmegnies, N.F., Duviviet, D.H., Vandenput, S.N. *et al.* (2002) Exercise-induced pulmonary perfusion redistribution in heaves. *Equine vet. J., Suppl.* **34**, 478-484.
13. Derksen, F.J. and Robinson, N.E. (1980) Esophageal and intrapleural pressures in the healthy conscious pony. *Am. J. vet. Res.* **41**, 1756-1761.
14. Fazio, F. and Jones, T. (1975) Assessment of regional ventilation by continuous inhalation of radioactive krypton-81m. *Br. med. J.* **3**, 673-675.
15. Burch, W.M., Sullivan, P.J. and McLaren, C.J. (1986) Technegas - a new ventilation agent for lung scanning. *Nucl. med. Comm.* **7**, 865-871.
16. Strong, J.C. and Agnew, J.E. (1989) The particle size distribution of Technegas and its influence on regional lung deposition. *Nucl. med. Comm.* **10**, 425-430.
17. Coghe, J., Votion, D. and Lekeux, P. (2000) Comparison between radioactive aerosol, Technegas and krypton for ventilation imaging in healthy calves. *Vet. J.* **160**, 25-32.
18. Amis, T.C. and Jones, T. (1980) Krypton-81m as a flow tracer in the lung: theory and quantitation. *Bull. Eur. Physiopathol. Respir.* **16**, 245-259.
19. Votion, D., Vandenput, S., Duvivier, D.H. *et al.* (1997) Analysis of equine scintigraphical lung images. *Vet. J.* **153**, 49-61.
20. O'Callaghan, M.W., Hornof, W.J., Fisher, P.E. *et al.* (1987) Exercise-induced pulmonary haemorrhage in the horse: results of a detailed clinical, post mortem and imaging study. VII. Ventilation/perfusion scintigraphy in horses with EIPH. *Equine vet. J.* **19**, 423-427.
21. Votion, D., Vandenput, S., Duvivier, D.H. *et al.* (1998) Scintigraphical evaluation of alveolar clearance in horses. *Vet. J.* **156**, 51-58.
22. Nelson, R. and Hampe, D.W. (1983) Measurement of tracheal mucous transport rate in the horse. *Am. J. vet. Res.* **44**, 1165-1166.
23. Willoughby, R.A., Erker, G.L., McKee, S.L. *et al.* (1991) Use of scintigraphy for the determination of mucociliary clearance rates in normal, sedated, diseased and exercised horses. *Can. J. vet. Res.* **55**, 315-320.
24. Coombs, S.L. and Webbon, P.M. (1987) Observations on tracheal mucociliary

clearance in horses. *Tierarztl. Prax., Suppl.* **2**, 5-9.

25. Willoughby, R., Ecker, G., McKee, S. *et al.* (1992) The effects of equine rhinovirus (ERhv-2), influenza (EIV) virus and herpesvirus (EHV-4) infection on tracheal clearance rate (TCR) in horses. *Can. J. vet. Res.* **56**, 115-121.
26. Sweeney, C.R. (1989) Tracheal mucus transport rate in healthy horses. *Am. J. vet. Res.* **50**, 2135-2137.
27. Duvivier, D.H., Votion, D., Vandenput, S. *et al.* (1997) Aerosol therapy in the equine species. *Vet. J.* **154**, 189-202.
28. Lekeux, P. and Duvivier, D.H. (2001) Aerosol therapy. In: *Equine Respiratory Diseases*, Ed: P. Lekeux, International Veterinary Information Service, Ithaca.
29. Newman, S.P. (1993) Scintigraphic assessment of therapeutic aerosols. *Crit. Rev. Ther. Drug Carrier Syst.* **10**, 65-109.
30. Votion, D. (1998) Aerosol deposition in the horse lung. In: *Proceedings of the World Equine Airways Symposium*, Guelph, Canada (CD-ROM). p 21.
31. Coyne, C.P., Kelly, A.B., Hornof, W.J. *et al.* (1987) Radiolabeling of equine platelets in plasma with ^{111}In-(2-mercaptopyridine-N-oxide) and their *in vivo* survival. *Am. J. vet. Res.* **48**, 385-391.
32. Daniel, G.B., Tucker, R.L., Buckman, T. *et al.* (1992) *In vitro* comparison of equine granulocytes labeled with ^{99m}Tc-hexamethylpropyleneamine oxime or ^{111}In-oxine. *Am. J. vet. Res.* **53**, 871-876.
33. Fairbairn, S.M., Page, C.P., Lees, P. *et al.* (1993) Early neutrophil but not eosinophil or platelet recruitment to the lungs of allergic horses following antigen exposure. *Clin. expt. Allergy* **23**, 821-828.
34. Butson, R.J., Webbon, P.M. and Fairbairn, S.M. (1995) ^{99m}Tc-HMPAO labelled leucocytes and their biodistribution in the horse: a preliminary investigation. *Equine vet. J.* **27**, 313-315.
35. Votion, D.M., Harmegnies, N.F. and Lekeux, P.M. (2000) A simple method for neutrophil isolation in horse. *Eur. J. Nucl. Med.* **27**, 1089.
36. Votion, D.M., Roberts, C.A., Marlin, D.J. *et al.* (1999) Feasibility of scintigraphy in exercise-induced pulmonary detection and quantification; preliminary studies. *Equine vet. J., Suppl.* **30**, 137-142.
37. Votion, D.M., Harmegnies, N.F. and Lekeux, P.M. (2000) Feasibility of monitoring neutrophils' migration into the lung with immunoscintigraphy: preliminary study. *Eur. J. Nucl. Med.* **27**, 1089.
38. Sampson, C.B. (1996) Complications and difficulties in radiolabelling blood cells: a review. *Nucl. med. Comm.* **17**, 648-658.

EQUINE SCINTIGRAPHY INDEX

INDEX

NB: Page numbers in italics refer to illustrations.

This is the first book ever devoted entirely to equine scintigraphy. Written by experienced clinicians working in this field, it covers the basic science of radiopharmaceuticals and scintigraphy in the horse. Chapters on the mechanism and action of the gamma camera, and quality control, are followed by sections on patient preparation, how to carry out effective scintigraphic examinations, and how to interpret and understand the images acquired. Section Two of the book goes on to study the normal appearance of the skeleton in the horse, as well as the most common examples of abnormality. Separate chapters address the performance sports horse, the racing Thoroughbred, and the Standardbred. In addition, information on radiation safety issues, the doses staff are likely to receive, and steps which can be taken to minimise these doses is included.

Nuclear scintigraphy has been widely used in equine veterinary medicine in institutions and referral practices for approximately 15 years, and in recent years more private practices have been establishing nuclear medicine facilities. It has become very apparent to us that although a number of excellent general review papers and chapters in books discuss the potential usefulness of equine nuclear scintigraphy, and some much more specific articles have been published, there has been a lack of a general text covering all aspects of equine nuclear medicine. We are also aware that, as with many imaging modalities, practitioners sometimes attempt to diagnose abnormalities without a comprehensive knowledge of normal, and the full range of normal variations, and sometimes without adequately criticising their own basic image quality. We therefore set out to harness the collective expertise of a number of people experienced with nuclear scintigraphy from a variety of geographical locations, and involved with different populations of sports and pleasure horses.

We feel strongly that nuclear scintigraphy is not a tool to be used in isolation. It should be used selectively and the results must always be related to those of clinical examination and other diagnostic techniques. It is not going to provide an answer in every horse and we have attempted to highlight both the limitations of nuclear scintigraphy and some artefacts that may confound interpretation.

We, the Editors, learnt a lot by sharing our collective experiences and sincerely hope that anyone reading this text or browsing through the figures will be both stimulated and challenged to improve their level of diagnosis.